

NIST GCR 07-914

A Computational Model for Fire Growth and Spread On Thermoplastic Objects

Michael Bockelie
Qing Tang
Reaction Engineering International
77 West 200 South
Suite 210
Salt Lake City, UT 84101

NIST
**National Institute of
Standards and Technology**
U.S. Department of Commerce

NIST GCR 07-914

A Computational Model for Fire Growth and Spread On Thermoplastic Objects

Prepared for
*U.S. Department of Commerce
Building and Fire Research Laboratory
National Institute of Standards and Technology
Gaithersburg, MD 20899-8665*

By
Michael Bockelie
Qing Tang
Reaction Engineering International
*77 West 200 South
Suite 210
Salt Lake City, UT 84101*

November 2007



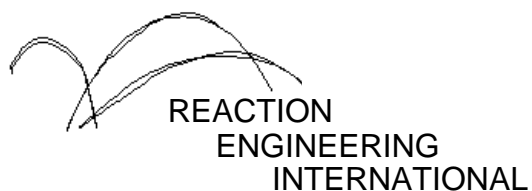
U.S. Department of Commerce
Carlos M. Gutierrez, Secretary

National Institute of Standards and Technology
James M. Turner, Acting Director

Notice

This report was prepared for the Building and Fire Research Laboratory of the National Institute of Standards and Technology under Contract number SB1341-05-C-0041. The statement and conclusions contained in this report are those of the authors and do not necessarily reflect the views of the National Institute of Standards and Technology or the Building and Fire Research Laboratory.

Committed Individuals Solving Challenging Problems



A Computational Model for Fire
Growth and Spread on Thermoplastic Objects

Final Report

By

Mike Bockelie and Qing Tang

Reaction Engineering International
Salt Lake City, Utah

October 31, 2007

Prepared for

National Institute of Standards and Technology
Contract No. SB1341-05-C-0041
REI Project No. 4716

77 West 200 South, Suite 210 - Salt Lake City, Utah 84101
Telephone: (801) 364-6925 FAX: (801) 364-6977
<http://www.reaction-eng.com>

DISCLAIMER

“This report was prepared as an account of work sponsored by an agency of the United States Government. Neither the United States Government nor any agency thereof, nor any of their employees, makes any warranty, express or implied, or assumes any legal liability or responsibility for the accuracy, completeness, or usefulness of any information, apparatus, product, or process disclosed, or represents that its use would not infringe privately owned rights. Reference herein to any specific commercial product, process, or service by trade name, trademark, manufacturer, or otherwise, does not necessarily constitute or imply its endorsement, recommendation, or favoring by the United States Government or any agency thereof. The views and opinions of authors expressed herein do not necessarily state or reflect those of the United States Government or any agency thereof.”

EXECUTIVE SUMMARY

In this report is described the work effort by Reaction Engineering International (REI) to develop, demonstrate and deliver to the National Institute of Standards and Technology (NIST) a condensed phase computational fluid dynamics (CFD) based tool to model the processes of melting, flow and gasification of thermoplastic materials exposed to a high heat flux. Potential applications of the tool include investigating the behavior of polymer materials commonly used in personal computers and computer monitors if exposed to an intense heat flux, such as occurs during a fire

The model delivered to NIST is based on a time dependent (time varying) grid CFD method.

- The model is written in FORTRAN 90 in an object-oriented form. A 3D, finite volume, multi-block body-fitted time dependent (time varying) grid formulation is used to solve the unsteady Navier Stokes equations. The time integration, spatial discretization and overall solution procedure are based on standard CFD methods from the literature. A multi-grid method is used to accelerate convergence at each time step.
- Sub-models are included to describe the temperature dependent viscosity relationship and in-depth gasification and absorption of thermoplastic materials, free surface flows and surface tension. NIST data is used for key material properties of the thermoplastic materials of interest.
- A variety of boundary conditions can be used for the velocity field (no-slip, free-slip) and heat transfer to the object (adiabatic, heat loss, specified heat flux).
- Model outputs include the time dependent velocity, temperature and position (displacement) at points in the thermoplastic body which can be imported to standard CFD visualization packages. Additional outputs include the time history of the mass loss rate and heat fluxes.
- The accuracy and capabilities of the modeling tool are demonstrated on a series of test cases of increasing complexity. The test cases include grid sensitivity studies, adding heat loss boundary conditions, simulations for two thermoplastic materials (PP702N, PP6523), different heat flux scenarios and test problem configurations.

Comparisons of model results to NIST experimental data indicate discrepancies between the model and experimental results, particularly for the rate of mass loss. To match NIST data for mass loss rate large changes were required to the parameters originally used in the in-depth absorption model and kinetic rate parameters in the in-depth gasification model. In addition, for simulations in which the free surface of the melt flow is parallel to the direction of gravity a grid smoothing operation needed to be applied to the free surface to control grid skewness that would lead to simulation divergence. For simulations that did not include models for all key physics (e.g., no in-depth absorption, no in-depth gasification) the simulations would develop a large deformation ("belly") at the free surface. For carefully selected model parameters and procedures, comparisons of the model results and NIST data show favorable agreement. However, the research effort was un-able to provide satisfactory explanations for the need to significantly increase the model parameters for the in-depth absorption and in-depth gasification models or the presence of the "belly" at the free surface of the thermoplastic object. These issues remain un-resolved though some efforts continue at NIST to address these issues.

The source code, documentation, test problems (all needed files) and presentation material have been delivered to NIST.

In the future, it may be possible to couple models such as the condensed phase CFD code to the NIST Fire Dynamics Simulator (FDS) code, a CFD model that solves for gas phase transport and combustion. The combined tools would enable high-fidelity simulations for fire spread scenarios in office environments populated with desktop/deskside personal computers.

TABLE OF CONTENTS

	Page
DISCLAIMER	i
EXECUTIVE SUMMARY	ii
TABLE OF CONTENTS.....	iv
LIST OF FIGURES	vi
LIST OF TABLES.....	viii
ACRONYMS AND ABBREVIATIONS.....	ix
1. BACKGROUND	1
1.1 Introduction.....	1
1.2 Project Management - Statement of Work, Deliverables and Reporting.....	2
1.3 Report Organization.....	3
2. METHODS AND APPROACH	4
2.1 Overview of Time Varying Grid CFD Model (CPCFD) model.....	5
2.2 Details of CPCFD model	7
2.2.1 Tracking The Free Surface	7
2.2.2 Wall Boundary Condition.....	10
2.2.3 Time Integration Algorithm.....	12
3. RESULTS AND DISCUSSION.....	14
3.1 Task 0.....	15
3.2 Task 1.....	18
3.2.1 Task Overview	18
3.2.2 Free Surface Smoothing.....	19
3.2.3 Tracking Free Surface at the Edges	21
3.2.4 Task 1B: Modeling Results of Resin PP702.....	25
3.2.5 Task 1C: Moedling Results of Resin PP6523.....	32
3.3 Task 2.....	34
3.3.1 Task Overview	34
3.3.2 Heat Loss and In-depth Absorption Models	35
3.3.3 Computational Grid and Case Summary	37
3.3.4 Results and Discussion	38
3.4 Task 3.....	41
3.4.1 Task Overview	41
3.4.2 In-depth Gasification Model.....	42
3.4.3 Task 3A – CFD Simulation of Resin PP702N.....	43
3.4.4 Task 3B – CFD Simulation of Resin PP6523.....	50
3.5 Task 4.....	51
3.5.1 Task Overview	51
3.5.2 Conjugate Flow-Heat Transfer Problem.....	53
3.5.3 Computational Grid, Melt Flow Source, Boundary and Initial Conditions.....	55
3.5.4 Implementation of Surface Tension Model	57
3.5.5 Parametric Study of Grid Sensitivity and Time Accuracy	59

3.5.6 Task 4A, 4B and 4C Results and Discussions	63
4. CONCLUSIONS.....	67
5. LITERATURE REFERENCES.....	69
APPENDIX A – Detailed PowerPoint Summary of Modeling Results	A-1
Task 0.....	A-2
Task 1.....	A-9
Task 2.....	A-83
Task 3.....	A-153
Task 4.....	A-224
APPENDIX B – Code Documentation.....	B-1
1.0 Instructions for using the CPCFD code to solve problems of Task 1, 2 and 3.....	B-2
2.0 Instructions for using the CPCFD code to solve problems of Task 4.....	B-8
3.0 Instructions for adjusting control parameters to avoid divergence.....	B-15

LIST OF FIGURES

	Page
Figure 2.1 Sketch of free surface correction procedure.....	8
Figure 2.2 Sketch of interior grid adjustment.....	9
Figure 2.3 Sketch of the sheme to enforce adiabatic wall boundary condition.....	11
Figure 3.1 Sketch of 2D test problem used in Task 0.....	15
Figure 3.2 Object height as a function of time.....	16
Figure 3.3 Temperature distribution at a selected time (1000s).....	16
Figure 3.4 Velocity vectors colored by velocity magnitude at a selected time (1000s).....	17
Figure 3.5 Geometry and boundary conditions of the 2D test problem for Task 1.....	18
Figure 3.6 Surface smoothing scheme.....	19
Figure 3.7 Fluctuations in free surface will small blending factors.....	19
Figure 3.8 Free surface evolution with large blending factors (0.1,0.5,1.0).....	20
Figure 3.9 Schematic for tracking the free surface at the edge.....	21
Figure 3.10 Free surface evolution using three different surface tracking algorithms.....	23
Figure 3.11 Mass loss percentage as function of time for three surface tracking algorithms.....	23
Figure 3.12 Viscosity-temperature relationships for PP702.....	25
Figure 3.13 Computational grids used in Task 1A and Task 1B.....	26
Figure 3.14 Typical residual histories in one time step.....	27
Figure 3.15 Mass loss percentage as function of time on four grids (PP702N).....	28
Figure 3.16 Free surface location and temperature field as a function of time (PP702N).....	29
Figure 3.17 Velocity vectors at Time = 220 seconds (PP702N).....	30
Figure 3.18 Temperature profiles on the free surface at selected times (PP702N).....	31
Figure 3.19 Viscosity-temperature relationships for PP6523.....	32
Figure 3.20 Mass loss percentage as function of time on four grids (PP6523).....	32
Figure 3.21 Sketch of in-depth absorption and heat loss models.....	35
Figure 3.22 Incident heat flux distribution in the horizontal direction.....	36
Figure 3.23 Task 2 computational grid at t = 0 sec.....	37
Figure 3.24 Mass loss percentage as a function of time for Task 2 cases.....	38
Figure 3.25 Surface temperature and velocity magnitude profiles along the free surface.....	39
Figure 3.26 Velocity vectors in Case 2A and Case 2B.....	40
Figure 3.27 Sketch of in-depth absorption, gasification, and surface heat loss models.....	42
Figure 3.28 Sketch of modeled resin in Task 3.....	43
Figure 3.29 Normalized incident heat flux profile as a function of distance from free surface ...	44
Figure 3.30 Impacts of changing gasification and absorption models in Task 3A.....	45
Figure 3.31 Impacts of external heat flux in Task 3A.....	46
Figure 3.32 Comparison of predicted and measured total mass loss rate, fraction of mass loss occurring as melt flow and surface temperature for four cases in Task 3A.....	47
Figure 3.33 Data for fraction of incident radiation versus depth used to define in-depth absorption model A4.....	48
Figure 3.34 Comparison of predicted and measured total mass loss rate, fraction of mass loss occurring as melt flow and the surface temperature for two additional cases in Task 3A.....	49
Figure 3.35 Sketch of two scenarios of melt flow with a catch surface.....	51
Figure 3.36 Sketch of Task 4 experiment.....	53

Figure 3.37 Conjugated computational model used in Task 4.....	54
Figure 3.38 Sketch of computational grids adopted in Task 4 modeling	55
Figure 3.39 1-D heat transfer problem for the catch plate.....	56
Figure 3.40 Diagram of the algorithm for calculating surface curvature	58
Figure 3.41 Free surface shapes at selected times for different time-step sizes	60
Figure 3.42 Mean spreading velocity as a function of the square of the maximum time-step size	60
Figure 3.43 Free surface shapes at selected times using different grid. No surface tension effects included.....	61
Figure 3.44 Free surface shapes at selected times using different grid. Surface tension effects included	61
Figure 3.45 Mean spreading velocity as a function of the square of the normalized grid size.....	62
Figure 3.46 Melt flow rate used in Case 4A and Case 4C.....	64
Figure 3.47 Melt flow rate used in Case 4B	64
Figure 3.48 Temperature contours of the melt pool and catch plate	65
Figure 3.49 Mean velocity of melt front as a function of time	66

LIST OF TABLES

	Page
Table 1.1 Project Tasks and Status	2
Table 3.1 Clock Time and Memory Requirement for Task 1B	31
Table 3.2 Calculated Steady-State Mass Loss Rate.....	33
Table 3.3 Task 2 Case Summary	37
Table 3.4 Calculated Steady-State Mass Loss Rate.....	38
Table 3.5 In-Depth Gasification Model Constants in Task 3A	43
Table 3.6 Task 3A Case Summary	45
Table 3.7 Task 3A Additional Case Summary	48
Table 3.8 In-Depth Gasification Model Constants in Task 3B.....	50
Table 3.9 Task 3B Case Summary	50
Table 3.10 Task 3B Results Summary	50
Table 3.11 Material Properties Used in Task 4 CFD Model	54
Table 3.12 Parametric Cases for Studying Grid Sensitivity and Time Accuracy.....	59
Table 3.13 Task 4 Case Summary	63

ACRONYMS AND ABBREVIATIONS

BFC	Body Fitted Coordinate
CFD	Computational Fluid Dynamics
CPCFD	Condensed Phase Computational Fluid Dynamics code
FDS	Fire Dynamics Simulator
NIST	National Institute of Standards and Technology
PP702N	Polypropylene resin 702N
PP6523	Polypropylene resin 6523
REI	Reaction Engineering International
SIMPLE	Semi-Implicit Method for Pressure Linked Equations
TVD	Total Variation Diminishing
VOF	Volume of Fluid
1D	One Dimensional
2D	Two Dimensional
3D	Three Dimensional

1. BACKGROUND

1.1 Introduction

This report describes the work effort by Reaction Engineering International (REI) to develop, demonstrate and deliver to the National Institute of Standards and Technology (NIST) a condensed phase computational fluid dynamics (CFD) based tool to model the processes of melting, flow and gasification of thermoplastic materials exposed to a high heat flux. This work effort is in response to NIST solicitation PWS SB1341-05-C-0041. Potential applications of the tool include investigating the behavior of polymer materials commonly used in personal computers and computer monitors if exposed to an intense heat flux, such as occurs during a fire

The condensed phase CFD (CPCFD) model delivered to NIST is based on a time dependent (time varying) grid CFD method. The time dependent grid CFD model provides a rigorous approach, enabling detailed studies of the melting and melt flow processes for thermoplastic materials. The model was developed by re-using portions of an existing CFD tool and enhancing it with sub-models required to address the specific needs of modeling thermoplastic flows. The time integration, spatial discretization and overall solution procedure are based on standard CFD methods from the literature.

CPCFD is written in FORTRAN 90 in an object-oriented form. A 3D, finite volume, multi-block body-fitted time dependent (time varying) grid formulation is used to solve the unsteady Navier Stokes equations. A multi-grid method is used to accelerate convergence at each time step. Sub-models are included to describe the temperature dependent viscosity relationship and in-depth gasification and absorption of thermoplastic materials, free surface flows and surface tension. NIST data has been used for key material properties as well as to develop and benchmark the sub-models for thermoplastic materials. A variety of boundary conditions can be used for the velocity field (no-slip, free-slip) and heat transfer to the object (adiabatic, heat loss, specified heat flux).

Model outputs include the time dependent velocity, temperature and position (displacement) at points in the thermoplastic body. The model outputs can be imported to standard CFD visualization packages. Depending on the sophistication of the visualization software, either static images at a selected point in time or animations that highlight the time-varying behavior of the thermoplastic object can be produced. The CFD images contained in this report have been generated using FIELDVIEW, a CFD visualization package available from Intelligent Light (<http://www.ilight.com>). Additional model outputs include the time history of the mass loss rate and heat fluxes that can be used in comparisons to experimental data.

The accuracy and capabilities of the modeling tool are demonstrated on a series of test cases of increasing complexity. The test cases include grid sensitivity studies, adding heat loss boundary conditions and in-depth gasification and adsorption. Simulations for two thermoplastic materials (PP702N, PP6523) are performed for different heat flux scenarios and test problem configurations.

All calculations presented in this report have been performed with computational resources typical of what is found in an engineering office (i.e., a high end personal computer).

1.2 Project Management - Statement of Work, Deliverables and Reporting

Highlighted in Table 1.1 are the tasks that were to be performed to execute this project. Included in the table is a summary of the status of each Task. The work effort for the project was divided into a Base Period, with a subsequent Option Period. As noted in the table, some tasks in the Base Period were deleted from the statement of work by NIST. In addition, NIST elected not to fund the tasks in the Option Period.

Table 1.1. Project Tasks and Status.

	Status
Task 0: Port CPCFD computer code to Fortran 90	Completed
Task 1: 2D condensed phase melt-drip model with steady imposed heat flux.	
• Task 1A = visit NIST for project kickoff meeting/discussion	Completed
• Task 1B = Perform model for Resin 1	Completed
• Task 1C = Perform model for Resin 2	Completed
Task 2: Add radiative and convective heat losses and in-depth absorption of radiative heat flux	
• Task 2A = perform model for Resin 1 using heat loss boundary condition at the heated surface	Completed
• Task 2B = perform model for Resin 1 using heat loss boundary condition at the heated surface and in-depth absorption	Completed
• Task 2C = perform model for Resin 2 using heat loss boundary condition at the heated surface and in-depth absorption	Completed
Task 3: Add gasification	
• Task 3A = Perform model for Resin 1	Completed
• Task 3B = Perform model for Resin 2	Completed
Task 4: Include melt pool on catch surface	
• Task 4A = perform model for resin 1 with gap 1	Completed
• Task 4B = perform model for resin 2 with gap 1	Completed
• Task 4C = perform model for resin 1 with gap2	Completed
• Task 4D = NIST Site visit – Project update	Deleted from SOW by NIST
• Task 4E = NIST Site visit – Base Period Program Review	Deleted from SOW by NIST
• Task 4F = Base Period Summary Report	Completed
Option Period	
Task 5: Provide expertise during coupling of condensed phase model with gas phase model	Option Period Not Exercised by NIST
Task 6: 3D flame spread model	Option Period Not Exercised by NIST
Summary Report – Final	Option Period Not Exercised by NIST

Project Kick-off meeting

A project kick-off meeting was held at the start of the project, on November 2, 2005 at the NIST offices in Gaithersburg, Maryland, to discuss project plan, technical approach and deliverables.

Deliverables and Reporting

All contractually required reports, forms, technical updates and source code, documentation and supporting files for CPCFD have been provided to the NIST COTR.

The NIST COTR has been provided with the materials listed below.

1. A one page monthly progress report for each month of the project.
2. Detailed PowerPoint summaries containing quantitative results as the work was performed (technical updates) and at Task completion. The summaries included descriptions of model enhancements and model results (e.g., CFD plots for velocity, temperature field, animations of solution variables, computational run time, XY plots for key results such as mass loss rate, comparisons to NIST data).
3. The CPCFD computational model at the completion of each Task; provided were all needed source code, input files and output files.
4. A Final Report (i.e., this document) that includes a description of the modeling method, test problems for each Task, quantitative results for each task and difficulties encountered during model development.

During the course of the project, conference call based meetings were conducted that included NIST and REI technical personnel in which technical updates and technical details of the modeling effort were discussed. The conference call meetings were held on an as-needed basis (e.g., one to two conference calls per month).

1.3 Report Organization

The remainder of this document is organized as follows:

- Chapter 2 - a description of the methods and approach used in CPCFD;
- Chapter 3 – a detailed description of the modeling results for each Task performed during the Base Period;
- Chapter 4 – conclusions from the project;
- Appendix A – a detailed PowerPoint summary for the work effort, model enhancements and model results for this project; portions of the material in Appendix A were provided to and discussed with Dr. Kathy Butler (NIST COTR) and Dr. Tom Ohlemiller (NIST) during the course of the project;
- Appendix B – CPCFD code documentation, including information on:
 - Instructions for Using CPCFD to Solve Problems of Task 1, 2 and 3;
 - Instructions for Using CPCFD to Solve Problems of Task 4; and
 - Instructions for Adjusting Control Parameters to Avoid Divergence.

2. METHODS AND APPROACH

The general approach used in CPCFD is based on standard finite volume CFD methods, the details of which are available in many references and thus only briefly described here. Two topics that merit a more detailed discussion are the technique used to generate and smooth the free surface of the time varying grid and the algorithm used to advance the solution through time in a time-accurate manner.

In the following sections, a description of the numerical details used within CPCFD are described. Provided are:

- an overview of the time varying grid CFD model;
- details for:
 - tracking the free surface;
 - wall boundary conditions; and
 - the time integration algorithm.

The description of the methods assumes the reader is familiar with CFD modeling techniques. Literature references are noted where appropriate.

2.1 Overview of Time Varying Grid CFD Model (CPCFD) model

A numerical method featuring a time-varying grid system was employed to solve the targeted thermoplastic melting problems. In the method, a grid with a body fitted coordinate (BFC) system was used to discretize the thermoplastic object. As the object deforms the grid deforms accordingly, i.e. the free surface of the object is always a boundary of the computational domain. The coordinate transformation for a three-dimensional case can be written as

$$\begin{aligned}\xi_1 &= \xi_1(x_1, x_2, x_3, t) \\ \xi_2 &= \xi_2(x_1, x_2, x_3, t) \\ \xi_3 &= \xi_3(x_1, x_2, x_3, t) \\ \tau &= t\end{aligned}\quad (1)$$

where t is time, (x_1, x_2, x_3) is another notation for the Cartesian coordinates (x, y, z) , and τ is the time in the curvilinear coordinate system (ξ_1, ξ_2, ξ_3) . Note that ξ_1 , ξ_2 and ξ_3 are functions of time. The Navier-Stokes equations in the new coordinate system is written as

$$\begin{aligned}\frac{1}{J} \frac{\partial \rho}{\partial \tau} + \frac{1}{J} \frac{\partial \rho}{\partial \xi_k} \frac{\partial \xi_k}{\partial t} + \frac{\partial}{\partial \xi_j} \left(\rho u_k \frac{1}{J} \frac{\partial \xi_j}{\partial x_k} \right) &= 0 \\ \frac{1}{J} \frac{\partial \rho u_i}{\partial \tau} + \frac{1}{J} \frac{\partial \rho u_i}{\partial \xi_k} \frac{\partial \xi_k}{\partial t} + \frac{\partial}{\partial \xi_j} \left[\left(\rho u_i u_k + p \delta_{ij} \right) \frac{1}{J} \frac{\partial \xi_j}{\partial x_k} \right] &= \frac{\partial}{\partial \xi_j} \left(\sigma_{ik} \frac{1}{J} \frac{\partial \xi_j}{\partial x_k} \right) + \rho g_i \\ \frac{1}{J} \frac{\partial \rho c_p T}{\partial \tau} + \frac{1}{J} \frac{\partial \rho c_p T}{\partial \xi_k} \frac{\partial \xi_k}{\partial t} + \frac{\partial}{\partial \xi_j} \left(\rho c_p T u_k \frac{1}{J} \frac{\partial \xi_j}{\partial x_k} \right) &= \frac{\partial}{\partial \xi_j} \left(k \frac{\partial T}{\partial \xi_m} \frac{\partial \xi_m}{\partial x_k} \frac{1}{J} \frac{\partial \xi_j}{\partial x_k} \right)\end{aligned}\quad (2)$$

where $J = \left| \frac{\partial(\xi_1, \xi_2, \xi_3)}{\partial(x_1, x_2, x_3)} \right|$ is the Jacobian of the transformation, and $\sigma_{ik} = \mu \left(\frac{\partial u_i}{\partial x_k} + \frac{\partial u_k}{\partial x_i} \right)$ is the viscous stress tensor [5]. The second term at the left-hand-side of each of three equations above comes from the time-dependent coordinate transformation. It represents the additional fluxes of mass, momentum and enthalpy (for continuity, momentum and energy equations, respectively) introduced by the moving coordinates. It should be noted that the coordinate transformation (time varying grid) introduces no approximation to the NS equations.

A pressure correction method [6] was used to solve the governing equations. All equations are discretized using a finite volume method. For the momentum equations the second-order central difference scheme is used for spatial discretization due to the large viscosity that occurs in thermoplastic flow problems [10]. For the energy equation a second-order Total Variation Diminishing (TVD) scheme is applied [10]. Time integration is performed with a fully implicit three-level method that gives second-order temporal accuracy [5]. The solution must be tightly converged at each time step to maintain numerical stability over long time periods. Hence, a multi-grid algorithm is applied to accelerate the convergence of the solution at each time step [5], [10].

The solution algorithm follows the well-known Semi-Implicit Method for Pressure Linked Equations (SIMPLE) approach [6]. In the SIMPLE the solution is advanced through time using a series of inner iteration loops and outer iteration loops. For a moving grid where the time history of the grid movement is prescribed (e.g., a piston moving in a chamber), the SIMPLE scheme can be described as follows:

- Step 1: All variables are assigned initial values at $t = t_0$.
- Step 2: Time is advanced to $t_1 = t_0 + \Delta t$, the grid is moved to the new position and an iterative procedure is performed to determine the solution of the coupled non-linear equations at the new time level.

(Note: for the first time step, a first-order Euler backward scheme is used for the time integration instead of the three-level method which requires information at two previous time levels).

➤ Within each time step, the following steps are repeated:

(Steps 2a to 2d constitute one *outer iteration* loop)

- 2a The momentum equations are discretized and linearized, leading to an algebraic equation system for each velocity component. These linear equation systems are solved iteratively in turn to obtain an improved estimate of the velocity at the new time level. Here, a multi-grid algorithm is used to accelerate the convergence. The iterations in the linear equation solver are called *inner iterations*
 - 2b The improved velocity field is used to calculate new mass fluxes through the control volume faces and to invoke the mass-conservation equation; the result is the pressure-correction equation. Upon solving for the pressure correction, the mass fluxes, cell-center velocities, and pressure are corrected.
 - 2c The energy transport equation is solved in the same manner as per step (a) to obtain better estimates for the temperature.
 - 2d Fluid properties (e.g., viscosity) and source terms (e.g., gasification mass loss rate) are updated.
- The *outer iteration* loop (steps 2a to 2d) is repeated until the residual level computed before the first inner iteration in each equation becomes sufficiently small.

When the non-linear, coupled equations are satisfied to a desired tolerance, the time is advanced by another Δt , and the above described process (Steps 1-2) repeated. The solution from the previous time step serves as the initial guess for the solution at the next time level.

For the thermoplastic melt flow problems of interest in this report, the grid does not move in a prescribed manner. Instead, the grid movement is calculated as part of the solution. The arbitrary grid movement complicates the solution procedure. Furthermore, as described in this report, special grid smoothing procedures must be performed to avoid simulation divergence. The SIMPLE solution procedure used for the melt flow problems performed in this report is described in the next section.

2.2 Details of CPCFD model

2.2.1 Tracking The Free Surface

The following boundary conditions have to be satisfied at the free surface:

- kinematic condition: this boundary condition implies that the free surface is an interface between two fluids with no flow through it, i.e.:

$$\dot{m}_{fs} = 0 \quad (3)$$

where “fs” denotes the free surface.

- dynamic condition: this boundary condition implies that the forces acting on the fluid at the free surface are in equilibrium. If the surface tension force and the viscous stresses at the free surface are neglected, the dynamic condition reduces to the statement that the pressure on both sides of the free surface must be the same.

In CPCFD, the dynamic boundary condition is implemented by treating the free surface as a boundary with a prescribed pressure. In the discretized continuity equation the velocity of the fluid at the free surface boundary is obtained with a one-sided extrapolation from the interior. The pressure-correction equation employs a Dirichlet boundary condition at the free surface.

With this approach, at the end of a SIMPLE-step the dynamic condition is satisfied - but not the kinematic condition. The grid cell face velocities at the free surface, which are corrected after solving the pressure-correction equation to enforce local and global mass conservation, can lead to non-zero mass fluxes (\dot{m}_{fs}). To satisfy the kinematic condition, the grid cell vertices which define the boundary cell face must be moved so that the correction of the volume swept by the free surface (\dot{V}'_{fs}) compensates for the mass flux created in the preceding step:

$$\dot{m}_{fs} + \dot{V}'_{fs} = 0 \quad (4)$$

An iterative procedure for correcting the free surface is used in CPCFD. The procedure is incorporated into the *outer iteration* loop of the SIMPLE algorithm described in Section 2.1.

The SIMPLE solution algorithm, including free surface tracking, used to perform the melt flow simulations in this report is summarized below.

- Step 1: All variables are assigned initial values at $t = t_0$.
- Step 2: Time is advanced to $t_1 = t_0 + \Delta t$, the grid is moved to the new position and an iterative procedure is performed to determine the solution of the coupled non-linear equations at the new time level.

(Note: for the first time step, a first-order Euler backward scheme is used for the time integration instead of the three-level method which requires information at two previous time levels).

- Within each time step, the following steps are repeated:

(Steps 2a to 2e constitute one *outer iteration* loop)

- 2a Solve the momentum equations using the geometry defined by the current shape of the free surface and the prescribed pressure on it. This replaces the *inner iteration* loop (step 2a) outlined in Section 2.1.

- 2b Enforce local mass conservation in each control volume by solving the pressure-correction equation, using the prescribed pressure boundary condition at the current free surface. Mass is conserved both globally and in each control volume, but non-zero mass fluxes through the free surface can result.
 - 2c Correct the position of the free surface so that the volume defined by its corrected and previous position compensates for the mass fluxes through the free surface obtained in the preceding step.
 - 2d The energy transport equation is solved in the same manner as per step 2a to obtain better estimates for the temperature.
 - 2e Fluid properties (e.g., viscosity) and source terms (e.g., gasification mass loss rate) are updated.
- The *outer iteration* loop (steps 2a-2e) are repeated until all equations and boundary conditions are satisfied (i.e., until the mass fluxes are zero and the residual of each equation is smaller than a threshold value).

The time is advanced by another Δt , and the above described process (Steps 1-2) repeated. The solution from the previous time step serves as the initial guess for the solution at the next time level.

The free surface correction procedure described in step 2c (above) is illustrated in Figure 2.1.

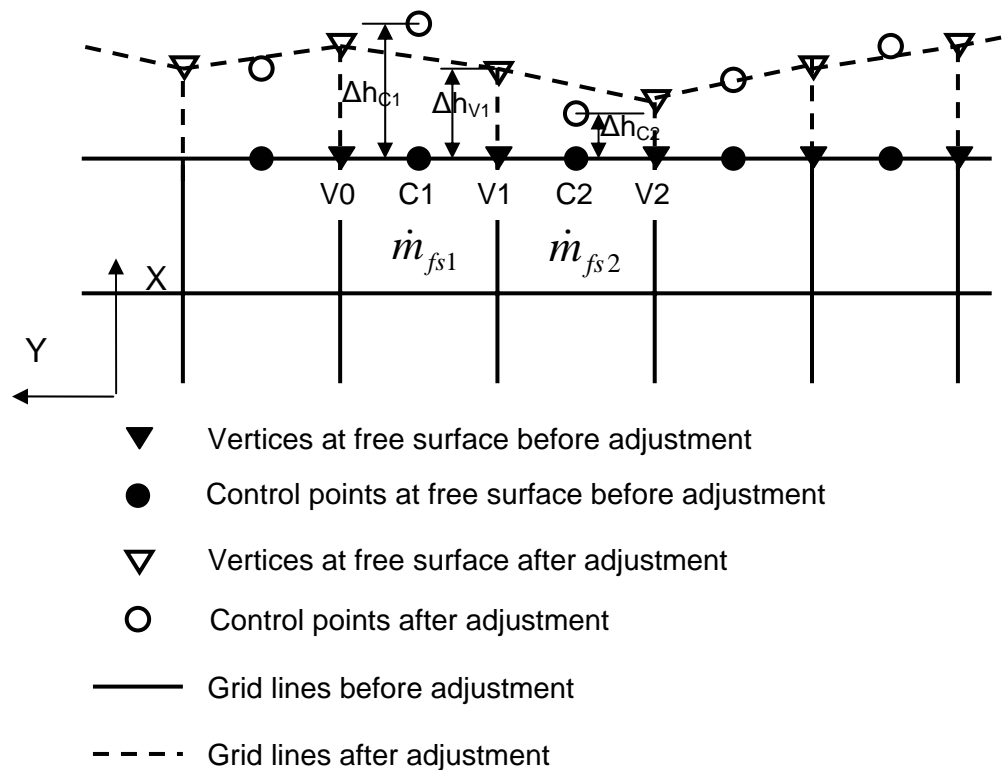


Figure 2.1 Sketch for free surface correction procedure.

In the current implementation, the vertices that define the free surface are only allowed to move in one direction (i.e., in the X direction in Figure 2.1). This significantly simplifies the re-

meshing algorithm and has been shown to be adequate for modeling the targeted thermoplastic deformation problems.

- The first step in the free surface correction algorithm is to define a set of control points along the current free surface. The current cell face centers are selected for this purpose. The corrected positions of the control points defined by the displacement Δh_C are calculated as

$$\Delta h_C = \frac{\dot{m}_{fs} \Delta t}{\rho A}, \quad (5)$$

where \dot{m}_{fs} is the mass flux through the cell face, Δt is the time step, ρ is the density, and A is the area of the cell face.

- The corrected positions of vertices are defined by the displacement Δh_V , which is computed by averaging neighboring Δh_C 's. If uniform grid spacing is used in the Y direction, such as shown in Figure 2.1, then Δh_V is expressed as

$$\Delta h_{V,n} = \frac{1}{2} (\Delta h_{C,n} + \Delta h_{C,n+1}), \quad (6)$$

where n is the index of the vertex.

- The free surface after correction is defined by the corrected vertices shown as dashed line in Figure 2.1.

The grid in the interior of the solution domain must respond to the movement of the vertices in the free surface, to preserve its good quality (i.e., avoid grid skewness). A simple and general re-meshing technique for the internal grid, which can be successfully applied in all situations and for all geometries, is difficult to devise. The current algorithm simply re-adjusts the location of the inner vertices to preserve the same relative position between the free surface and the opposite boundary. In addition to the adjustment of the interior grid, the mass fluxes through the interior cell faces may also need adjustment to maintain mass conservation in the new control volume. As shown in Figure 2.2, the mass flux \dot{m}^{k+1} after the grid adjustment is calculated as

$$\dot{m}^{k+1} = \dot{m}^k - \frac{\rho V}{\Delta t}. \quad (7)$$

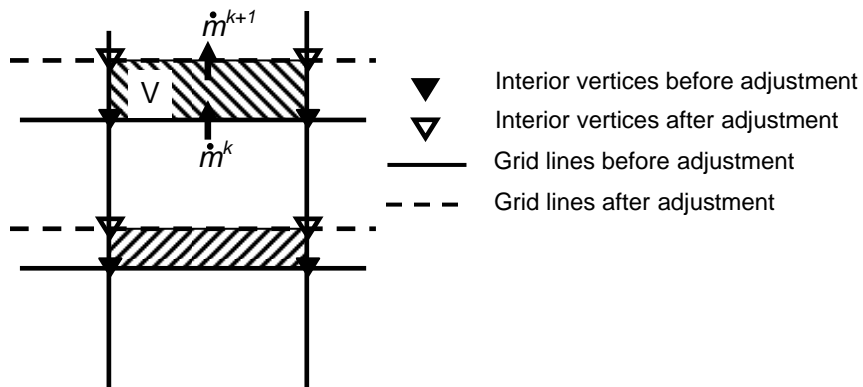


Figure 2.2 Sketch of interior grid adjustment.

2.2.2 Wall Boundary Condition

In CPCFD, the wall boundary conditions are implemented by using “ghost” cells. Ghost cells are grid cells that form the boundary of the computational domain. The cell center quantities such as velocity and temperature of a ghost cell are not updated in the procedure of solving the governing partial differential equations (PDEs). A “wall cell” is a ghost cell that forms the solid wall surrounding the computational domain. A “fluid cell” is a grid cell in the interior of the computational domain whose cell center quantities are the solution of the governing PDEs.

In this project, wall boundary conditions are characterized as no-slip/slip, no-penetration, and adiabatic/constant temperature.

- In CPCFD, the slip wall boundary condition is implemented by equating the cell-center velocity components in a wall cell (i.e., ghost cell) with its neighboring fluid cell.
- The constant temperature condition is implemented by setting the temperature at the wall cell (i.e., ghost cell) cell-center to a given temperature.
- The no-slip, no-penetration wall boundary is implemented by setting the cell-center velocity components in the wall cells (i.e., ghost cells) of the boundary to zero. When calculating the diffusive source terms in the momentum equations, the velocity components at the wall cell face-center are needed. In CPCFD, the velocity components at a grid cell face-center are obtained by interpolating the velocity components at the two grid cell-centers that share the same grid cell-face. The interpolation factor is determined by the respective distances between the grid cell face-center and the two grid cell-centers. For the velocity at the wall cell face-center, the interpolation factor is either 0 or 1 depending on where the wall cell lies relative to the fluid cell. For example, if the grid cell above (north of) the fluid cell is a wall cell (i.e., ghost cell) then the interpolation factor is 1. With this approach, the velocity components at a wall cell face-center is always set equal to the velocity components at the wall cell cell-center, which is always zero for a no-slip, no-penetration wall.
- The adiabatic wall boundary condition is implemented by setting the neighboring coefficient associated with the wall cell to zero. For example, the 1D generic transport equation (Eq. (10)) can be written as a discretized algebraic equation for cell P as follows:

$$A_E T_E + A_W T_W - (A_E + A_W - S_P) T_P = S_U, \quad (8)$$

where T is the cell center fluid temperature to be solved; A_E , A_W , and $A_P = (A_E + A_W - S_P)$ are the coefficients; S_U and S_P are the source terms; and cell E and cell W are the neighboring cells of cell P and lie to the east and west of cell P , respectively.

For illustration purposes, it is assumed the east side of cell P is an adiabatic wall. Thus, cell E is a wall cell (i.e., ghost cell) and its cell center temperature T_E must be equal to T_P . Substituting the condition $T_E = T_P$ into Eq. (8) results in

$$A_w T_w - (A_w - S_p) T_p = S_U, \quad (9)$$

which implies $A_p = -(A_w - S_p)$. This is equivalent to assigning A_E to 0 before A_p is calculated. In CPCFD, Eq. (9) is used to construct the linear equation system for the unknowns and is solved iteratively.

The above implementation for the adiabatic wall boundary condition implies that the zero heat flux condition (i.e., adiabatic condition) at the wall face is satisfied along the line that connects the fluid cell cell-center and the wall cell (i.e., ghost cell) cell-center. However, if the line is not perpendicular to the wall surface, an error is introduced into the solution. In CPCFD, this error is eliminated by adjusting the wall cell (i.e., ghost cell) cell-center positions during the re-meshing step so that the line connecting a fluid cell and its wall cell (i.e., ghost cell) counterpart is always normal to the wall cell cell-face. This is illustrated in Figure 2.3. Here, the wall cell cell-face is defined by vertices **a** and **b**, and point **c** is the cross point of the wall cell cell-face and the line connecting the two cell centers. As long as point **c** is within face **ab**, the scheme remains first-order accurate. If point **c** lies outside **ab**, then grid refinement in the vertical direction is needed to maintain first-order accuracy.

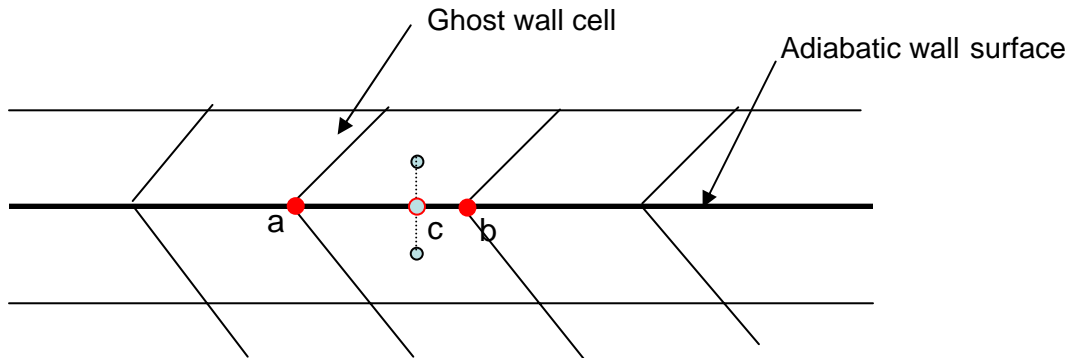


Figure 2.3 Sketch of the scheme to enforce adiabatic wall boundary condition.

2.2.3 Time Integration Algorithm

As noted above, two time integration methods are used in CPCFD. The first order, implicit Euler method is used for the first time step of the solution. A second order implicit method is used for all subsequent time steps.

First Order Euler Method

Originally, the first order implicit Euler method was the only time integration method available in CPCFD [5]. For illustration purposes, we consider a one dimensional (1D) generic transport equation with constant velocity, constant fluid properties, and no source terms:

$$\frac{\partial \phi}{\partial t} = -u \frac{\partial \phi}{\partial x} + \frac{\Gamma}{\rho} \frac{\partial^2 \phi}{\partial x^2}. \quad (10)$$

If a central differencing scheme is used for the spatial derivatives, the discretized algebraic equations in the implicit Euler method are written as:

$$A_P \phi_i^{n+1} + A_E \phi_{i+1}^{n+1} + A_W \phi_{i-1}^{n+1} = Q_P, \quad (11)$$

where

$$\begin{aligned} A_E &= \frac{\rho u}{2\Delta x} - \frac{\Gamma}{(\Delta x)^2}; \\ A_W &= -\frac{\rho u}{2\Delta x} - \frac{\Gamma}{(\Delta x)^2}; \\ A_P &= -(A_E + A_W) + \frac{\rho}{\Delta t}; \\ Q_P &= \frac{\rho}{\Delta t} \phi_i^n. \end{aligned} \quad (12)$$

The above method is unconditionally stable but has a first order truncation error.

Second Order Implicit Method

To achieve higher time accuracy, a fully implicit scheme of second order accuracy [5] is used in CPCFD. By using a quadratic backward approximation in time and central differencing in space, the resulting algebraic equation for the 1D generic transport equation is written as:

$$A_P \phi_i^{n+1} + A_E \phi_{i+1}^{n+1} + A_W \phi_{i-1}^{n+1} = \frac{2\rho}{\Delta t} \phi_i^n - \frac{\rho}{2\Delta t} \phi_i^{n-1} \quad (13)$$

where the coefficients A_E and A_W are the same as in case of the implicit Euler scheme. However, the central coefficient now has a stronger contribution from the time derivative:

$$A_P = -(A_E + A_W) + \frac{3\rho}{2\Delta t}, \quad (14)$$

and the source term contains contribution from time level t_{n-1} . The implementation of the second order scheme on top of the implicit Euler scheme is straightforward.

Stability and Time Step Size

Although both methods are unconditionally stable, it was found that the solution may diverge if the time step is too large. This can occur due to the free surface tracking scheme being an explicit procedure (see Eq. (5)). In the current model, the time step is determined by

$$\Delta t = \min \left(\Delta t_{\max}, c \frac{\Delta x}{|u|} \right) \quad (15)$$

where Δt_{\max} is a user supplied maximum time step and c is the Courant number. In simulating the targeted thermoplastic deformation problem, if oscillations occur or the solution diverges, the user must either reduce the maximum time step or reduce the Courant number.

3. RESULTS AND DISCUSSION

In this section the modeling results for the different test cases investigated are provided. The material in this section is organized by Task (see Table 1.1). Provided, in order, are descriptions of the work effort and example results for:

- Task 0: Port CPCFD computer code to Fortran 90
- Task 1: 2D condensed phase melt-drip model with steady imposed heat flux.
 - Task 1A = visit NIST for project kickoff meeting/discussion
 - Task 1B = Perform model for Resin 1
 - Task 1C = Perform model for Resin 2
- Task 2: Add radiative and convective heat losses and in-depth absorption of radiative heat flux
 - Task 2A = perform model for Resin 1 using heat loss boundary condition at the heated surface
 - Task 2B = perform model for Resin 1 using heat loss boundary condition at the heated surface and in-depth absorption
 - Task 2C = perform model for Resin 2 using heat loss boundary condition at the heated surface and in-depth absorption
- Task 3: Add gasification
 - Task 3A = Perform model for Resin 1
 - Task 3B = Perform model for Resin 2
- Task 4: Include melt pool on catch surface
 - Task 4A = perform model for resin 1 with gap 1
 - Task 4B = perform model for resin 2 with gap 1
 - Task 4C = perform model for resin 1 with gap 2

3.1. Task 0: Port CPCFD to Fortran 90

The CPCFD code was originally written in C++. To reduce concerns about future enhancements and support, NIST required that the delivered computational model be written in Fortran 90. Hence, the first task performed by REI was to re-write the code in Fortran 90. The Fortran 90 version of CPCFD retains the object-oriented design of the C++ code and is organized into two subroutines and a main program. The test problem from the NIST RFP is used to demonstrate the consistency between the C++ code and the Fortran code. The results are described below.

The test problem is a triangular object resting in a flat container. The object is 5 cm high and makes an angle of 45° with the container surface. Figure 3.1 below illustrates the right half of the problem. A constant heat flux is applied to the surface of the object, and heat losses due to radiation and convection are taken into account. Free-slip boundary conditions and adiabatic boundary conditions are applied to the plane of symmetry along the left face of the object and also to the base and side wall of the container.

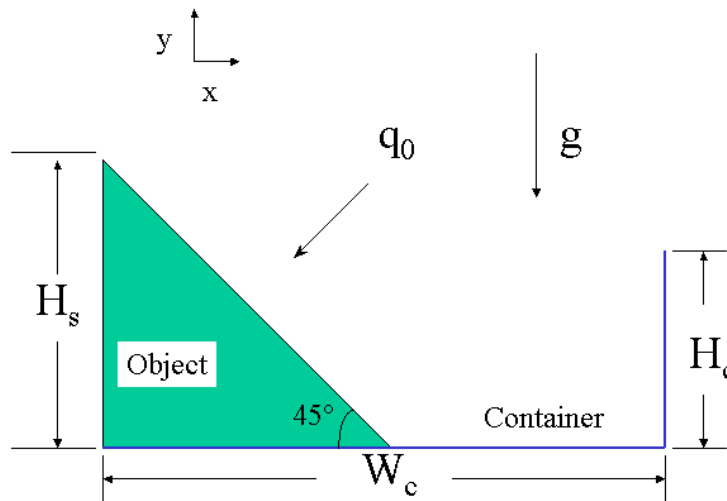


Figure 3.1 Sketch of 2D test problem used in Task 0.

A 102×52 grid is used to model the test problem. A constant time step of 2 seconds is used. The convergence criterion for each time step in the simulation is that at least five significant digits remain unchanged from iteration to iteration. The simulation was run for 1300 time steps (2600 seconds in integration time).

Shown in Figure 3.2 is the object height as a function of time. The result from the C++ code is plotted as a solid line and the result from the Fortran code is plotted as a dotted line. The difference between the two solutions are negligible. It requires 2502 seconds for the object height, H , to be reduced down to $0.26H_s$ (0.013m), after which the object height decreases at a smaller rate as it approaches steady state. Shown in Figure 3.3 and Figure 3.4 are the temperature contours and velocity vectors, respectively, at 1000 s. Again, the results are almost identical. It should be pointed out that the Fortran code runs slightly slower than the C++ code.

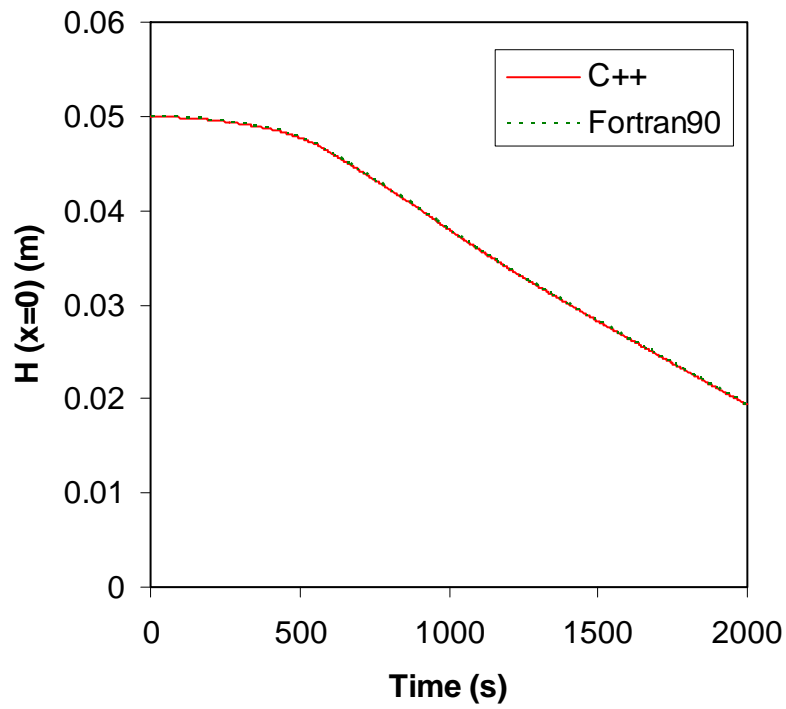


Figure 3.2 Object height as a function of time.

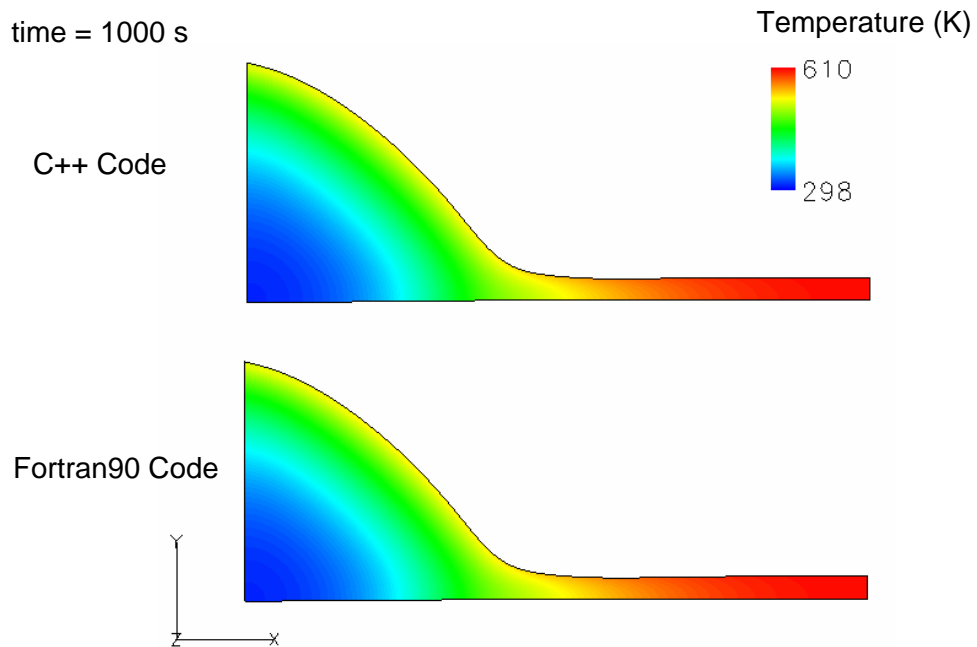


Figure 3.3 Temperature distribution at selected time (1000 s).

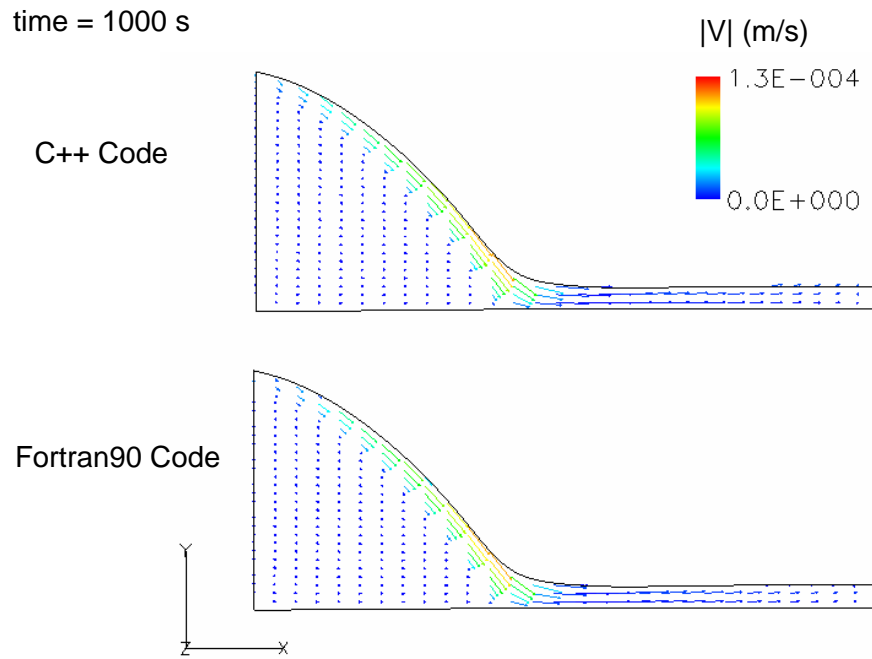


Figure 3.4 Velocity vectors colored by velocity magnitude at selected time (1000 s).

3.2. Task 1: 2D model with steady imposed heat flux

3.2.1 Task Overview

In this section, the CPCFD code is used to solve for the flow and temperature field that results for an upright 2D thermoplastic slab exposed to a steady heat flux on one side. The Task 1 test problem is illustrated Figure 3.5. The slab rests on a fixed boundary surface on the right and bottom faces with adiabatic heat properties. The geometry of the catch surface is ignored in this task. The viscosity of the slab is strongly dependent on temperature, and the material flows out over the bottom boundary when its temperature is sufficiently high. The steady imposed heat flux is applied directly to the material surface regardless of its shape.

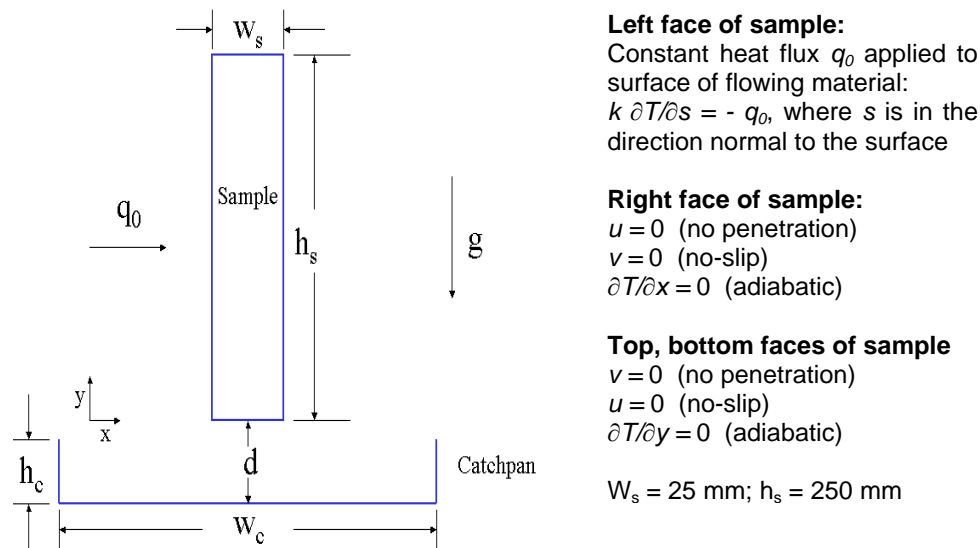


Figure 3.5 Geometry and boundary conditions of the 2D test problem for Task 1.

The behavior of two polypropylene resins, PP702N and PP6523, are examined. As described below these two resins have very different viscosity-temperature relationships. This task was performed in three steps:

- Task 1A = visit NIST for project kickoff meeting/discussion;
The project kick-off meeting was held at the start of the project, on November 2, 2005 at the NIST offices in Gaithersburg, Maryland, to discuss project plan, technical approach and deliverables.
- Task 1B = Perform model for Resin PP702; and
- Task 1C = Perform model for Resin PP6523.

Provided, in order, in the remainder of this section are:

- the free surface smoothing scheme used to ensure stability during simulations;
- improvements to the free surface tracking algorithm used to determine the locations of vertices that are common to the free surface and a no-slip wall;
- model results for Task 1B (for PP702N); and
- model results for Task 1C. (for PP6523).

3.2.2 Free Surface Smoothing

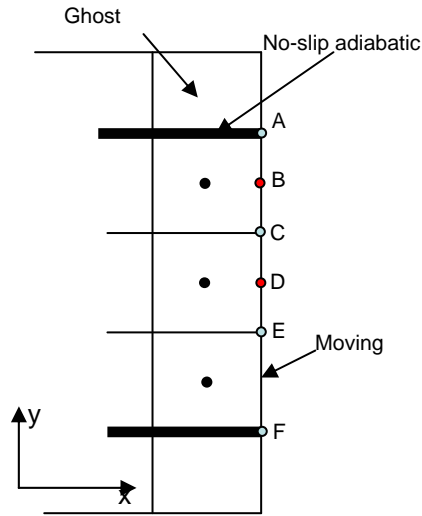


Figure 3.6 Surface smoothing scheme.

Modeling experience highlighted the need to develop a grid smoothing scheme that could be applied to the free surface to avoid fluctuations in the solution when the free surface is almost parallel to the gravitational force. As shown in Figure 3.6, the new location of vertex C in the X direction after one time step is calculated as follows:

1. Calculate the new face center locations

$$x_D^{new} = x_D^{old} + \frac{\dot{m}_D}{\rho A_{CE}} \Delta t \quad (16)$$

2. Calculate the temporary vertex point locations

$$x_C^* = \frac{1}{2} (x_B^{new} + x_D^{new}) \quad (17)$$

3. Smooth the moving boundary

$$x_C^{new} = (1 - \alpha) \cdot x_C^{old} + \alpha \cdot \frac{1}{4} (x_A^{old} + 2x_C^* + x_E^*), \quad (18)$$

where α is a blending factor, \dot{m}_D is the mass flux through the cell face, Δt is the time step, ρ is the density, and A_{CE} is the area of the cell face. Note that in Step 2 and Step 3 the positions of the boundary vertex point (e.g., point A in Figure 3.6) are not updated and x_A^{old} is used in Eq. (18). The algorithms used to calculate the positions of the boundary vertex are described in the next section.

Figure 3.7 shows the evolution of the free surface in two test cases similar to the Task 1 test problem. The value of the blending factor α is set to 0.0 and 0.01, respectively. Furthermore, note that for $\alpha = 0.0$ no smoothing is performed at the free surface.

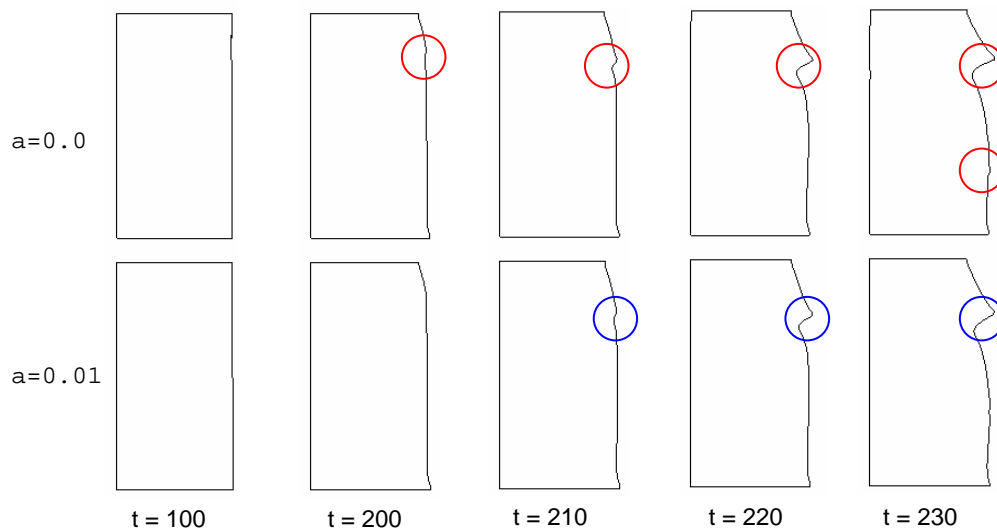


Figure 3.7 Fluctuations in free surface with small blending factors. The top row uses a blending factor of 0.0 and the bottom row uses a blending factor of 0.01.

From Figure 3.7, it can be seen that with no smoothing, or a very small blending factor, fluctuations develop along the free surface at a very early stage of the simulation.

Figure 3.8 shows the results for using three larger blending factors. It is found that, when $\alpha > 0.1$, the free surface becomes very smooth and no fluctuations occur during the calculations. For most simulations, a blending factor of 1.0 is used. The blending factor is set within the source code for CPCFD.

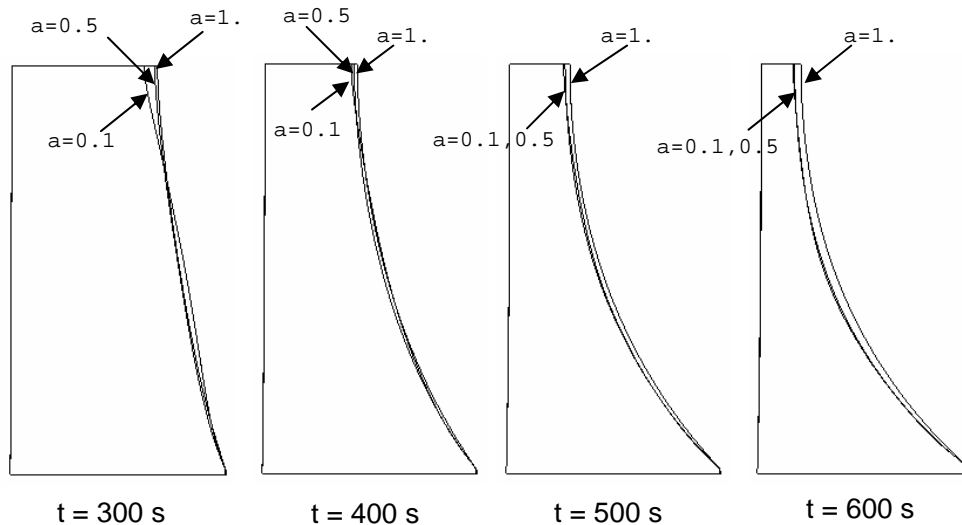


Figure 3.8 Free surface evolution with large blending factors (0.1, 0.5, 1.0).

3.2.3 Tracking the Free Surface at the Edges

As outlined in Section 2.2.1, the kinematic condition is used to move the control points (i.e., free surface cell face centers). The cell vertices between these control points are then moved to locations obtained by interpolating coordinates of neighbor control points, but it remains open how to move the points at the edges of the free surface. For points on the free surface the vertex moves the same distance as the neighboring control point. However, the edges between free surface and the solid wall require special attention.

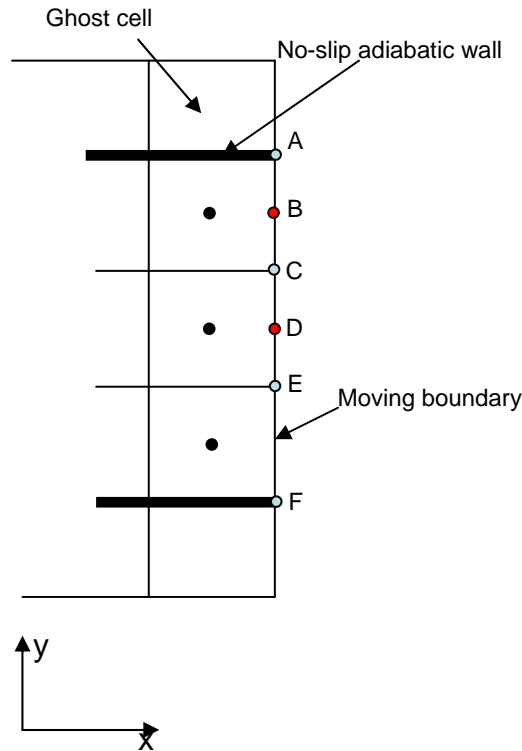


Figure 3.9 Schematic for tracking the free surface at the edge.

For the vertex point on the free surface that resides on the solid wall the grid vertex point is allowed to move along the wall, but the movement is performed in a manner that enforces the “no-slip” condition. Simply fixing the location of this grid point is not adequate; such an approach results in significant grid skewness that leads to divergence of the simulation.

Three models (algorithms) have been investigated to move the vertex points at the solid wall-free surface vertices. In Figure 3.9, point A is a vertex shared by the no-slip wall and the free surface, vertices A, C, E, and F lie on the free surface, and points B and D are cell face centers that serve as control points.

As outlined in Section 2.2.1, the first step in determining the moving boundary after each time step is to calculate the new control point locations, for example

$$x_B^{new} = x_B^{old} + \frac{\dot{m}_B}{\rho A_{AC}} \Delta t \quad (19)$$

where \dot{m}_B is the mass flux through face AC obtained by solving the momentum equations and pressure-correction equation. It should be noted that, in solving for \dot{m}_B , the no-slip boundary condition is satisfied. The second step is to calculate new locations of the vertices by interpolating the positions of neighbor control points. However, for vertex point A on the edge, special treatment is needed. The three models tested pertain to step 2 in the free surface correction algorithm in section 2.2.1.

Model 1

In this algorithm vertex point A is simply moved by the same amount as its neighboring vertex (i.e., point C), resulting in:

$$x_A^{new} = x_C^* = \frac{1}{2}(x_B^{new} + x_D^{new}). \quad (20)$$

After computing x_A^{new} , a smoothing step is applied which updates the locations of the interior vertices (e.g., point A and point E) and x_A^{new} from Eq. (20) is used instead of x_A^{old} in Eq. (18). No smoothing is applied to x_A^{new} .

Model 2

The second approach investigated assumes that vertex A moves the same amount as the control point next to it (i.e., cell face-center point B). In this approach, Eq. (20) is replaced by

$$x_A^{new} = x_B^{new} = x_B^{old} + \frac{\dot{m}_B}{\rho A_{AC}} \Delta t. \quad (21)$$

After computing x_A^{new} , a smoothing step is applied which updates the locations of the interior vertices (e.g., point A and point E) and x_A^{new} from Eq. (21) is used instead of x_A^{old} in Eq. (18). No smoothing is applied to x_A^{new} .

Model 3

The last approach investigated involves applying the smoothing process to the interior vertices *before* updating the position of the edge vertex. In this approach, Eq. (17) and Eq. (18) are applied as described in Section 2.2.1, after which x_A^{new} is computed from:

$$x_A^{new} = x_C^{new} = \frac{1}{4}(x_A^{old} + 2x_C^* + x_E^*). \quad (22)$$

No smoothing is applied to x_A^{new} .

Comparison of the Three Models

Figure 3.10 shows the test results using these three models. The test case is similar to the Task 1 problem, where the top boundary is a no-slip wall and the right side boundary is the free surface exposed to a constant heat flux.

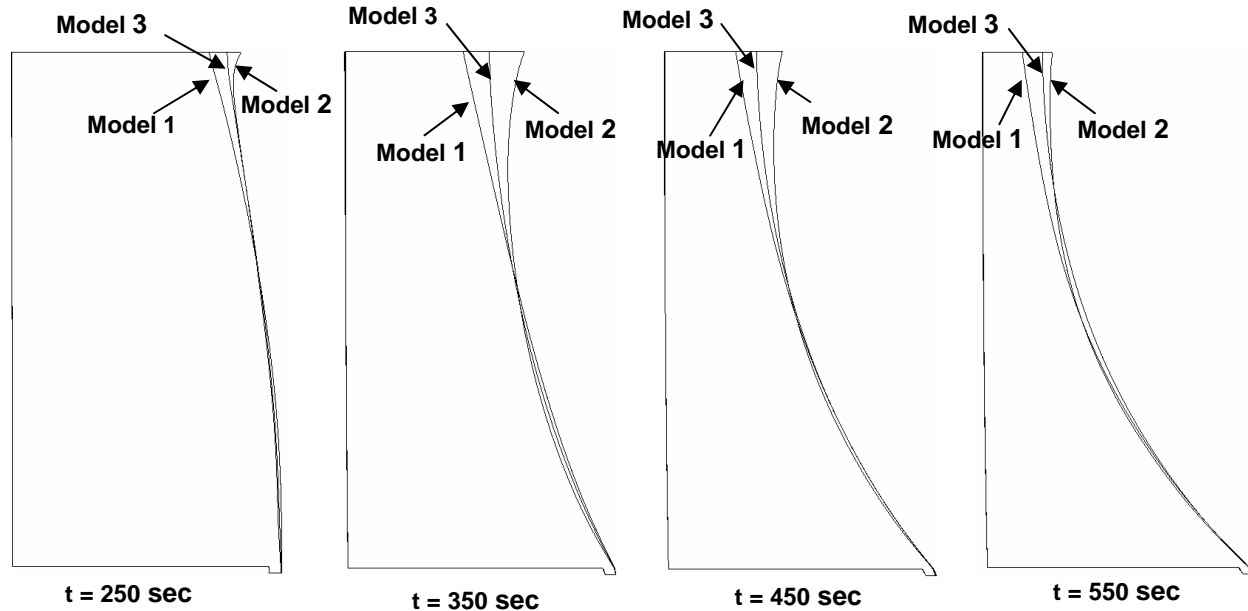


Figure 3.10 Free surface evolution using three different surface tracking algorithms.

In Figure 3.10, it can be seen that the edge vertex at the top-right corner retreats much faster in Model 1 than in Model 2. This is because in Model 2, the movement of point A is approximated by the movement of point B rather than point C (see Figure 3.9). The no-slip wall boundary condition has a stronger influence on point B than point C because point B is halfway closer to the wall than point C. The different melting behaviors observed in Figure 3.10 for Model 1 and Model 3 are a result of the surface smoothing process.

Figure 3.11 shows the mass loss histories obtained from the test case using the three different surface tracking models described above. Although the different models strongly impact the shape of the free surface (i.e., Figure 3.10), the differences in the mass loss histories are very small for these simulations.

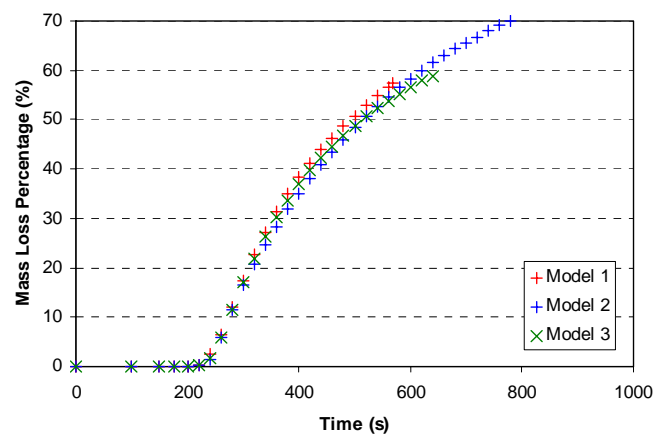


Figure 3.11 Mass loss percentage as function of time for three surface tracking algorithms.

Model 1 is used for the simulations performed for the Task 1, mainly because the issue of tracking the edge vertex was not raised until the simulations for Task 2 were being performed. Furthermore, Model 1 was adequate for the problem addressed in Task 1. During the work effort for Task 2 it became necessary to develop a better method to treat the vertex point at the edge of the free surface. In the parametric study described in this section, the simulation using Model 3 predicted a free surface shape that, qualitatively, better agreed with observed behavior in NIST experiments and with simulation results obtained by NIST using a volume of fluid (VOF) method [1]. Therefore Model 3 is used for the simulations presented for Task 2 and Task 3. None of the models were needed for the simulations performed for Task 4.

3.2.4 Task 1B: Modeling Results for Resin PP702

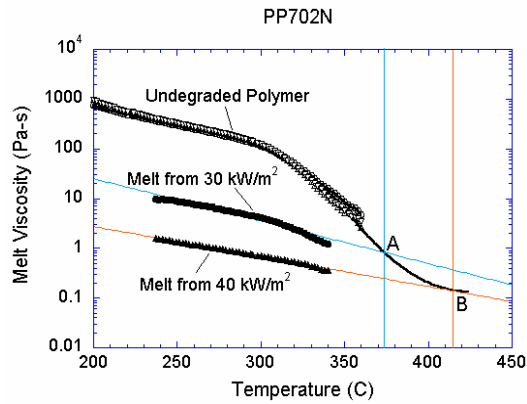


Figure 3.12 Viscosity-temperature relationships for PP702.

Figure 3.12 shows the measured viscosity of the PP702 polymer as a function of temperature with a fixed shear rate of 0.1 [13]. Note that in the figure the melt viscosity uses a log scale. In addition, the figure highlights a highly non-linear temperature-viscosity relationship; that is, small changes in temperature result in very large changes in viscosity. The solid line in Figure 3.12 is used in the CFD model to describe the highly non-linear viscosity-temperature relationship, which can be expressed as

$$\mu = \begin{cases} 10^6 & T < 25^\circ\text{C} \\ 10^6(200 - T)/(200 - 25) + f_1(200) & 25^\circ\text{C} \leq T < 200^\circ\text{C} \\ f_1(T) & 200^\circ\text{C} \leq T < 350^\circ\text{C} \\ f_2(T) & 350^\circ\text{C} \leq T < 425^\circ\text{C} \\ f_2(425) & T \geq 425^\circ\text{C} \end{cases}$$

$$f_2(T) = 10^{(53.19 - 0.2542 T + 2.9879 \times 10^{-4} T^2)}$$

$$f_1(T) = 10^{(14.48 - 0.13858 T + 5.5960 \times 10^{-4} T^2 - 7.8665 \times 10^{-7} T^3)}$$

The width and height of the 2D object are 25 mm and 250 mm, respectively. All material properties are constant except the viscosity; the density (ρ) is 900 kg/m³, the heat capacity (C_p) is 2400 J/kg-K, and the heat conductivity (k) is 0.5W/m-K. The initial temperature is 300 K and the external heat flux is 20,000 W/m². The external heat flux is implemented as a source term in the energy equation, and it only affects the control volumes immediately next to the free surface (i.e., in-depth absorption is not modeled and all the energy is absorbed in the free surface). No heat loss is considered in this task. Due to the lack of key physical models such as radiative heat loss in the model, overheating of the material (i.e., the temperature rises to more than 1000 K) occurs when the width of the object becomes too small). Overheating causes sharp changes in viscosity (e.g., one order of magnitude change in viscosity due to several degrees difference in temperature) along the free surface. The material with low viscosity tends to roll-over the material with high viscosity, which cannot be handled by CPCFD. To overcome this problem, an artificial heat sink term is added to the energy transport equation. The heat sink term is constructed to mimic the gasification heat loss term. However, no mass loss is involved in the model for this Task. The heat sink term can be expressed as a function of temperature (T) as :

$$q = -B \exp\left(-\frac{E}{T}\right). \quad (23)$$

For Task 1B and Task 1C, the constants in Eq. (23) are chosen as $B = 6.276 \times 10^{20}$ and $E = -25350$. The heat sink term is negligible when the temperature is below 700 K and becomes significant when the temperature exceeds 750 K.

To evaluate the sensitivity of the model results (e.g., mass loss rate) to grid resolution, four grids - 14×200 , 15×200 , 19×200 and 21×200 - with different levels of grid resolution near the free surface are used in the calculations. The latter three grids are shown in Figure 3.13. Note that the lines shown in the figures connect cell centers instead of vertices. In the vertical direction the

grid cell spacing is uniform with 200 cells. In the horizontal direction the grid cell spacing is biased (i.e., non-uniform). In the 15×200 grid, the first three layers of cells next to the free surface have a cell size of 0.625 mm in the horizontal direction. In the 19×200 grid and the 21×200 grid, the cell size near the surface reduces to 0.5 mm and 0.3125 mm, and the number of cells with these cell sizes increases to 4 and 6, respectively. These small cells form a layer along the free surface with a width of about 2 mm, which is adequate to cover the melt flow based on the experience gained in a trial-and-error process. The initial width of the outlet boundary is set to a small value, i.e., 0.5 mm. There are 3, 4, and 6 cells in the outlet boundary in the three grids, respectively. The ratio of the cell sizes in the horizontal direction is fixed throughout the calculation, thus increasing the number of small cells near the free surface leads to higher resolution of the sharp gradient near the surface. Because CPCFD uses a moving grid method, the region of high grid resolution tracks the time dependent location of the free surface.

Because the interface is always a boundary in the interface tracking method implemented in CPCFD, high grid resolution is only required near the moving boundary. This is not the case for methods such as VOF in which high grid resolution must be used throughout the computational domain because the interface lies inside the domain and the location of the interface changes with time [1]. Hence, using grids with biased cell spacing with dimensions of 15×200 , 19×200 , and 21×200 in the CPCFD simulations provides a grid resolution at the free surface that is equivalent to that of grids with a uniform cell spacing with dimensions of, respectively, 40×200 , 50×200 , and 80×200 . Note that VOF simulations typically require a grid with a uniform grid cell spacing.

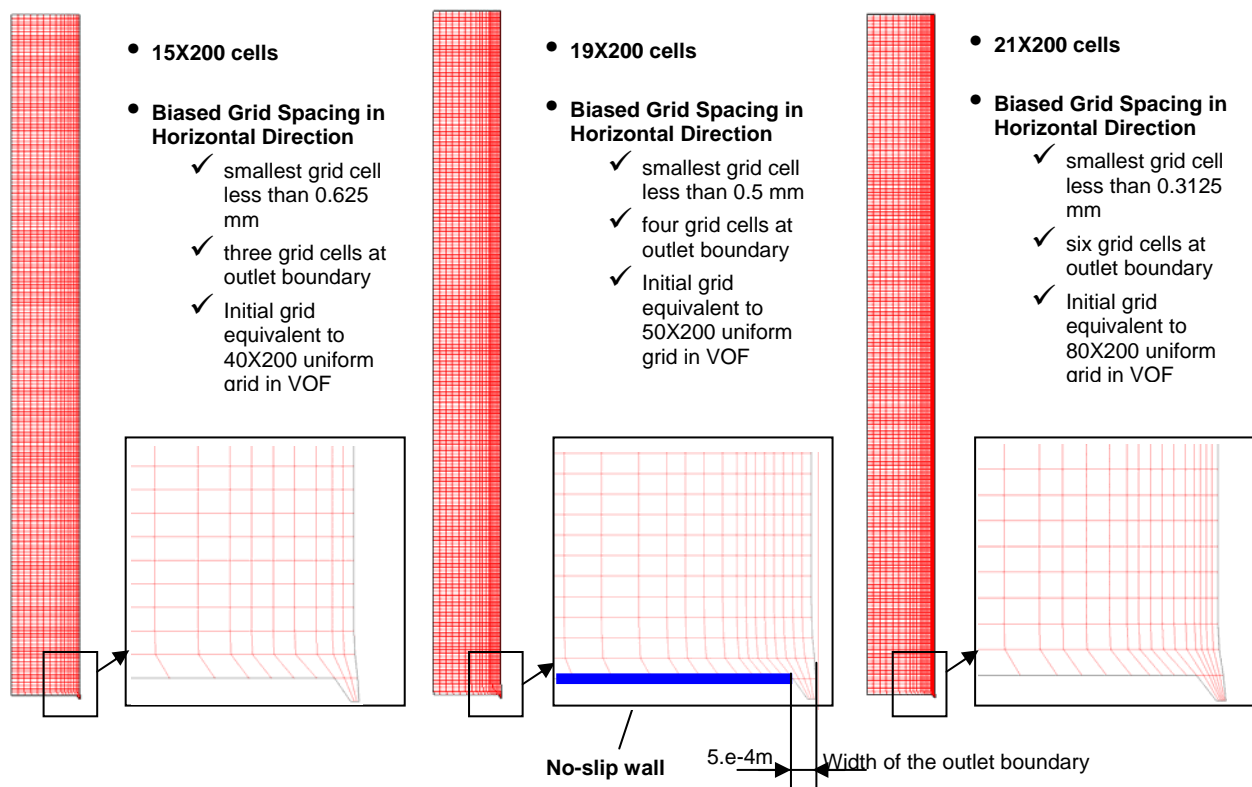


Figure 3.13 Computational grids used in Task 1A and Task 1B.

In the calculation, the residual is used to determine convergence. The residual for a solved quantity Y is defined by the coefficients and source terms of the discretized equation (i.e., A_E , A_W , A_N , A_S , and S_u) and the solved quantities at the cell centers (i.e., Y_p) and at each cell face center (i.e., Y_E , Y_W , Y_N and Y_S):

$$R_Y^\Psi \equiv 7 + \log_{10} \left(\frac{\sum_{\text{Calculation domain}} R_Y^0}{\sum_{\text{Calculation domain}} \Psi_Y} \right), \quad (24)$$

where $R_Y^0 \equiv A_E Y_E + A_W Y_W + A_N Y_N + A_S Y_S + S_U - A_P Y_P$, and $\Psi_Y \equiv A_P Y_P$. During each time step, iteration is terminated when residuals of all solved quantities are below 1 (i.e., at least six significant digits of the solution remain unchanged from iteration to iteration). Figure 3.14 shows a typical residual history for a single time step. The number of iterations required to reach convergence depends on many factors. Typically, during the early stages of a simulation many iterations (e.g., more than 200) are required to converge the solution at each time step. After the resin starts to flow, typically less than ten iterations are required. A minimum number of iterations in each time step can be set in the input data file to force CPCFD to always perform a minimum number of iterations at each time step regardless of the convergence criteria. Other factors that impact the convergence history include the under-relaxation factor, time step size, and characteristics of the problem itself (e.g., type of resin, external heat flux).

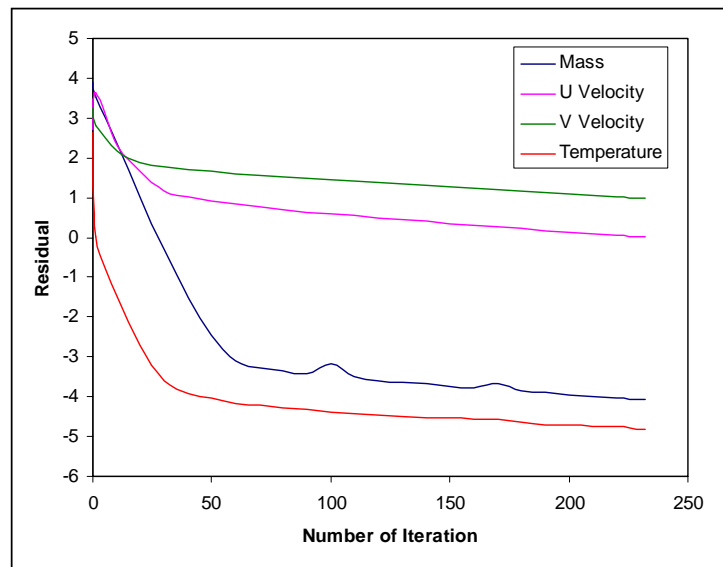


Figure 3.14 Typical residual histories in one time step.

Model Results

The calculated mass loss (i.e., the mass leaving the computational domain) percentage as a function of time is shown in Figure 3.15 for each of the four grids described above.

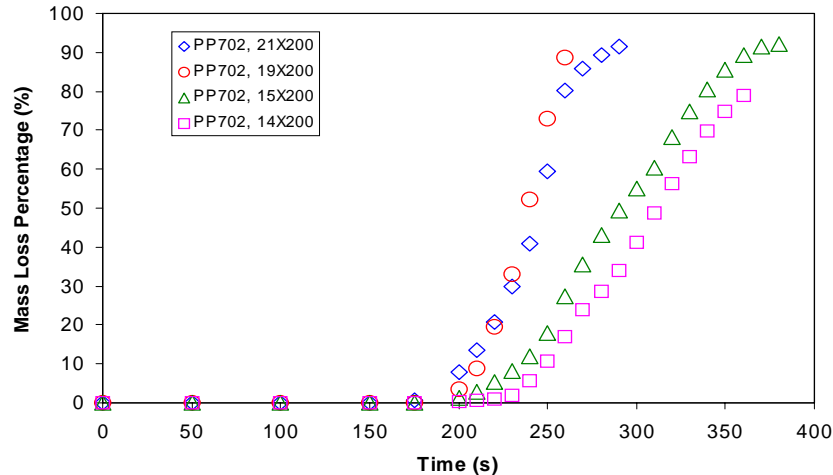


Figure 3.15 Mass loss percentage as a function of time on four grids (PP702N).

It can be seen that the results are very sensitive to the grid resolution near the free surface. The two coarser grids (14x200, 15x200) are not adequate to resolve the sharp temperature gradient near the surface and lead to very different melt behaviors. The two finer grids (19x200, 21x200) yield similar results in terms of mass loss history and “steady state” mass loss rate (i.e., grid convergence). In CPCFD, the size of the time-step is determined based on the CFL constraint, which is a model input. The above four cases all used the same CFL number, resulting in each case using a different time step. In general, the 21x200 grid case has the smallest time step size. Hence the temporal error also plays a role in making the mass loss histories different.

Figure 3.16 shows the calculated free surface location and the temperature field as a function of time for the case where a 21x200 grid is used. Within the first 100 seconds, the movement of the free surface is negligible under the simulated condition (i.e., 30 KW/m² heat flux). However, the temperature in the thin layer neighboring the free surface can be seen to build up due to the external heat flux. As the temperature rises, the viscosity of the resin decreases rapidly. At about 120 seconds, noticeable movement of the free surface can be seen at the top-right corner. At about 200 seconds, the melt material starts to flow rapidly downwards along the free surface. A thin layer of melted polymer with high temperature can be seen near the free surface. From about 200 to 250 second, the mass loss rate appears to reach steady state. After 260 seconds, the flow slows down as most of the material has now left the computational domain.

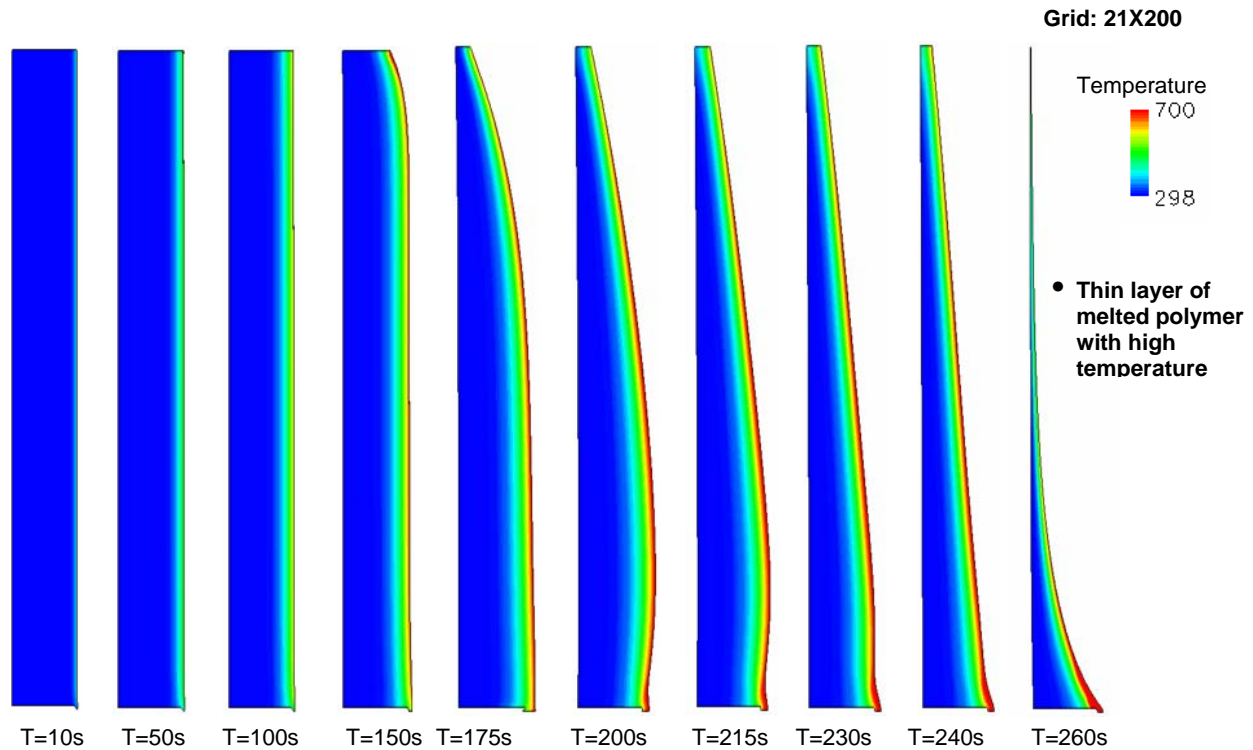


Figure 3.16 Free surface location and temperature field as function of time (PP702N).

In Figure 3.16, it can be seen that the top of the free surface retreats much faster than the other part of the surface once the thin melt layer is formed. Between 200s and 215s, a “belly” (or bulge) develops in the lower part of the free surface. These phenomena have not been observed in experiments or VOF simulations performed by NIST [13]. The cause for this predicted behavior is not known. However, parametric studies indicate that:

1. the free surface smoothing algorithm and the free surface edge tracking algorithm described in the previous two sections (i.e., Section 3.2.2 and Section 3.2.3, respectively) have great impacts on the shape of the free surface, particularly near the boundary at the top wall; and
2. the inclusion of more physical processes, such as in-depth absorption (see Section 3.3.2 for details), can help avoid the development of the “belly” that is observed in the simulations.

Snap shots of the velocity field (displayed with velocity vectors) are shown in Figure 3.17, which shows the melt flow along the free surface. The results shown are from the 21×200 case and are taken at time 220 seconds. Note that the velocity magnitude is zero everywhere except near the free surface. Note that the grid lines in the figure connect the cell centers and the vectors are formed by using cell center velocity components. In the figure, all velocity vectors are scaled by the same factor and the grid cell size varies along the extent of the free surface due to the moving grid algorithm used in the solution procedure.

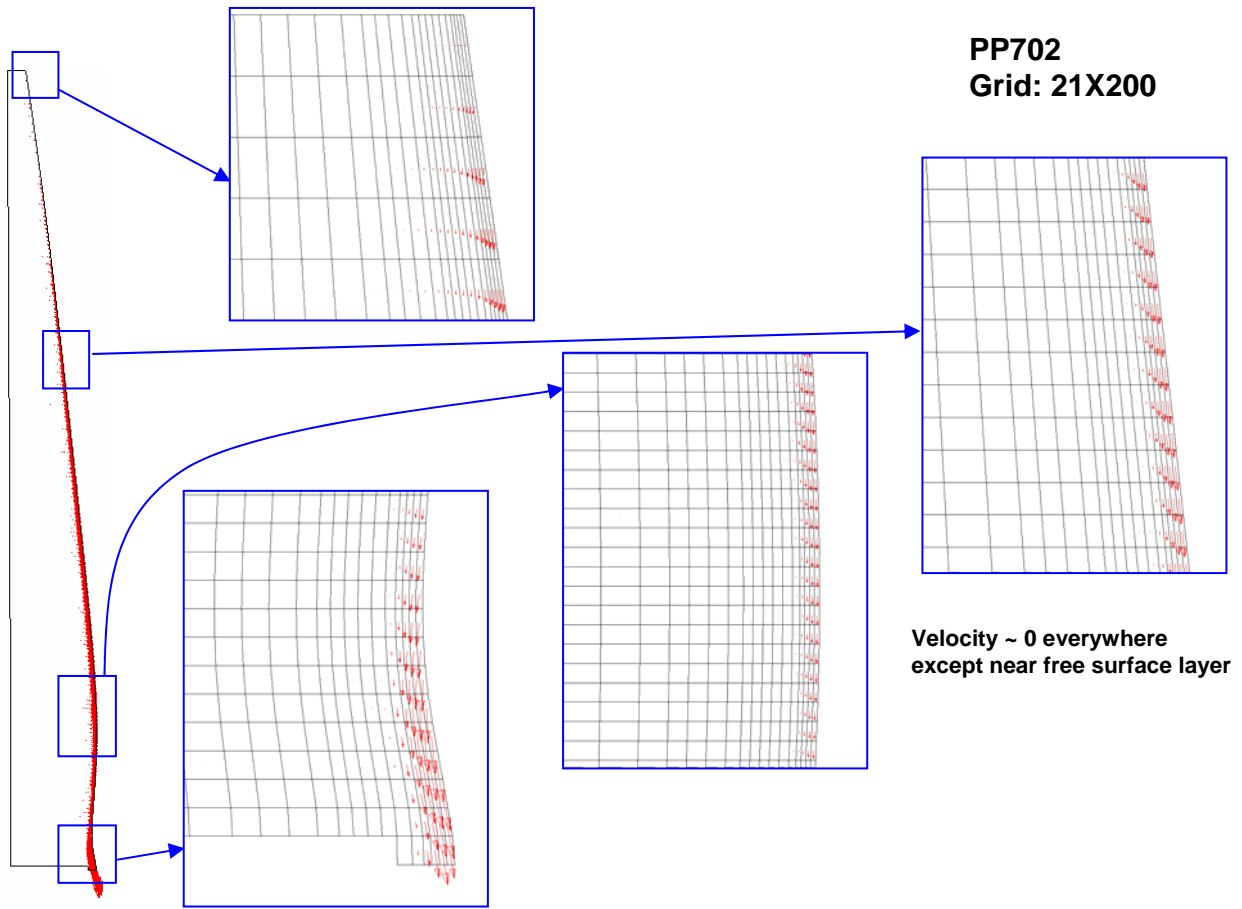


Figure 3.17 Velocity vectors at time = 220 seconds (PP702N).

Compare Model Results and NIST Experimental Data

The temperature profiles on the free surface from the above case (21x200 grid) at selected times (200 seconds, 230 seconds, 240 seconds) are plotted in Figure 3.18. The predicted results show that, at the early stage when conduction is the main heat transfer mode inside the material, the surface temperature distribution is more uniform than that at a later stage, when convective heat transfer becomes stronger. The average free surface temperature observed in similar experiments at NIST was about 613 K (Ohlmiller FAX 01-18-06). The predicted average surface temperatures as shown in the figure are in the range from 675 K to 700 K. The higher average surface temperature calculated by the code may be due to the lack of critical models, such as radiative heat loss on the surface, gasification, etc.

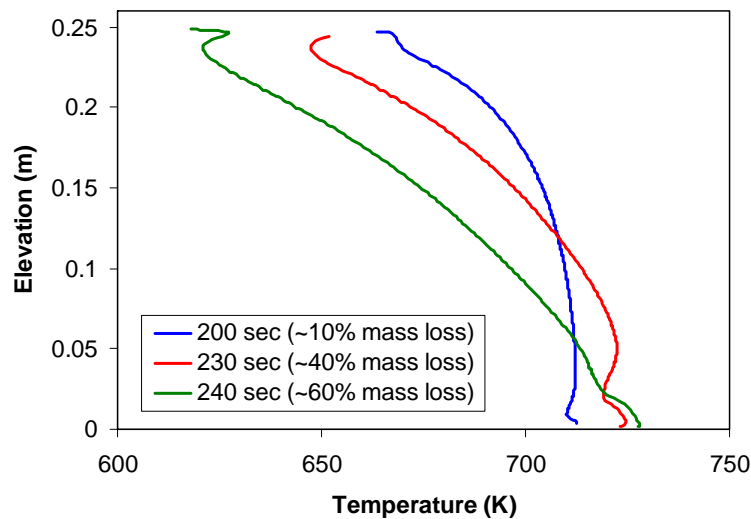


Figure 3.18 Temperature profiles on the free surface at selected times (PP702N).

Computational Resources

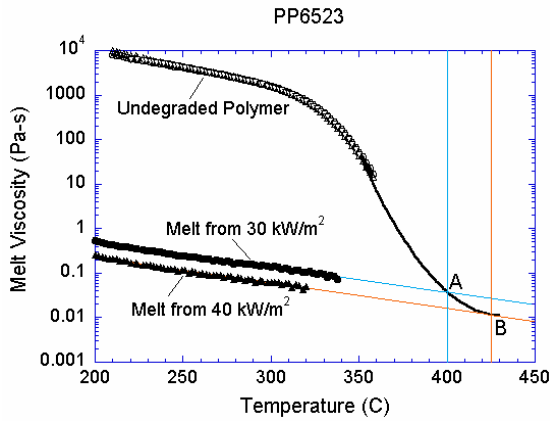
The computational times and memory requirements for the cases performed in Task 1B are summarized in Table 3.1. All calculations were run on a Dell Precision 450 Desktop PC with a Xeon 3 GHz CPU.

Table 3.1 Clock Time and Memory Requirement for Task 1B Cases.

Case	Wall Clock Time (hr)	Memory Requirement (MB)
14 X 200	24	1
15 X 200	36	1
19 X 200	100	2
21 X 200	120	2

3.2.5 Task 1C: Modeling Results of Resin PP6523

Figure 3.19 shows the measured viscosity of PP6523 polymer as a function of temperature with a fixed shear rate of 0.1 [13]. The solid line in Figure 3.19 is used in the CFD model to describe the highly non-linear viscosity-temperature relationship, which can be expressed as



$$\mu = \begin{cases} 10^6 & T < 25^\circ\text{C} \\ 10^6(220 - T)/(220 - 25) + f_1(220) & 25^\circ\text{C} \leq T < 220^\circ\text{C} \\ f_1(T) & 220^\circ\text{C} \leq T < 350^\circ\text{C} \\ f_2(T) & 350^\circ\text{C} \leq T < 430^\circ\text{C} \\ f_2(430) & T \geq 430^\circ\text{C} \end{cases}$$

$$f_1(T) = 10^{(-85.843 + 1.3870T - 7.979 \times 10^{-3}T^2 + 2.0286 \times 10^{-5}T^3 - 1.9344 \times 10^{-8}T^4)}$$

$$f_2(T) = 10^{(100.90 - 0.4771T + 5.533 \times 10^{-4}T^2)}$$

Figure 3.19 Viscosity-temperature relationships for PP6523.

Model Results

Comparing the viscosity-temperature relationship used for PP6523 with that for PP702N, it can be seen that the viscosity of PP6523 is much greater than that of PP702N when the temperature is below 620 K, but is an order of magnitude smaller than that of PP702N when temperature is above 700 K.

The grids used in Task 1b are re-used in the current task. Figure 3.20 shows the calculated mass loss histories. The case with the coarsest grid (14x200) predicts a very different melting behavior as compared to the other three grids; a much longer time is required before the polymer flows and the mass loss rate is also much smaller. The differences among the three cases with finer grids are much smaller than the differences between them and the case with the coarsest grid, indicating grid convergence has been achieved. Again, because the time-step size varies differently in each case, temporal error also plays a role in making the mass loss histories different.

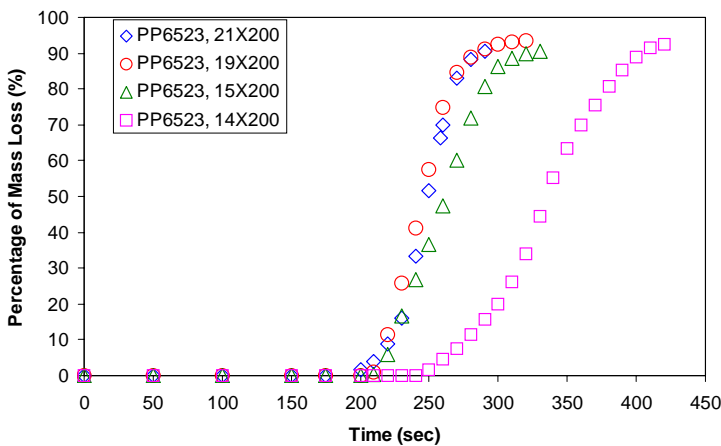


Figure 3.20 Mass loss percentage as a function of time for PP6523 on four grids.

Compare Model Results for PP702N (Task 1B) and PP6523 (Task 1C)

A “steady-state” mass loss rate (i.e. averaged mass loss rate) is calculated for certain time periods and summarized in Table 3.2. For the cases using the finest grids (19x200, 21x200), the steady-state mass loss rates are very close to each other. The results also show that PP65223 flows slightly faster than does PP702N under the same external heat flux, which may be caused by the lower viscosity of PP6523 at temperatures above 650K.

Table 3.2 Calculated Steady-State Mass Loss Rate.

Case	PP702N		PP6523	
	Mass loss rate (g/s m)	Time period (second)	Mass loss rate (g/s m)	Time period (second)
14X200	28.1	220 - 330	33.8	250 - 400
15X200	31.5	210 - 320	59.1	200 - 290
19X200	63.3	180 - 260	70.7	200 - 270
21X200	62.4	180 - 260	70.5	200 - 270

Computational Resources

The computational time and memory requirement for the cases performed in Task 1C are comparable to those of Task 1B (see Table 3.1).

3.3. Task 2: Surface Heat Loss and In-depth Absorption of Radiative Heat Flux

3.3.1 Task Overview

For Task 2, the CPCFD model established in Task 1 is modified to include the radiative and convective heat losses from the heated surface and to include in-depth absorption into the polymer of the imposed radiative heat flux. Computational results have been obtained for two polymer resins (i.e., PP702N and PP6523). The task was performed in three steps

- Task 2A: perform model for PP702N with heat loss boundary condition at the heated surface
- Task 2B: perform model for PP702N with heat loss boundary condition at the heated surface and in-depth absorption
- Task 2C: perform model for PP6523 with heat loss boundary condition at the heated surface and in-depth absorption

Several modeling issues were investigated during the performance period of Task 2. These include the following:

- a free surface tracking scheme for the no-slip boundary at the top wall;
- implementation of an adiabatic wall boundary condition for grid lines that are not orthogonal to the solid wall; and
- the free surface smoothing function

Although not included in the original statement of work, simulation of a third polymer resin (PP23K) was also performed to investigate particular aspects of the model. Results and discussions for the investigations of the PP23K resin can be found in Section 3.2 and in the PowerPoint progress reports and e-mails with NIST dated between May and June, 2006.

In this section, provided are

- a description of the surface heat loss model and the in-depth absorption model; and
- modeling results from Task 2A, 2B, and 2C.

3.3.2 Heat Loss and In-depth Absorption Models

The heat loss model added in Task 2 accounts for the heat transfer processes occurring between the heated free surface and the surrounding environment. Two heat transfer processes are considered - free convection and heat radiation.

In Task 1, the external heat flux is applied only on the free surface and the energy transmitted into the interior of the material occurs only through heat conduction and heat convection. However, in experiments, it has been observed that the heated polymer becomes semi-transparent and thus allows the external radiative energy to penetrate the exposed surface [13]. The in-depth absorption model developed in this task accounts for this mode of energy distribution, in addition to heat conduction and heat convection.

Figure 3.21 is a sketch of the new models developed in this task. A 2D 5.0 cm × 10.0 cm (width × height) polymer sample is modeled with the free surface facing right. The other three sides of the sample are modeled as no-slip adiabatic wall boundaries. The free surface is exposed to an

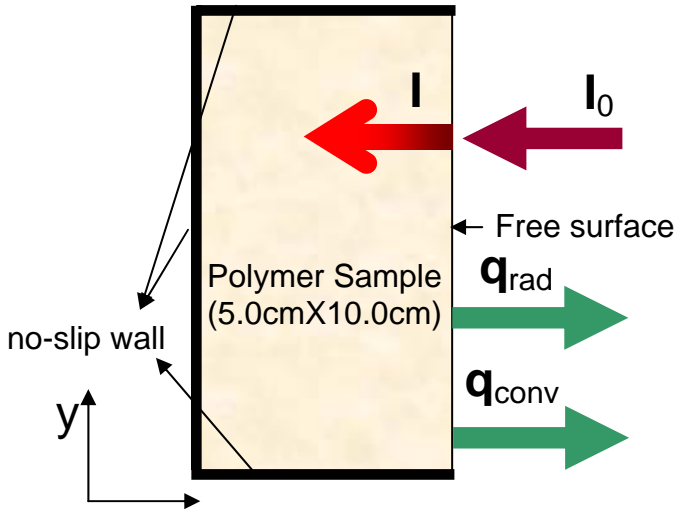


Figure 3.21 Sketch of in-depth absorption and heat loss models.

external heat flux represented by I_0 , which penetrates the surface and its intensity (i.e. I) reduces with increasing depth due to the in-depth absorption effect of the material. Heat losses due to heat radiation and free convection are represented by q_{rad} and q_{conv} , respectively. These heat loss effects are only applied to the free surface. Within the CPCFD code, q_{rad} and q_{conv} are treated as additional source terms in the energy transport equation and can be expressed as:

$$\dot{q}_{radiation} = -A\varepsilon\sigma(T^4 - T_0^4), \quad (25)$$

and

$$\dot{q}_{convection} = -Ah_{conv}(T - T_0). \quad (26)$$

In the above equations, A is the surface area; ε is the emissivity ($=1.0$); σ is the Stefan-Boltzmann Constant ($=5.67e-8 \text{ Wm}^{-2}\text{K}^{-4}$); T_0 is the ambient temperature ($=298 \text{ K}$); and h_{conv} is the convective heat transfer coefficient ($=8.0 \text{ Wm}^{-2}\text{K}^{-1}$).

The in-depth absorption effect is modeled using an additional heat source term in the energy transport equation. The source term can be written as

$$\dot{q}_{absorption} = \int_{\Omega} \frac{dI}{dx} d\Omega, \quad (27)$$

where I is the incident heat flux and Ω is the control volume. The model assumes that the in-depth absorption effect only happens in the x-direction (i.e., perpendicular to the free surface). The magnitude of the incident heat flux inside the material is a function of the distance from the free surface in the x-direction and is based on NIST data [13]:

$$\left\{ \begin{array}{l} \frac{I}{I_0} = 10^{(-5.17x+6.964x^2)}, \quad 0 \leq x < 0.3 \text{ (cm)} \\ \frac{I}{I_0} = 10^{(-0.5154-1.473x+0.4339x^2)}, \quad 0.3 \leq x < 1.3 \text{ (cm)} \end{array} \right., \quad (28)$$

where I_0 is the external heat flux and x represents the distance from the free surface.

The relationship between the normalized incident heat flux and distance x is plotted in Figure 3.22. It can be seen that within 2 mm of the free surface about 80% of the energy has been absorbed by the polymer, even though the radiative heat continues more than 10 mm into the material. Because Eq. (28) does not extend to the total depth of the object modeled (i.e. 5 cm), the remaining incident heat flux beyond 1.3 cm is neglected in the current implementation; the incident heat flux at this point is less than 2% of the initial external heat flux.

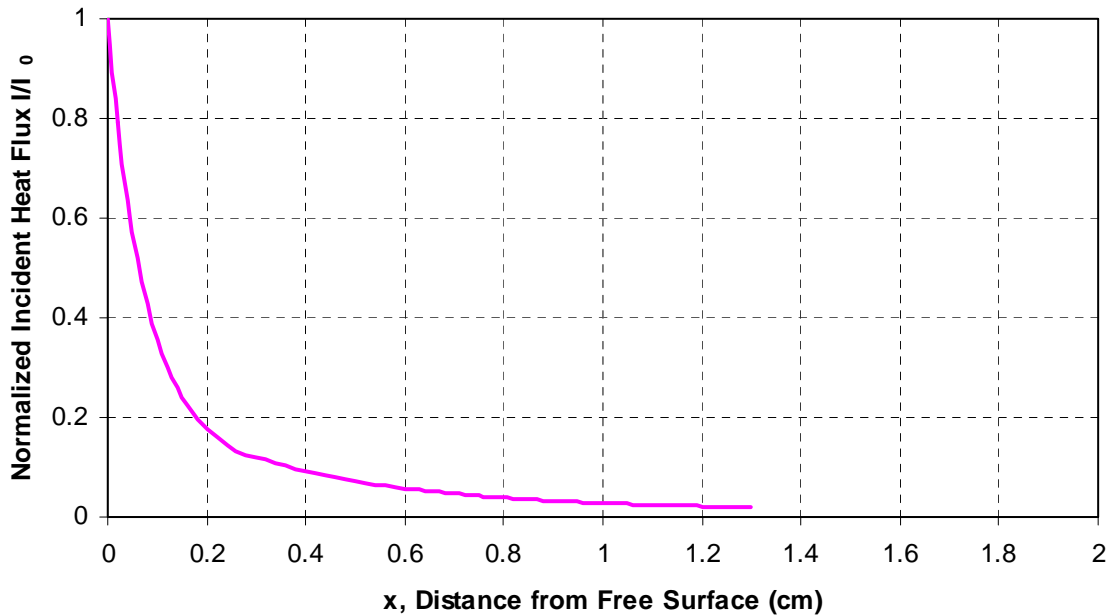


Figure 3.22 Incident heat flux distribution in the horizontal direction.

3.3.3 Computational Grid and Case Summary

As noted above, a 5.0 cm × 10.0 cm (width × height) 2D block is modeled in Task 2. The computational grid is 30 × 80 cells as shown in Figure 3.23. The initial grid resolution is the same as the 19 × 200 grid used in Task 1, and provides resolution equivalent to a 100 × 80 grid if uniform grid cell spacing is used in the horizontal direction and the grid cell size is equal to the smallest cell near the surface. The size of the outlet boundary at the bottom-right corner, which contains four outlet cells, is set to 0.5 mm initially.

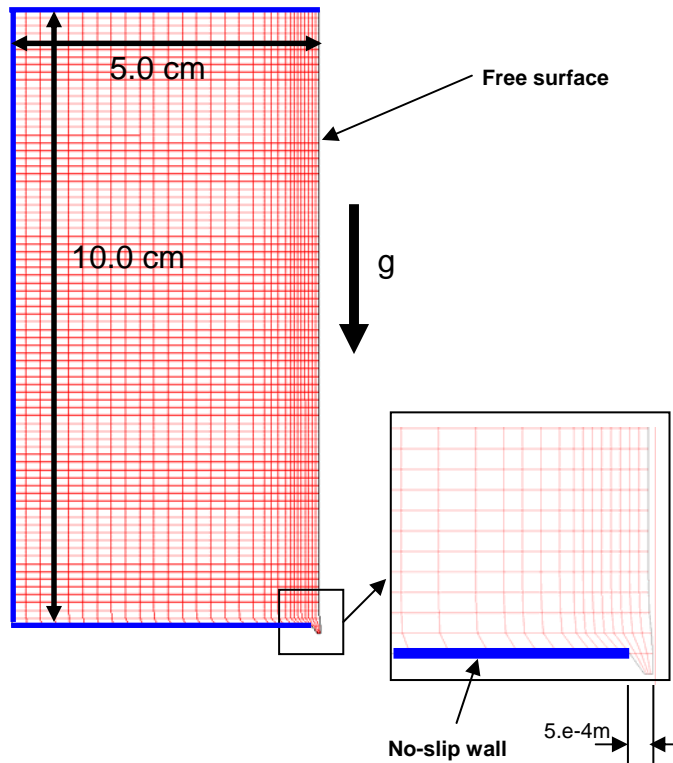


Figure 3.23 Task 2 computational grid at $t = 0$ sec.

The material properties and external heat flux are the same as per Task 1. The three cases performed in Task 2 are summarized in Table 3.3. All cases were run on a 3.0 GHz Intel Xeon workstation.

Table 3.3 Task 2 Case Summary.

Sub-task	Resin	Case	Radiative and convection heat losses	In-depth absorption	Surface smoothing blending factor *	Mass loss and simulated time period	Estimated wall clock time
Task 2A	PP702N	Case 2A	Included	Not included	1.0	60%, 370 s	~50 hrs
Task 2B	PP702N	Case 2B	Included	Included	1.0	65%, 700 s	~26 hrs
Task 2C	PP6523	Case 2C	Included	Included	0.1	70%, 700 s	~28 hrs

* See Section 3.2.2 for details

3.3.4 Results and Discussion

Plotted in Figure 3.24 are the mass loss histories for the three cases listed in Table 3.3. Comparing the results of Case 2A and Case 2B, it can be seen that the inclusion of the in-depth absorption model significantly slows down the melting process. The mass loss histories in Case 2B and Case 2C are about the same. The steady-state mass loss rate of PP6523 from Case 2C is slightly larger than that of PP702N from Case 2B, probably due to the lower viscosity of PP6523 at high temperature. On the other hand, PP702N in Case 2B starts to flow slightly earlier than does PP6523 in Case 2C, which may be due to the fact that at low temperatures the viscosity of PP6523 is much higher than that of PP702N.

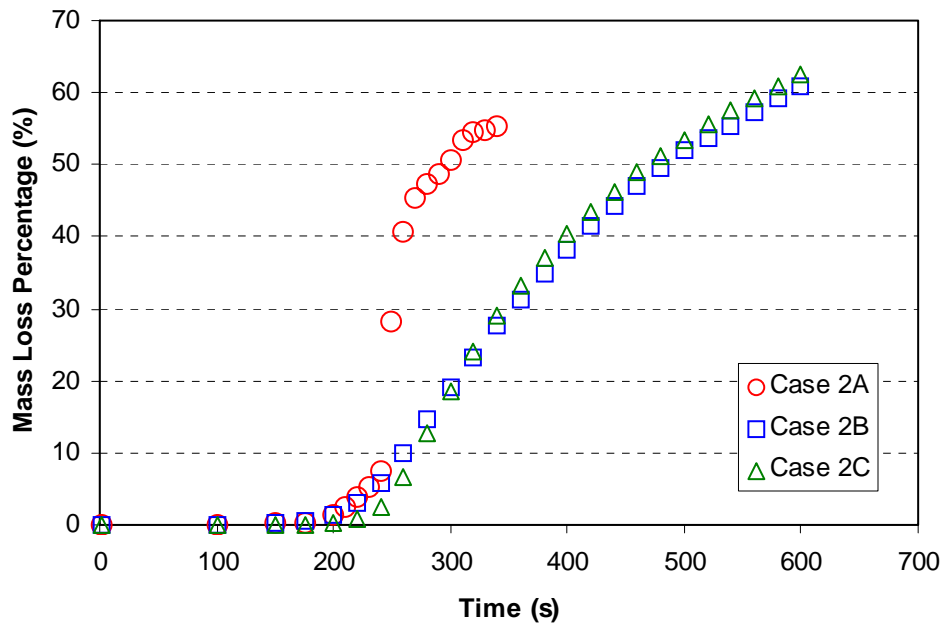


Figure 3.24 Mass loss percentages as a function of time for Task 2 cases.

Listed in Table 3.4 is the “steady-state” mass loss rates calculated from the modeling results. In the table, average mass loss rate reported in columns 2-3 are for the time period shown in column 4. Comparison of the predicted mass loss rate with the experimental data shows that, even with the inclusion of the in-depth absorption model, the predicted melt mass flow rate is still much higher than the measured data. The lack of other key physical processes in the model such as in-depth gasification may explain the discrepancy.

Table 3.4 Calculated Steady-State Mass Loss Rate.

Case	Mass loss rate ($\text{gs}^{-1}\text{m}^{-1}$)	Mass loss rate (gs^{-1}) [*]	Time period
Case 2A	24.0	2.4	200 s – 300 s
Case 2B	6.5	0.65	200 s – 600 s
Case 2C	7.5	0.75	240 s – 600 s
Measurement [13]	-	0.15	-

^{*} assumes the depth of the object is 0.1m

Impact of In-Depth Absorption on Model Results

One of the main goals of Task 2 is to assess the impact of the in-depth absorption model on the computational results. The in-depth absorption model enables the external energy to be distributed within the object beyond the free surface, without resorting to heat conduction and heat convection from the surface thus decreasing the temperature gradient near the free surface.

The impact of including in-depth absorption on the computational results is two-fold.

1. It reduces the surface temperature and increases the viscosity in the melting layer substantially, which in turn slows down the melting flow. This can be seen in Figure 3.25, which depicts the temperature and velocity profiles along the free surface. All profiles are taken at 35% mass loss. Comparison between the temperature profiles in Case 2A and Case 2B shows that the average temperature of the free surface drops about 75 K due to including in-depth absorption in the model. The cooler temperature changes the viscosity by at least one order of magnitude, which leads to a significantly different surface flow velocity. The velocity magnitude in Case 2A is six times larger than that in Case 2B at the same mass loss percentage. In addition, the average surface temperature predicted in Case 2B (i.e., about 640 K) is much closer to that observed in similar experiments conducted by NIST, which is 648 K (Ohlemiller FAX 01-18-2006).

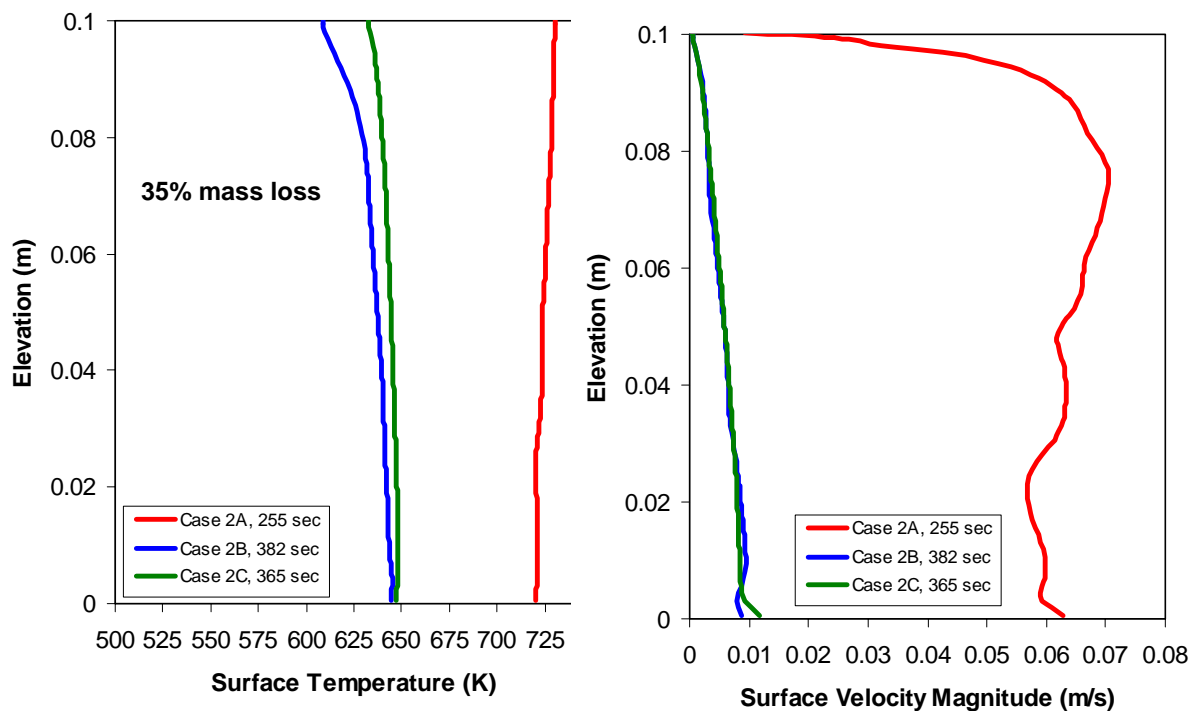


Figure 3.25 Surface temperature and velocity magnitude profiles along the free surface at a time corresponding to 35% mass loss.

- The second impact of the in-depth absorption model is that it broadens the thickness of the melting layer because it distributes radiative energy further into the thermoplastic object (i.e., beyond the free surface). This can be seen in Figure 3.26, which shows the velocity vectors near the free surface for Case 2A (left) and Case 2B (right) at points in time corresponding to (about) 51% and 19% mass loss, respectively. The velocity vectors plotted in Figure 3.26 are scaled about the same. The general location of the melting layers can be identified by the red vectors in the two large pictures. The four small (inset) pictures show that the velocity magnitude in the melting layer for Case 2B is smaller than that in Case 2A because the in-depth absorption model reduces the temperature near the free surface, which in turn makes the melt flow more viscous. Although both cases started with the same initial grid, the grid cell spacing for Case 2A is different than the grid cell spacing for Case 2B due to the free surface evolving at a different rate.

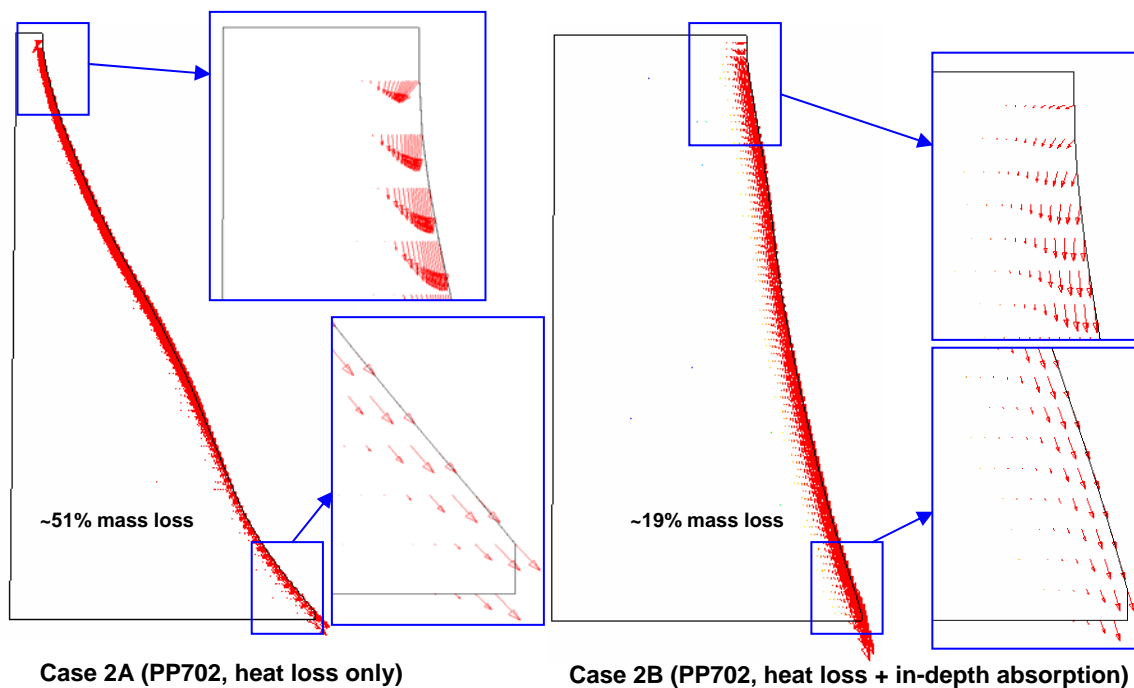


Figure 3.26 Velocity vectors in Case 2A and Case 2B.

3.4. Task 3: In-depth Gasification

3.4.1 Task Overview

In Task 3, a model describing the in-depth gasification of the thermoplastic material is implemented into CPCFD. An empirical Arrhenius expression is used to implement the chemistry into the mass and energy equations. Results have been obtained for two polymer resins. The task was performed in two steps

- Task 3A = Perform model for PP702N
- Task 3B = Perform model for PP6523

With guidance from the NIST COTR, a parametric study has been performed to select the best available rates and parameters for the expressions for the in-depth gasification. Predicted results are compared with experimental data provided by NIST.

In the following are provided:

- A description of the in-depth gasification model;
- Model results for resin PP702N (Task 3A); and
- Model results for resin PP6523 (Task 3B).

3.4.2 In-depth Gasification Model

In CPCFD, the gasification process is represented by the removal of polymer mass and energy using sink terms in the mass and energy equations. Figure 3.27 is a sketch of the models used in the Task 3 simulations. The in-depth gasification model is represented by \mathbf{q}_{gas} and \mathbf{m}_{gas} , which

describe the heat and mass losses due to the pyrolysis of the polymer melt material. The two sink terms are computed as

$$\dot{q}_{\text{gasification}} = -\int_{\Omega} H_v \rho B \exp\left(-\frac{E}{RT}\right) d\Omega, \quad (29)$$

and

$$\dot{m}_{\text{gasification}} = -\int_{\Omega} \rho B \exp\left(-\frac{E}{RT}\right) d\Omega. \quad (30)$$

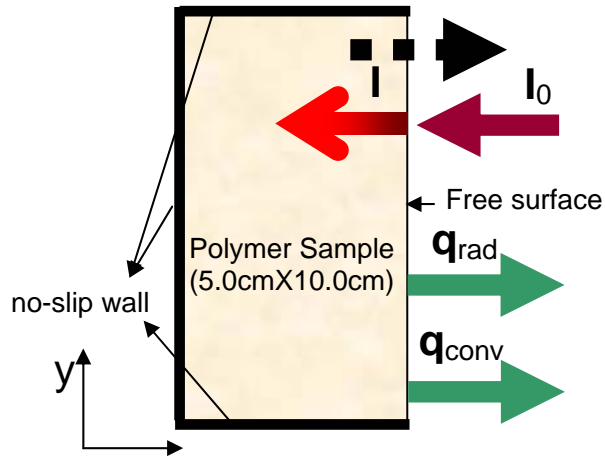


Figure 3.27 Sketch of in-depth absorption, gasification, and surface heat loss models.

In the above two equations, H_v is the gasification heat (=1250 J/g), ρ is the density, and B and E/R are model constants.

3.4.3 Task 3A – CFD Simulation of Resin PP702N

The computational domain adopted in Task 3 is shown in Figure 3.28. As per Task 2, a 10 cm (H) × 5 cm (D) 2D “slice” of the 3D object is modeled. The width of the object (i.e., W = 10 cm) is only used to compare to test data. The 2D grid is the same as that used in Task 2.

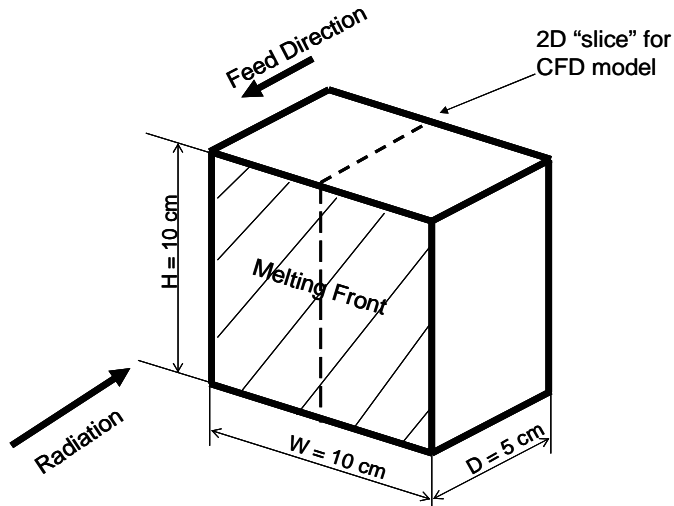


Figure 3.28 Sketch of modeled resin in Task 3.

Multiple gasification models have been investigated in order to achieve better agreement with measured data. The results shown in this section use two of them. Both models used the same functional form, but different numerical parameters. The model constants are summarized in Table 3.5. The mass loss rate due to gasification per unit volume y is related to temperature T as:

$$y = \rho B \exp\left(-\frac{E}{RT}\right). \quad (31)$$

Table 3.5 In-Depth Gasification Model Constants in Task 3A.

	A (s ⁻¹)	E/R
Model G1	2.18e+12	24,400
Model G6	3.27e+14	24,400

Model G1 is the base model provided by NIST [13]. Model G6 increases the magnitude of the gasification rate by a factor of 150. For information on the other in-depth gasification models investigated, see Appendix A.

Description of In-Depth Absorption Models A1 and A3

Several in-depth absorption models have also been used in this Task to study their impacts on the gasification process. The results from three of the models are discussed in this section; results obtained using the other models can be found in Appendix A.

1. The first model - Model A1 – was used in Task 2 and is referred to as the base model. The normalized incident heat flux can be written as a function of the distance from the free surface:

$$\begin{cases} \frac{I}{I_0} = 10^{(-5.17x+6.964x^2)}, & 0 \leq x < 0.3 \text{ (cm)} \\ \frac{I}{I_0} = 10^{(-0.5154-1.473x+0.4339x^2)}, & 0.3 \leq x < 1.3 \text{ (cm)} \end{cases} \quad (32)$$

2. The second model – Model A3– is different from Model A1 in that the incident heat flux dissipates much quicker inside the polymer resin. The relationship between the normalized incident heat flux and the distance from the free surface is

$$\frac{I}{I_0} = \exp(-11.513x), \quad 0 \leq x < 0.4 \text{ (cm)} \quad (33)$$

The model constant (i.e., -11.513) used in Model A3 is obtained by requiring 99% absorption at $x = 0.4$ cm. This model appears to give the best simulation results when combined with model G6 when comparing to experimental data.

A third model (Model A4) and its simulation results will be described at the end of the section.

Figure 3.29 shows a comparison of the two in-depth absorption models. It can be seen that the base model (i.e., Model A1) allows the incident heat flux to penetrate much further beyond the free surface than does Model A3.

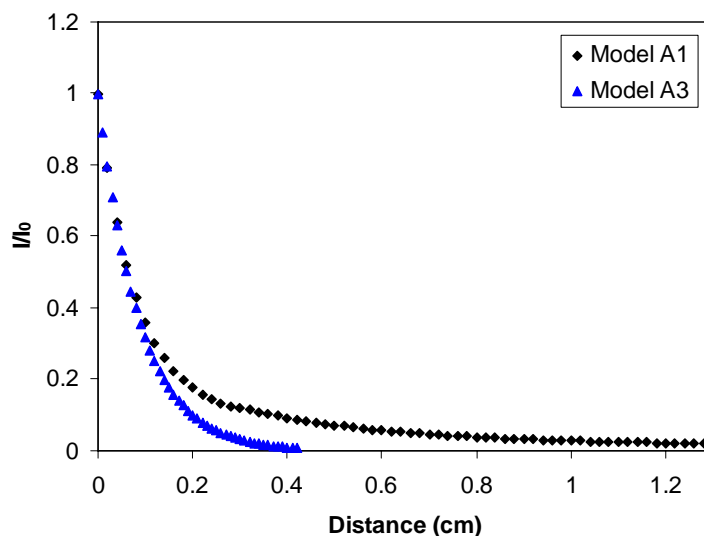


Figure 3.29 Normalized incident heat flux profile as a function of distance from free surface.

Model Results and Comparison to Experimental Data for Models (G1, A1) and (G6, A3)

Four cases have been performed in Task 3A and are listed in Table 3.6. Radiative and convective heat losses at the free surface are included in all cases using the model established in Task 2. Case 3A is the baseline case using base models for gasification and absorption. Model G6 and Model A3 in Case 3N are developed to match measured mass loss rates at 30 KWm⁻² heat flux. Case 3P and 3Q are the same as Case 3N but have different heat flux boundary conditions. All calculations were run on a Dell Precision 450 Desktop PC with a Xeon 3 GHz CPU.

Table 3.6 Task 3A Case Summary.

Case	Gasification model	Absorption model	External heat flux (KWm^{-2})	Simulated time period	Wall clock time
Case 3A	G1	A1	30	550 sec	~24 hrs
Case 3N	G6	A3	30	800 sec	~36 hrs
Case 3P	G6	A3	46	1000 sec	~42 hrs
Case 3Q	G6	A3	20	1000 sec	~42 hrs

Figure 3.30 shows the mass loss histories for Case 3A and 3N. The two cases use different combinations of gasification and absorption models and the results are vastly different. In the plot, the solid lines represent the total mass loss (i.e., material leaving the computational domain due to gasification and melting). The dashed lines represent the mass loss occurring as melt flow only. The difference between solid and dashed line represents the mass loss due to gasification. In Case 3A, the fraction of mass loss occurring as melt flow is more than 99% while the mass loss due to gasification is negligible. However, the experimental data suggests that, at 30 KWm^{-2} heat flux, about 30% mass loss is caused by gasification.

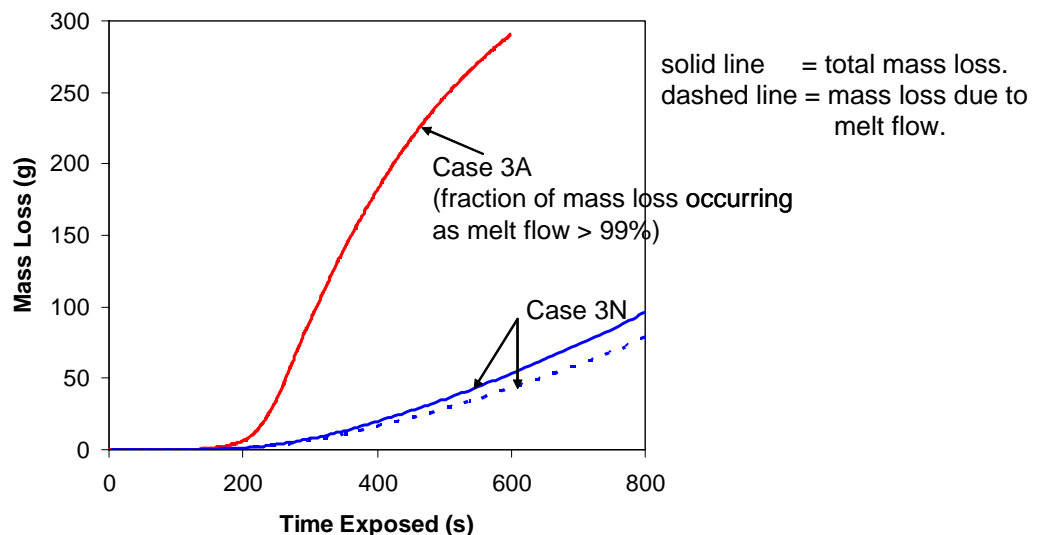


Figure 3.30 Impacts of changing gasification and absorption models in Task 3A.

To match the experimental data, the base models in Case 3A were adjusted to form Model A3 and Model G6. In Model A3, the penetration length of the incident heat flux is significantly shortened to increase the temperature near the free surface. In Model G6, the in-depth gasification process is intensified by two orders of magnitude. As noted in Table 3.6, Case 3N uses these models. From Figure 3.30, it can be seen that for Case 3N that: 1) the overall mass loss rate becomes much smaller than that of Case 3A; and 2) the mass loss due to gasification becomes more significant.

The impacts of different external heat fluxes on the simulation results are shown in Figure 3.31. Three cases, i.e., Case 3P, 3N and 3Q, are compared with each other. Again, the solid lines in the plot represent the total mass loss and the dashed lines represent the mass loss occurring as melt flow. It can be seen that the overall mass loss rate increases as external heat flux increases. The results also suggest that higher external heat flux leads to higher gasification mass loss

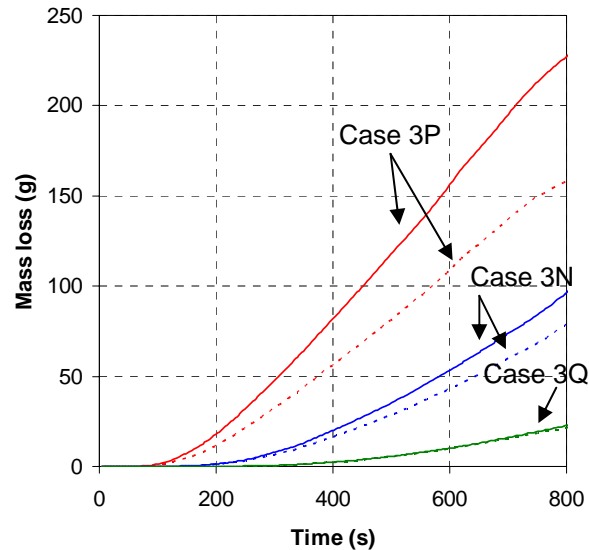


Figure 3.31 Impacts of external heat flux in Task 3A.

Illustrated in Figure 3.32 are comparisons of the simulation results (i.e., total mass loss rate, fraction of mass loss occurring as melt flow, and average free surface temperature) for Case 3A, Case 3N, Case 3P and Case 3Q with NIST experimental data. In the figure, the predicted overall mass loss rate and the fraction of mass loss occurring as melt flow are calculated from 200 seconds to the end time of each simulation. The predicted average surface temperatures are calculated at 25% total mass loss.

For the baseline case (Case 3A), the predicted overall mass loss rate and the fraction of mass loss occurring as melt flow are too high as compared to the experimental data. After adjusting the gasification and absorption models, the agreement between the data and the calculated results from Case 3N is satisfactory. Both Case 3A and Case 3N predict the correct average surface temperature.

It is interesting to see that, although Case 3P and 3Q share the same gasification and absorption models with Case 3N which are only “optimized” for the 30 KWm^{-2} data point, they nevertheless predict the correct trend shown in the experimental data set.

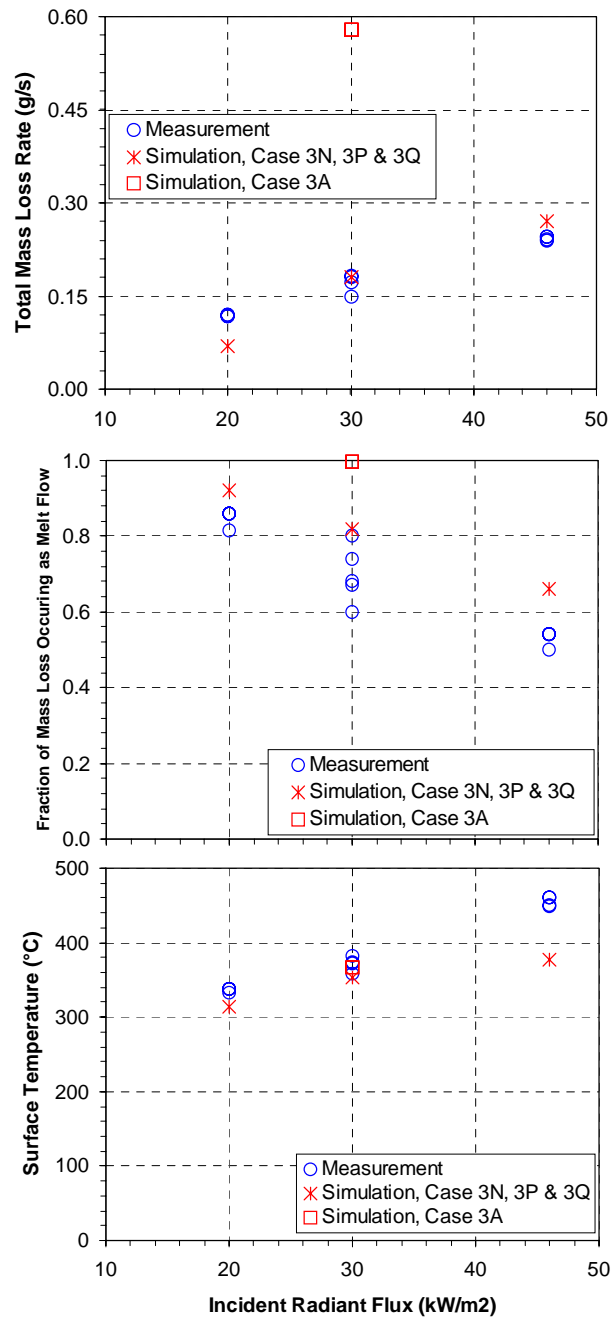


Figure 3.32 Comparison of predicted and measured total mass loss rate, fraction of mass loss occurring as melt flow and the surface temperature for four cases in Task 3A.

Description of In-Depth Absorption Model A4

A third in-depth absorption model – Model A4 – was used in for simulations. Model A4 is based on data obtained in a recent experiment conducted at NIST [13]. The model is shown in Figure 3.33. A mathematical description for Model A4 is provided in Eq. (34) and shown in Figure 3.33 where y represents I/I_0 in the model formulation.

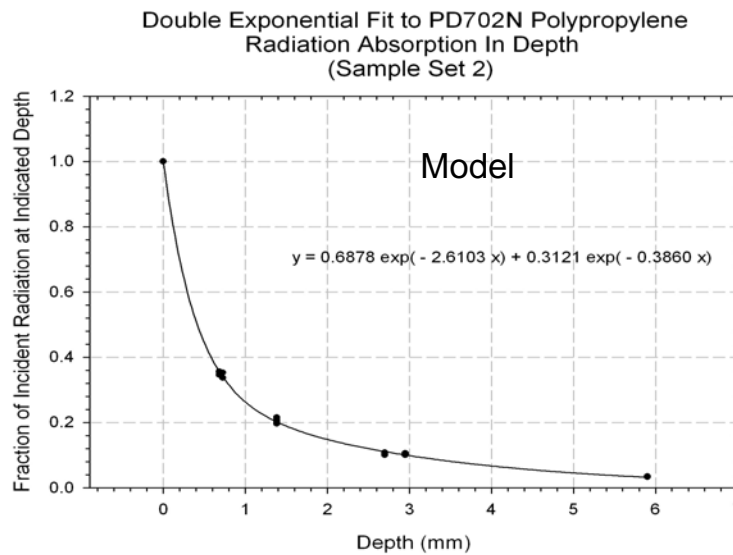


Figure 3.33 Data for fraction of incident radiation versus depth used to define in-depth absorption model A4.

$$\frac{I}{I_0} = 0.6878 \exp(-2.6103x) + 0.3121 \exp(-0.386x), \quad 0 \leq x < 0.6 \text{ (cm)} \quad (34)$$

Model Results and Comparison to Experimental Data for Model (G6, A4)

Two cases are summarized in Table 3.7. Both simulations were performed assuming an external heat flux at 30 KWm^{-2} .

Table 3.7 Task 3A Additional Case Summary.

Case	Gasification model	Absorption model	External heat flux (KWm^{-2})	Simulated time period	Wall clock time
Case 3R	G6	A4	30	1000 sec	~20 hrs
Case 3S	G1	A4	30	600 sec	~10 hrs

Illustrated in Figure 3.34 are comparisons of the simulation results (i.e., total mass loss rate, fraction of mass loss occurring as melt flow, and average free surface temperature) for Case 3R and Case 3S with NIST experimental data. In the figure, the predicted overall mass loss rate and the fraction of mass loss occurring as melt flow are calculated from 200 seconds to the end time of each simulation. The predicted average surface temperatures are calculated at 25% total mass loss. It can be seen that using the original in-depth gasification model G1 (i.e., Case 3S), the predicted total mass loss rate is four times higher than the measured value and the predicted fraction of mass loss due to gasification is negligible and much smaller than the measured value. However, the predicted surface temperature appears to be in good agreement with the data. By

increasing the gasification rate by a factor of 150 in Model G6 (i.e., Case 3R), the predicted total mass loss rate is 50% higher than the measurement and the predicted fraction of mass loss occurring as melt flow and the surface temperature are in good agreement with the data.

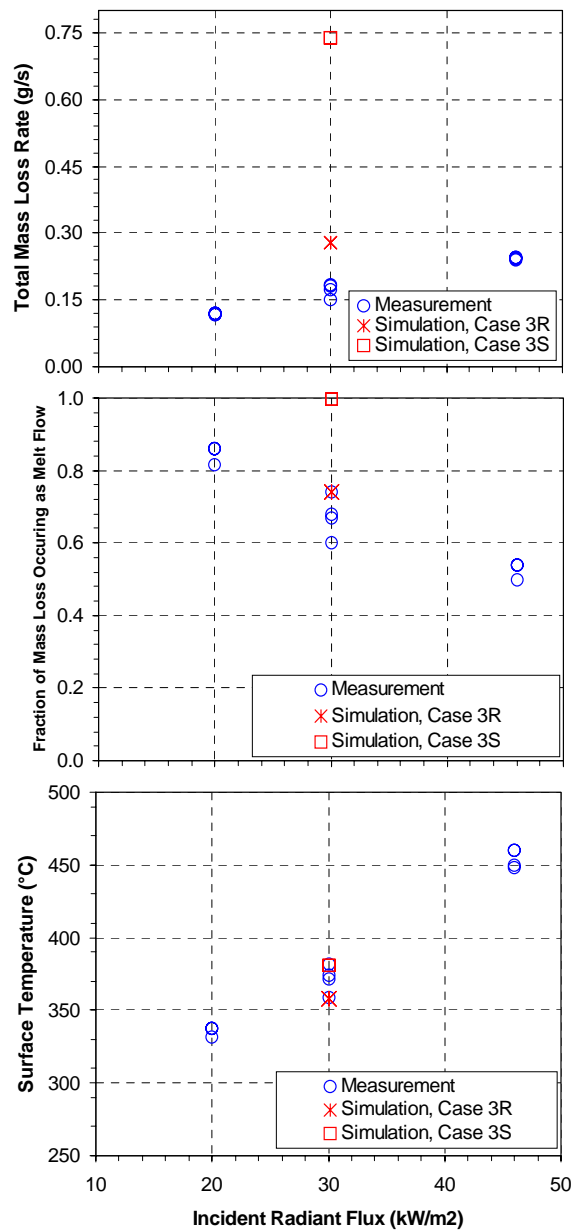


Figure 3.34 Comparison of predicted and measured total mass loss rate, fraction of mass loss occurring as melt flow and the surface temperature for two additional cases in Task 3A.

The results from Case 3A, Case 3P, Case 3R, and Case 3S presented in this section suggest that, to match the experimental data, the kinetic parameter for the in-depth gasification in the base model (G1) has to be changed significantly. The reason why an adjustment to the in-depth gasification model parameter was necessary remains unsolved.

3.4.4 Task 3B – CFD Simulation of Resin PP6523

Simulations have also been performed for resin PP6523. The model constants in the gasification model used in this task are listed in Table 3.8. Model G7 is the base model provided by NIST [13]. The magnitude of the gasification rate is increased by a factor of 150 in Model G8 based on the experience of modeling PP702N in Task 3A.

Table 3.8 In-Depth Gasification Model Constants in Task 3B.

	B (s ⁻¹)	E/R
Model G7	2.23e+13	26,000
Model G8	3.35e+15	26,000

The absorption models are the same as those used in Task 3A. Two cases were run and are summarized in Table 3.9. Case 3C is the baseline case.

Table 3.9 Task 3B Case Summary.

Case	Gasification model	Absorption model	External heat flux (KWm-2)	Simulated time period (s)	Wall clock time (hr)
Case 3C	G7	A1	30	500	~24
Case 3I	G8	A3	30	2000	~60

The simulation results are summarized in Table 3.10., which are calculated in the same manner as those calculated in Task 3A. For the baseline case (Case 3C), behavior that is very similar to that of Case 3A is observed; that is, the melting process is very fast and the mass loss due to gasification is negligible. In Case 3I, by shortening the heat flux penetration length and strengthening the gasification process, the melting process slows down dramatically and more than 70% of the overall mass loss is caused by gasification. The baseline case also predicts a higher surface temperature (e.g., 20 K higher at 25% mass loss). No experimental data has been provided to REI to compare with the model results.

Table 3.10 Task 3B Results Summary.

Case	Total mass loss rate (gs ⁻¹)	Fraction of mass loss due to melt flow	Average surface temperature at 25% mass loss (°C)
Case 3C	0.69	0.99	382
Case 3I	0.065	0.28	362

3.5. Task 4: Modeling Melt Pool on Catch Surface

3.5.1 Task Overview

In Task 4, CPCFD is modified to include the flow of melt on the solid catch surface. Included in the model are the catch surface material properties and finite thickness, melt solidification and surface tension gradient effects. The model also includes a nonzero tilt angle for the catch surface. Results are presented for three cases: the two polymer resins with a single specified tilt angle of the catch surface, and one of these polymer resins with a different surface tilt angle. The Task was performed through the following steps:

- Task 4A = perform model for resin 1 (PP702N) with angle 1
- Task 4B = perform model for resin 2 (PP6523) with angle 1
- Task 4C = perform model for resin 1 (PP702N) with angle 2
- Task 4D = site visit to NIST by REI
- Task 4E = site visit to NIST by REI for Base Period project review
- Task 4F = base period summary report.

Note that NIST deleted Task 4D and Task 4E from the statement of work and thus are not described here. Task 4F (Summary Report) resulted in this document.

The original plan was to use one grid block (Block 1) to represent the melting slab (as per Tasks 1-3), a second (Block 2) to represent the overhanging melt flow, and a third (Block 3) to represent the flow on the catch surface, as sketched in Figure 3.35.

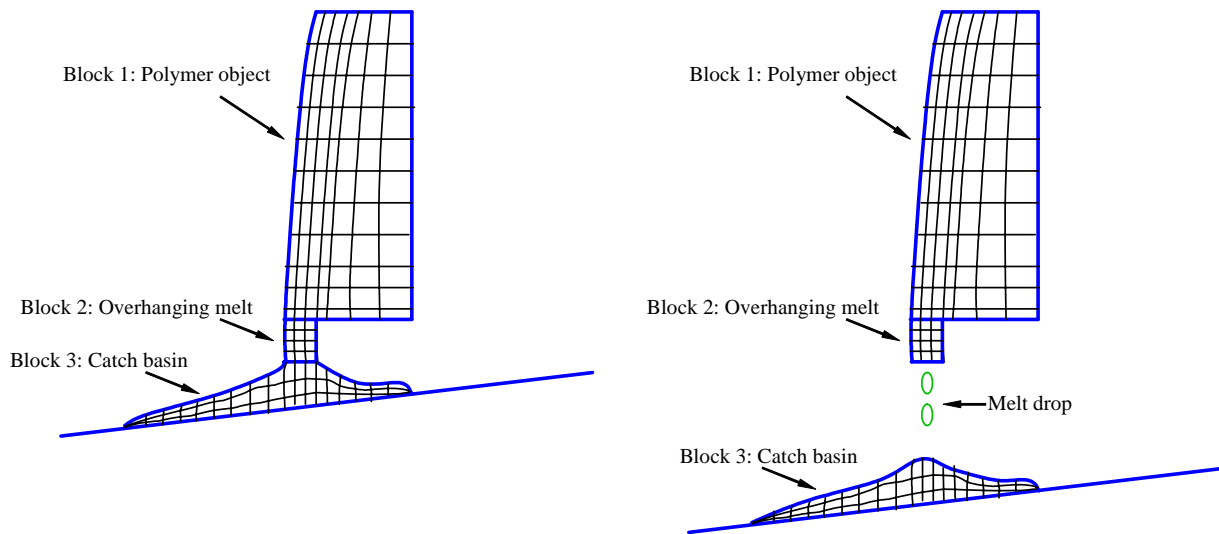


Figure 3.35 Sketch of two scenarios of melt flow with a catch surface. In schematic at left the melt flow spans the gap. In schematic at right the melt flow drips.

After a feasibility study and discussions with NIST, the following decisions were made regarding the Task 4 modeling approach.

1. The simultaneous processes of melt flowing along the free surface of the polymer object and the melt flowing along the catch surface should be decoupled and modeled as two separate problems. The melt flow on the free surface of the polymer object is to be solved using the

approach established in Task 1, 2 and 3. In Task 4, the focus is to use CPCFD to model the melt flow on the catch surface only.

2. The overhanging melt is a great challenge to CPCFD and will not be included in the CFD calculation because it merely provides a bridge to transport the melt flow from the polymer object to the catch surface.
3. The coupling between the simulations of Block 1 and Block 3 is implemented through additional source terms in the governing equations. These source terms are computed during the process of solving the Block 1 melt problem (i.e., Task 3). These source terms are time dependent and are stored in an output/input data file. When solving the Block 3 melt flow problem (i.e., Task 4), these time dependent source terms (i.e., mass source, energy source) are read into the model at the beginning of the simulation. As the Task 4 simulation progresses, the source terms are tabulated and added to the corresponding governing equations to mimic the melt flow from the polymer object landing on the catch basin.
4. The Task 4 simulations also include the heat transfer process occurring within the catch plate. The heat transfer and melt flow of the polymer resin on the catch surface and the heat transfer inside the catch plate are modeled as a conjugate heat transfer problem.

In the following sections are provided:

- a brief description of the conjugate flow-heat transfer problem;
- a discussion of the surface tension models used in the model of melt flow on the catch basin;
- a grid sensitivity study;
- a study of the time accuracy of the simulation; and
- model results and discussions for Task 4A, Task 4B and Task 4C.

3.5.2 Conjugate Flow-Heat Transfer Problem

A sketch of the experimental configuration to be used by NIST is shown in Figure 3.36. In the experiment, the hot melt from the polymer slab will flow down and spread on the ceramic catch plate. The catch plate has insulated sides and is heated from below by an aluminum plate that is attached to the bottom of the ceramic plate. The temperature of the catch surface will be sufficient to allow the hot melt to spread without piling up. The temperature distribution along the interface between the ceramic plate and the aluminum plate is assumed to be uniform and constant due to the large heat conductivity of the aluminum.

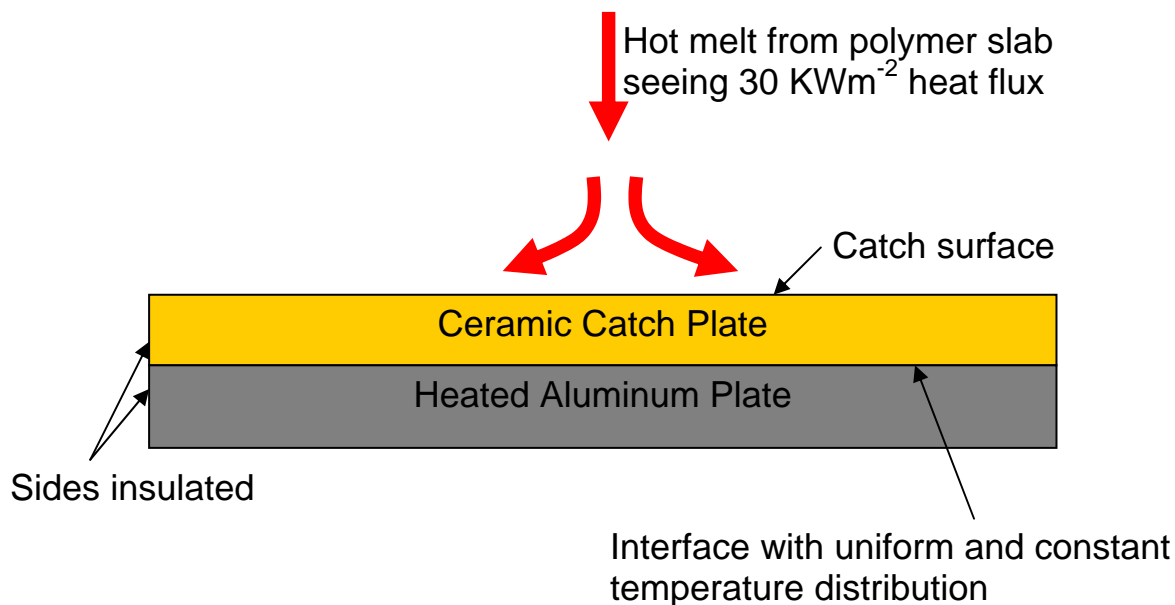


Figure 3.36 Sketch of Task 4 experiment.

At the start of the experiment, the catch plate is heated by the aluminum plate and the temperature distribution inside the catch plate is in steady state. After the hot melt (from the test piece located above the catch plate) lands on the catch surface, coupled transient heat transfer processes occur within the hot melt and the catch plate due to the temperature difference between the two materials and the heat losses that occur at the melt pool surface.

The heat transfer process inside the ceramic catch plate plays a vital role in the formation of the melt pool on the catch surface. To calculate the temperature distribution in the catch plate accurately, the heat transfer problem in the catch plate and the hot melt flow problem are solved simultaneously. A sketch of the computational model is shown in Figure 3.37. It should be noted that only a 2D “slice” in the L-H plane is solved in the Task 4 simulations. The width of the domain (i.e., $W = 7$ cm) is used to facilitate the comparisons with data from future experiments. In this model, the computational domain includes both the catch plate and the melt pool on the catch surface. The bottom of the catch plate is assumed to be a constant temperature boundary. The interface between the melt pool and the catch plate lies within the problem domain and does not need any special treatment. The upper boundary of the melt pool is treated as a free surface with radiative and convective heat losses.

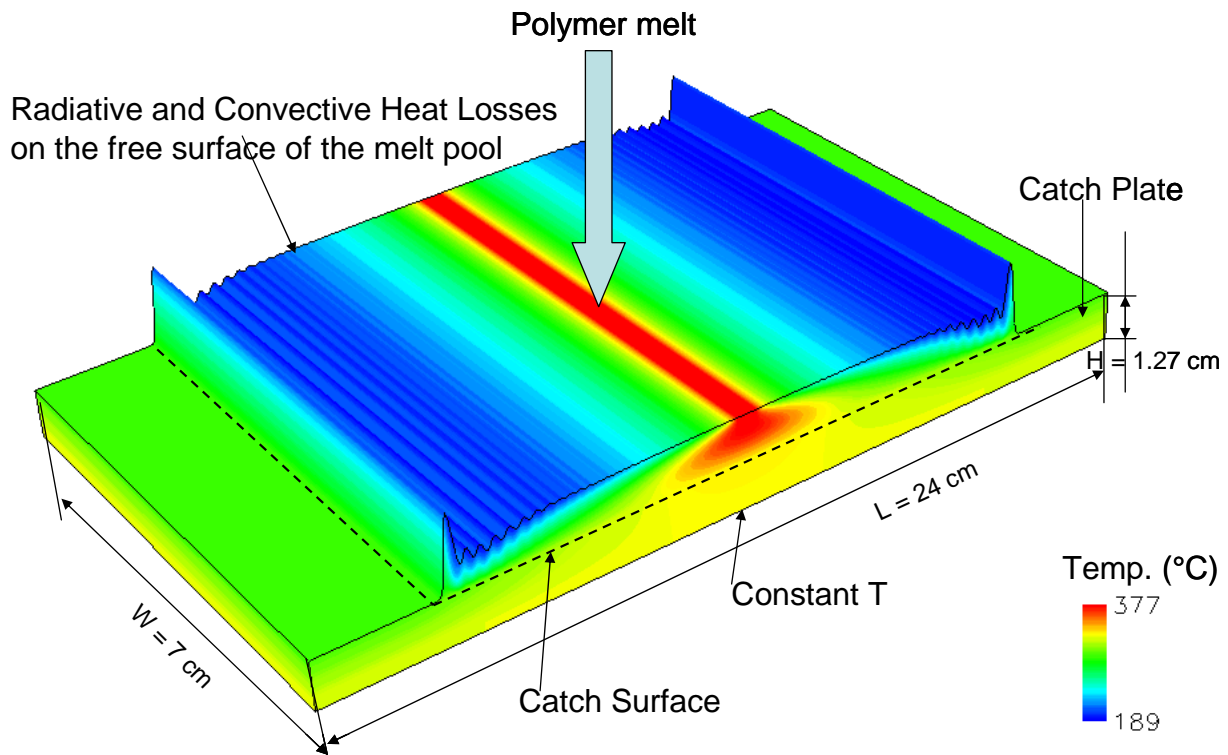


Figure 3.37 Conjugated computational model used in Task 4.

The material properties of the polymer melt and the catch plate used in the CFD calculations are listed in Table 3.11. Because the catch plate must remain solid during the calculation, its viscosity is set to a very large value to suppress motion in the catch plate.

Table 3.11 Material Properties Used in Task 4 CFD Model.

	Polymer melt	Catch plate
Heat capacity ($\text{J kg}^{-1} \text{K}^{-1}$)	2400	961
Density (kg m^{-3})	900	2800
Heat conductivity ($\text{W m}^{-1} \text{K}^{-1}$)	0.25	1.26
Viscosity (Pa-s)	Temperature dependent	1.e6

3.5.3 Computational Grid, Melt Flow Source, Boundary and Initial Conditions

A sketch of the 2D computational grid is shown in Figure 3.38. The grid lines in the picture connect cell centers. The grid consists of two parts.

- The bottom part ($L \times H2$, $24\text{cm} \times 1.27\text{cm}$) uses a fixed grid to model the catch plate. In the $H2$ direction, there are 10 internal cells and the grid cells are stretched with the finest grid spacing near the interface between the catch plate and the melt pool. In the L direction, uniform grid cell spacing is used.
- The top part ($L \times H1$) uses a moving grid to model the melt pool. In the $H1$ direction, there are 20 internal cells with uniform spacing. The initial value of $H1$ is 0.1 mm. The grid in the L direction uses the same number of cells and the same grid cell spacing as the $L \times H2$ part of the grid.

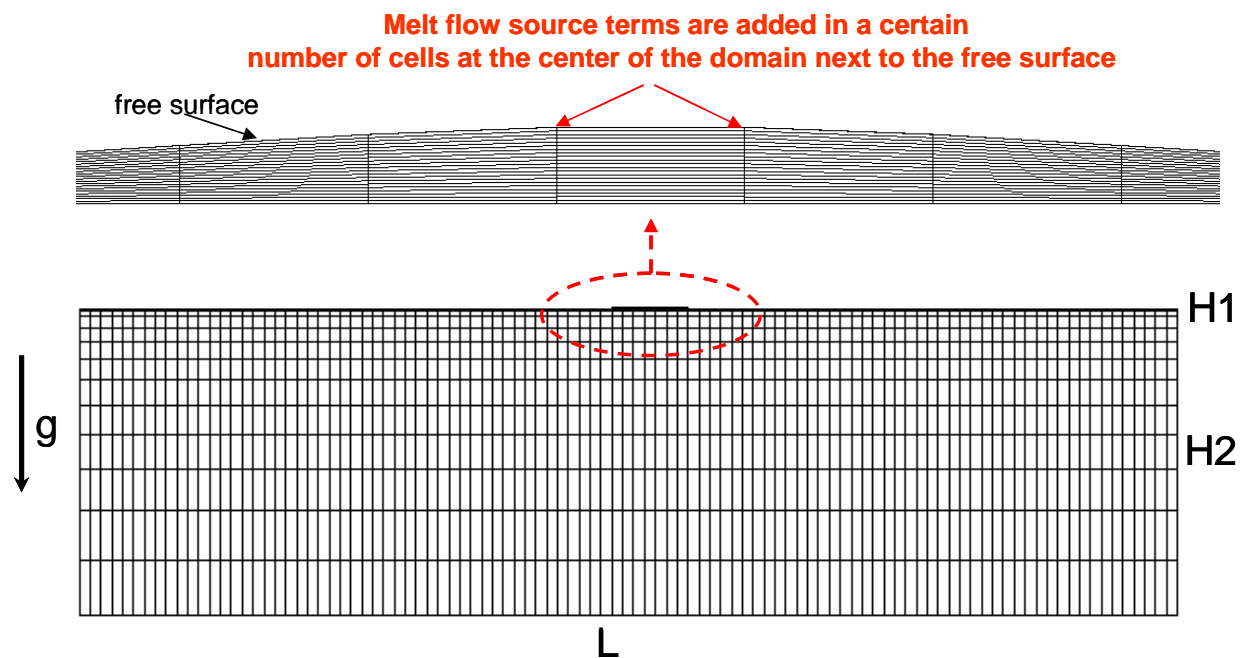


Figure 3.38 Sketch of computational grids adopted in Task 4 modeling.

The melt flow sources (i.e., mass source and energy source), which approximate the melt flow from the polymer slab, are added to the discretized governing equations in selected cells at the center of the domain in the L direction next to the free surface. The source terms added to the momentum and energy equations can be expressed as $\dot{m}(U_{flow} - U)$ and $\dot{m}(T_{flow} - T)$, respectively, where \dot{m} is the mass flow rate (i.e., the mass loss rate computed in Task 3), U_{flow} ($= 0 \text{ ms}^{-1}$) and T_{flow} ($= 650 \text{ K}$) are the velocity and temperature of the hot melt, and U and T are the solved variables. The melt flow temperature is estimated based on the simulation results from Task 3.

The top boundary of the melt pool is a free surface with radiative and convective heat losses. The free surface is not exposed to any external radiative heat source. The convective heat loss rate \dot{q}_{conv} is computed as

$$\dot{q}_{conv} = -Ah(T_s - T_a), \quad (35)$$

where A is the surface area, h ($= 8 \text{ Wm}^{-2}\text{K}^{-1}$) is the convection heat transfer coefficient, T_s is the surface temperature and T_a ($=298 \text{ K}$) is the ambient temperature. The radiative heat loss rate \dot{q}_{rad} is calculated as

$$\dot{q}_{rad} = -A\varepsilon\sigma(T_s^4 - T_a^4), \quad (36)$$

where ε is the emissivity ($=1.0$); σ is the Stefan-Boltzmann Constant ($=5.67\text{e-}8 \text{ Wm}^{-2}\text{K}^{-4}$).

The bottom boundary of the catch plate is treated as a no-slip constant temperature boundary. For resin PP702N the bottom temperature is set to 675 K and for PP6523 the temperature is set to 700 K. It has been found that these temperatures have a great impact on the simulation. In particular, if the bottom temperature is too low, the melt material will pile up on the surface and the simulation will diverge. The values used in Task 4 were obtained via a trial-and-error process. The two sides of the domain are modeled as outlet boundaries. Here, a zero-gradient condition is used on by assigning the cell-centered quantities of the fluid cells next to the outlet boundary to the neighboring ghost cells.

The initial temperature distribution of the catch plate is obtained by solving a 1-D steady state heat transfer problem, the results of which are shown in Figure 3.39.

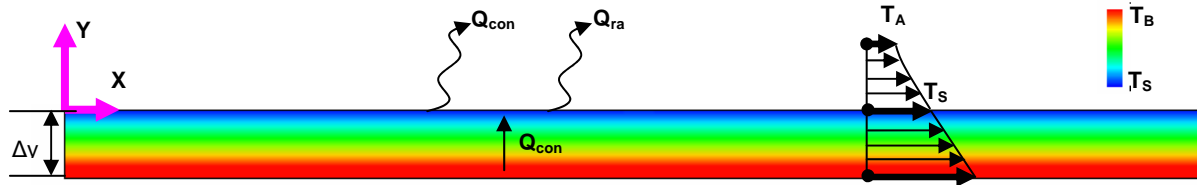


Figure 3.39 1-D heat transfer problem for the catch plate.

The energy balance equation for the above problem can be written as:

$$k \frac{dT}{dy} = h(T_s - T_a) + \varepsilon\sigma(T_s^4 - T_a^4), \quad (37)$$

where k ($= 1.26 \text{ Wm}^{-1}\text{K}^{-1}$) is the heat conductivity of the catch plate, and Δy ($=1.27 \text{ cm}$) is the height of the plate. If the bottom temperature T_B is 675 K as in modeling PP702N, the initial catch plate temperature T can be expressed as

$$T = T_B - 6860.63(y + 0.0127), \quad -0.0127 \text{ m} \leq y \leq 0.0 \text{ m} \quad (38)$$

For a 700 K backside temperature as in modeling PP6523, the initial temperature is

$$T = T_B - 7570.87(y + 0.0127), \quad -0.0127 \text{ m} \leq y \leq 0.0 \text{ m} \quad (39)$$

The initial cell center temperature for the melt pool is set to the surface temperature T_s computed using Eq. (38) and Eq. (39) at $y = 0 \text{ m}$.

3.5.4 Implementation of Surface Tension Model

Two surface tension effects have been considered in the current task.

The first one is the surface tension force normal to the interface that balances the pressure difference across the interface. The resulting equation is known as the Young-Laplace equation [10]:

$$\Delta P = \gamma \left(\frac{1}{R_1} + \frac{1}{R_2} \right), \quad (40)$$

where ΔP is the pressure difference over the interface; R_1 and R_2 are the principle radii of the curvature of the surface; and γ is the surface tension. In the CFD implementation, the pressure difference is modeled as a body force in the momentum equations as:

$$\begin{aligned} \vec{F}_{vol} &= -\Delta P \cdot A \cdot \hat{n} = -\gamma \cdot \kappa \cdot A \cdot \hat{n} \\ \kappa &= \nabla \cdot \hat{n} \\ \hat{n} &= \frac{\vec{n}}{|\vec{n}|} \end{aligned} \quad (41)$$

where A is the surface area; κ is the curvature of the free surface; and \vec{n} is the normal vector of the free surface.

The second effect is the so-called surface tension gradient effect in fire spreading studied by Sirignano and Glassman [11]. They found that the variation of the surface tension due to the temperature gradient along the surface amounts to a stress by which the surface liquid is pulled away from the flame front. Thus, the hot liquid is carried forward in the direction of flame propagation and energy is transported by convection. At the surface, the stress resulting from the variation of the surface tension equals the viscous stress:

$$\mu \frac{\partial U}{\partial n} = \frac{d\gamma}{d\tau} \equiv \gamma_\tau, \quad (42)$$

where μ is viscosity, U is the velocity, n is the normal direction and τ is the tangential direction. In the CFD implementation, the additional surface shear stress term due to the surface tension gradient is modeled as a body force term in the momentum equations as follows:

$$\begin{aligned} \vec{S} &= \gamma_\tau \cdot \hat{\tau} = \gamma_x \vec{i} + \gamma_y \vec{j} \\ \hat{\tau} &= \frac{\vec{\tau}}{|\vec{\tau}|} \end{aligned} \quad (43)$$

where $\vec{\tau}$ is the tangential vector of the free surface. γ_x and γ_y are the additional source terms in the u - and v -momentum equations, respectively. Note that the surface tension models are only applied to cells that form the free surface (i.e., these source terms are zero for internal cells).

In CPCFD, the surface tension is correlated to the temperature as [12]:

$$\gamma = -0.04T(^{\circ}\text{C}) + 29.10 \quad (165 - 220^{\circ}\text{C}). \quad (44)$$

The correlation has been suggested by NIST [13] and is valid for Eastman Epolene D-10 atactic polypropylene. For temperatures outside the range of 165 to 220°C, extrapolation is used in the CFD modeling.

Another important quantity in the surface tension model described above is the surface curvature. Figure 3.40 is a diagram of the algorithm developed to calculate the surface curvature κ . Note that the current implementation of the algorithm is only valid for the 2D problems solved in Task 4. The extension of the algorithm to 3D geometries is straightforward. In the algorithm, the surface is approximated by line segments that connect vertices. Referring to Figure 3.40, the normal vector n_1 is calculated based on the vertices (x_1, y_1) and (x_2, y_2) and the normal vector n_2 is calculated based on the vertices (x_2, y_2) and (x_3, y_3) . The curvature at vertex (x_2, y_2) can then be approximated as:

$$\kappa_2 = \nabla \cdot n = \frac{\partial n_x}{\partial x} + \frac{\partial n_y}{\partial y} = \frac{\Delta n_x}{\Delta x} + \frac{\Delta n_y}{\Delta y} = \frac{n_{x2} - n_{x1}}{\Delta x} + \frac{n_{y2} - n_{y1}}{\Delta y} . \quad (45)$$

The terms Δx and Δy are computed from the cell center locations as shown in Figure 3.40. The curvature at vertices (x_3, y_3) , (x_4, y_4) is obtained in a similar manner. The face center curvature is calculated by taking the average of the curvature at nearby vertices.

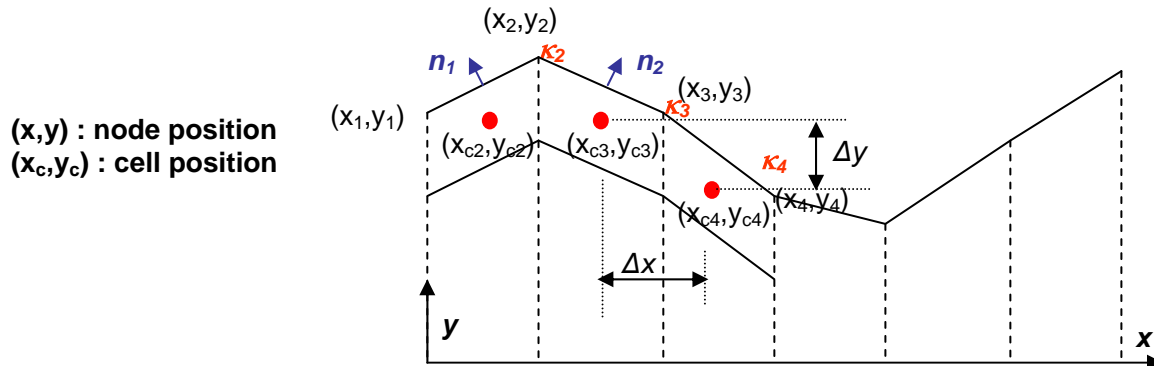


Figure 3.40 Diagram of the algorithm for calculating surface curvature.

3.5.5 Parametric Study of Grid Sensitivity and Time Accuracy

In Task 1 to Task 3, it was observed that the CPCFD simulation results are sensitive to grid resolution and time step size. In Task 4, a set of carefully chosen parametric cases have been performed to investigate the grid sensitivity and time accuracy of CPCFD before tackling the three required sub-tasks. These parametric cases are summarized in Table 3.12.

Table 3.12 Parametric Cases for Studying Grid Sensitivity and Time Accuracy.

Case	Time Step	Grid	CPU time (hr)	Surface tension effects
T7	$\Delta t_{\max}=0.1$; CFL=0.5	400X30	8.5	Not included
T18	$\Delta t_{\max}=0.045$; CFL=0.5	400X30	15.0	Not included
T8	$\Delta t_{\max}=0.02$; CFL=0.5	400X30	15.0	Not included
T13	$\Delta t_{\max}=0.01$; CFL=0.5	400X30	34.0	Not included
T19	$\Delta t_{\max}=0.02$; CFL=0.5	533X30	15.0	Not included
T14	$\Delta t_{\max}=0.02$; CFL=0.5	600X30	17.0	Not included
T15	$\Delta t_{\max}=0.02$; CFL=0.5	800X30	21.0	Not included
T9	$\Delta t_{\max}=0.02$; CFL=0.5	400X30	21.0	Included
T16	$\Delta t_{\max}=0.02$; CFL=0.5	600X30	36.0	Included
T17	$\Delta t_{\max}=0.02$; CFL=0.5	800X30	48.0	Included

All cases were performed for the PP702N resin. The simulated time period is 250 seconds and all cases were run on a Dell Precision 450 Desktop PC with a Xeon 3 GHz CPU. Note that the time-step size is determined by two factors, namely the maximum time-step size Δt_{\max} and the CFL number. The grid refinement is only performed in the horizontal direction.

The melt flow rate is a constant at 0.14 gs^{-1} , which is an estimate of the mean mass flow rate based on the simulation results from Task 3. In Case 3R (see Figure 3.34), the predicted mean total mass loss rate is 0.27 gs^{-1} , the fraction of melt flow occurring as melt flow is 0.74. Considering the object modeled in Task 3 has a width (W) of 10 cm and the object modeled in Task 4 has a width of 7 cm, the melt flow rate used in Task 4 can be calculated as $0.27 \times 0.74 \times 7/10 = 0.14 \text{ gs}^{-1}$.

The mass sources are distributed in the 10 cells at the center of the top surface in the 400X30 grid and the 20 center cells at the center of the top surface in the 800X30 grid. A 2.5 degree tilt angle is applied to the catch plate by adjusting the direction of the gravity force.

Figure 3.41 shows the impact of the time-step size on the free surface shape. The “ringing” effects observed at the two edges of the melt pool are non-physical; these are caused by numerical errors in the solution algorithm. It can be seen that, due to the tilted catch plate, the right edge of the melt pool spreads faster than the left edge. As the time-step gets smaller, the spreading velocity of the melt pool increases.

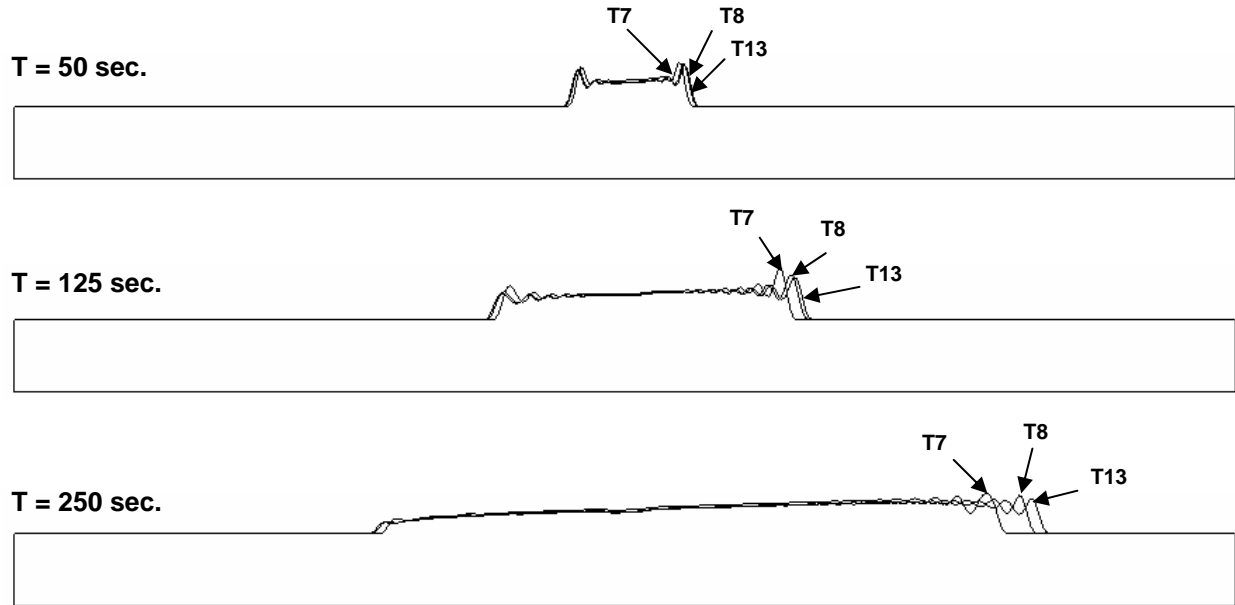


Figure 3.41 Free surface shapes at selected times for different time-step sizes.

To quantify the impact of the time-step size on the calculated melt pool behavior, the mean velocity of the right edge of the melt is plotted against the square of the maximum time-step size in Figure 3.42. The cases plotted are for cases T7, T18, T8 and T13. The mean velocity of the edge is obtained by dividing the moving distance of the edge by the time difference. It can be

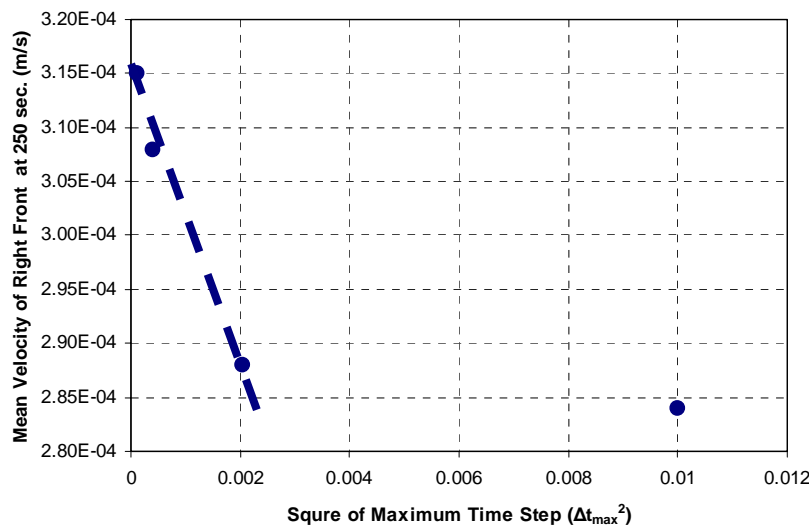


Figure 3.42 Mean spreading velocity as a function of the square of the maximum time-step size.

be seen that the mean velocity at 250 seconds increases linearly as the square of the maximum time-step size decreases, which indicates that the numerical scheme is second order accurate in time for this Task 4 problem. The time-step size used in Case T7 is too large and causes significant errors in predicting the melt pool spreading rate. Note that surface tension effects were not included in the four test cases.

Figure 3.43 and Figure 3.44 show the free surface shapes for simulations performed with different grid resolutions in the horizontal direction. The surface tension effects are included in the three cases shown in Figure 3.44 but not included in the three cases shown in Figure 3.43. Note that the time-step size criteria for all six cases are the same. The first observation from the two figures is that the surface tension effects make the shape at the edge of the melt pool smoother. The second observation is that the “ringing” phenomenon becomes more severe as the grid resolution increases. The “ringing” effects are similar to that of the well-known Gibbs phenomenon for discontinuous functions [14].

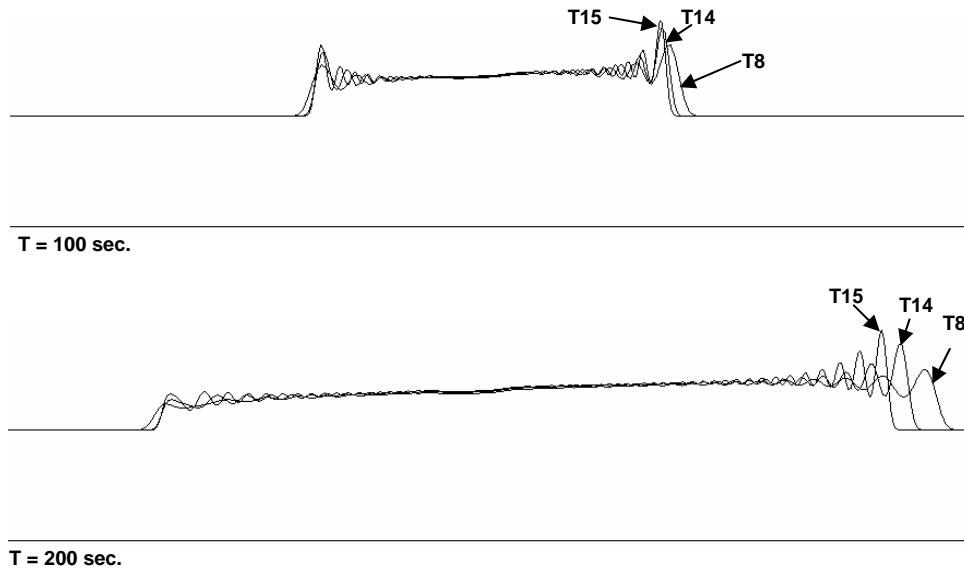


Figure 3.43 Free surface shapes at selected times using different grid. No surface tension effects included.

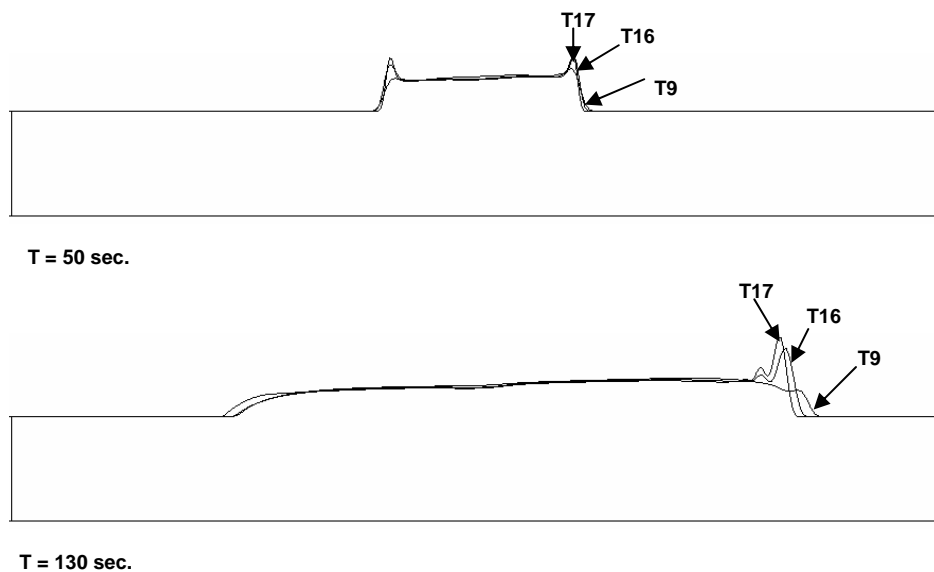


Figure 3.44 Free surface shapes at selected times using different grid. Surface tension effects included.

To quantify the impacts of the grid resolution on the predicted melt pool behavior, plotted in Figure 3.45 is the mean velocity of the right edge of the melt versus the square of the normalized grid size. The normalized grid size is defined as the horizontal grid cell size divided by the horizontal grid cell size for the 400×30 grid (i.e., 0.6mm). The data points for surface tension not included correspond to simulations T7, T19, T14 and T15 and the data points for surface tension included correspond to simulations T9, T16 and T17. From the figure it can be seen that a linear relationship exists between the data points, indicating that the numerical scheme used in CPCFD is second order accurate in space.

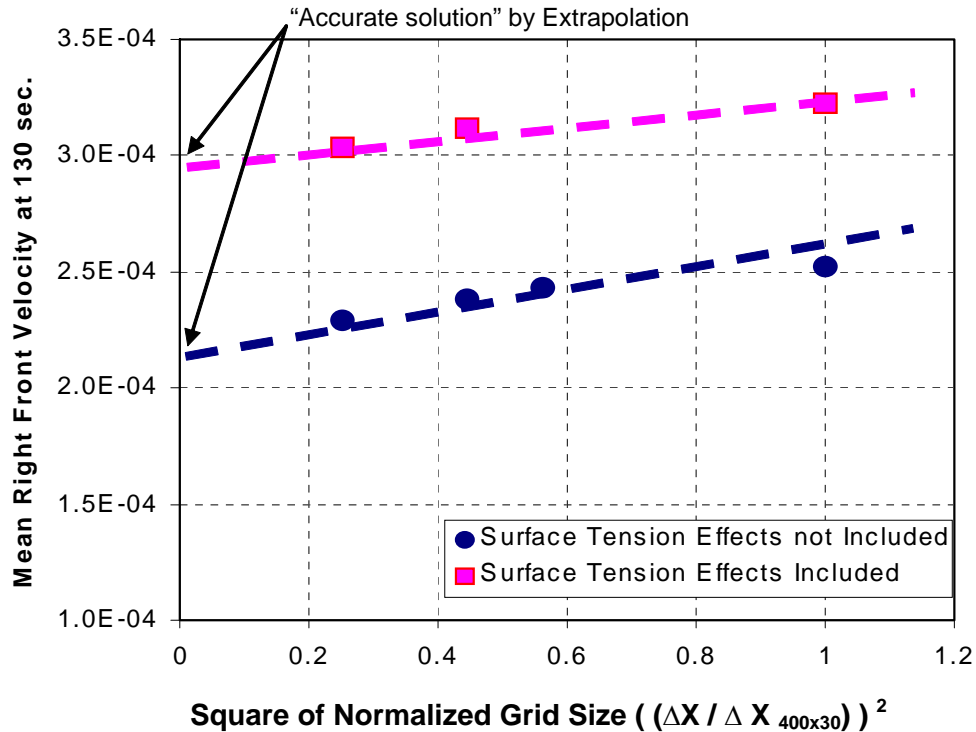


Figure 3.45 Mean spreading velocity as a function of the square of the normalized grid size.

3.5.6 Task 4A, 4B and 4C Results and Discussions

In Tasks 4A-4C, simulations are performed for two polymer resins with different catch plate tilt angles. Three cases have been performed and are summarized in Table 3.13. A 400×30 grid is used in all cases, where the time dependent mass source is distributed among the ten center cells near the free surface. It was found that the small melt flow rate onto the catch plate at the beginning (i.e., < 100 sec.) caused the case to crash because the melt temperature became too low due to heat loss. To overcome this difficulty, the melt flow on the catch surface from 0 seconds to 200 seconds is modeled using a constant melt flow rate in all cases to create an initial amount of mass on the catch plate. The simulations are performed in the following steps:

1. Compute the melt flow using a large constant melt flow rate (i.e., 0.14gs^{-1}) for 30 seconds. This will result in about 5 grams of melt on the catch plate.
2. Stop simulation.
3. Restart simulation using the time dependent melt flow rate profile, starting at 200 seconds.
4. Continue simulation until melt front approaches end of plate.

Table 3.13 Task 4 Case Summary.

Case	Resin	Melt Flow Rate	Time Step Size	Tilt Angle	Simulated Time Period	Wall Clock Time
4A	PP702N	From Case 3R	$\Delta t_{\max}=0.02$; CFL=0.5	2.5°	200 s – 430 s	~19 hrs
4B	PP6523	From Case 3I	$\Delta t_{\max}=0.02$; CFL=0.5	2.5°	700 s – 1350 s	~36 hrs
4C	PP702N	From Case 3R	$\Delta t_{\max}=0.01$; CFL=0.5	0.0°	200 s – 540 s	~40 hrs

The time dependent melt flow rates are obtained from the Task 3 modeling results. For Case 4A and 4C, the melt flow rate is computed from the mass loss history predicted by Case 3R (see Figure 3.46); additional details on the Case 3R results can be found in Section 3.4.3 and Figure 3.34. The melt flow rate used in Case 4B (see Figure 3.47) is calculated from the Case 3I results, which can be found in Section 3.4.4 and in Appendix A.

In Figure 3.46 and Figure 3.47, the solid lines represent the total mass loss from the polymer slab. The dashed lines are the mass loss occurring as melt flow. The difference between the solid line and dashed line is the mass loss due to gasification. The melt flow rate is calculated as the first derivative of the dashed line and is stored in a look-up table, which is read-in as input data by CPCFD at the beginning of the simulation. During the simulation, the flow rate is tabulated from the table given at a certain point in time.

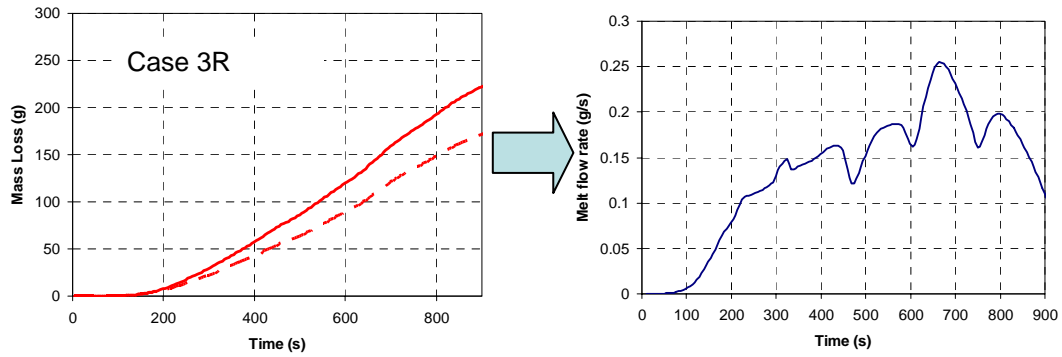


Figure 3.46 Melt flow rate used in Case 4A and Case 4C.

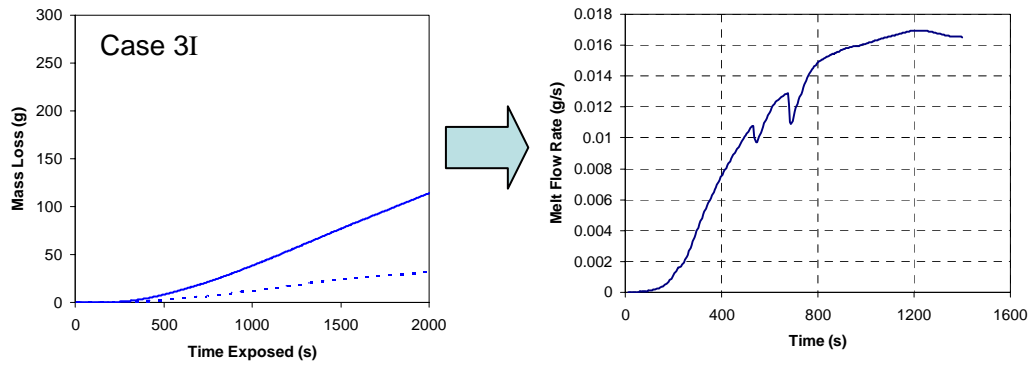


Figure 3.47 Melt flow rate used in Case 4B.

Figure 3.48 shows the temperature contours of the melt pool and the catch plate calculated in the three cases. For all cases, the temperature at the center of the melt pool near the free surface is higher than the other part of the melt pool because the hot melt from the polymer slab enters the melt pool at this location. Away from the center, the free surface becomes cool due to heat loss to the environment. The melt pool is heated by the catch plate where a temperature gradient in the vertical direction can be seen. Due to the tilted catch plate in Case 4A and 4B, the right front of the melt pool moves faster than the left front. In Case 4C, the two fronts of the melt pool move at the same pace and the shape of the melt pool as well as the temperature distribution are symmetric with respect to the center of the domain in the horizontal direction. The surfaces in all three cases are very smooth.

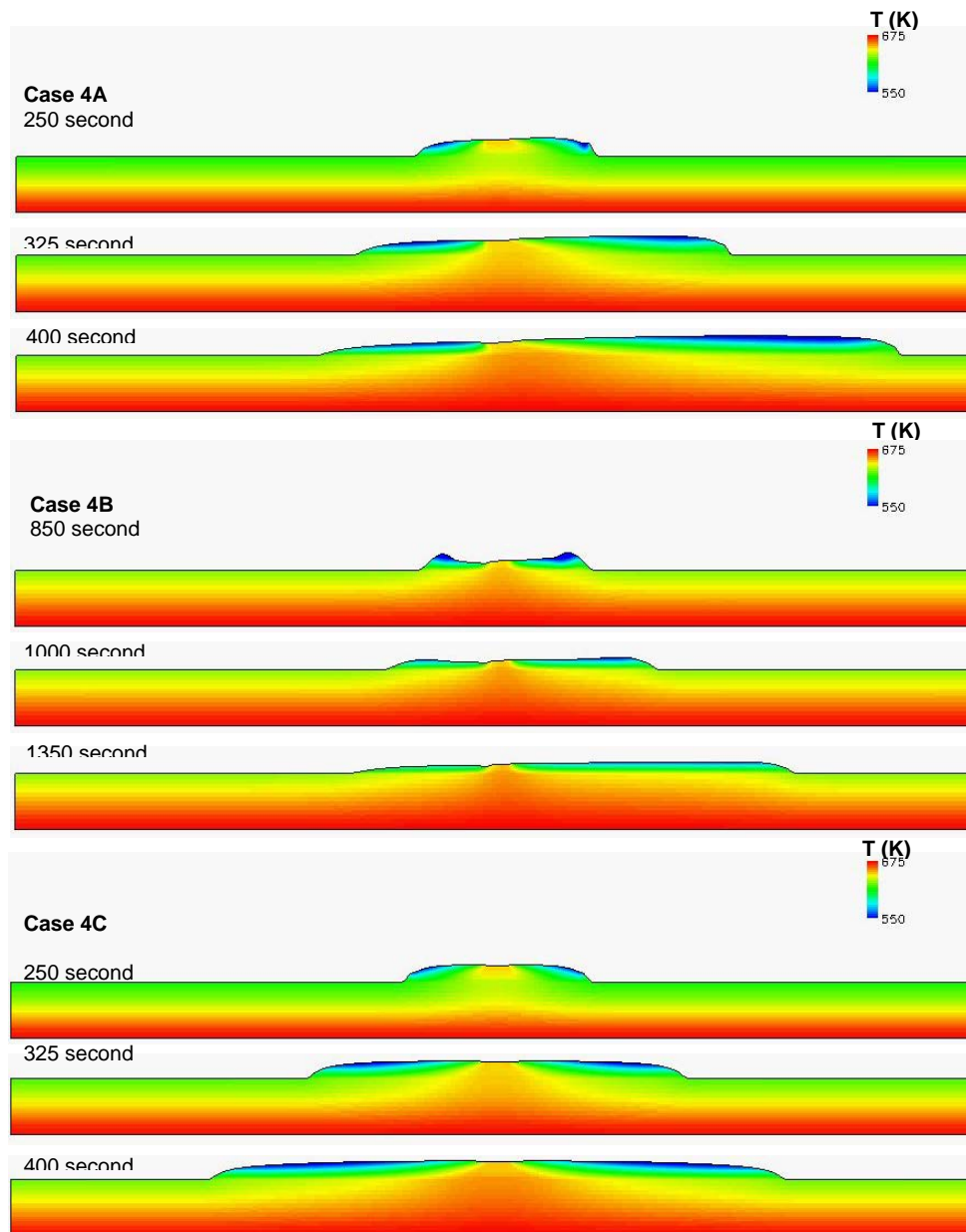


Figure 3.48 Temperature contours of the melt pool and catch plate.

Comparing Case 4A and 4B in Figure 3.48, it can be seen that: 1) the overall height of the melt pool in Case 4A is larger than that in Case 4B; and 2) the right front in Case 4A moves faster than the right front in Case 4B. This is caused by the different viscosity-temperature relationships of PP702N and PP6523, and the different melt flow rates used in the two cases.

Illustrated in Figure 3.49 is the time history of the melt front velocities for Case 4A, Case 4B and Case 4C. The plots show that the right melt front moves faster than the left melt front for Case 4A and Case 4B. However, for Case 4C the two melt fronts move at the same speed. In the future, when the data becomes available, it will be possible to compare these plots to NIST experimental data.

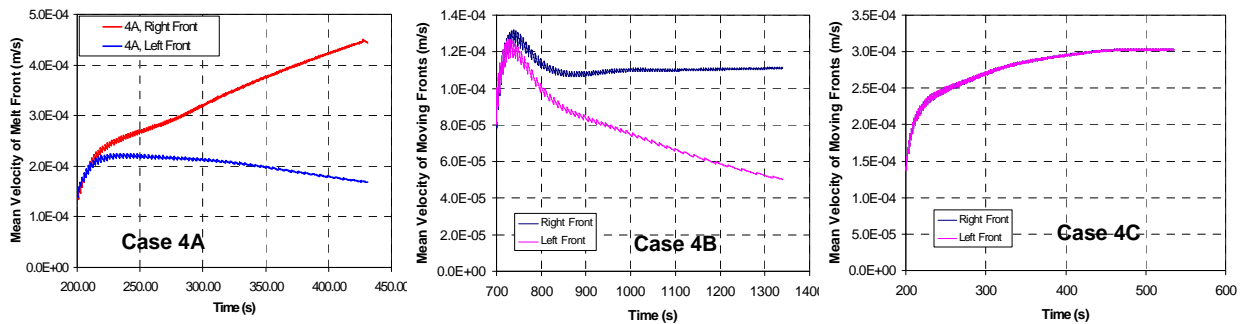


Figure 3.49 Mean velocity of melt front as a function of time.

The “zigzag” appearance of the curves plotted in Figure 3.49 is a result of the melt front tracking algorithm used in CPCFD. In the algorithm, the position of the melt front is “marked” by the coordinate of the grid point immediately behind the front. The “marked” position of the melt front remains unchanged until the melt front moves a distance Δx (i.e., one grid cell in the horizontal direction). The mean velocity reported in Figure 3.49 is obtained using the following formula:

$$V_{front} = \frac{x_t - x_{t_0}}{t - t_0} \quad (46)$$

where x_t and x_{t_0} are the positions of the front at the current time and at the beginning of the simulation, respectively. Because x_t is not updated continuously (i.e., not updated at every time step), the velocity vs. time curves appear squiggly.

4. CONCLUSIONS

In this report is described the work effort by REI to develop, demonstrate and deliver to NIST a condensed phase CFD based tool to model the processes of melting, flow and gasification of thermoplastic materials exposed to a high heat flux. Potential applications of the tool include investigating the behavior of polymer materials commonly used in personal computers and computer monitors if exposed to an intense heat flux, such as occurs during a fire

The model delivered to NIST is based on a time dependent (time varying) grid CFD method.

- The model is written in FORTRAN 90 in an object-oriented form. A 3D, finite volume, multi-block body-fitted time dependent (time varying) grid formulation is used to solve the unsteady Navier Stokes equations. The time integration, spatial discretization and overall solution procedure are based on standard CFD methods from the literature. A multi-grid method is used to accelerate convergence at each time step.
- Sub-models are included to describe the temperature dependent viscosity relationship and in-depth gasification and absorption of thermoplastic materials, free surface flows and surface tension. NIST data is used for key material properties of the thermoplastic materials of interest.
- A variety of boundary conditions can be used for the velocity field (no-slip, free-slip) and heat transfer to the object (adiabatic, heat loss, specified heat flux).
- Model outputs include the time dependent velocity, temperature and position (displacement) at points in the thermoplastic body which can be imported to standard CFD visualization packages. Additional outputs include the time history of the mass loss rate and heat fluxes.
- The accuracy and capabilities of the modeling tool are demonstrated on a series of test cases of increasing complexity. The test cases include grid sensitivity studies, adding heat loss boundary conditions, simulations for two thermoplastic materials (PP702N, PP6523), different heat flux scenarios and test problem configurations.

Comparisons of model results to NIST experimental data indicate discrepancies between the model and experimental results, particularly for the rate of mass loss. To match NIST data for mass loss rate large changes were required to the parameters originally used in the in-depth absorption model and kinetic rate parameters in the in-depth gasification model. In addition, for simulations in which the free surface of the melt flow is parallel to the direction of gravity a grid smoothing operation needed to be applied to the free surface to control grid skewness that would lead to simulation divergence. For simulations that did not include models for all key physics (e.g., no in-depth absorption, no in-depth gasification) the simulations would develop a large deformation ("belly") at the free surface. For carefully selected model parameters and procedures, comparisons of the model results and NIST data show favorable agreement. However, the research effort was un-able to provide satisfactory explanations for the need to significantly increase the model parameters for the in-depth absorption and in-depth gasification models or the presence of the "belly" at the free surface of the thermoplastic object. These issues remain un-resolved though some efforts continue at NIST to address these issues.

The current work effort has highlighted the importance of having accurate models to describe in-depth absorption, in-depth gasification and the highly non-linear viscosity-temperature relationship that exists for thermoplastic objects. Hopefully, future experiments can provide the necessary data to develop more accurate models for these items.

The source code, documentation, test problems (all needed files) and presentation material have been delivered to NIST.

In the future, it may be possible to couple models such as the condensed phase CFD code to the NIST FDS code, a CFD model that solves for gas phase transport and combustion. The combined tools would enable high-fidelity simulations for fire spread scenarios in office environments populated with desktop/deskside personal computers.

5. LITERATURE REFERENCES

1. Butler, K. M.; Ohlemiller, T. J.; Linteris, G. T., "Progress Report on Numerical Modeling of Experimental Polymer Melt Flow Behavior," Interflam 2004. International Interflam Conference, 10th Proceedings, Volume 2, July 5-7, 2004. Edinburgh, Scotland, Interscience Communications Ltd., London, England, 937-948 pp, 2004. <http://fire.nist.gov/bfrlpubs/fire04/PDF/f04032.pdf>
2. Ohlemiller, T. J.; Shields, J. R.; Butler, K. M.; Collins, B.; Seck, M., "Exploring the Role of Polymer Melt Viscosity in Melt Flow and Flammability Behavior," New Developments and Key Market Trends in Flame Retardancy. Fall Conference. Proceedings. Fire Retardant Chemicals Association. October 15-18, 2000, Ponte Vedra, FL, Fire Retardant Chemicals Assoc., Lancaster, PA, 1-28 pp, 2000. <http://fire.nist.gov/bfrlpubs/fire00/PDF/f00128.pdf>
3. Ohlemiller, T. J.; Butler, K. M., "Influence of Polymer Melt Behavior on Flammability," U.S./Japan Government Cooperative Program on Natural Resources (UJNR). Fire Research and Safety. 15th Joint Panel Meeting. Volume 1. Proceedings. March 1-7, 2000, San Antonio, TX, Bryner, S. L., Editor(s), 81-88 pp, 2000. <http://fire.nist.gov/bfrlpubs/fire00/PDF/f00129.pdf>
4. Yan, Z., "CFD Fire Simulation and Its Recent Development", Dept. of Fire Safety Engineering, Lund University, Sweden. Chapter to be included in upcoming *Developments in Heat Transfer Series* published by WIT press.
5. Ferziger, J.H., and Peric, M., "Computational Methods For Fluid Dynamics", Springer, 3rd Edition, 2002.
6. Patankar, S.V., "Numerical heat transfer and fluid flow". McGraw-Hill, New York, 1980
7. J.U. Brackbill, D.B. Kothe, & C. Zemach, "A continuum method for modeling surface tension", J. Comput. Phy., 100, pp335-354, 1992.
8. Tang, Q., "MEPDF Method for Modeling Turbulent Combustion Using Detailed Chemistry", NSF SBIR Phase I Final Report, DMI-0441833, July, 2005.
9. W. Zhao, C. Zhang, S. H. Frankel, & L. Mongeau. Computational Aeroacoustics of phonation, I: Numerical methods, acoustic analogy validation, and effects of glottal geometry. J. Acoust. Soc. Am., 112(5), pp2134-2146, 2002.
10. W. Zhao. A numerical investigation of sound radiation from subsonic jets with application to human speech production, PhD thesis, Purdue University, West Lafayette, 2000.
11. Pierre-Gilles de Gennes, Françoise Brochard-Wyart, David Quéré (2002). *Capillary and Wetting Phenomena -- Drops, Bubbles, Pearls, Waves*. Springer.
12. W.A. Sirignano and I. Glassman, *Combustion Sci. and Tech.*, Vol. 1, pp. 307-312, 1970.

13. Thomas Ohlemiller, Kathy Butler, NIST, private communication.

14. J.W., Gibbs, "*Fourier Series*". Nature 59, 200, 1898 and 606, 1899.

APPENDIX A

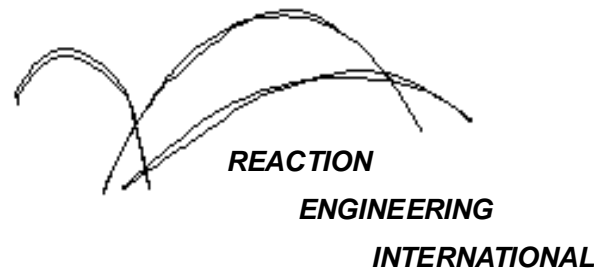
Detailed PowerPoint Summary of Modeling Results

Task 0



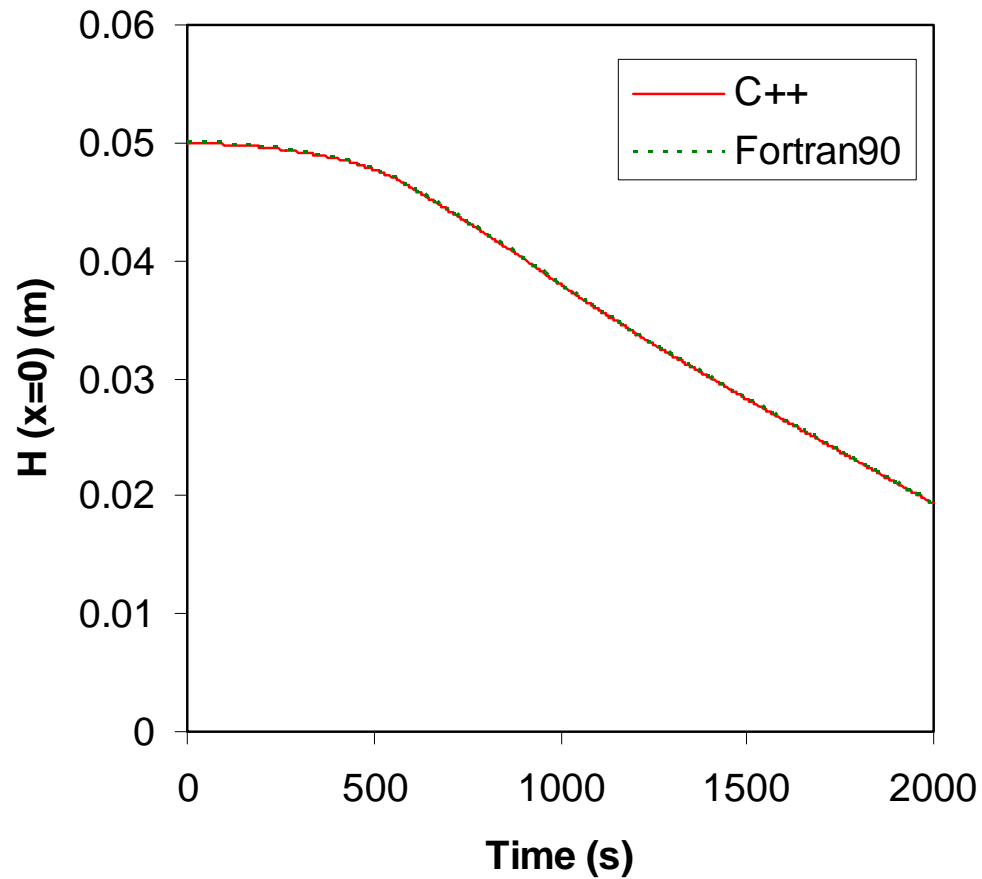
A Computational Model For Fire Growth and Spread On Thermoplastic Objects

Task 0: port CPCFD to Fortran 90
(10/01/05 ~ 10/25/05)



*

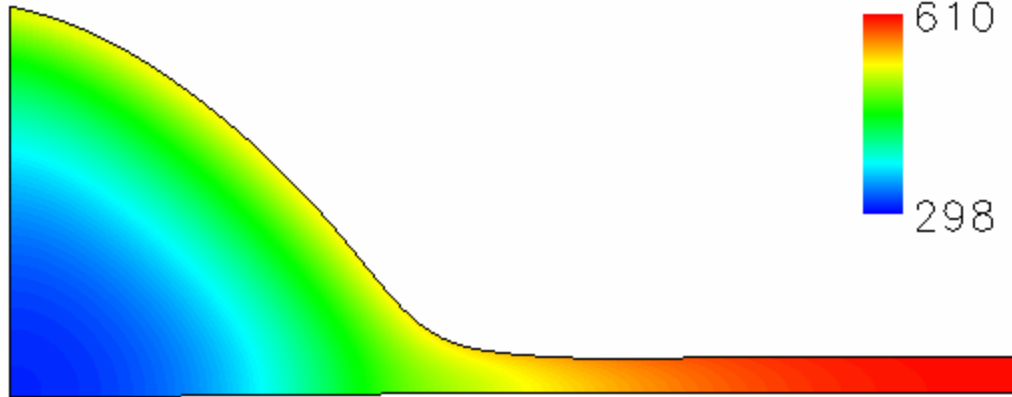
Object height as a function of time



Object Temperature Contour

time = 1000 s

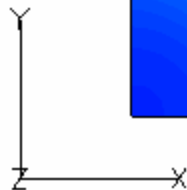
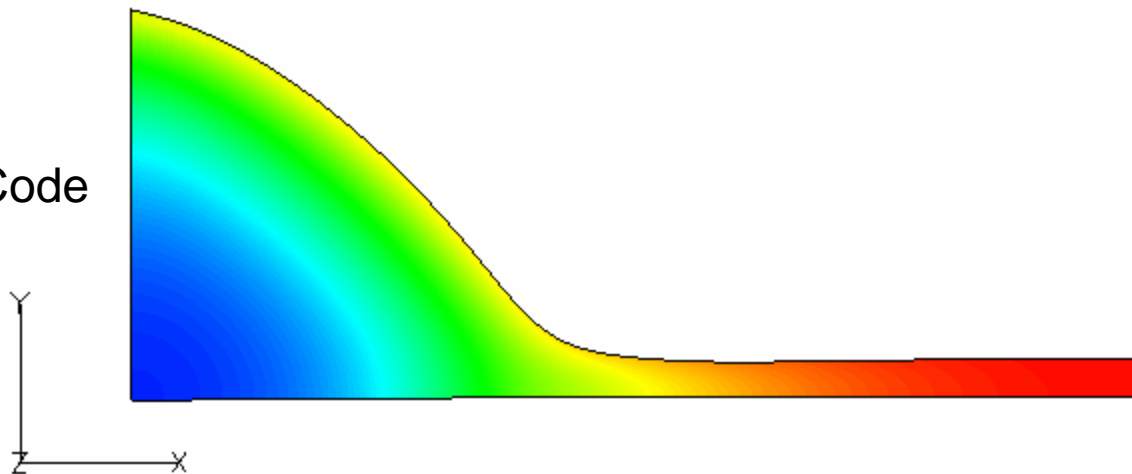
C++ Code



Temperature (K)



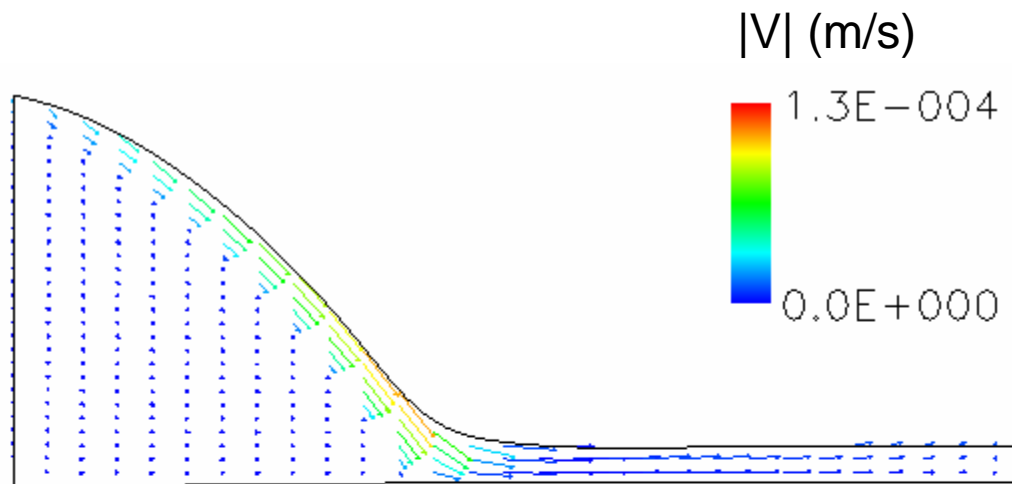
Fortran90 Code



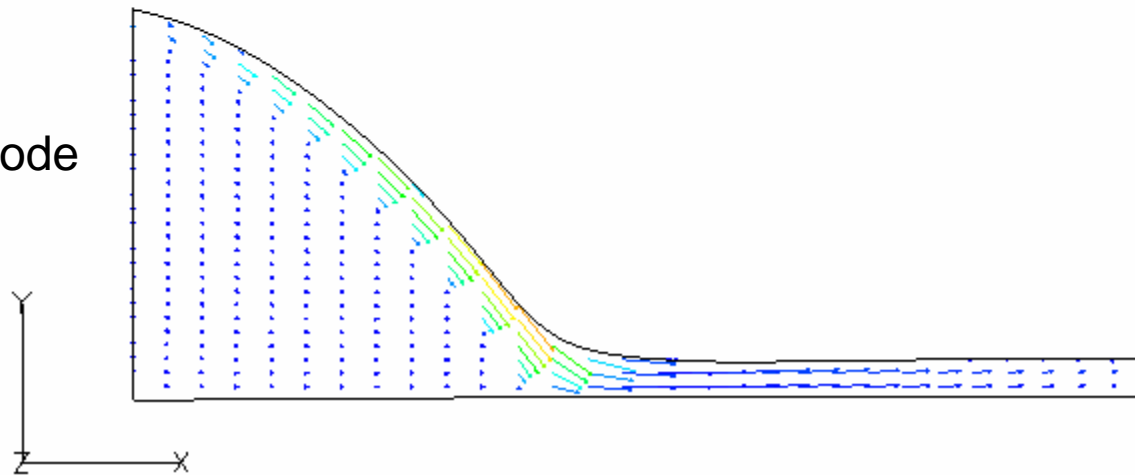
Velocity Vector Field

time = 1000 s

C++ Code



Fortran90 Code



Summary

During this performance period, we have

- ❑ converted the C++ version CPCFD code to a Fortran 90 version (task 1 option)
- ❑ compared the performance of the two codes on the triangle test problem
 - ❑ the two codes give exactly the same results (within the round-off error of double precision floating point)
- ❑ corrected several coding errors in the original C++ code
- ❑ identified several areas that need improvement or modification (see future work)
 - ❑ these improvements and modifications are necessary for the melt-drip test problem in task 1 and other future work



Future Work

- ❑ Test numerical scheme for implicit updating free surface position
 - ❑ Currently using explicit scheme that requires **small time step** to avoid instability
- ❑ Test generalized algorithms for tracking free surface position and generating grids
 - ❑ Current algorithm is **specifically designed for the triangle test problem**
- ❑ Test methods for assigning **stress free** boundary condition to free surface
 - ❑ Currently, free surface boundary is treated as outlet boundary (zero gradient) that is not stress free (though zero mass flow rate across the free surface is guaranteed).
 - ❑ The current method may cause problem in cases where surface tension is important or if the effects of surface tension are required to study in the future
- ❑ 2D condensed phase melt-drip model with steady heat flux

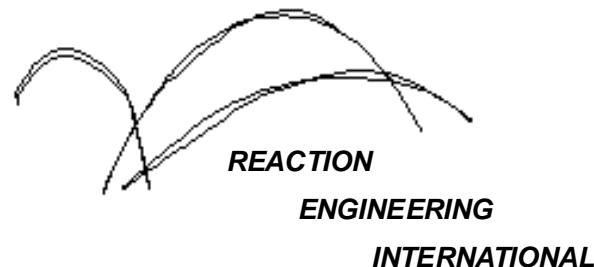


Task 1



A Computational Model For Fire Growth and Spread On Thermoplastic Objects

Task 1: 2D condensed phase melt-drip model with steady heat flux
(1/13/06)



x

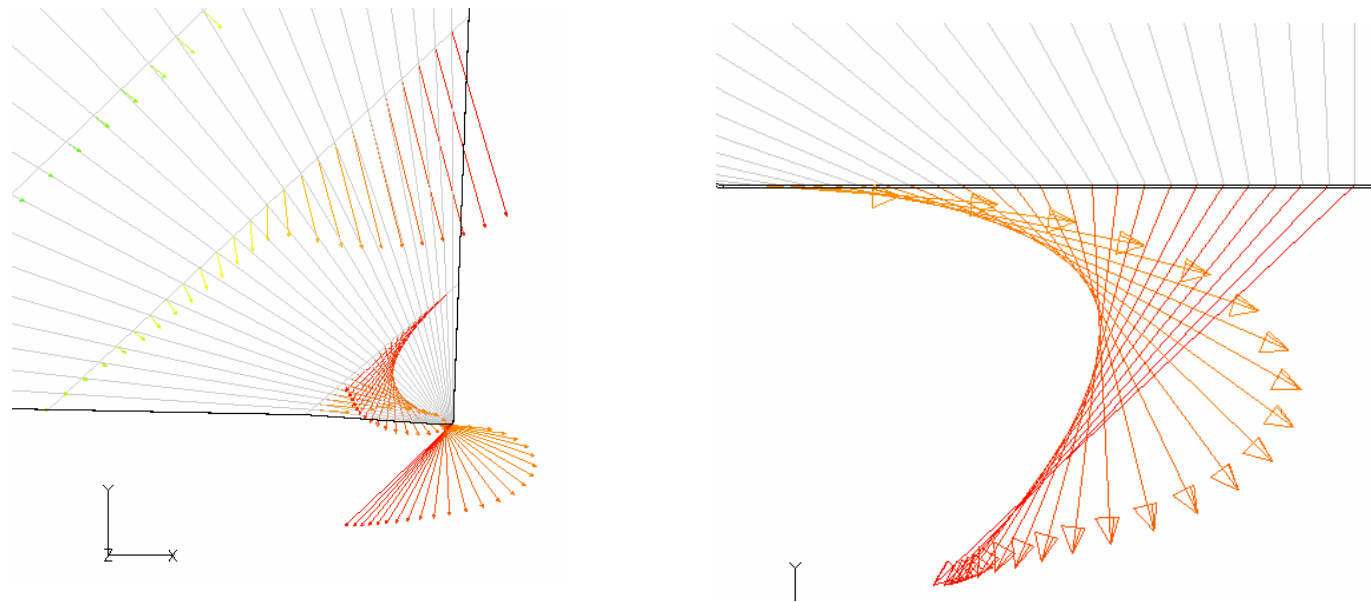
Status Summary

- ❑ Investigated “Model 2” (see Progress Report – Dec, 2005)
 - Solution diverged at about $t = 230$ s

- ❑ Investigated a simplified problem
 - Replaced bottom no-slip wall BC with an outlet boundary
 - Used rectilinear grid
 - Simulation ran successfully
 - Identified deficiencies in code and model that lead to instability (grid skewness may not be the only reason!)
 - ✓ fluctuations in free surface shape
 - ✓ time step too large
 - ✓ localized over-heating of polymer in very thin regions
 - Enhanced robustness of solver
 - ✓ a filtering function to suppress fluctuation of free surface shape
 - ✓ improved time step size selection
 - ✓ special treatment to avoid over-heating in very thin regions



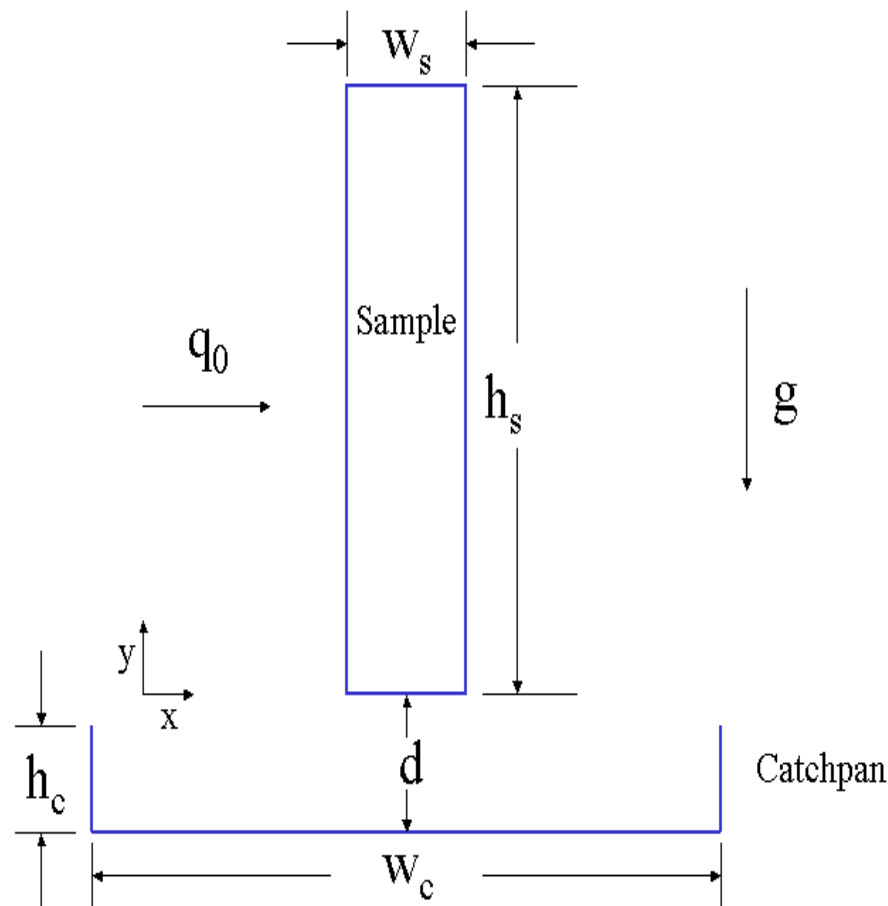
Recall “Model 2” and problems encountered



Velocity vectors at the corner of the model

Solution diverged

A Simplified Problem



Left face of sample:

Constant heat flux q_0 applied to surface of flowing material:
 $k \partial T / \partial s = -q_0$, where s is in the direction normal to the surface

Right face of sample:

$u = 0$ (no penetration)
 $v = 0$ (no-slip)
 $\partial T / \partial x = 0$ (adiabatic)

Top face of sample

$v = 0$ (no penetration)
 $u = 0$ (no-slip)
 $\partial T / \partial y = 0$ (adiabatic)

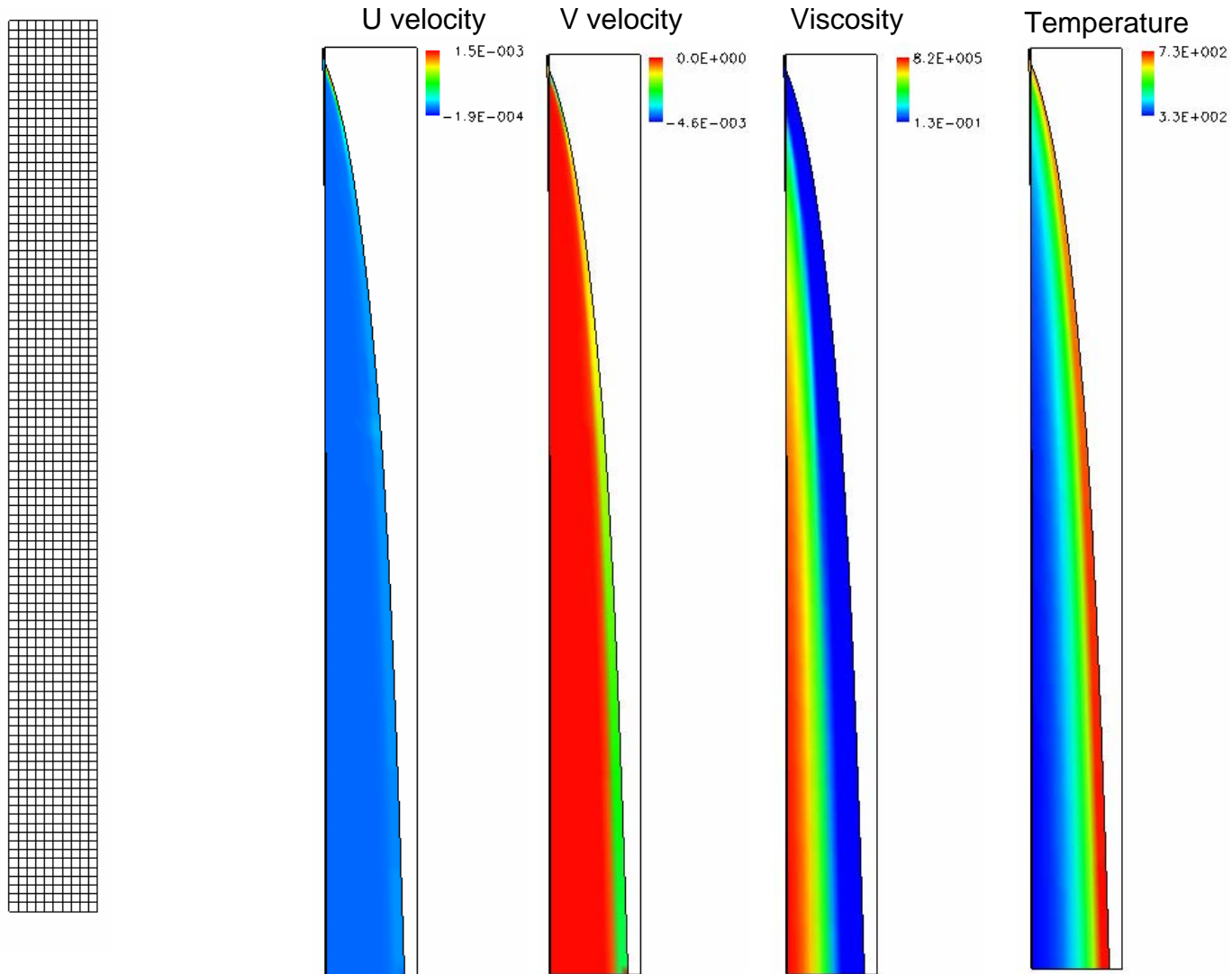
Bottom face of sample

Zero gradient (outlet)

All other parameters same as before



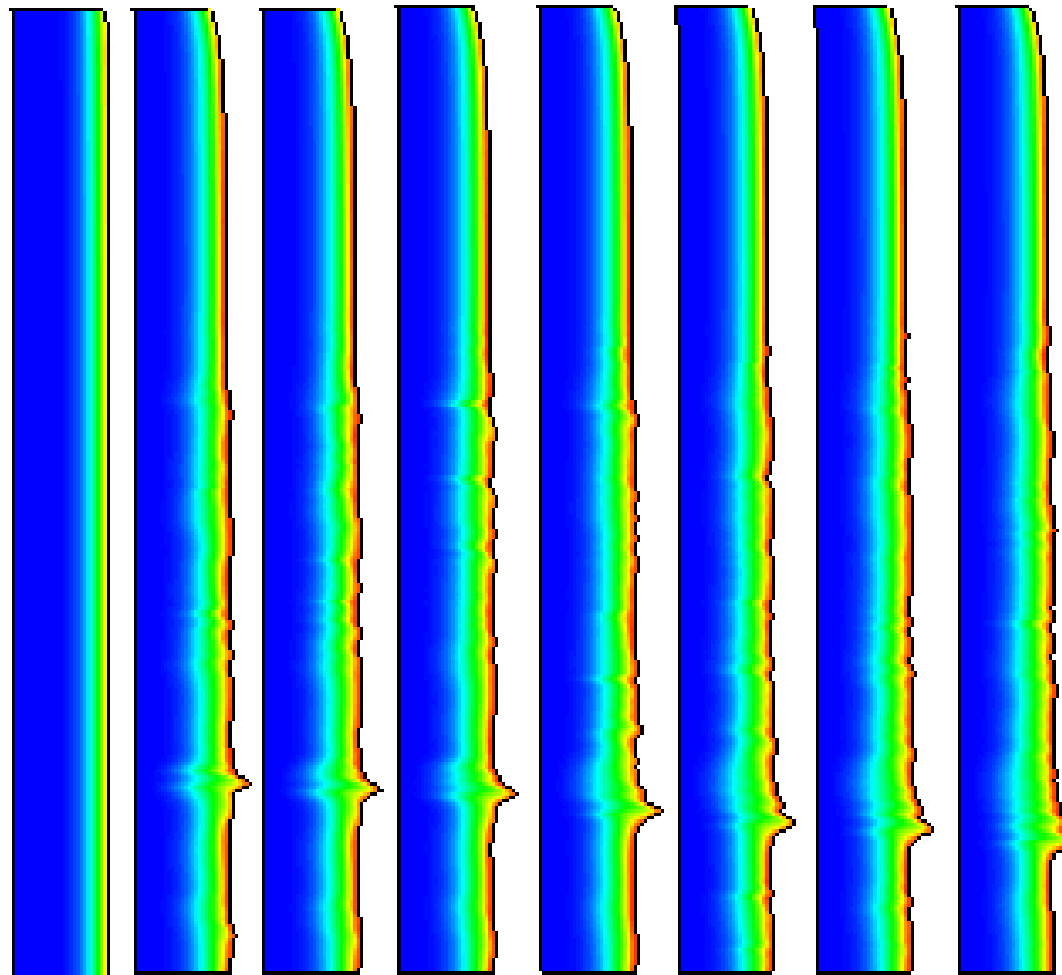
Rectilinear Grid and Solution



$T = 710$ s



Example – fluctuations of moving boundary

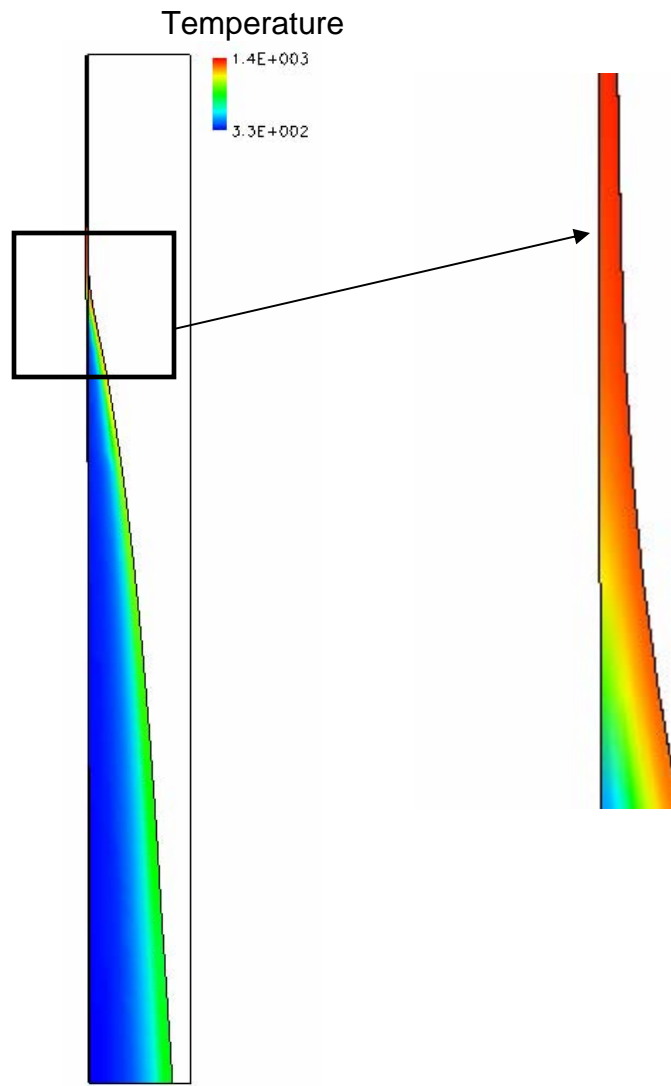


T=140s

T=260s

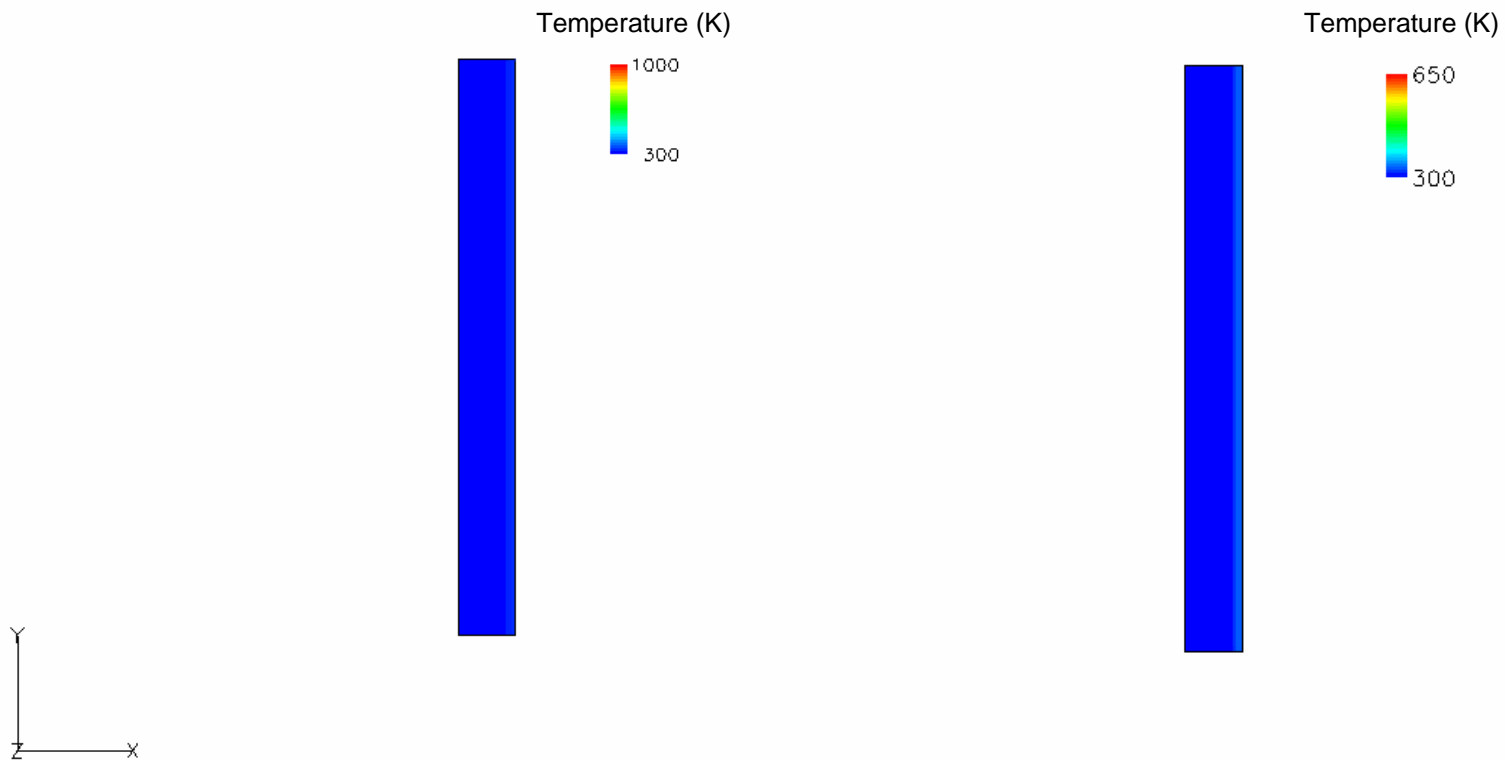
Use filtering function to
suppress the fluctuation

Example - local over heating



- Temperature can reach more than 2000 K in regions where polymer is extremely thin
- Leads to instability
- Results in very small time step
- **Special treatment:**
when material thickness is less than a small value, set the heat flux to zero

Movies – polymer temperature

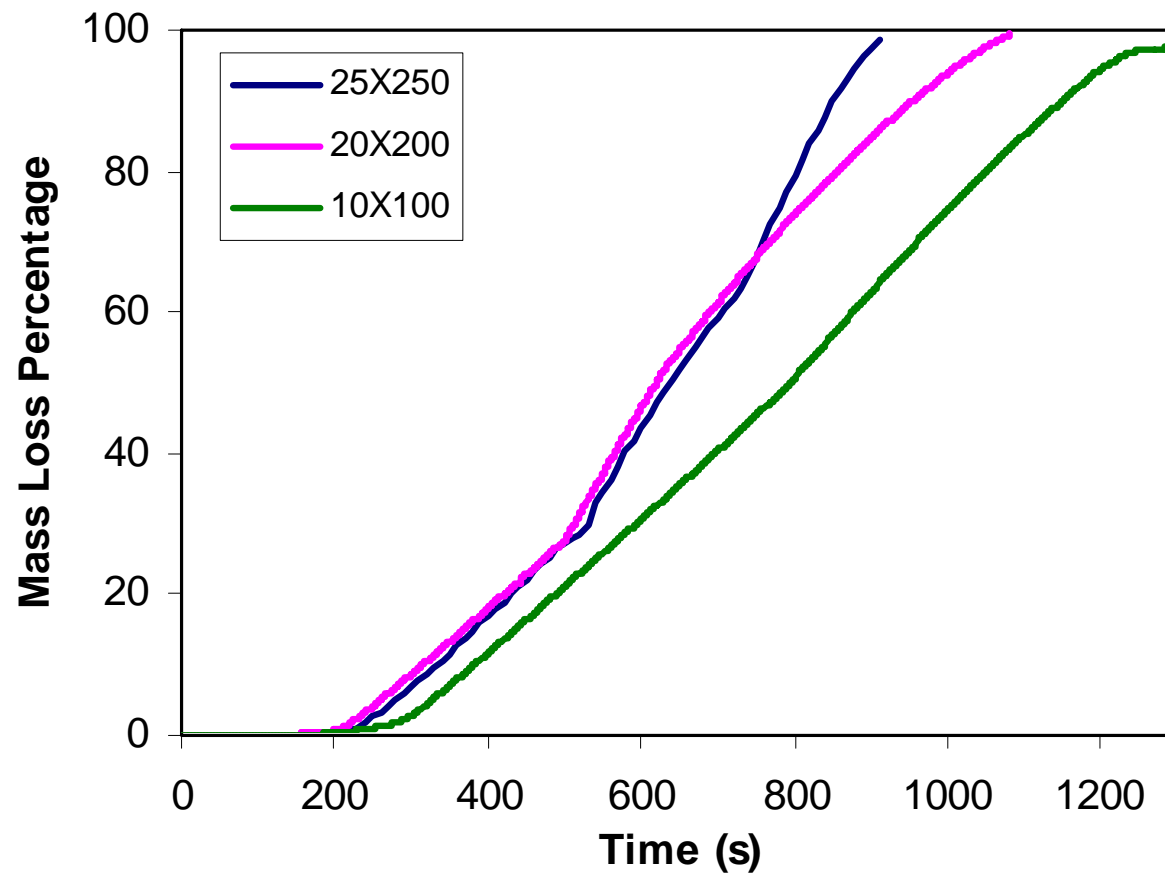


Without special treatment
To avoid local over-heating

With special treatment
To avoid local over-heating



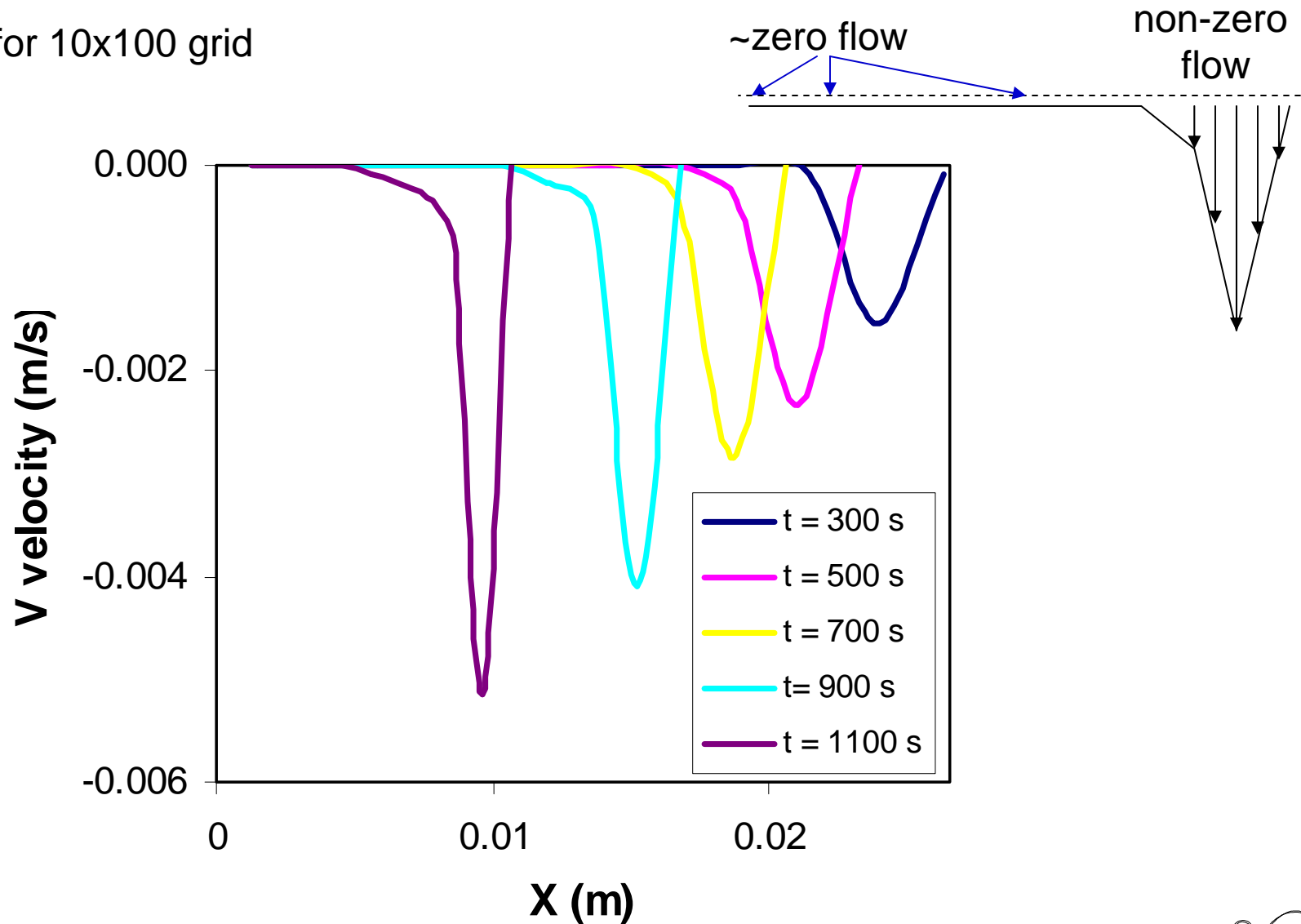
Mass Loss vs. Time



Velocity Profile at Outlet

Non-zero velocity only occurs near free surface region

Results for 10x100 grid



Next Steps

- ❑ Comparison to NIST data
 - NIST to provide data for mass loss vs. time
 - NIST experimental data
 - NIST VOF numerical model results (if available)

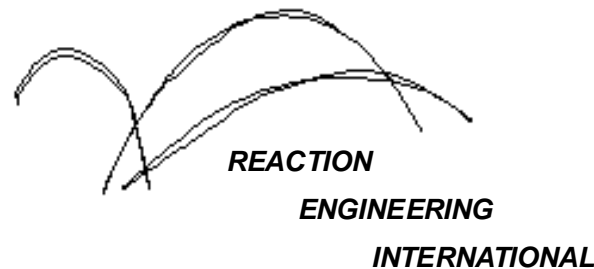
- ❑ Use improved solver to re-visit original problem (with no-slip BC) using single block rectilinear grid

- ❑ If needed, switch to multi-block model
 - current work will be very useful to guide multi-block simulation



A Computational Model For Fire Growth and Spread On Thermoplastic Objects

Task 1: 2D condensed phase melt-drip model with steady heat flux
(1/20/06)



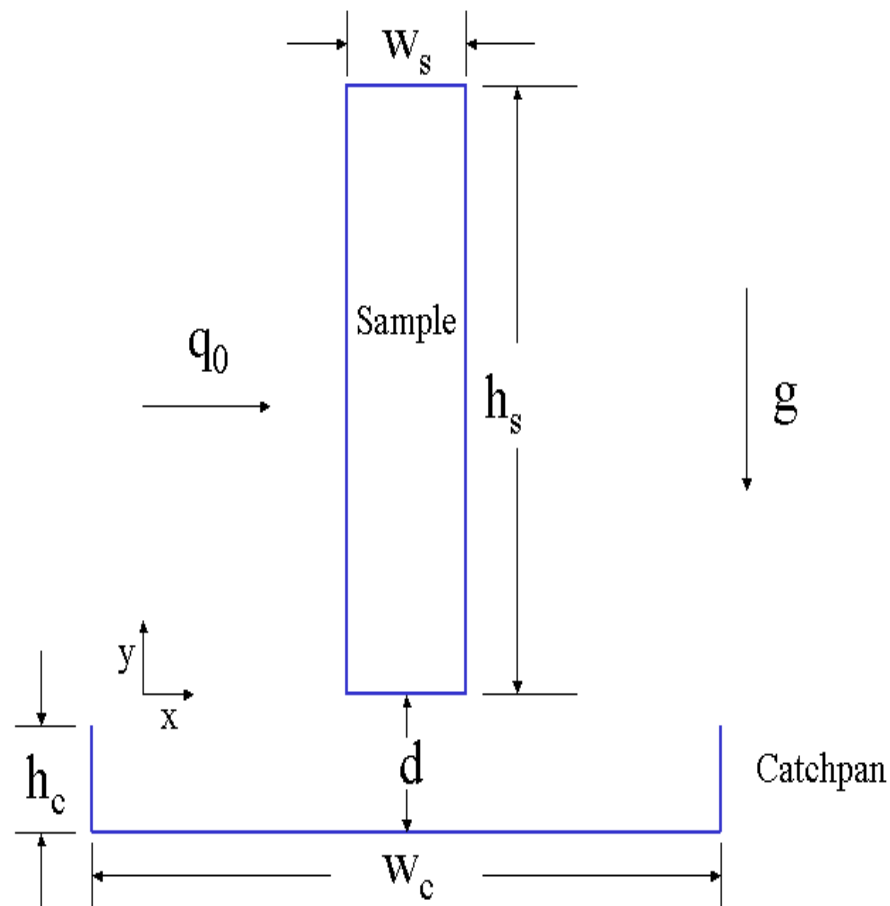
Status Summary

- ❑ Investigated 2D problem with no-slip wall BC at bottom of slab (holder)
 - used improved code (see 11/13/06 report)
 - modified re-meshing strategy near bottom wall boundary
 - modified implementation of the outlet boundary condition

- 100x10 grid used to investigate feasibility of model
- model with biased grid (i.e., fine grid near slab surface) in progress



Problem



Left face of sample:

Constant heat flux q_0 applied to surface of flowing material:
 $k \frac{\partial T}{\partial s} = -q_0$, where s is in the direction normal to the surface

Right face of sample:

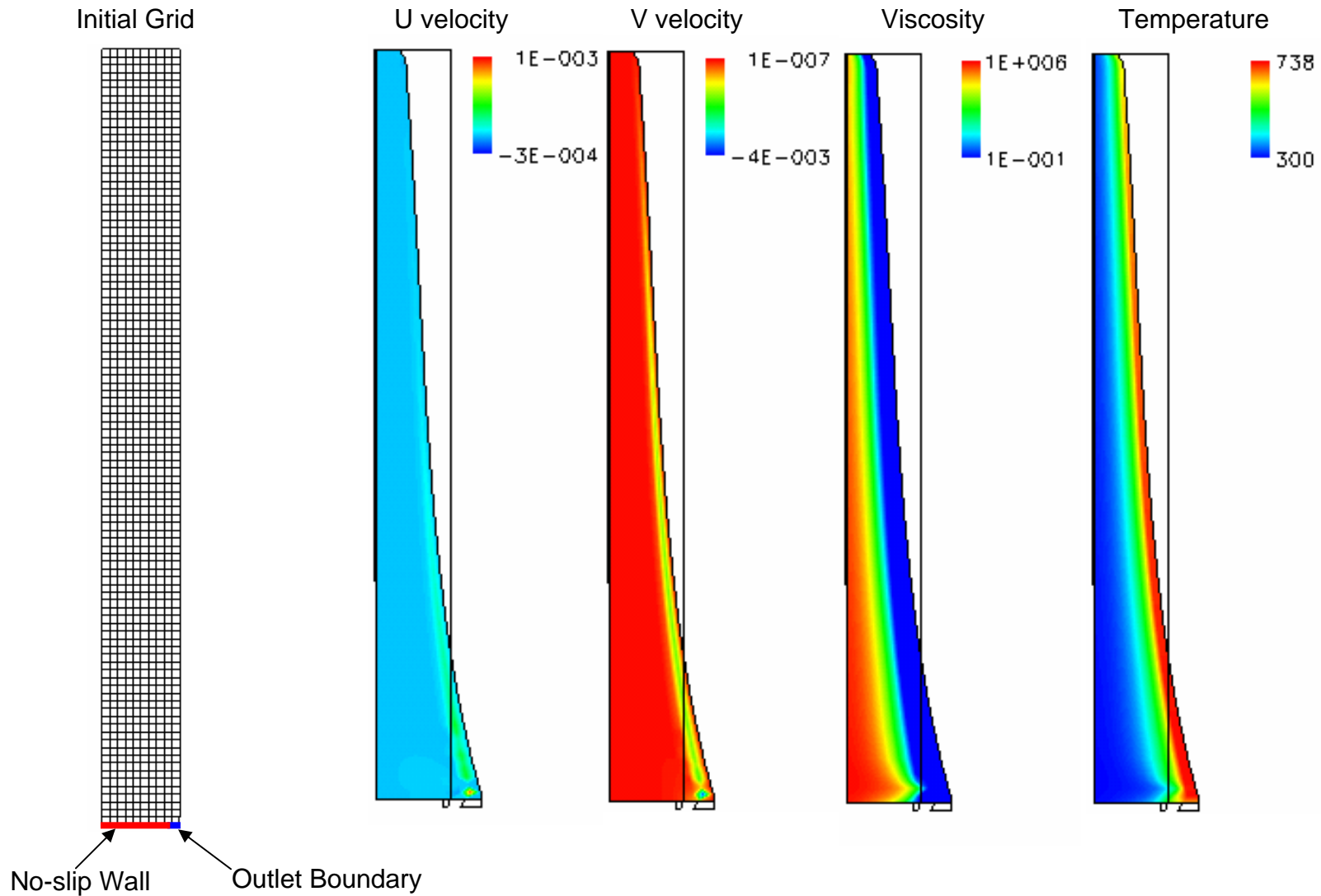
$u = 0$ (no penetration)
 $v = 0$ (no-slip)
 $\frac{\partial T}{\partial x} = 0$ (adiabatic)

Top and Bottom face of sample

$v = 0$ (no penetration)
 $u = 0$ (no-slip)
 $\frac{\partial T}{\partial y} = 0$ (adiabatic)



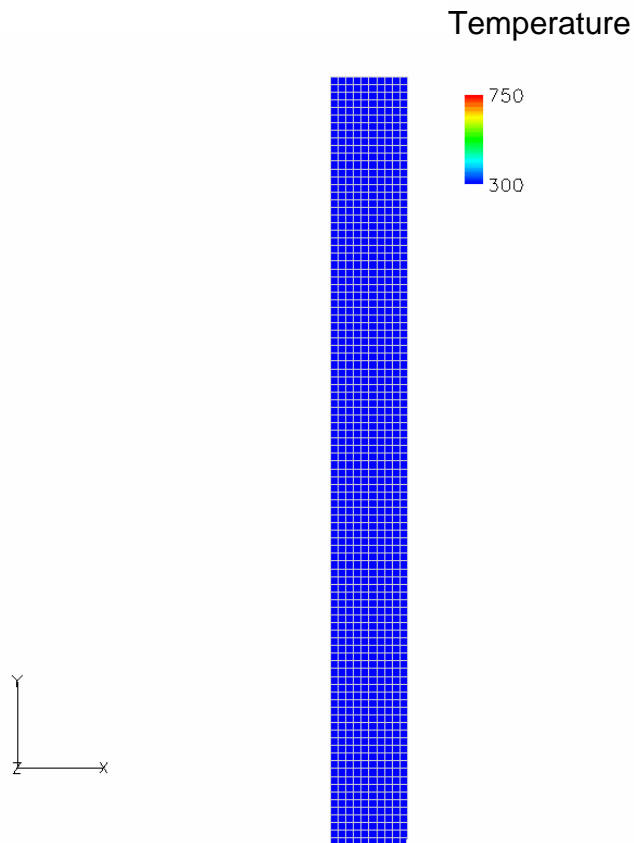
Rectilinear Grid and Solution



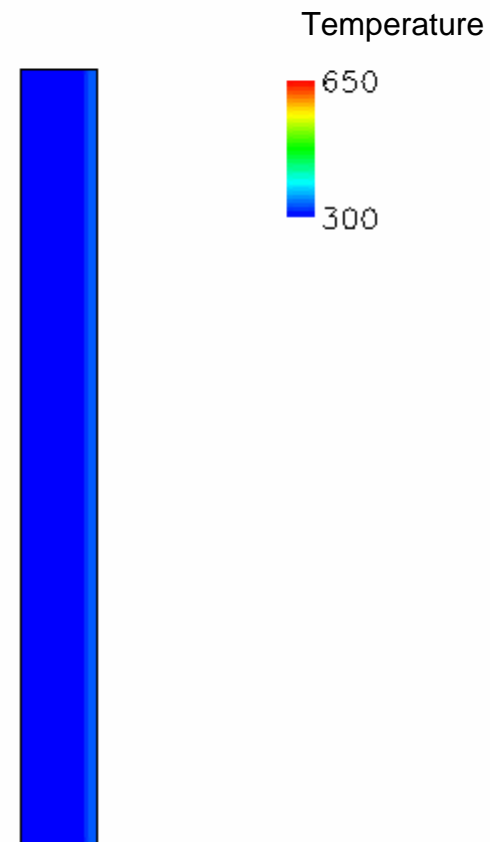
T = 500 s



Movies – polymer temperature



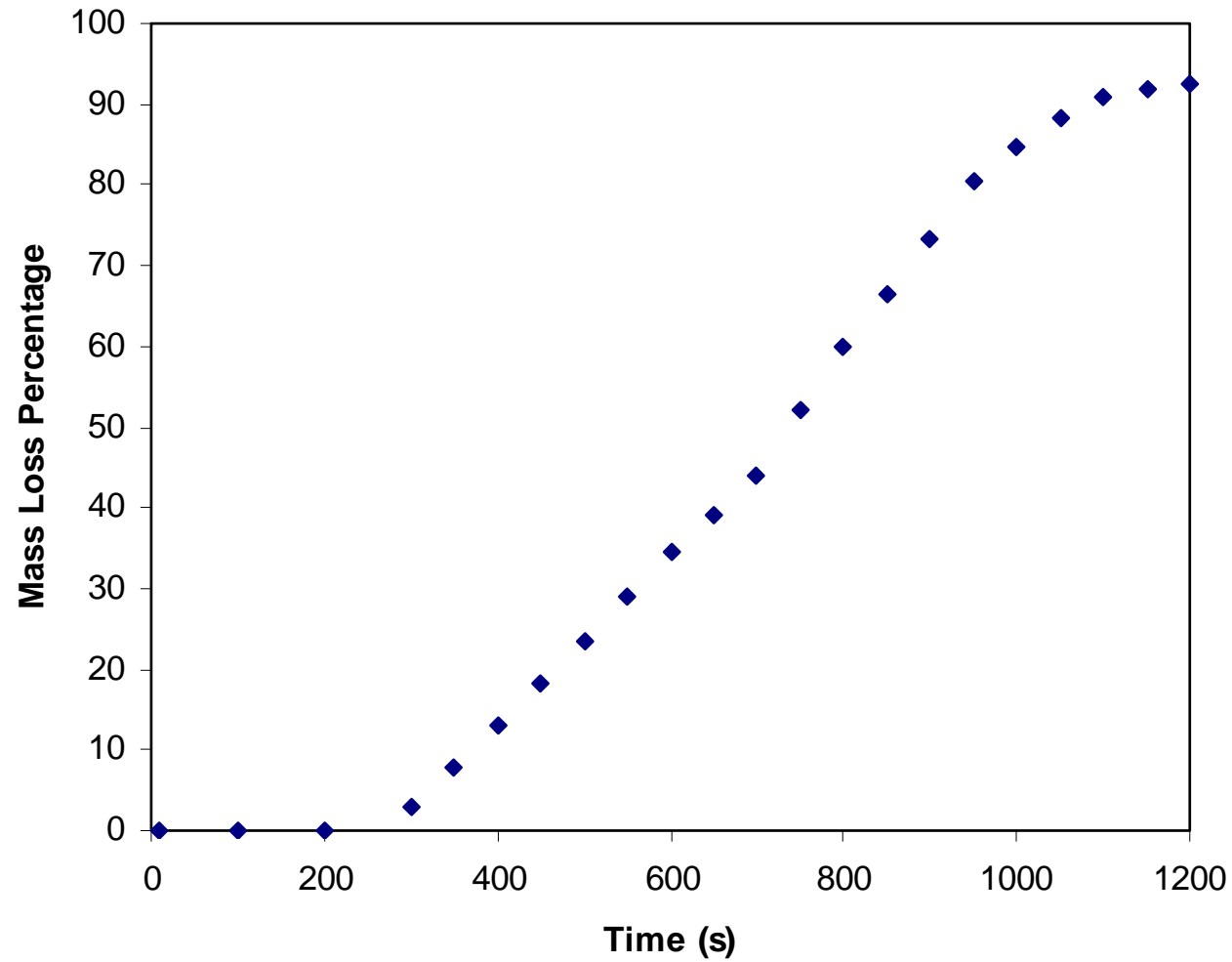
With no-slip bottom wall



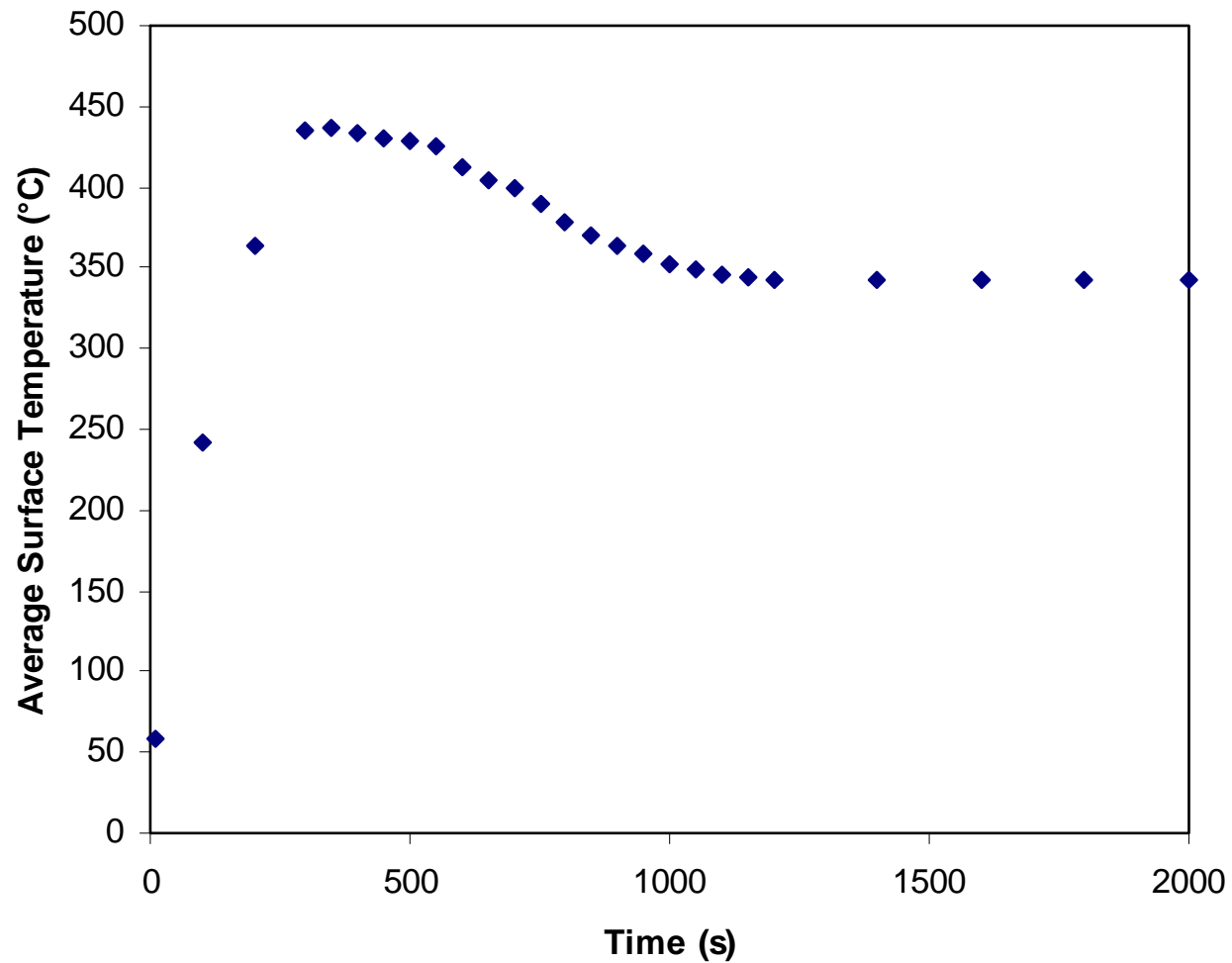
Without no-slip bottom wall



Mass Loss vs. Time



Ave. Surface Temperature vs. Time



Comparisons

- ❑ Slip and No Slip Models
 - Flow begins at about $t \sim 200$ sec
 - $\sim 95\%$ Mass Loss at $t \sim 1200$ sec
 - No Slip – time to achieve 95% Mass Loss less for finer grid
 - Ave. Surface Temperature : 250 – 450 °C during mass loss time period

- ❑ NIST Test Data
 - ❑ Flow starts at $t \sim 200$ sec
 - ❑ $\sim 95\%$ Mass Loss at $t \sim 2300$ sec
 - ❑ Ave. Mass loss rate ~ 0.12 g/sec
 - ❑ Surface Temperature ~ 350 °C

- ❑ Physics Not Included in current model
 - ✓ radiative, convective heat transfer at surface
 - ✓ gasification
 - ✓ vaporization of polymer



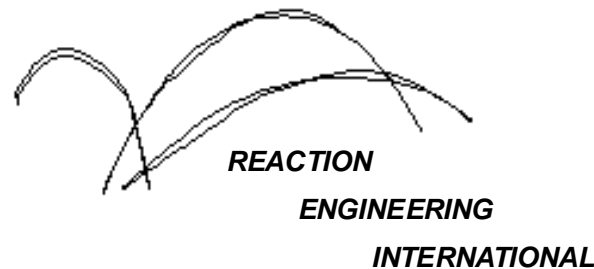
Next Steps

- ❑ Complete grid sensitivity study for current polymer
- ❑ Comparison to NIST data
 - Compare mass loss or surface temperature vs. time ? Other ?
 - NIST experimental data = what is thickness of test piece ?
- ❑ Repeat tests using improved solver for second polymer
 - Need NIST data for material properties
- ❑ Conf. Call by Jan. 30
- ❑ Complete Task 1 Jan. 31

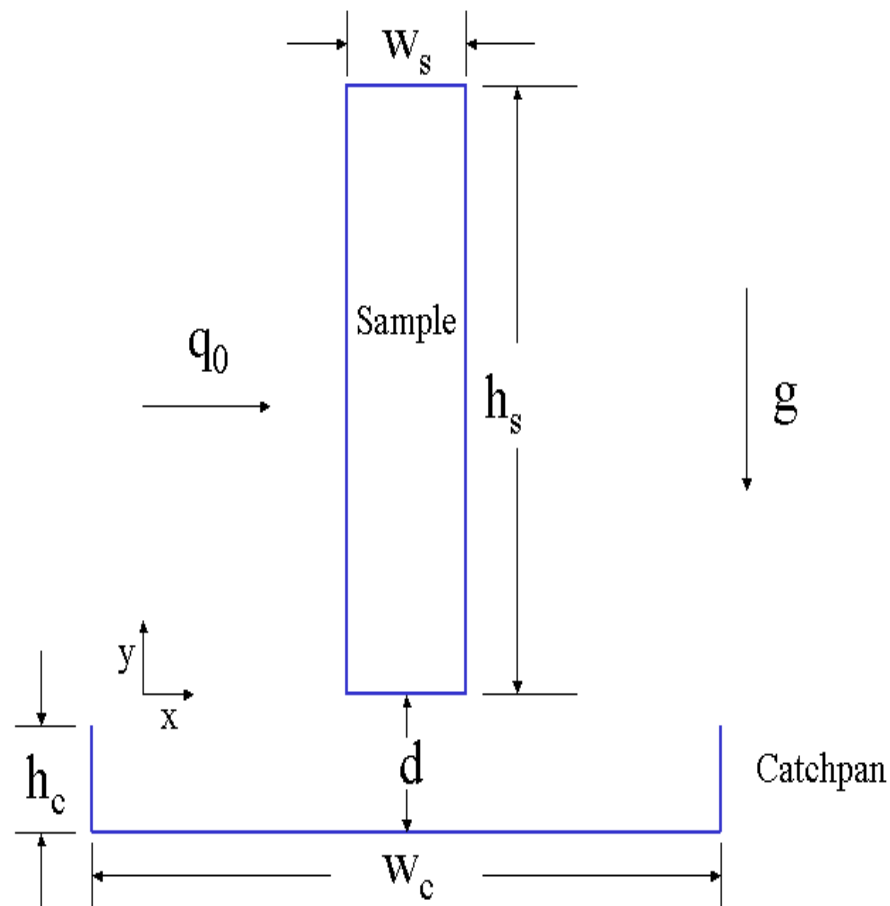


A Computational Model For Fire Growth and Spread On Thermoplastic Objects

**Task 1: 2D condensed phase melt-drip model
with steady heat flux
(1/26/06)**



Modeled Problem



Left face of sample:

Constant heat flux q_0 applied to surface of flowing material:
 $k \frac{\partial T}{\partial s} = -q_0$, where s is in the direction normal to the surface ($q_0 = 20000 \text{ w/m}^2$)

Right face of sample:

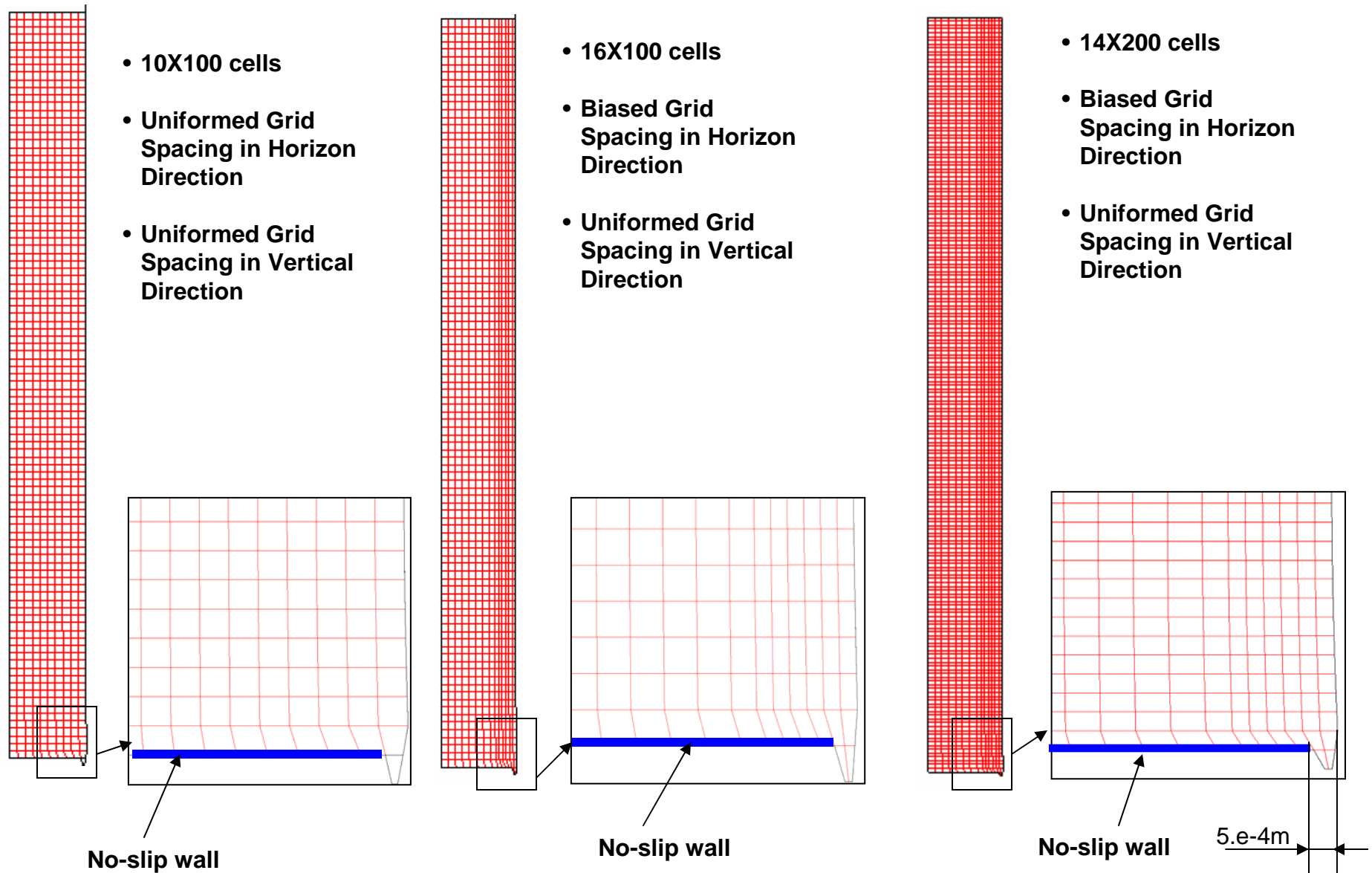
$u = 0$ (no penetration)
 $v = 0$ (no-slip)
 $\frac{\partial T}{\partial x} = 0$ (adiabatic)

Top and Bottom face of sample

$v = 0$ (no penetration)
 $u = 0$ (no-slip)
 $\frac{\partial T}{\partial y} = 0$ (adiabatic)



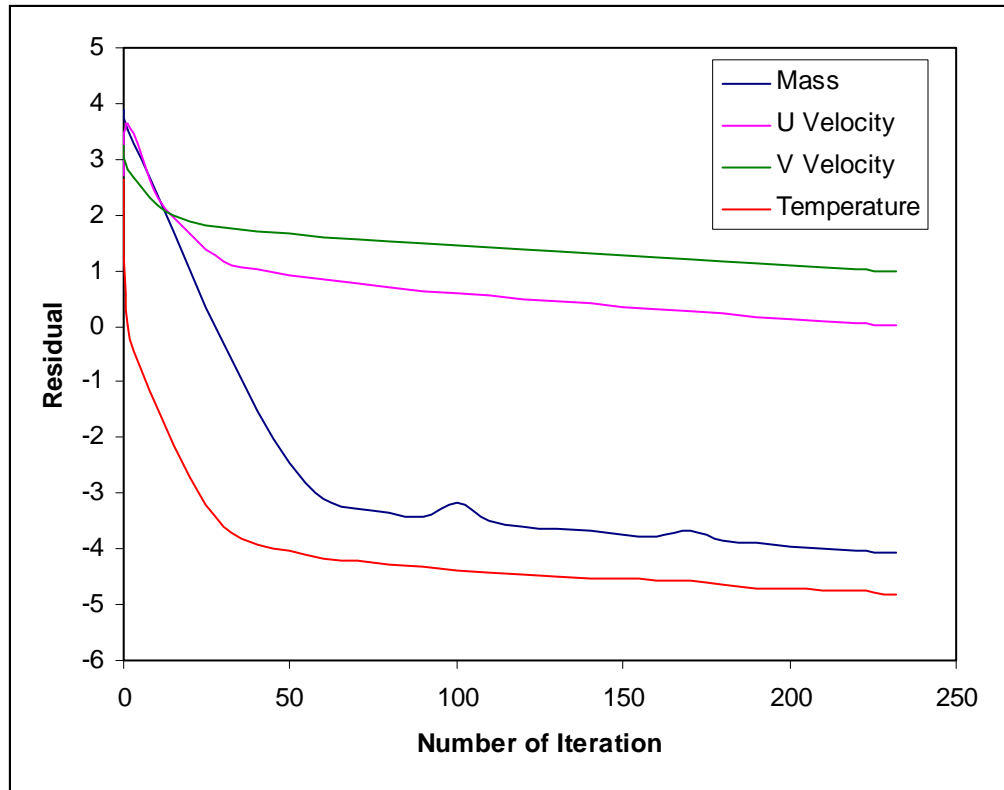
Computation Domain and Grids



* Grid lines in the plots connect cell centers



Residual History



- During each time step, iteration is terminated when residuals of all solved quantity are below 1 (i.e., at least six significant digits remain unchanged from iteration to iteration)

A typical residual history in one time step

Residual definition

$$R_Y^\psi \equiv \log_{10} \left(\frac{\sum_{\text{Calculation domain}} R_Y^0}{\sum_{\text{Calculation domain}} \psi_Y} \right)$$

Where $R_Y^0 \equiv A_E Y_E + A_W Y_W + A_N Y_N + A_S Y_S + A_T Y_T + A_B Y_B + S_U - A_P Y_P$

And $\psi_Y = A_P Y_P$

Y is the solved quantity



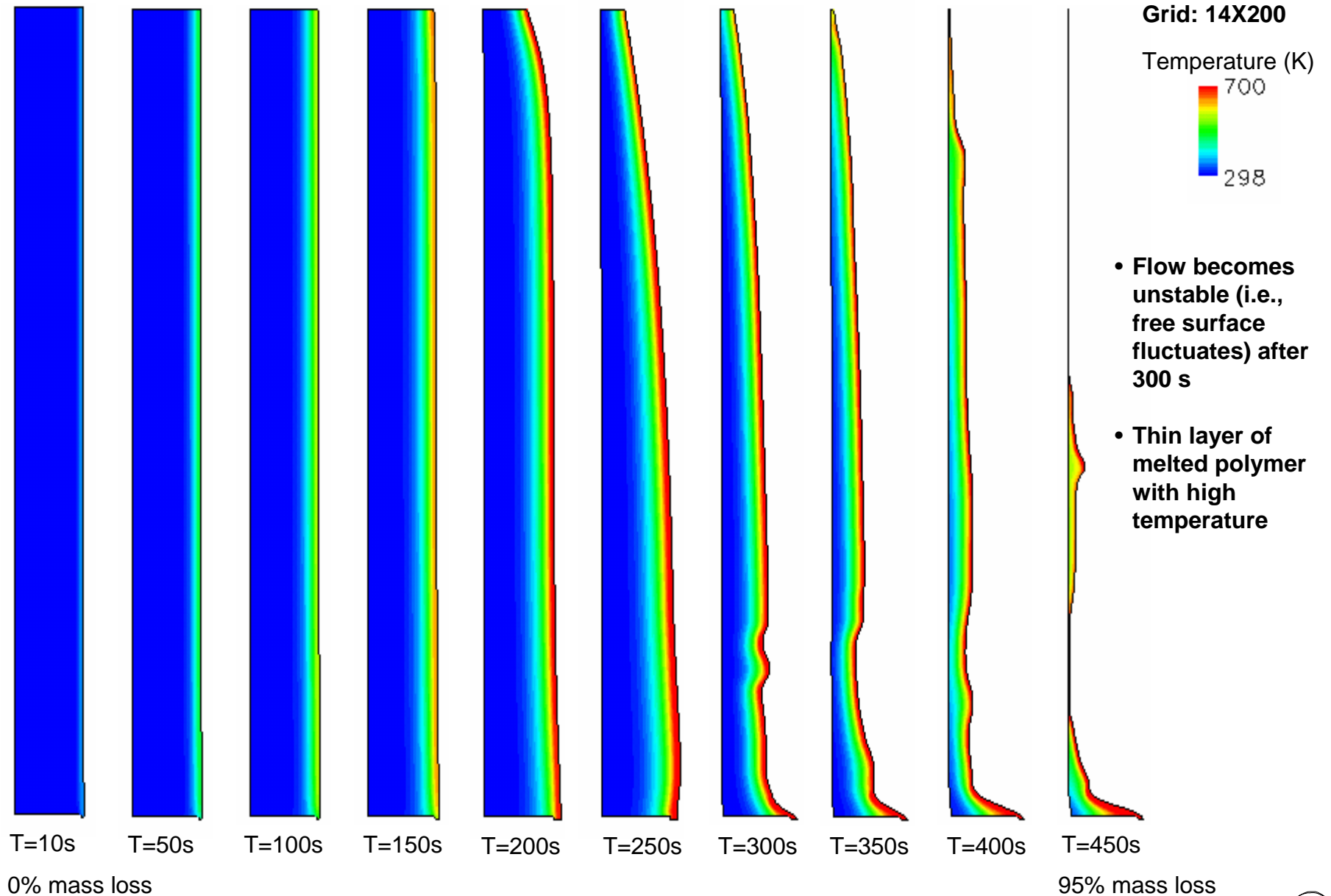
Computational Cost

- All Cases were run on a Dell Precision 450 Desktop PC with a Xeon 3GHz CPU

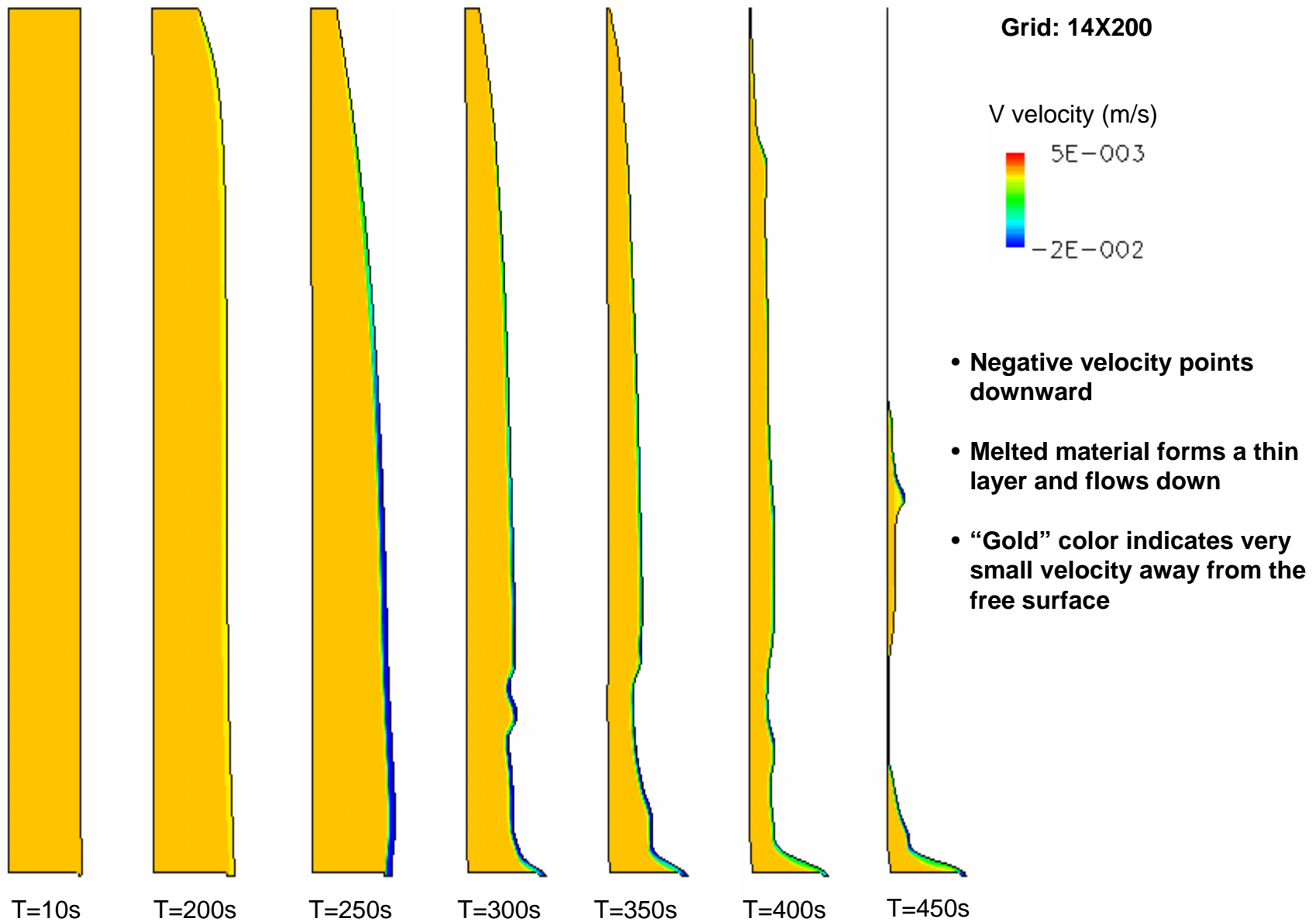
Case	Wall Clock Time	Memory Requirement
10X100	4 hours	< 1MB
14X100	6 hours	~1 MB
14X200	12 hours	~2 MB



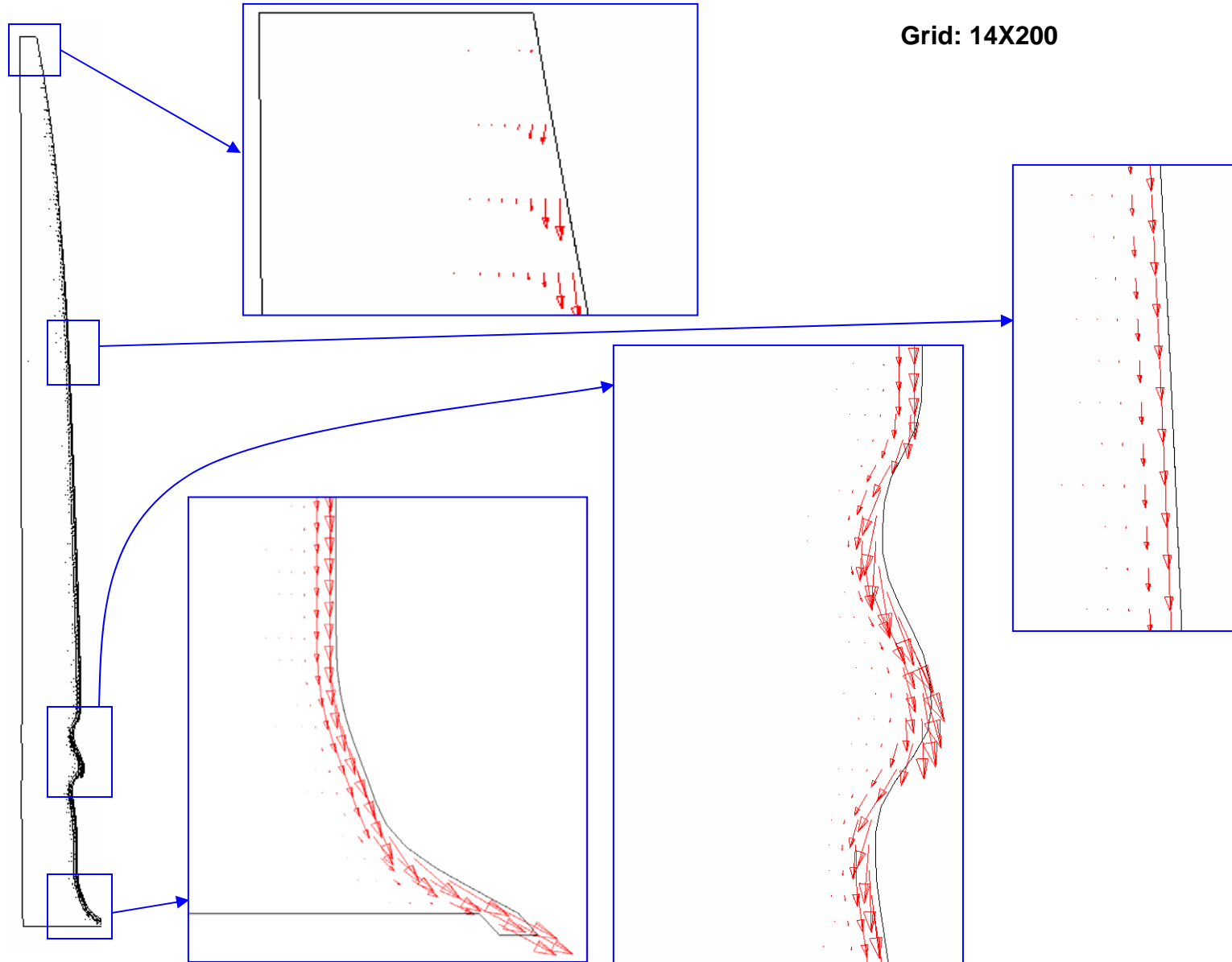
Free Surface Location and Temperature Field Against Time



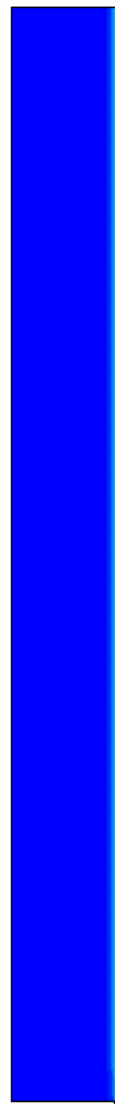
Free Surface Location and Velocity Field Against Time



Velocity Vectors at Time = 300 s

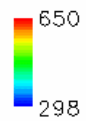


Movie: Free Surface Location and Temperature Contour



Grid: 14X200

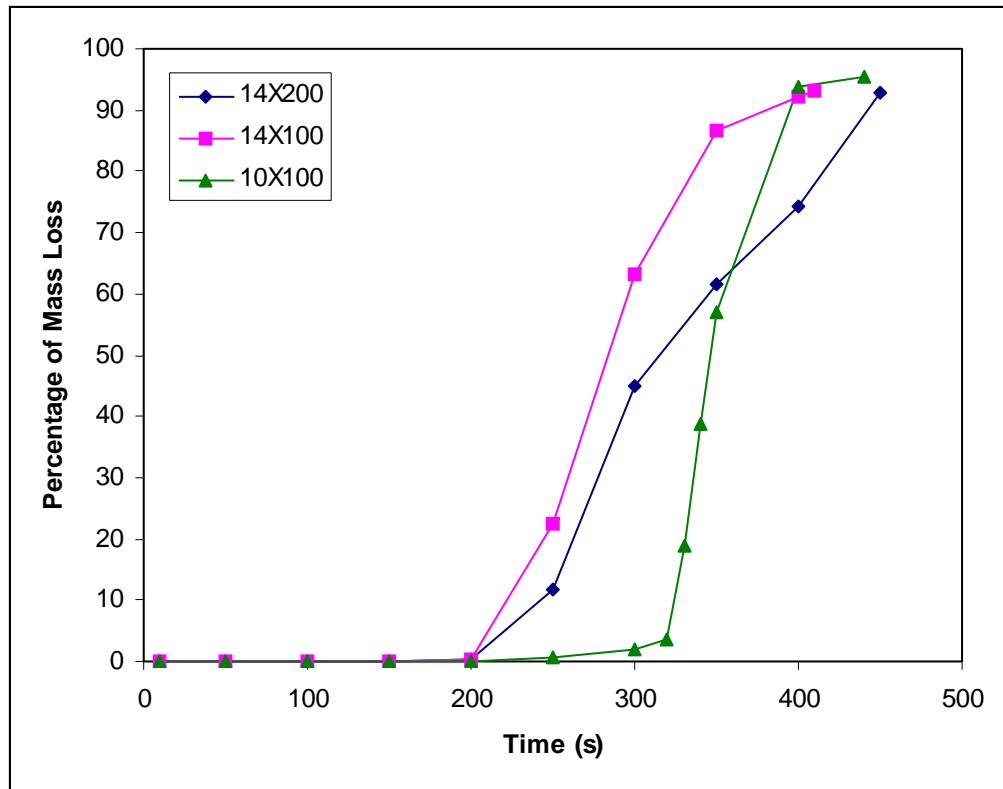
Temperature (K)



- Free surface fluctuation (wave) starts at the outlet and propagates upwards



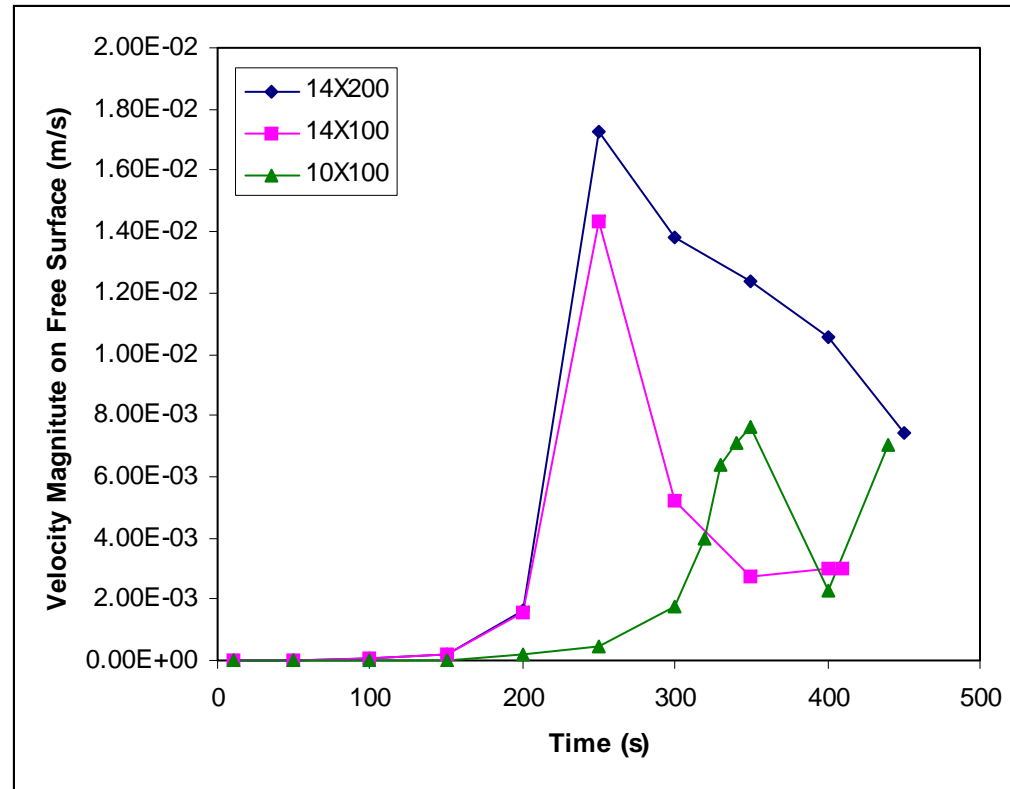
Mass Loss as Function of Time



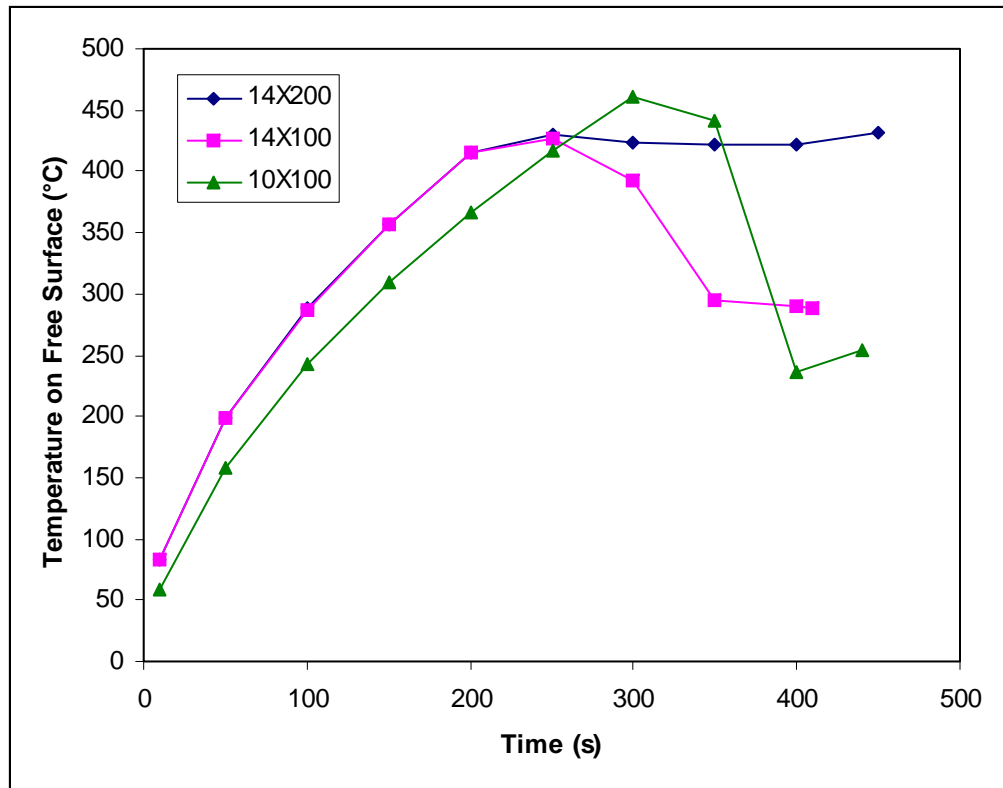
Grid	Mass Loss Rate	Comments
10X100	28.1*	Computed from 250 s to 440 s,
14X100	25.4*	Computed from 200 s to 410 s
14X200	21.4*	Computed from 200 s to 450 s
Experiment	0.12	

* per unit length (g/s m)

Area Weighted Average Velocity on Free Surface as Function of Time



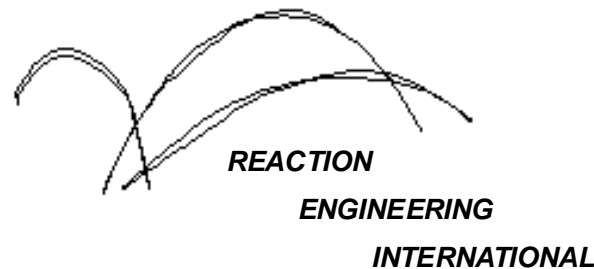
Area Weighted Average Temperature on Free Surface as Function of Time



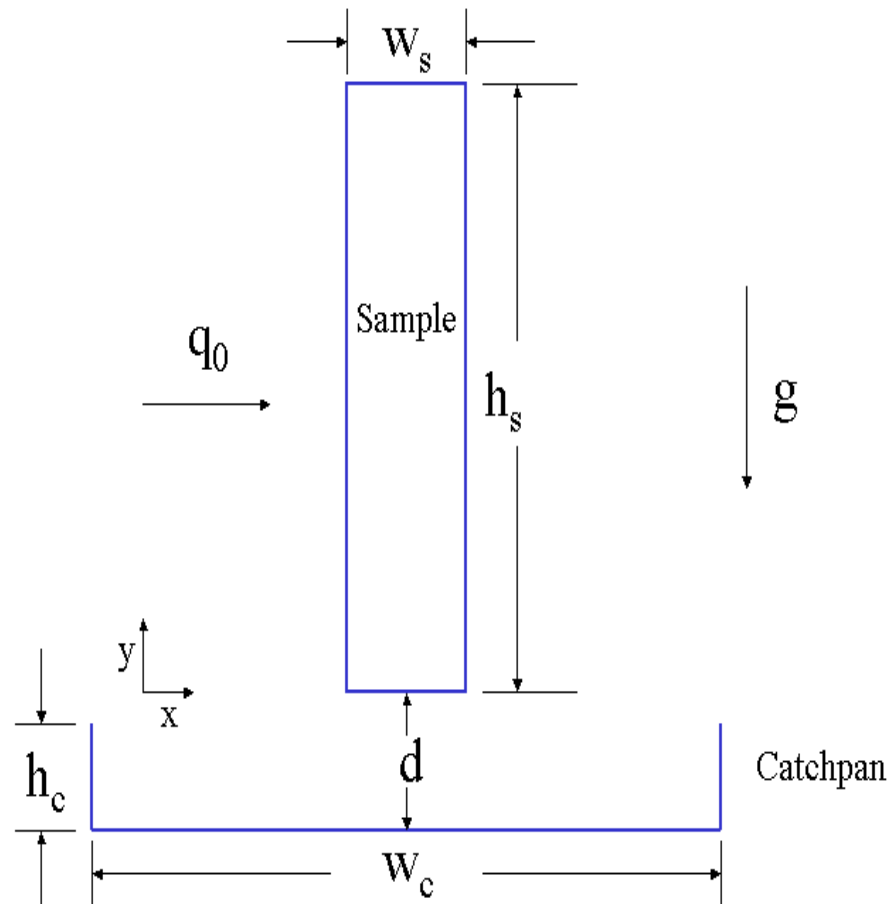
Grid	Surface Temperature	Comments
10X100	295 °C	Averaged from 0 to 95% mass loss
14X100	303 °C	
14X200	347 °C	
Experiment	340 °C	

A Computational Model For Fire Growth and Spread On Thermoplastic Objects

Task 1: 2D condensed phase melt-drip model with steady heat flux (PP702)
(3/06/06)



Modeled Problem



Left face of sample:

Constant heat flux q_0 applied to surface of flowing material:
 $k \frac{\partial T}{\partial s} = -q_0$, where s is in the direction normal to the surface ($q_0 = 20000 \text{ w/m}^2$)

Right face of sample:

$u = 0$ (no penetration)
 $v = 0$ (no-slip)
 $\frac{\partial T}{\partial x} = 0$ (adiabatic)

Top and Bottom face of sample

$v = 0$ (no penetration)
 $u = 0$ (no-slip)
 $\frac{\partial T}{\partial y} = 0$ (adiabatic)

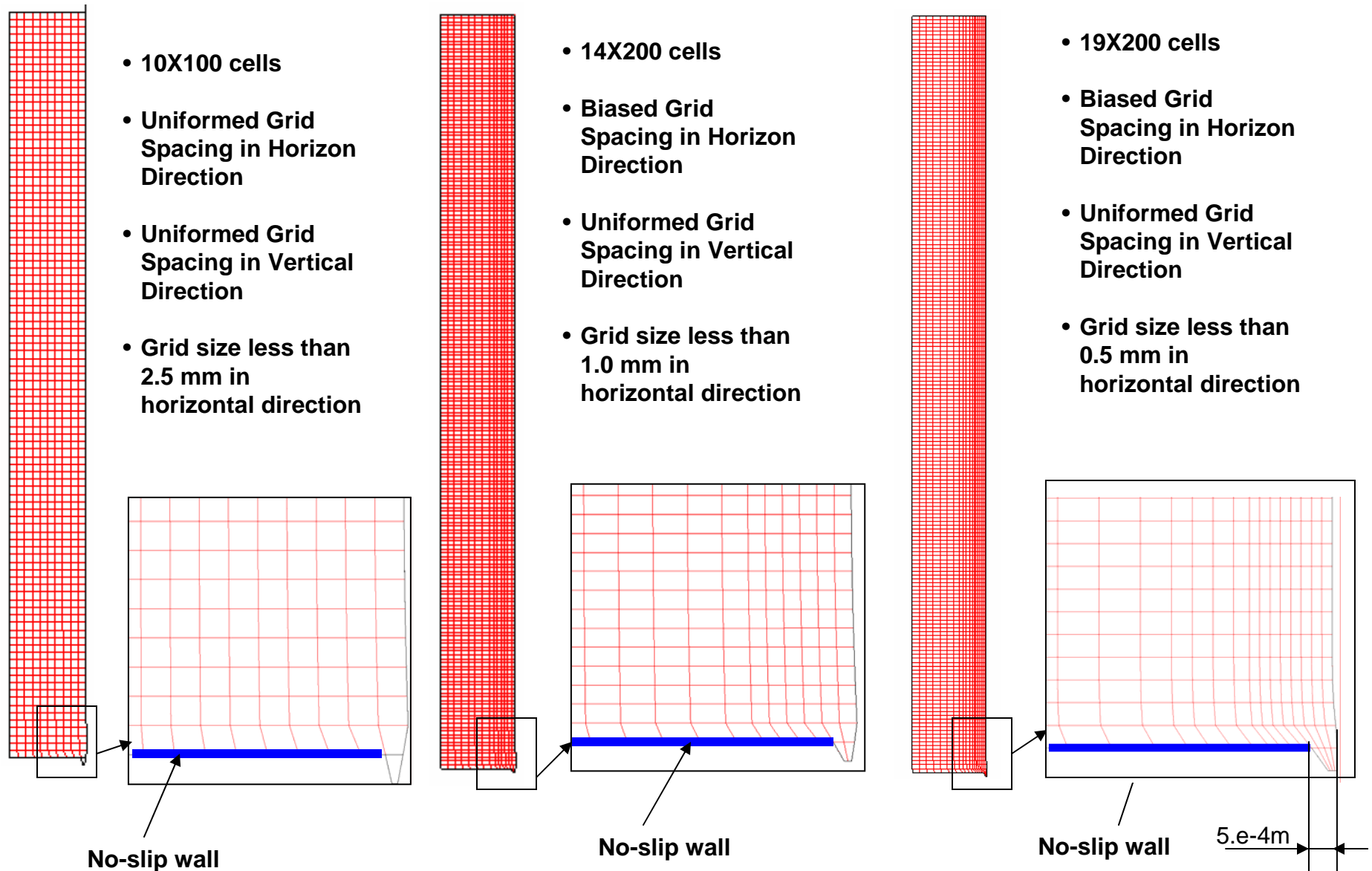


Solution Algorithm

1. Solve the momentum equations using the geometry defined by the current shape of the free surface and the prescribed pressure at it
2. Enforce local mass conservation in each CV by solving the pressure-correction equation, using the prescribed pressure boundary condition on the current free surface. Mass is conserved both globally and in each CV, but the non-zero mass fluxes through the free surface may result.
3. Correct the position of the free surface so that the volume defined by its corrected and previous position (i.e., at previous time step) compensates the mass fluxes through the free surface obtained in the preceding step.
4. Re-mesh the grids based on the corrected free surface position and update the transformation Jacobian matrix.
5. Return to step 1 and repeat until all equations and boundary conditions are satisfied.
6. Advance to the next time step



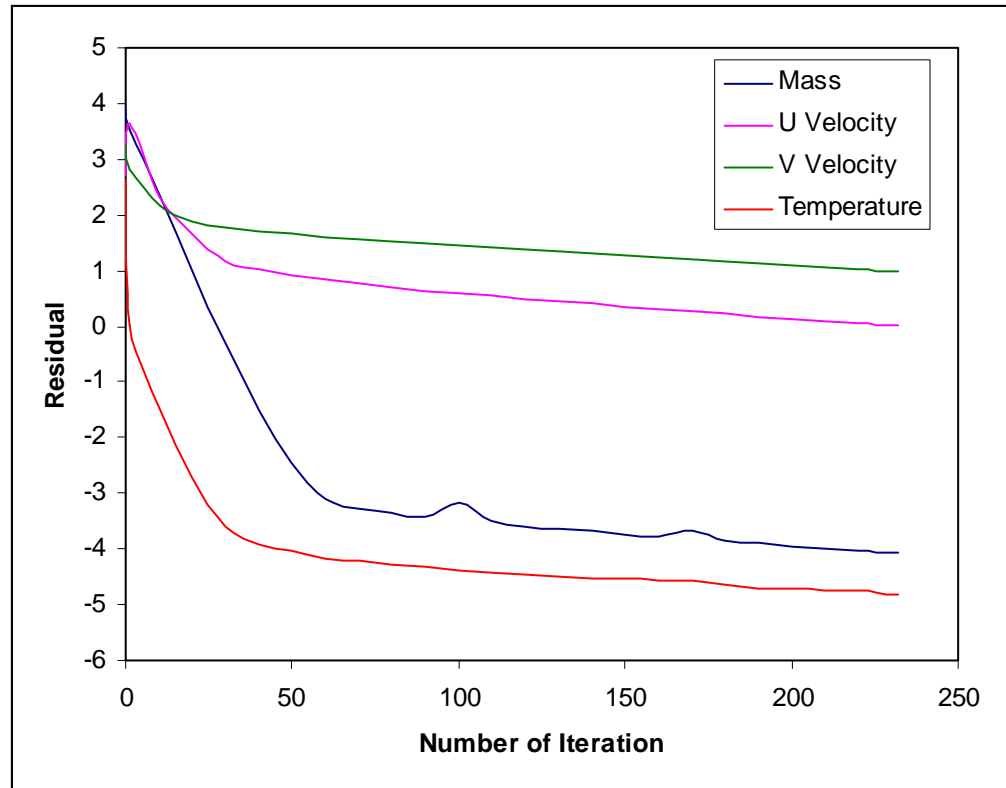
Computation Domain and Grids



* Grid lines in the plots connect cell centers



Residual History



- During each time step, iteration is terminated when residuals of all solved quantity are below 1 (i.e., at least six significant digits remain unchanged from iteration to iteration)

A typical residual history in one time step

Residual definition

$$R_Y^\psi \equiv 7 + \log_{10} \left(\frac{\sum_{\text{Calculation domain}} R_Y^0}{\sum_{\text{Calculation domain}} \psi_Y} \right)$$

Where $R_Y^0 \equiv A_E Y_E + A_W Y_W + A_N Y_N + A_S Y_S + A_T Y_T + A_B Y_B + S_U - A_P Y_P$

And $\psi_Y = A_P Y_P$

Y is the solved quantity



Computational Cost

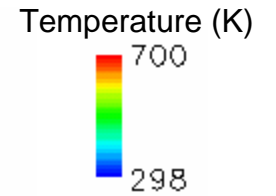
- All Cases were run on a Dell Precision 450 Desktop PC with a Xeon 3GHz CPU

Case	Wall Clock Time	Memory Requirement
10X100	~ 4 hours	< 1MB
14X200	~ 30 hours	~1 MB
19X200	~100 hours	~2 MB

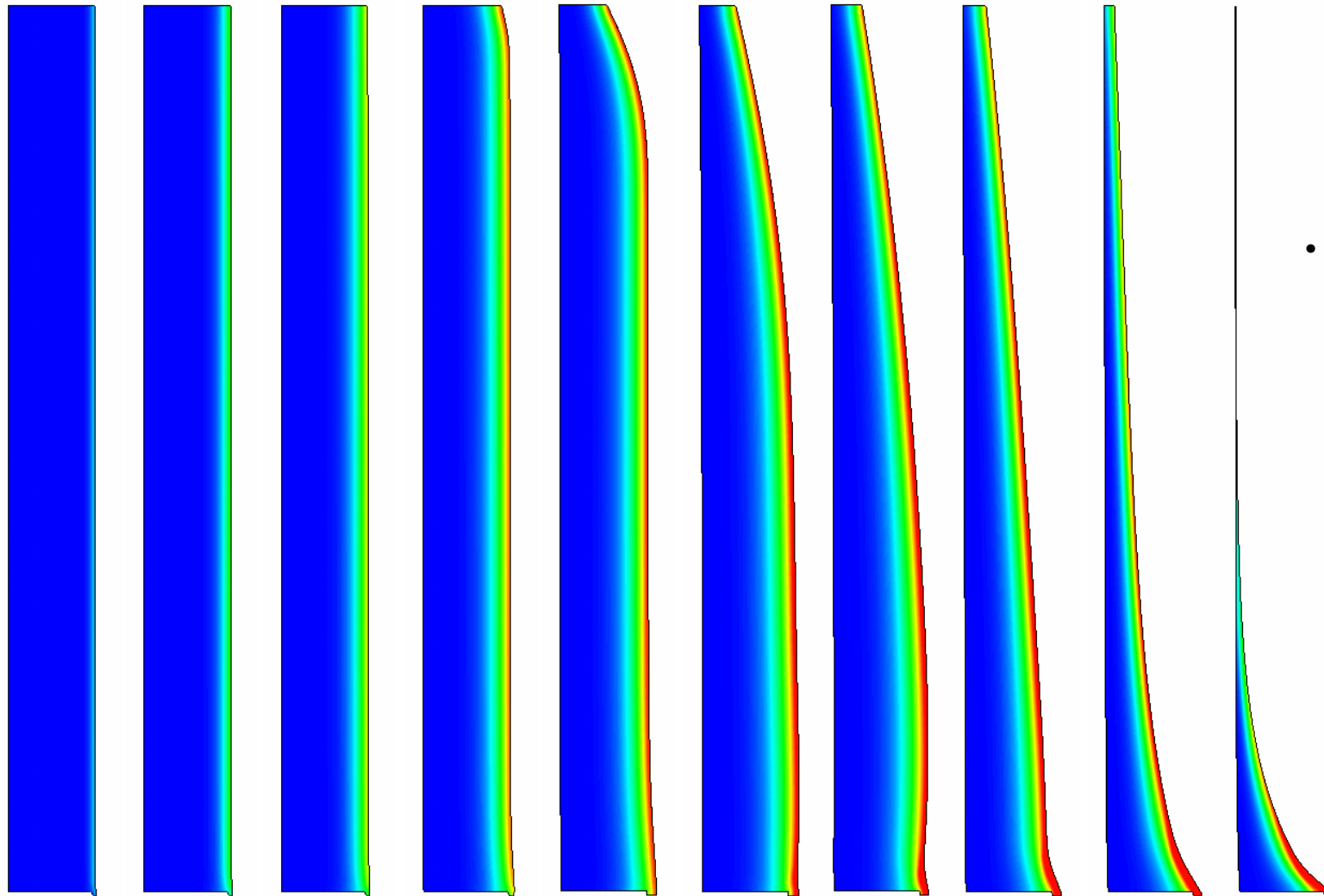


Free Surface Location and Temperature Field vs. Time

Grid: 19X200



- Thin layer of melted polymer with high temperature



T=10s

T=50s

T=100s

T=150s

T=175s

T=200s

T=215s

T=230s

T=240s

T=260s

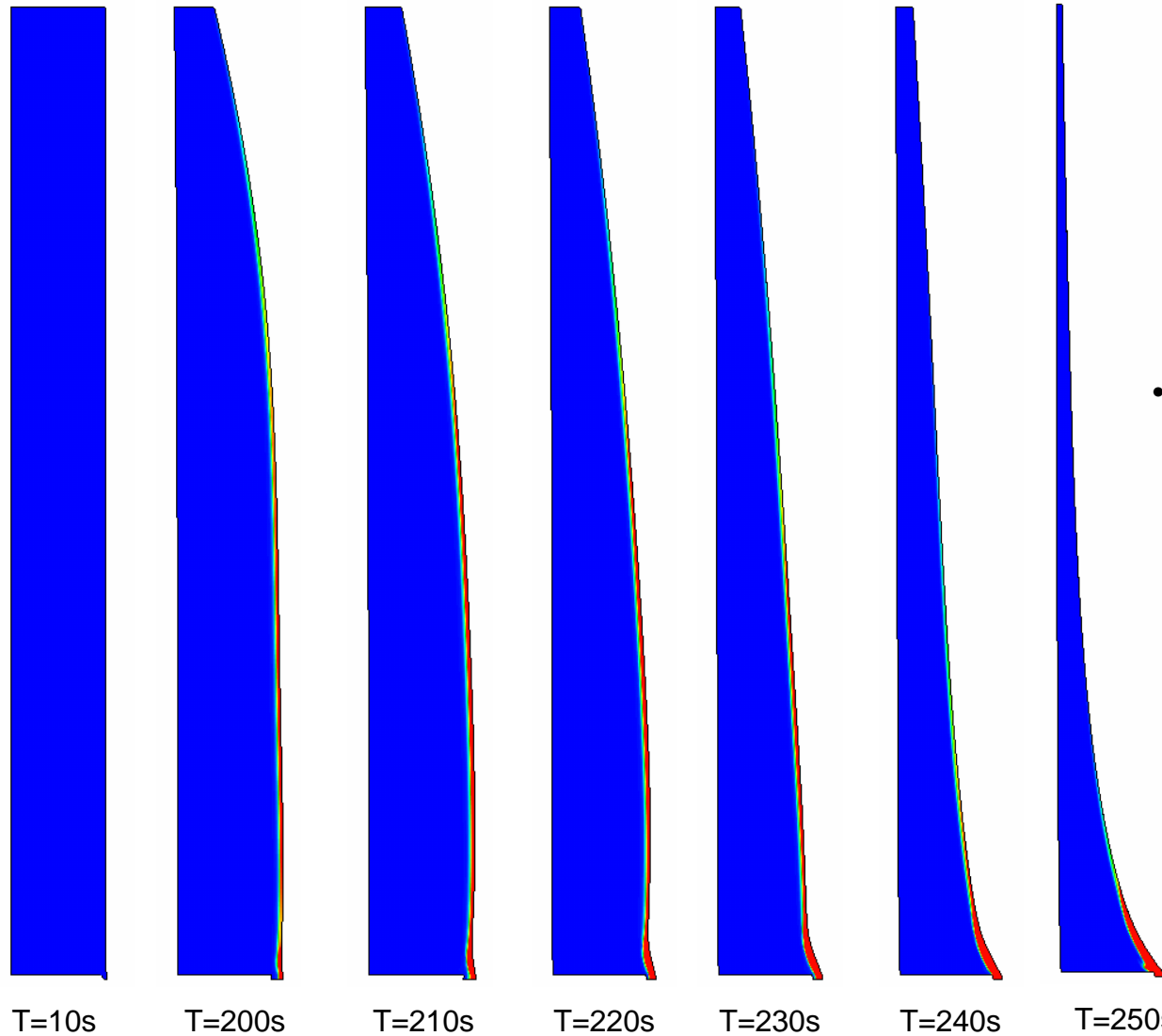
0% mass loss

85% mass loss



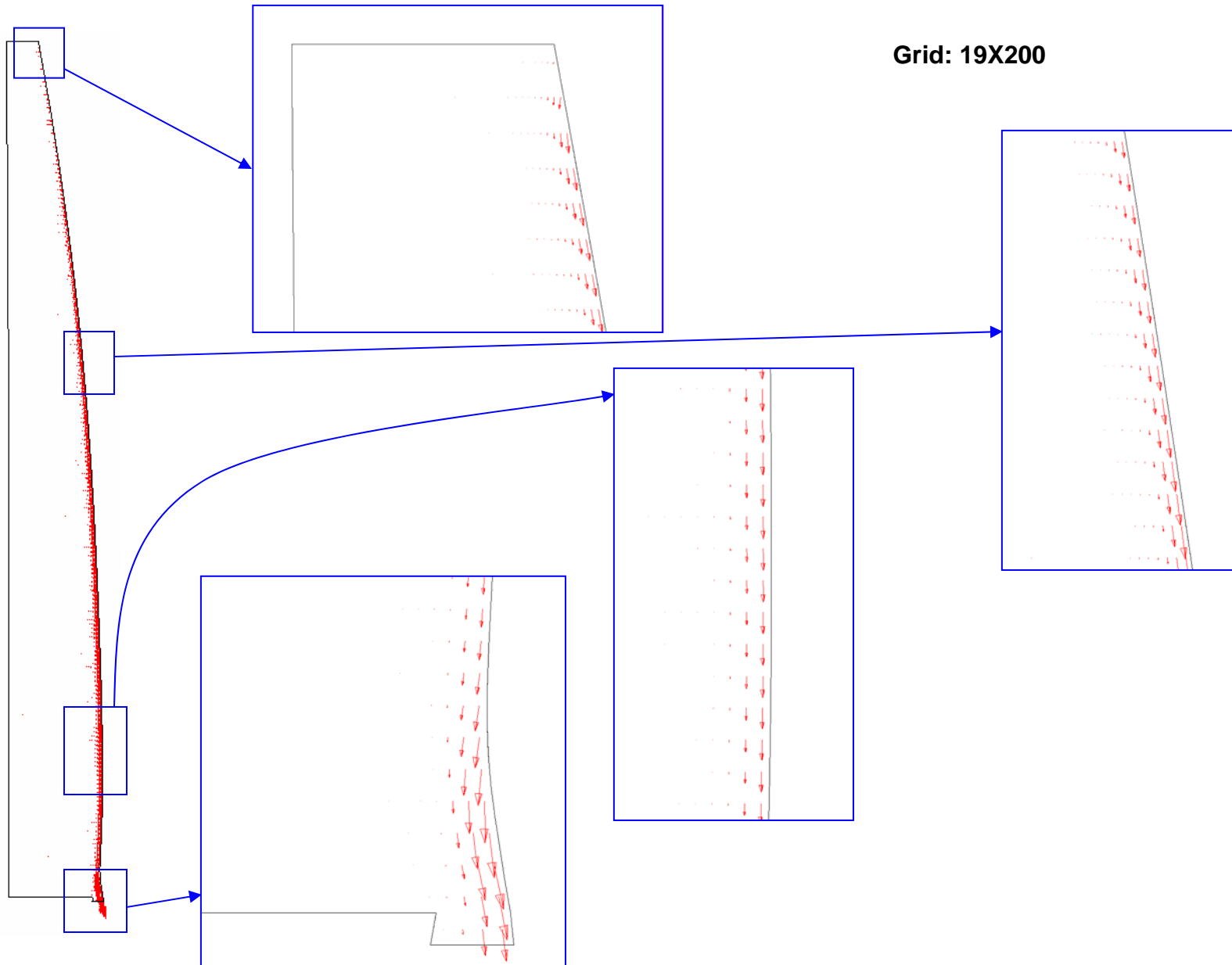
Free Surface Location and Velocity Magnitude vs. Time

Grid: 19X200

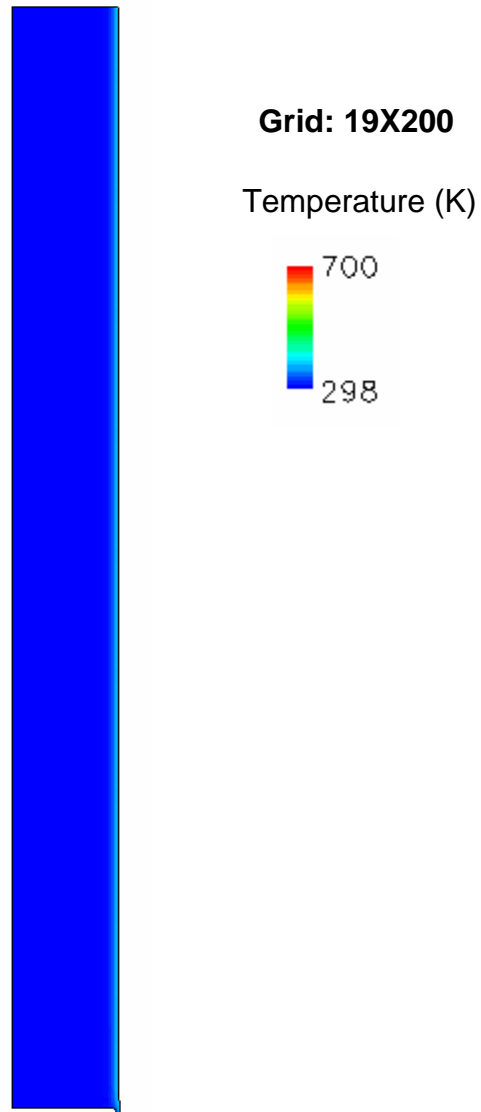


- Melted material forms a thin layer and flows down

Velocity Vectors at Time = 300 s

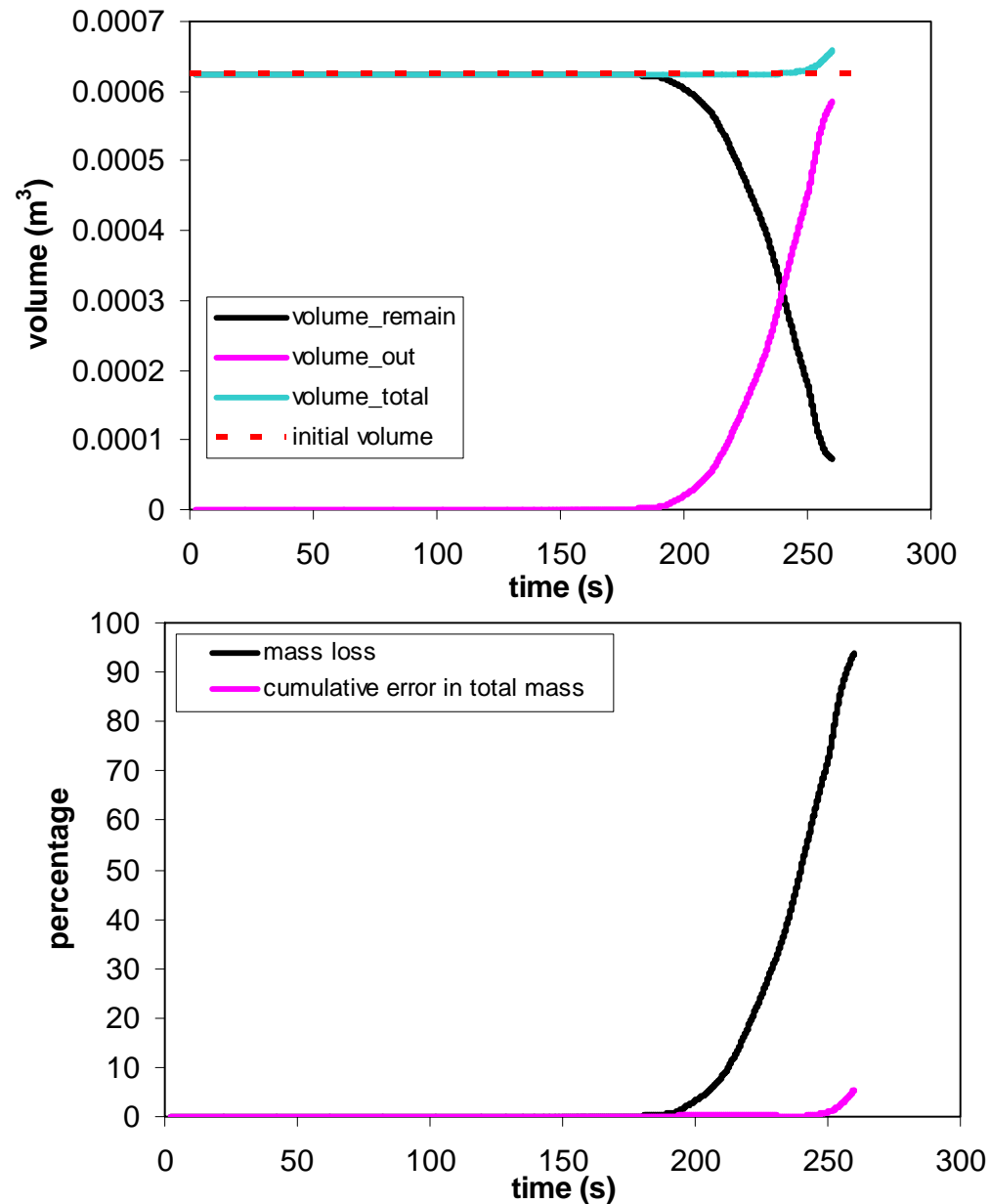


Movie: Free Surface Location and Temperature Contour



A small, handwritten mark or signature in the bottom right corner of the page, consisting of several overlapping, curved lines.

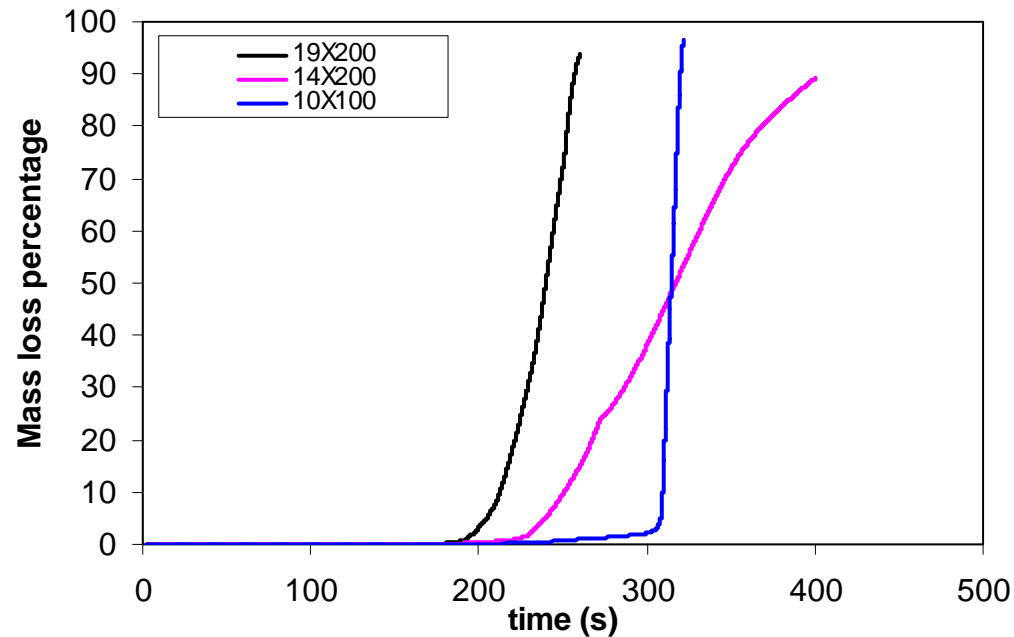
Volume/Mass Change as Function of Time



- Cumulative error of mass conservation is defined as the normalized difference between the initial mass within the domain and the sum of the mass out of the domain and the mass within the domain.
- Cumulative error is less than 1% before reaching 88% mass loss and is less than 5% at 95% mass loss. The increasing cumulative error in mass conservation at the end of the calculation is due to the significant grid skewness



Mass Loss as Function of Time

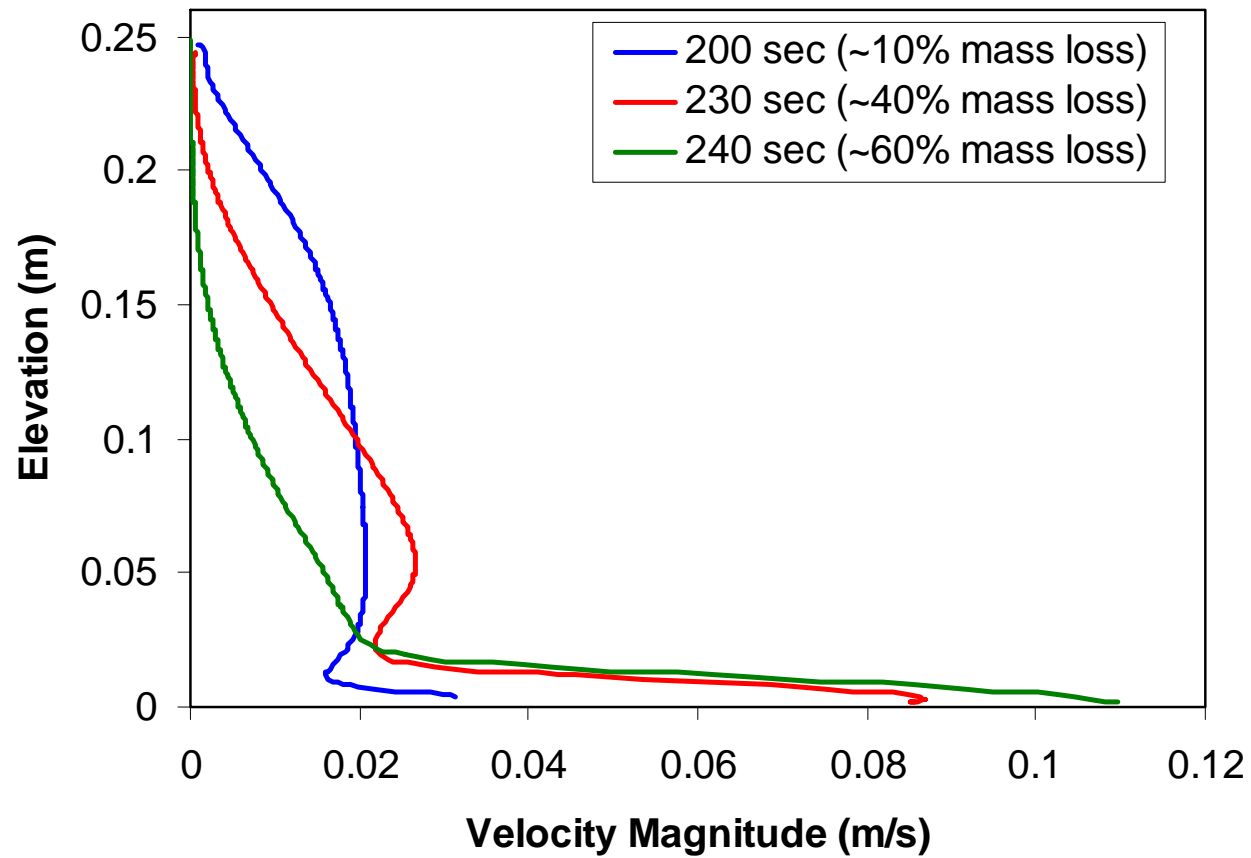


- The mass loss rate is 0.28 g/(s, m) in the case with 19X200 grid cells, while the number in the experiment is 0.12 g/s
- The three cases do not show grid convergence. Further refine the grids beyond 19X200 is computationally prohibitive at this point to investigate this issue.

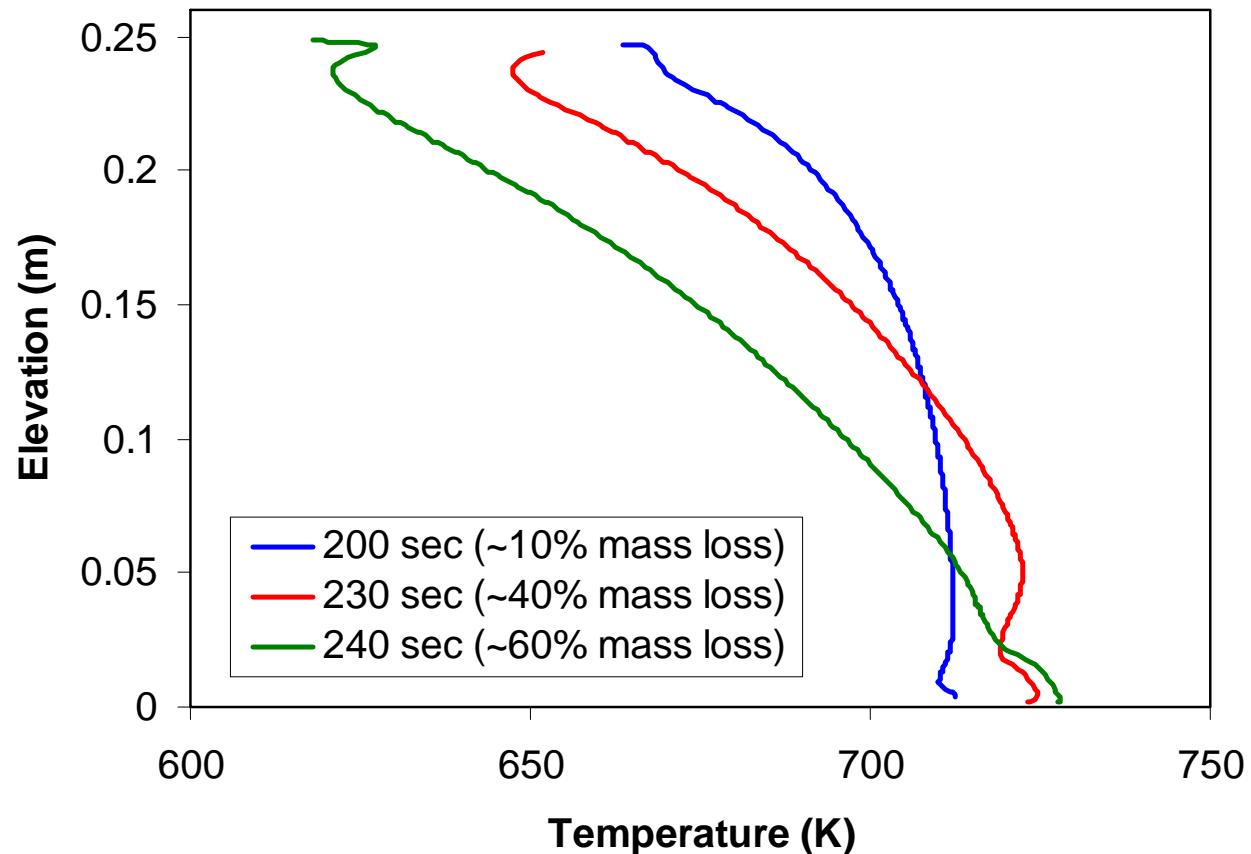
* per unit length (g/s m)



Velocity Magnitude Profiles on Free Surface at Different Time



Temperature Profiles on Free Surface at Different Times

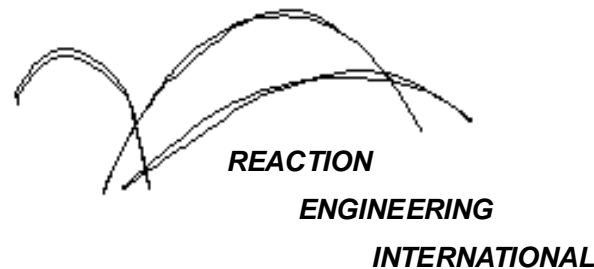


- Average free surface temperature observed in experiment was around 613 K
- The computation model does not include processes such as radiant and convective heat loss, gasification, etc., which may be the cause of the higher temperature calculated on the free surface.



A Computational Model For Fire Growth and Spread On Thermoplastic Objects

Task 1: 2D condensed phase melt-drip model with steady heat flux
(4/03/06)

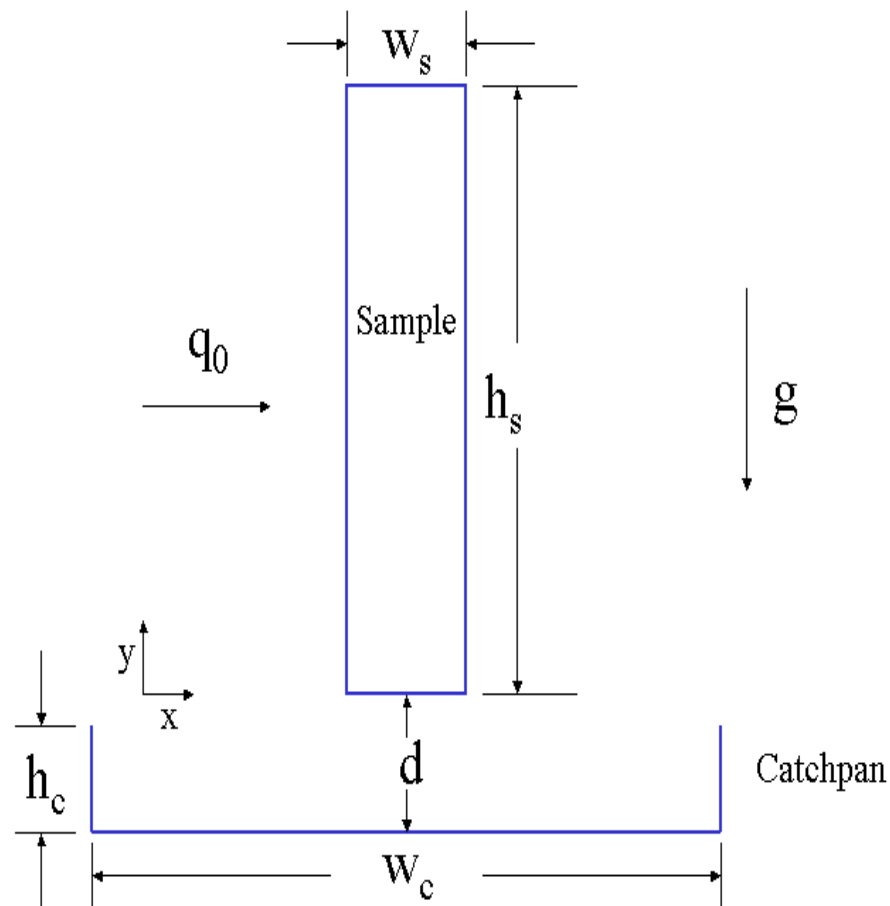


Outline

- Problem Definition
- Solution Algorithm
- Three Computational Grids
- Example Convergence History
- Computational Cost
- Example Results
 - Free surface location, temp., velocity - selected times
 - Movie of free surface location and temperature
 - Mass loss, surface temperature, surface velocity
- Summary



Modeled Problem



Left face of sample:

Constant heat flux q_0 applied to surface of flowing material:
 $k \frac{\partial T}{\partial s} = -q_0$, where s is in the direction normal to the surface ($q_0 = 20000 \text{ w/m}^2$)

Right face of sample:

$u = 0$ (no penetration)
 $v = 0$ (no-slip)
 $\frac{\partial T}{\partial x} = 0$ (adiabatic)

Top and Bottom face of sample

$v = 0$ (no penetration)
 $u = 0$ (no-slip)
 $\frac{\partial T}{\partial y} = 0$ (adiabatic)



Parameter Values – PP702 Resin

Initial conditions:

$$T_0 = 25 \text{ }^\circ\text{C}$$

$$u = 0$$

$$v = 0$$

$$\rho = 10^5 \text{ Pa}$$

Problem parameters:

$$q_0 = 20,000 \text{ W/m}^2$$

$$g = 9.8 \text{ m/s}^2$$

$$h_s = 0.25 \text{ m}$$

$$w_s = 0.025 \text{ m}$$

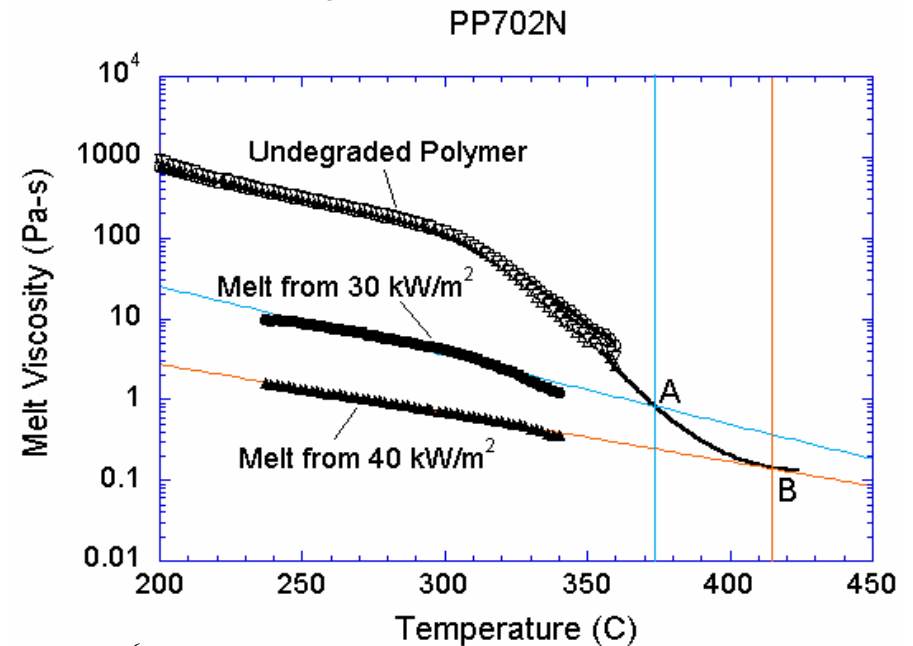
Material properties: All parameters are constant except for viscosity.

$$\rho = 900 \text{ kg/m}^3$$

$$c_p = 2400 \text{ J/kg-K}$$

$$k = 0.25 \text{ W/m-K}$$

Viscosity:



$$\mu = \begin{cases} 10^6 & T < 25^\circ\text{C} \\ 10^6(200 - T)/(200 - 25) + f_1(200) & 25^\circ\text{C} \leq T < 200^\circ\text{C} \\ f_1(T) & 200^\circ\text{C} \leq T < 350^\circ\text{C} \\ f_2(T) & 350^\circ\text{C} \leq T < 425^\circ\text{C} \\ f_2(425) & T \geq 425^\circ\text{C} \end{cases}$$

$$f_2(T) = 10^{\wedge}(53.19 - 0.2542T + 2.9879 \times 10^{-4} T^2)$$

$$f_1(T) = 10^{\wedge}(14.48 - 0.13858T + 5.5960 \times 10^{-4} T^2 - 7.8665 \times 10^{-7} T^3)$$

Parameter Values – PP6523 Resin

Initial conditions:

$$\begin{aligned} T_0 &= 25 \text{ }^\circ\text{C} \\ u &= 0 \\ v &= 0 \\ \rho &= 10^5 \text{ Pa} \end{aligned}$$

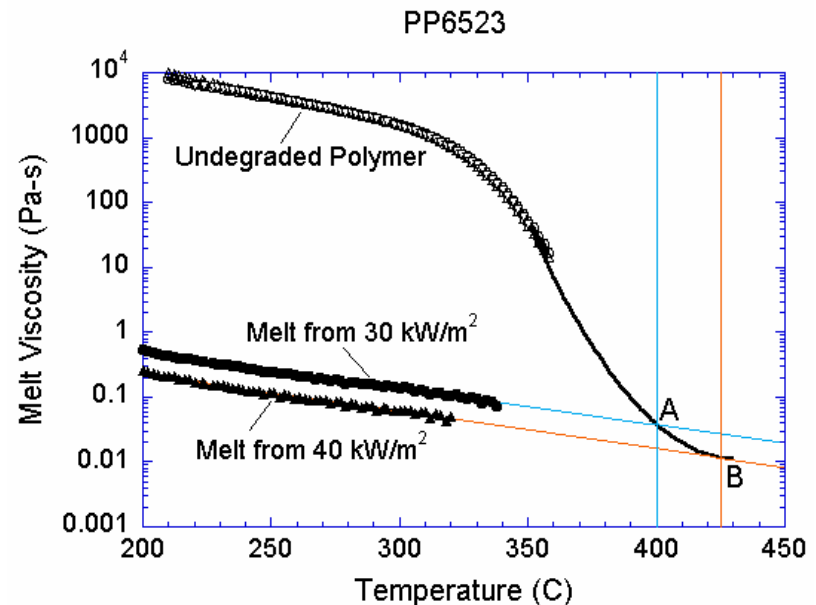
Problem parameters:

$$\begin{aligned} q_0 &= 20,000 \text{ W/m}^2 \\ g &= 9.8 \text{ m/s}^2 \\ h_s &= 0.25 \text{ m} \\ w_s &= 0.025 \text{ m} \end{aligned}$$

Material properties: All parameters are constant except for viscosity.

$$\begin{aligned} \rho &= 900 \text{ kg/m}^3 \\ c_p &= 2400 \text{ J/kg-K} \\ k &= 0.25 \text{ W/m-K} \end{aligned}$$

Viscosity:



$$\mu = \begin{cases} 10^6 & T < 25^\circ\text{C} \\ 10^6(220-T)/(220-25) + f_1(220) & 25^\circ\text{C} \leq T < 220^\circ\text{C} \\ f_1(T) & 220^\circ\text{C} \leq T < 350^\circ\text{C} \\ f_2(T) & 350^\circ\text{C} \leq T < 430^\circ\text{C} \\ f_2(430) & T \geq 430^\circ\text{C} \end{cases}$$

$$f_1(T) = 10^{\left(-85.843 + 1.3870T - 7.979 \times 10^{-3}T^2 + 2.0286 \times 10^{-5}T^3 - 1.9344 \times 10^{-8}T^4\right)}$$

$$f_2(T) = 10^{\left(100.90 - 0.4771T + 5.533 \times 10^{-4}T^2\right)}$$

Solution Algorithm

1. Solve the momentum equations using the geometry defined by the current shape of the free surface and the prescribed pressure at it
2. Enforce local mass conservation in each CV by solving the pressure-correction equation, using the prescribed pressure boundary condition on the current free surface. Mass is conserved both globally and in each CV, but non-zero mass fluxes through the free surface may result.
3. Correct the position of the free surface so that the volume defined by its corrected and previous position (i.e., at previous time step) compensates the mass fluxes through the free surface obtained in the preceding step.
4. Re-mesh the grids based on the corrected free surface position and update the transformation Jacobian matrix.
 - Grid smoothing to avoid gridline entanglement
5. Return to step 1 and repeat until all equations and boundary conditions are satisfied.
6. Advance to the next time step

Discretization Schemes

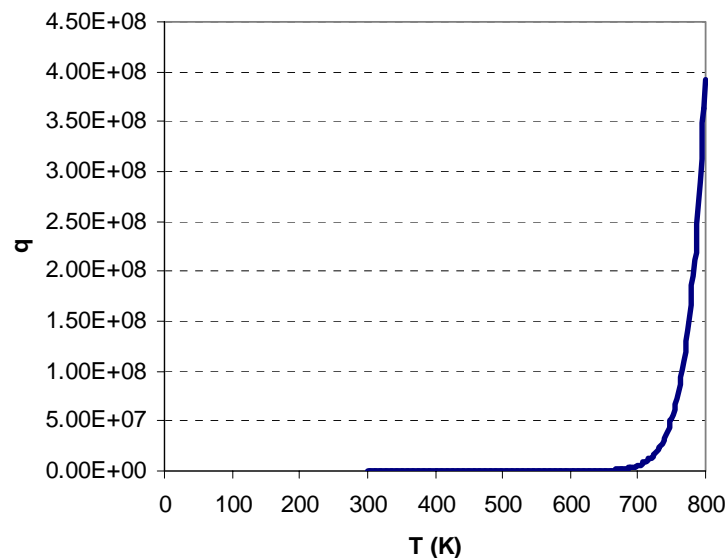
- Second-order central difference scheme used for spatial discretization of momentum equations
- Second-order Total Variation Diminishing (TVD) scheme used for spatial discretization of energy equation
- Second-order (three level) scheme used for time integration



Heat Sink Term for Energy Equation

□ A heat sink term in Arrhenius form is added to the energy equation to alleviate overheating

- Overheating results in non-physical temperatures along the free surface due to lacking of other physical models, which in-turn creates sharp changes in viscosity (e.g., one order of magnitude change in viscosity due to several degrees difference in temperature) along the free surface. The material with low viscosity tends to roll-over the material with high viscosity, which can not be handled by the current algorithm.
- The material roll-over may not cause problem for the VOF method.
- The overheating problem becomes significant when grid size becomes smaller near the free surface due to the large temperature gradient near the surface

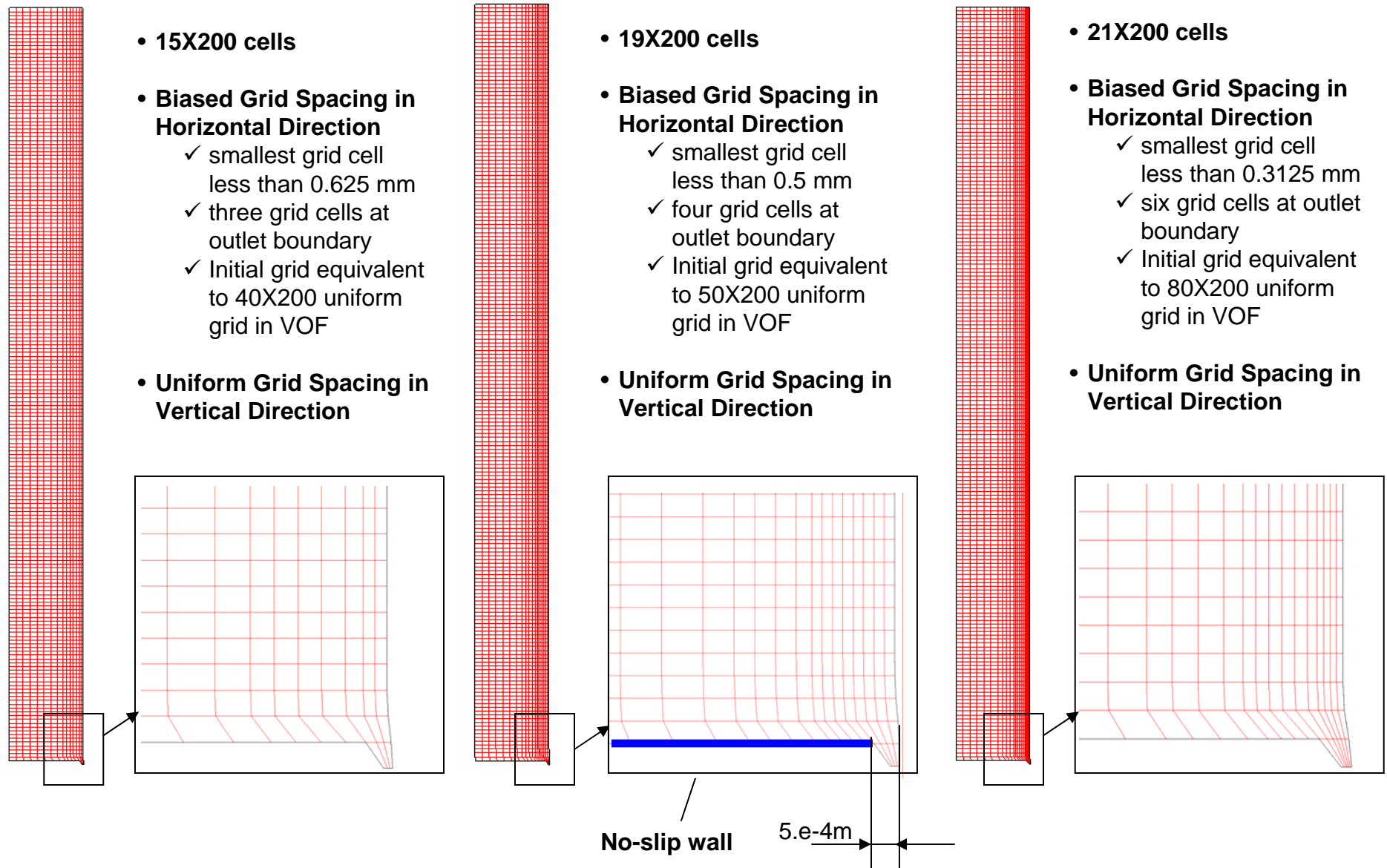


- The heat sink term in the energy equation is constructed to mimic the gasification heat loss term. However, no mass loss is involved in the model currently. The heat sink term can be expressed as $q = H\rho B \exp(-E / RT)$
- The left figure shows the model used in the simulations presented in this report. In the model, the sink term is negligible when temperature is below 700 K and becomes significant when temperature exceeds 750 K. We found this model works fine for PP702 and PP6523 which have similar melting temperatures around 700 K. Different model must be used for PP23 because it has a much lower melting temperature at 460 K

- Melting temperature can be found from the viscosity-temperature relationship where viscosity becomes constant when temperature exceeds the melting temperature



Computation Domain and Grids



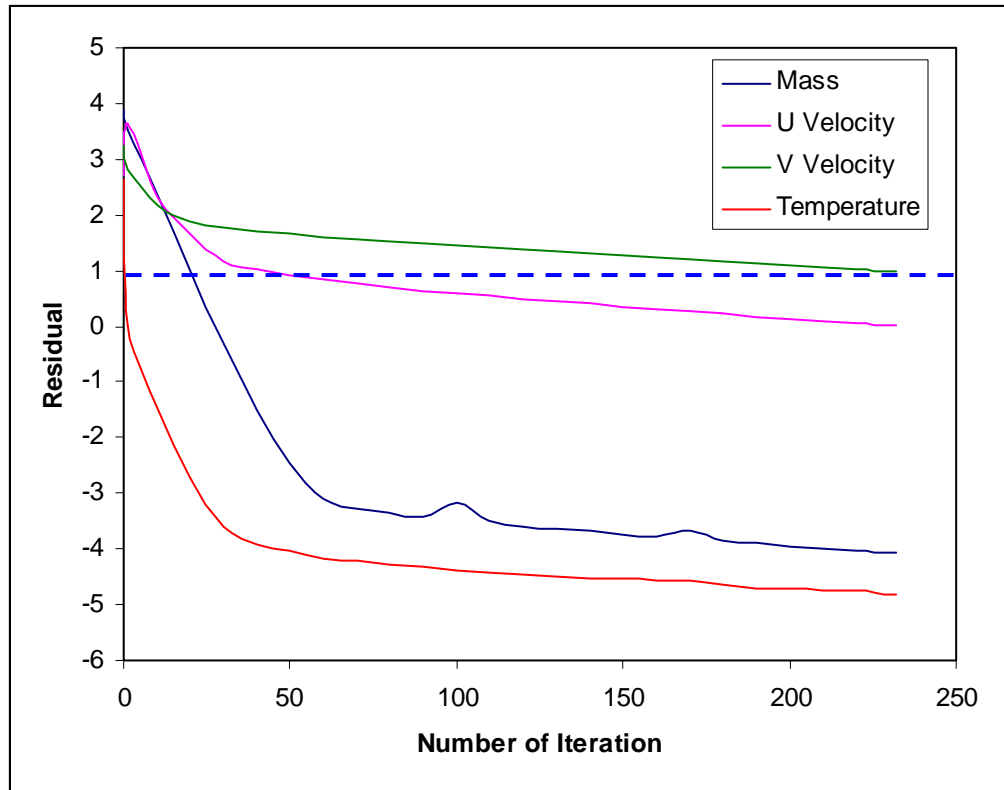
* Grid lines in the plots connect cell centers



Case Summary

Polymer	Grid	# of cells at outlet boundary	Initial Finest Grid Size (mm)	Equiv. Uniform Grid in VOF	Status as of 03/29/06	Comments
PP6523	14X200 (biased)	2	1.25	20X200	Done	
PP6523	15X200 (biased)	3	0.625	40X200	Done	
PP6523	19X200 (biased)	4	0.5	50X200	Done	
PP6523	21X200 (biased)	6	0.3125	80X200	Done	
PP702	10X100 (uniform)	1	2.5	10X100	Done	Too coarse
PP702	14X200 (biased)	2	1.25	20X200	Done	
PP702	15X200 (biased)	3	0.625	40X200	Done	
PP702	19X200 (biased)	4	0.5	50X200	Done	
PP702	21X200 (biased)	6	0.3125	80X200	Done	
PP23	10X100 (uniform)	1	2.5	10X100	Failed	
PP23	14X200 (biased)	2	1.25	20X200	Done	On hold
PP23	19X200 (biased)	4	0.5	50X200	10% mass loss	On hold
PP23	21X200 (biased)	6	0.3125	80X200	5% mass loss	On hold

Residual History



- PP702, Grid = 19x200
- During each time step, iteration is terminated when residuals of all solved quantity are below 1 (i.e., at least six significant digits remain unchanged from iteration to iteration)

A typical residual history in one time step

Residual definition

$$R_Y^\psi \equiv 7 + \log_{10} \left(\frac{\sum_{\text{Calculation domain}} R_Y^0}{\sum_{\text{Calculation domain}} \psi_Y} \right)$$

Where $R_Y^0 \equiv A_E Y_E + A_W Y_W + A_N Y_N + A_S Y_S + A_T Y_T + A_B Y_B + S_U - A_P Y_P$

And $\psi_Y = A_P Y_P$

Y is the solved quantity



Computational Cost

- All Cases were run on a Dell Precision 450 Desktop PC with a Xeon 3GHz CPU

PP702

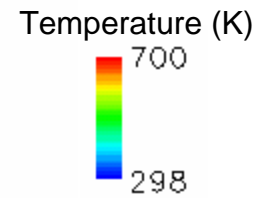
Case	Wall Clock Time	Memory Requirement
10X100	~ 4 hours	< 1MB
14X200	~ 24 hours	~1 MB
15X200	~ 36 hours	~1 MB
19X200	~100 hours	~2 MB
21X200	~120 hours	~2 MB

- Run times are comparable between cases of PP702 and PP6523 with same grid

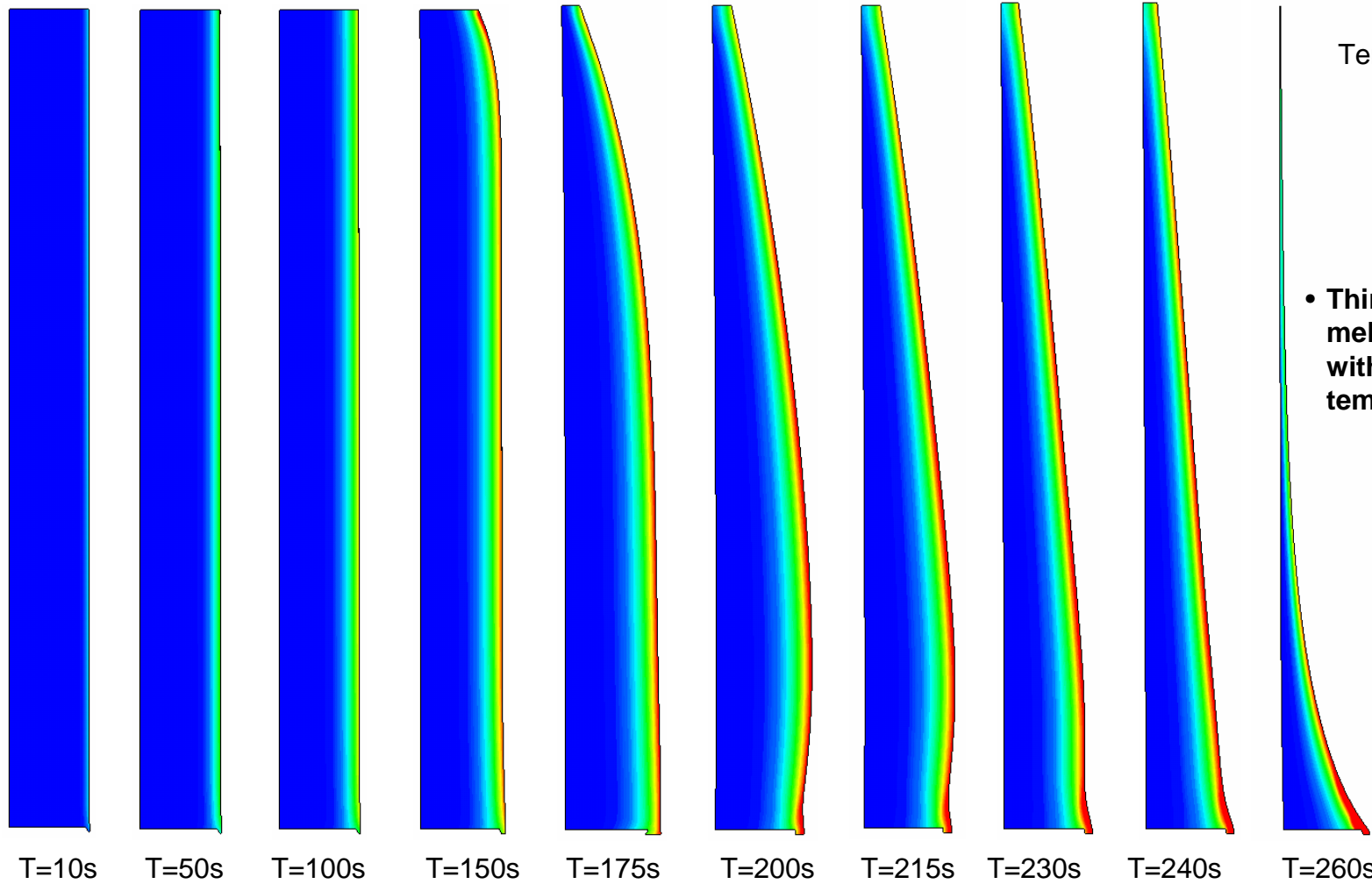


Free Surface Location and Temperature Field vs. Time – PP702

Grid: 21X200

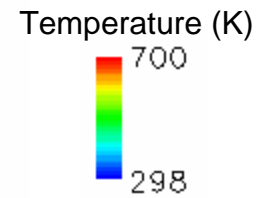


- Thin layer of melted polymer with high temperature

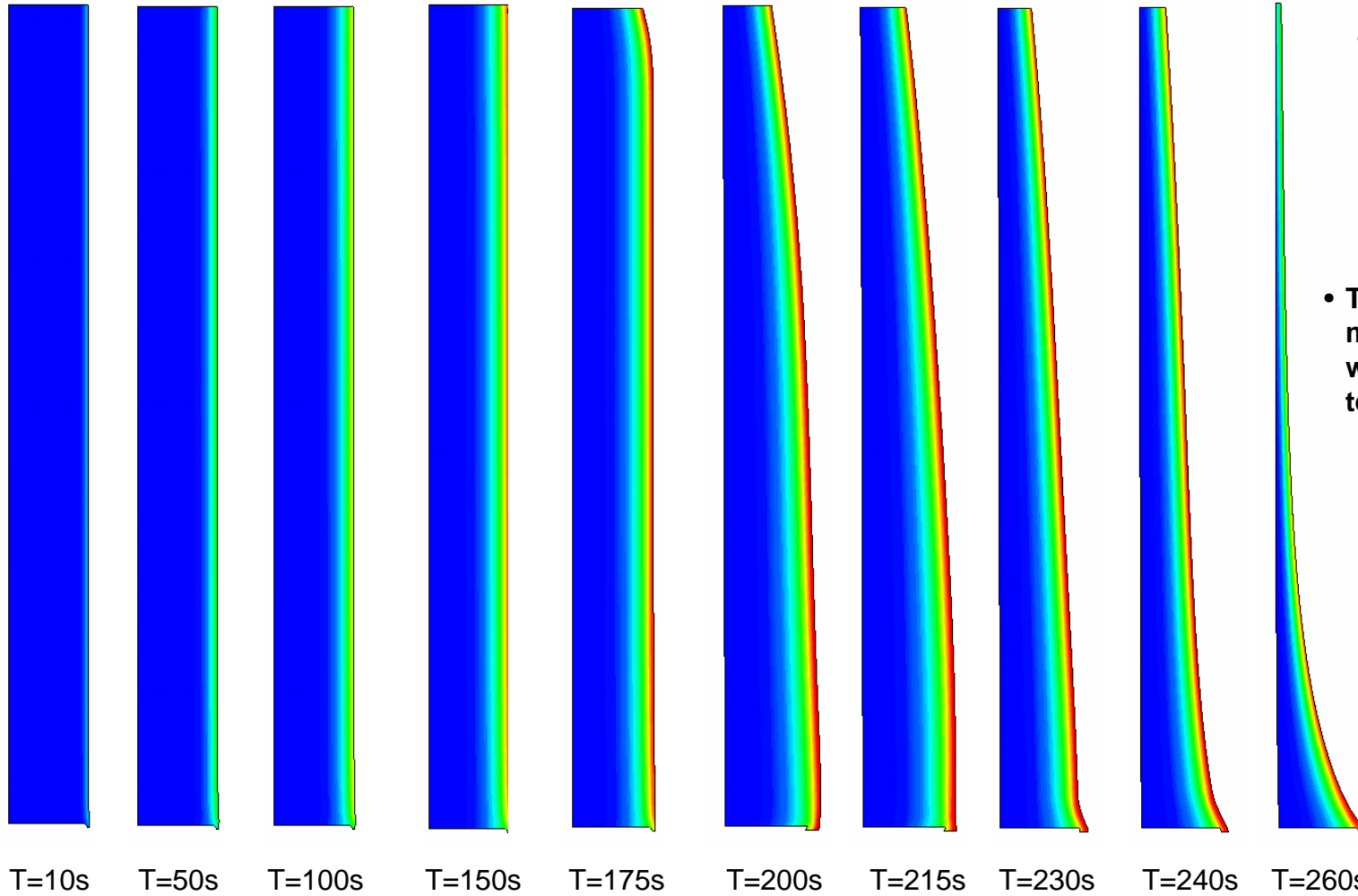


Free Surface Location and Temperature Field vs. Time – PP6523

Grid: 19X200

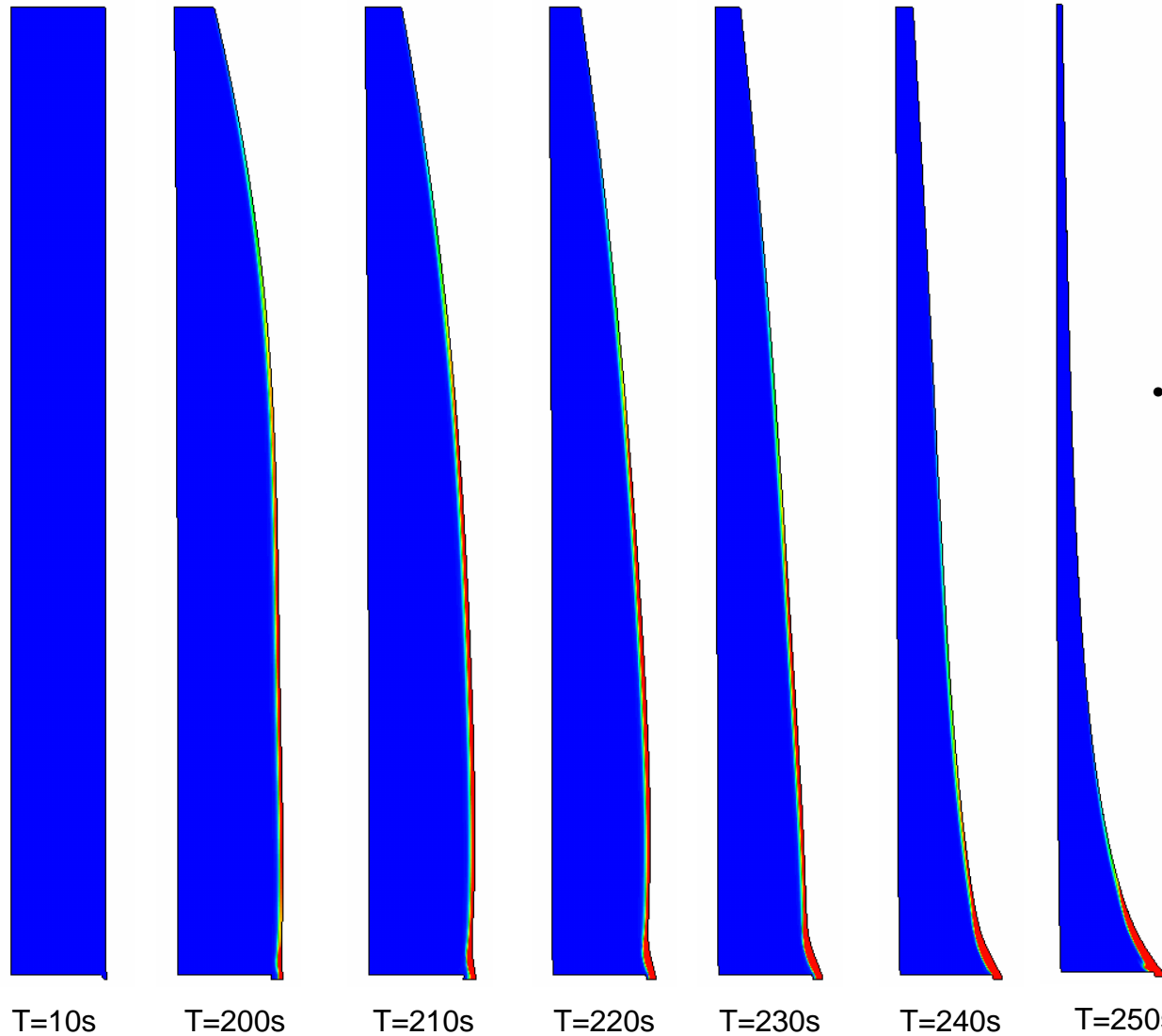


- Thin layer of melted polymer with high temperature



Free Surface Location and Velocity Magnitude vs. Time – 702

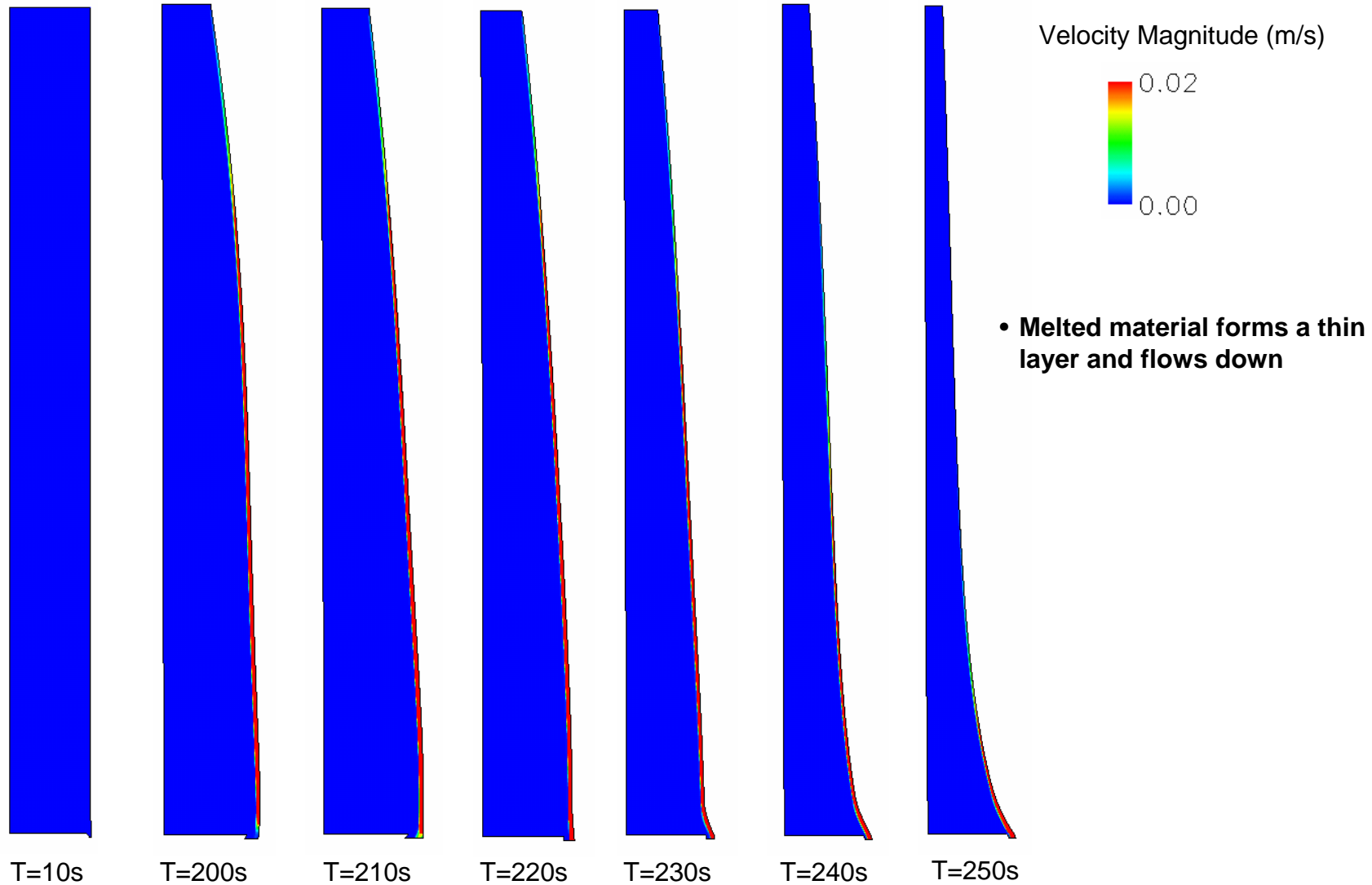
Grid: 19X200



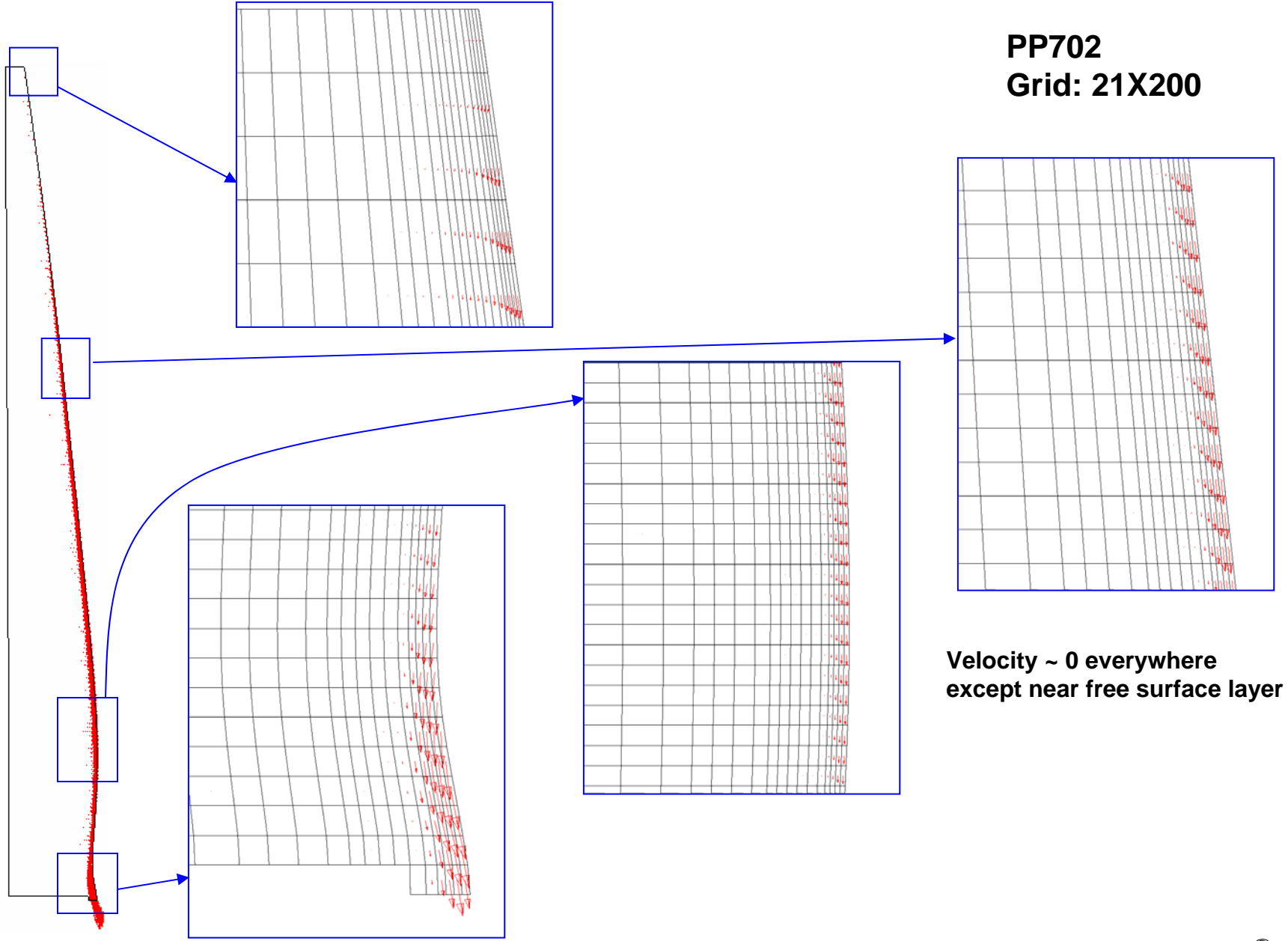
- Melted material forms a thin layer and flows down

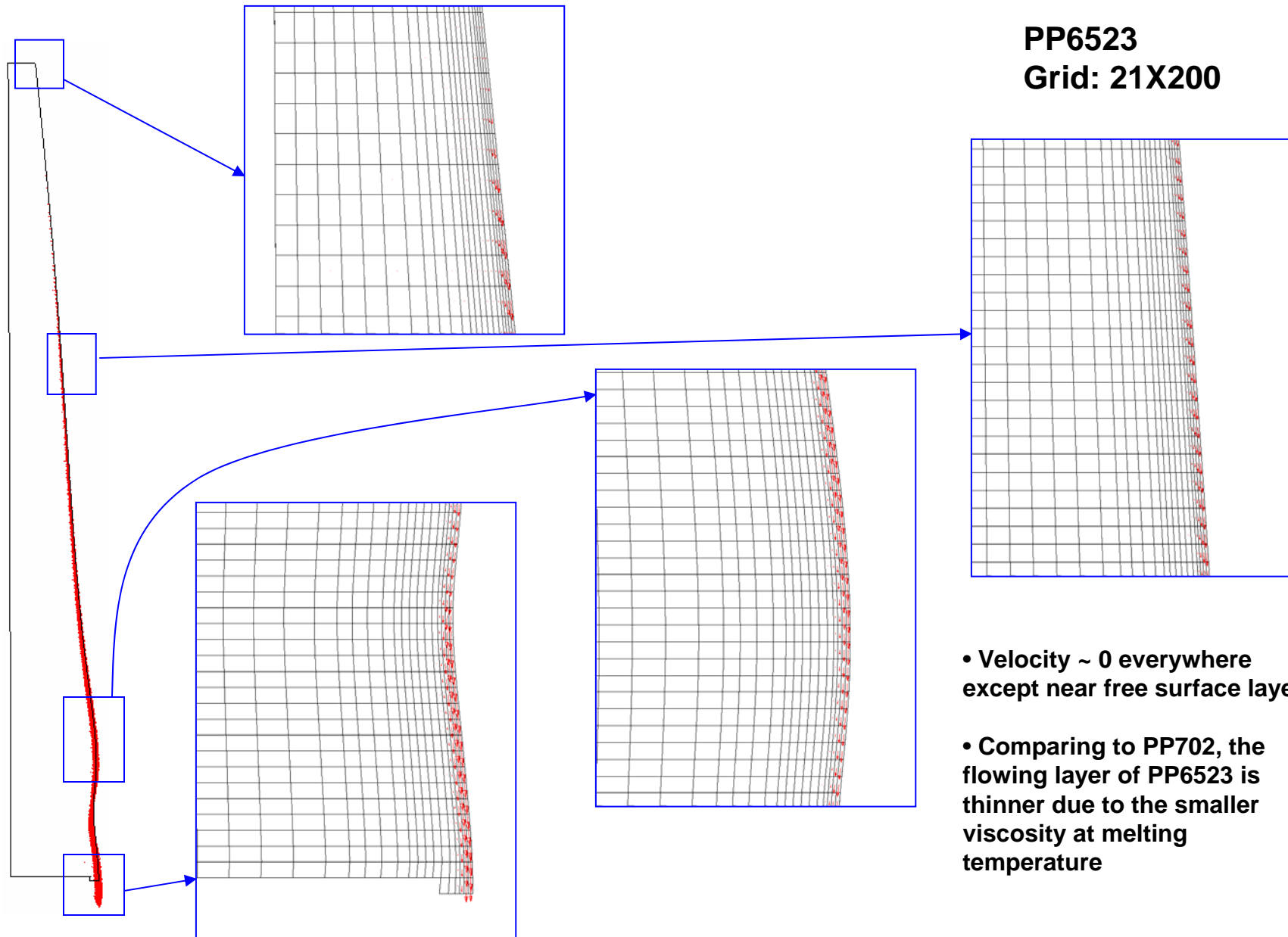
Free Surface Location and Velocity Magnitude vs. Time – PP6523

Grid: 19X200

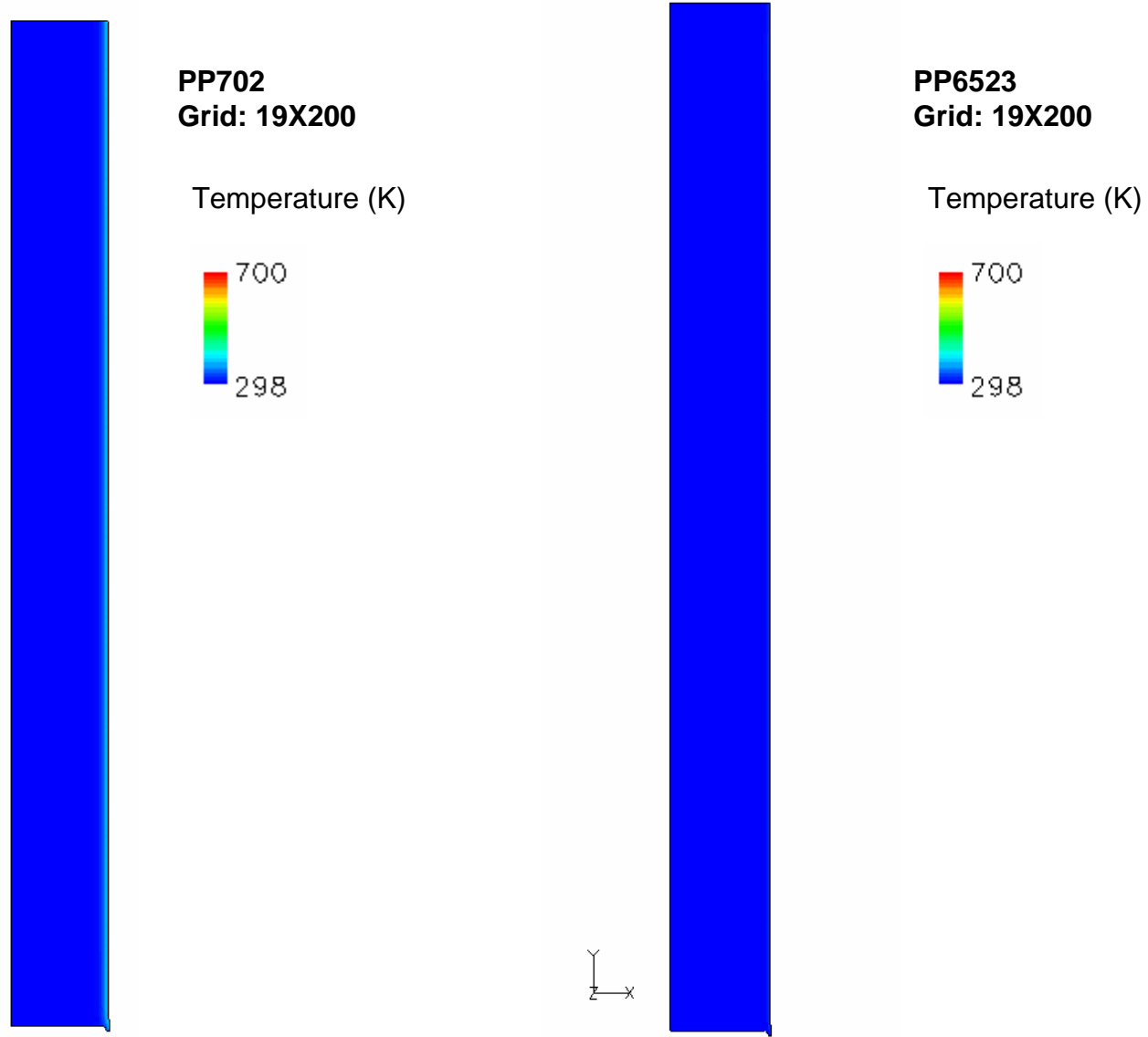


Example: Velocity Vectors at Time = 220 s (Zoom to 200% for better view)



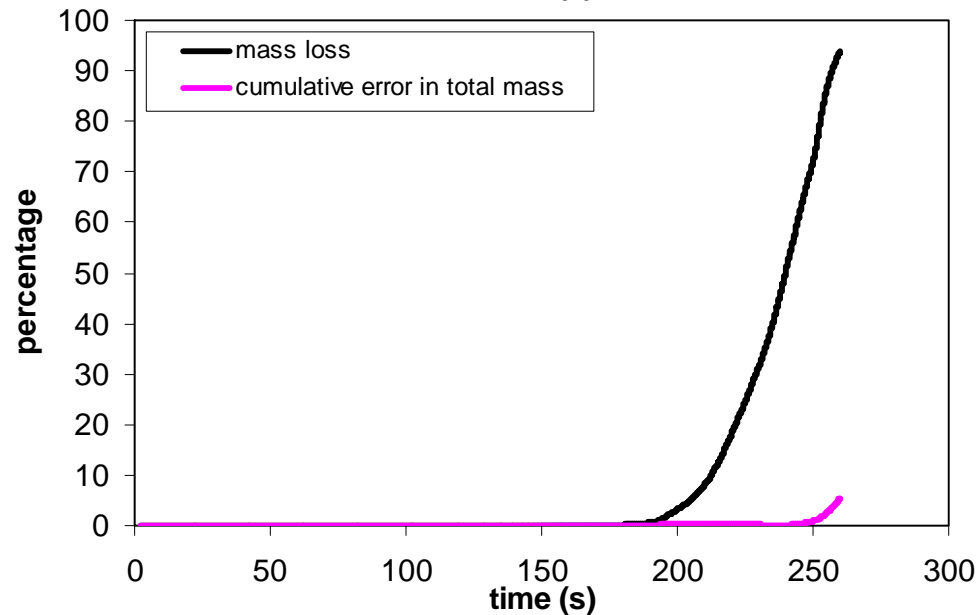
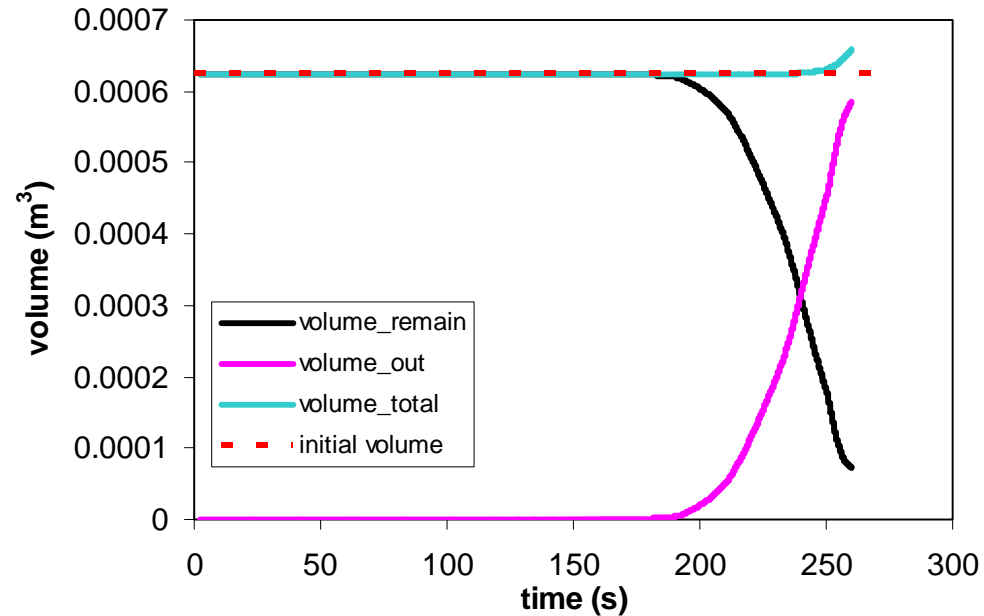
Example: Velocity Vectors at Time = 235 s (Zoom to 200% for better view)

Movie: Free Surface Location and Temperature Contour



Volume/Mass Change as Function of Time

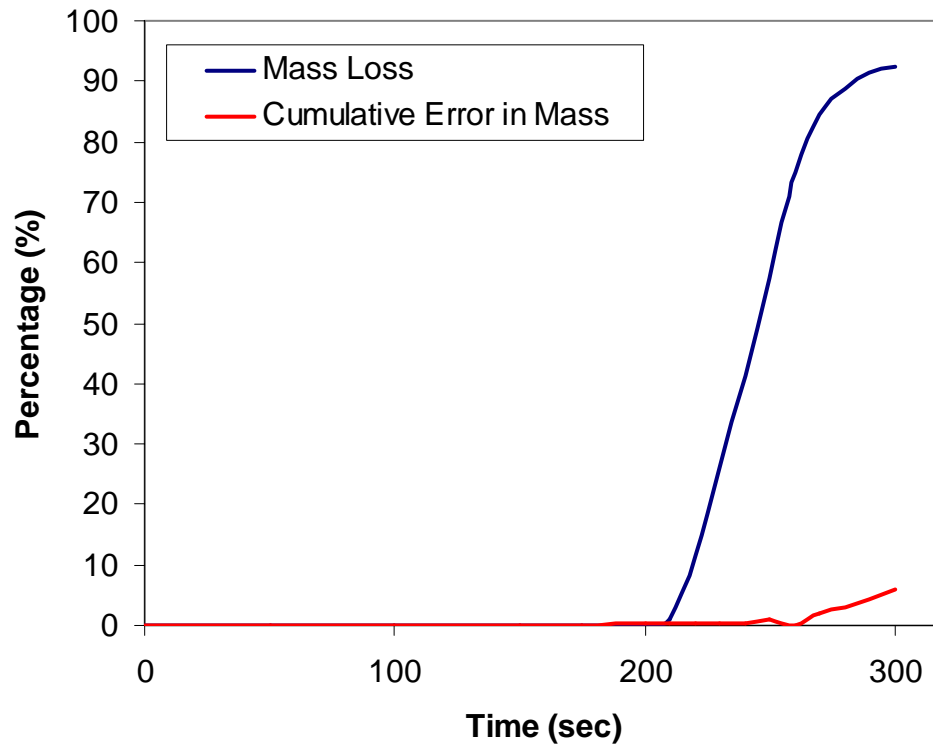
PP702
Grid: 19X200



- Cumulative error of mass conservation is defined as the normalized difference between the initial mass within the domain (at $t=0$) and the sum of the mass out of the domain and the mass within the domain.
- Cumulative error is less than 1% before reaching 88% mass loss and is less than 5% at 95% mass loss. The increasing cumulative error in mass conservation at the end of the calculation is due to the significant grid skewness around the bottom lip



Volume/Mass Change as Function of Time

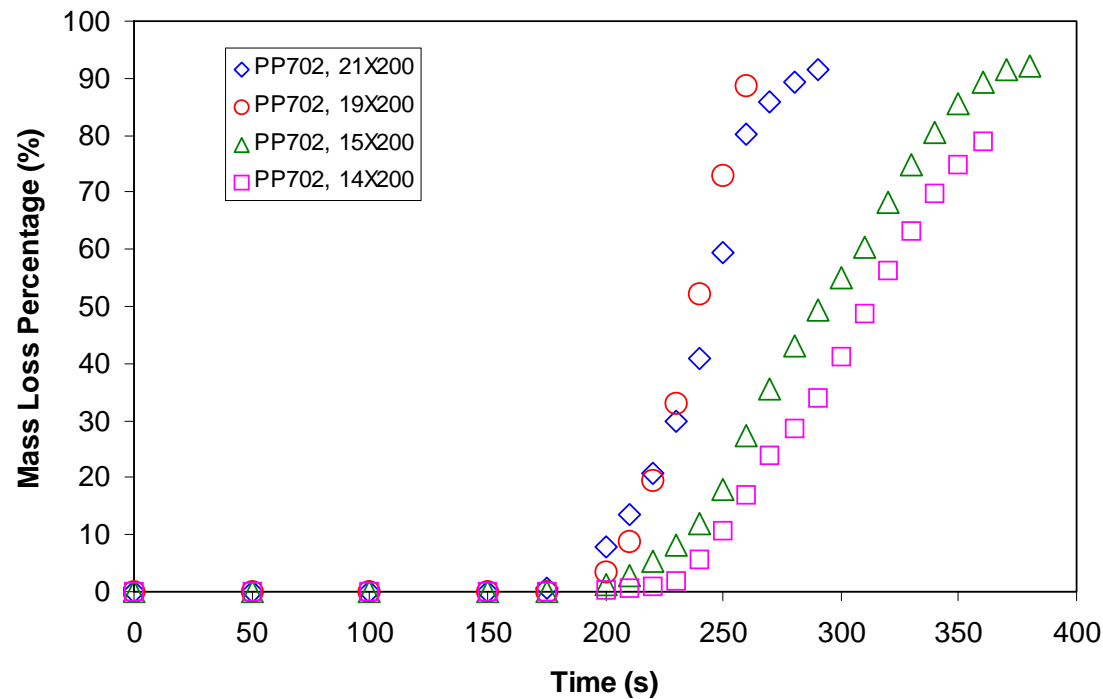


PP6523

Grid: 19X200

- Cumulative error is less than 1% before reaching 82% mass loss and is less than 5% at 92% mass loss. The increasing cumulative error in mass conservation at the end of the calculation is due to the significant grid skewness around the bottom lip

Mass Loss as Function of Time – PP702



Grid	“steady state” Mass Loss Rate	Comments
14X200	28.1*	Computed from 220 s to 330 s,
15X200	31.5*	Computed from 210 s to 320 s
19X200	63.3*	Computed from 180 s to 260 s
21X200	62.4*	Computed from 180 s to 260 s
Experiment	0.12**	Ohlemiller FAX 01-18-06

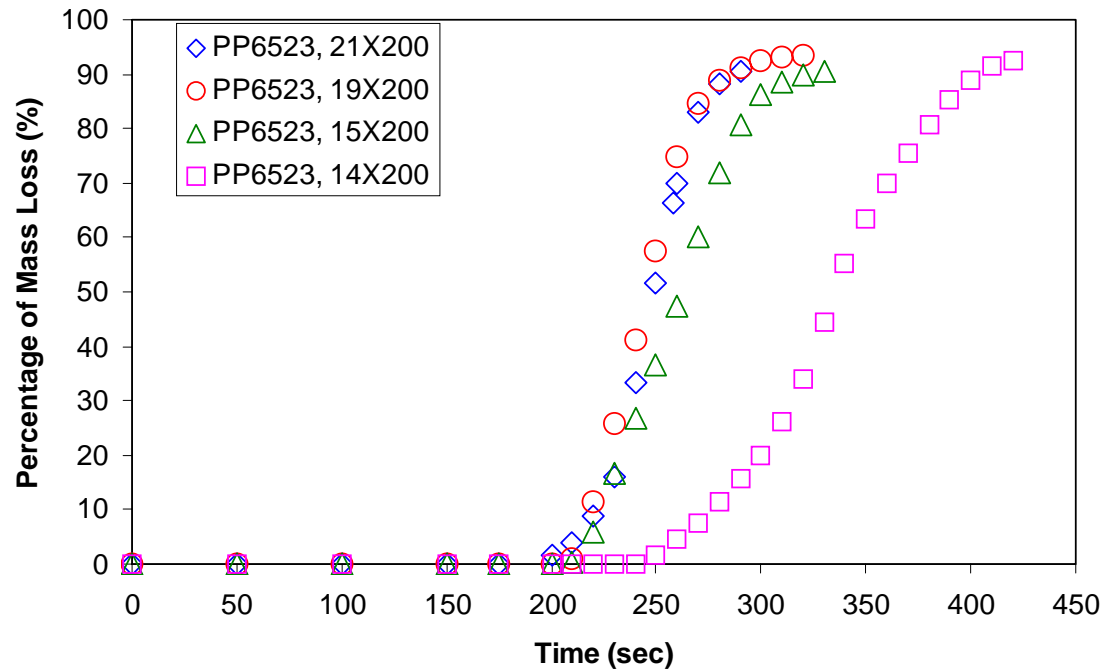
* per unit length (g/s m)

** g/s

PP702

- The results are very sensitive to the grid resolution near the free surface. The resolution of the two coarser grids are not adequate to resolve the sharp temperature gradient near the surface.
- The two cases with finer grids yield similar results in terms of mass loss history and “steady state” mass loss rate, which indicates grid convergence to some extent.
- The code chooses time-step size based on a constant CFL number in all three cases. The time step sizes are not constant in each case and they are also very different in different cases. In general, the 21X200 case has the smallest time step size. Hence temporal error also plays a role in make the mass loss history different.
- The predicted mass loss rate should not be directly compared to the experimental observation due to (1) this is a 2-D simulation; (2) some critical physical models are missing in the numerical model such as heat loss, radiation absorption, and pyrolysis.

Mass Loss as Function of Time – PP6523



PP6523

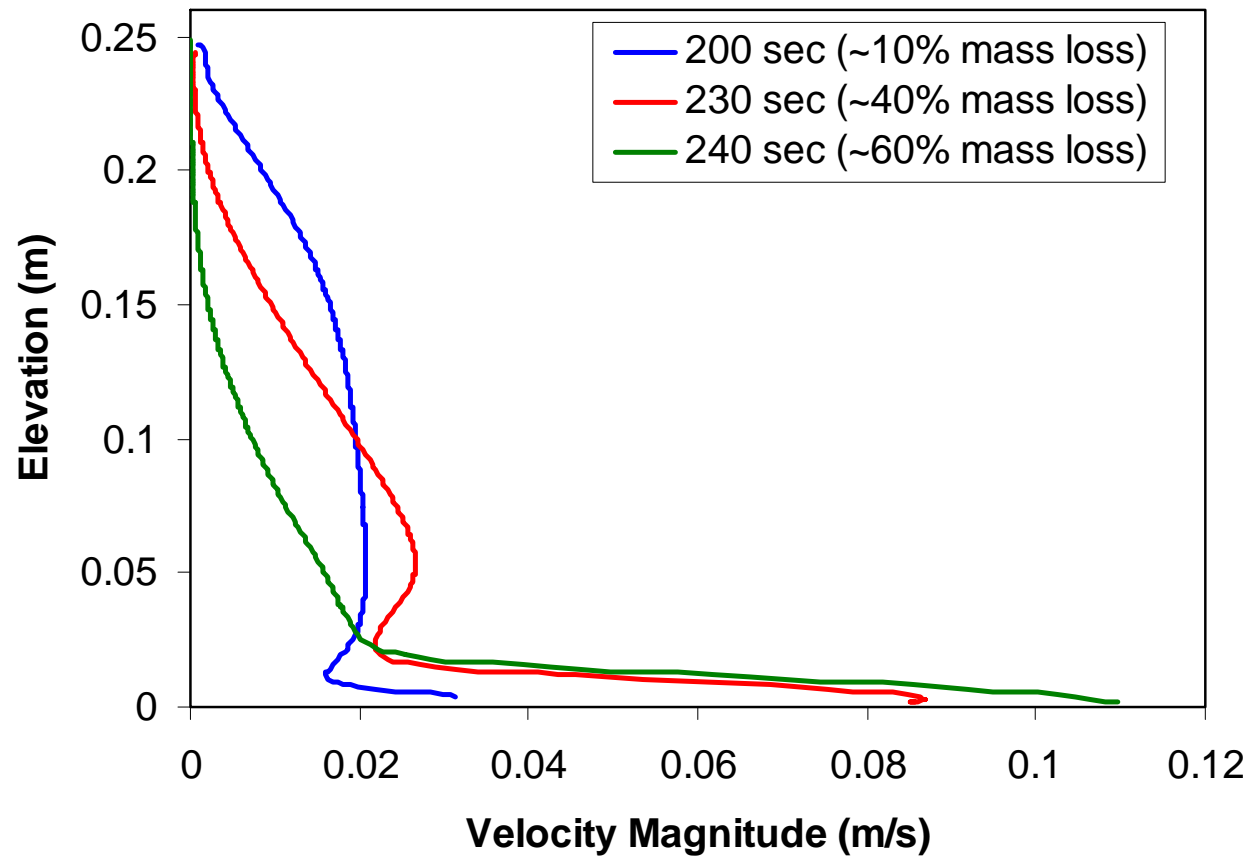
- The case with coarsest grid predicted very different melting behavior comparing to the other three cases. It took much longer time for the polymer to flow and the mass loss rate was also much smaller.
- The differences among the three cases with finer grids are much smaller than the differences between them and the case with the coarsest grid in terms of the starting time of melted flow, 'steady state' mass loss rate, and mass loss history, which indicates grid convergence to some extent.

Grid	"steady state" Mass Loss Rate	Comments
14X200	33.8*	Computed from 250 s to 400 s,
15X200	59.1*	Computed from 200 s to 290 s
19X200	70.7*	Computed from 200 s to 270 s
21X200	70.5*	Computed from 200 s to 270 s
Experiment	N/A	

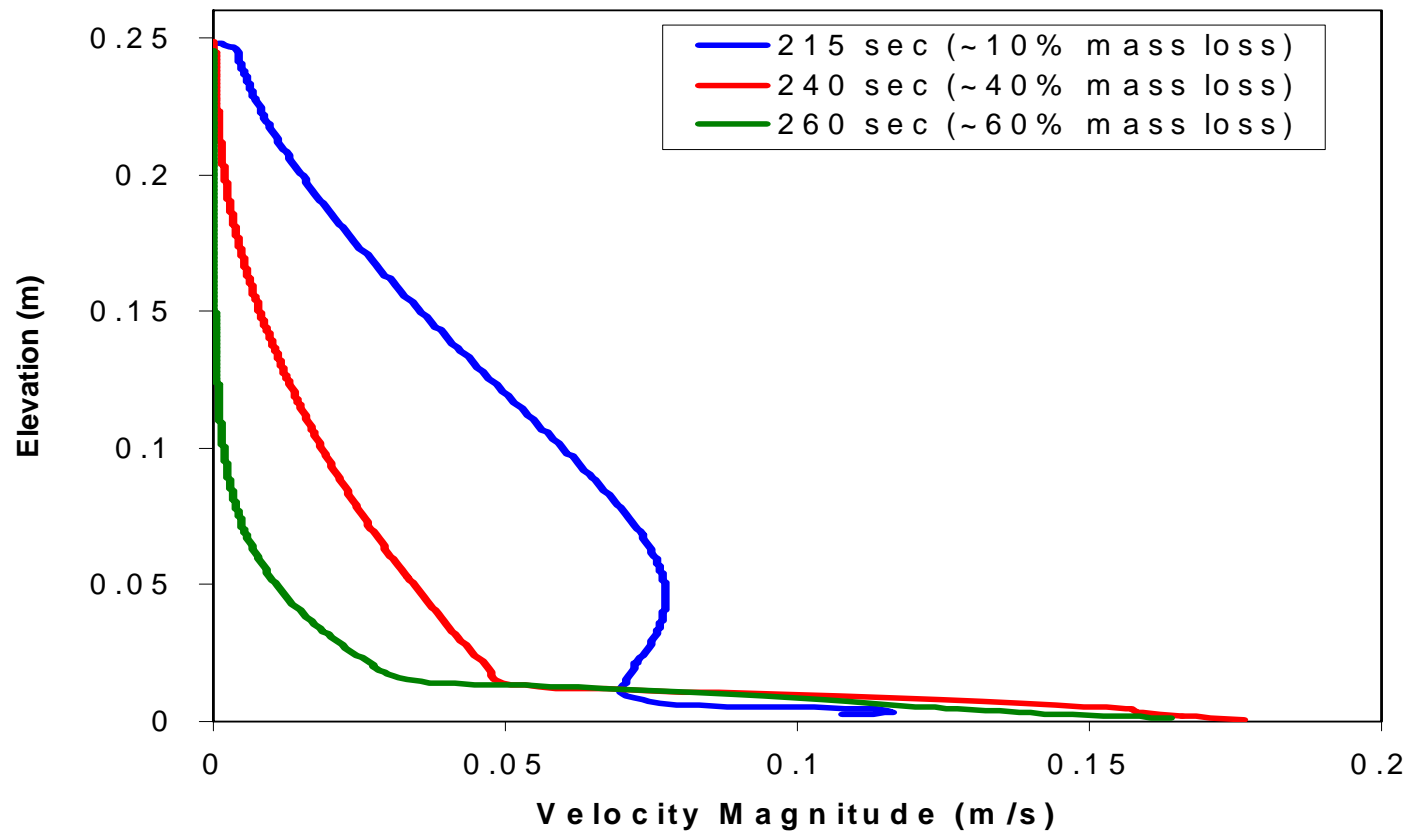
* per unit length (g/s m)

** g/s

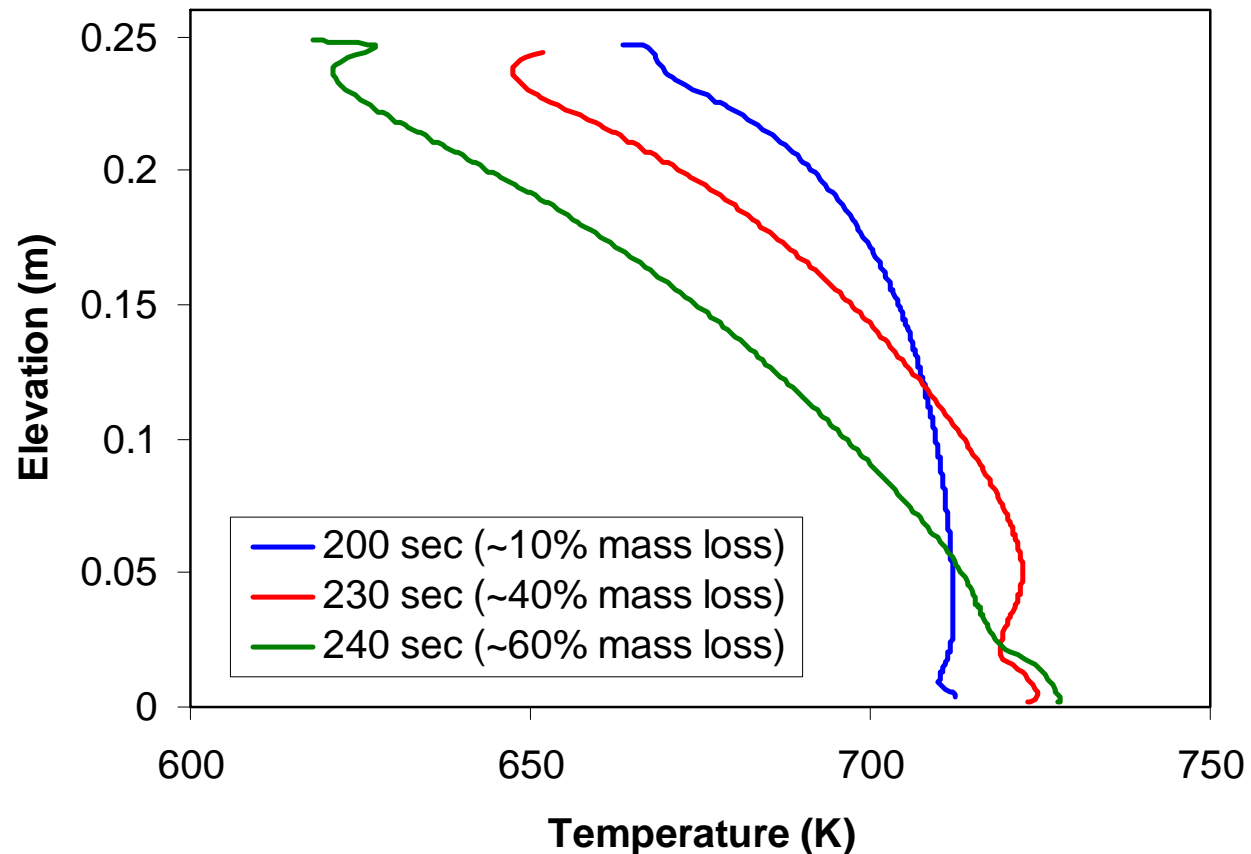
Velocity Magnitude Profiles on Free Surface at Selected Times



Velocity Magnitude Profiles on Free Surface at Selected Times



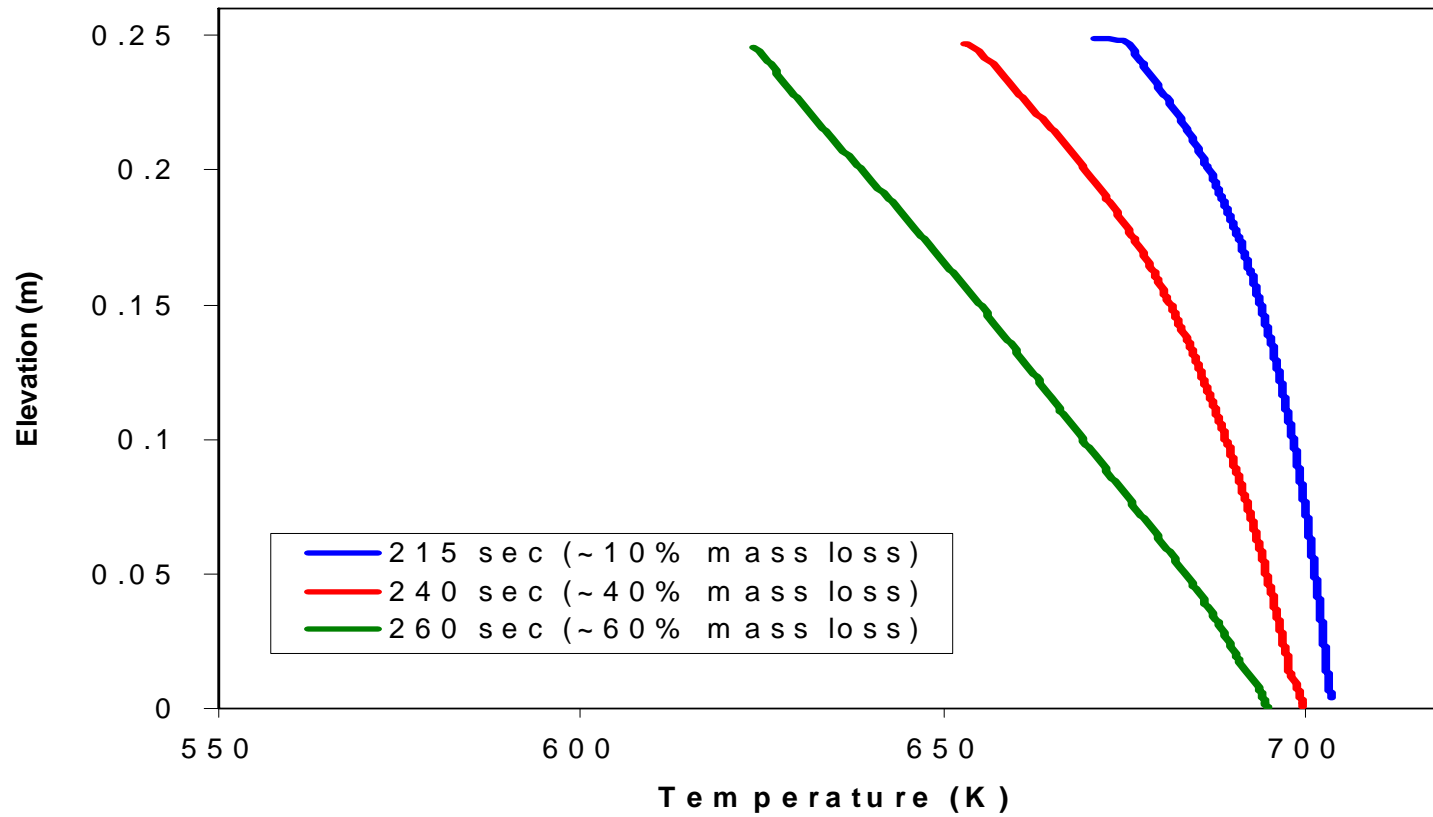
Temperature Profiles on Free Surface at Selected Times



- Average free surface temperature observed in experiment (Ohlmeir FAX 01-18-06) was ~613 K
- The computation model does not include processes such as radiant and convective heat loss, gasification, etc., which may be the cause of the higher temperature calculated on the free surface.



Temperature Profiles on Free Surface at Selected Times



Summary

- Completed Two Resins on Multiple Grids
- Grid Sensitivity / Convergence
 - 15x200 possibly too coarse
 - 19x200 and 21 x200 => about same mass loss rate
- Computational Cost highlighted
 - About same cost for both resins
- Model features highlighted
 - Solution algorithm
 - Typical convergence history
 - Solutions at selected times
 - Velocity field resolution across melt boundary layer
- Example Results
 - Free surface location, temp., velocity - selected times
 - Movie of free surface location and temperature
 - Mass loss, surface temperature, surface velocity



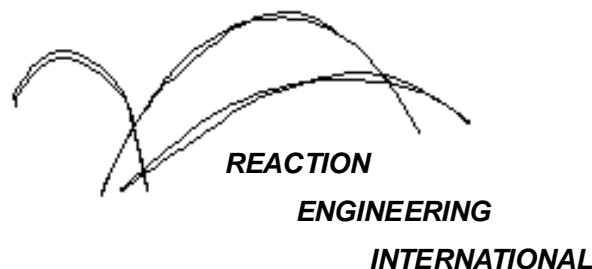
Task 2



A Computational Model For Fire Growth and Spread On Thermoplastic Objects

**Task 2: 2D model with steady heat flux, radiative
and convective heat losses, and in-depth
absorption of radiative heat flux**

(5/31/06)



Outline

⊕ Radiative and convective heat loss, In-depth absorption models

- ⊕ Only impacts energy equation
- ⊕ Both radiative and convective heat losses are only applied to the free surface
- ⊕ A heat source term is added to the energy equation to account for in-depth absorption.
- ⊕ Absorption coefficient is a function of the distance from the free surface

⊕ Absorption coefficient models

- ⊕ In-depth absorption coefficient data for one polymer resin provided by NIST
 - ⊕ Email sent by Kathy to Bockelie on 2/22/2006
 - ⊕ Data applicable to PP23K in the HIFT apparatus
- ⊕ Three models constructed based on the NIST data

⊕ Cases studied

- ⊕ Computational grid
- ⊕ Case summary
- ⊕ Example results:
 - ⊕ Free surface location, temp., velocity
 - ⊕ Mass loss, surface temperature, surface velocity, and comparisons with data

⊕ Summary



Heat loss and In-depth absorption models

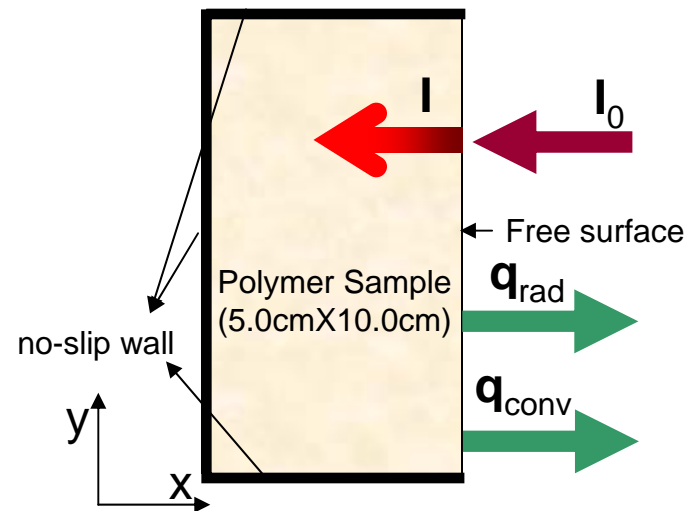


Figure 1, Sketch of in-depth absorption and heat loss model

⊕ Energy equation source terms due to in-depth absorption, radiative and convective heat losses

- ⊕ In-depth absorption: $\dot{q}_{\text{absorption}} = \int_{\Omega} \frac{dI}{dx} d\Omega$, assuming absorption process in x-direction only
- ⊕ Radiative heat loss: $\dot{q}_{\text{radiation}} = -A\epsilon\sigma(T^4 - T_0^4)$, assuming radiative heat loss only on free surface
- ⊕ Convective heat loss: $\dot{q}_{\text{convection}} = -Ah_{\text{conv}}(T - T_0)$

⊕ Parameters: A – surface area; Ω - volume; ϵ - emissivity (=1.0); σ - Stefan-Boltzmann Constant (=5.67e-8); T_0 – ambient temperature (=298 K); h_{conv} – convective heat transfer coefficient (= 8.0)

⊕ A heat sink term is added to the energy equation to prevent overheating (i.e., $T > 750\text{K}$)

⊕ The models are implemented in subroutine ***fbck_bc_sca***



Absorption Coefficient Models

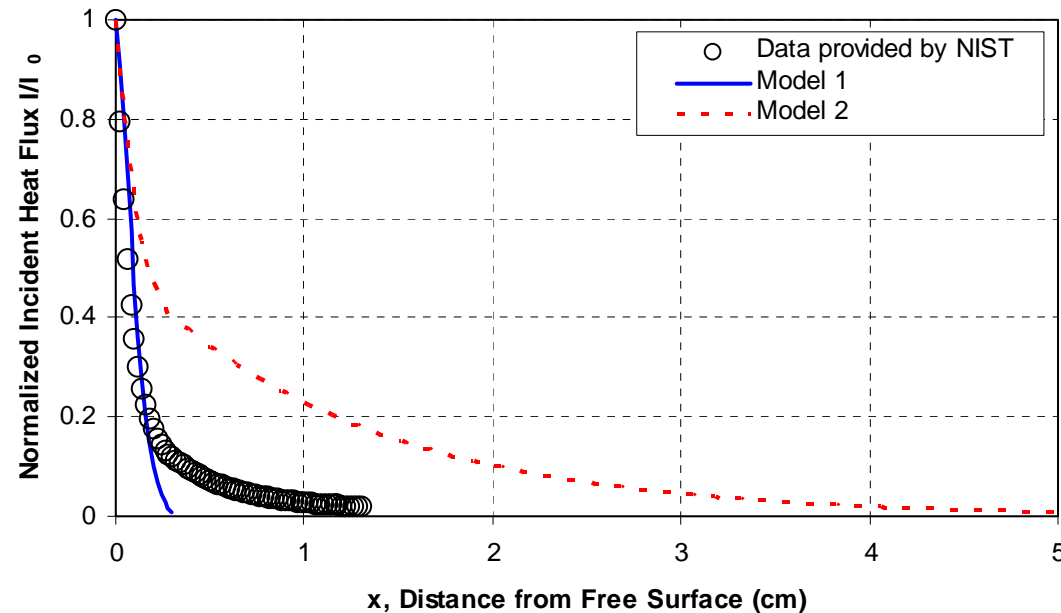


Figure 2, Incident heat flux distribution in the horizontal direction

⊕ Original data (symbols in Figure 2) is roughly applicable to the PP23K resin at the HIFT apparatus

$$\Phi \begin{cases} I/I_0 = 10^{(-5.17x + 6.964x^2)}, & 0 \leq x < 0.3 \text{ (cm)} \\ I/I_0 = 10^{(-0.5154 - 1.473x + 0.4339x^2)}, & 0.3 \leq x < 1.3 \text{ (cm)} \end{cases}$$

• Three incident heat flux distribution functions are used in the CFD model

• Model 1 is differentiable, and all models are well defined over the entire thickness of the sample

• Model 1: $I/I_0 = \exp(-3.843x - 38.36x^2)$, $0 \leq x \leq 3.0$ (cm)

• Model 2: $\begin{cases} I/I_0 = \exp(-5.17x + 6.964x^2), & 0 \leq x < 0.3 \text{ (cm)} \\ I/I_0 = \exp(-0.6814 - 0.7802x - 0.009333x^2), & 0.3 \leq x < 5.0 \text{ (cm)} \end{cases}$

• Model 3: use the original fitted data



Computational Grid

- ⊕ Polymer sample dimension:
5.0cm X 10.0cm
- ⊕ 30X80 Grid (biased)
- ⊕ Initial grid resolution the same
as the 19X200 grid used in
Task 1
- ⊕ Equivalent to 100X80 grid if
using uniform grid spacing and
fixed grid

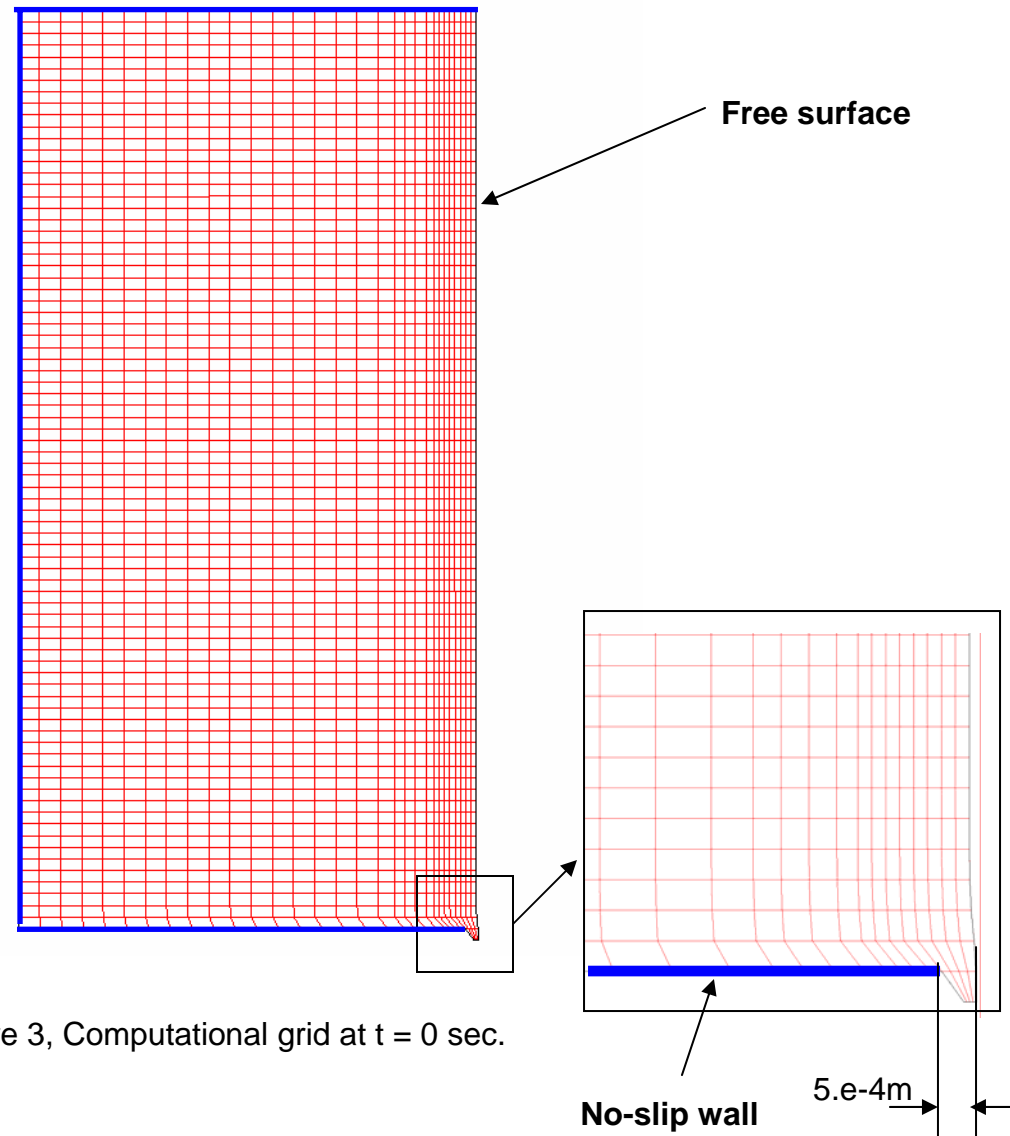


Figure 3, Computational grid at t = 0 sec.

Case Summary

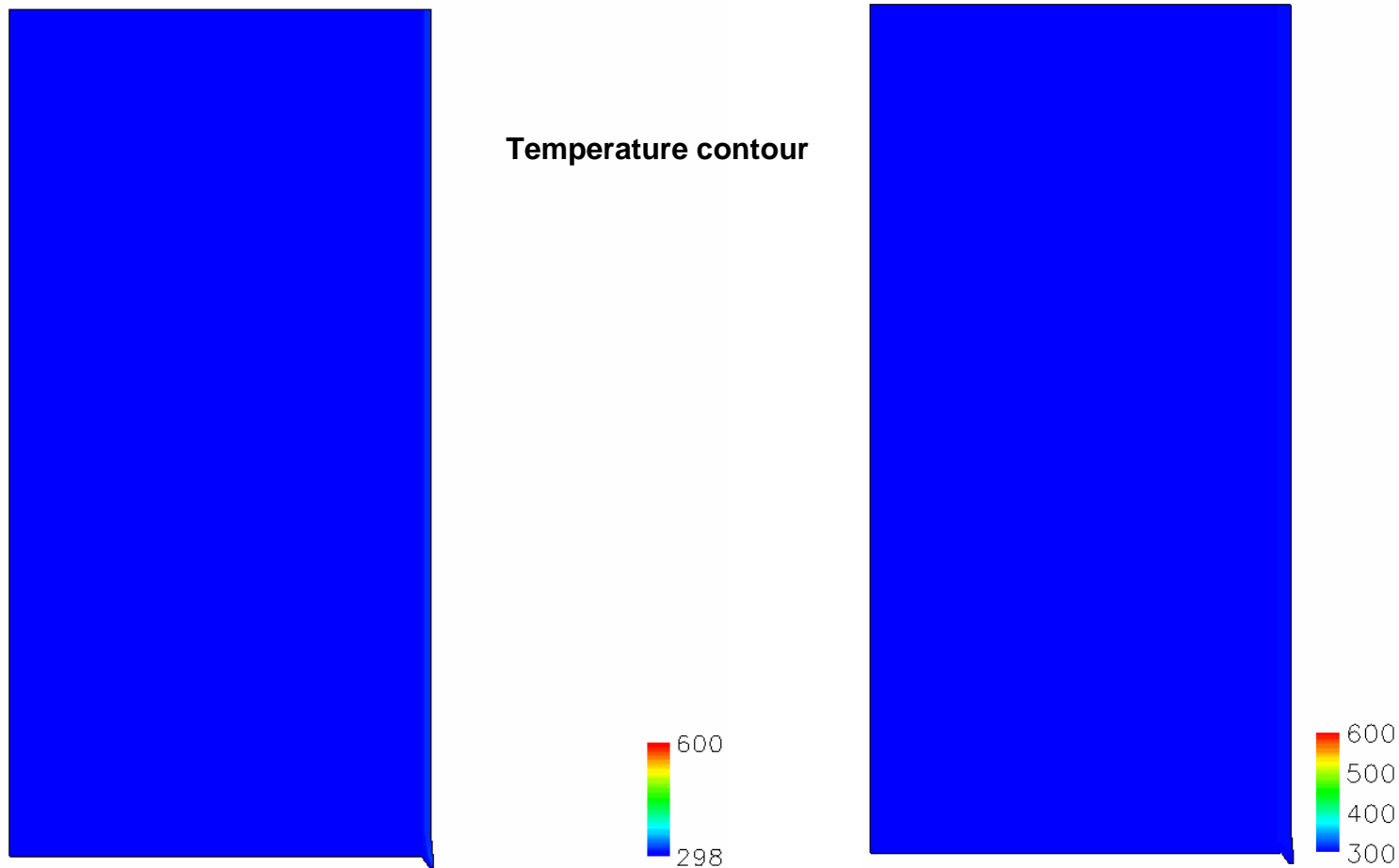
⊕ All cases are run with a external Incident heat flux of 30KW/m²

Case	Polymer Resin	Radiative and Convective Heat Losses	In-depth Absorption	In-depth Absorption Coefficient Model	Mass Loss and Elapsed Time	Estimated CPU Time	Case Status
Case 2A	PP702	Included	Not included	N/A	65%, 400 sec	~ 48 h	Stopped*
Case 2B	PP702	Included	Included	Model 1	58%, 650 sec	~ 30 h	Stopped*
Case 2C	PP6523	Included	Included	Model 1	55%, 460 sec	~ 16 h	Stopped*
Case 2D	PP702	Included	Included	Model 2	27%, 480 sec	~ 2 h	Diverged
Case 2E	PP702	Included	Included	Model 3	N/A	N/A	In progress

* Manually stopped because calculation become extremely slow when mass loss exceeds 50%



Impact of In-depth Absorption on Melting Process



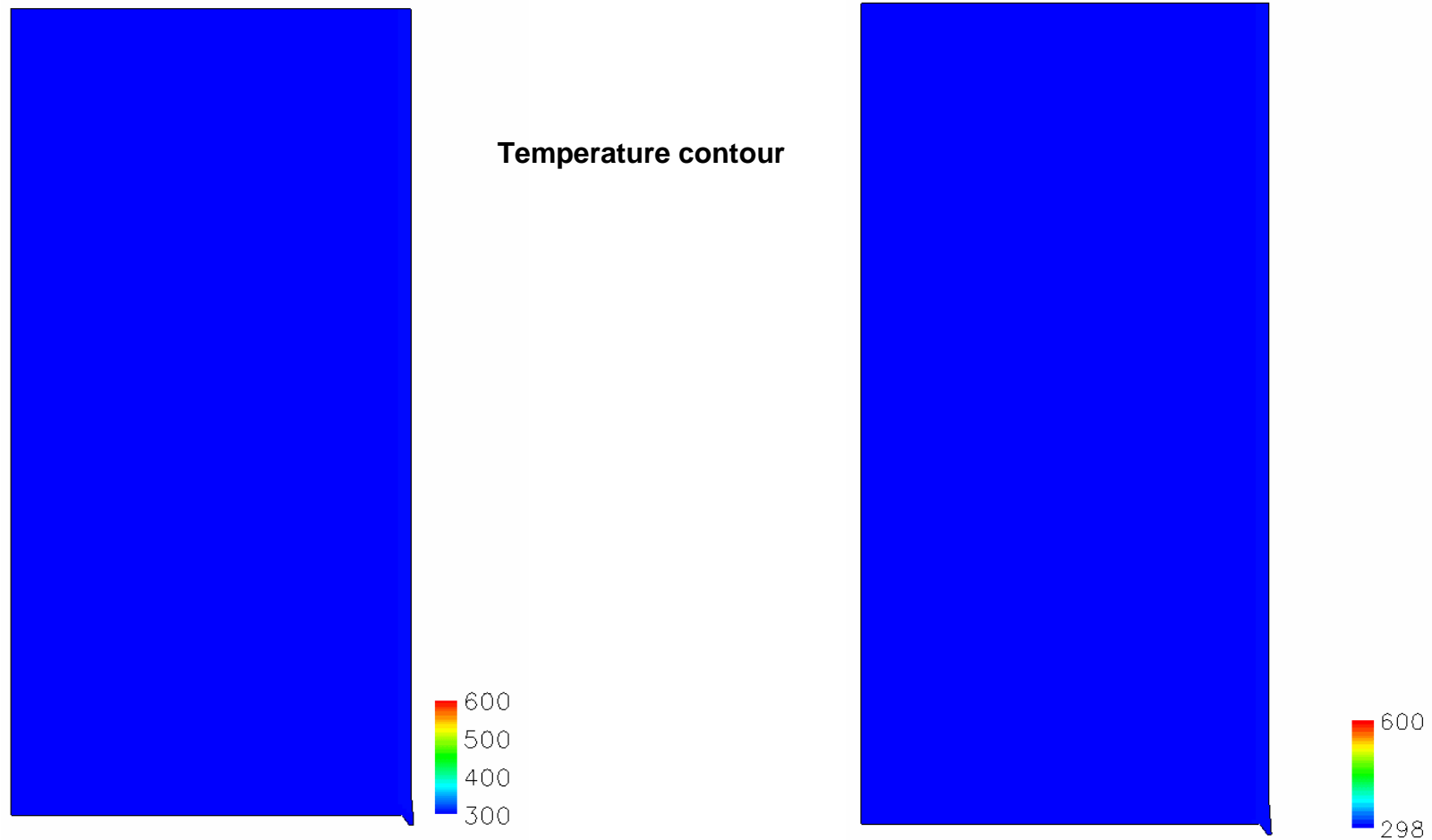
Case 2A (PP702, heat loss only)

Case 2B (PP702, heat loss + in-depth absorption)

- ⊕ Time interval between movie frames: 5 seconds
- ⊕ The inclusion of in-depth absorption leads to significant difference in shape change history
 - ⊖ Melting process slows down
 - ⊖ Upper free surface moves much slower towards the back wall
 - ⊖ Melting layer becomes thicker



Impact of Different Resin on Melting Process

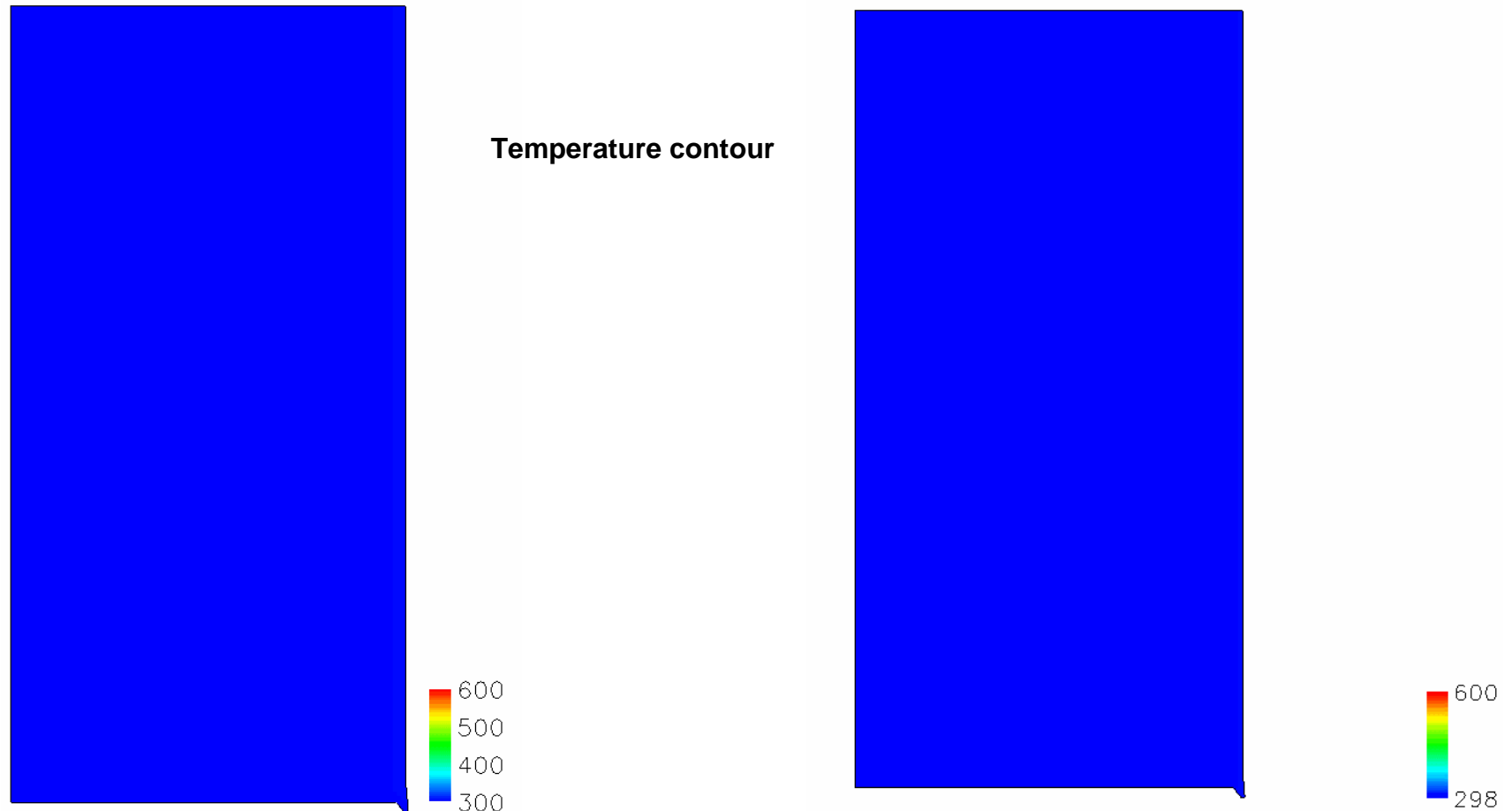


Case 2B (PP702, heat loss + in-depth absorption) Case 2C (PP6523, heat loss + in-depth absorption)

- ⊕ Time interval between movie frames: 5 seconds
- ⊕ PP6523 has a much lower viscosity at high temperature, which leads to faster melting process



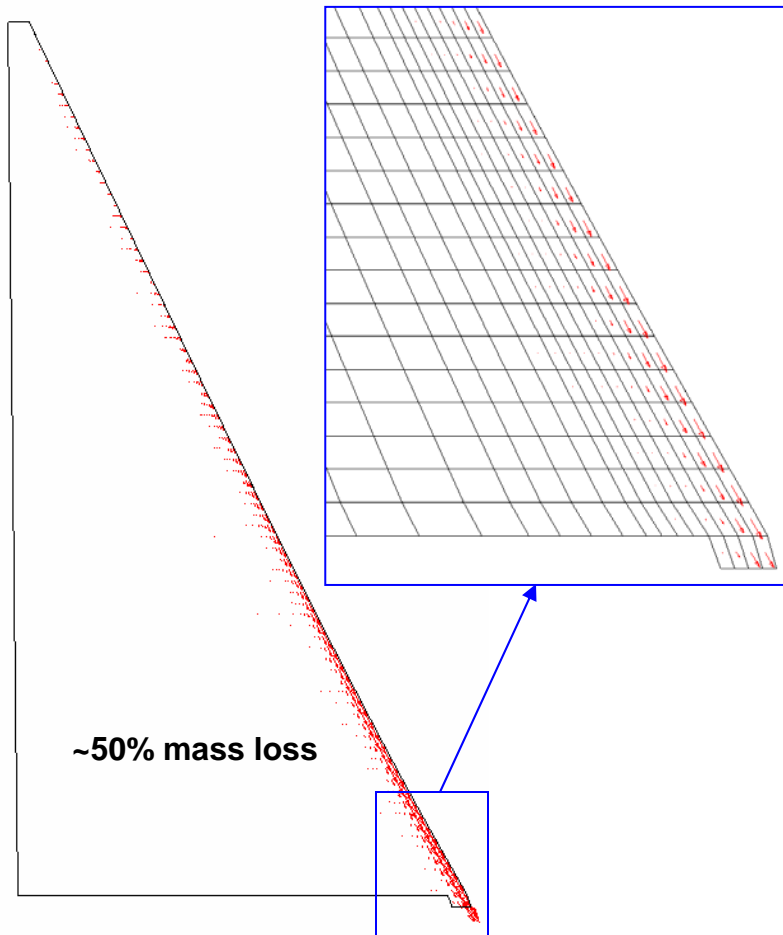
Impact of Different Absorption Coefficient Models



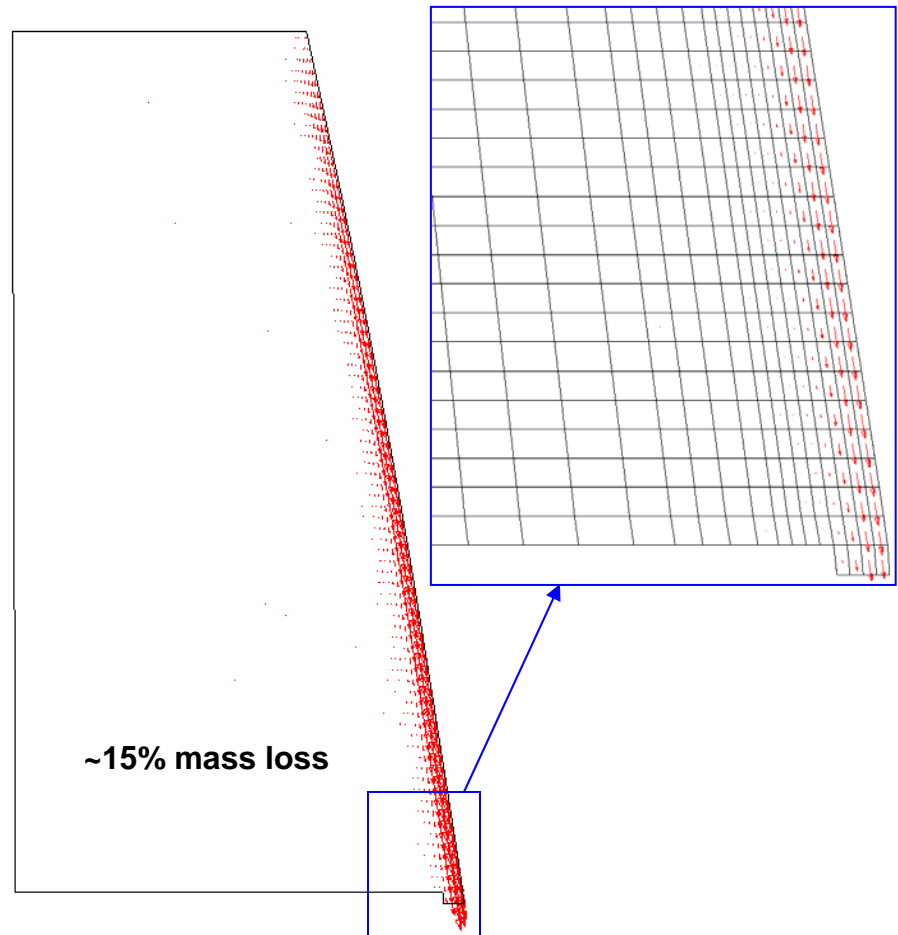
- ⊕ Time interval between movie frames: 5 seconds
- ⊕ Model 2 (Case 2D) has a much larger optical thickness than that in Model 1, which leads to
 - ⊖ deeper penetration of incident heat flux below the surface
 - ⊖ thicker melting layer and slower melting process
 - ⊖ large amount of material bulge over the bottom lip and causes the calculation to diverge



Example: Velocity Vectors at $t = 300$ sec (zoom to 200% for better viewing)



Case 2A (PP702, heat loss only)

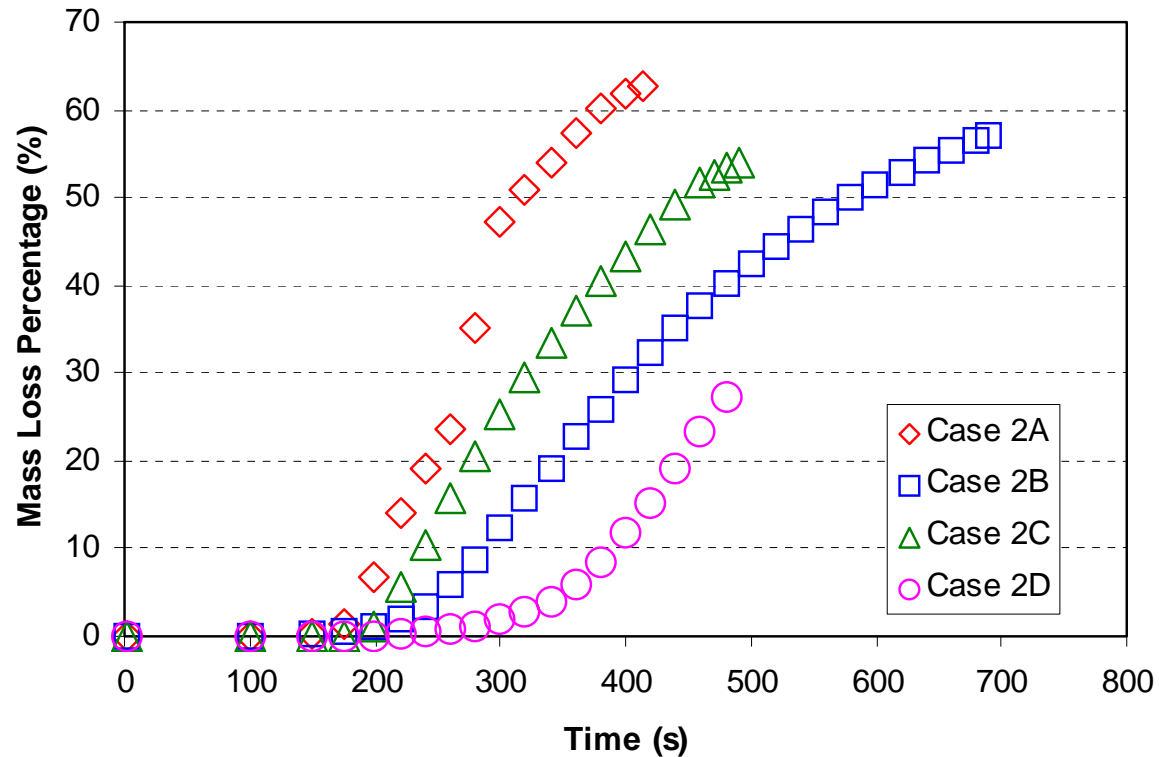


Case 2B (PP702, heat loss + in-depth absorption)

⊕ The addition of in-depth absorption leads to

- ⊖ slower melting process
- ⊖ thicker melting layer below free surface

Mass Loss as Function of Time

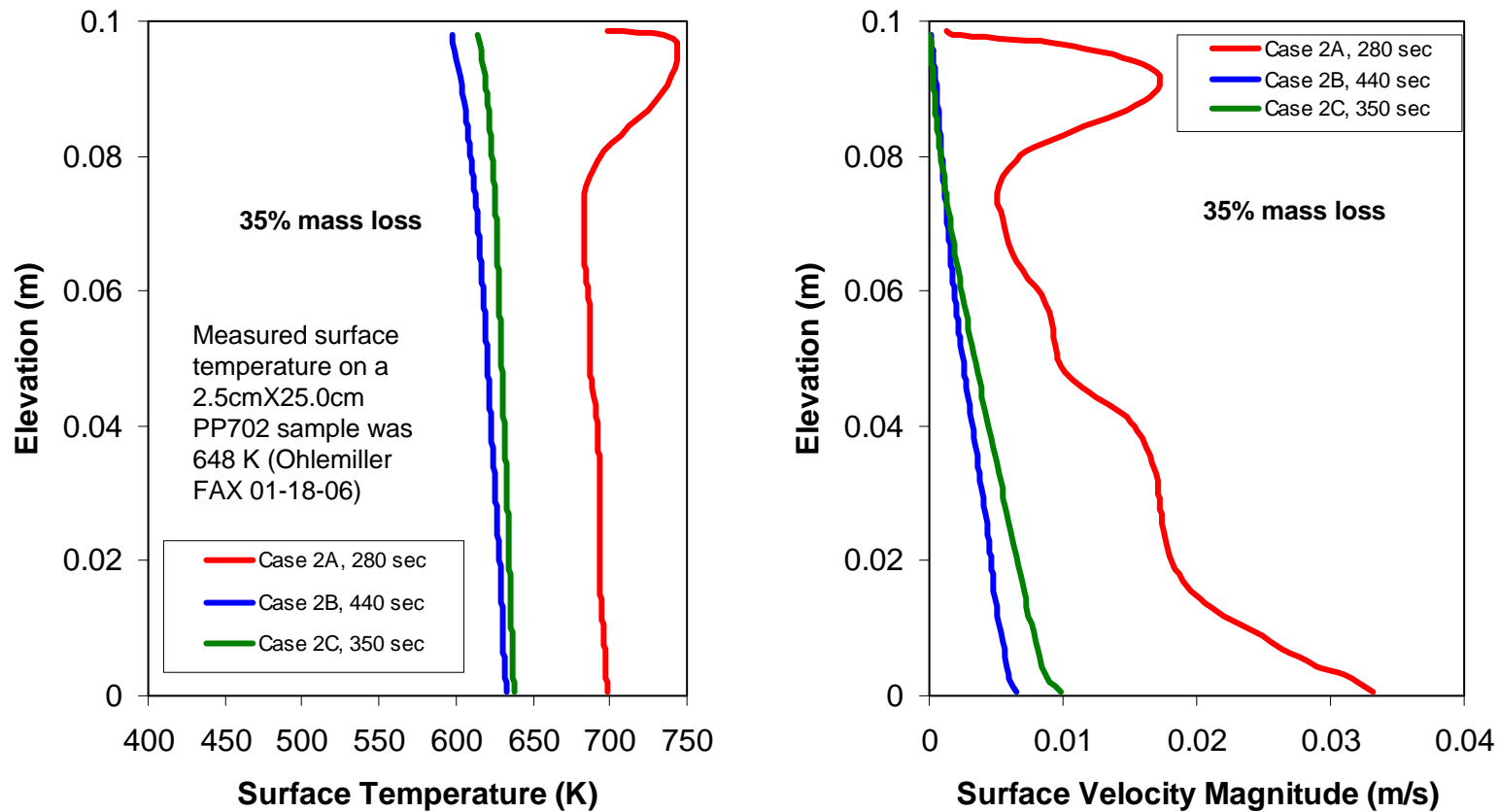


Grid	"steady state" Mass Loss Rate	Comments
Case 2A	36.0*	Computed from 200 s to 300 s,
Case 2B	11.2*	Computed from 220 s to 660 s
Case 2C	18.0*	Computed from 220 s to 440 s
Case 2D	14.8*	Computed from 340 s to 480 s
Experiment	0.15** +	Ohlemiller FAX 01-18-06

* per unit length (g/s m) ** g/s + measured on a 2.5cmX25.0cm PP702 sample



Example: Surface Temperature and Velocity Magnitude



Surface temperature and velocity magnitude profiles at 35% mass loss

- ⊕ Velocity magnitudes approach zero at upper no slip wall
- ⊕ Temperature monotonically distributed along the surface in Case 2B and 2C
- ⊕ Inclusion of in-depth absorption decreases surface temperature and velocity
- ⊕ Over-heating ($T > 698\text{K}$) occurs in Case 2A at upper portion of the free surface
- ⊕ Case 2C has higher surface temperature and velocity than Case 2B due to low viscosity



Summary

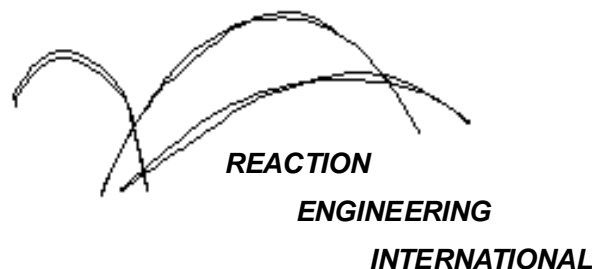
- ⊕ Studied Two Resins with Heat Losses and In-depth Absorption of Heat Flux
- ⊕ Most Cases were run to at least 50% mass loss
 - ⊕ Calculation becomes extremely slow when mass loss exceeds 50%
 - ⊕ One case (Case 2D) diverged at 27% mass loss due to large optical thickness considered
 - ⊕ One case (Case 2E) is in progress using fitted absorption coefficient data
- ⊕ Computational Cost highlighted
 - ⊕ Less expensive than Task 1
 - ⊕ Smaller computational domain
 - ⊕ Larger time step due to lower velocity caused by heat losses and in-depth absorption
- ⊕ Model features highlighted
 - ⊕ Heat loss models and in-depth absorption models
 - ⊕ Impacts of different models on melting processes
 - ⊕ Solutions at selected times
 - ⊕ Velocity field resolution across melt boundary layer
- ⊕ Example Results
 - ⊕ Free surface location, temp., velocity - selected times
 - ⊕ Movie of free surface location and temperature
 - ⊕ Mass loss, surface temperature, surface velocity, and comparison with experimental data



A Computational Model For Fire Growth and Spread On Thermoplastic Objects

**Task 2: 2D model with steady heat flux, radiative
and convective heat losses, and in-depth
absorption of radiative heat flux**

(6/01/06)



Outline

⊕ Radiative and convective heat loss, In-depth absorption models

- ⊕ Only impacts energy equation
- ⊕ Both radiative and convective heat losses are only applied to the free surface
- ⊕ A heat source term is added to the energy equation to account for in-depth absorption.
- ⊕ Absorption coefficient is a function of the distance from the free surface

⊕ Absorption coefficient models

- ⊕ In-depth absorption coefficient data for one polymer resin provided by NIST
 - ⊕ Email sent by Kathy to Bockelie on 2/22/2006
 - ⊕ Data applicable to PP23K in the HIFT apparatus
- ⊕ Three models constructed based on the NIST data

⊕ Cases studied

- ⊕ Computational grid
- ⊕ Case summary
- ⊕ Example results:
 - ⊕ Free surface location, temp., velocity
 - ⊕ Mass loss, surface temperature, surface velocity, and comparisons with data

⊕ Summary



Heat loss and In-depth absorption models

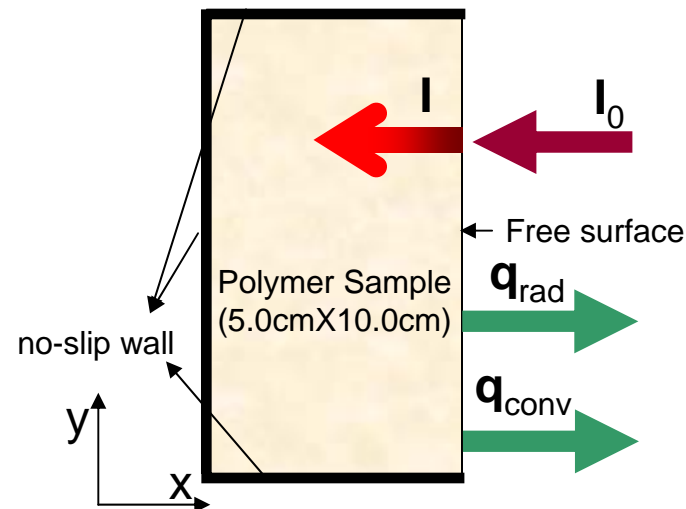


Figure 1, Sketch of in-depth absorption and heat loss model

⊕ Energy equation source terms due to in-depth absorption, radiative and convective heat losses

- ⊕ In-depth absorption: $\dot{q}_{\text{absorption}} = \int_{\Omega} \frac{dI}{dx} d\Omega$, assuming absorption process in x-direction only
- ⊕ Radiative heat loss: $\dot{q}_{\text{radiation}} = -A\epsilon\sigma(T^4 - T_0^4)$, assuming radiative heat loss only on free surface
- ⊕ Convective heat loss: $\dot{q}_{\text{convection}} = -Ah_{\text{conv}}(T - T_0)$

⊕ Parameters: A – surface area; Ω - volume; ϵ - emissivity (=1.0); σ - Stefan-Boltzmann Constant (=5.67e-8); T_0 – ambient temperature (=298 K); h_{conv} – convective heat transfer coefficient (= 8.0)

⊕ A heat sink term is added to the energy equation to prevent overheating (i.e., $T > 750\text{K}$)

⊕ The models are implemented in subroutine ***fbck_bc_sca***



Absorption Coefficient Models

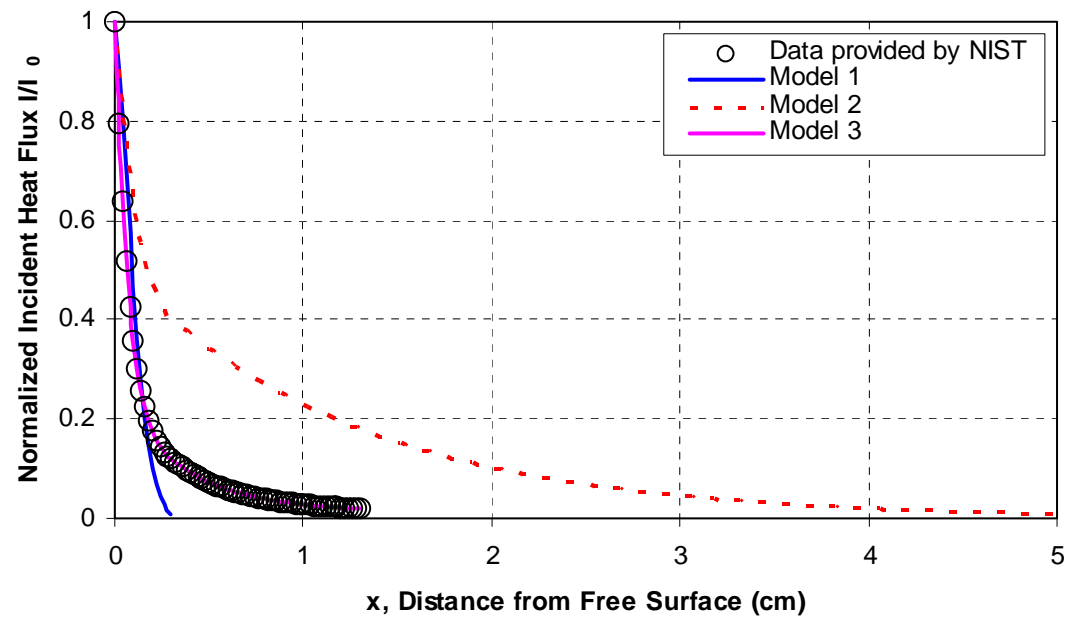


Figure 2, Incident heat flux distribution in the horizontal direction

⊕ Original data (symbols in Figure 2) is roughly applicable to the PP23K resin at the HIFT apparatus

$$\Phi \begin{cases} I/I_0 = 10^{(-5.17x + 6.964x^2)}, & 0 \leq x < 0.3 \text{ (cm)} \\ I/I_0 = 10^{(-0.5154 - 1.473x + 0.4339x^2)}, & 0.3 \leq x < 1.3 \text{ (cm)} \end{cases}$$

• Three incident heat flux distribution functions are used in the CFD model

• Model 1 is differentiable, and all models are well defined over the entire thickness of the sample

• Model 1: $I/I_0 = \exp(-3.843x - 38.36x^2)$, $0 \leq x \leq 3.0$ (cm)

• Model 2: $\begin{cases} I/I_0 = \exp(-5.17x + 6.964x^2), & 0 \leq x < 0.3 \text{ (cm)} \\ I/I_0 = \exp(-0.6814 - 0.7802x - 0.009333x^2), & 0.3 \leq x < 5.0 \text{ (cm)} \end{cases}$

• Model 3: use the original fitted data



Computational Grid

- ⊕ Polymer sample dimension:
5.0cm X 10.0cm
- ⊕ 30X80 Grid (biased)
- ⊕ Initial grid resolution the same
as the 19X200 grid used in
Task 1
- ⊕ Equivalent to 100X80 grid if
using uniform grid spacing and
fixed grid

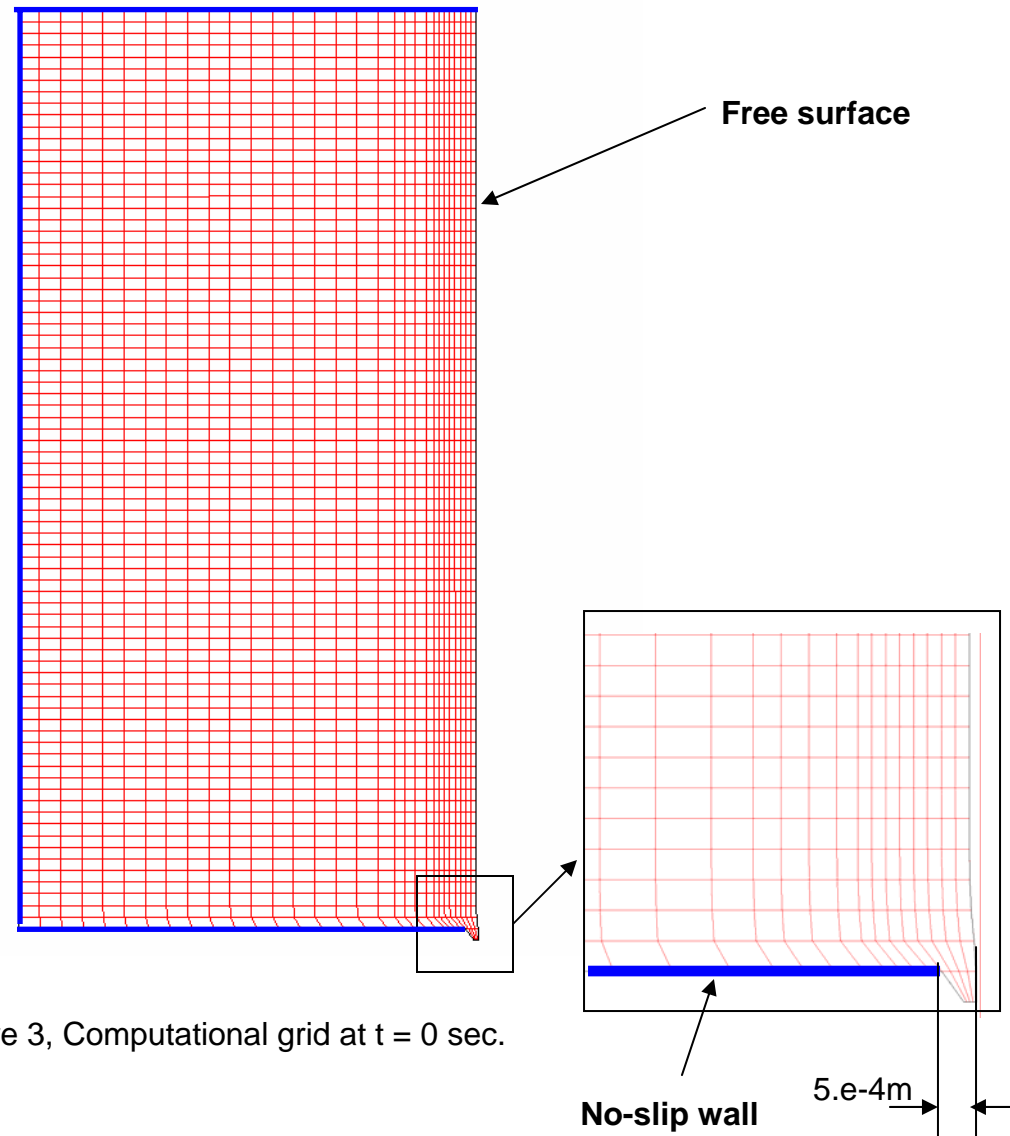


Figure 3, Computational grid at t = 0 sec.

Case Summary

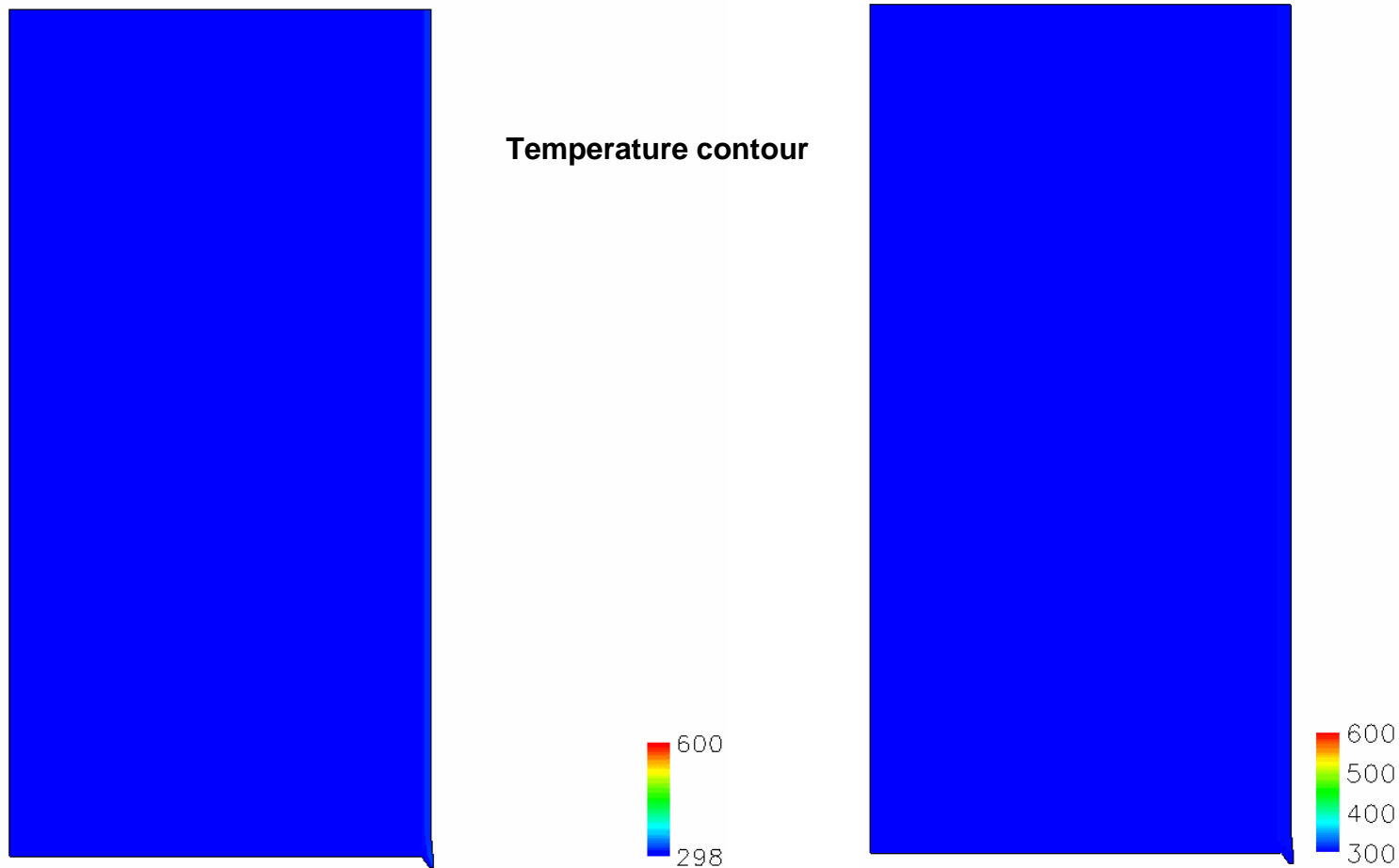
⊕ All cases are run with a external Incident heat flux of 30KW/m²

Case	Polymer Resin	Radiative and Convective Heat Losses	In-depth Absorption	In-depth Absorption Coefficient Model	Mass Loss and Elapsed Time	Estimated CPU Time	Case Status
Case 2A	PP702	Included	Not included	N/A	65%, 400 sec	~ 48 h	Stopped*
Case 2B	PP702	Included	Included	Model 1	58%, 650 sec	~ 30 h	Stopped*
Case 2C	PP6523	Included	Included	Model 1	55%, 460 sec	~ 16 h	Stopped*
Case 2D	PP702	Included	Included	Model 2	27%, 480 sec	~ 2 h	Diverged
Case 2E	PP702	Included	Included	Model 3	55%, 700 sec	~ 21 h	Stopped*
Case 2F	PP6523	Included	Included	Model 3	57%, 570 sec	~ 7 h	Stopped*

* Manually stopped because calculation become extremely slow when mass loss exceeds 50%



Impact of In-depth Absorption on Melting Process



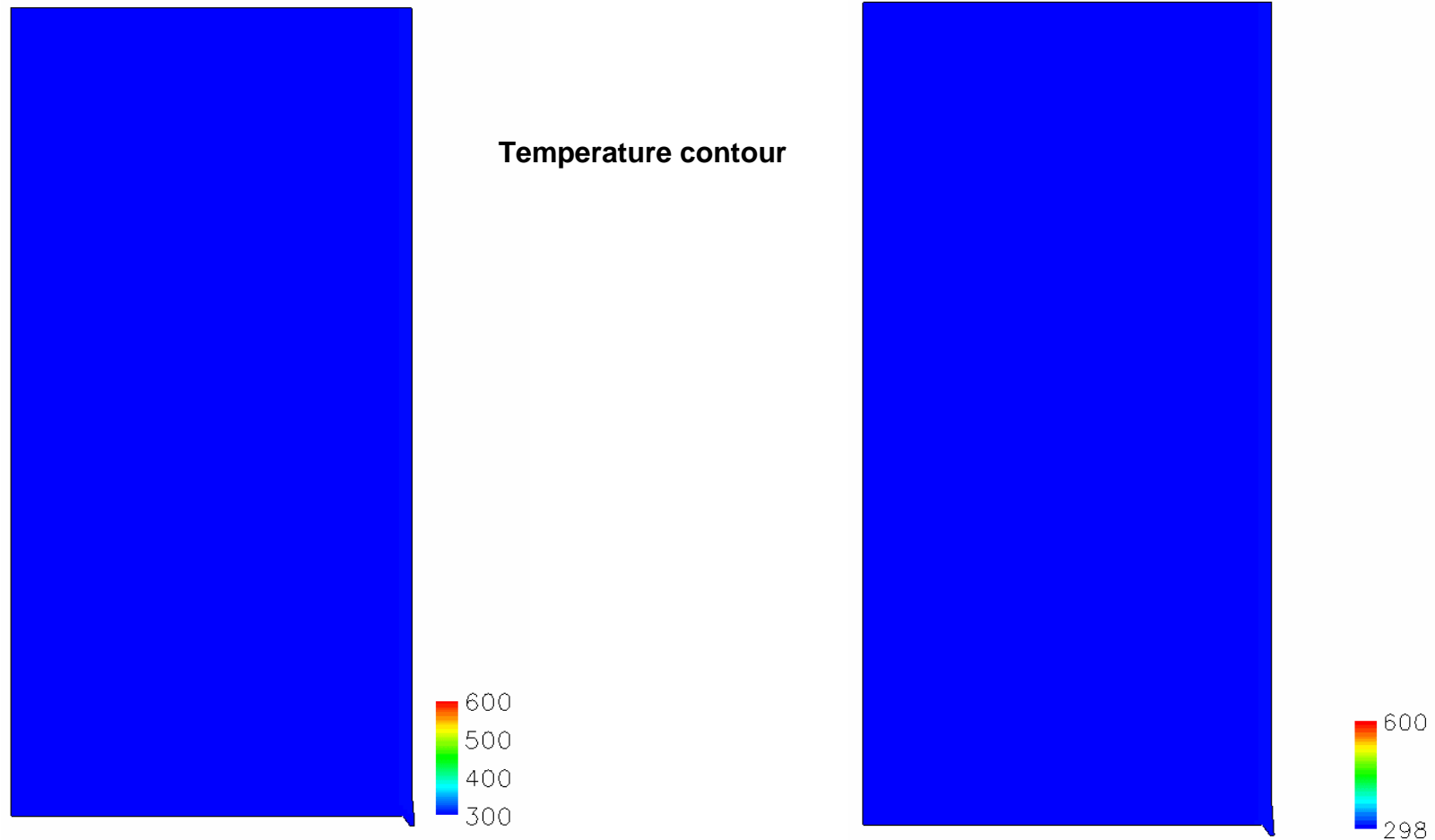
Case 2A (PP702, heat loss only)

Case 2B (PP702, heat loss + in-depth absorption)

- ⊕ Time interval between movie frames: 5 seconds
- ⊕ The inclusion of in-depth absorption leads to significant difference in shape change history
 - ⊖ Melting process slows down
 - ⊖ Upper free surface moves much slower towards the back wall
 - ⊖ Melting layer becomes thicker



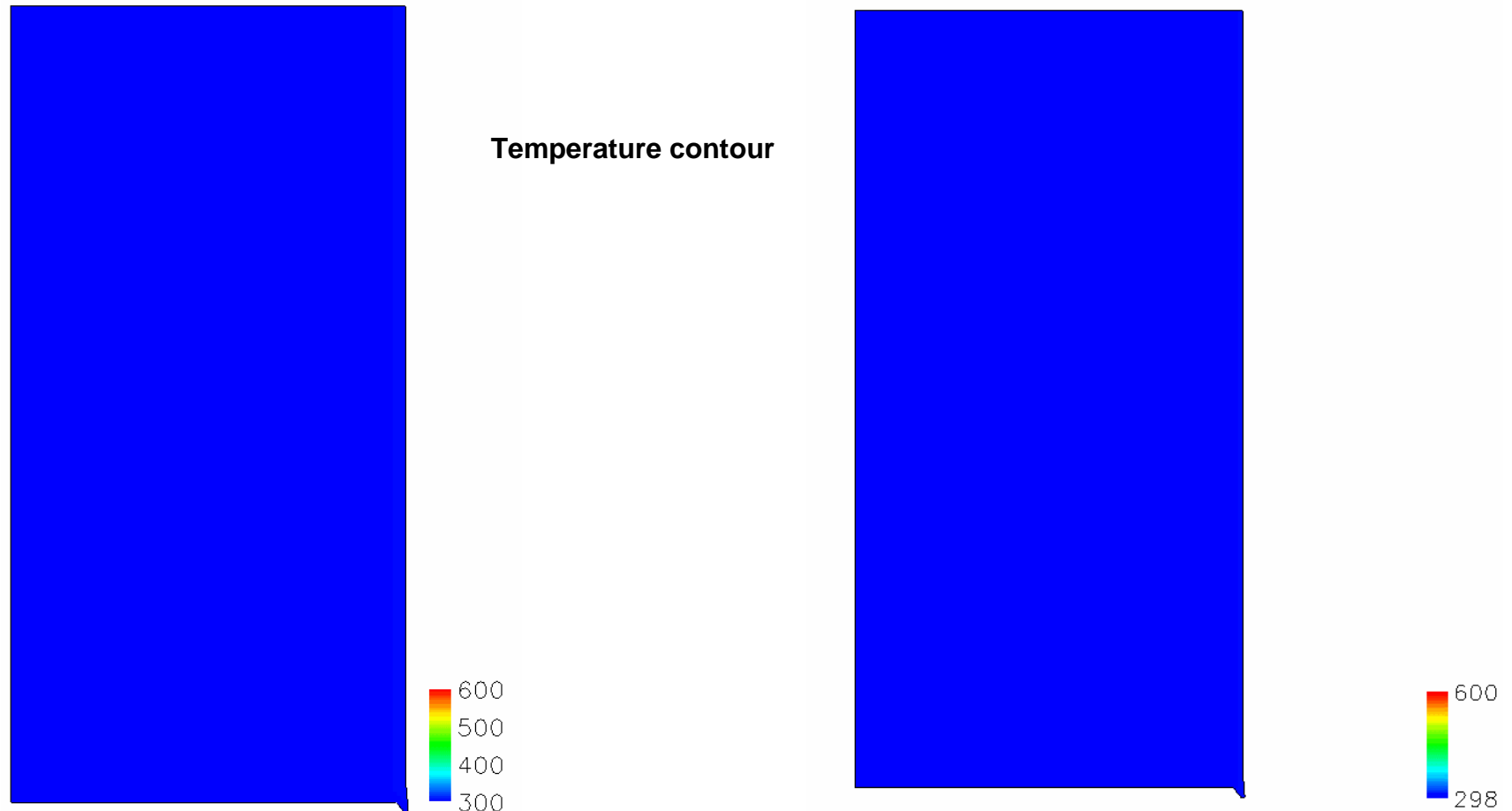
Impact of Different Resin on Melting Process



- ⊕ Time interval between movie frames: 5 seconds
- ⊕ PP6523 has a much lower viscosity at high temperature, which leads to faster melting process



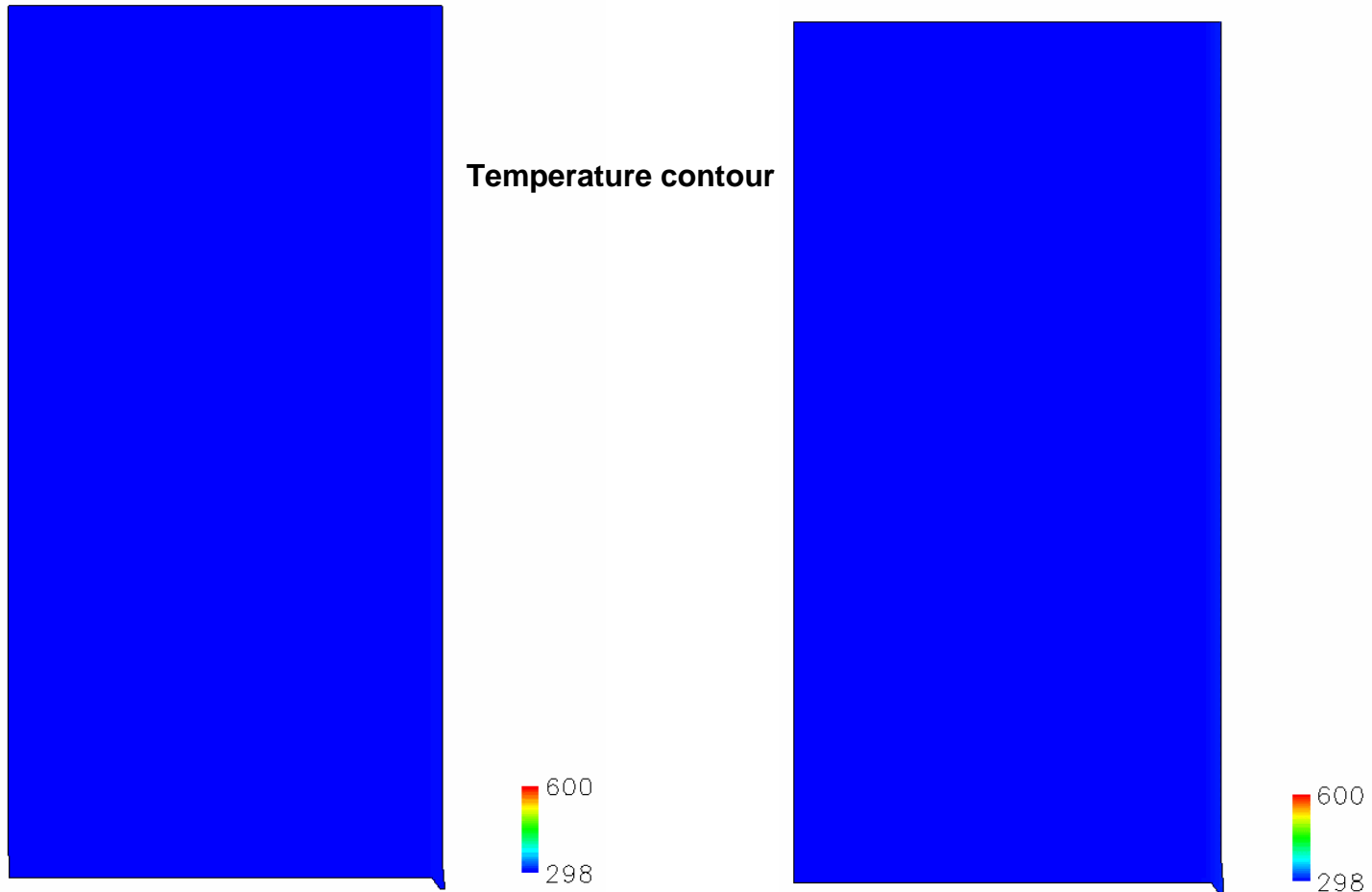
Impact of Different Absorption Coefficient Models



- ⊕ Time interval between movie frames: 5 seconds
- ⊕ Model 2 (Case 2D) has a much larger optical thickness than that in Model 1, which leads to
 - ⊖ deeper penetration of incident heat flux below the surface
 - ⊖ thicker melting layer and slower melting process
 - ⊖ large amount of material bulge over the bottom lip and causes the calculation to diverge



Impact of Different Absorption Coefficient Models



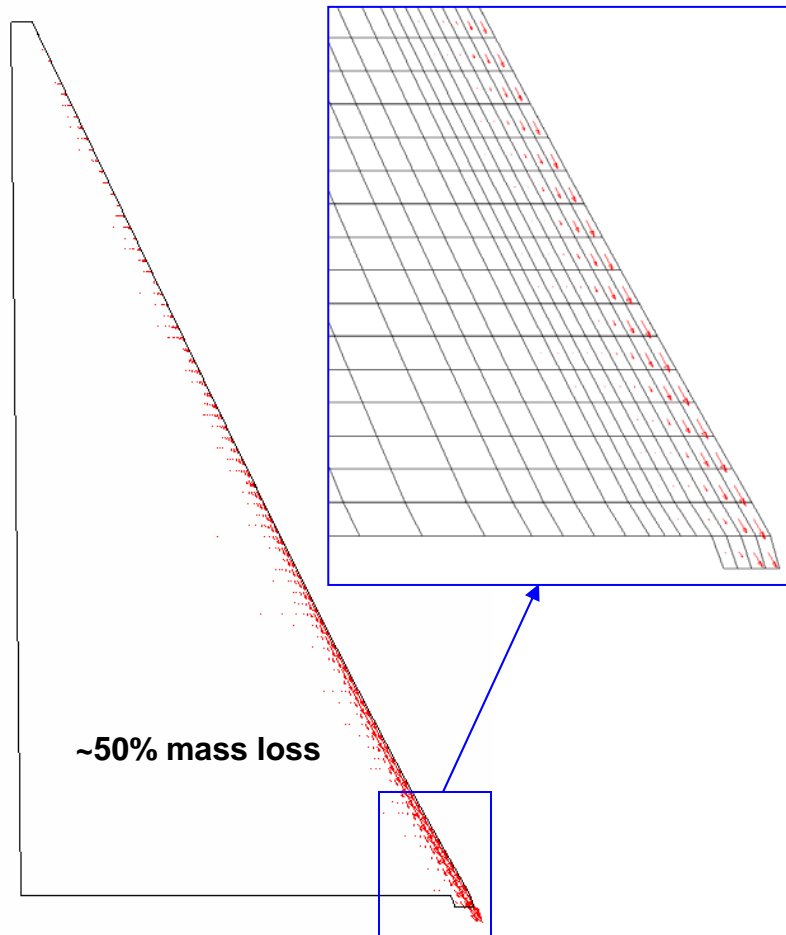
Case 2E (PP702, in-depth absorption model 3)

Case 2F (PP6523, in-depth absorption model 3)

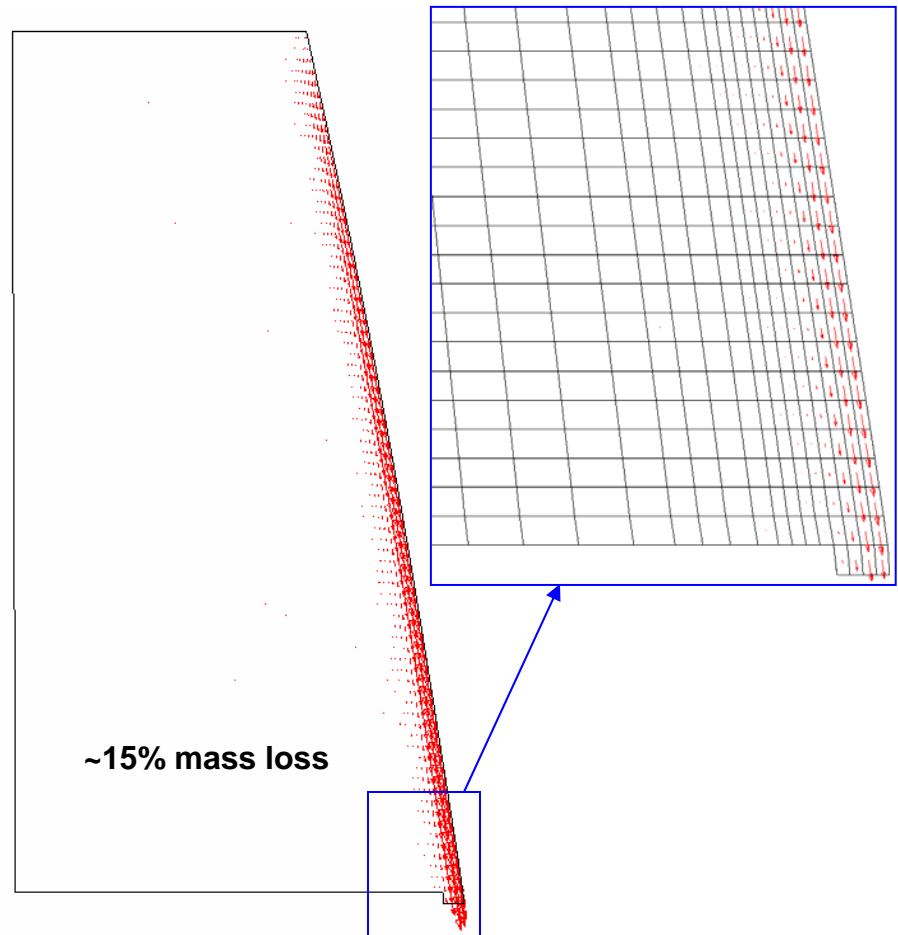
⊕ Time interval between movie frames: 5 seconds



Example: Velocity Vectors at $t = 300$ sec (zoom to 200% for better viewing)



Case 2A (PP702, heat loss only)

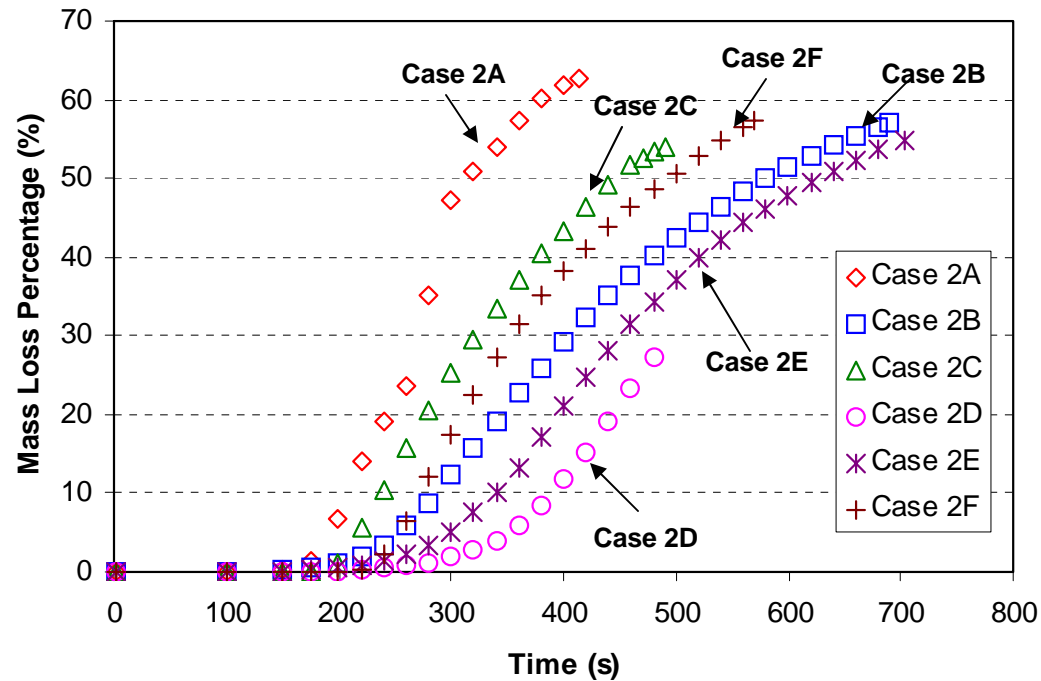


Case 2B (PP702, heat loss + in-depth absorption)

⊕ The addition of in-depth absorption leads to

- ⊖ slower melting process
- ⊖ thicker melting layer below free surface

Mass Loss as Function of Time



Grid	“steady state” Mass Loss Rate	Comments
Case 2A	18.0*	Computed from 200 s to 300 s,
Case 2B	5.6*	Computed from 220 s to 660 s
Case 2C	9.0*	Computed from 220 s to 440 s
Case 2D	7.4*	Computed from 340 s to 480 s
Case 2E	5.3*	Computed from 260 s to 700 s
Case 2F	8.8*	Computed from 250 s to 560 s
Experiment	0.15** +	Ohlemiller FAX 01-18-06

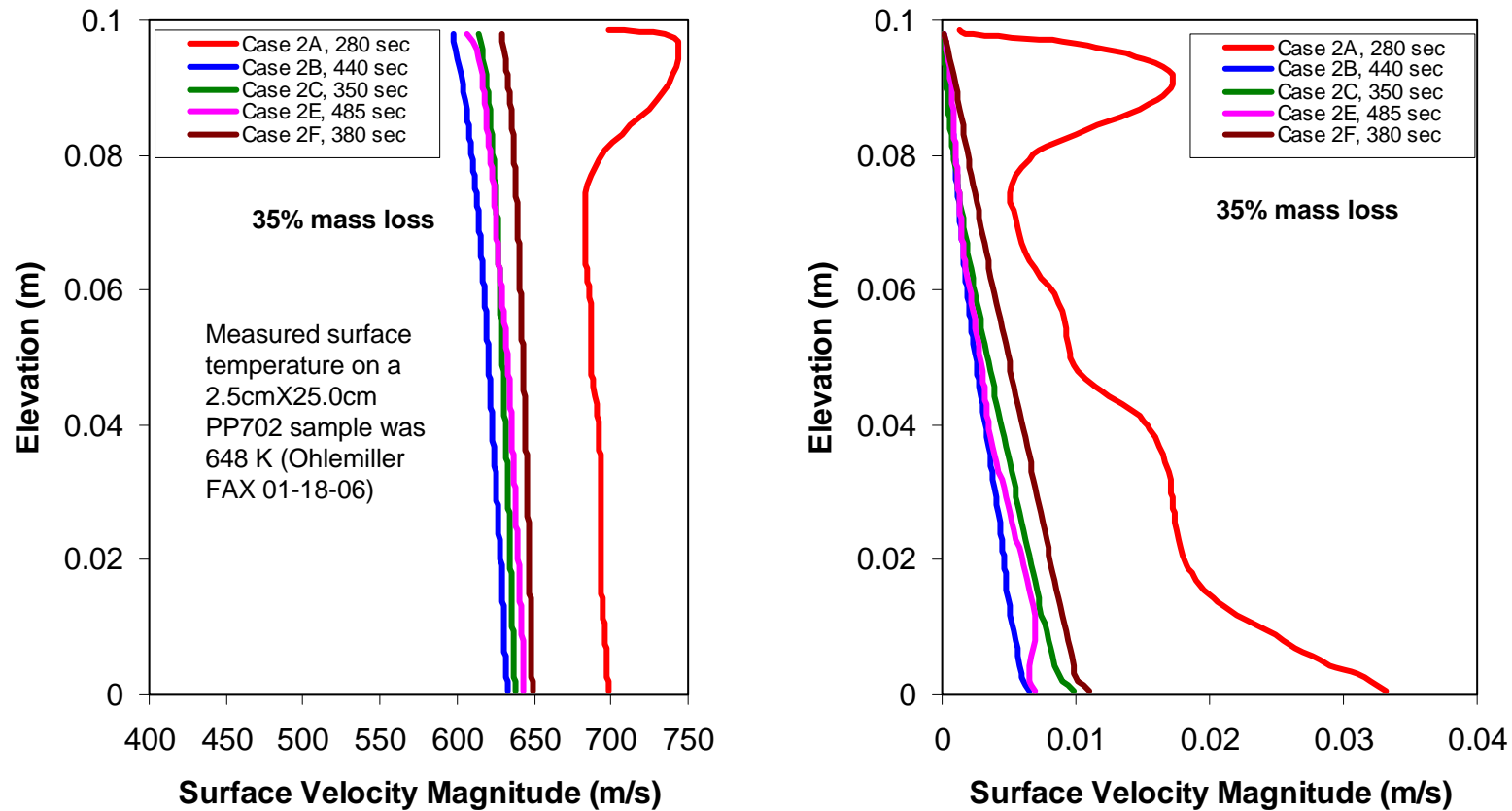
* per unit length (g/s m)

** g/s

+ measured on a 2.5cmX25.0cm PP702 sample



Example: Surface Temperature and Velocity Magnitude



Surface temperature and velocity magnitude profiles at 35% mass loss

- ⊕ Velocity magnitudes approach zero at upper no slip wall
- ⊕ Temperature monotonically distributed along the surface in Case 2B, 2C, 2E, and 2F
- ⊕ Inclusion of in-depth absorption decreases surface temperature and velocity
- ⊕ Over-heating ($T > 698\text{K}$) occurs in Case 2A at upper portion of the free surface

Summary

- ⊕ Studied Two Resins with Heat Losses and In-depth Absorption of Heat Flux
- ⊕ Most Cases were run to at least 50% mass loss
 - ⊕ Calculation becomes extremely slow when mass loss exceeds 50%
 - ⊕ One case (Case 2D) diverged at 27% mass loss due to large optical thickness considered
 - ⊕ One case (Case 2E) is in progress using fitted absorption coefficient data
- ⊕ Computational Cost highlighted
 - ⊕ Less expensive than Task 1
 - ⊕ Smaller computational domain
 - ⊕ Larger time step due to lower velocity caused by heat losses and in-depth absorption
- ⊕ Model features highlighted
 - ⊕ Heat loss models and in-depth absorption models
 - ⊕ Impacts of different models on melting processes
 - ⊕ Solutions at selected times
 - ⊕ Velocity field resolution across melt boundary layer
- ⊕ Example Results
 - ⊕ Free surface location, temp., velocity - selected times
 - ⊕ Movie of free surface location and temperature
 - ⊕ Mass loss, surface temperature, surface velocity, and comparison with experimental data

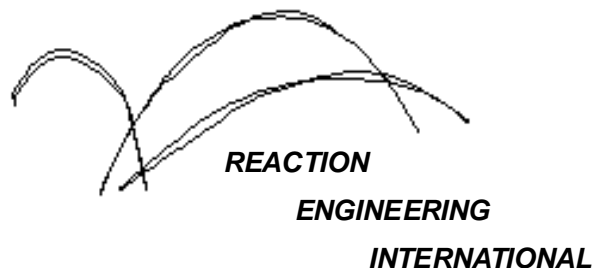


A Computational Model For Fire Growth and Spread On Thermoplastic Objects

Investigating Impact of Different Moving
Boundary Tracking Schemes on Predicted
Melting Behaviors

Contract No. SB1341-05-C-0041

06/22/2006

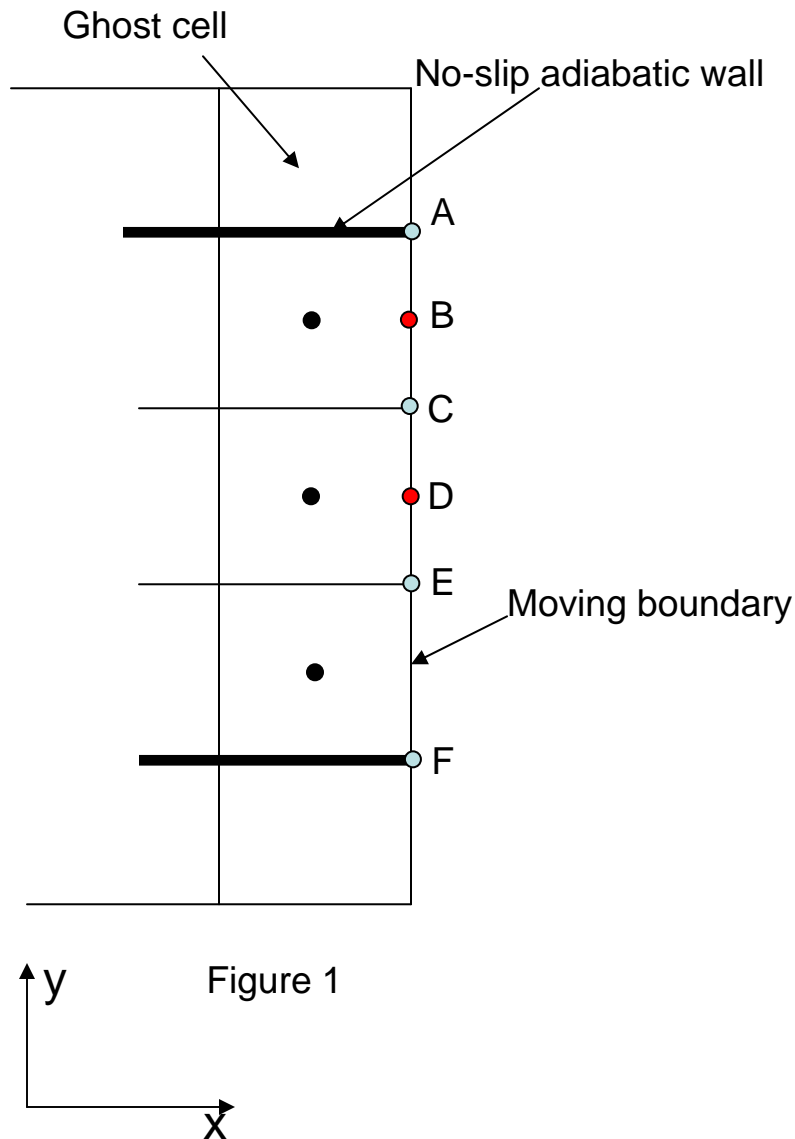


Outline

- Models for moving boundary tracking
- Slumping problem with zero heat flux
- Melting behaviors using different tracking models



Models for tracking moving boundary location



- The shape and location of moving boundary are represented by grid point ACEF in Figure 1
- The algorithm for determining moving boundary after each time step is described below (**Model 1**):

- calculating new face center locations, for example

$$x_D^{new} = x_D^{old} + \frac{\dot{m}_D}{\rho A_{CE}} \Delta t$$

- calculating new grid vertex point location, for example

$$x_C = \frac{1}{2} (x_B^{new} + x_D^{new})$$

- Constrain grid vertex point to no-slip wall:

$$x_A = x_C$$

- Smooth moving boundary:

$$x_c^{new} = \frac{1}{4} (x_A + 2x_C + x_E)$$

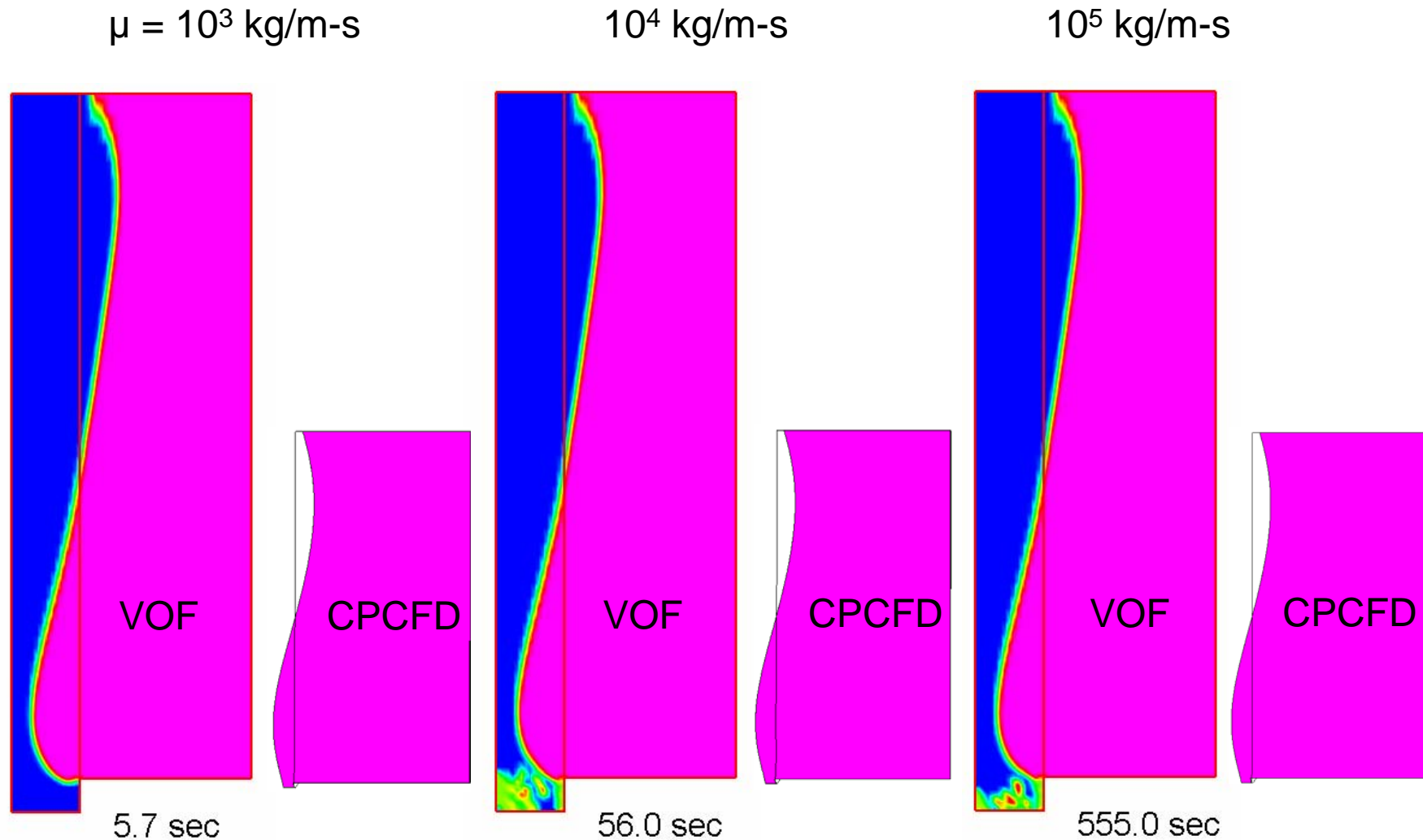
- To investigate the impact of the model on tracking moving boundary location, two more models are created:

- Model 2:** $x_A = x_B^{new}$ in step 3
- Model 3:** step 1-4 above then re-apply constraint on wall point: $x_A^{new} = x_C^{new}$

- No-slip wall boundary affects the solution of the mass flux across the face center on the moving boundary, but has no direct impact on the movement of point A



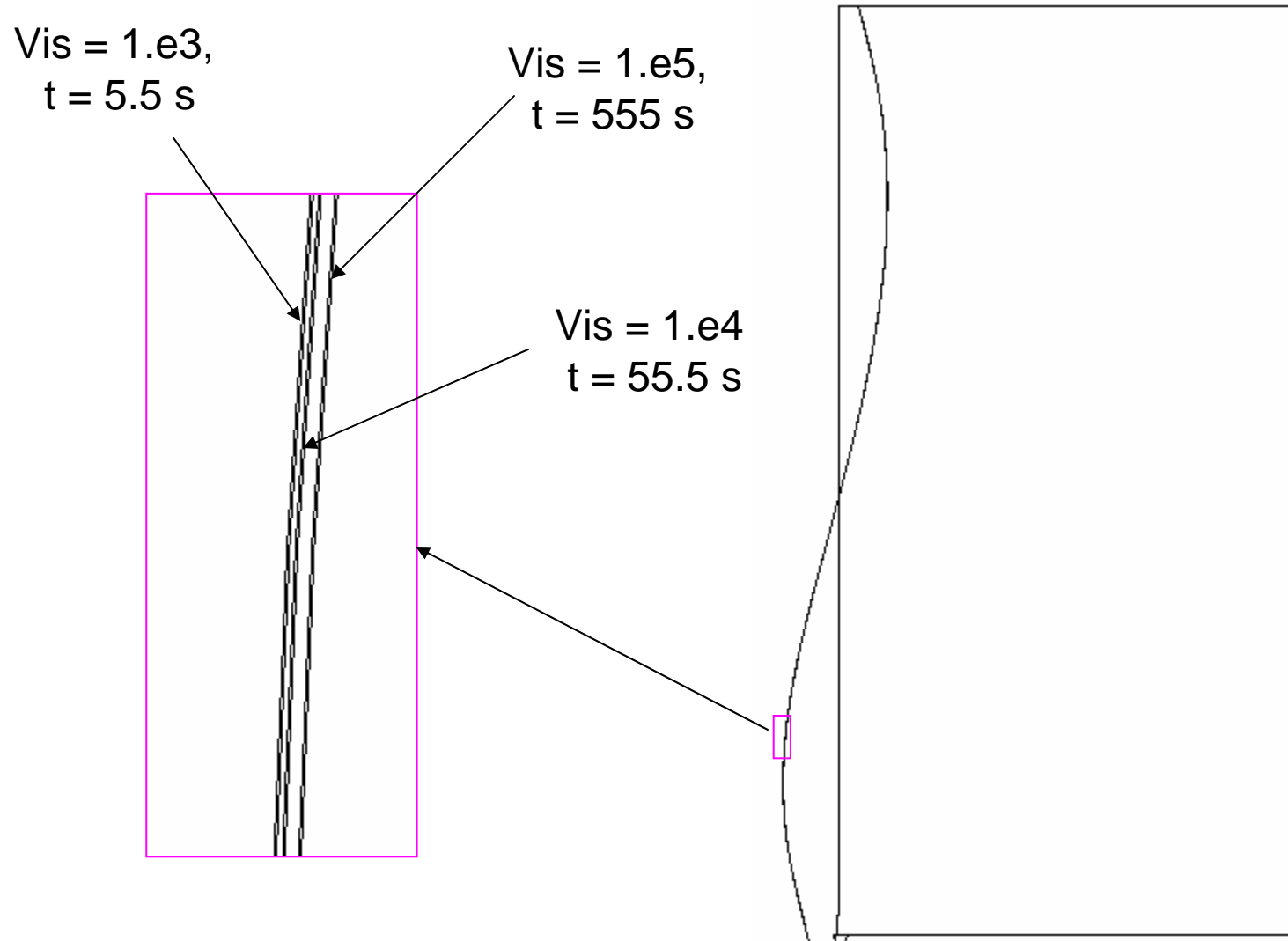
Slumping behavior as a function of viscosity



- External incident heat flux is set to zero in the CPCFD simulations
- Model 1 for tracking moving boundary is used in all CPCFD simulations



Slumping behavior as a function of viscosity

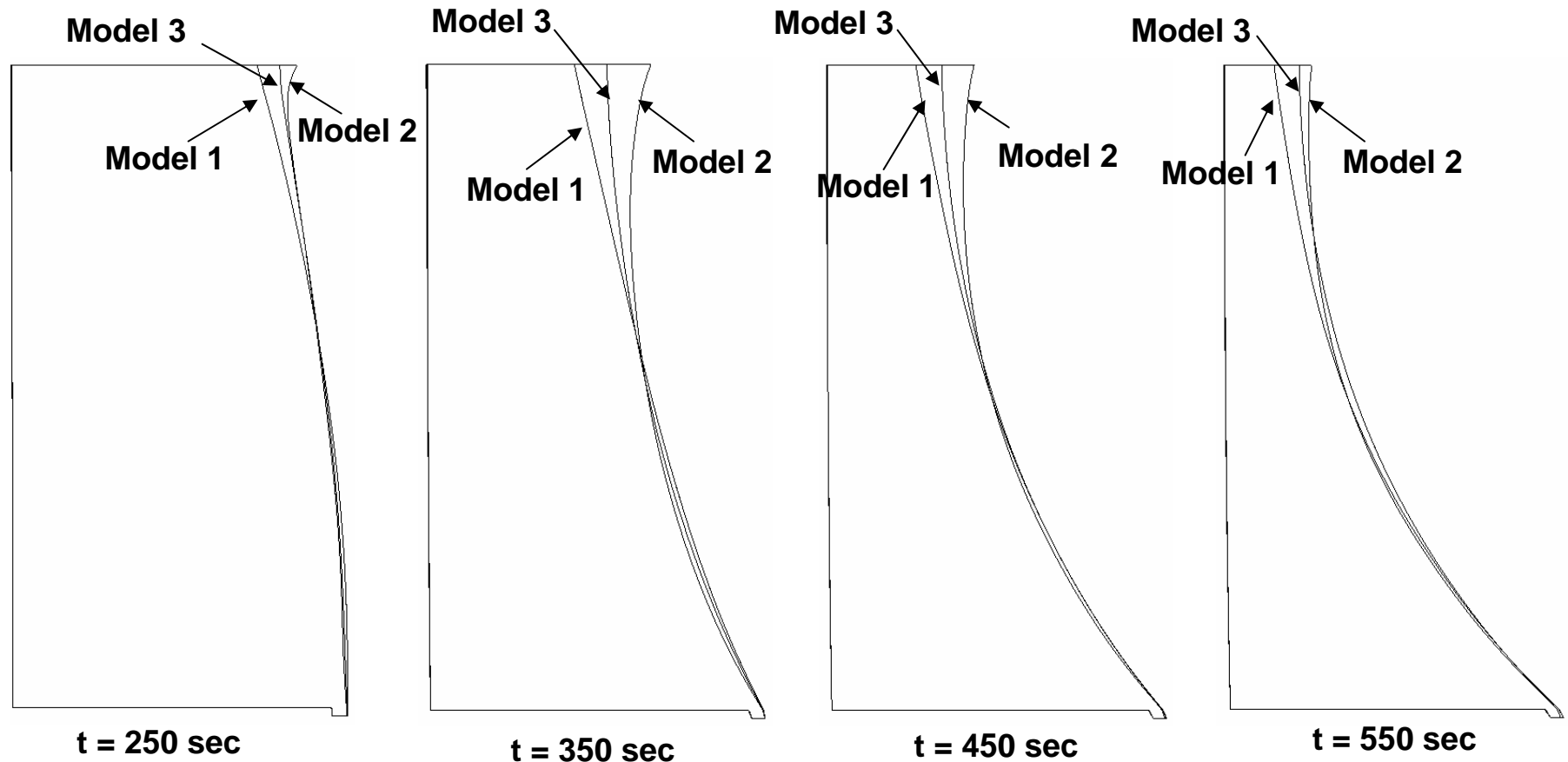


- External incident heat flux is set to zero in the CPCFD simulations
- Model 1 of tracking moving boundary is used in all CPCFD simulations
- Similarity solutions have been achieved



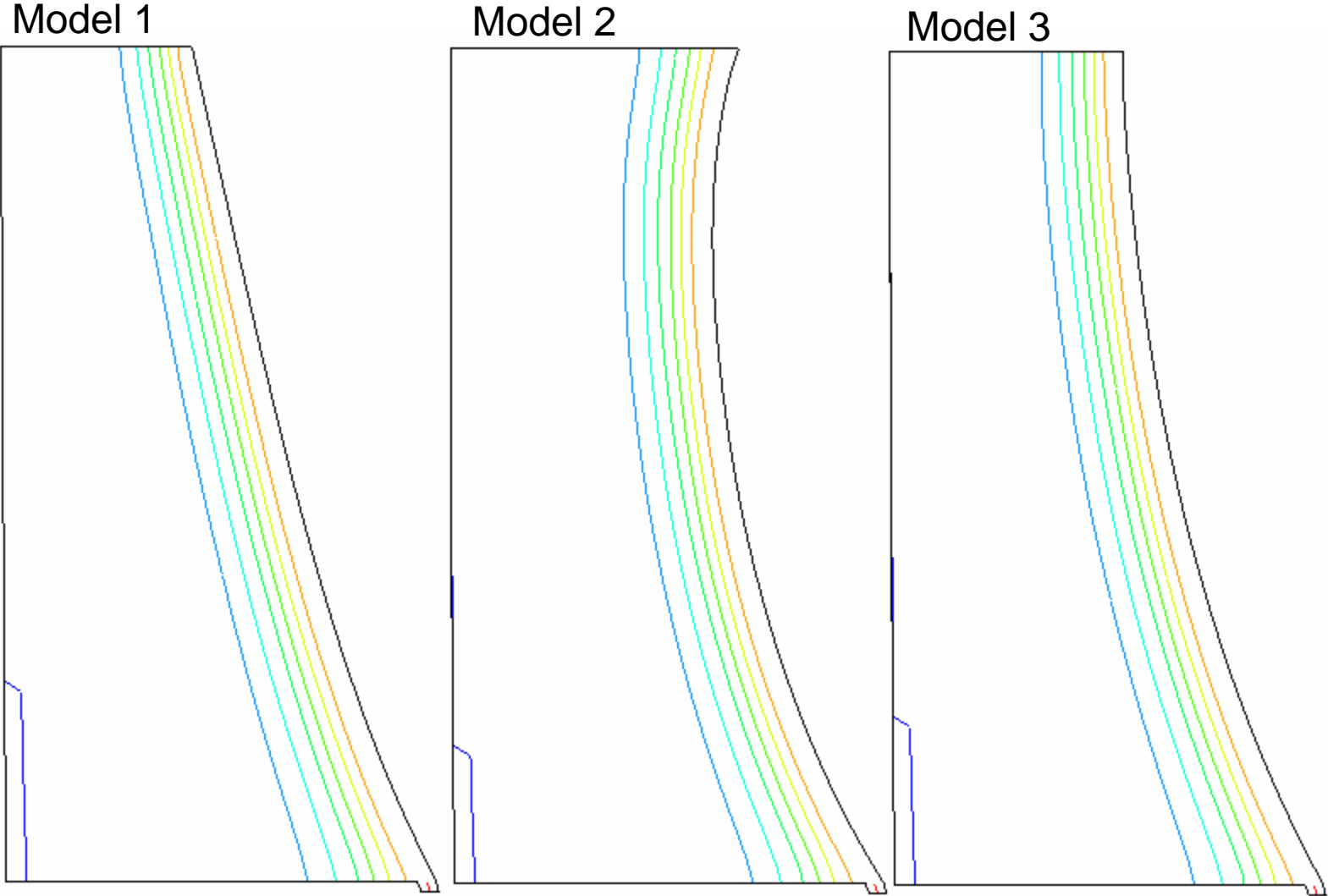
Melting behavior with 30KW/m² Heat Flux

PP6523



- The movement of the moving boundary at the top in Model 2 is significantly slower than that in Model 1. This is because, in Model 2 (see figure 1), the movement of point A is approximated by point B rather than point C in model 1. Point B is halfway closer to the no-slip wall than point C.
- The different melting behaviors of Model 1 and Model 3 are caused by the surface smoothing process.

Temperature Contour

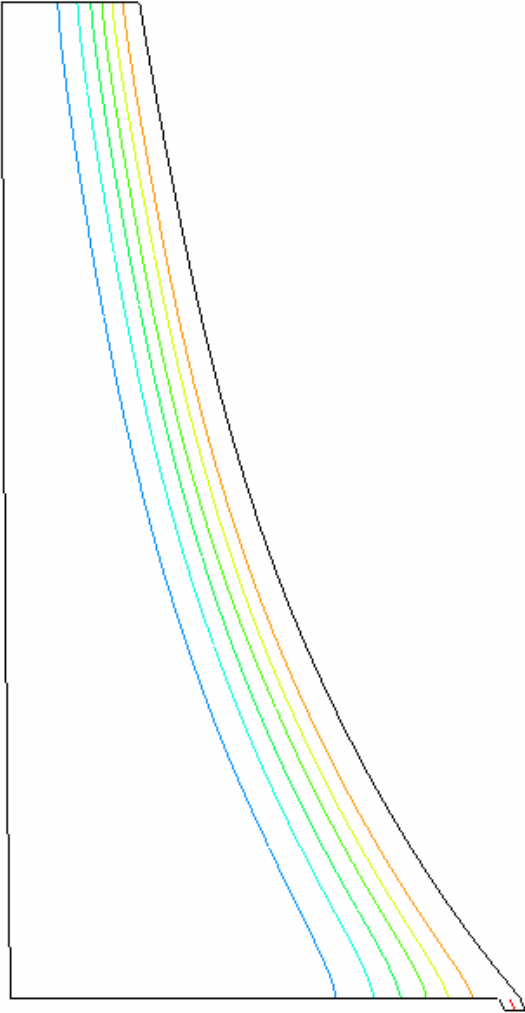


Contours drawn using only the interior cell center values $T = 350 \text{ sec}$

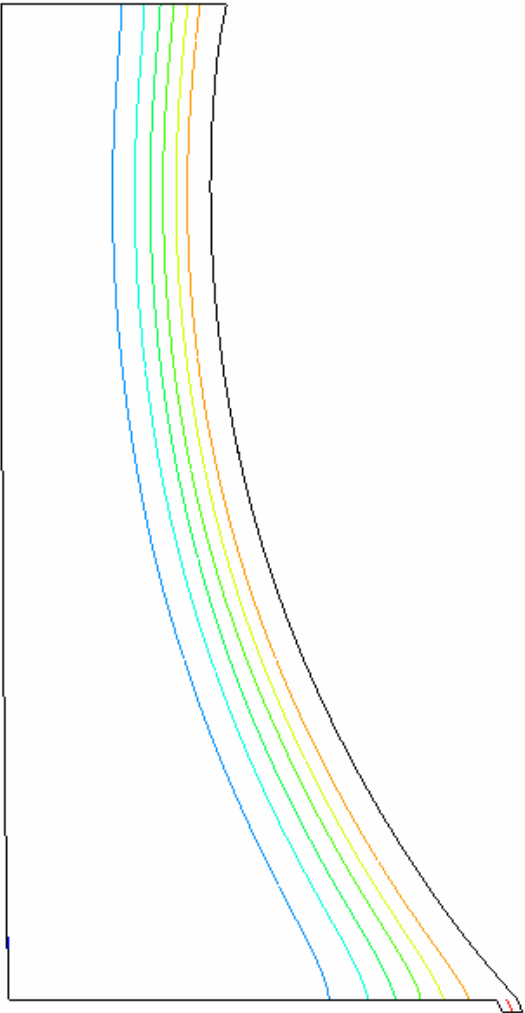


Temperature Contour

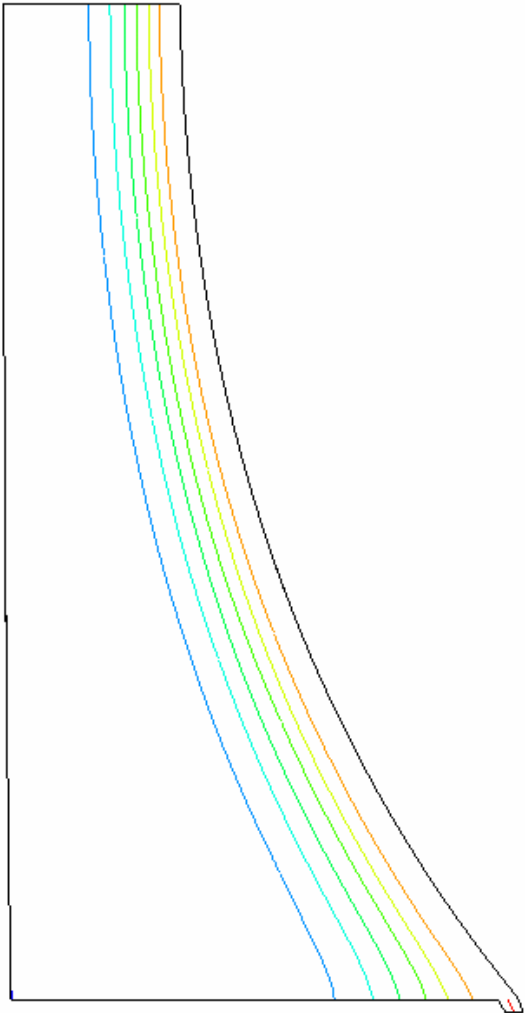
Model 1



Model 2



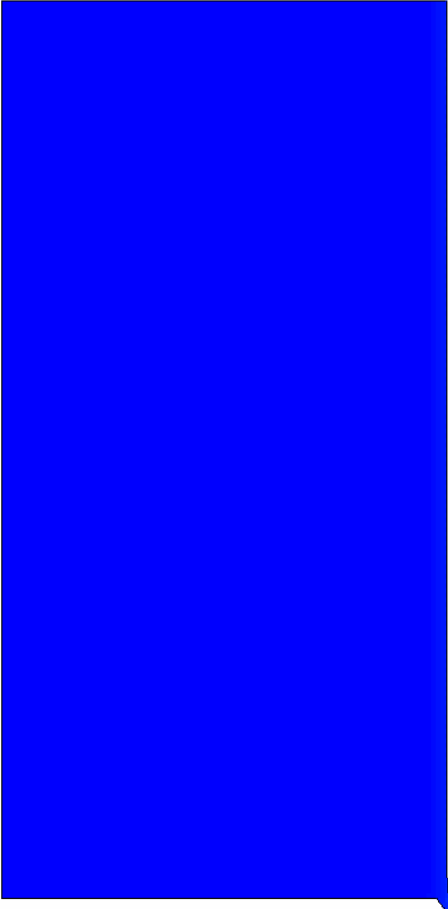
Model 3



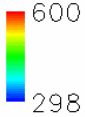
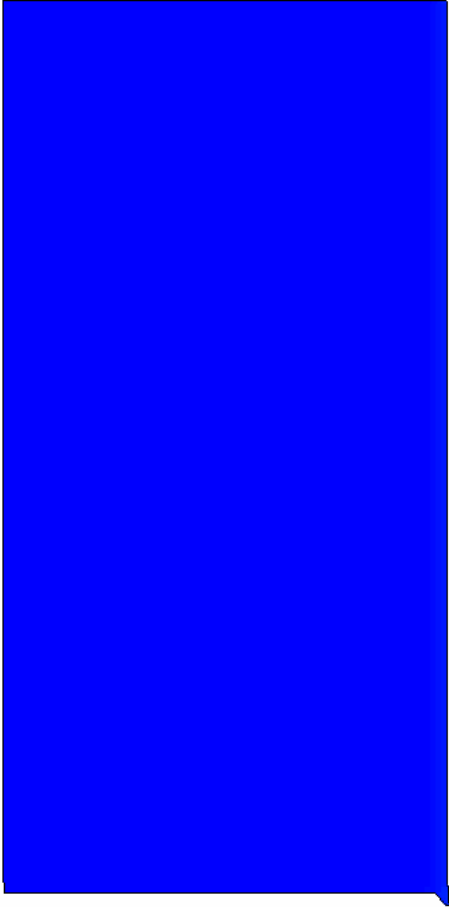
Contours drawn using only the interior cell center values $T = 450 \text{ sec}$



Model 1



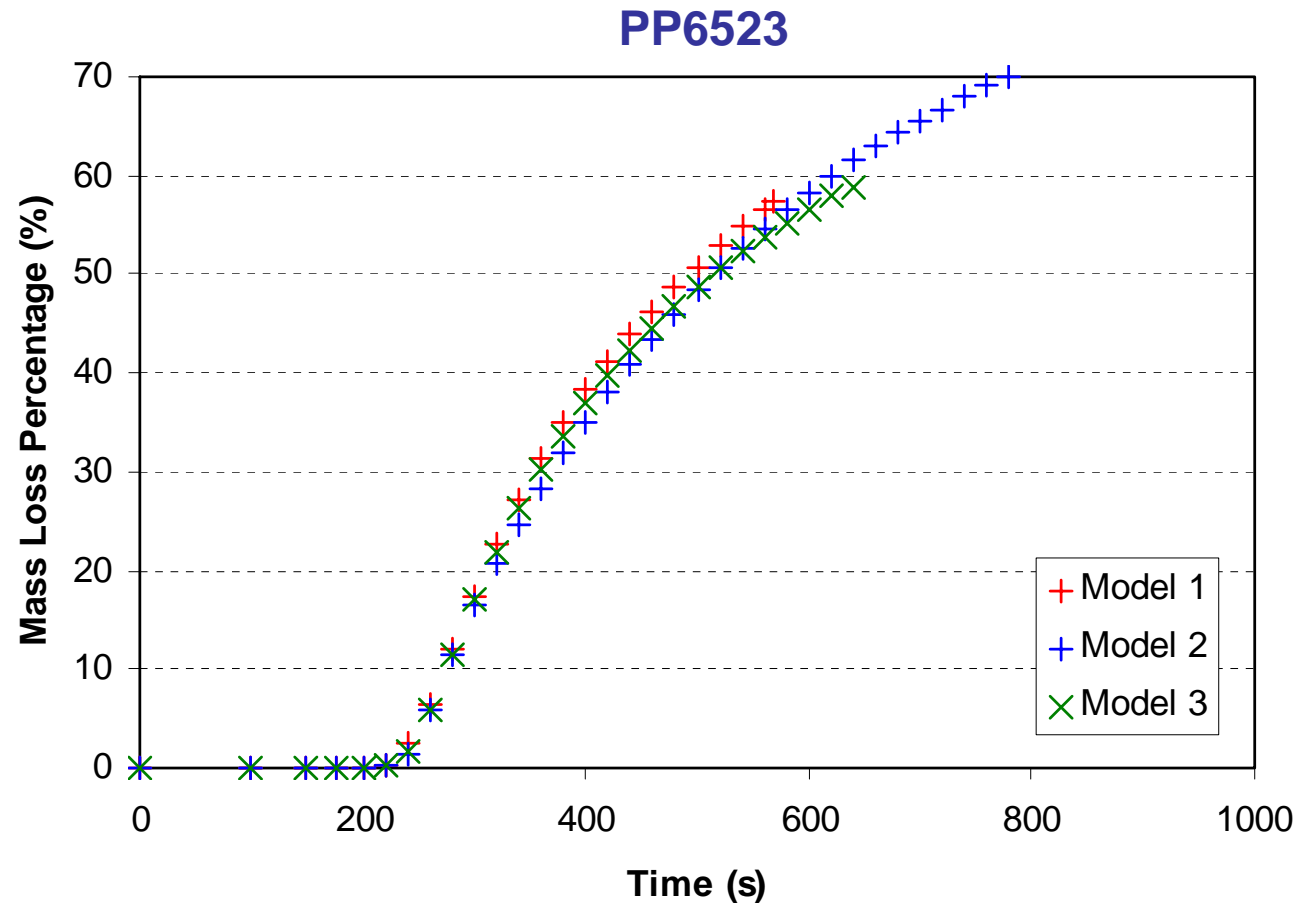
Model 3



PP6523

A small, handwritten mark or signature in the bottom right corner of the page.

Melting behavior with 30KW/m² Heat Flux

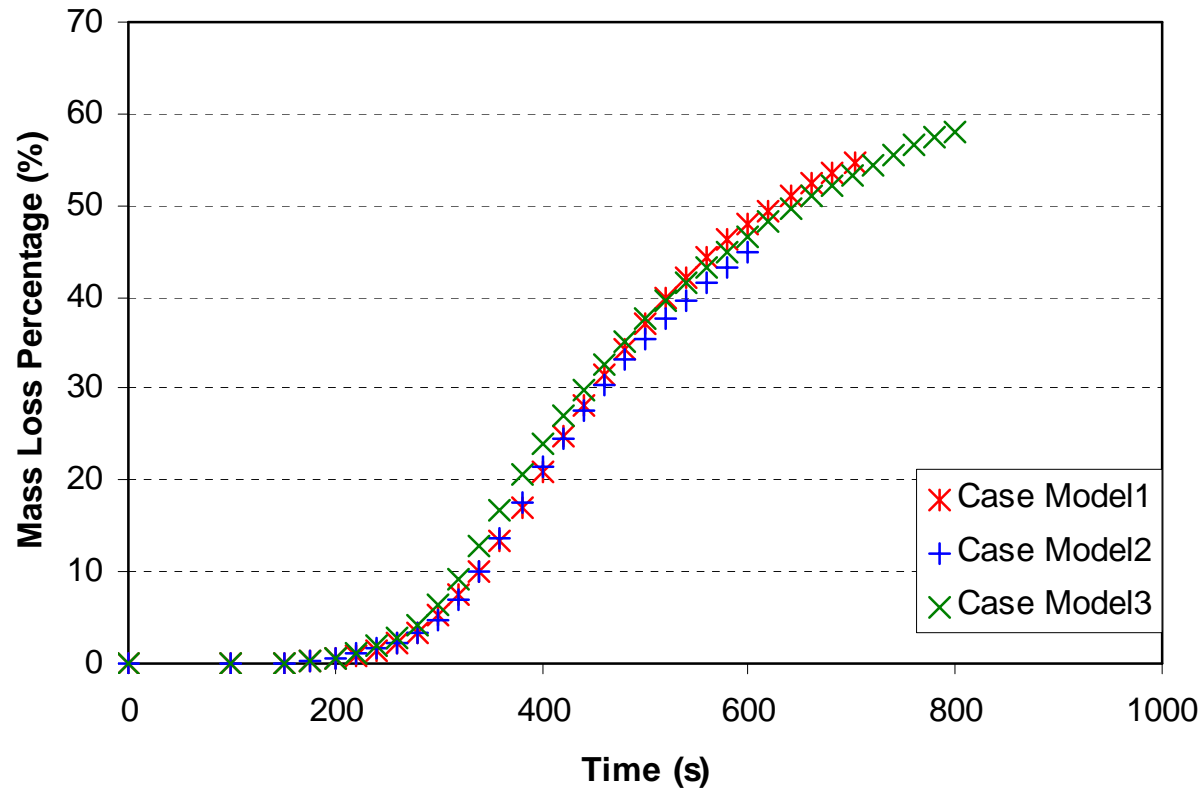


- Although the shape changes are very different (see the previous slide) when using different models to track the moving boundary, the differences in mass loss histories are within 4% throughout the simulations.



Melting behavior with 30KW/m² Heat Flux

PP702N



- The different models for computing the location of the wall grid vertex point result in mass loss histories that are in close agreement for the duration of the simulations.

Parametric Study of Moving Boundary Tracking Algorithm

Qing Tang

REI

6/22/2006



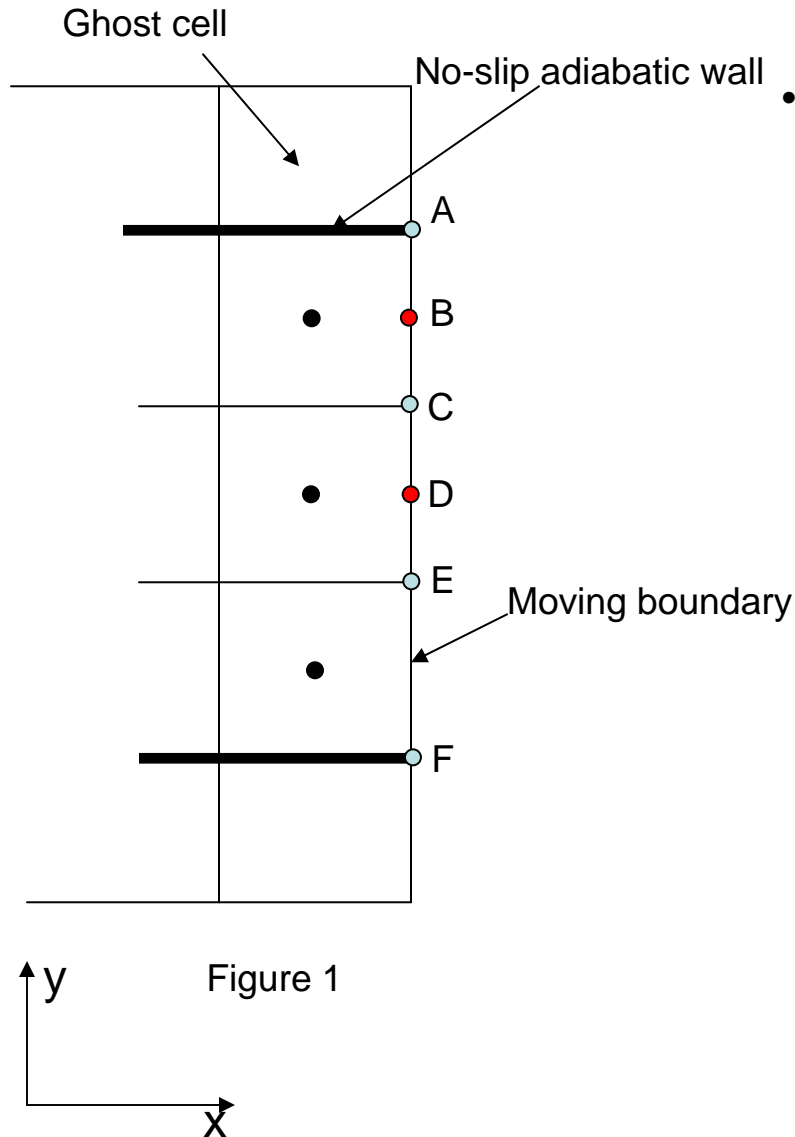
Outline

- Under Relaxation (or Blending) of the Smoothing Function
- Impact of Grid Refinement in the Vertical Direction
- Impact of Under Relaxation of the Smoothing Function
- Summary and Future Work

* PP6523 is modeled in all cases



Under Relaxation of Smoothing Function



The algorithm for determining moving boundary after each time step is described below

1. calculating new face center locations, for example

$$x_D^{new} = x_D^{old} + \frac{\dot{m}_D}{\rho A_{CE}} \Delta t$$

2. calculating new grid vertex point location, for example

$$x_C = \frac{1}{2} (x_B^{new} + x_D^{new})$$

3. Constrain grid vertex point to no-slip wall:

$$x_A = x_C$$

4. Smooth moving boundary with **under relaxation**:

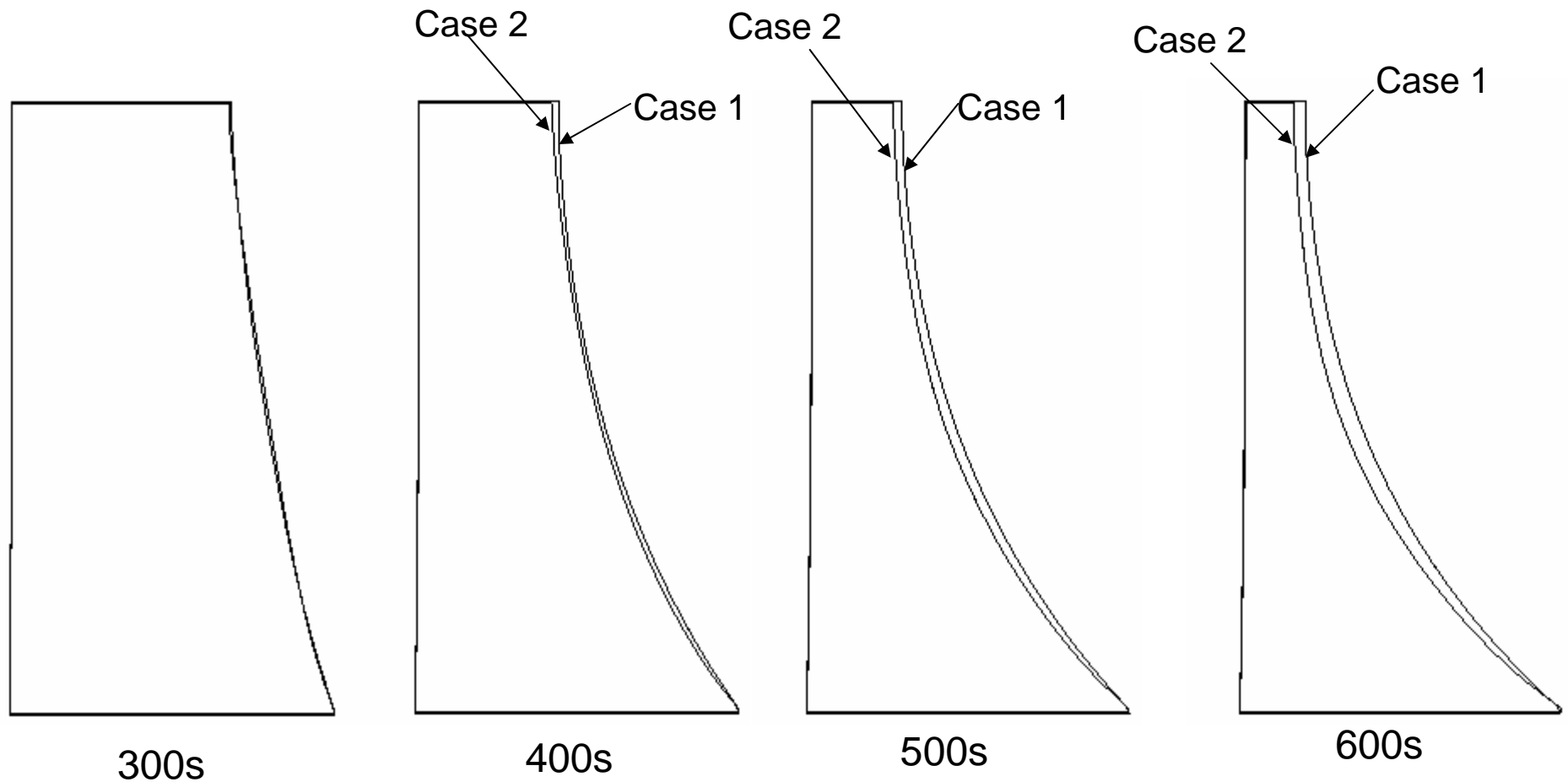
$$x_c^{new} = \alpha \cdot x_c^{old} + (1 - \alpha) \cdot \frac{1}{4} (x_A + 2x_C + x_E)$$

5. re-apply constraint on wall point:

$$x_A^{new} = x_c^{new}$$

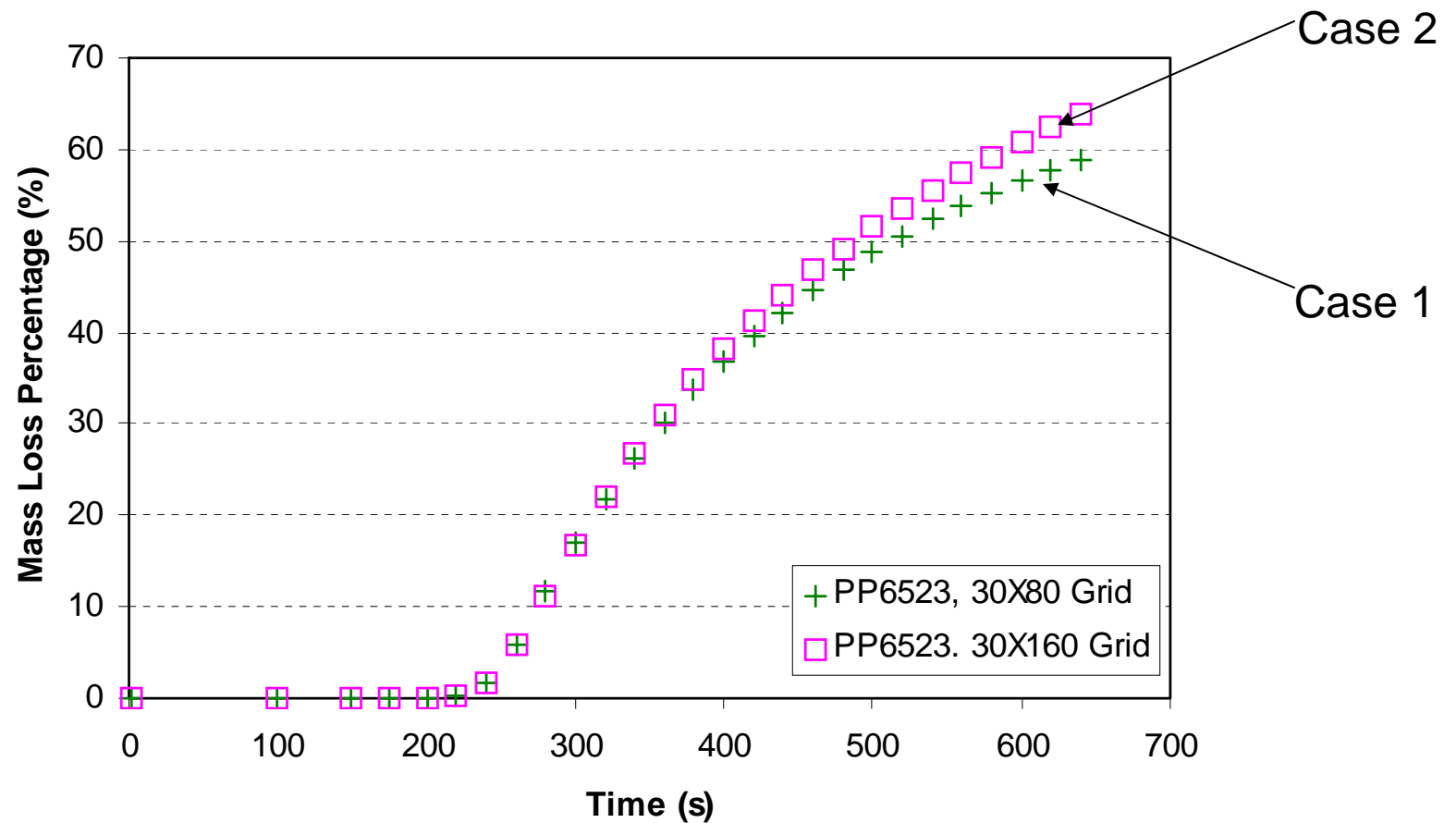


Impact of Grid Refinement on Free Surface



Case 1: 30X80 Grid
Case 2: 30X160 Grid
 $a=0.0$

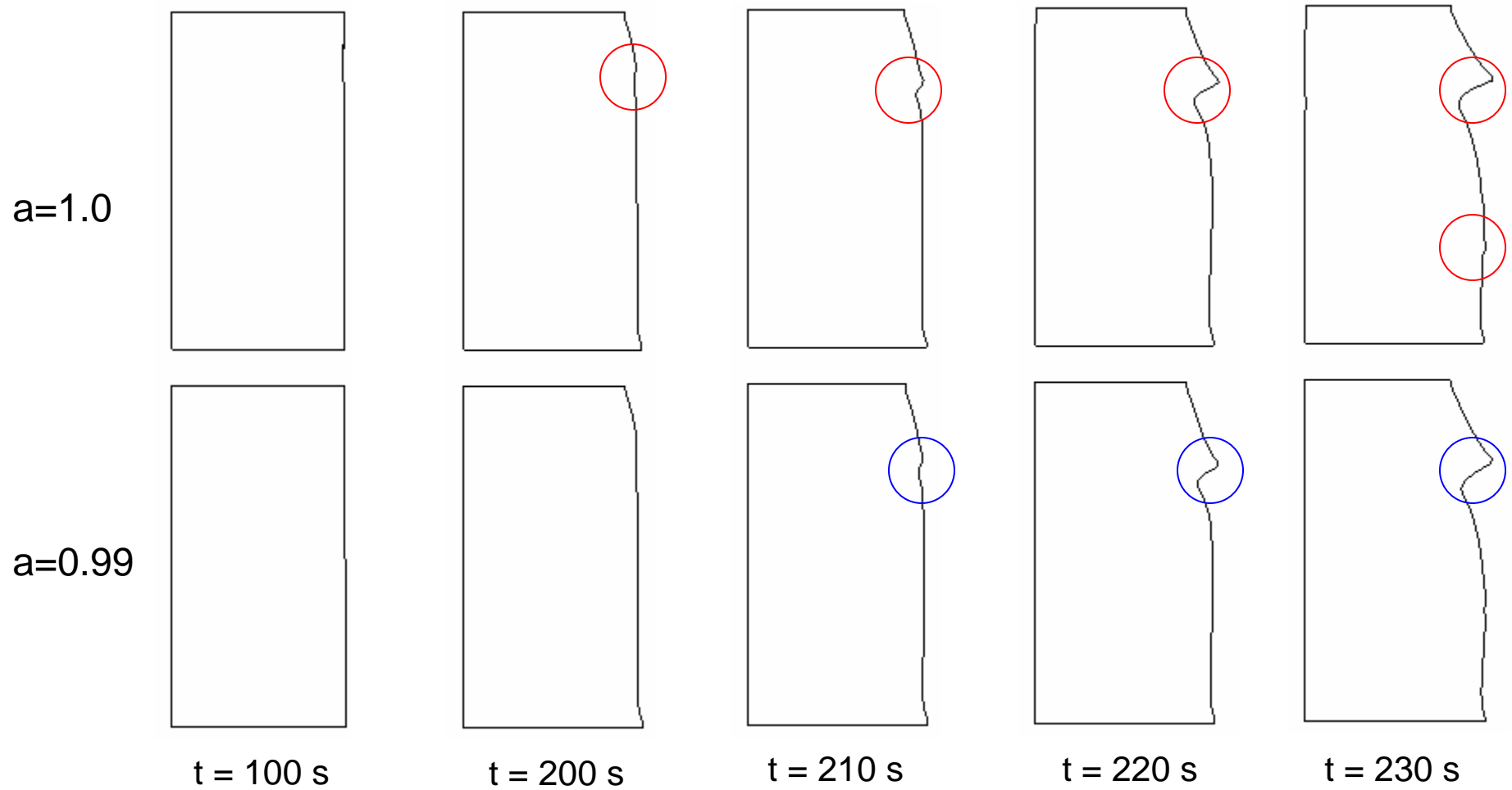
Impact of Grid Refinement on Mass Loss Rate



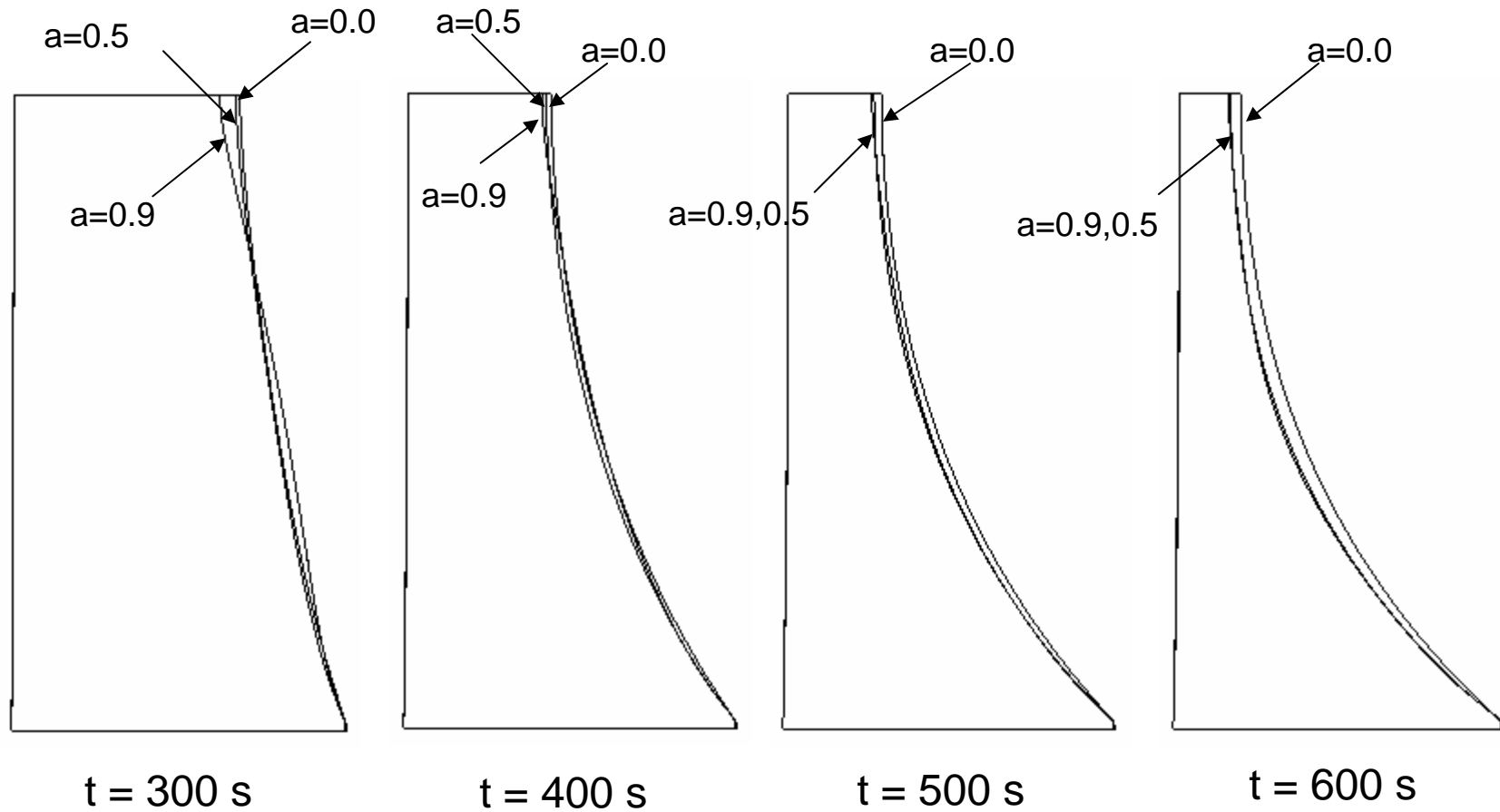
Case 1: 30X80 Grid
Case 2: 30X160 Grid
a=0.0



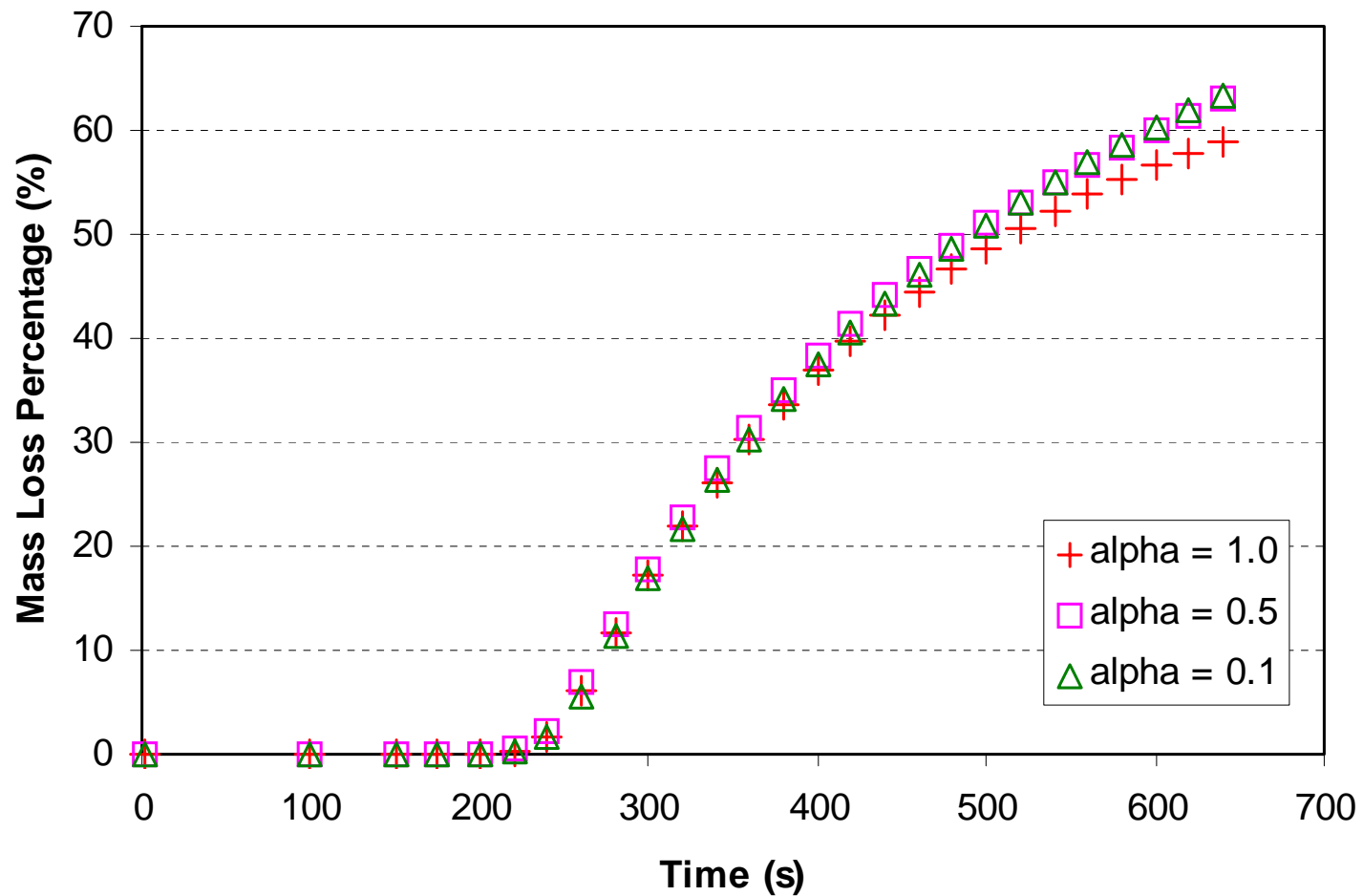
Under Relaxation Factor $a=1.0, 0.99$



Under Relaxation Factor $a=0.9, 0.5, 0.0$



Impact of Under Relaxation Factor on Mass Loss Rate



Summary and Future Work

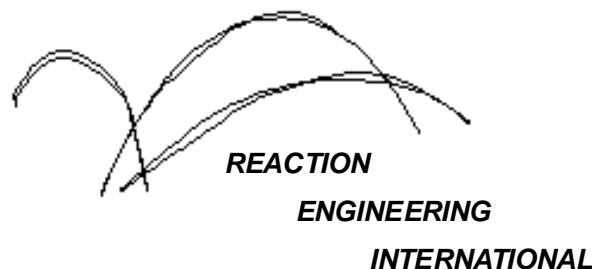
- Refining grid in the vertical direction does not have a significant impact on the shape of the moving boundary
- Refining grid in the vertical direction changes the mass loss rate slightly after the total mass loss reaches 30%, and makes the mass loss process closer to steady state
- Smoothing the moving boundary is crucial to numerical stability.
- Three different under relaxation factors in the smoothing function are tested
 - Using small under relaxation factor, the moving boundary is slightly different during the early melting stage.
 - They all lead to similar moving boundary shapes when mass losses become significant
 - smaller under relaxation factors lead to slightly faster mass loss rate
- Future Work: Test refined grid with small under relaxation factor



A Computational Model For Fire Growth and Spread On Thermoplastic Objects

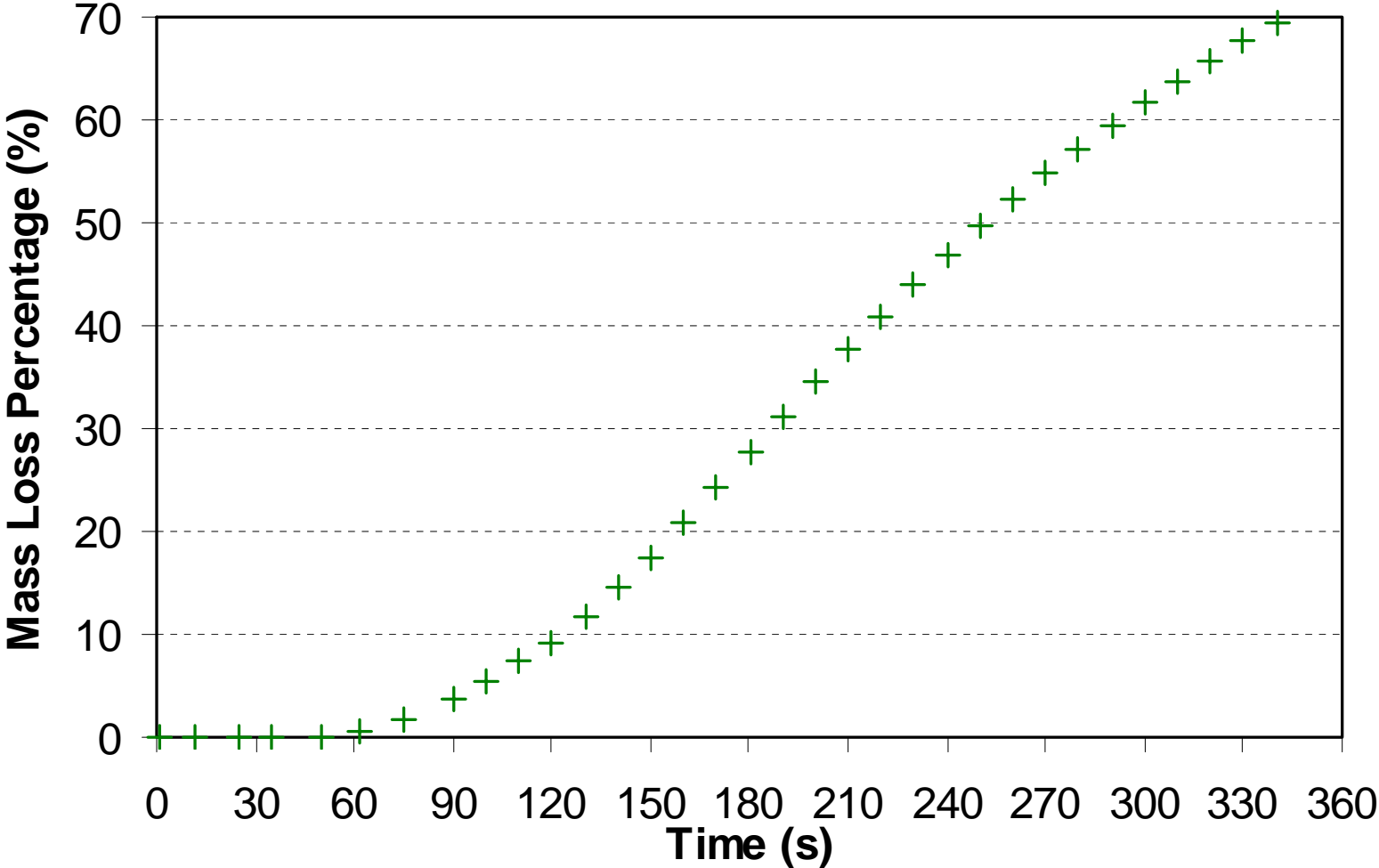
**CFD Simulation of PP23K with steady heat flux,
radiative and convective heat losses, and in-
depth absorption of radiative heat flux**

(6/30/06)

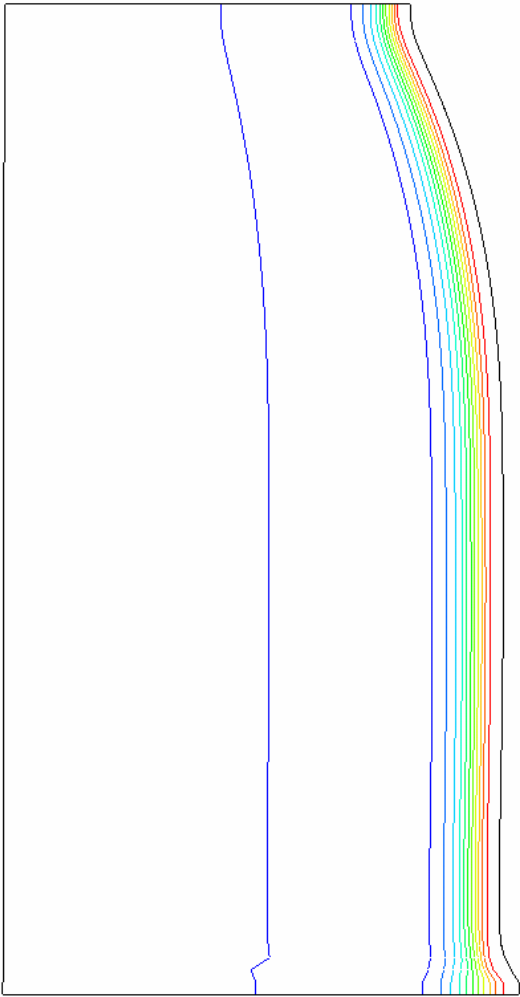


Mass Loss vs. Time

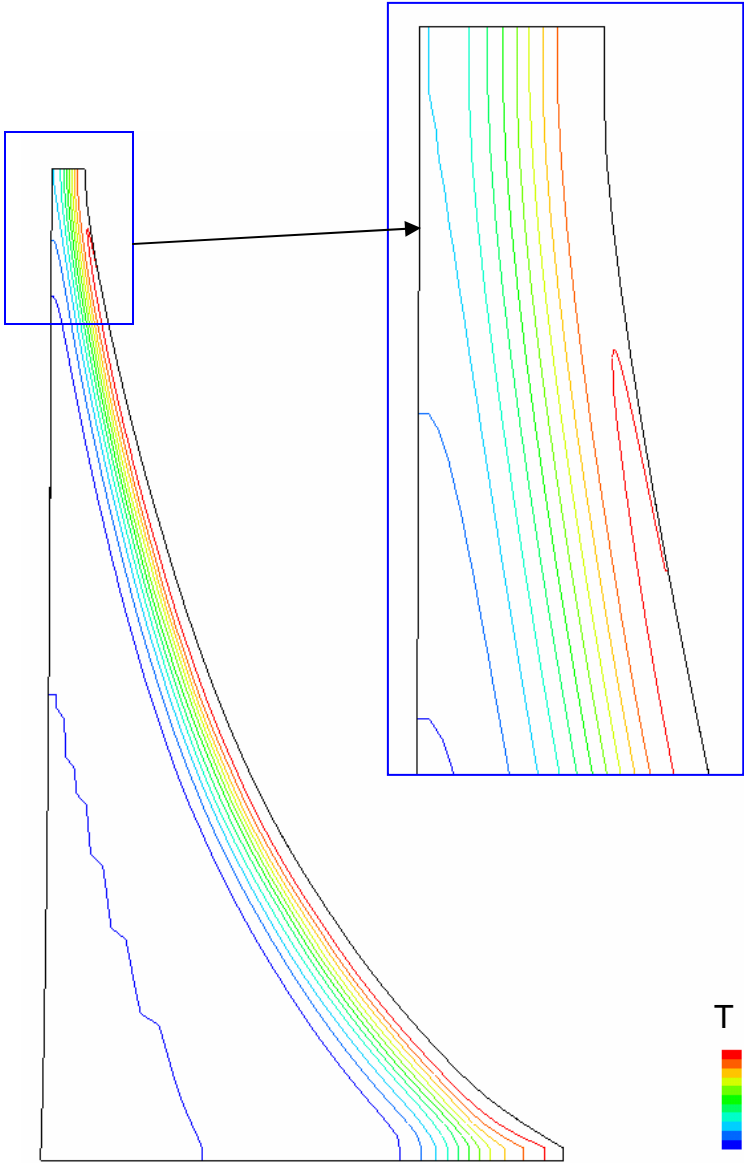
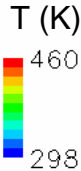
PP23K, 30X80 Grid



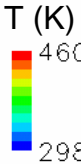
Temperature Contours



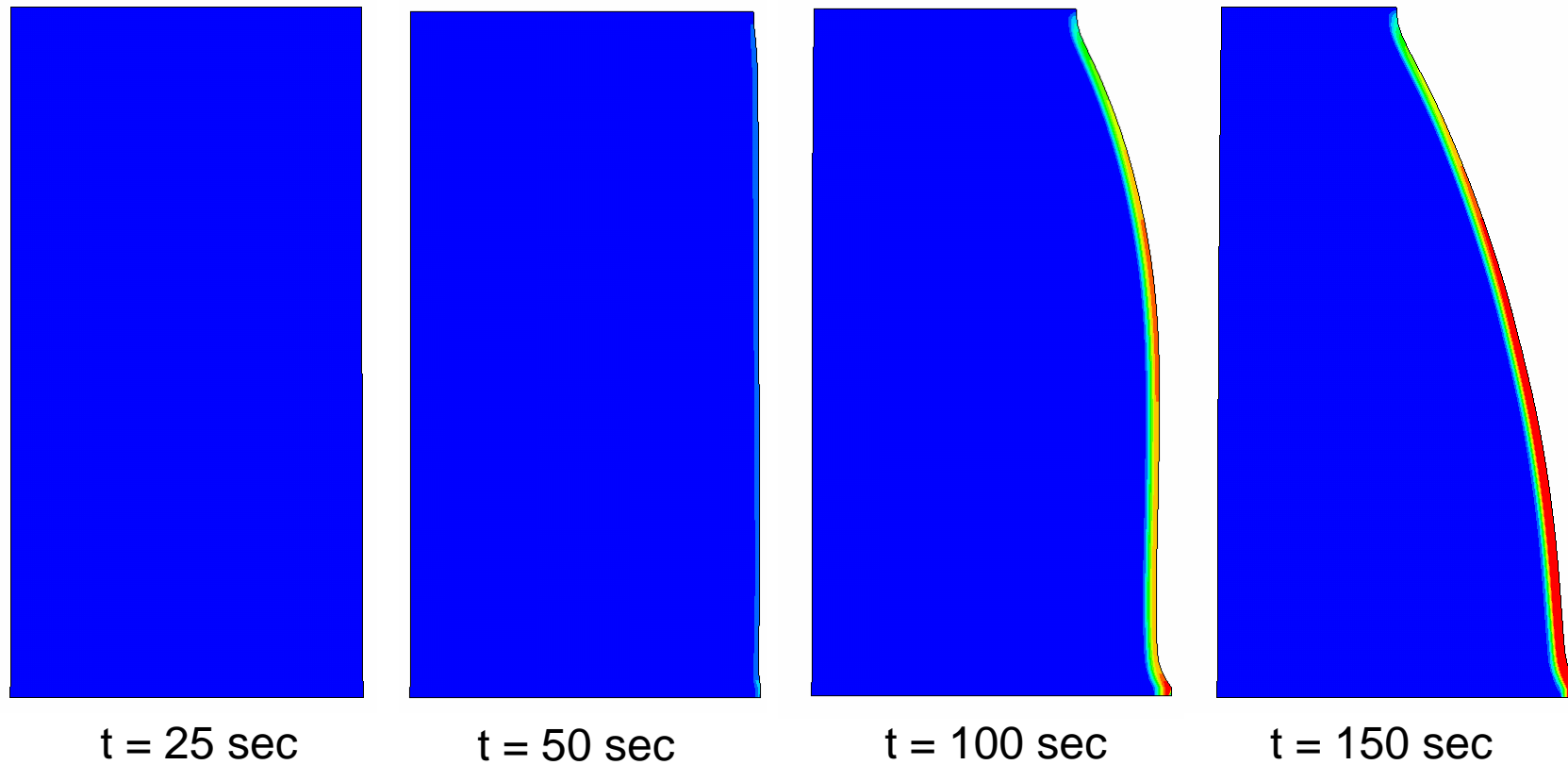
t = 100 sec.



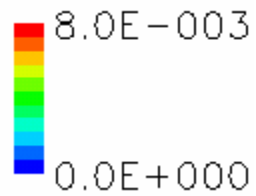
t = 300 sec.



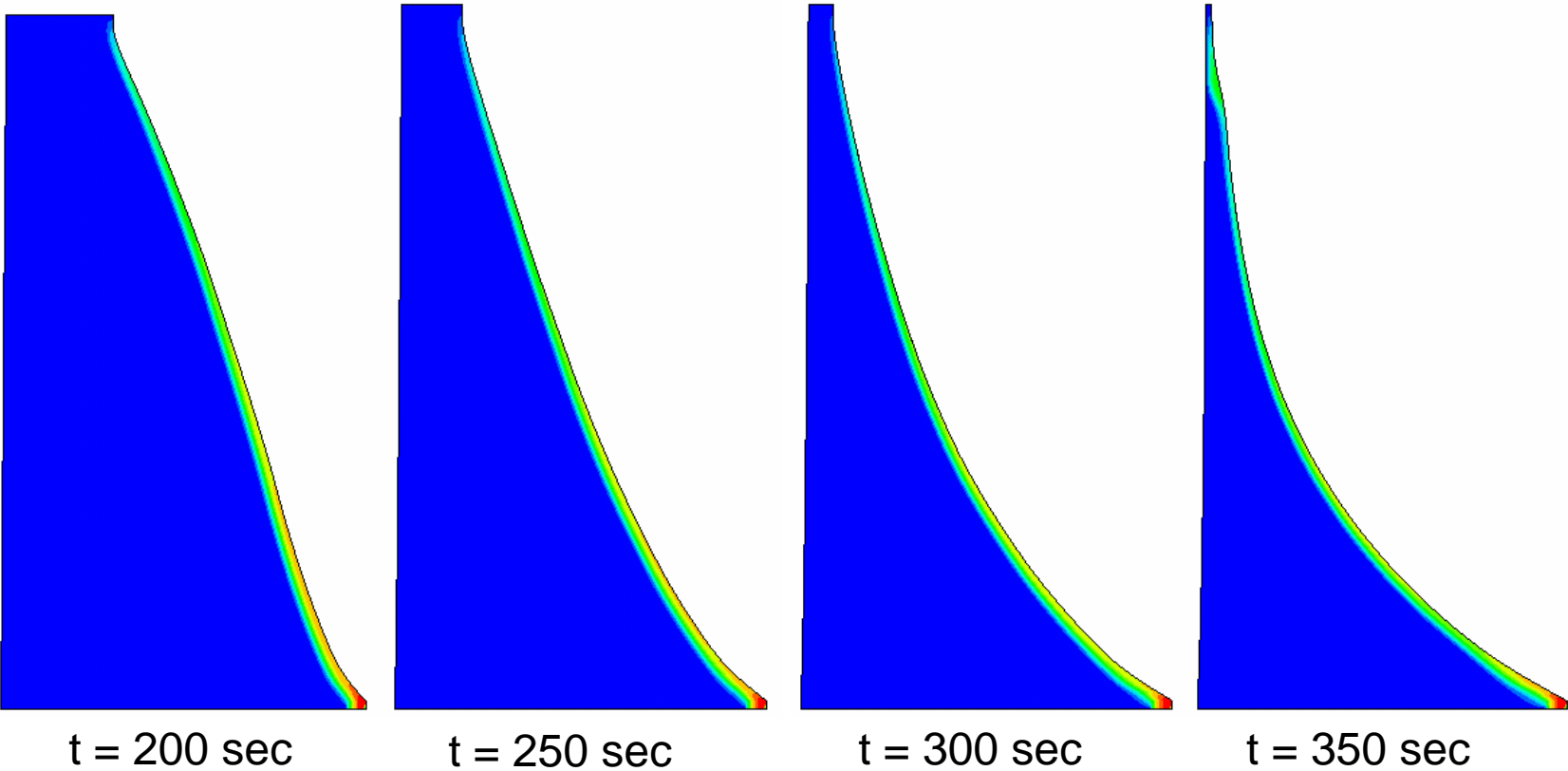
Free Surface Evolution



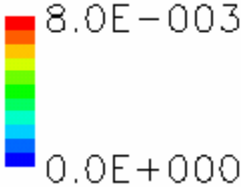
Velocity Magnitude (m/s)



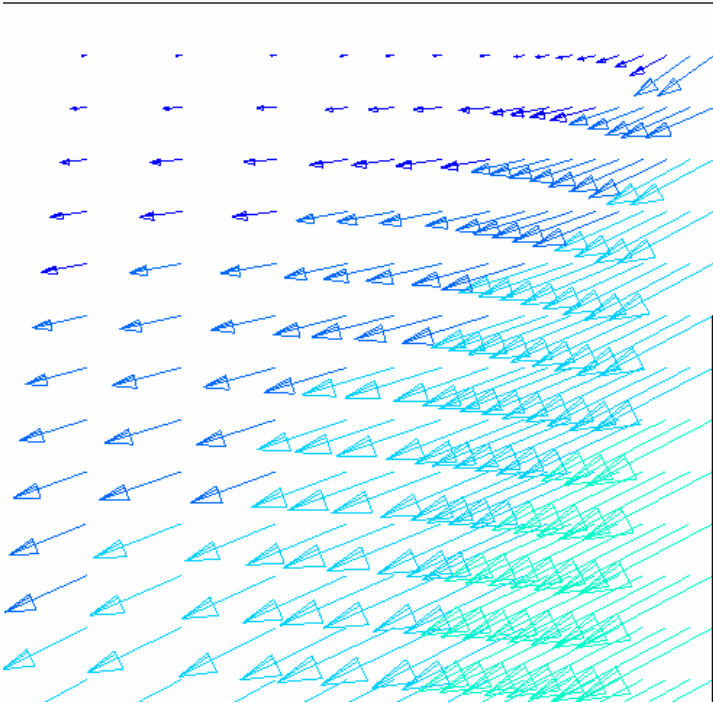
Free Surface Evolution



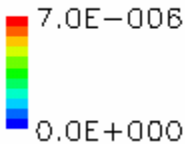
Velocity Magnitude (m/s)



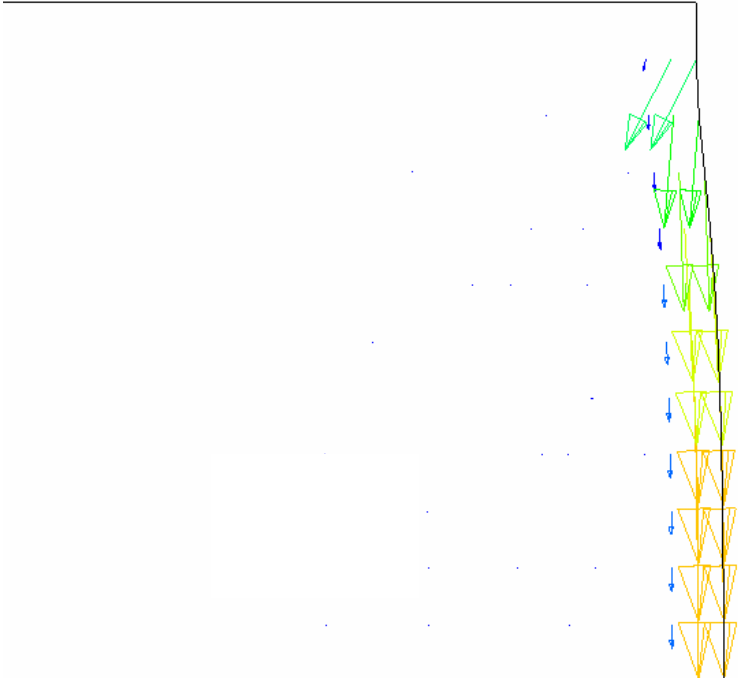
Velocity Vectors Near Top Boundary



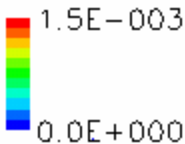
Velocity Magnitude (m/s)



t = 25 sec



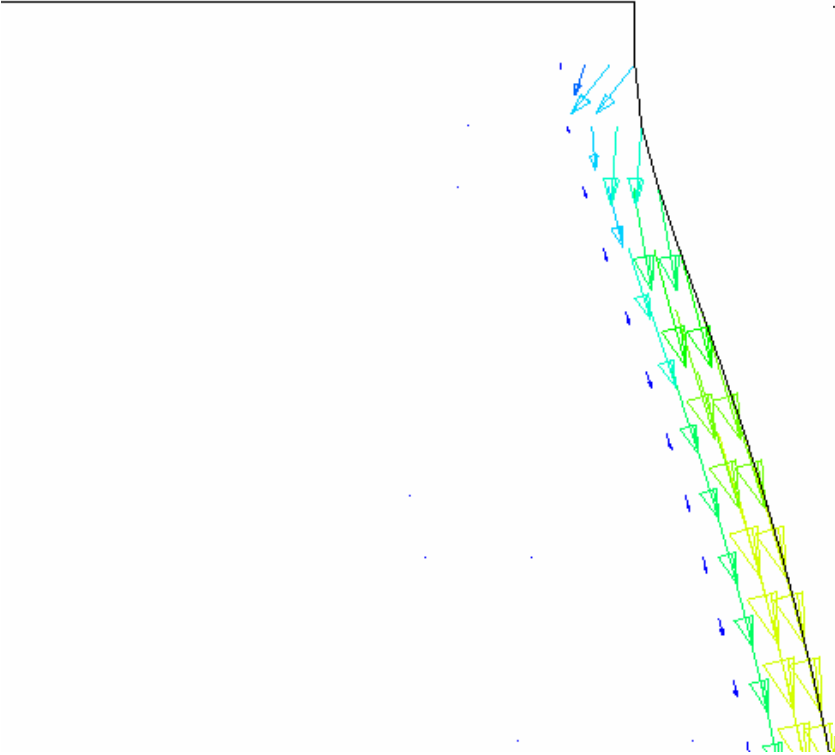
Velocity Magnitude (m/s)



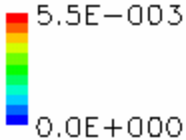
t = 50 sec



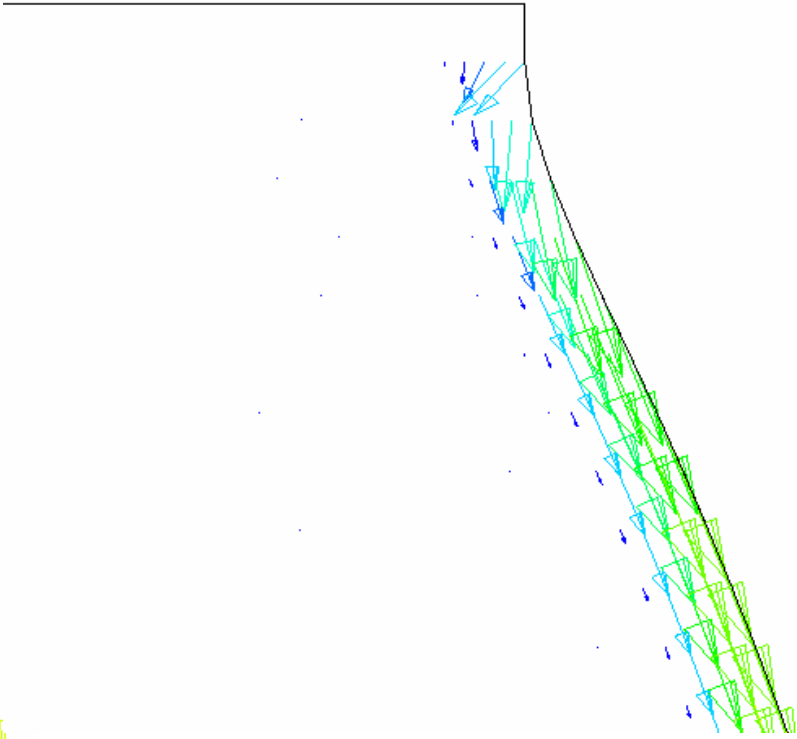
Velocity Vectors Near Top Boundary



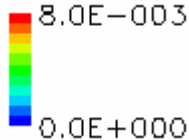
Velocity Magnitude (m/s)



t = 75 sec



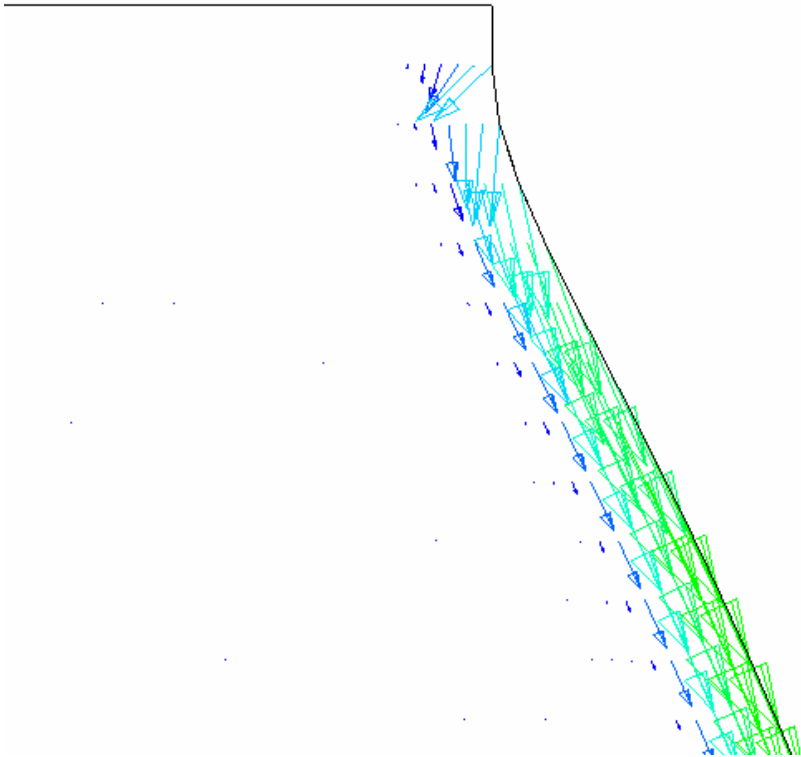
Velocity Magnitude (m/s)



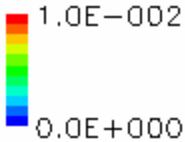
t = 100 sec



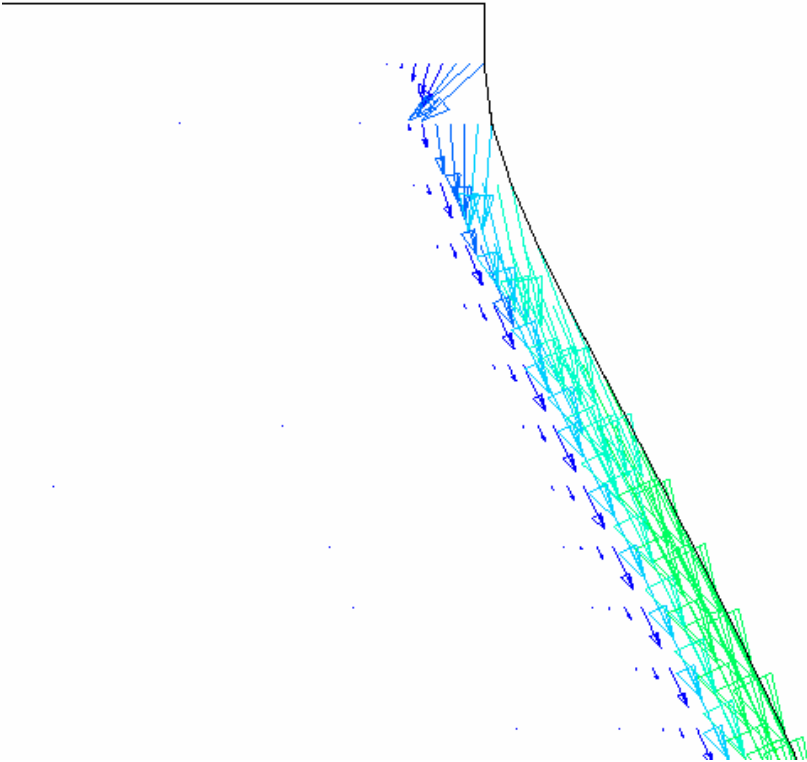
Velocity Vectors Near Top Boundary



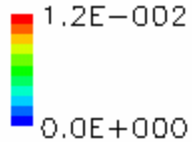
Velocity Magnitude (m/s)



t = 125 sec



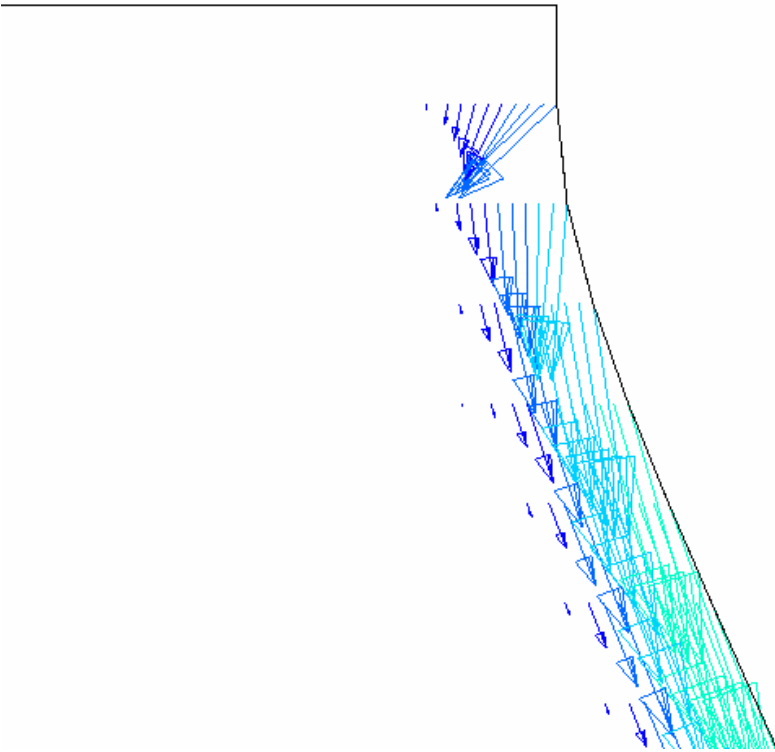
Velocity Magnitude (m/s)



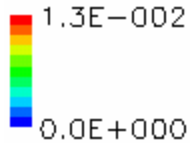
t = 150 sec



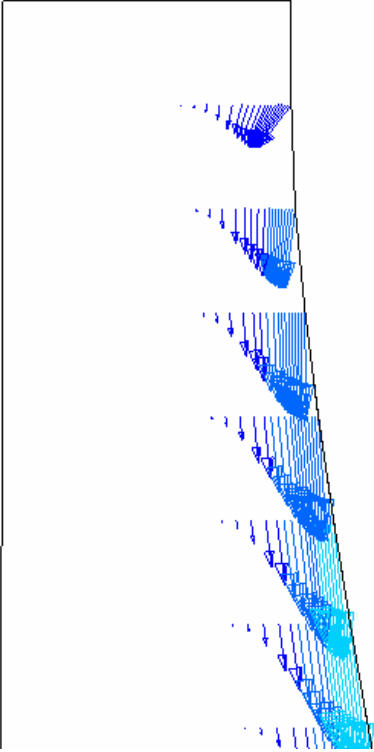
Velocity Vectors Near Top Boundary



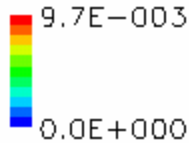
Velocity Magnitude (m/s)



t = 200 sec



Velocity Magnitude (m/s)



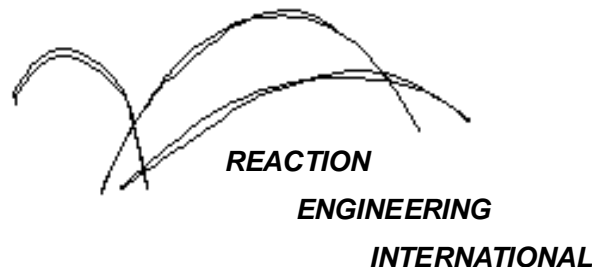
t = 300 sec



A Computational Model For Fire Growth and Spread On Thermoplastic Objects

**Task 2: 2D model with steady heat flux, radiative
and convective heat losses, and in-depth
absorption of radiative heat flux**

(7/11/06)



Outline

⊕ Introduction

⊕ Radiative and convective heat loss, In-depth absorption models

- ⊕ Only impacts energy equation
- ⊕ Both radiative and convective heat losses are only applied to the free surface
- ⊕ A heat source term is added to the energy equation to account for in-depth absorption.
- ⊕ Absorption coefficient is a function of the distance from the free surface

⊕ Absorption coefficient models

- ⊕ In-depth absorption coefficient data for one polymer resin provided by NIST
 - ⊕ Email sent by K. Butler to M. Bockelie on 2/22/2006
 - ⊕ Data applicable to PP23K in the HIFT apparatus

⊕ Cases studied

- ⊕ Computational grid
- ⊕ Case summary
- ⊕ Example results:
 - ⊕ Free surface location, temp., velocity
 - ⊕ Mass loss, surface temperature, surface velocity, and comparisons with data

⊕ Summary



Introduction

- ⊕ Several modeling issues have been investigated during the performance period of Task 2, they are
 - ⊕ In-depth absorption model
 - ⊕ Implementation of top no-slip wall boundary
 - ⊕ Adiabatic wall boundary
 - ⊕ Grid smoothing function
 - ⊕ Grid sensitivity

- ⊕ Simulation of a third polymer raisin (PP23K) has also been performed

- ⊕ Results and discussions about these investigations can be found in previous PowerPoint progress reports and e-mails with NIST during May and June, 2006

- ⊕ Results shown in this report represent the latest from simulating polymer raisin PP702 and PP6523 based on the experience gained through the study.



Heat loss and In-depth absorption models

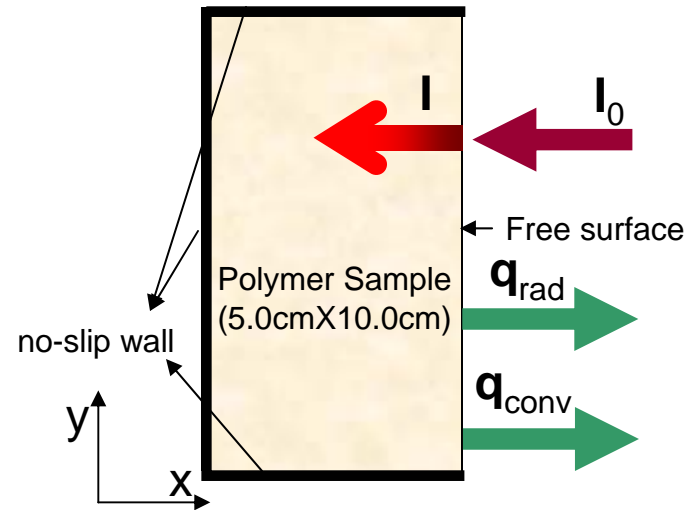


Figure 1, Sketch of in-depth absorption and heat loss model

⊕ Energy equation source terms due to in-depth absorption, radiative and convective heat losses

- ⊕ In-depth absorption: $\dot{q}_{\text{absorption}} = \int_{\Omega} \frac{dI}{dx} d\Omega$, assuming absorption process in x-direction only
- ⊕ Radiative heat loss: $\dot{q}_{\text{radiation}} = -A\varepsilon\sigma(T^4 - T_0^4)$, assuming radiative heat loss only on free surface
- ⊕ Convective heat loss: $\dot{q}_{\text{convection}} = -Ah_{\text{conv}}(T - T_0)$
- ⊕ Parameters: A – surface area; Ω - volume; ε - emissivity (=1.0); σ - Stefan-Boltzmann Constant (=5.67e-8); T_0 – ambient temperature (=298 K); h_{conv} – convective heat transfer coefficient (= 8.0)
- ⊕ A heat sink term is added to the energy equation to prevent overheating (i.e., $T > 750\text{K}$)
- ⊕ The models are implemented in subroutine ***fblick_bc_sca***



Absorption Coefficient Model

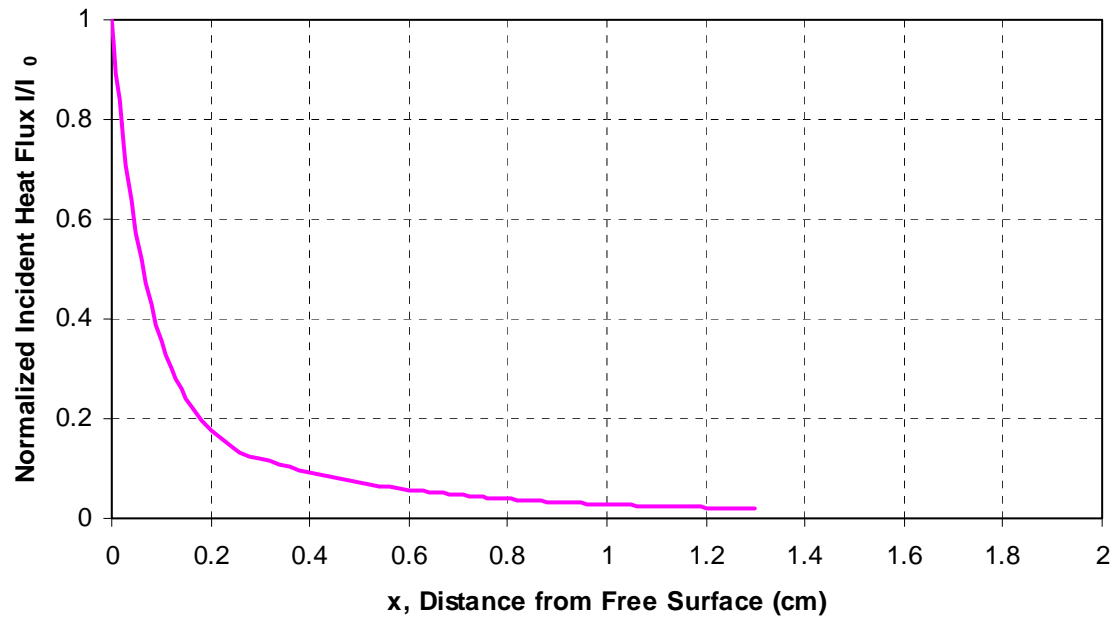


Figure 2, Incident heat flux distribution in the horizontal direction

⊕ In-depth absorption model

$$\oplus \begin{cases} I/I_0 = 10^{(-5.17x+6.964x^2)}, & 0 \leq x < 0.3 \text{ (cm)} \\ I/I_0 = 10^{(-0.5154-1.473x+0.4339x^2)}, & 0.3 \leq x < 1.3 \text{ (cm)} \end{cases}$$



Computational Grid

- ⊕ Polymer sample dimension:
5.0cm X 10.0cm
- ⊕ 30X80 Grid (biased)
- ⊕ Initial grid resolution the same
as the 19X200 grid used in
Task 1
- ⊕ Equivalent to 100X80 grid if
using uniform grid spacing and
fixed grid

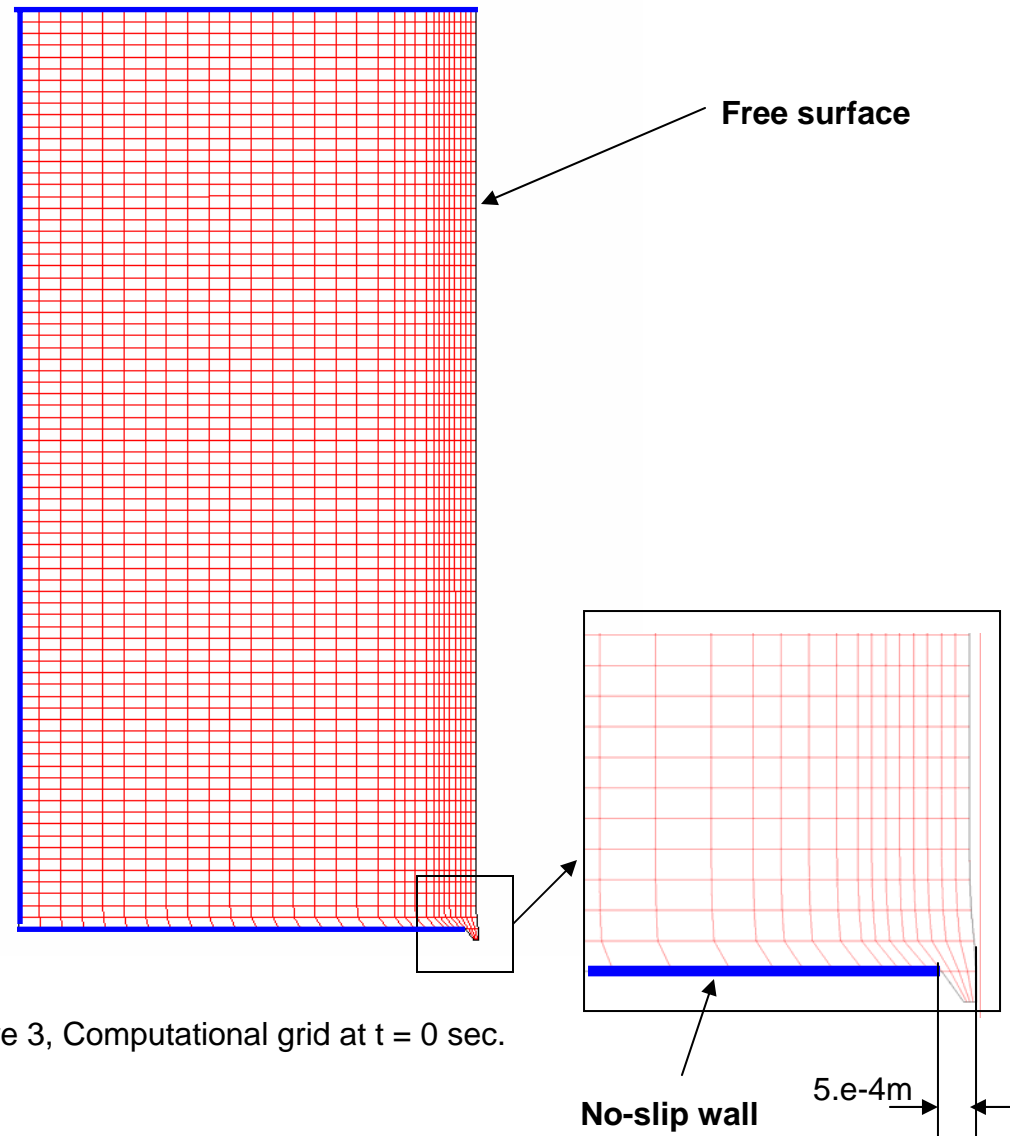


Figure 3, Computational grid at $t = 0$ sec.

Handwritten signature

Case Summary

⊕ External Incident heat flux: 30KW/m²

Case	Polymer Resin	Radiative and Convective Heat Losses	In-depth Absorption	Surface Smoothing Under-relaxation Factor (α)*	Mass Loss and Simulated Time	Estimated CPU Time**
Case 2A	PP702	Included	Not included	0.0	60%, 370 sec	~ 50 h
Case 2B	PP702	Included	Included	0.0	65%, 700 sec	~ 26 h
Case 2C	PP6523	Included	Included	0.9	70%, 700 sec	~ 28 h

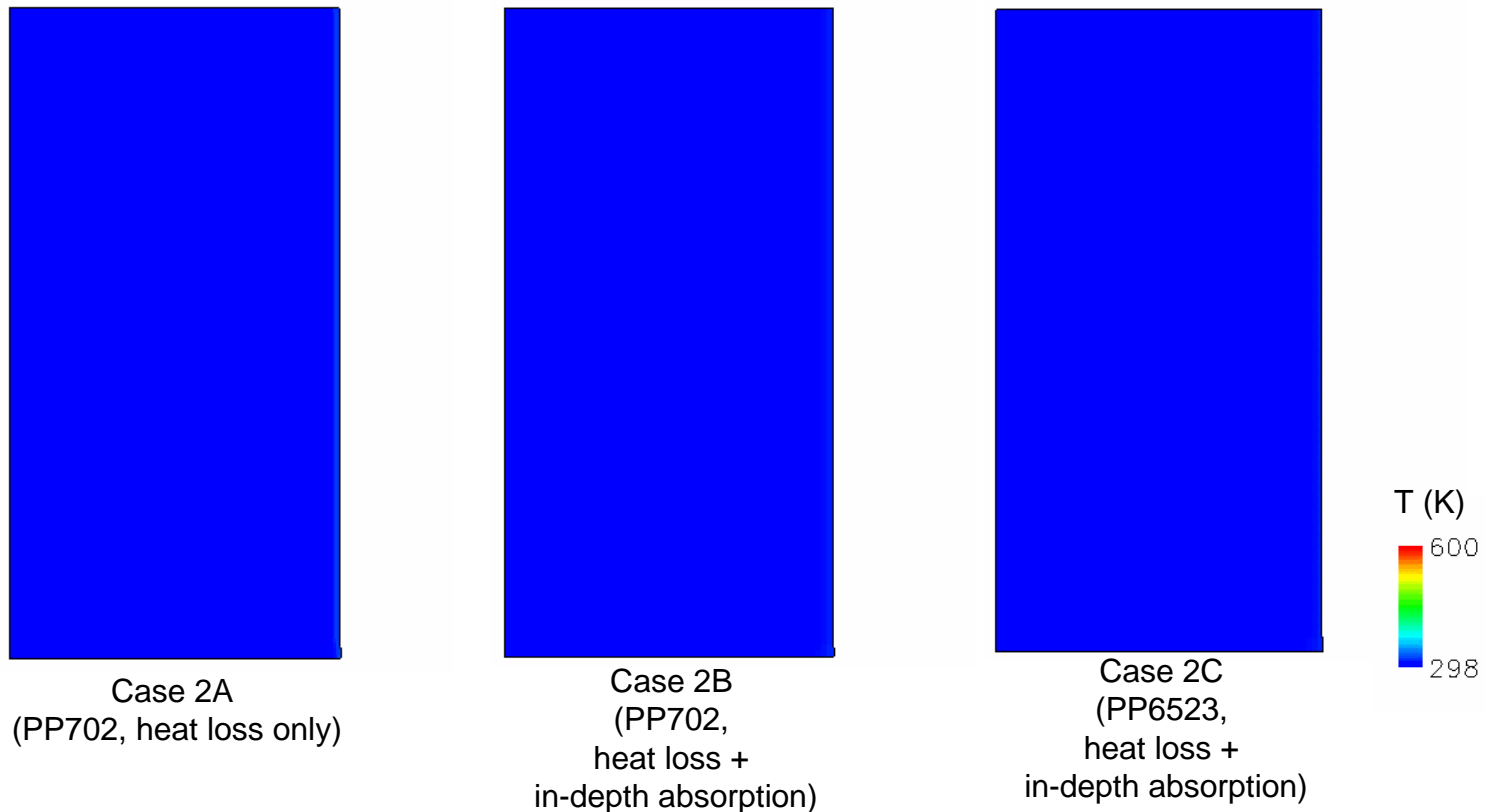
* As per PowerPoint progress report 06-22-2006: $x_C^{new} = \alpha \cdot x_C^{old} + (1 - \alpha) \cdot \frac{1}{4} (x_A^{old} + 2x_C^{old} + x_E^{old})$

** all cases were run on a 3.0GHz Intel Xeon workstation



Impact of In-depth Absorption on Melting Process

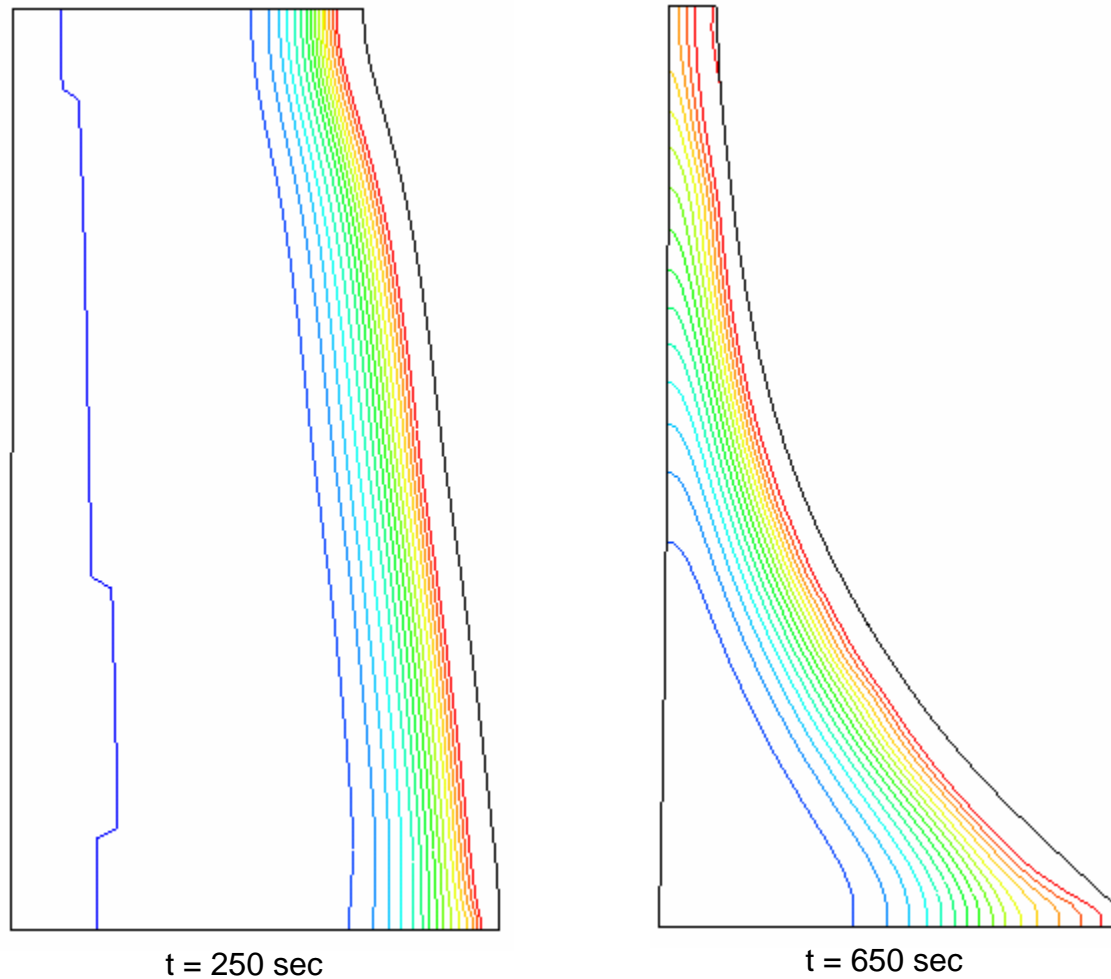
Temperature contour



- ⊕ Time interval between movie frames: 5 seconds
- ⊕ The inclusion of in-depth absorption leads to significant difference in shape change history
 - ⊕ **Melting process slows down**
 - ⊕ **Upper free surface moves much slower towards the back wall**
 - ⊕ **Melting layer becomes thicker**



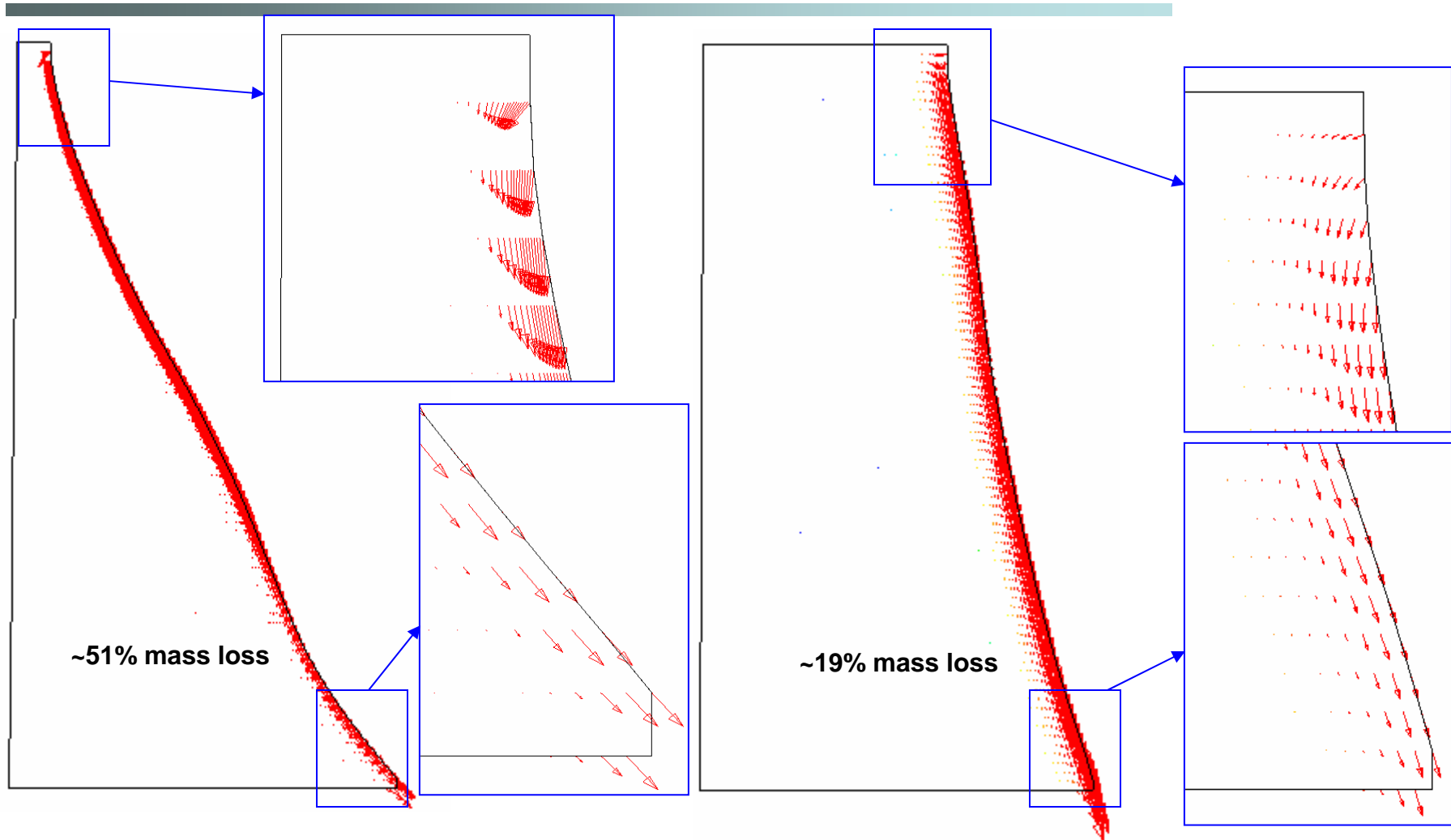
Example: Temperature Contours at $t = 250$ and 650 sec



Case 2B (PP702, heat loss + in-depth absorption)

Contour lines are perpendicular to the solid walls in the near wall regions, which indicates the walls are adiabatic

Example: Velocity Vectors at t = 300 sec



Case 2A (PP702, heat loss only)

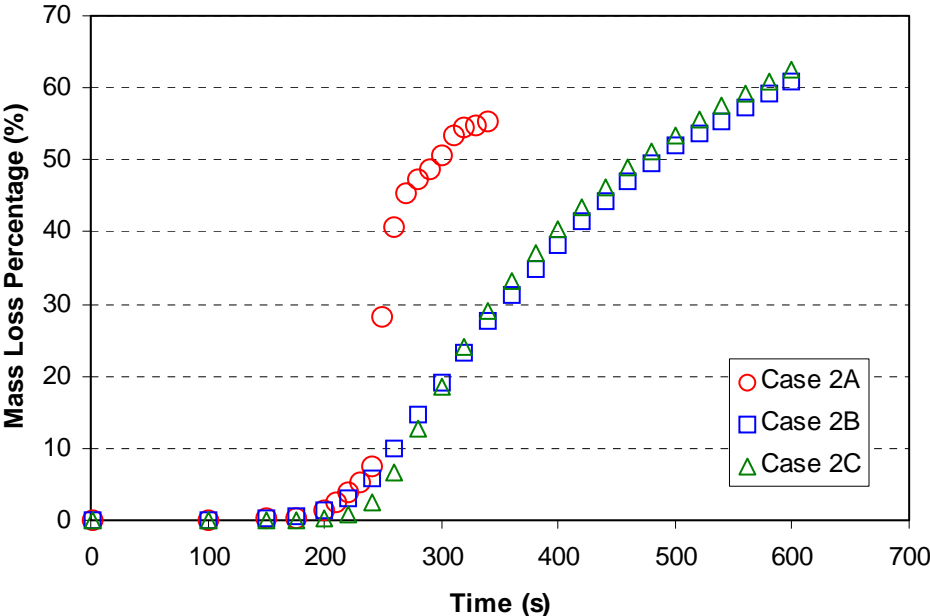
Case 2B (PP702, heat loss + in-depth absorption)

- ⊕ The addition of in-depth absorption leads to
 - ⊕ slower melting process
 - ⊕ thicker melting layer below free surface

Vectors in different boxes are not the same scale



Mass Loss as Function of Time



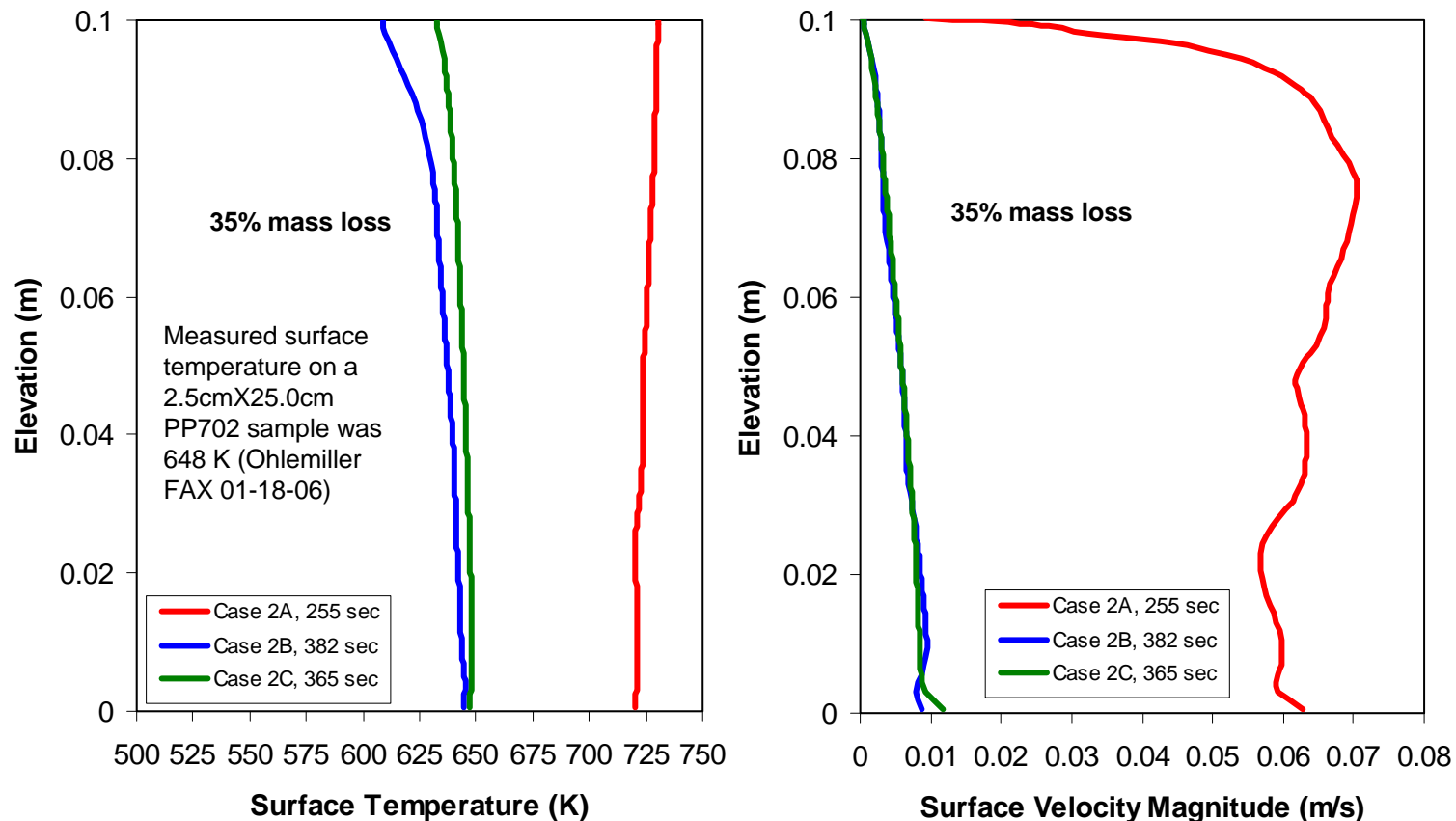
Grid	“steady state” Mass Loss Rate	Comments
Case 2A	24.0*	Computed from 200 s to 300 s,
Case 2B	6.5*	Computed from 200 s to 600 s
Case 2C	7.5*	Computed from 240 s to 600 s
Experiment	0.15**	Ohlemiller FAX 01-18-06

* per unit length (g/s m)

** g/s



Example: Surface Temperature and Velocity Magnitude



- ⊕ Velocity magnitudes approach zero at upper no slip wall
- ⊕ Inclusion of in-depth absorption decreases surface temperature and velocity magnitude
- ⊕ Over-heating ($T > 698\text{K}$) occurs in Case 2A where surface temperature is at the highest near the top

Summary

- ⊕ Results presented for Two Resins with Heat Losses and In-depth Absorption of Heat Flux
- ⊕ Cases were run to at least 60% mass loss
- ⊕ Computational Cost highlighted
 - ⊕ Less expensive than Task 1
 - ⊕ Smaller computational domain
 - ⊕ Larger time step due to lower velocity caused by heat losses and in-depth absorption
- ⊕ Model features highlighted
 - ⊕ Heat loss model and in-depth absorption model
 - ⊕ Impacts of different models on melting processes
 - ⊕ Solutions at selected times
 - ⊕ Velocity field resolution across melt boundary layer
- ⊕ Example Results
 - ⊕ Free surface location, temp., velocity - selected times
 - ⊕ Movie of free surface location and temperature
 - ⊕ Mass loss, surface temperature, surface velocity, and comparison with experimental data
- ⊕ CPCFD source code for Task 2 has been provided to NIST via Email (6/30/06)



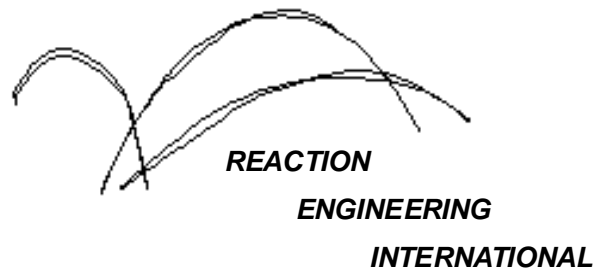
Task 3



A Computational Model For Fire Growth and Spread On Thermoplastic Objects

Task 3: 2D model with in-depth gasification

(8/11/06)



Outline

- ⊕ Introduction
- ⊕ In-depth gasification models
- ⊕ Cases studied
 - ⊕ Computational grid
 - ⊕ Case summary
 - ⊕ Example results:
 - ⊕ Free surface location, temp
 - ⊕ Mass loss, surface temperature, and comparisons with data
- ⊕ Summary



Introduction

- ⊕ In-depth gasification model has been implemented into the CPCFD code. Gasification is represented by the removal of polymer mass and energy using sink terms in both mass and energy equations.
- ⊕ Simulations of two polymer raisins (PP702N and PP6523) have been performed
- ⊕ Impact of in-depth absorption on gasification has been investigated.
- ⊕ Results shown in this report represent the latest from simulating polymer raisin PP702N and PP6523 based on the experience gained through Task 1 and Task 2.



Gasification, absorption and heat losses models

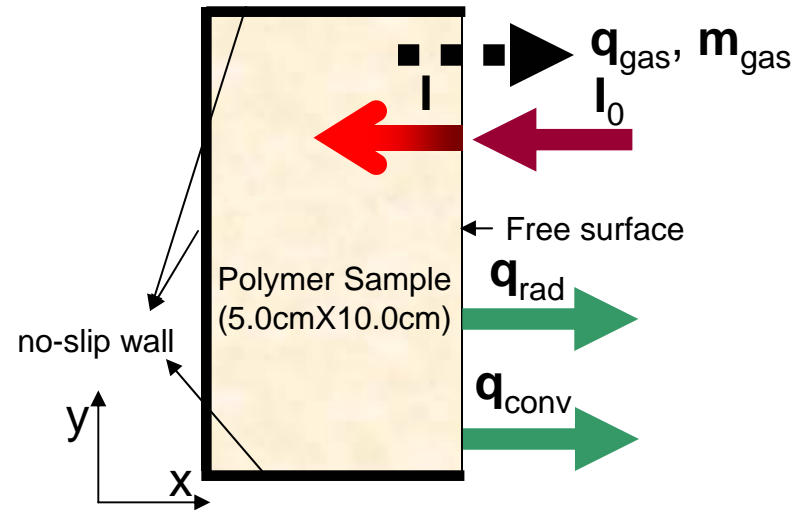


Figure 1, Sketch of gasification, absorption and heat loss model

⊕ Energy source/sink terms due to gasification, absorption, and heat losses

⊕ **In-depth gasification:** $\dot{q}_{\text{gasification}} = -\int_{\Omega} H_v \rho A e^{(-E/RT)} d\Omega$

⊕ In-depth absorption: $\dot{q}_{\text{absorption}} = \int_{\Omega} \frac{dI}{dx} d\Omega$, assuming absorption process in x-direction only

⊕ Radiative heat loss: $\dot{q}_{\text{radiation}} = -A \varepsilon \sigma (T^4 - T_0^4)$, assuming radiative heat loss only on free surface

⊕ Convective heat loss: $\dot{q}_{\text{convection}} = -A h_{\text{conv}} (T - T_0)$

⊕ Heat sink term to avoid over heating in Task 1 and 2 has been deactivated in this study

⊕ **Mass sink terms due to gasification:** $\dot{m}_{\text{gasification}} = -\int_{\Omega} \rho A e^{(-E/RT)} d\Omega$



Gasification Model Parameters

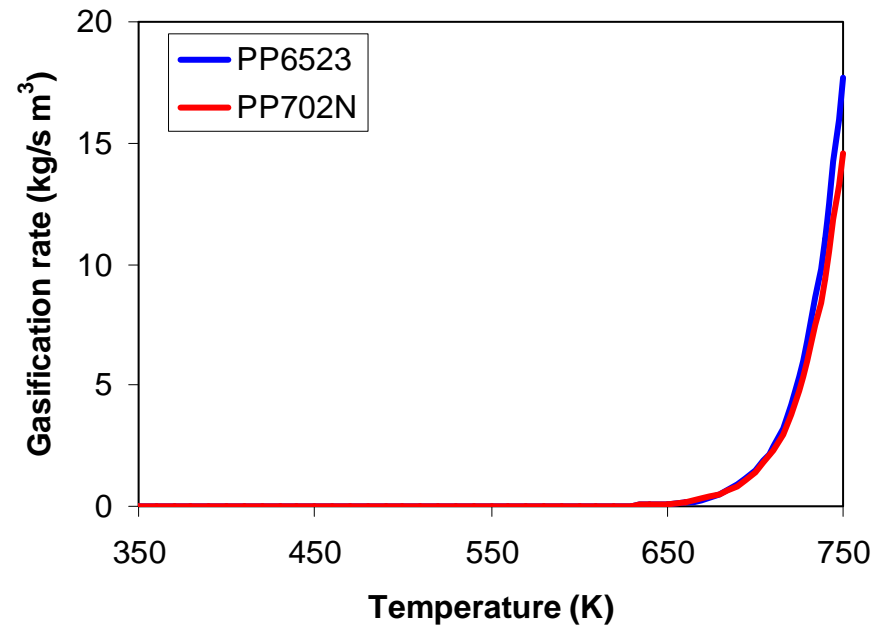


Figure 2, Mass loss rate due to gasification as functions of time

Gasification model parameters

Polymer Raisin	A (1/s)	E/R	H _v (J/kg)	r (kg/m ³)
PP702N	2.18e+12	24400	8.0e+5	900
PP6523	2.23e+13	26000	8.0e+5	900

Computational Grid

- ⊕ Polymer sample dimension:
5.0cm X 10.0cm
- ⊕ 30X80 Grid (biased)
- ⊕ Initial grid resolution the same
as the 19X200 grid used in
Task 1
- ⊕ Equivalent to 100X80 grid if
using uniform grid spacing and
fixed grid

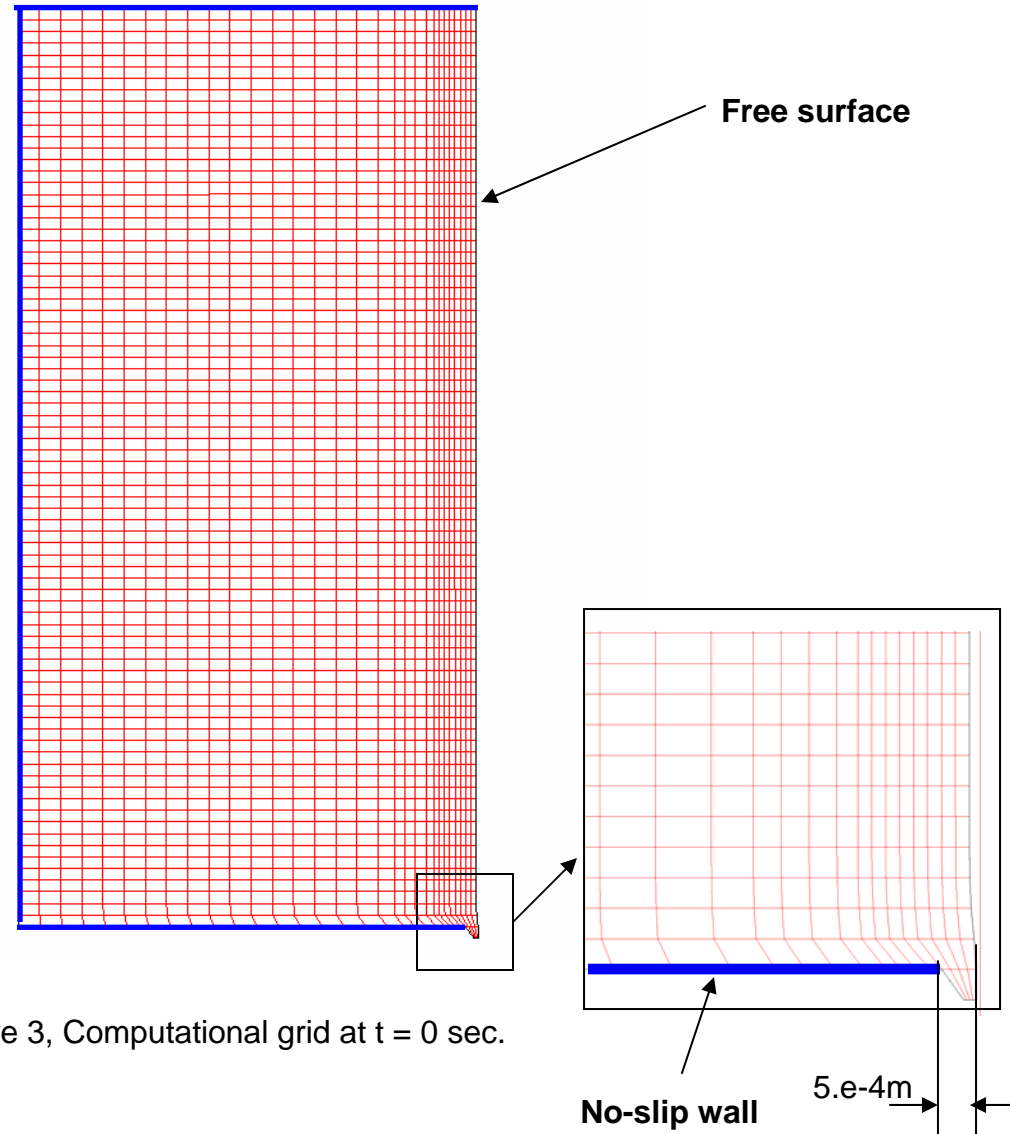


Figure 3, Computational grid at $t = 0$ sec.

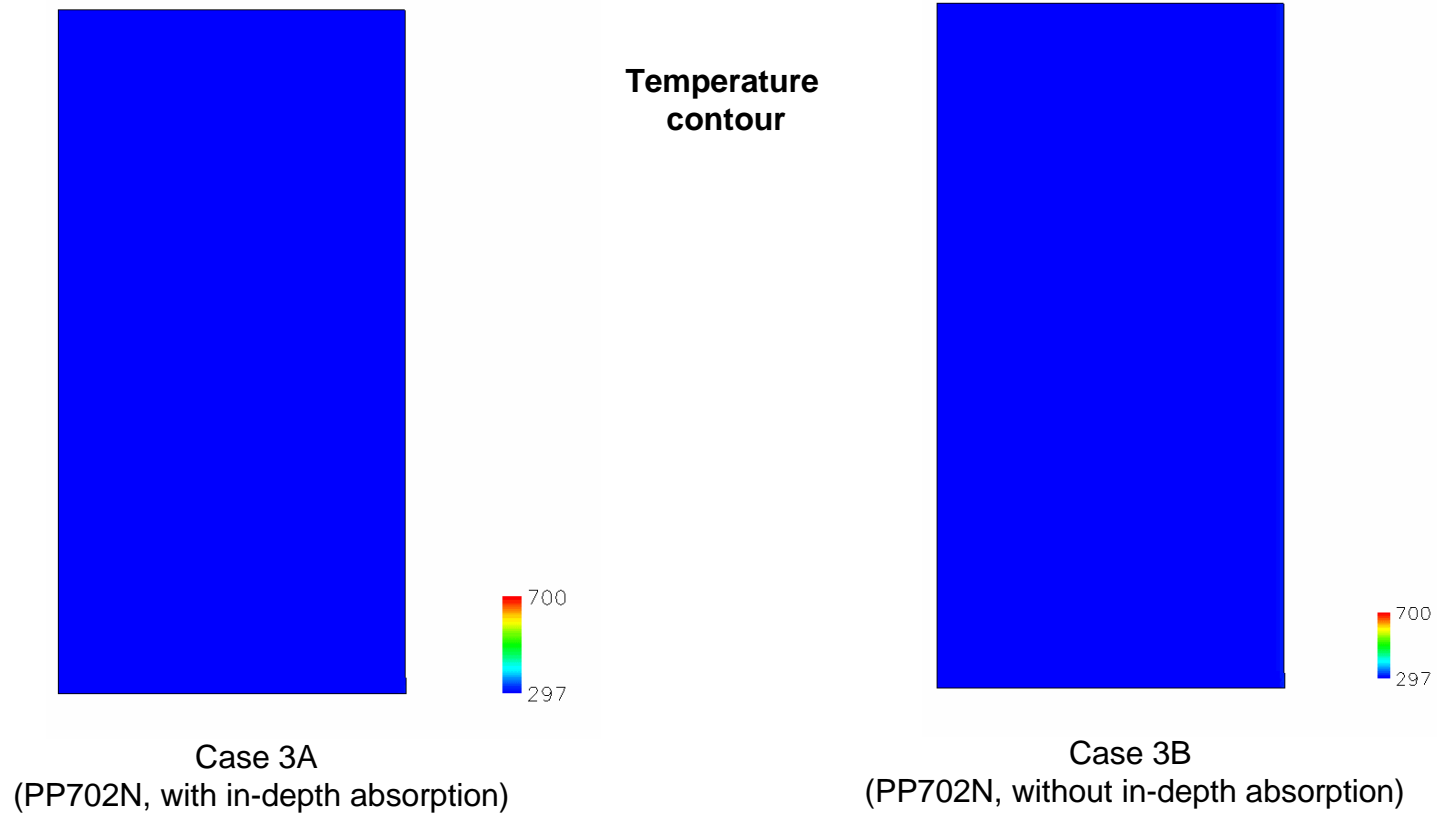
[Handwritten signature]

Case Summary

⊕ External Incident heat flux: 30KW/m²

Case	Polymer Resin	In-depth Gasification	Radiative and Convective Heat Losses	In-depth Absorption	Mass Loss and Simulated Time	Estimated CPU Time
Case 3A	PP702N	Included	Included	Included	65%, 600 sec	~ 24 h
Case 3B	PP702N	Included	Included	Not included	55%, 230 sec	~ 36 h
Case 3C	PP6523	Included	Included	Included	65%, 600 sec	~ 24 h
Case 3D	PP6523	included	Included	Not included	60%, 280 sec	~ 30 h

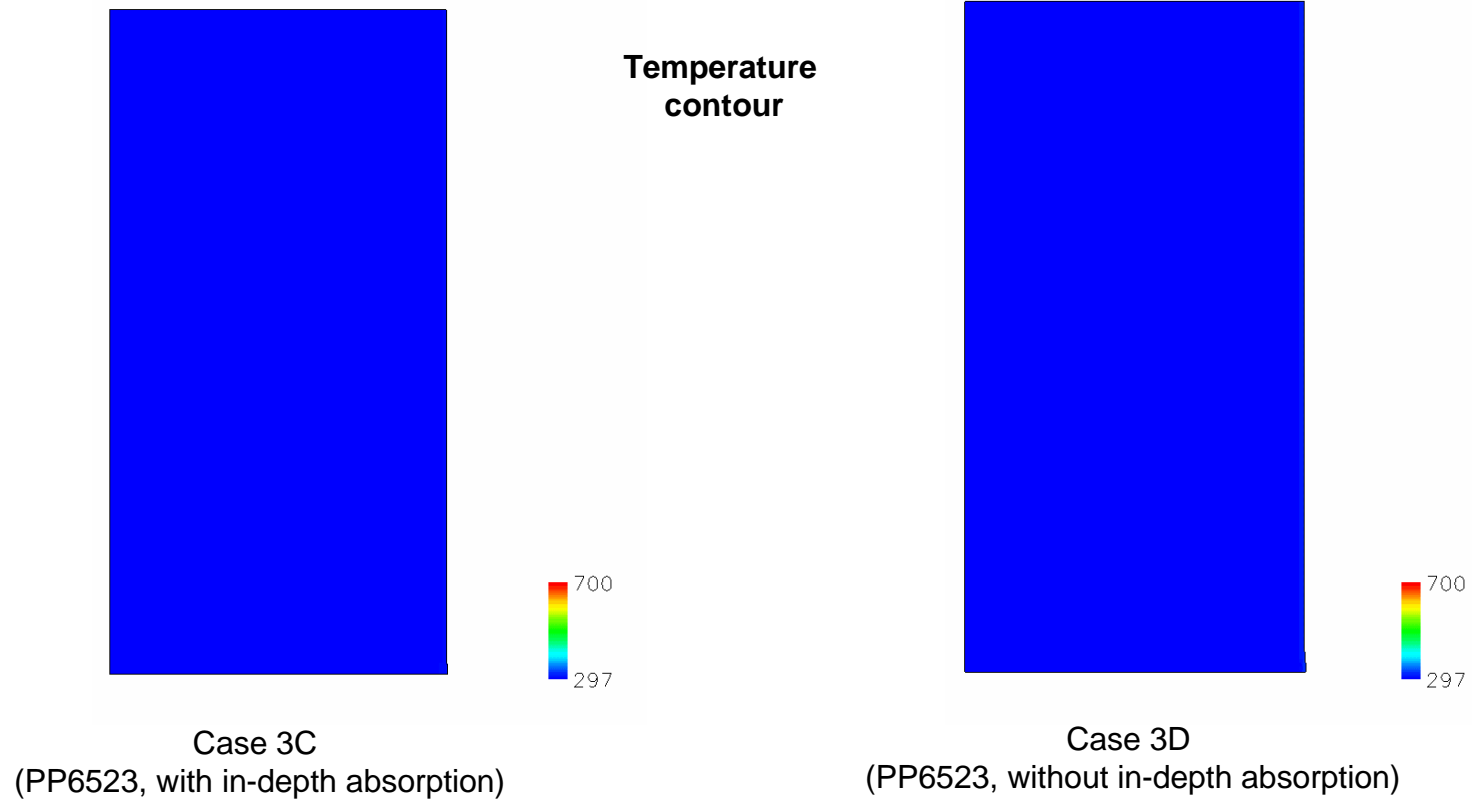
Simulated Melting Process (PP702N)



⊕ Time interval between movie frames: 5 seconds



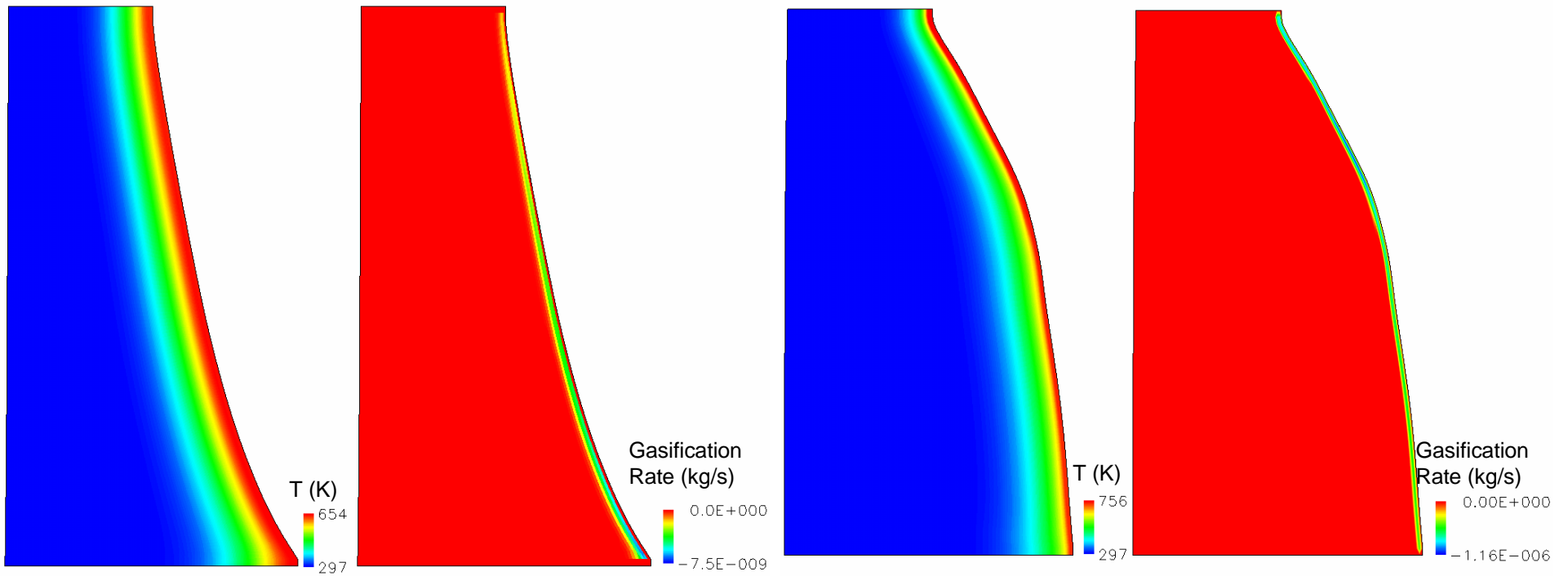
Simulated Melting Process (PP6523)



⊕ Time interval between movie frames: 5 seconds



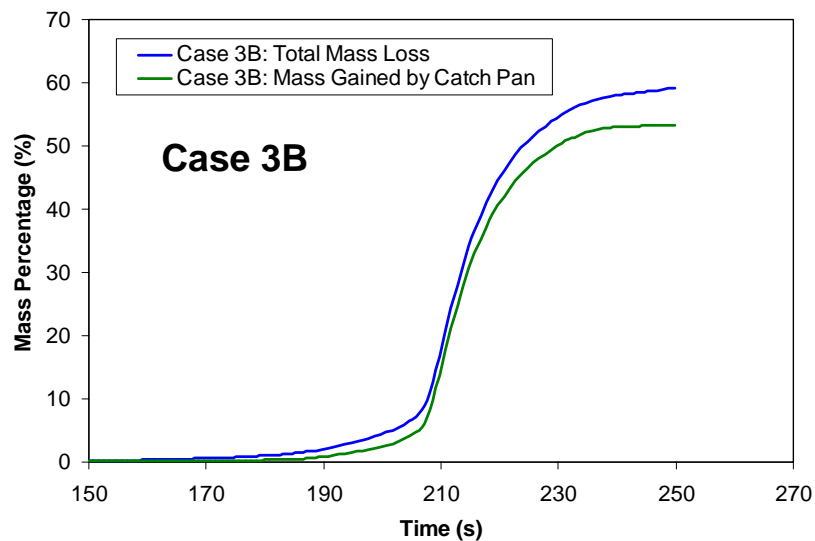
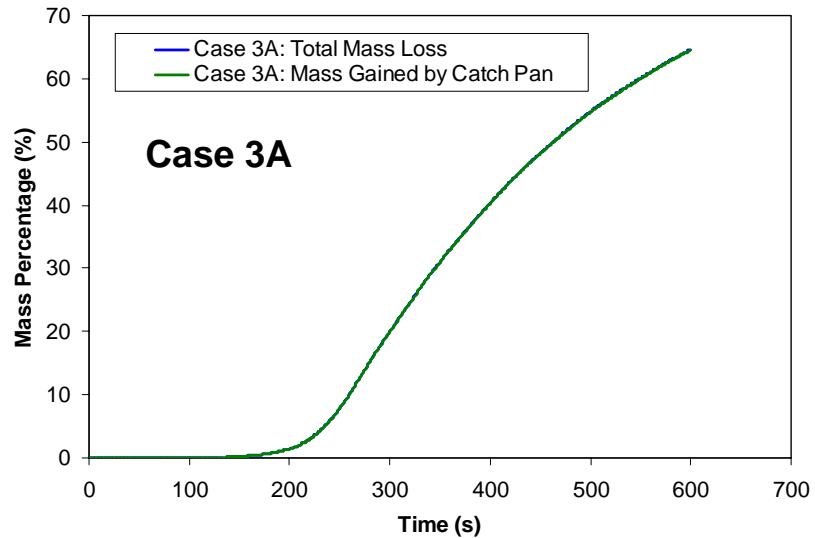
Gasification Rate (kg/s) (PP6523)



Case 3C
(PP6523, with in-depth absorption)

Case 3D, 255 sec.
(PP6523, without in-depth absorption)

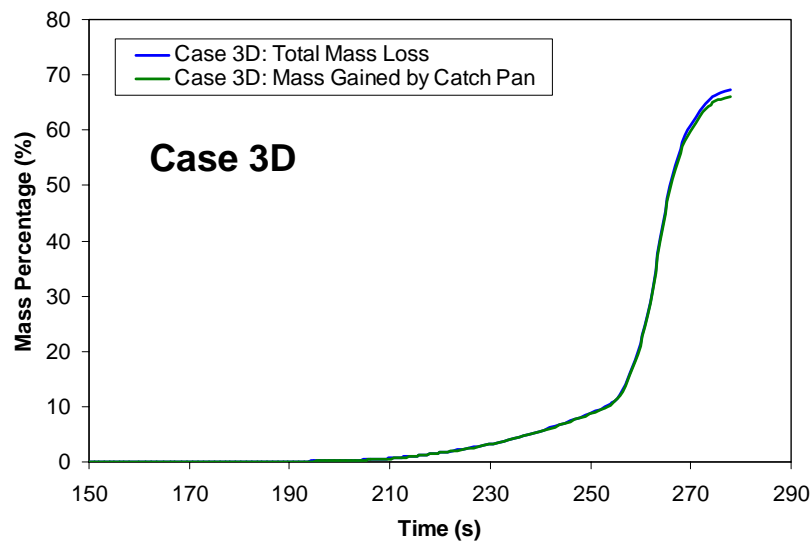
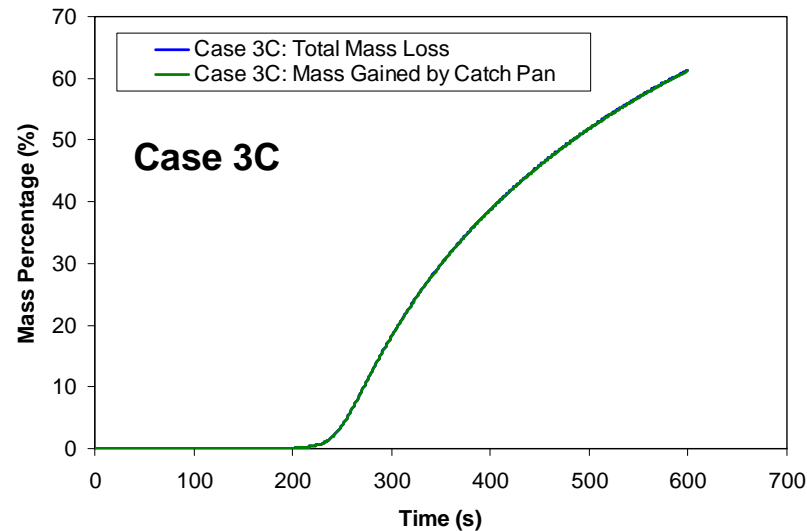
Mass Loss as Function of Time (PP702N)



- The differences between the blue curve and the green curve represent the mass loss due to gasification
- Mass loss due to gasification is negligible in Case 3A. In Case 3B, about 8% mass loss is due to gasification at the end of the simulation
- Experimental data indicates that gasification accounts for 8 to 10% mass loss.



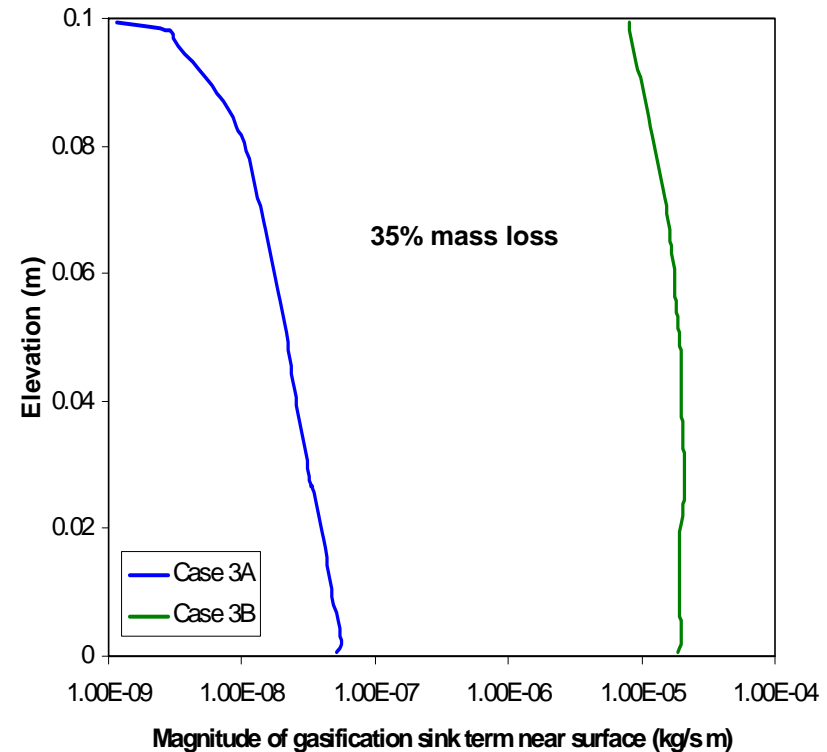
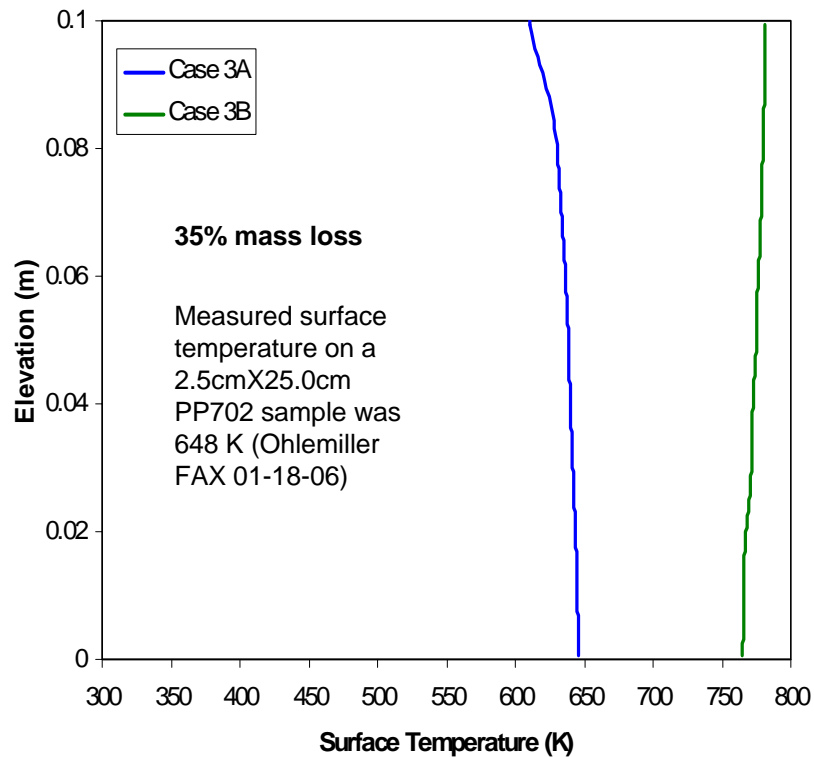
Mass Loss as Function of Time (PP6523)



- The differences between the blue curve and the green curve represent the mass loss due to gasification
- Mass loss due to gasification is negligible in Case 3C, and is very small in Case 3D (~3% at the end of the simulation)



Example: Surface Temperature and Gasification Sink Term

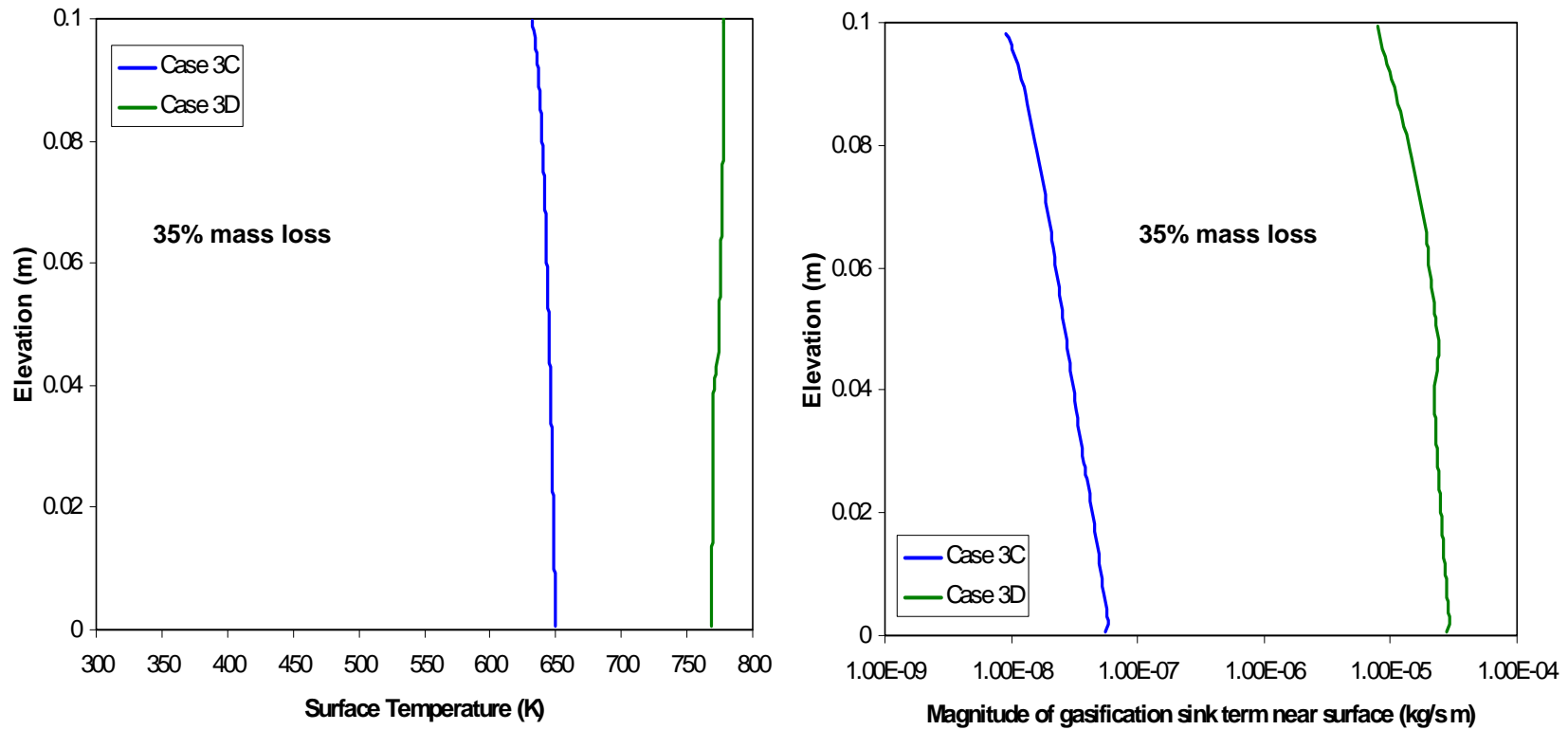


Surface temperature and gasification sink term profiles at 35% mass loss (PP702N)

- ⊕ Surface temperature increases more than 100 K when in-depth absorption model turned off
- ⊕ Magnitude of gasification sink term near the surface decreases by three orders of magnitude when in-depth absorption model turned off
- ⊕ Predicted surface temperature is in good agreement with measurement when in-depth absorption model turned on



Example: Surface Temperature and Gasification Sink Term



Surface temperature and gasification sink term profiles at 35% mass loss (PP6523)

Summary

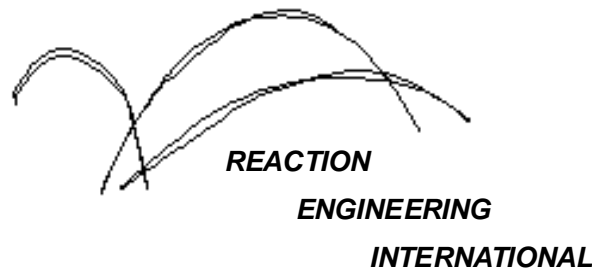
- ⊕ Results presented for two raisins with gasification, heat losses and in-depth absorption of external heat flux at 30 KW/m^2
- ⊕ Cases were run to at least 60% mass loss
- ⊕ Computational Cost highlighted
 - ⊕ Inclusion of gasification model does not have a big impact on run time.
- Example Results
 - ⊕ Free surface location, temp., gasification sink term
 - ⊕ Movie of free surface location and temperature
 - ⊕ Mass loss, surface temperature, gasification sink term
- ⊕ Discrepancy with measurement
 - ⊕ Measured surface temperature and gasification mass loss for PP702N are available
 - ⊕ Predicted surface temperature agrees well with measurement when all sub-models, i.e., gasification, heat loss, and in-depth absorption models, are included in the simulation. However, the predicted gasification mass loss is negligible.
 - ⊕ When turning off the in-depth absorption model, predicted gasification mass loss becomes significant. However, the predicted surface temperature is at least 100 K higher than the measurement
 - ⊕ The above observations suggest that, in order to match the experimental data, both the in-depth absorption model and the in-depth gasification model need improvements.



A Computational Model For Fire Growth and Spread On Thermoplastic Objects

**Task 3: 2D model with in-depth gasification
Parametric Study of model constants**

(8/31/06)



Outline

- ⊕ Introduction
- ⊕ In-depth absorption and gasification models in the parametric study
- ⊕ Parametric Cases studied
 - ⊕ Increase gasification rate
 - ⊕ Decrease heat flux penetration length
 - ⊕ Shift gasification to start at a lower temperature
 - ⊕ Increase external heat flux
- ⊕ Summary

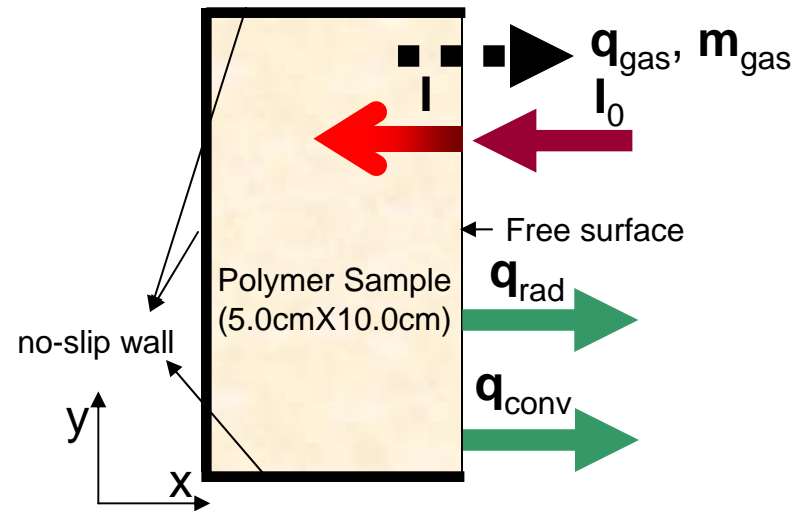


Introduction

- ⊕ In-depth absorption and gasification models provided by NIST has been implemented into the CPCFD code. See 8/11/06 report for detail.
- ⊕ As noted in 8-11-06 report, after simulating two polymer resins (PP702N and PP6523), it was found that
 - ⊕ Predicted surface temperature agrees well with measurement when all sub-models, i.e., gasification, heat loss, and in-depth absorption models, are included in the simulation. However, the predicted gasification mass loss is negligible.
 - ⊕ When turning off the in-depth absorption model, predicted gasification mass loss becomes significant. However, the predicted surface temperature is at least 100 K higher than the measurement
- ⊕ The above observations suggest that, in order to match the experimental data, both the in-depth absorption model and the in-depth gasification model need adjustments.
- ⊕ A parametric study regarding the two models is summarized in this report.
- ⊕ Simulations are performed for resin PP702N only



Gasification, absorption and heat losses models



Sketch of gasification, absorption and heat loss model

⊕ Energy source/sink terms due to gasification, absorption, and heat losses

⊕ **In-depth gasification:** $\dot{q}_{\text{gasification}} = -\int_{\Omega} H_v \rho A e^{(-E/RT)} d\Omega$

⊕ **In-depth absorption:** $\dot{q}_{\text{absorption}} = \int_{\Omega} \frac{dI}{dx} d\Omega$, assuming absorption process in x-direction only

⊕ Radiative heat loss: $\dot{q}_{\text{radiation}} = -A \varepsilon \sigma (T^4 - T_0^4)$, assuming radiative heat loss only on free surface

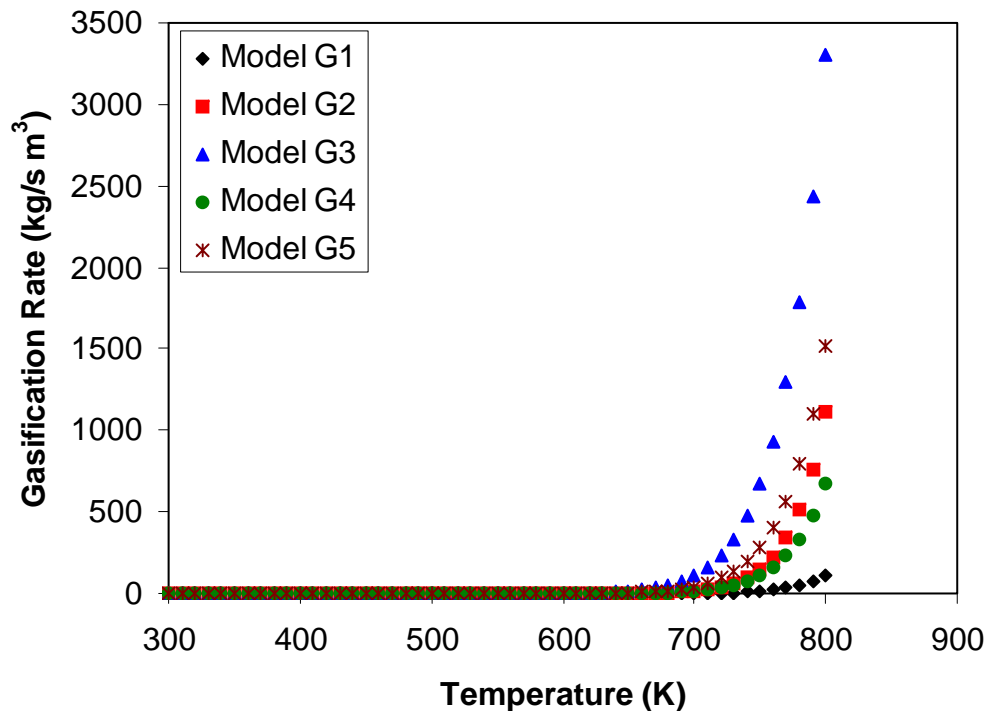
⊕ Convective heat loss: $\dot{q}_{\text{convection}} = -A h_{\text{conv}} (T - T_0)$

⊕ Heat sink term to avoid over heating in Task 1 and 2 has been deactivated in this study

⊕ **Mass sink terms due to gasification:** $\dot{m}_{\text{gasification}} = -\int_{\Omega} \rho A e^{(-E/RT)} d\Omega$



Gasification Models Used in Parametric Study



Mass loss rate due to gasification as functions of time

$$\text{Model expression: } y = A \exp\left(-\frac{B}{(x+C)}\right)$$

x : temperature (K)

y : gasification rate (kg/s m³)

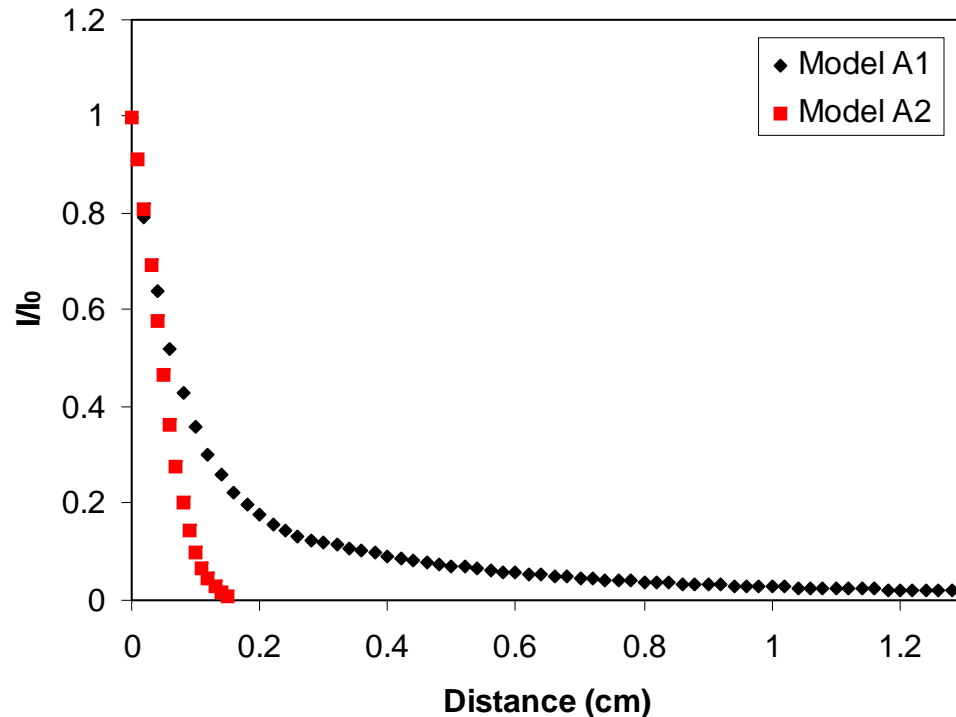
Gasification model parameters

	A (1/s)	B	C (K)
Model G1	2.18e+12	24400	0
Model G2	2.18e+13	24400	0
Model G3	2.18e+12	24400	100
Model G4	2.18e+12	24400	50
Model G5	2.18e+12	24400	75

- ⊕ Specific gasification heat increases from 800 J/g to 1260 J/g for calculating the gasification heat sink term in all models
- ⊕ Model G1 is the base model
- ⊕ Model G2 increases the magnitude of gasification rate by a factor of 10
- ⊕ Model G3, G4 and G5 shift the occurrence of gasification to lower temperature by 100, 50, and 75 K, respectively.



Absorption Models Used in Parametric Study



Normalized Incident Heat Flux Profile as a Function of Distance from Free Surface

Model expression:

Model A1:

$$\frac{I}{I_0} = 10^{(-5.17x + 6.964x^2)}, \quad 0 \leq x < 0.3$$

$$\frac{I}{I_0} = 10^{(-0.5154 - 1.473x + 0.4339x^2)}, \quad 0.3 < x \leq 1.3$$

Model A2:

$$\frac{I}{I_0} = \exp(-153.507x^2 - 7.6753x), \quad 0 \leq x < 0.15$$

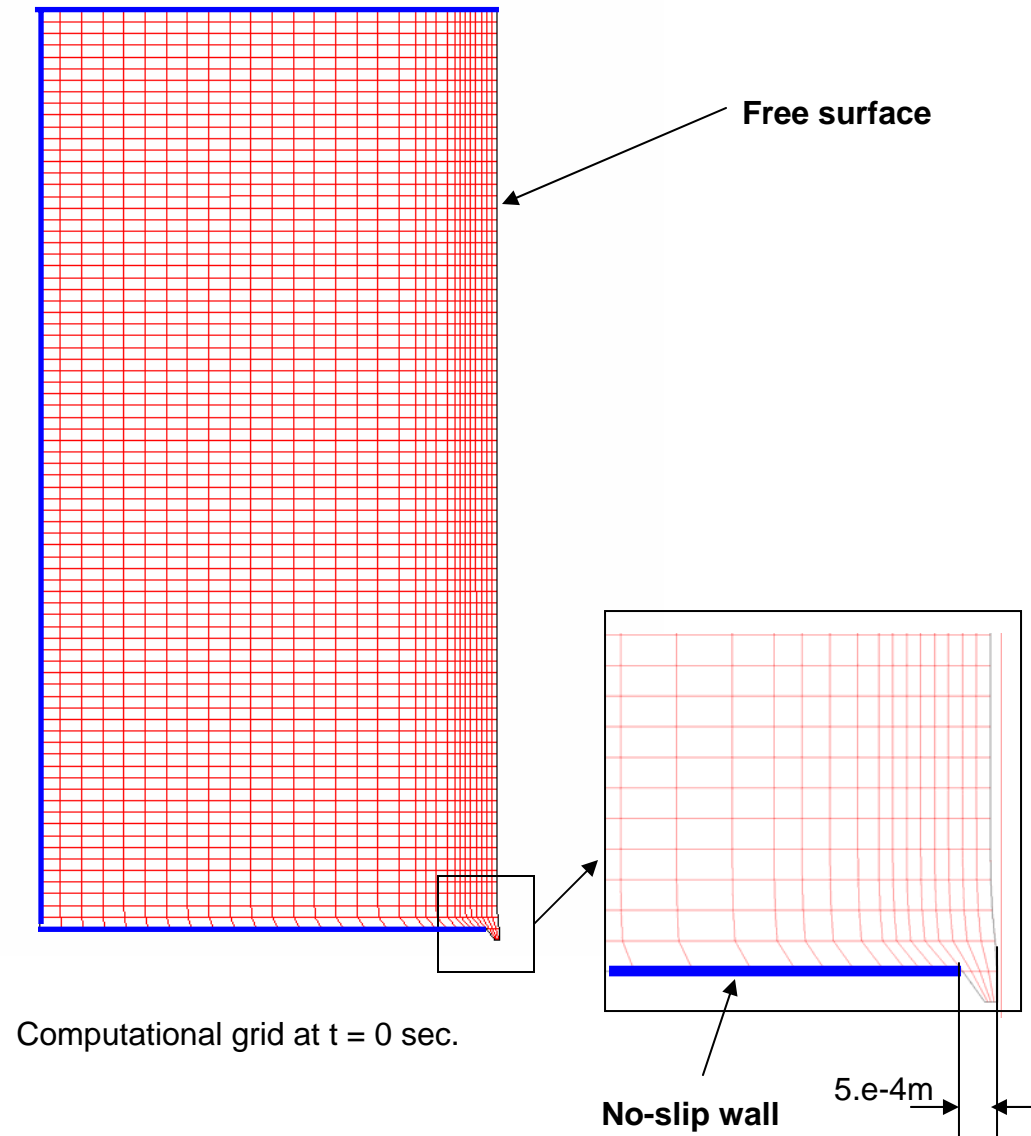
x : distance from free surface in cm

- ⊕ Model A1 is the base model
- ⊕ Model A2 shortens the penetration length of the incident heat flux
- ⊕ The heat flux penetration length covers at least 4 cells in the horizontal direction near the free surface



Computational Grid

- ⊕ Polymer sample dimension:
5.0cm X 10.0cm X 2.54cm
- ⊕ Modeled as a 2-D problem
with a computational domain
of 5.0cm X 10.0cm
- ⊕ 30X80 Grid (biased)
- ⊕ Initial grid resolution the same
as the 19X200 grid used in
Task 1
- ⊕ Equivalent to 100X80 grid if
using uniform grid spacing and
fixed grid



Case Summary

Case #	In-depth Gasification Model	In-depth Absorption Model	External heat flux (KW/m ²)
Case 3A	Model G1	Model A1	30
Case 3F	Model G2	Model A1	30
Case 3G	Model G1	Model A2	30
Case 3H	Model G3	Model A2	30
Case 3I	Model G4	Model A2	30
Case 3J	Model G5	Model A2	30
Case 3K	Model G3	Model A2	40
Case 3L	Model G5	Model A2	40

- ⊕ All cases are for PP702N
- ⊕ Radiation and convective heat losses at free surface are included in all cases
- ⊕ Case 3A is the baseline case



Simulation Results Summary

	Exposed time to reach 35% mass loss (s)	Average surface temperature at 35% mass loss (K)	Average surface gasification rate at 35% mass loss (g/s m)	Total mass loss rate* (g/s)	Mass loss rate due to flow* (g/s)
Case 3A	368	636	1.54e-7	0.18	0.18
Case 3F	383	634	1.44e-6	0.17	0.17
Case 3G	378	649	3.47e-7	0.18	0.18
Case 3H	806	625	1.53e-5	0.063	0.042
Case 3I	461	646	4.15e-6	0.15	0.14
Case 3J	675	637	9.10e-6	0.083	0.070
Measurement * +	N/A	648 !	N/A	0.053	0.035
Case 3K	602	640	2.93e-5	0.080	0.046
Case 3L	355	654	1.92e-5	0.15	0.13
Measurement * +	N/A	N/A	N/A	0.086	0.051

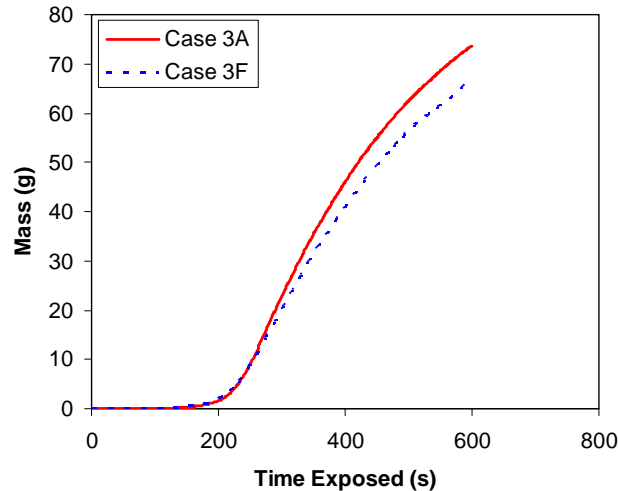
* mass loss rates are calculated from 200s to 600s for cases with 30KW/m² heat flux and from 100 to 600s for cases with 40KW/m² heat flux. The initial dimension of the simulated sample is 5.0cmX10.0cmX2.54cm.

+ measurement data was calculated based on data reported in "A Progress Report on Numerical Modeling of Experimental Polymer Melt Flow Behavior" by Kathryn M. Butler, et al. ***The initial dimension of the measured sample was not reported in the report and is assumed to be the same as that of the computational model.***

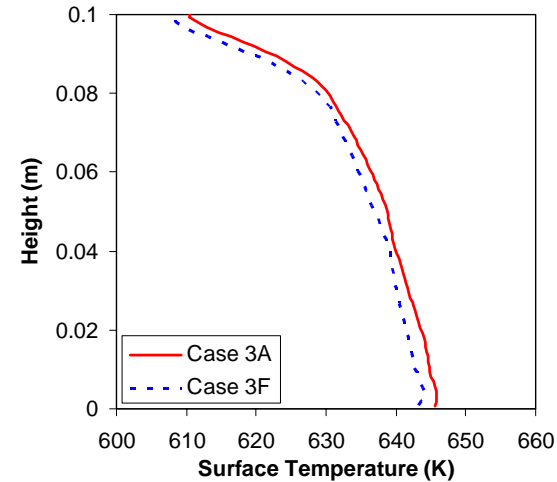
! Measured surface temperature was for a 2.5cmX25.0cm PP702 sample (Ohlemiller FAX 01-18-06). Most likely this was a point measurement (i.e., not a measurement of the average surface temperature). At what time or during what time period that this measurement was done was not available.



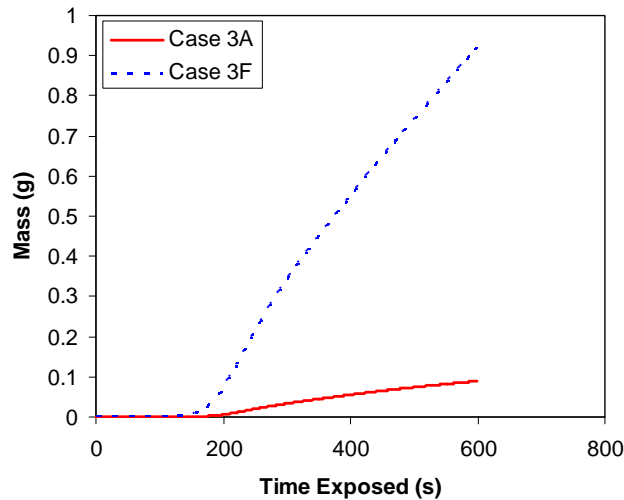
Impact of Increasing Gasification Rate



Mass gained by catch pan as a function of time



Surface Temperature Profile at 35% mass loss

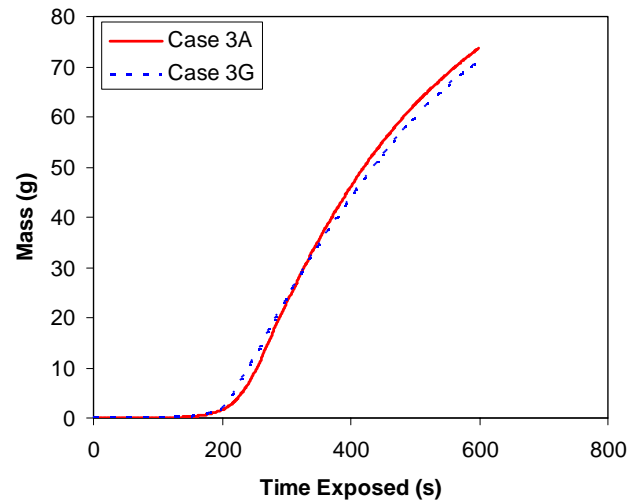


Gasification mass loss as a function of time

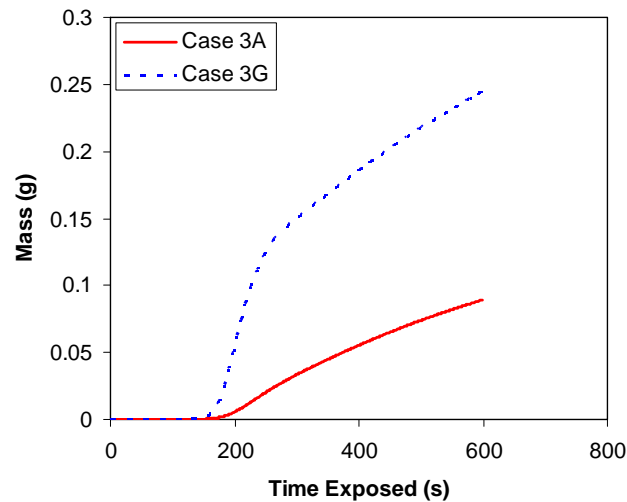
- ⊕ Increasing gasification rate by a factor of ten decreases surface temperature slightly
- ⊕ Gasification mass loss in Case 3F is ten times that of the baseline case
- ⊕ Compared to mass loss due to melting flow, gasification mass loss is still negligible in Case 3F
- ⊕ Overall mass loss rate in Case 3F is slightly smaller than that of Case 3A due to the slightly lower surface temperature and that melting flow still dominates the mass loss.



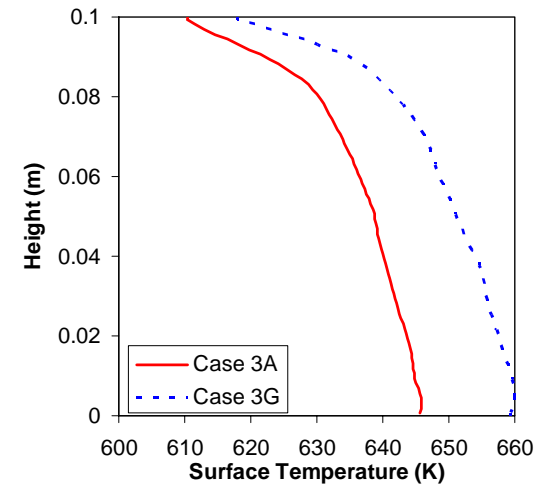
Impact of Decreasing Heat Flux Penetration Length



Mass gained by catch pan as a function of time



Gasification mass loss as a function of time

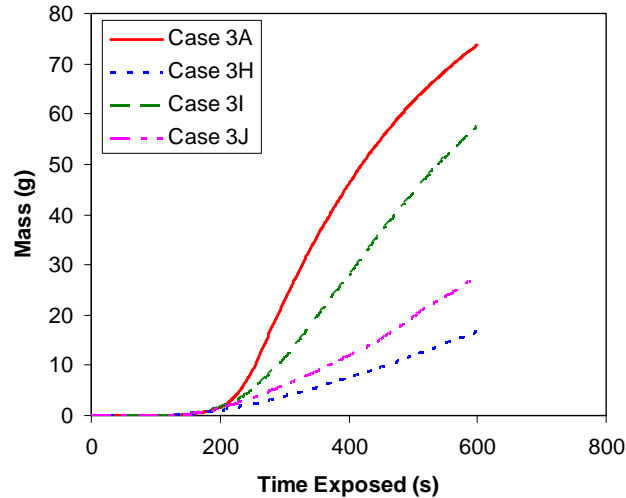


Surface Temperature Profile at 35% mass loss

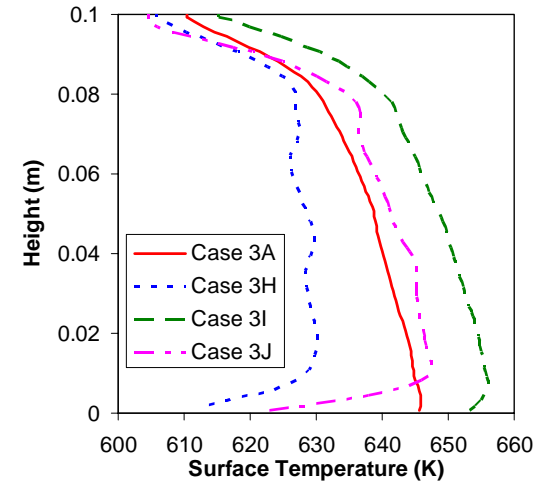
- ⊕ Decreasing incident heat flux penetration length increases surface temperature
- ⊕ Increased surface temperature leads to increased gasification mass loss
- ⊕ Compared to mass loss due to melting flow, gasification mass loss is still negligible
- ⊕ Decreasing heat flux penetration length alone does not have a big impact on overall mass loss history



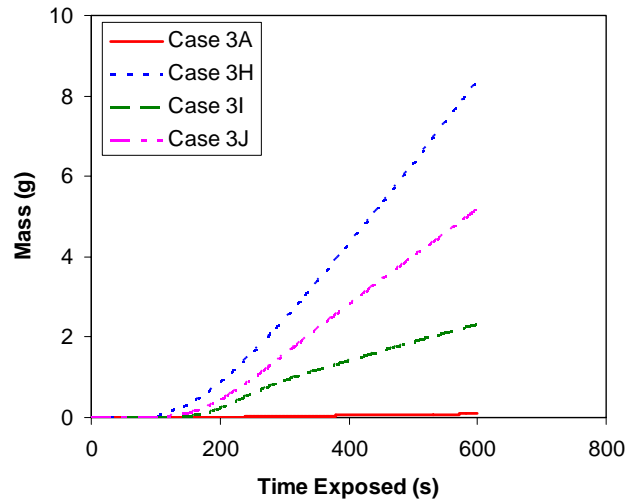
Impact of Shifting Gasification to Lower Temperature



Mass gained by catch pan as a function of time



Surface Temperature Profile at 35% mass loss

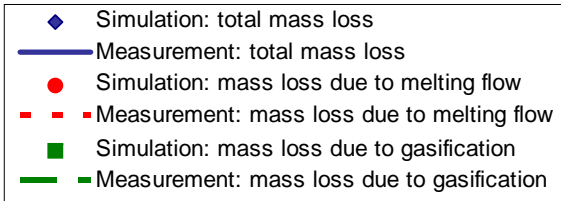
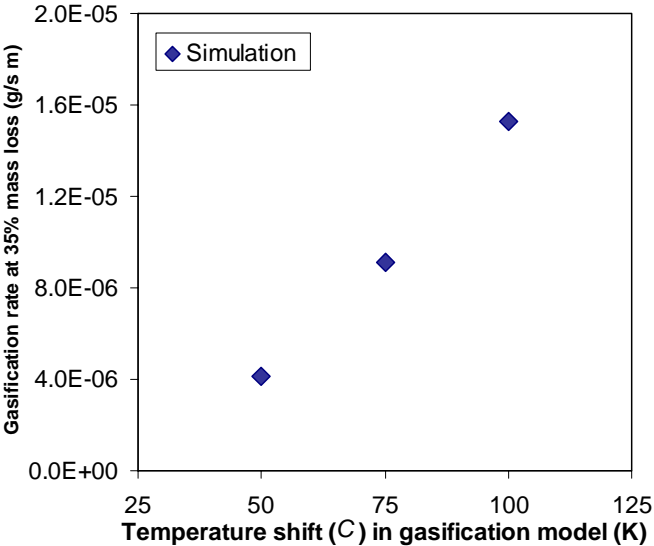
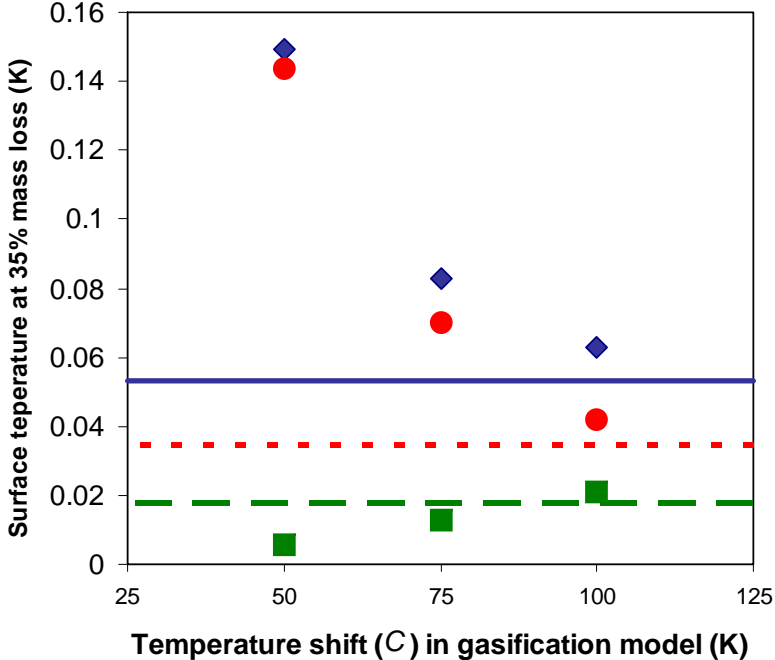
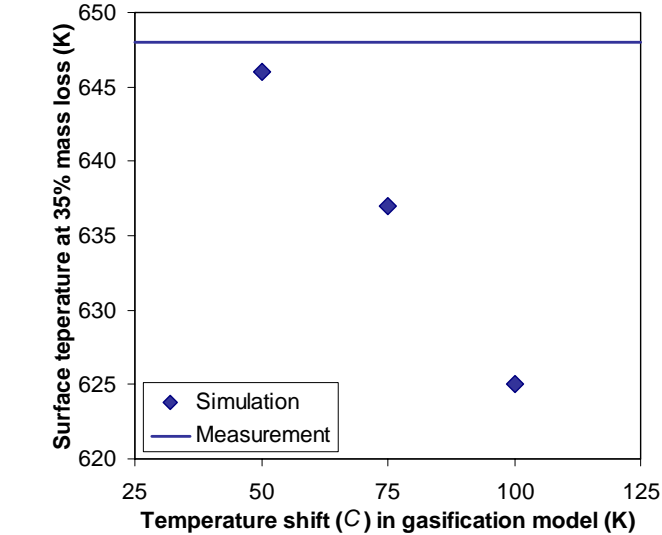


Gasification mass loss as a function of time

- ⊕ In Case H, I and J the modified absorption model is adapted
- ⊕ Shifting gasification to lower temperature range has a big impact on the melting process
- ⊕ Larger temperature shift (value of C in slide 5) leads to lower surface temperature, less mass loss due to melting flow, but more mass loss due to gasification



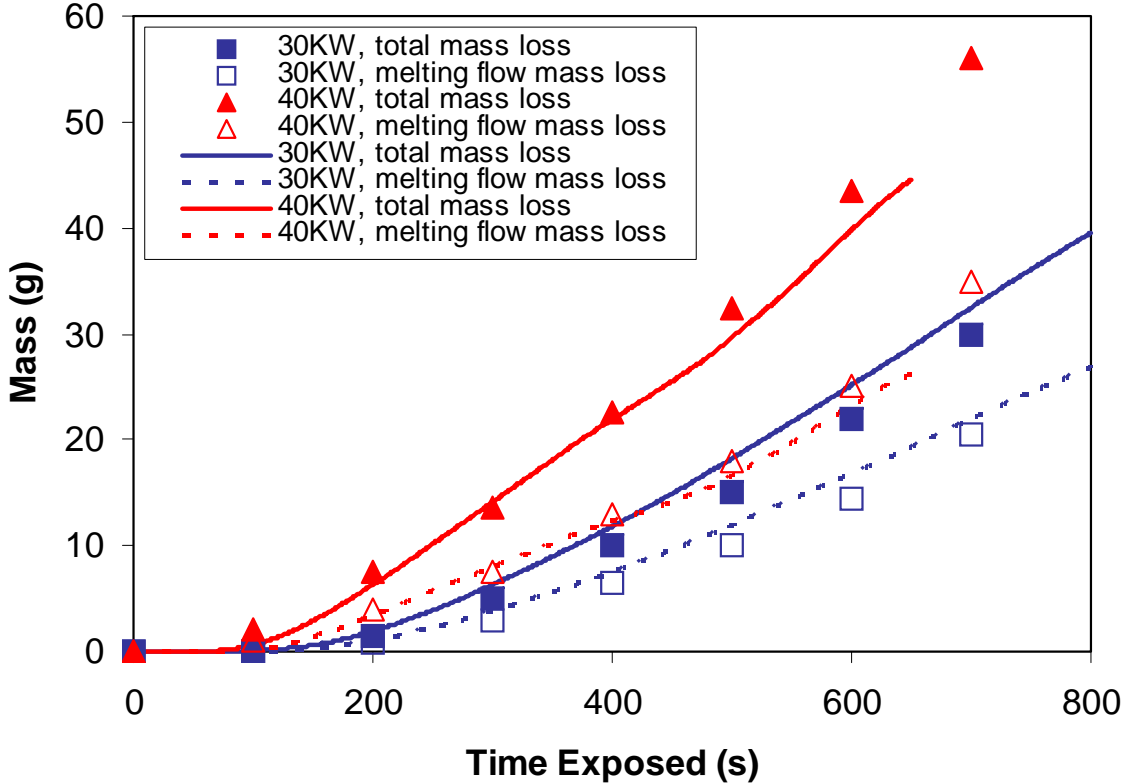
Close Look at Case H, I and J



⊕ Case 3H (C=100K) seems to yield fairly good agreement with the measured data in terms of mass loss rates



Mass Loss Histories at Different Heat Flux



- ⊕ Symbols – experimental data (“A Progress Report on Numerical Modeling of Experimental Polymer Melt Flow Behavior” by Kathryn M. Butler, et al)
- ⊕ Lines – Case 3H and Case 3K Simulation results



Summary

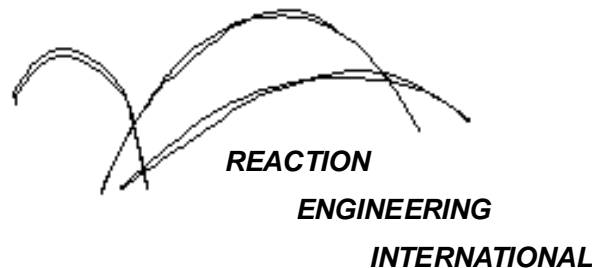
- ⊕ The impacts of different in-depth absorption and gasification models on the melting behavior have been studied
- ⊕ When only modifying one model, we have the following observation:
 - ⊕ Increasing the magnitude of the gasification rate by a factor of ten significantly enhances the gasification mass loss, which, however, is still negligible to the mass loss due to melting flow
 - ⊕ Shortening the penetration length of incident heat flux in the in-depth absorption model by a factor of at least three increases the surface temperature by about 15K, which leads to slightly more gasification mass loss. However, the overall mass loss history does not change much.
- ⊕ When modifying both models, we found that:
 - ⊕ Shifting the occurrence of gasification towards lower temperature range significantly altered the melting behavior.
 - ⊕ More temperature shifting towards lower temperature range -> lower surface temperature -> less mass loss due to melting flow -> more mass loss due to gasification -> slower overall melting process.
- ⊕ When combining model G3 for gasification and model A2 for absorption, the simulation results for PP702N seem to agree well with experimental data for heat flux of 30KW/m² and 40KW/m².



A Computational Model For Fire Growth and Spread On Thermoplastic Objects

**Task 3: 2D model with in-depth gasification
Parametric Study of model constants**

(9/14/06)

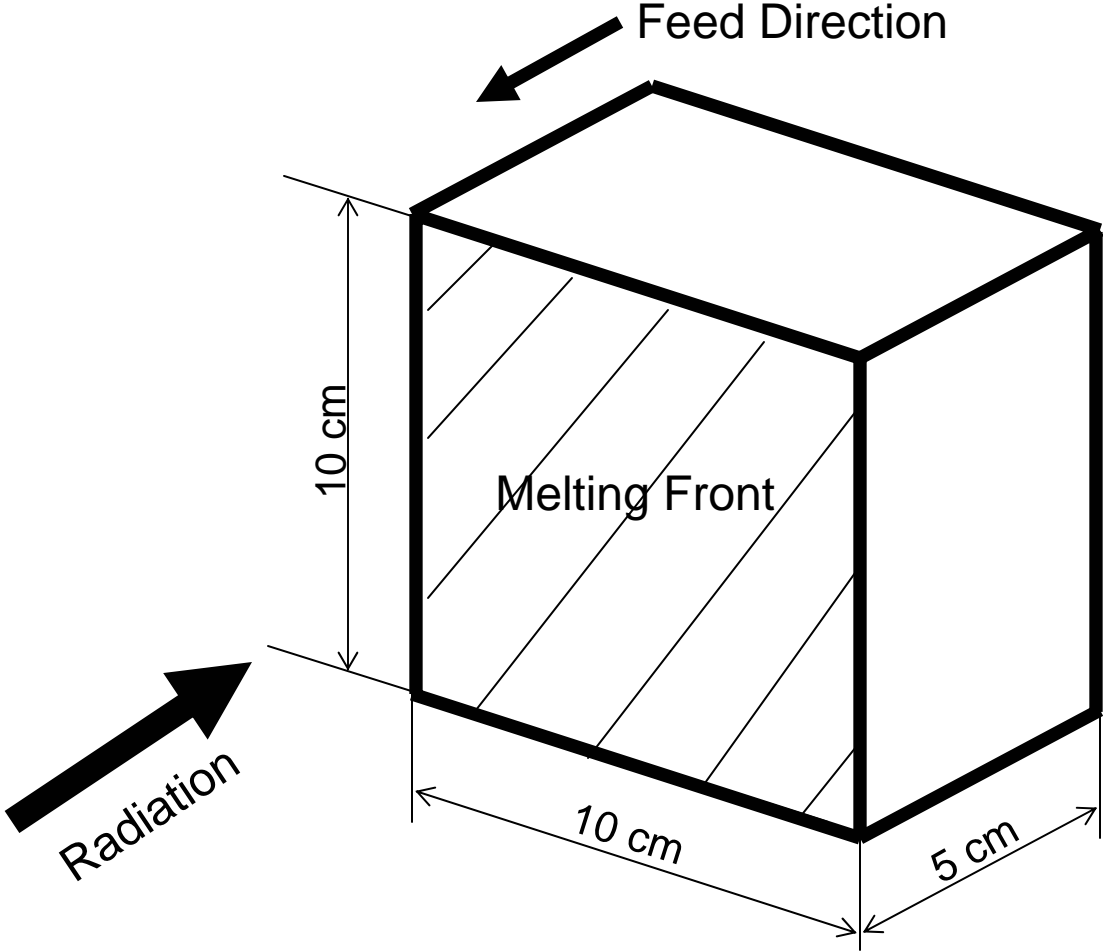


Outline

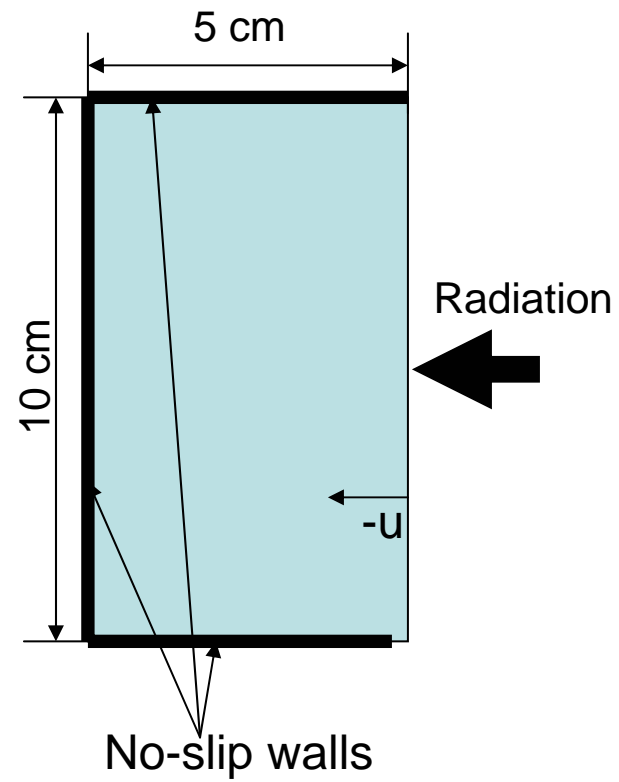
- ⊕ Physical Model
- ⊕ CFD Model
- ⊕ Comparison of previous simulation results with new experimental data
- ⊕ In-depth gasification models to be tested



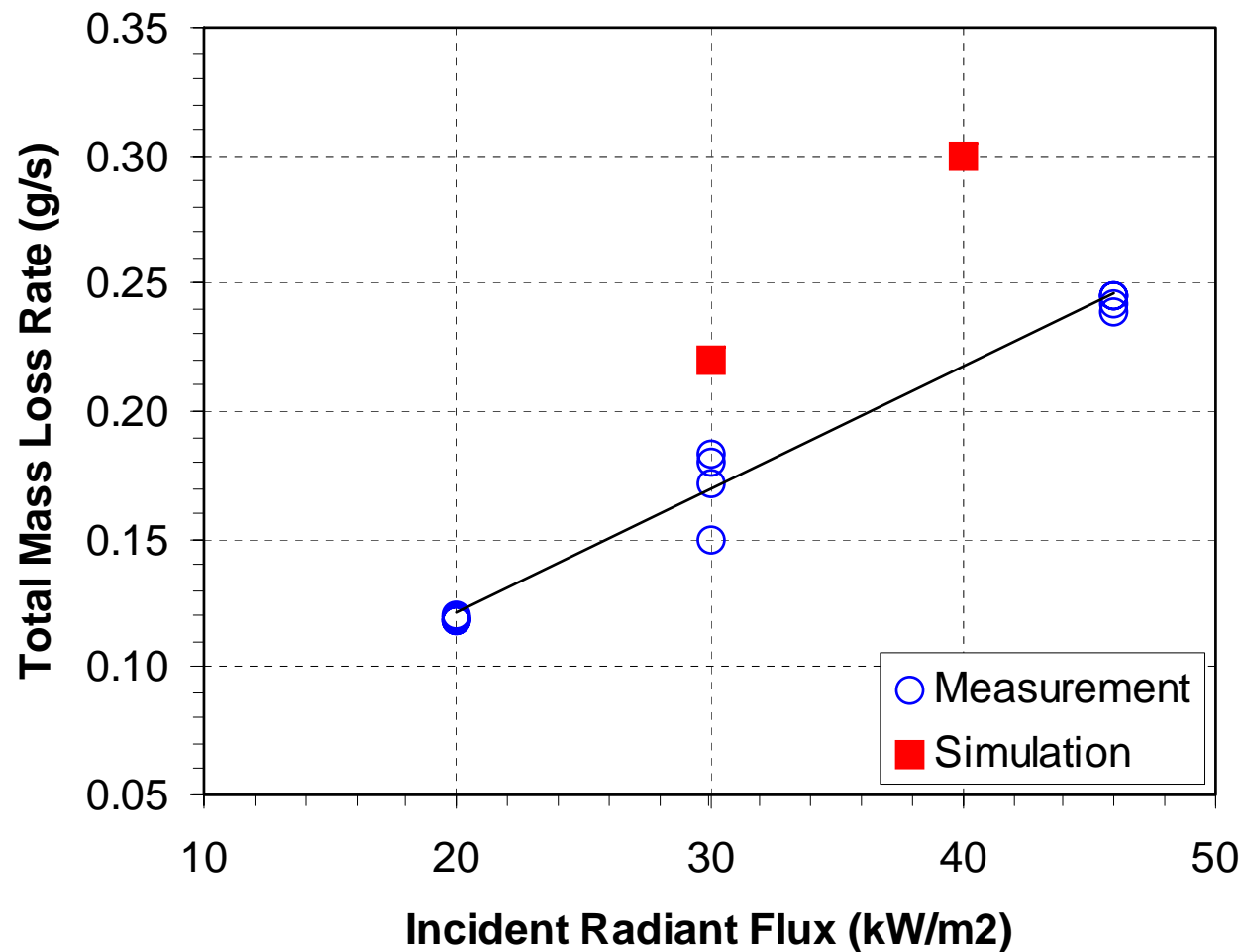
Physical Model



CFD Model

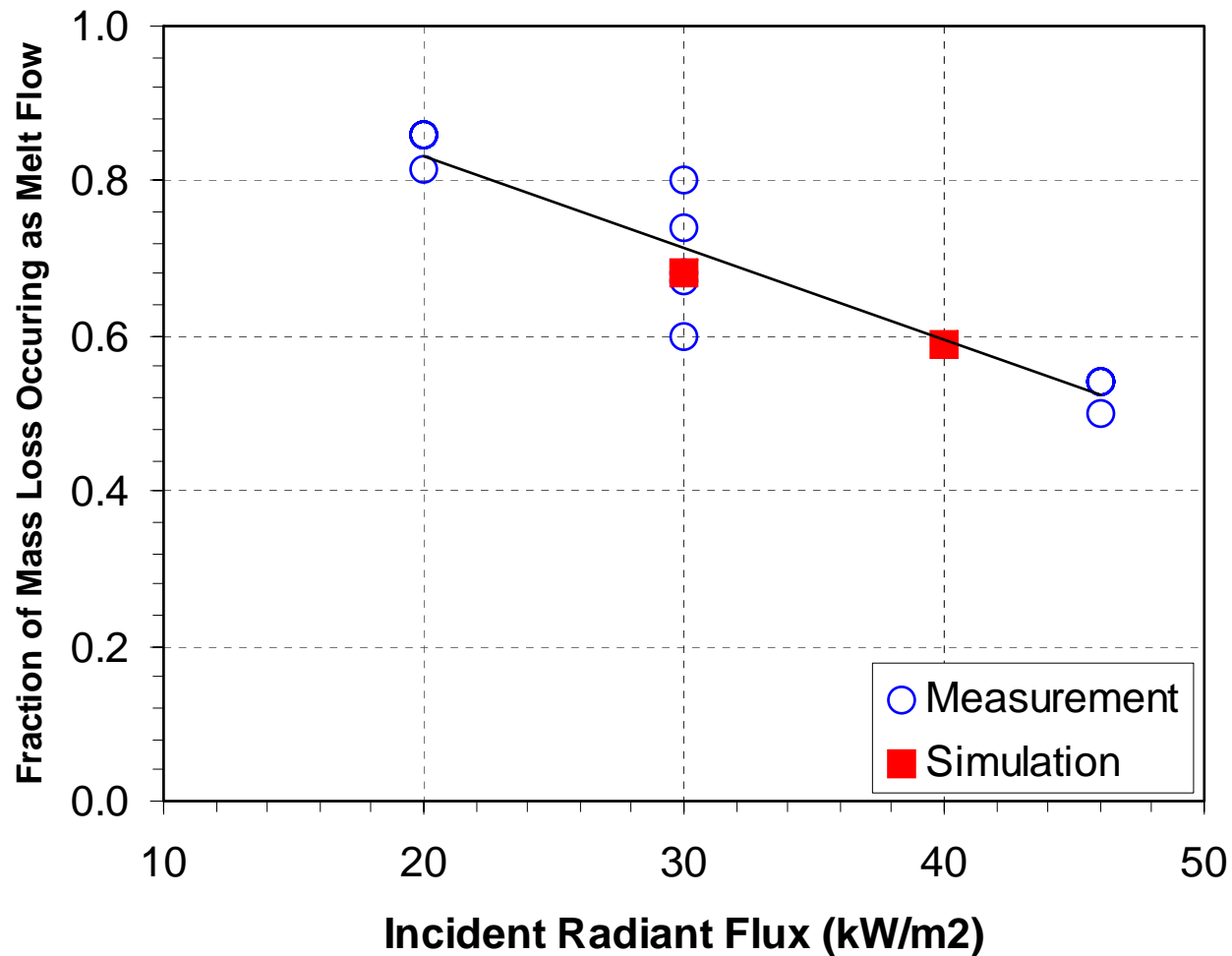


Comparison of CFD Results with Data



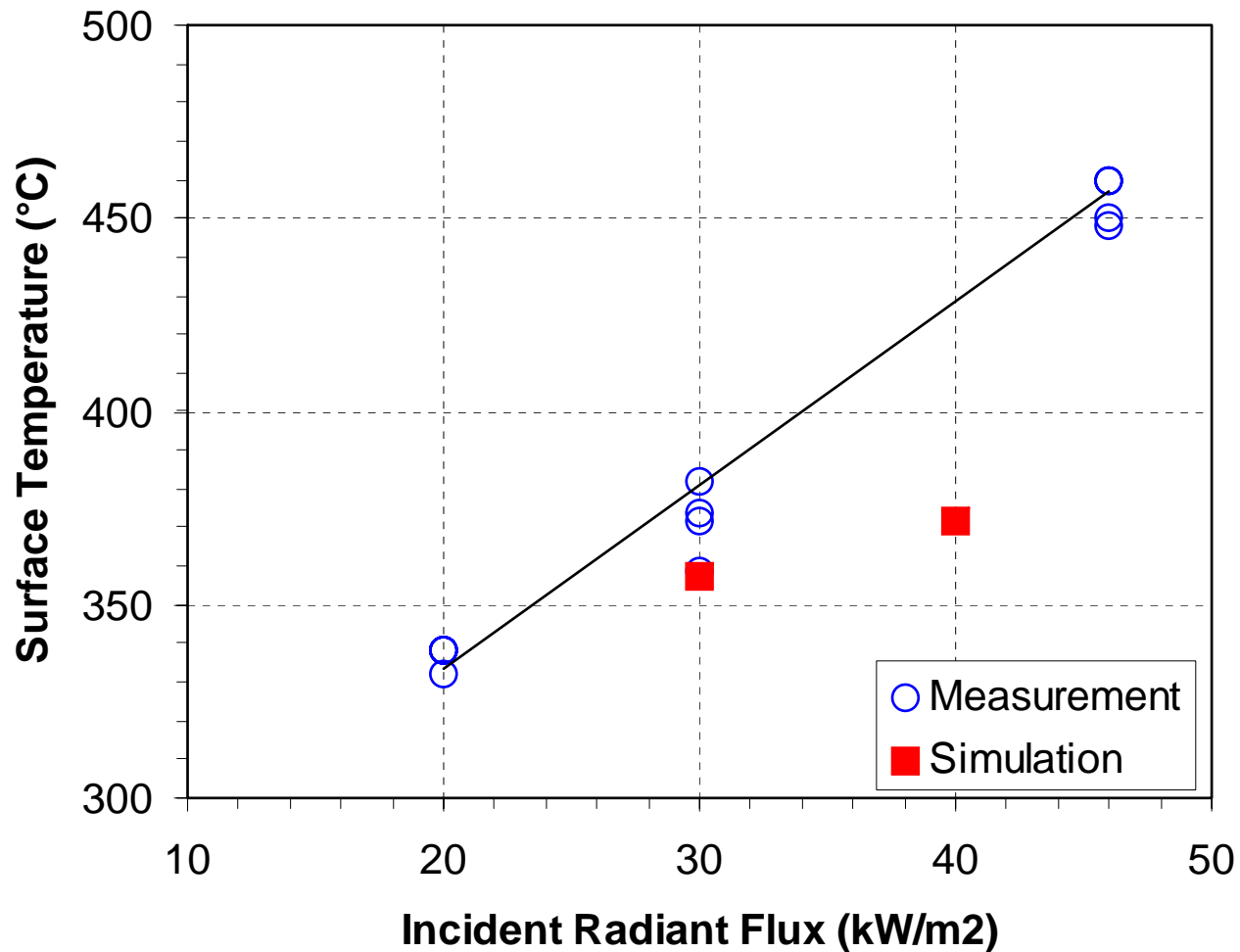
- ⊕ Simulation results are from Case 3H and Case 3K using CFD model 1 (see 8/31/06 report for detailed)
- ⊕ Measurement data provided by NIST (TOM, O., Fax 9/8/06)

Comparison of CFD Results with Data



- ⊕ Simulation results are from Case 3H and Case 3K using CFD model 1 (see 8/31/06 report for detailed)
- ⊕ Measurement data provided by NIST (TOM, O., Fax 9/8/06)

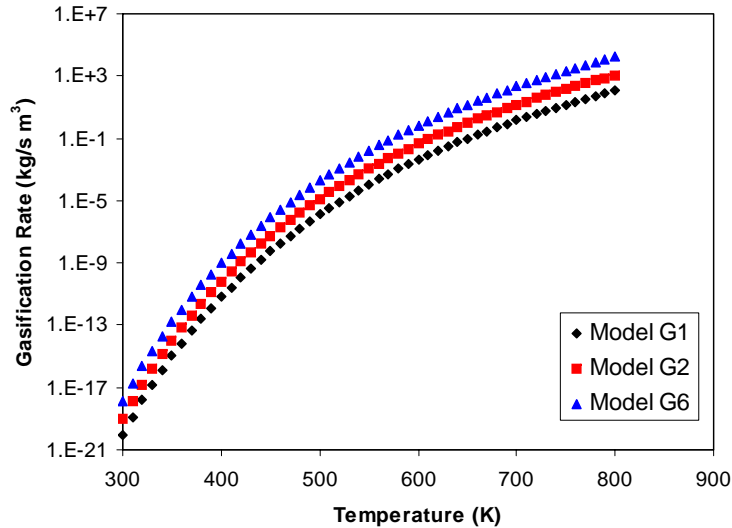
Comparison of CFD Results with Data



- ⊕ Simulation results are from Case 3H and Case 3K using CFD model 1 (see 8/31/06 report for detailed)
- ⊕ Measurement data provided by NIST (TOM, O., Fax 9/8/06)



Gasification Models for Future Work



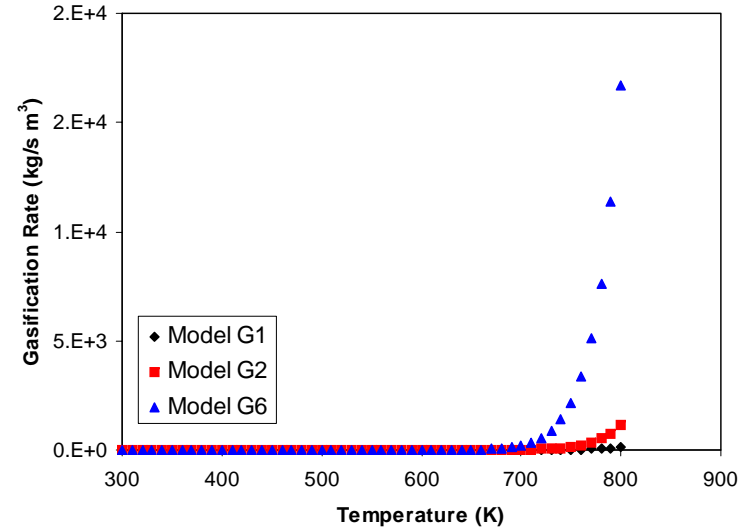
Mass loss rate (in log scale) due to gasification as functions of time

Model expression: $y = A \exp\left(-\frac{B}{x}\right)$

x : temperature (K)

y : gasification rate (kg/s m³)

- ⊕ Model G1 is the base model
- ⊕ Model G2 increases the magnitude of gasification rate by a factor of 10
- ⊕ Model G6 increases the magnitude of gasification rate by a factor of 150



Mass loss rate due to gasification as functions of time

Gasification model parameters

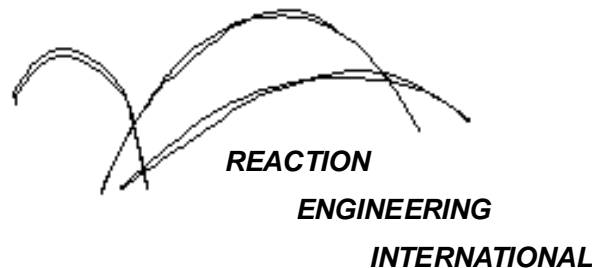
	A (1/s)	B
Model G1	2.18e+12	24400
Model G2	2.18e+13	24400
Model G6	3.27e+14	24400



A Computational Model For Fire Growth and Spread On Thermoplastic Objects

**Task 3: 2D model with in-depth gasification
Parametric Study of model constants**

(9/26/06)

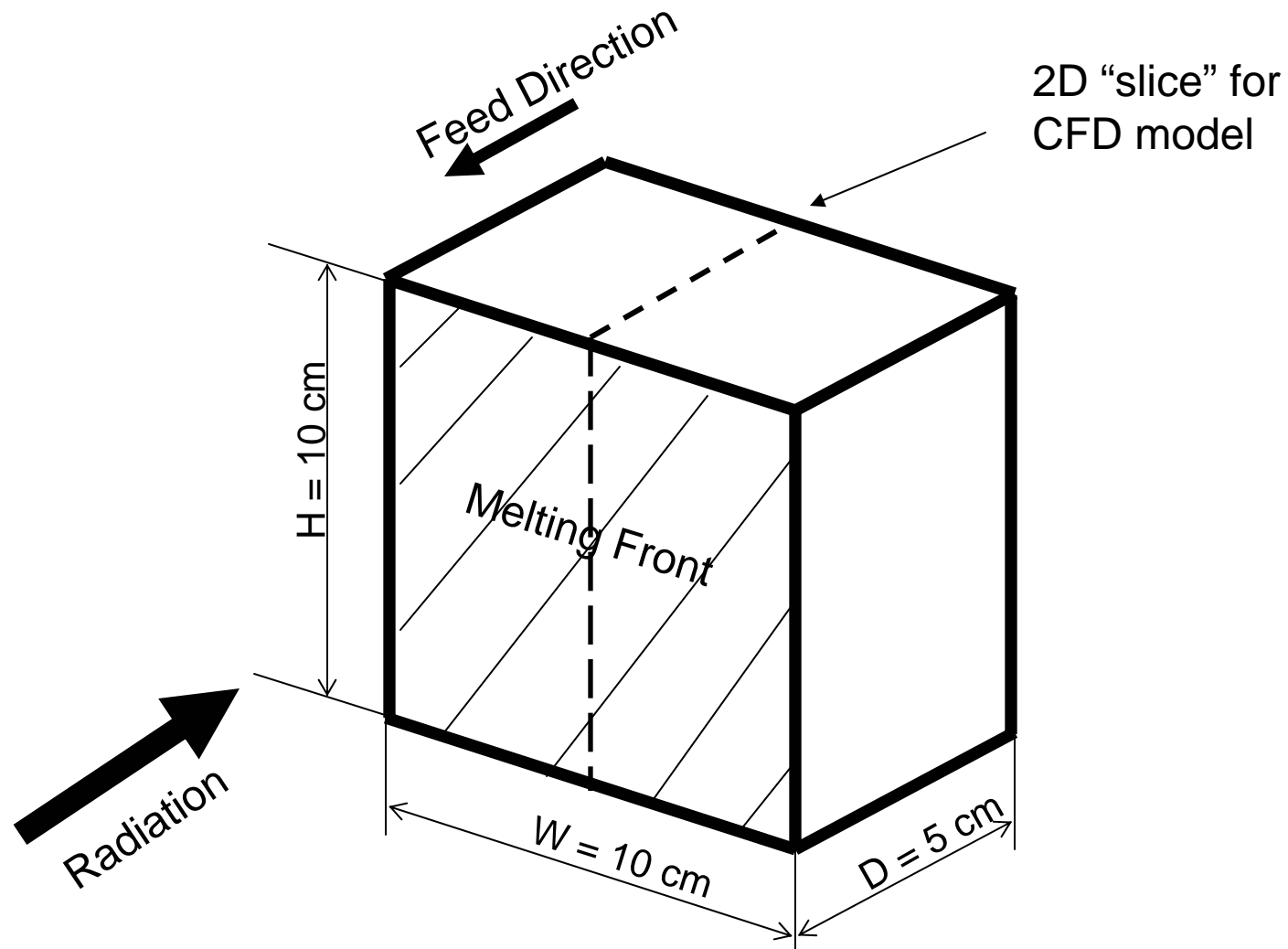


Outline

- ⊕ Physical Model
- ⊕ CFD Model
- ⊕ Modifications in absorption and gasification models
- ⊕ Selected simulation results and comparisons with data for PP702N
- ⊕ Selected simulation results for PP6523
- ⊕ Summary



Physical Model



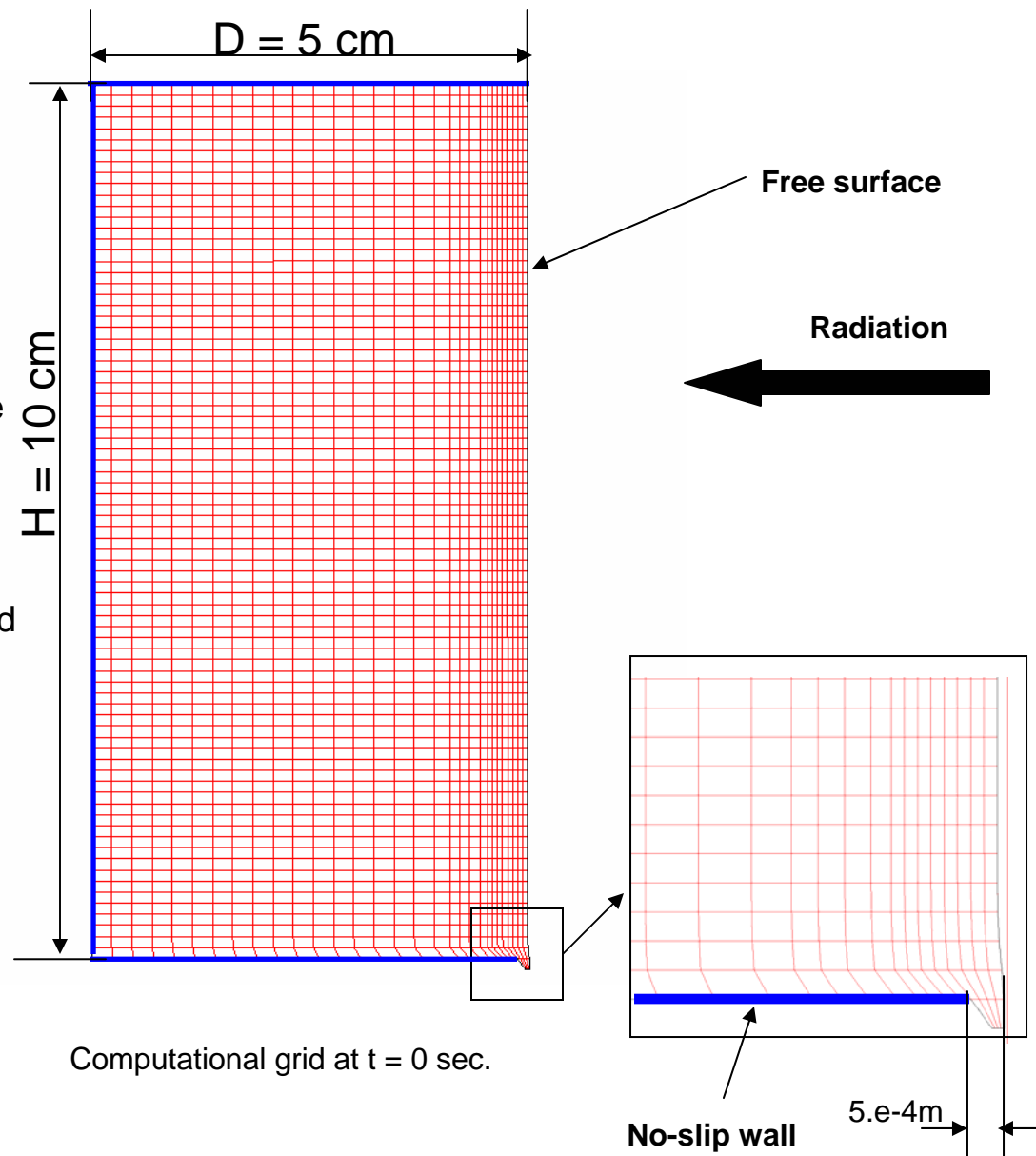
$h \times w \times d = 10\text{ cm} \times 10\text{ cm} \times 5\text{ cm}$

- in CFD model w only used to compare to test data

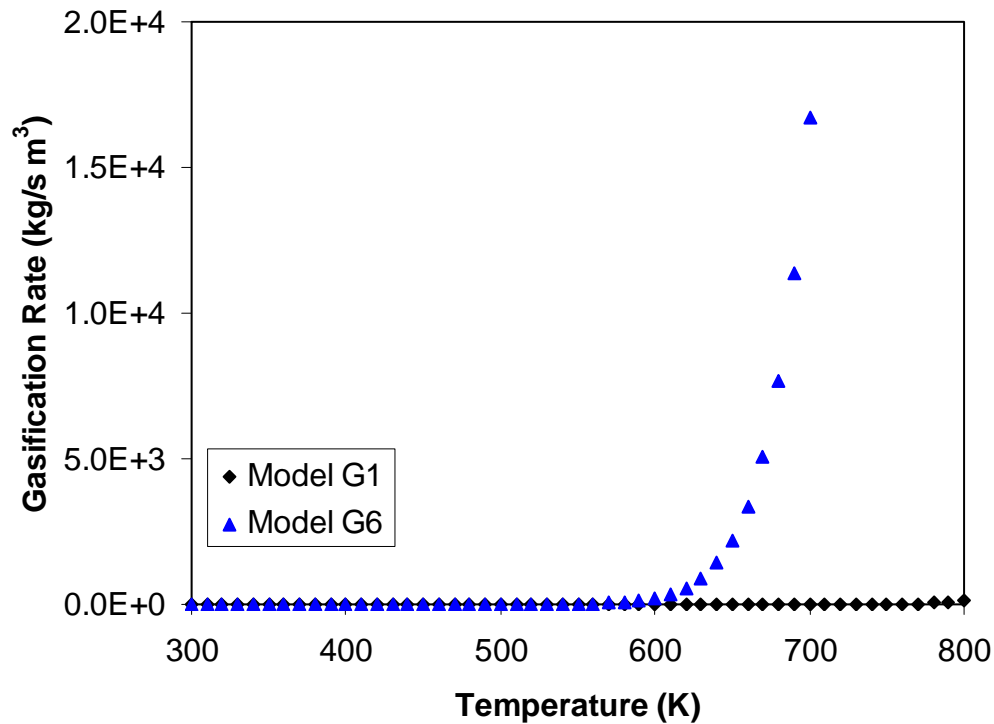


Computational Grid

- Modeled as a 2-D problem with a computational domain of 5.0cm X 10.0cm
- 30X80 Grid (biased)
- Initial grid resolution the same as the 19X200 grid used in Task 1
- Equivalent to 100X80 grid if using uniform grid spacing and fixed grid



Gasification Models



Mass loss rate (in log scale) due to gasification as functions of time

Model expression:

$$y = A \exp\left(-\frac{B}{x}\right)$$

x : temperature (K)

y : gasification rate (kg/s m³)

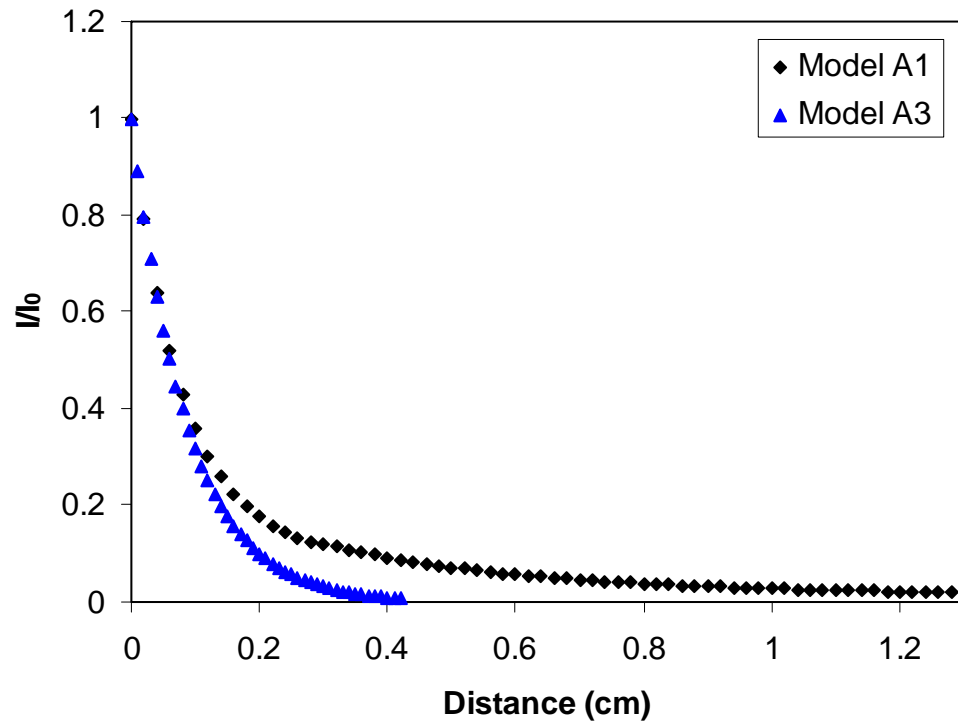
Gasification model parameters

	A (1/s)	B
Model G1	2.18e+12	24400
Model G6	3.27e+14	24400

- ⊕ Model G1 is the base model
- ⊕ Model G6 increases the magnitude of gasification rate by a factor of 150



Absorption Models



Normalized Incident Heat Flux Profile as a Function of Distance from Free Surface

- ⊕ Model A1 is the base model
- ⊕ Model A3 shortens the penetration length of the incident heat flux
- ⊕ The heat flux penetration length covers at least 4 cells in the horizontal direction near the free surface

Model expression:

Model A1:

$$\frac{I}{I_0} = 10^{(-5.17x + 6.964x^2)}, \quad 0 \leq x < 0.3$$

$$\frac{I}{I_0} = 10^{(-0.5154 - 1.473x + 0.4339x^2)}, \quad 0.3 < x \leq 1.3$$

Model A3:

$$\frac{I}{I_0} = \exp(-11.513x), \quad 0 \leq x < 0.4$$

x : distance from free surface in cm



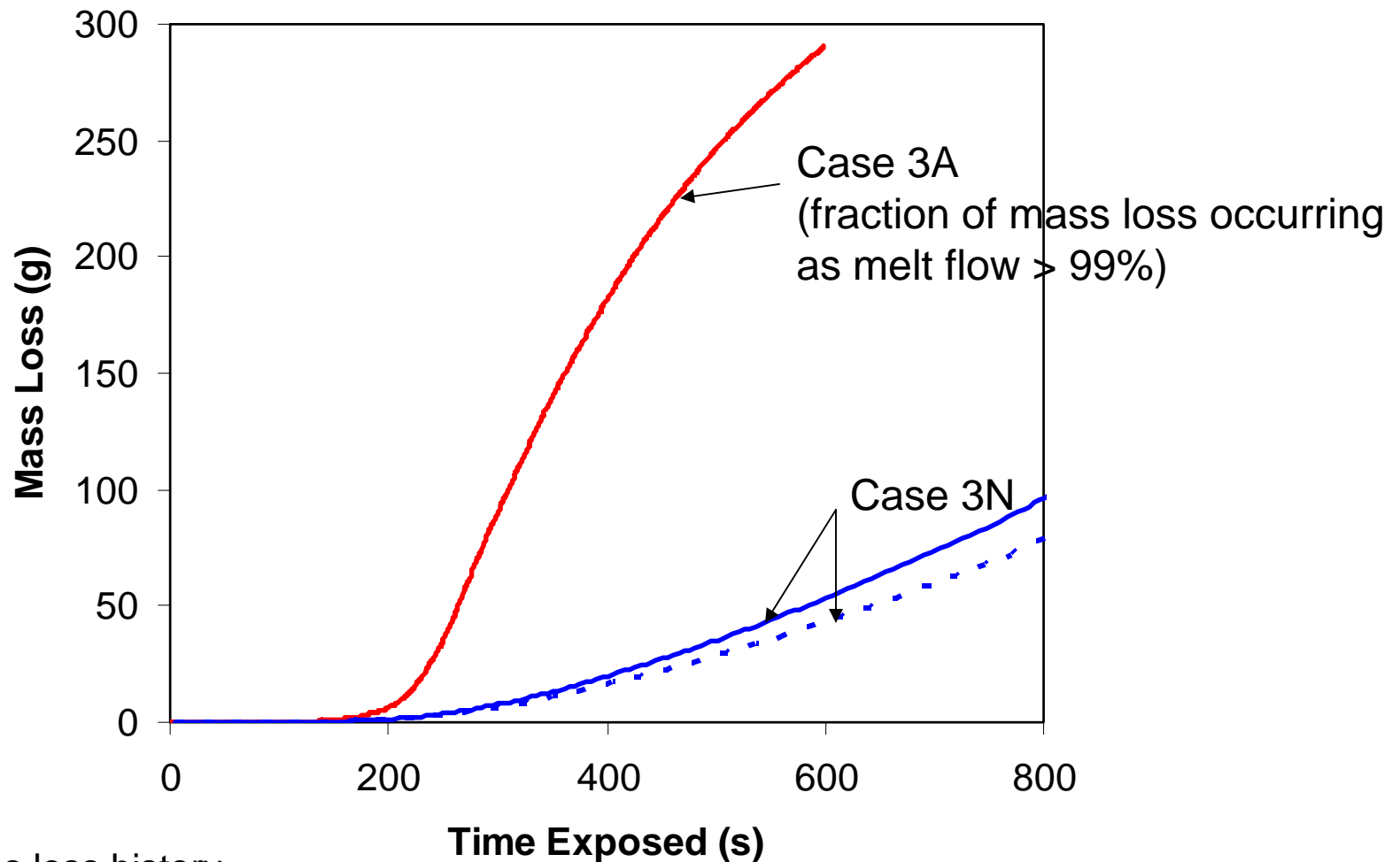
Case Summary (PP702N)

Case #	In-depth Gasification Model	In-depth Absorption Model	External heat flux (KW/m ²)
Case 3A	Model G1	Model A1	30
Case 3N	Model G6	Model A3	30
Case 3P	Model G6	Model A3	46
Case 3Q	Model G6	Model A3	20

- ⊕ All cases are for PP702N
- ⊕ Radiation and convective heat losses at free surface are included in all cases
- ⊕ Case 3A is the baseline case
- ⊕ Model G6 and A3 in Case 3N are developed to match measured mass loss rates at 30kW/m² heat flux
- ⊕ Case 3P and Case 3Q use same model parameters as Case 3N



Impacts of Changing Gasification and Absorption Models

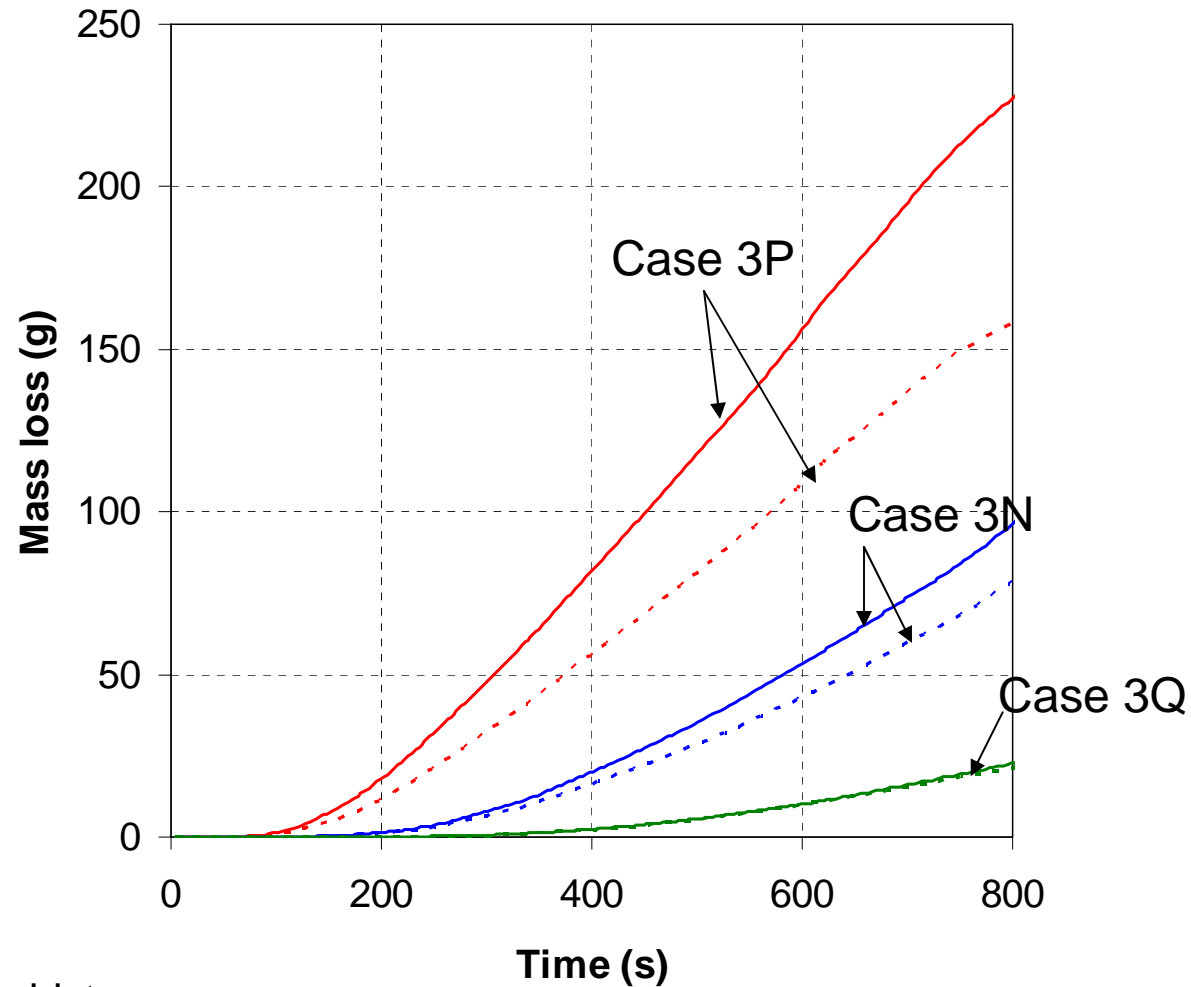


Mass loss history

- solid lines = total mass loss
- dashed lines = mass loss occurring as melt flow
- difference between solid and dashed line = mass loss due to gasification



Impacts of External Heat Flux (PP702N)

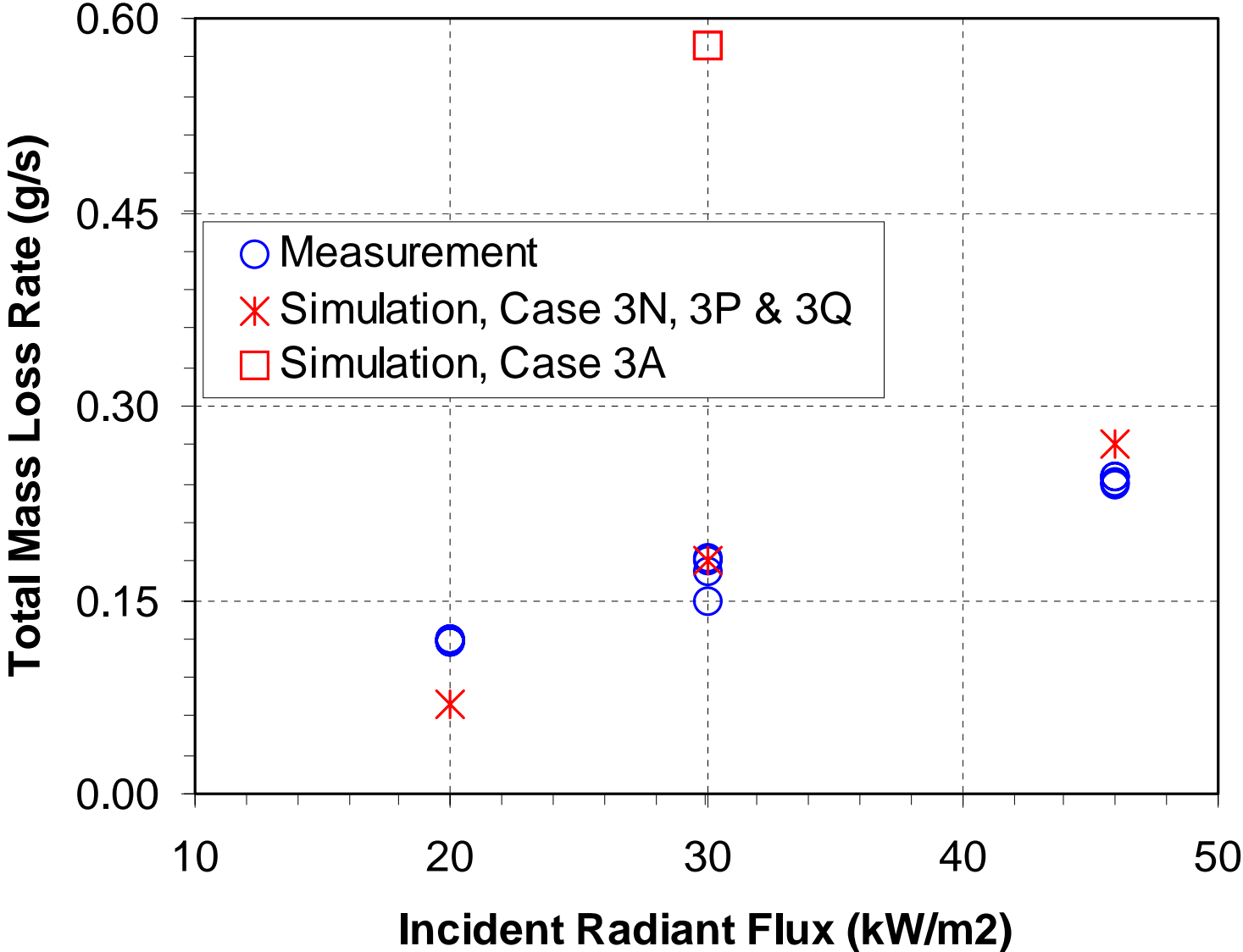


Mass loss history

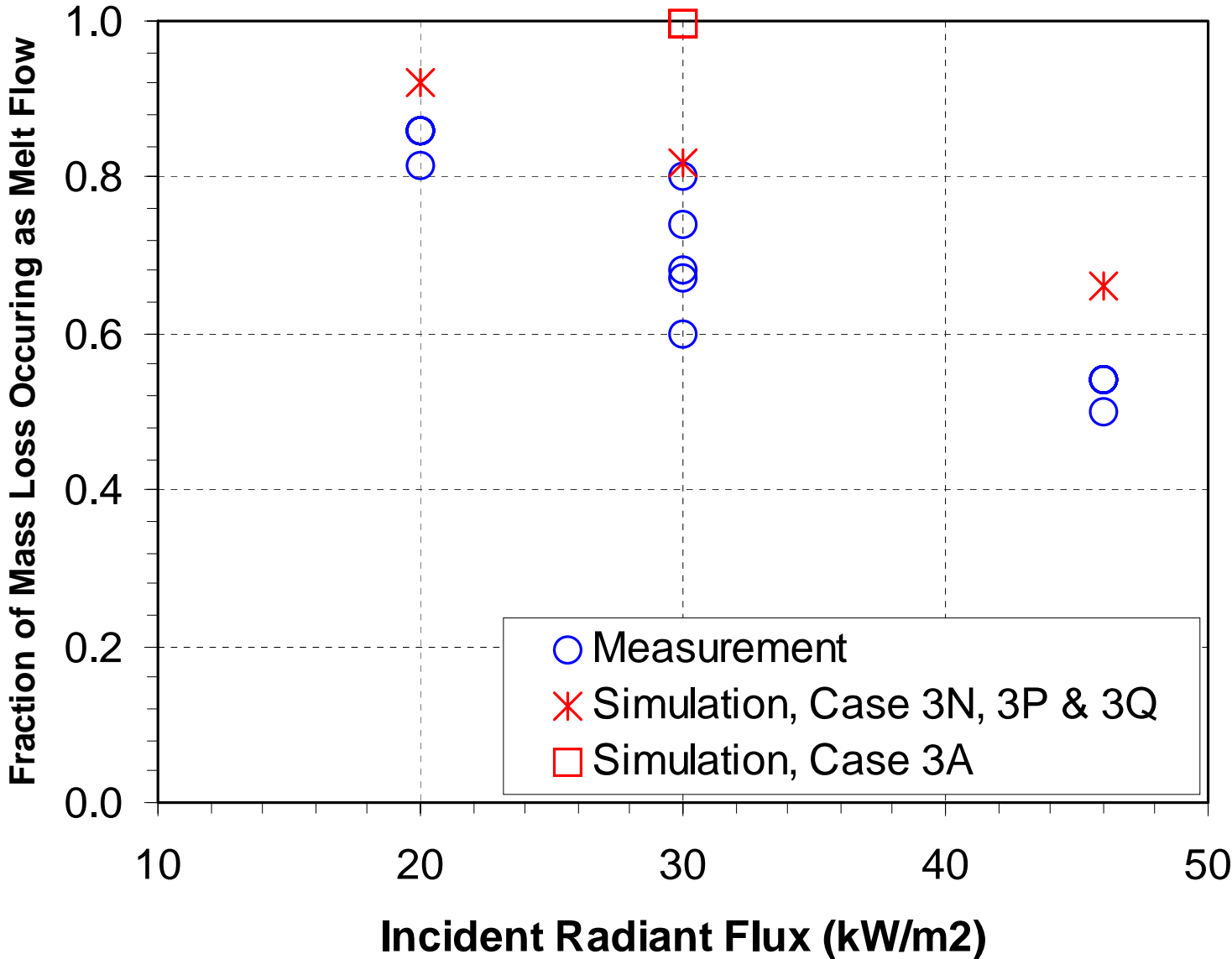
- solid lines = total mass loss
- dashed lines = mass loss occurring as melt flow
- difference between solid and dashed line = mass loss due to gasification



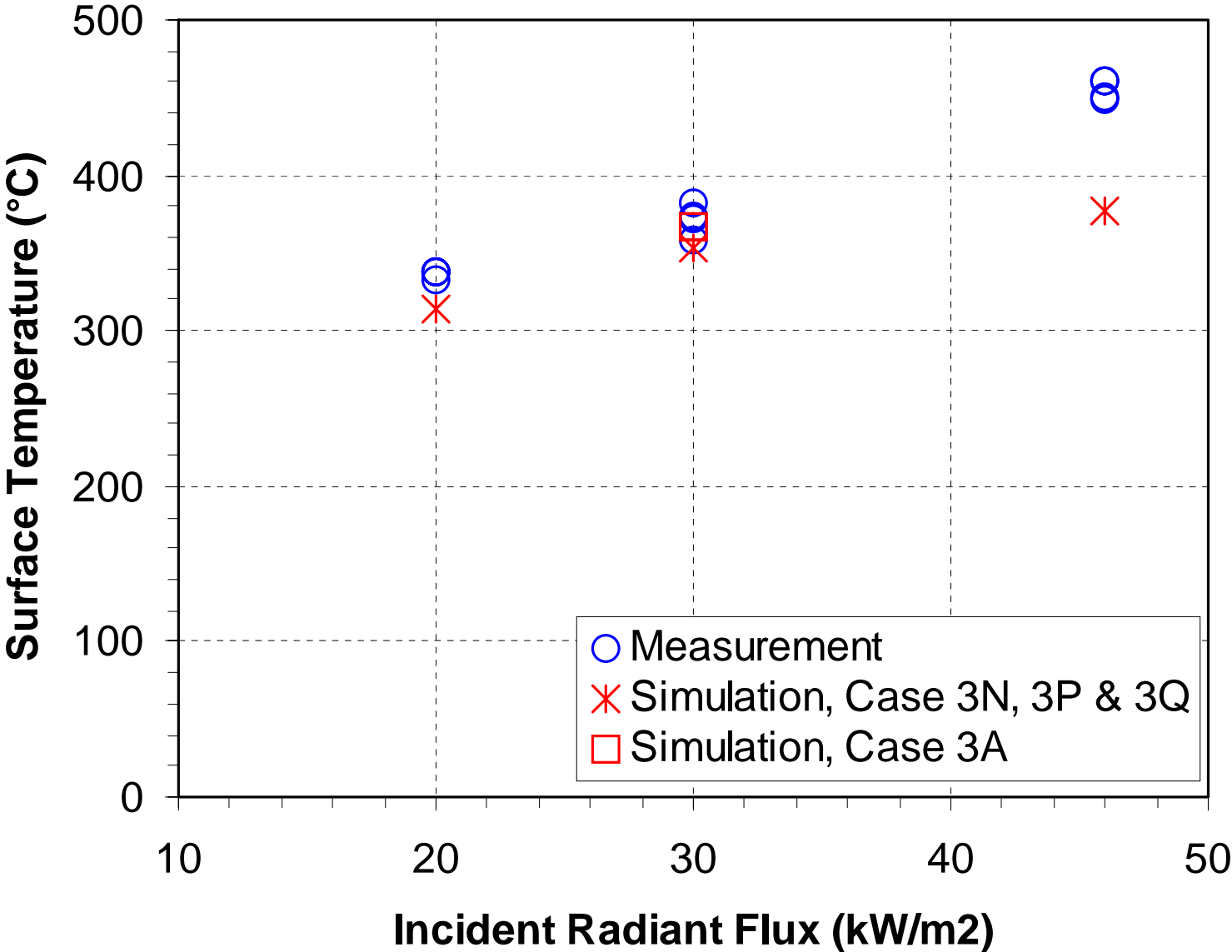
Simulation vs. Measurement (PP702N)



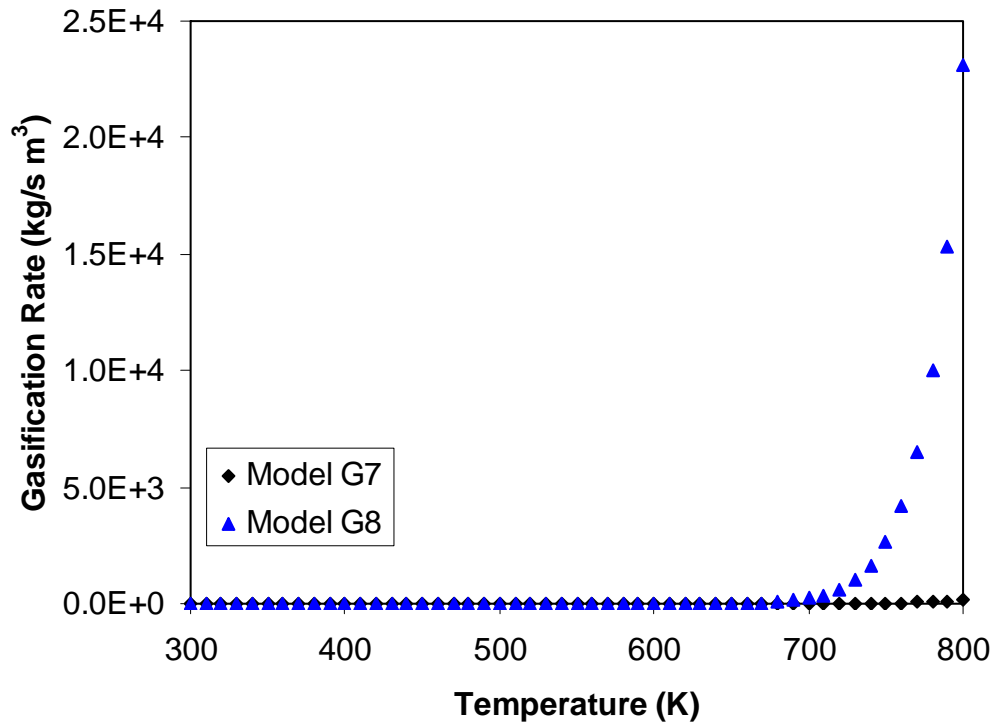
Simulation vs. Measurement (PP702N)



Simulation vs. Measurement (PP702N)



Gasification Models for PP6523



Mass loss rate (in log scale) due to gasification as functions of time

Model expression:

$$y = A \exp\left(-\frac{B}{x}\right)$$

x : temperature (K)

y : gasification rate (kg/s m³)

Gasification model parameters

	A (1/s)	B
Model G7	2.23e+13	26000
Model G8	3.35e+15	26000

- ⊕ Model G7 is the base model
- ⊕ Model G8 increases the magnitude of gasification rate by a factor of 150
- ⊕ Parameter for Model G8 is selected based on the experience of modeling PP702N



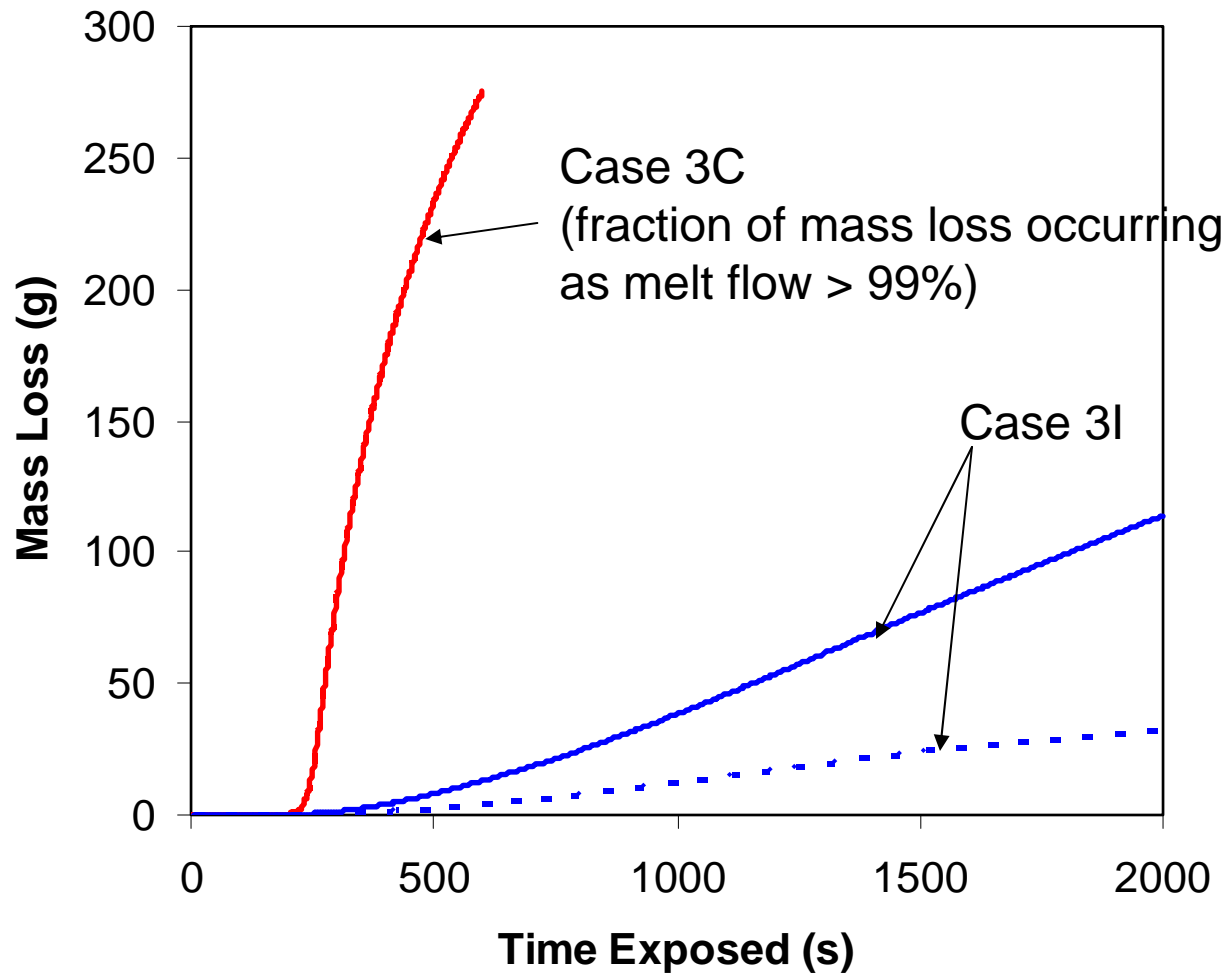
Case Summary (PP6523)

Case #	In-depth Gasification Model	In-depth Absorption Model	External heat flux (KW/m ²)
Case 3C	Model G7	Model A1	30
Case 3I	Model G8	Model A3	30

- ⊕ Radiation and convective heat losses at free surface are included in all cases
- ⊕ Case 3C is the baseline case



Predicted Mass Loss History for PP6523



Mass loss history

- solid lines = total mass loss
- dashed lines = mass loss occurring as melt flow
- difference between solid and dashed line = mass loss due to gasification



Case Summary (PP6523)

Case #	In-depth Gasification Model	In-depth Absorption Model	External heat flux (KW/m ²)	Total mass loss rate (g/s)	Fraction of mass loss due to melt flow	Surface Temperature at 25% mass loss (°C)
Case 3C	Model G7	Model A1	30	0.69	0.99	382
Case 3I	Model G8	Model A3	30	0.065	0.28	362

- ⊕ Radiation and convective heat losses at free surface are included in all cases
- ⊕ Case 3C is the baseline case



Summary

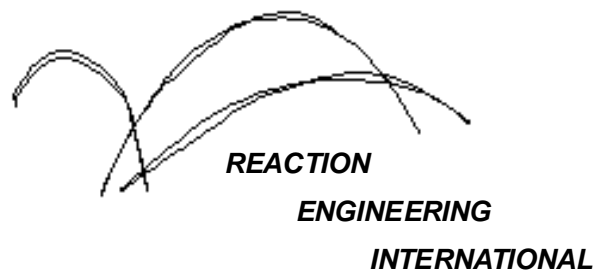
- ⊕ The in-depth absorption and gasification models are modified to match the measured total mass loss rate and the measured fraction of mass loss occurring as melt flow at 30 kW/m² external heat flux for PP702N
- ⊕ Case 3A (baseline) uses the absorption and gasification models provided by NIST does not match measured data for mass loss or surface temperature
- ⊕ Case 3N which uses the modified models shows
 - vastly different simulation results (compare to baseline)
 - matches the measured data reasonably well.
- ⊕ The same modified models developed for PP702N exposed to 30kW/m² heat flux have been applied to cases with 20 and 46 kW/m² heat flux. The predicted results agree reasonably well with measured data and show correct trends in total mass loss rate, fraction of mass loss due to melt flow, and surface temperature as a function of heat flux.
- ⊕ Two simulations have also been performed for PP6523 exposed to 30 kW/m² heat flux using different in-depth absorption and gasification models. It is found that the results are highly sensitive to the model parameters in the models



A Computational Model For Fire Growth and Spread On Thermoplastic Objects

Task 3: 2D model with in-depth gasification

(12/05/06)



Outline

- ⊕ Introduction
- ⊕ In-depth gasification models
- ⊕ In-depth absorption models
- ⊕ Cases studied
 - ⊕ Computational grid
 - ⊕ Case summary
 - ⊕ Example results:
 - ⊕ Free surface location, temperature contour
 - ⊕ Mass loss, surface temperature, and comparisons with data
- ⊕ Summary



Introduction

- ⊕ In-depth gasification model has been implemented into the CPCFD code. Gasification is represented by the removal of polymer mass and energy using sink terms in both mass and energy equations.
- ⊕ Simulation results of PP702N are presented in this report
- ⊕ A new in-depth absorption model is used in the simulations.



Gasification, absorption and heat losses models

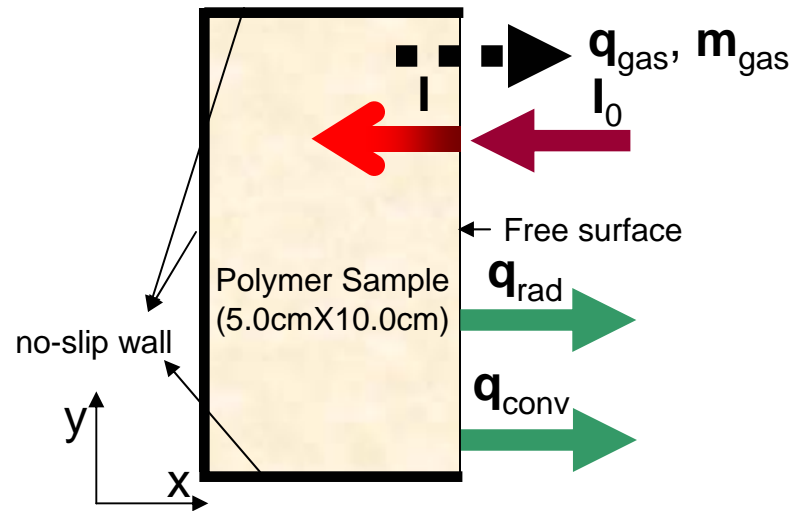


Figure 1, Sketch of gasification, absorption and heat loss model

- $\rho = 900 \text{ kg/m}^3$
- $c_p = 2400 \text{ J/kg-K}$
- $k = 0.25 \text{ W/m-K}$
- $q_0 = 30 \text{ kW/m}^2$
- $T_0 = 298 \text{ K}$
- $\varepsilon = 1.0$
- $\sigma = 5.67032 \times 10^{-8} \text{ W/m}^2\text{-K}^4$
- $h_{\text{conv}} = 8 \text{ W/m}^2\text{-K}$
- $H_v = 1250 \text{ J/g}$

⊕ Energy source/sink terms due to gasification, absorption, and heat losses

⊕ **In-depth gasification:** $\dot{q}_{\text{gasification}} = -\int_{\Omega} H_v \rho A e^{(-E/RT)} d\Omega$

⊕ In-depth absorption: $\dot{q}_{\text{absorption}} = \int_{\Omega} \frac{dI}{dx} d\Omega$ assuming absorption process in x-direction only

⊕ Radiative heat loss: $\dot{q}_{\text{radiation}} = -A \varepsilon \sigma (T^4 - T_0^4)$ assuming radiative heat loss only on free surface

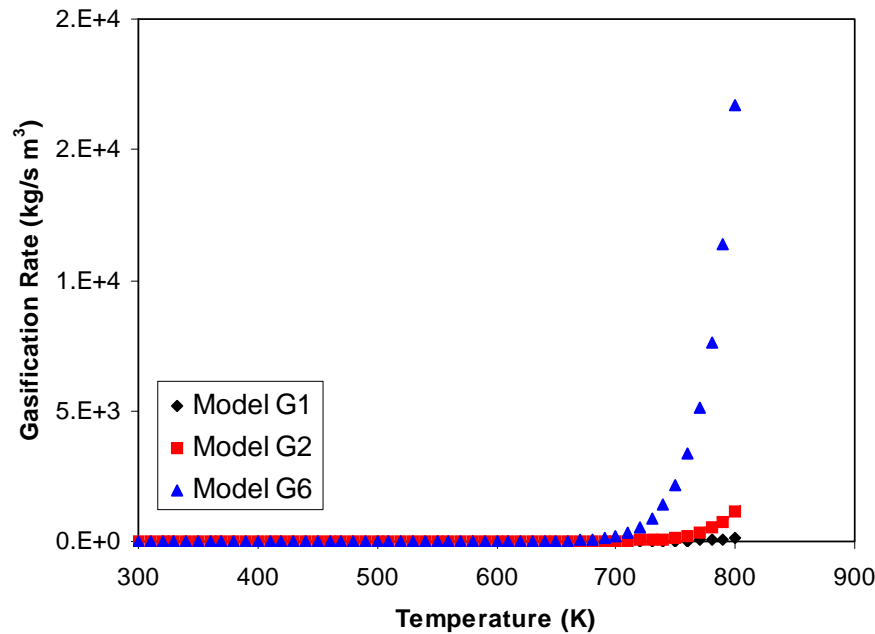
⊕ Convective heat loss: $\dot{q}_{\text{convection}} = -A h_{\text{conv}} (T - T_0)$

⊕ Heat sink term to avoid over heating in Task 1 and 2 has been deactivated in this study

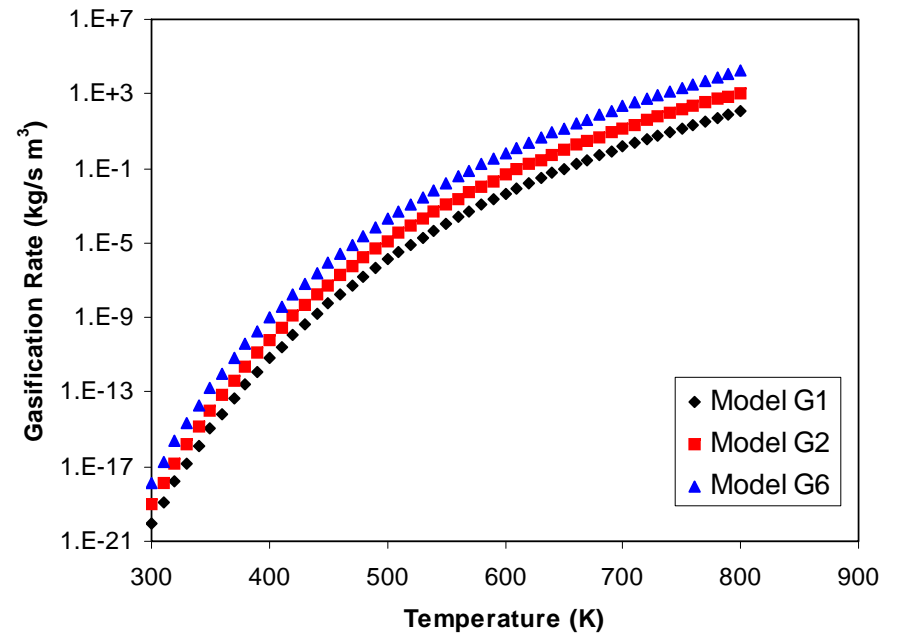
⊕ **Mass sink terms due to gasification:** $\dot{m}_{\text{gasification}} = -\int_{\Omega} \rho A e^{(-E/RT)} d\Omega$



Gasification Model Parameters



Mass loss rate due to gasification as function of time



Mass loss rate (in log scale) due to gasification as function of time

Model expression: $y = \rho A \exp\left(-\frac{B}{x}\right)$

x : temperature (K)

y : gasification rate (kg/s m³)

Gasification model parameters

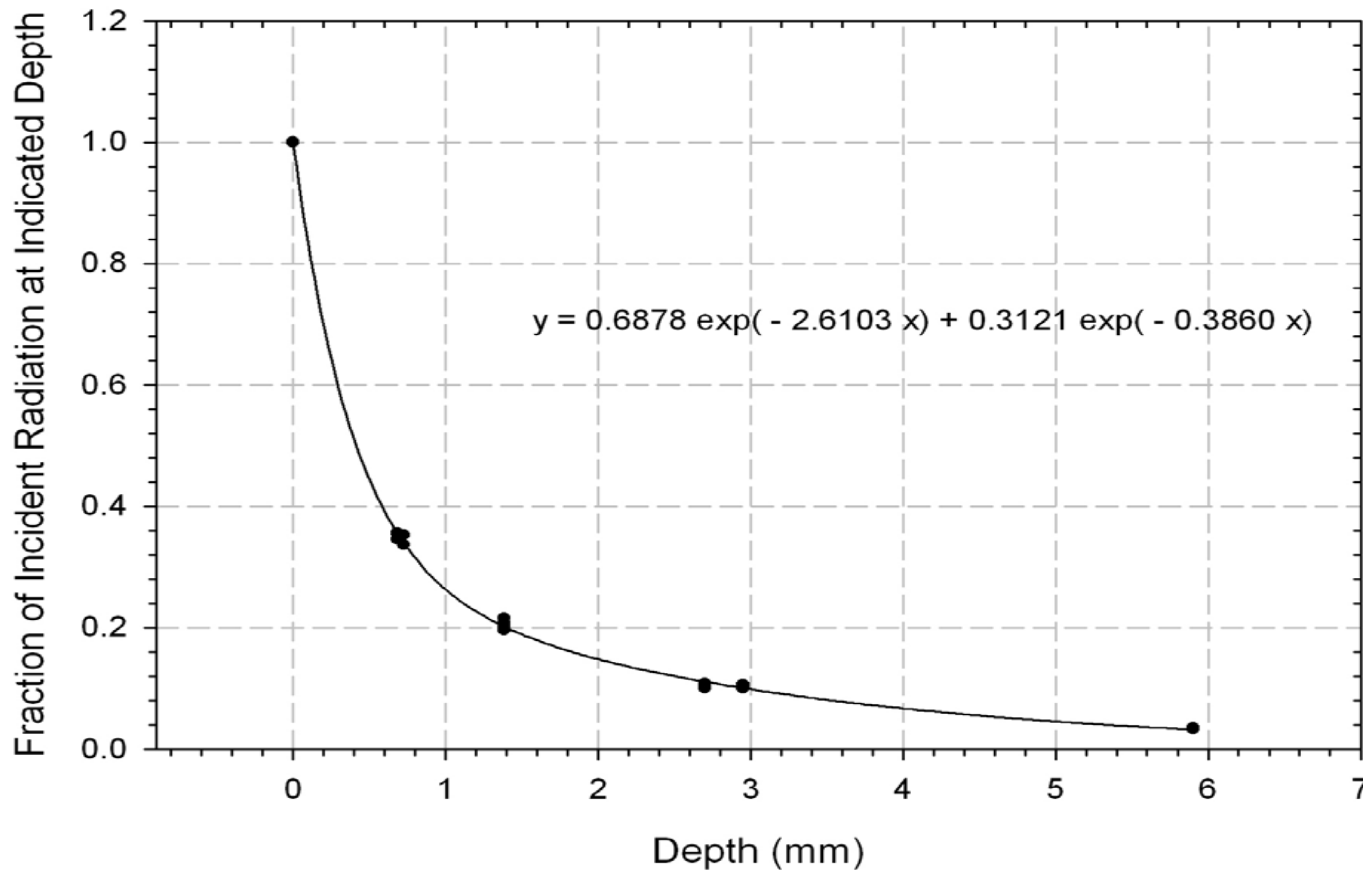
	A (1/s)	B
Model G1	2.18e+12	24400
Model G2	2.18e+13	24400
Model G6	3.27e+14	24400

- ⊕ Model G1 is the base model
- ⊕ Model G6 increases the magnitude of gasification rate by a factor of 150
- ⊕ G1 and G6 are used in the current calculations



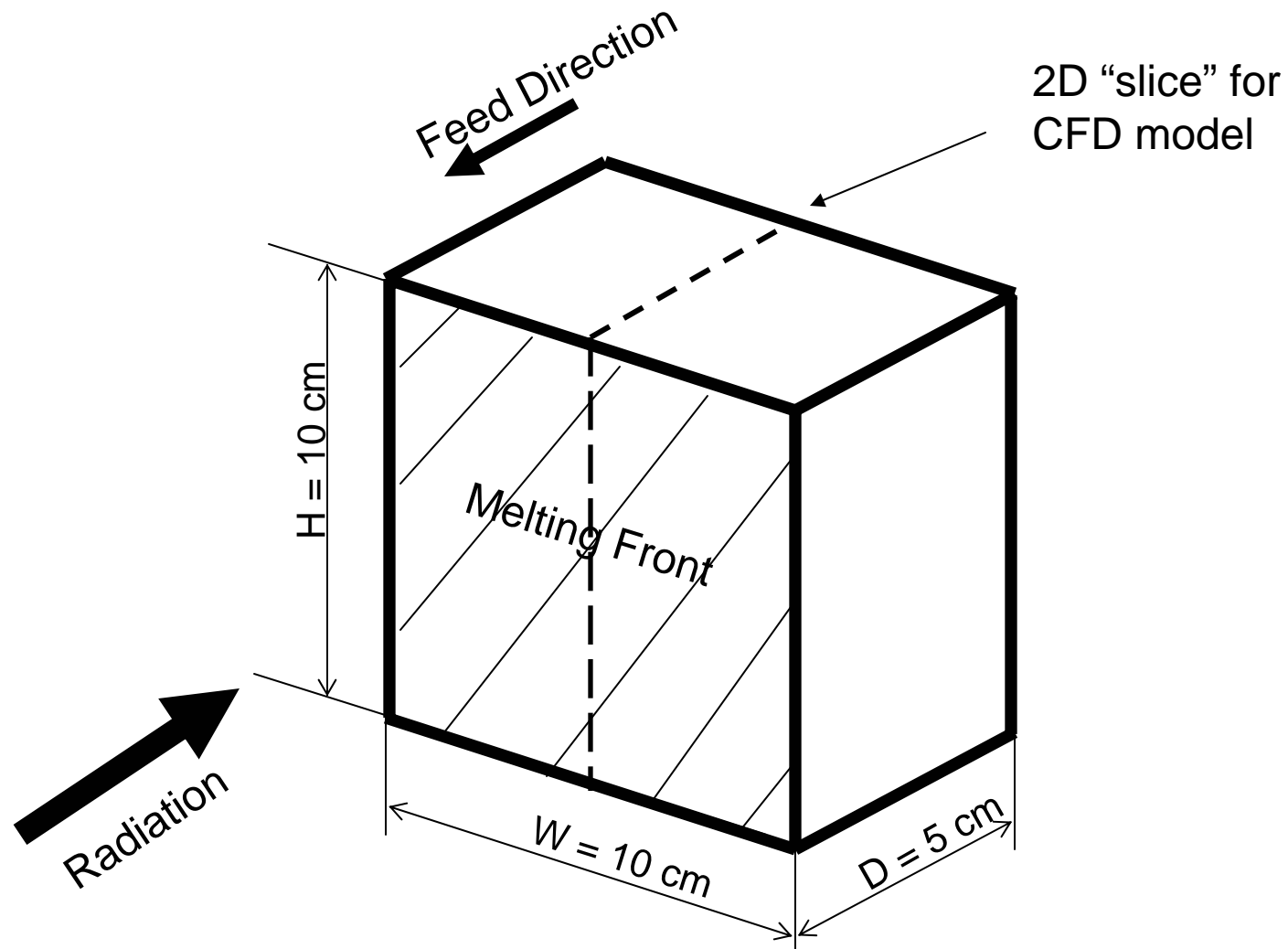
In-Depth Absorption Model

Model A4: Double Exponential Fit to PD702N Polypropylene
Radiation Absorption In Depth
(Sample Set 2)



from Tom Ohlemiller 10/25/06

Physical Model



$h \times w \times d = 10\text{ cm} \times 10\text{ cm} \times 5\text{ cm}$

- in CFD model w only used to compare to test data



Computational Grid

- ⊕ Modeled polymer sample dimension: 5.0cm X 10.0cm
- ⊕ 30X80 Grid (biased)
- ⊕ Initial grid resolution the same as the 19X200 grid used in Task 1
- ⊕ Equivalent to 100X80 grid if using uniform grid spacing and fixed grid

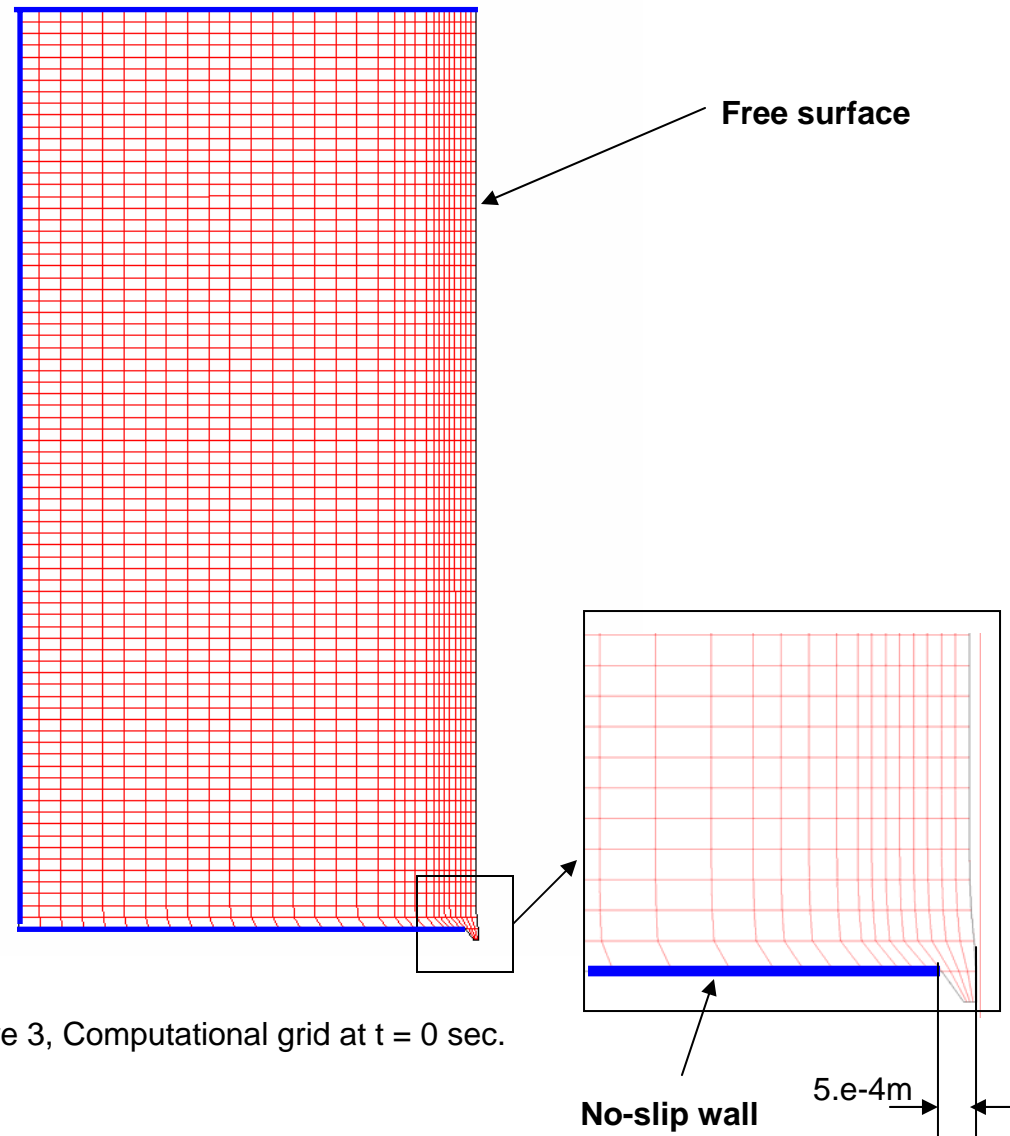


Figure 3, Computational grid at t = 0 sec.

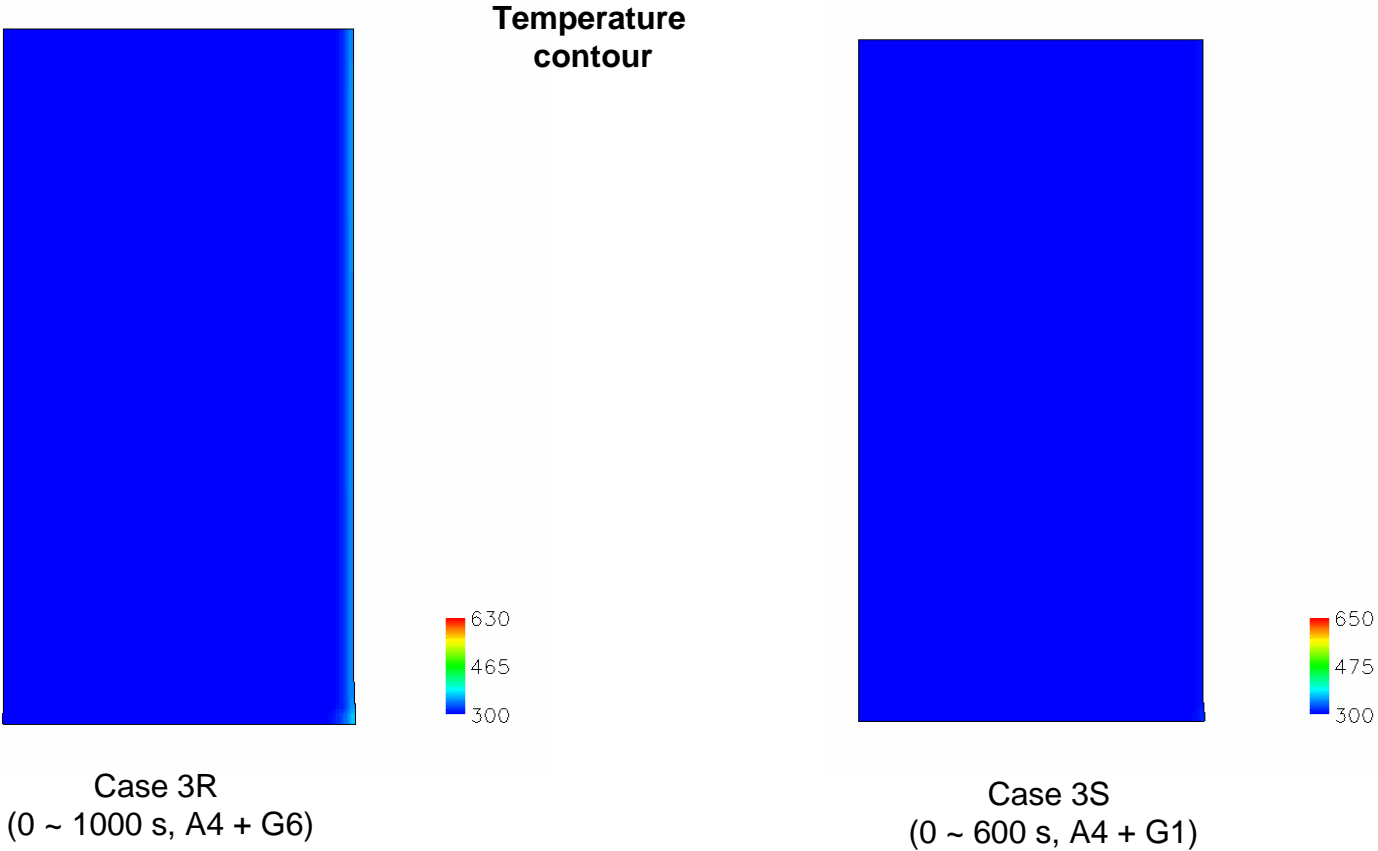
Case Summary

⊕ External Incident heat flux: 30KW/m²

Case	Polymer Resin	In-depth Gasification	Radiative and Convective Heat Losses	In-depth Absorption	Mass Loss and Simulated Time	Estimated CPU Time
Case 3R	PP702N	G6	Included	A4	55%, 1000 sec	~ 20 h
Case 3S	PP702N	G1	Included	A4	65%, 600 sec	~ 10 h



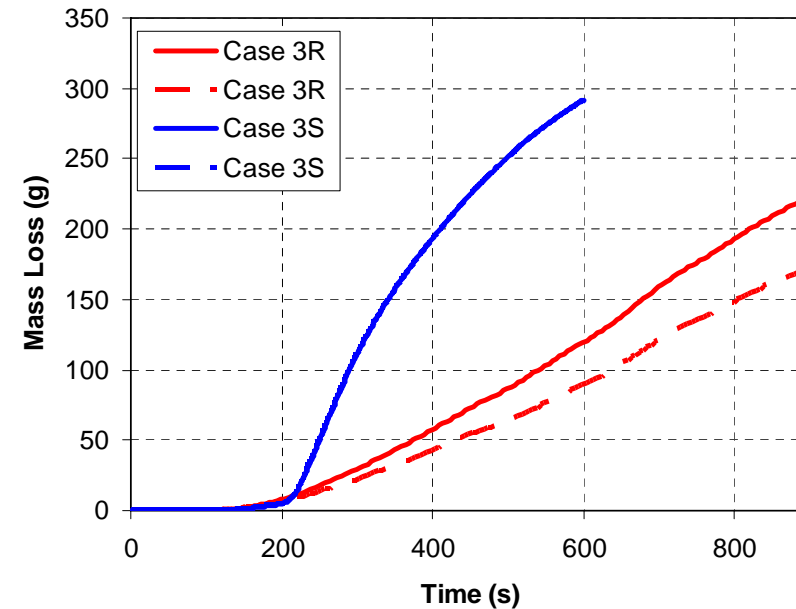
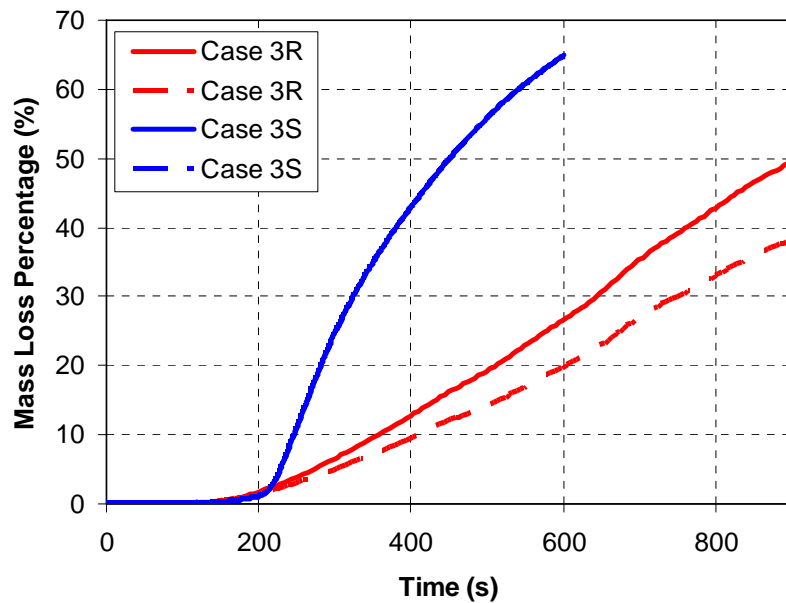
Simulated Melting Process (PP702N)



⊕ Time interval between movie frames: 5 seconds



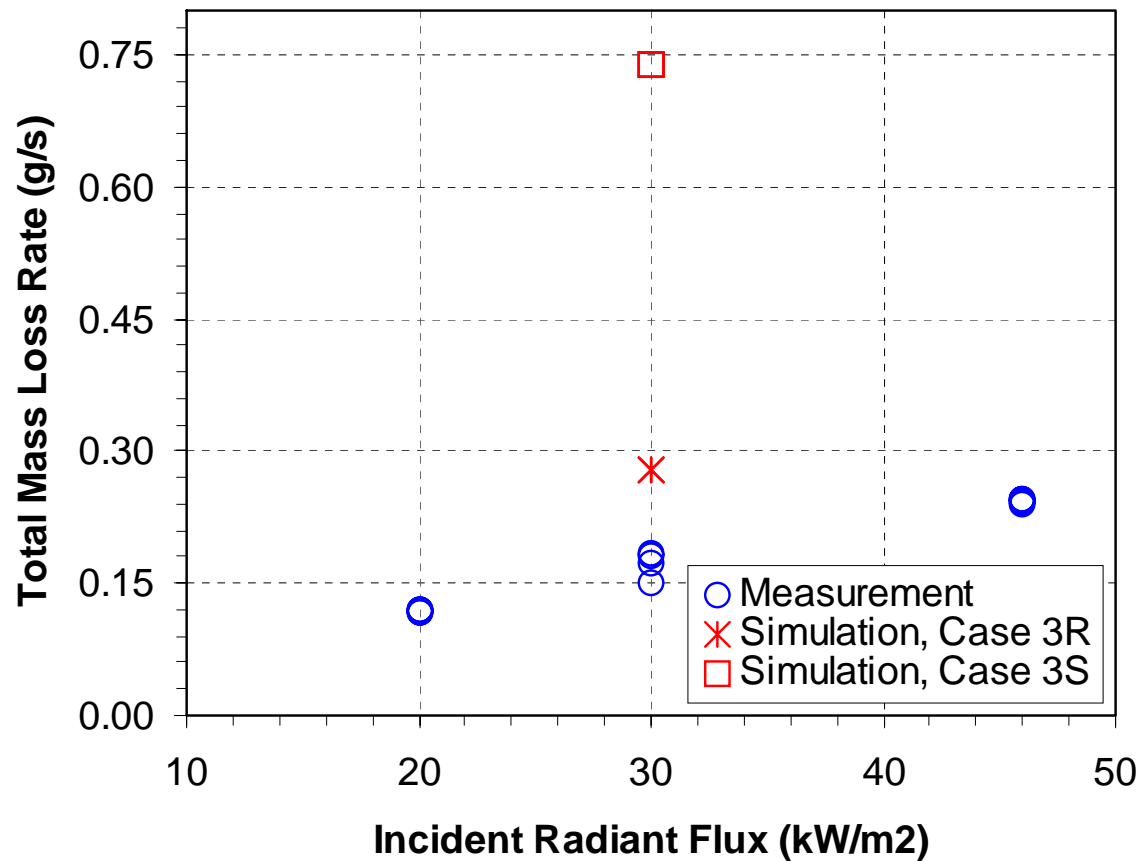
Mass Loss as Function of Time



Mass loss history

- solid lines = total mass loss
- dashed lines = mass loss occurring as melt flow
- difference between solid and dashed line = mass loss due to gasification

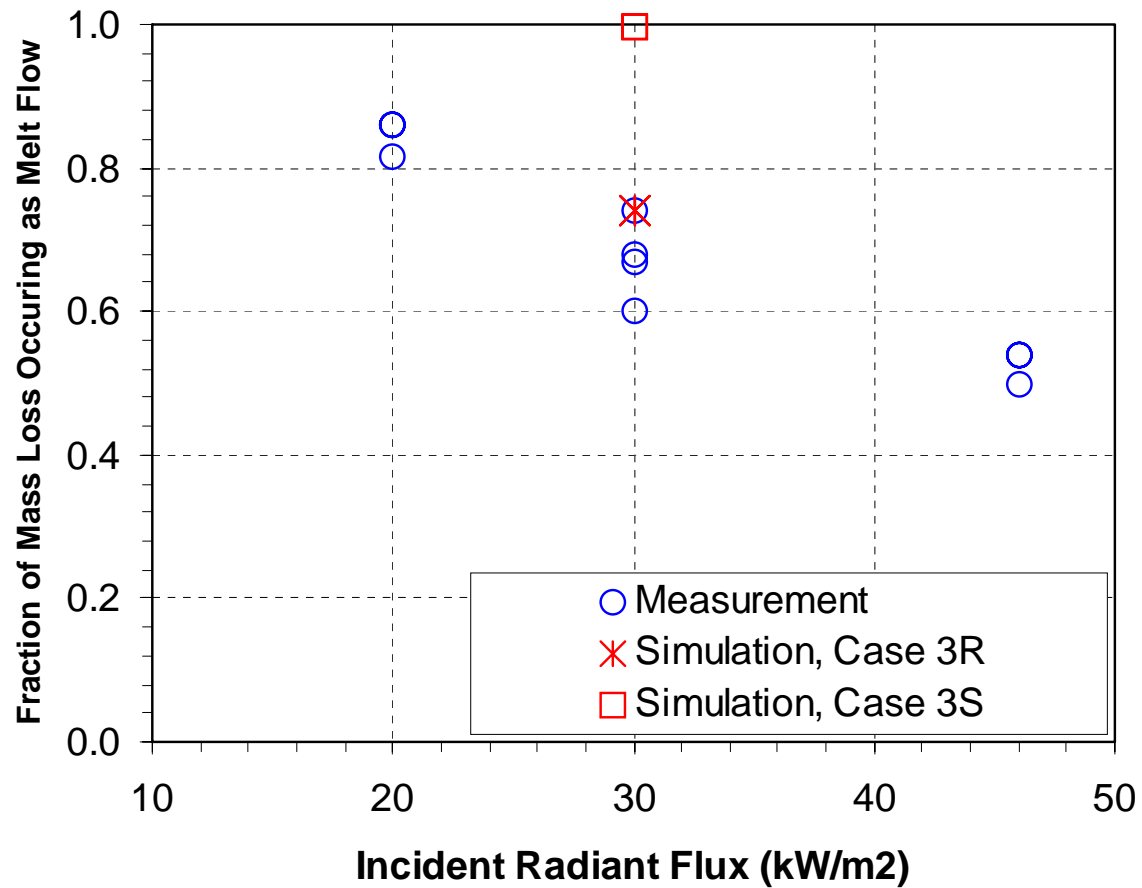
Simulation vs. Measurement



Case 3R, rate (0.28 g/s) computed using data from 110 s to 900 s
Case 3S, rate (0.74 g/s) computed using data from 210 s to 600 s



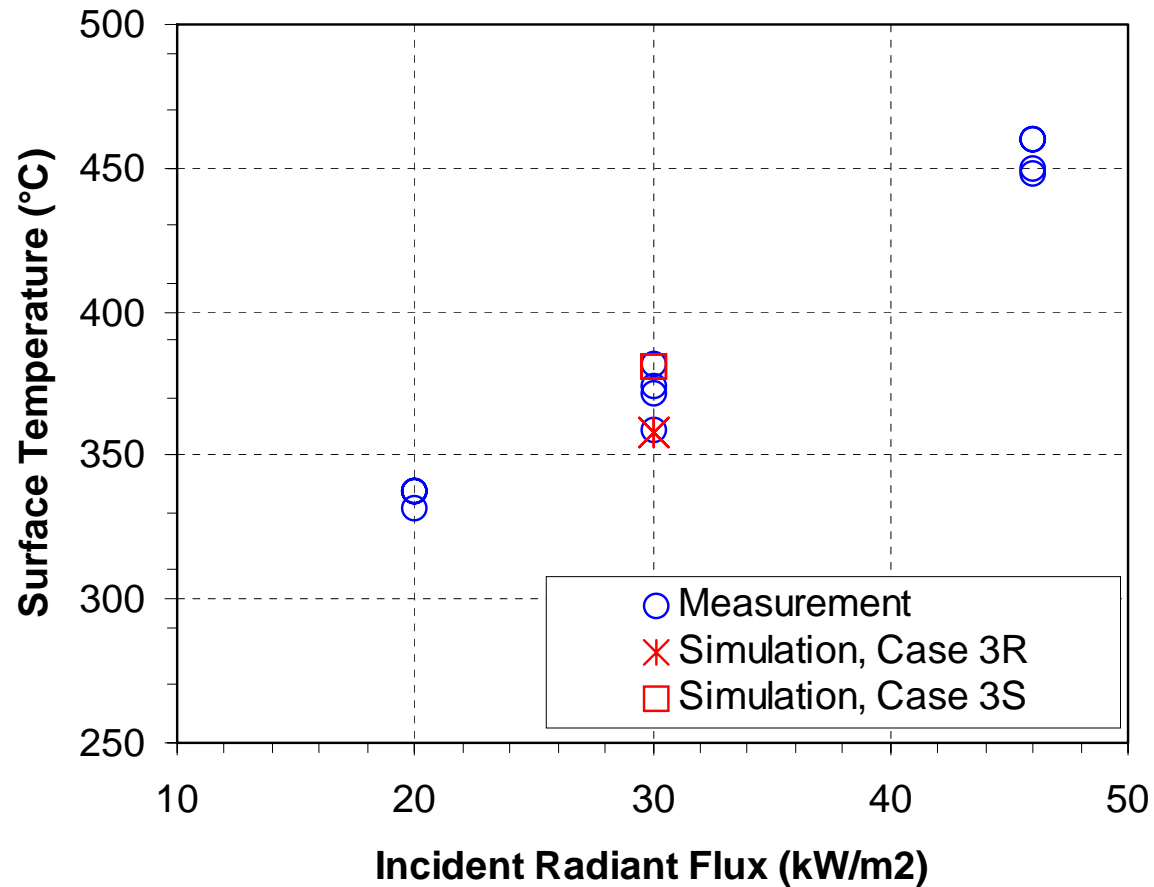
Simulation vs. Measurement (PP702N)



Case 3R, fraction (0.997) computed using data of 900 s
Case 3S, fraction (0.740) computed using data of 600 s



Simulation vs. Measurement (PP702N)



Predicted surface temperatures are area-averaged temperatures on the free surface at 450 s and 300 s for Case 3R (358°C) and Case 3S (381°C), respectively.



Summary

- ⊕ Results presented for PP702N with gasification, heat losses and in-depth absorption of external heat flux at 30 KW/m^2
- ⊕ Cases were run to at least 55% mass loss
- ⊕ Computational Cost highlighted
- ⊕ Example Results
 - ⊕ Movie of free surface location and temperature
 - ⊕ Mass loss rate, fraction of mass loss occurring as melt flow and surface temperature
- Observations
 - ⊕ Free surface near the top boundary recedes faster initially
 - ⊕ Free surface curvature near the bottom lip is suppressed artificially by the smoothing function used to stabilize the computation
 - ⊕ Increasing the gasification rate by a factor of 150 from model G1 to G6 leads to
 - ⊕ Lower surface temperature (i.e., decreasing by about 20°C)
 - ⊕ Lower total mass loss rate
 - ⊕ Higher fraction of mass loss occurring as melting flow
- ⊕ Comparison with data
 - ⊕ Using the original gasification model G1, the predicted total mass loss rate is four times higher than the measurement; the predicted fraction of mass loss due to gasification is negligible and much smaller than the measurement; though predicted surface temperature appears in good agreement with the data.
 - ⊕ Using the modified gasification model G6, the predicted total mass loss rate is 50% higher than the measurement; the predicted fraction of mass loss occurring as melt flow and surface temperature are in good agreement with the data.



Task 4

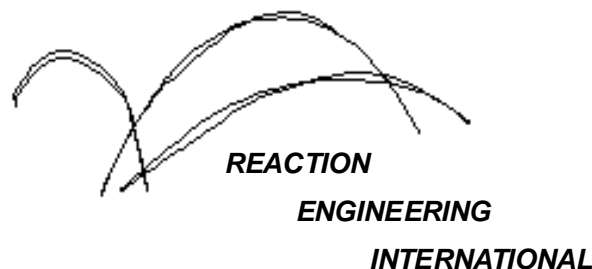


A Computational Model For Fire Growth and Spread On Thermoplastic Objects

Task 4: Include Melt Pool on Catch Surface

Goals, Methodology, and Plan

(01/10/07)



Outline

- ⊕ Task description
- ⊕ Modeling methodology
- ⊕ Preliminary plan



Task Description

- ⊕ Add to the existing model the flow of melt on the solid catch surface.
 - ⊕ Include catch surface material properties (slip/non-slip, surface temperature, ...)
 - ⊕ Finite thickness of catch basin
 - ⊕ Effects of surface tension
 - ⊕ Nonzero gap between sample and catch surface
 - ⊕ Nonzero tilt angle for the catch surface
 - ⊕ No change to in-depth absorption and in-depth gasification model

- ⊕ Task 4A – model PP702 with specified heat flux, gap and tilt angle
- ⊕ Task 4B – model PP6523 (same conditions as those used in Task 4A)
- ⊕ Task 4C – model PP702 or PP6523 with a different gap (no change in other conditions)

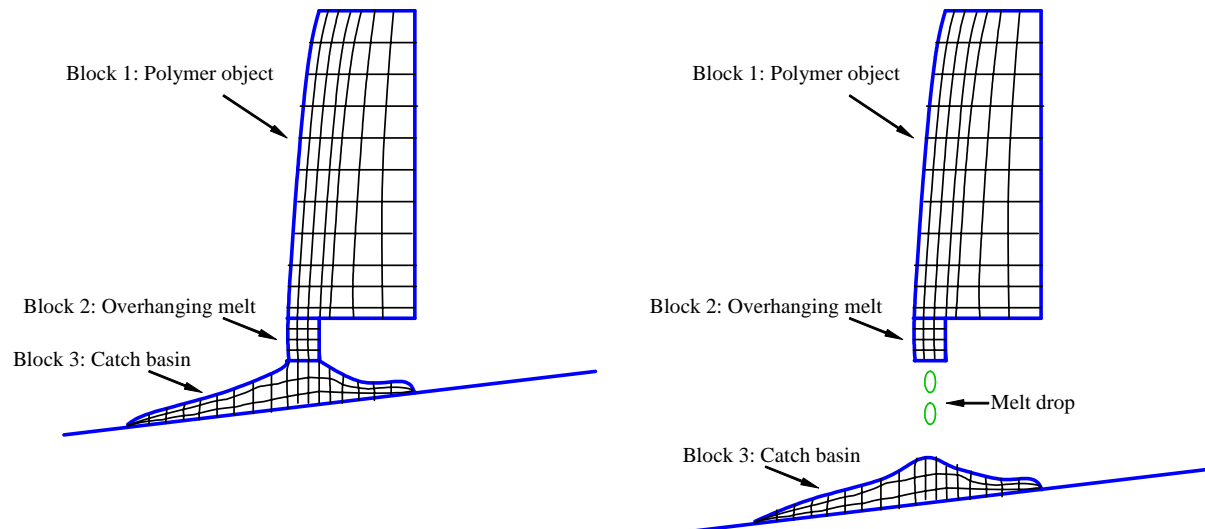
- ⊕ Task 4D – NIST site visit (project update)
- ⊕ Task 4E – NIST site visit (base period program review)
- ⊕ Task 4F – Base period summary report (first draft)

- ⊕ Due date – Four months after task 3



Modeling Methodology

- ⊕ Use the multi-block capability of the CPCFD code
 - ⊕ Two situations of melt flow may require different modeling approaches



- ⊕ The overhanging melt poses the biggest challenge
 - ⊕ Use engineering approximation for the overhanging melt can greatly simplify the problem
- ⊕ Need to know the heat and wall boundary conditions for the overhanging melt and the catch basin
- ⊕ What data is available from NIST for comparison?



Surface Tension Effects

- ⊕ Plan to implement the continuum surface force model proposed by Brackbill et al (1992)
 - ⊕ The addition of surface tension results in a pressure drop (or increase) across the free surface and can be treated as a Dirichlet boundary condition of the pressure equation. For 2-D problem,

$$p_i - p_o = \frac{\sigma}{R}$$

Diagram illustrating the equation $p_i - p_o = \frac{\sigma}{R}$ with labels for the variables:

- p_i : Pressure on the inside of the free surface
- p_o : Atmosphere pressure
- σ : Surface tension coefficient (temperature dependent)
- R : Radius of Surface curvature

- ⊕ Reference: J.U. Brackbill, D.B. Kothe, & C. Zemach, A continuum method for modeling surface tension, J. Comput. Phys., 100, pp335-354, 1992.
- ⊕ Need to know the surface tension coefficient for PP702 and PP6523
 - ⊕ NIST data available?
 - ⊕ If no data, how to estimate?



Preliminary Plan

- Work on Task 4A without surface tension effects
- Add surface tension model and complete Task 4A
- Complete Task 4B
- Complete Task 4C

⊕ Hurdles expected

- ⊕ Modeling overhanging melt
- ⊕ Surface tension model

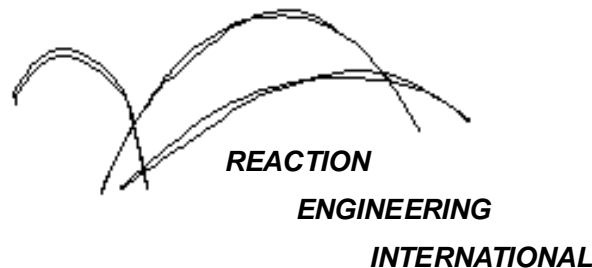


A Computational Model For Fire Growth and Spread On Thermoplastic Objects

Task 4: Include Melt Pool on Catch Surface

Feasibility Study

(02/22/07)



Outline

- ⊕ Model description
- ⊕ Test case results
- ⊕ Summary and future work



Model Description

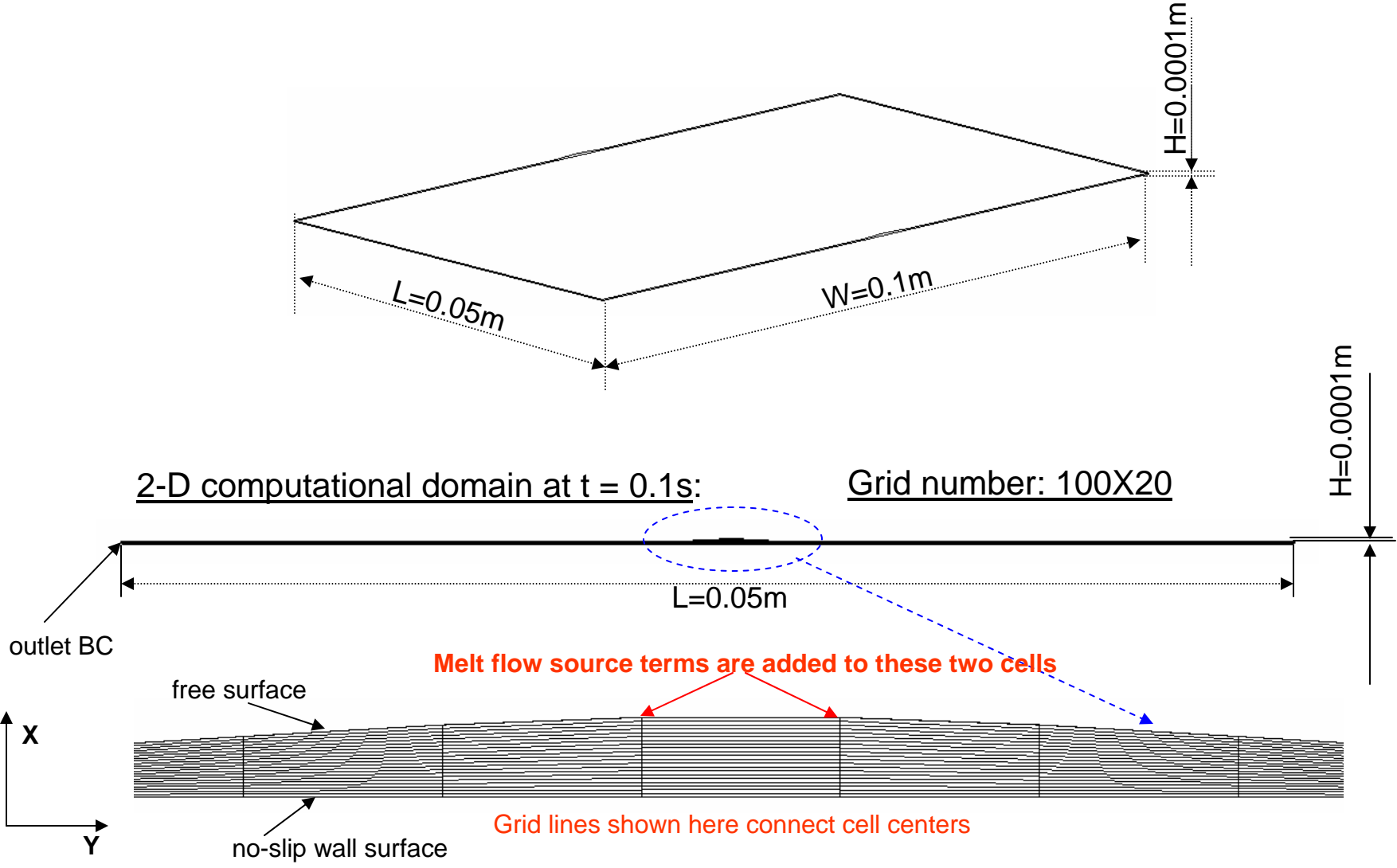
- ⊕ Study the feasibility of using CPCFD to model melt pool on catch surface.
 - ⊕ Case 1
 - ⊕ catch pan not included in the computational domain
 - ⊕ assume uniform constant melt temperature at 700K
 - ⊕ assume constant melt flow rate of 0.21 g/s (estimated from Task 3 results)
 - ⊕ assume melt flow velocity of $-1.e-3$ m/s perpendicular to the catch surface (estimated from Task3 results)
 - ⊕ no heat loss to environment
 - ⊕ catch surface tilt angle at 0°
 - ⊕ surface tension effects neglected
 - ⊕ Case 2
 - ⊕ catch pan included in the computational domain but has different properties (i.e., density, heat conductivity, and head capacity) than the polymer melt. viscosity of catch pan is set to be $1.e6$ pa-s and temperature of catch pan is 700K
 - ⊕ other conditions same as those in Case 1
- melt flow cumulated on the catch surface is treated as an additional mass source term of the continuity equation
 - ⊕ Additional source terms are added to momentum and energy equations to account for the impacts of the cumulated melt flow
 - ⊕ mass source term: \dot{m}
 - ⊕ momentum source term: $\dot{m}(u_{flow} - u)$
 - ⊕ energy source term: $\dot{m}(T_{flow} - T)$

$$\dot{m} = 0.21 \text{ g / s}; u_{flow} = -1.e-3 \text{ m / s}; T_{flow} = 700 \text{ K}$$



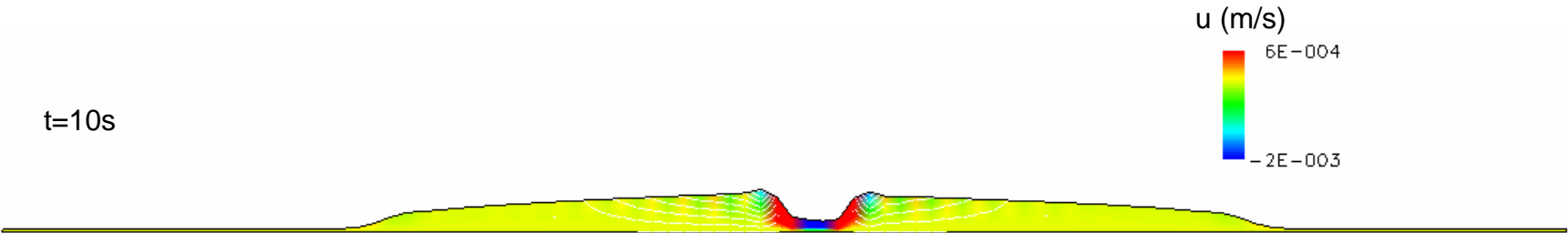
Case 1 Configuration

⊕ Initial dimension and grid

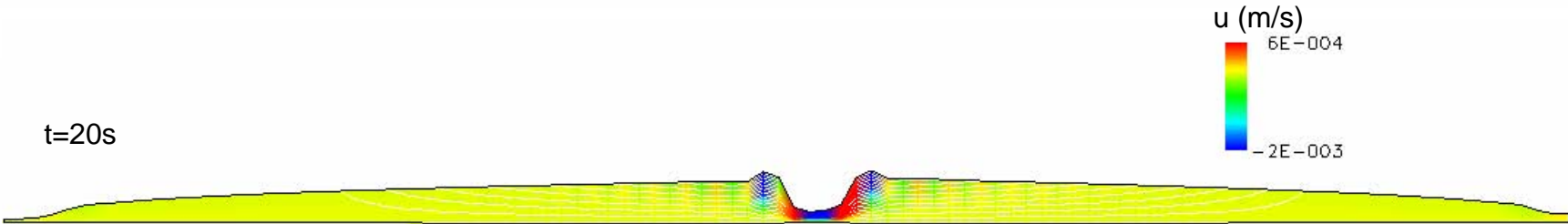


Case 1 Results

t=10s



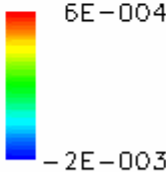
t=20s



Movie: 0 ~ 30 s (time interval between frames is 0.2 s)

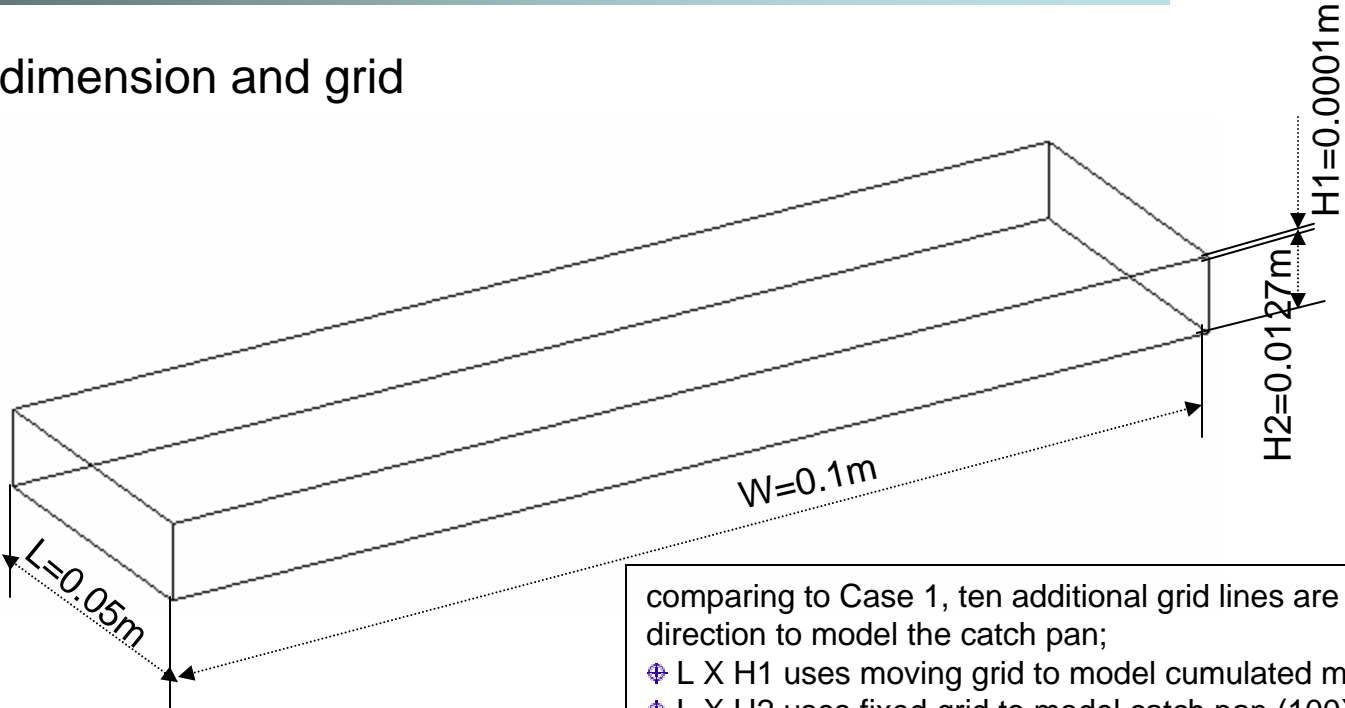
Takes 12 hrs to run on a P5 workstation

u (m/s)



Case 2 Configuration

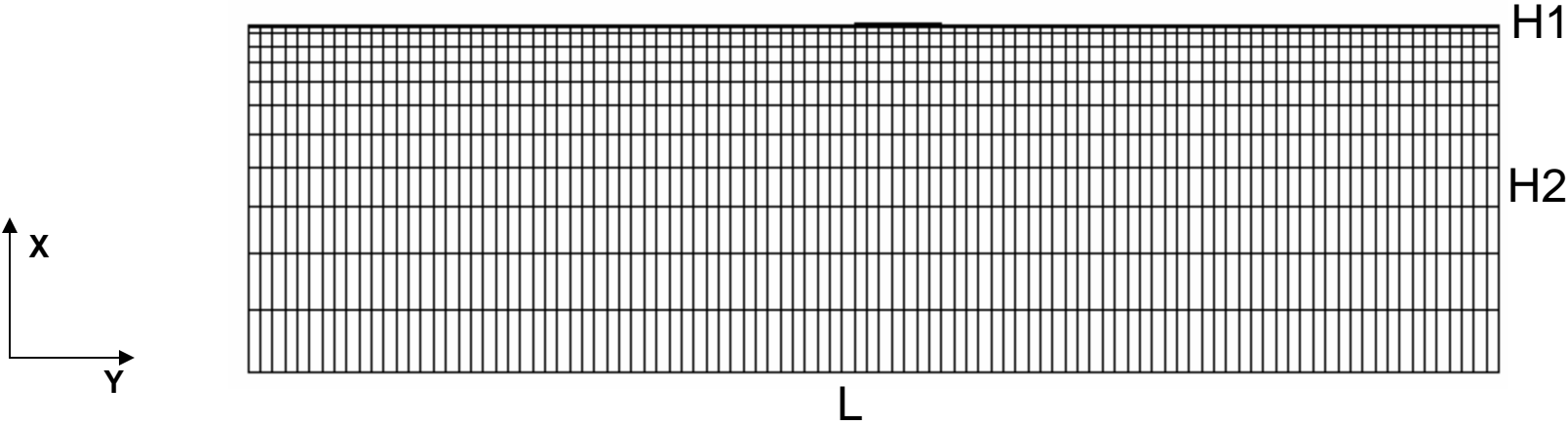
⊕ Initial dimension and grid



comparing to Case 1, ten additional grid lines are added in the x direction to model the catch pan;
 ⊕ L X H1 uses moving grid to model cumulated melt (100X20);
 ⊕ L X H2 uses fixed grid to model catch pan (100X10);

2-D computational domain at t = 0.1s:

Grid number: 100X30



Case 2 Material Properties

	Polymer melt	Catch pan*
Heat capacity (J/kg-K)	2400	961
Density (kg/m ³)	900	2800
Heat conductivity (W/m-K)	0.25	1.26
Viscosity (Pa-s)	0.13 ~1.e6	1.e6**

* data from NIST email (2/16/2007)

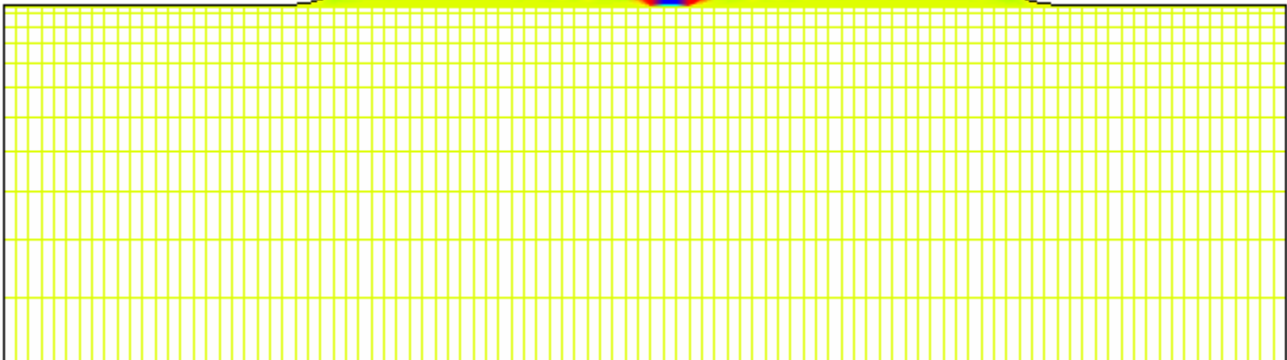
** arbitrarily chosen to suppress the flow

- ⊕ Material forming catch pan has smaller heat capacity and higher heat conductivity than the polymer melt. As a consequence, assuming 1-D heat conduction in the direction perpendicular to the catch surface inside the catch pan is invalid.
- ⊕ Case 2 includes the catch pan in the computational domain and may be more accurate in modeling the transient heat transfer in the catch pan.

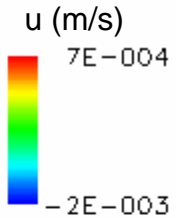
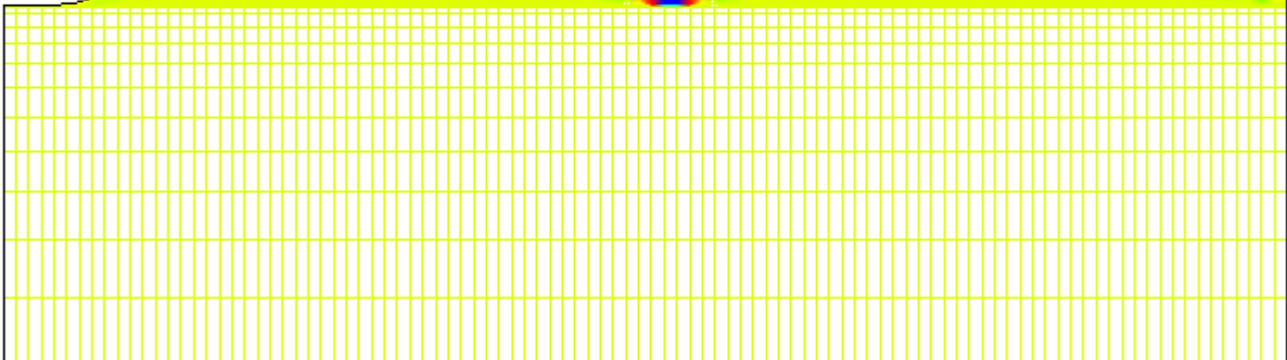


Case 2 Results

t=10s

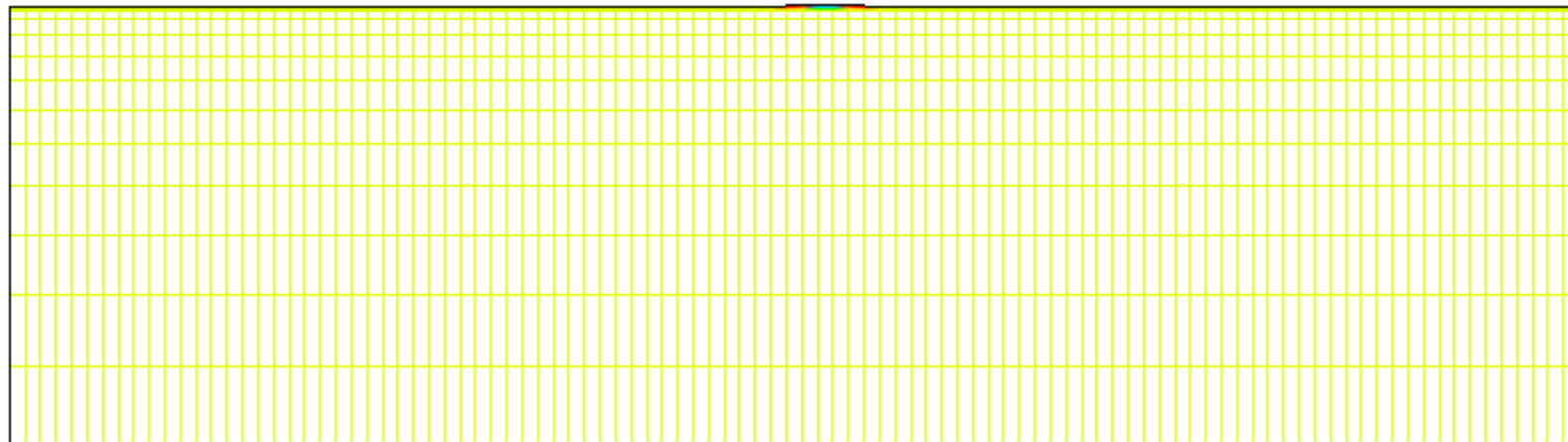
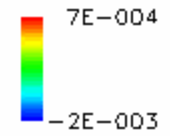


t=20s



Case 2 Results

Movie: 0 ~ 30 s (time interval between frames is 0.2 s)



Takes 12 hrs to run on a P5 workstation



Summary and Future Work

- ⊕ Two cases have been successfully performed, which show that the CPCFD is capable of modeling the melt flow on the catch surface under some simplified conditions

- ⊕ Future work includes:
 - ⊕ derive heat transfer coefficient on the melt surface (free convection on horizontal plate)
 - ⊕ incorporate more realistic boundary and initial conditions in the calculation
 - ⊕ surface heat loss
 - ⊕ constant temperature BC at the backside of the catch pan
 - ⊕ “cold” start (i.e., initial temperature of catch pan $\sim 250^{\circ}\text{C}$)
 - ⊕ tilt angle greater than 0°

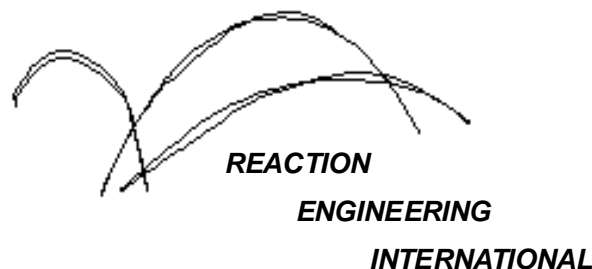


A Computational Model For Fire Growth and Spread On Thermoplastic Objects

Task 4: Include Melt Pool on Catch Surface

Task 4A (PP702N)

(03/21/07)

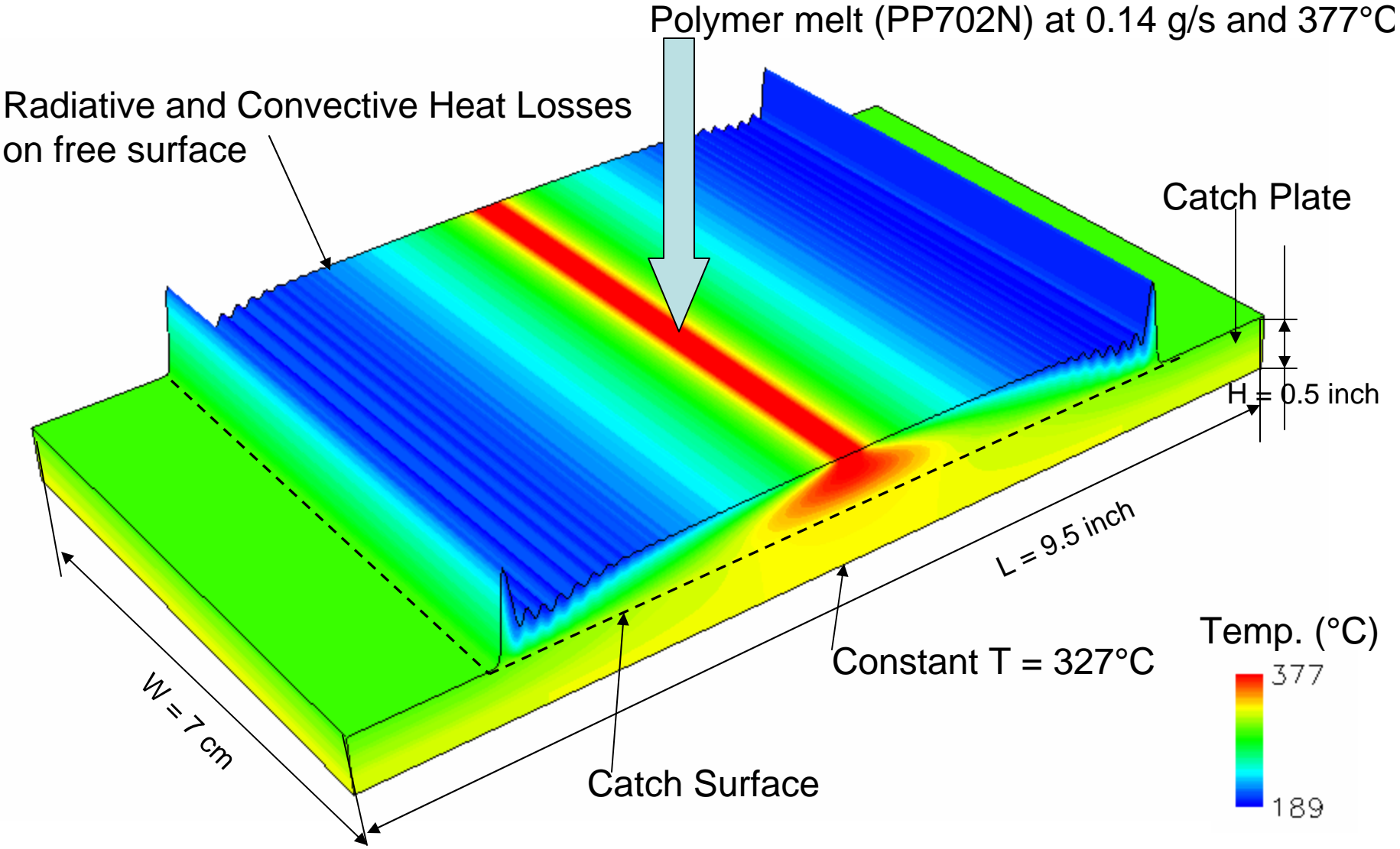


Outline

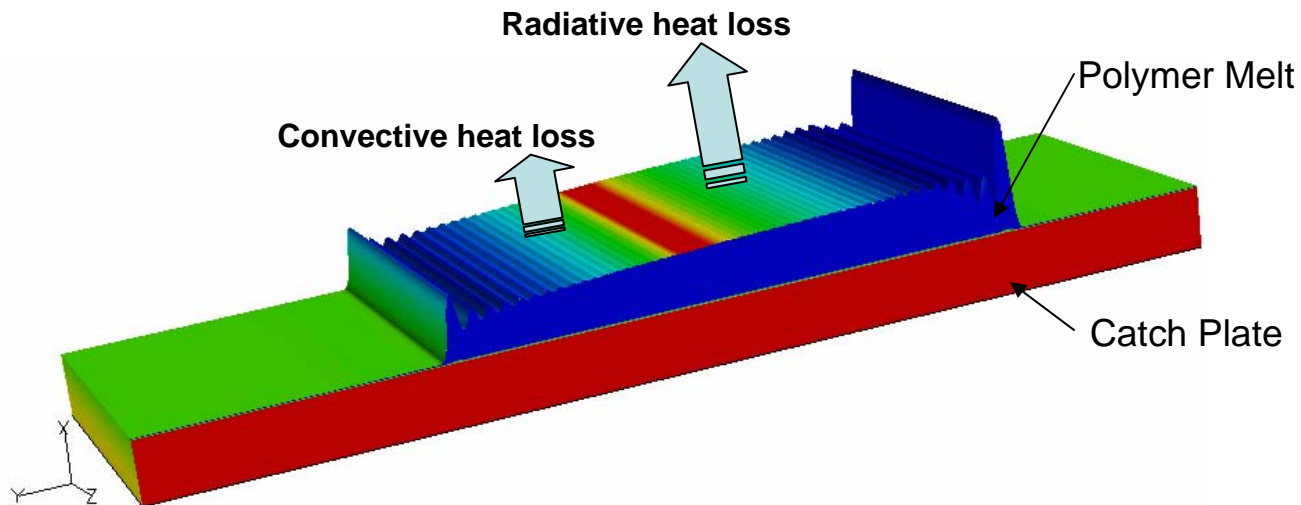
- ⊕ CFD model
- ⊕ Surface heat losses models
- ⊕ 2-D Computational grids
- ⊕ Test case results
 - ⊕ Case T1: All boundaries are adiabatic, Catch plate initial T at 600K
 - ⊕ Case T2: Free Convection on free surface and constant T (=600K) at the backside of catch plate
 - ⊕ Case T3: Free Convection and radiative heat losses on free surface and constant T (=600K) at the backside of catch plate
 - ⊕ Case T4: Same as Case T3 except the tilt angle of catch plate increases from 0° to 2.5°
 - ⊕ For all cases, polymer melt mass flow rate is 0.14g/s and its temperature is 650K
- ⊕ Summary and future work



CFD Model



Free Surface Heat Losses



⊕ Convective heat loss: $\dot{q}_{conv} = -h(T_{surf} - T_a)$, $T_a = 298^\circ\text{C}$

⊕ Approximate convection on the surface as “free convection on horizontal plate” *

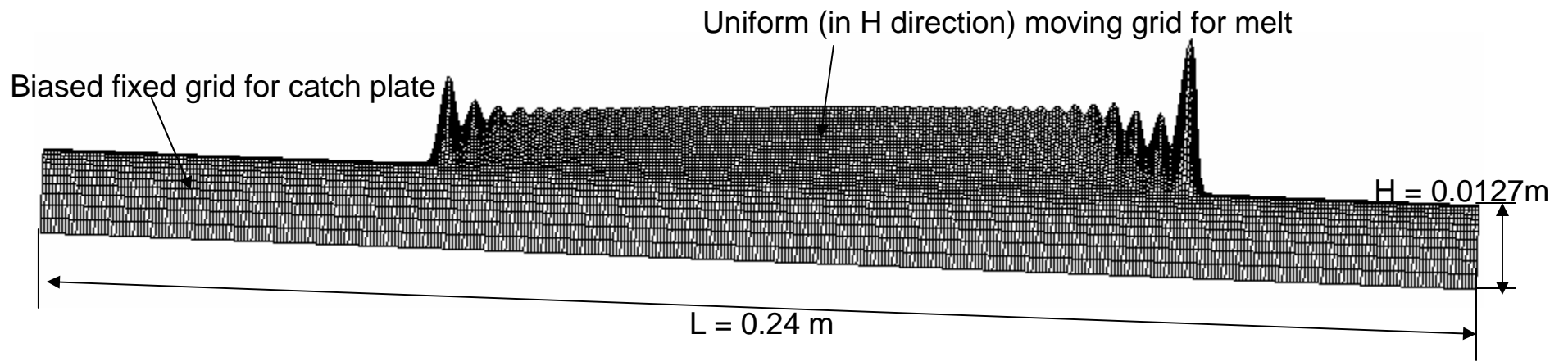
$$h = 1.32 \left(\frac{\Delta T}{L} \right)^{1/4} = 1.32 \left(\frac{400 - 27}{0.24} \right)^{1/4} \approx 8.0$$

⊕ Radiative heat loss: $\dot{q}_{rad} = -\varepsilon\sigma(T_{surf}^4 - T_a^4)$, $\varepsilon = 1.0$, $\sigma = 5.67\text{e-}8$

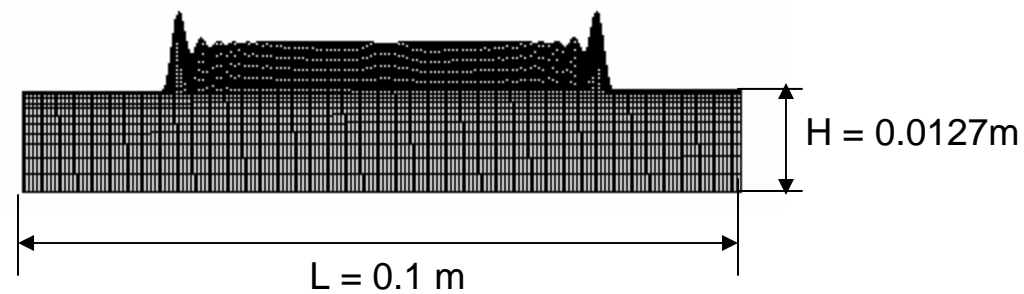
* Holman, J.P., Heat Transfer, McGraw-Hill, Inc., New York, 1981 (pp285)



2-D Computational Grids



400 X 30 (L X H) grid used in Case T3 and T4



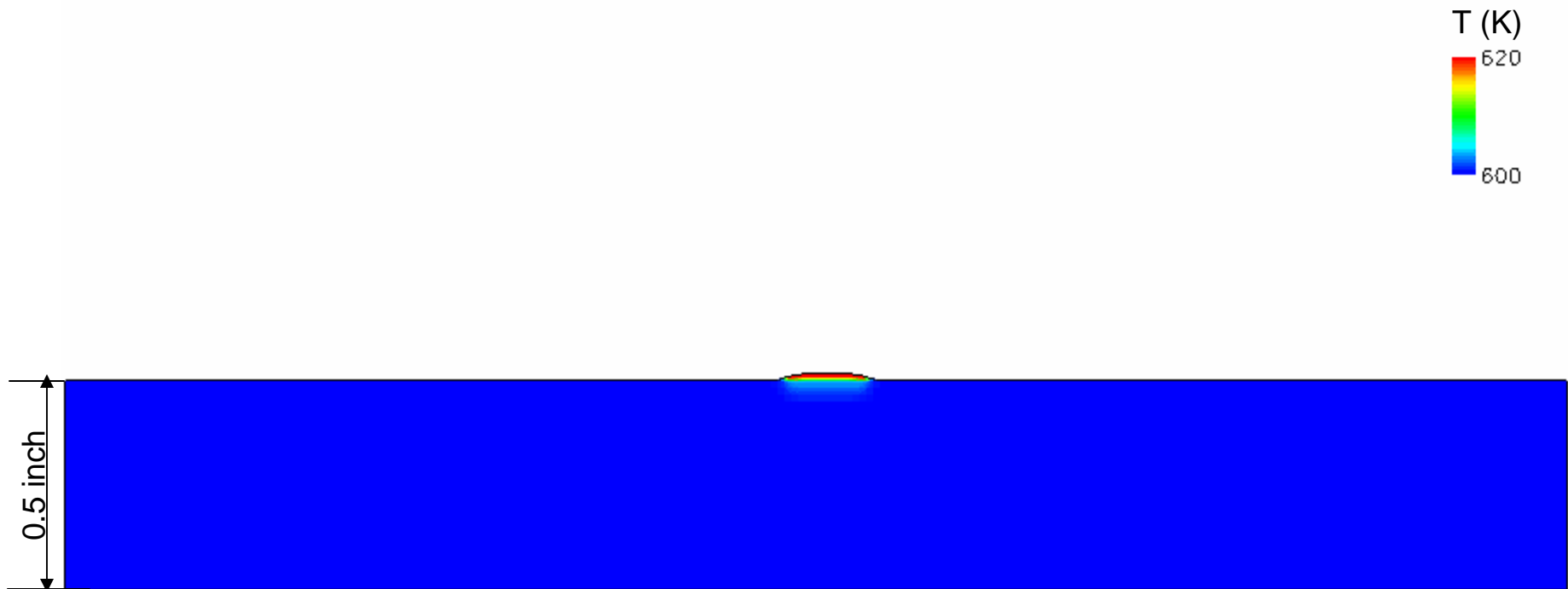
Reduced 200 X 30 (L X H) grid used in Case T1 and T2

Cases Summary

Case #	Description	Report
1	Adiabatic BC; Uniform $T_0=700\text{K}$; Catch plate not included; Reduced dimension; $\theta = 0^\circ$	02-23-2007
2	Adiabatic BC; Uniform $T_0=700\text{K}$; Catch plate included; Reduced dimension; $\theta = 0^\circ$	
T1	Adiabatic BC; Uniform $T_0=600\text{K}$; Catch plate included; Reduced dimension; $\theta = 0^\circ$	03-22-2007 (current)
T2	Convective heat loss; Uniform $T_0=600\text{K}$; Catch plate included; Backside constant T; Reduced dimension; $\theta = 0^\circ$	
T3	Convective and radiative heat losses; Uniform $T_0=600\text{K}$; Catch plate included; Backside constant T; NIST experiment dimension; $\theta = 0^\circ$	
T4	Convective and radiative heat losses; Uniform $T_0=600\text{K}$; Catch plate included; Backside constant T; NIST experiment dimension; $\theta = 2.5^\circ$	

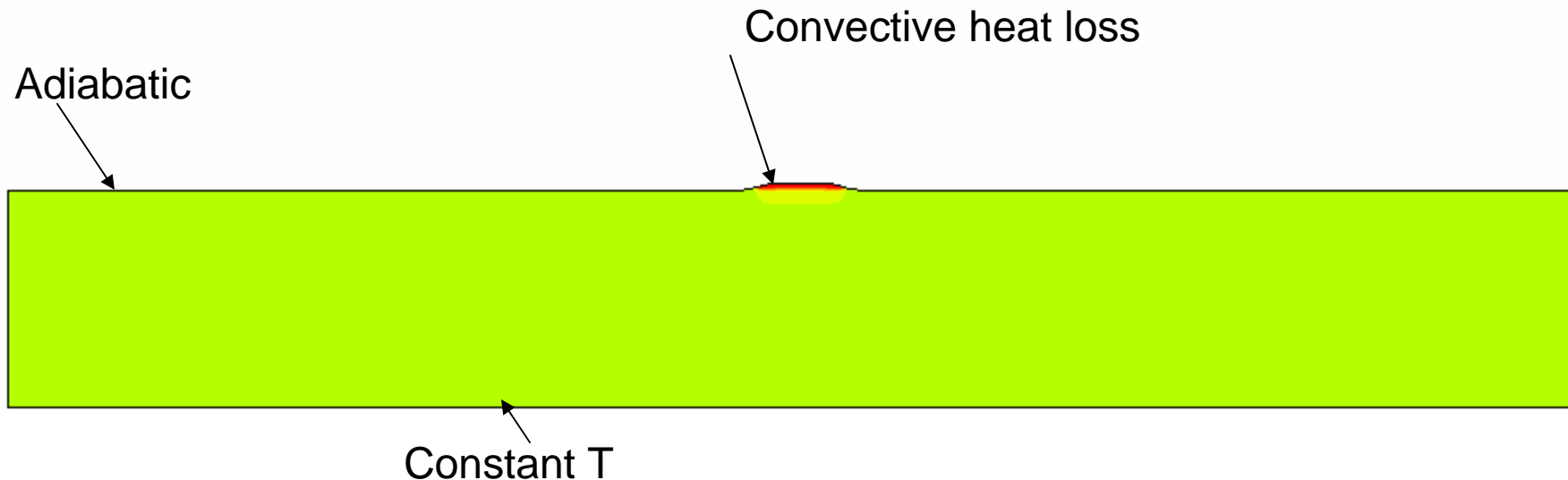


Case T1



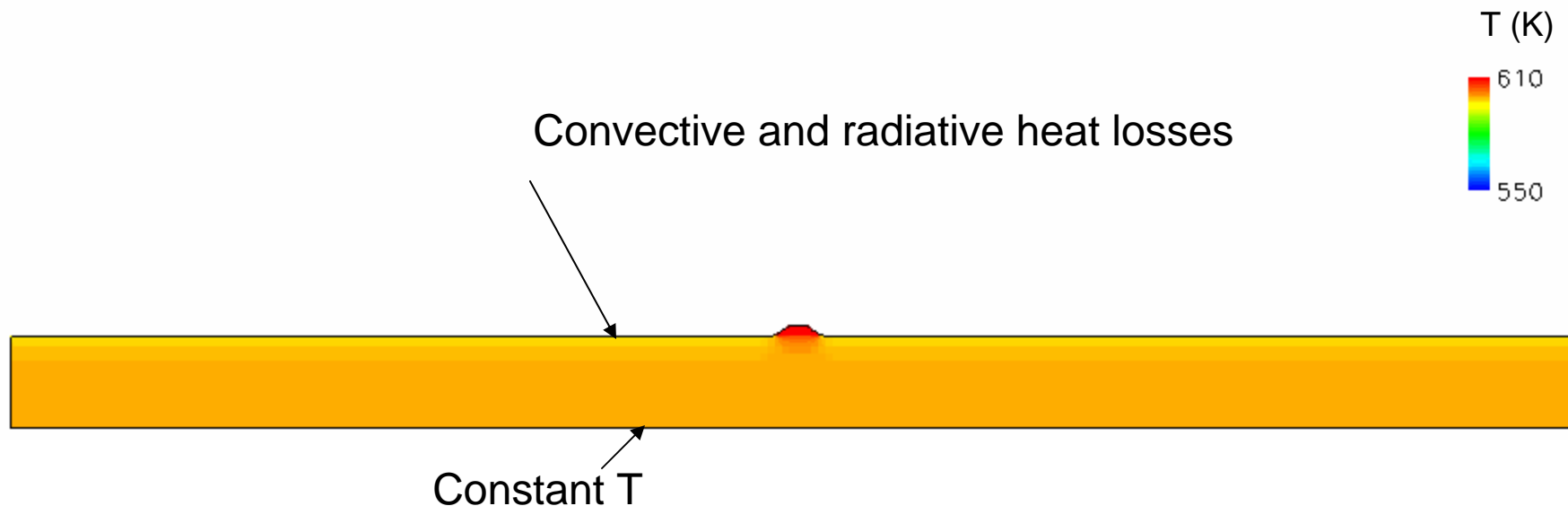
- ⊕ Adiabatic BC on melt free surface and catch plate surface; Uniform catch plate initial T at 600K
- ⊕ Reduced computational domain ($L = 0.1\text{m}$) w.r.t NIST experiment ($L = 0.24\text{ m}$) to save computational time
- ⊕ 2-dimensional grid: 200 X 30 (L X H)

Case T2



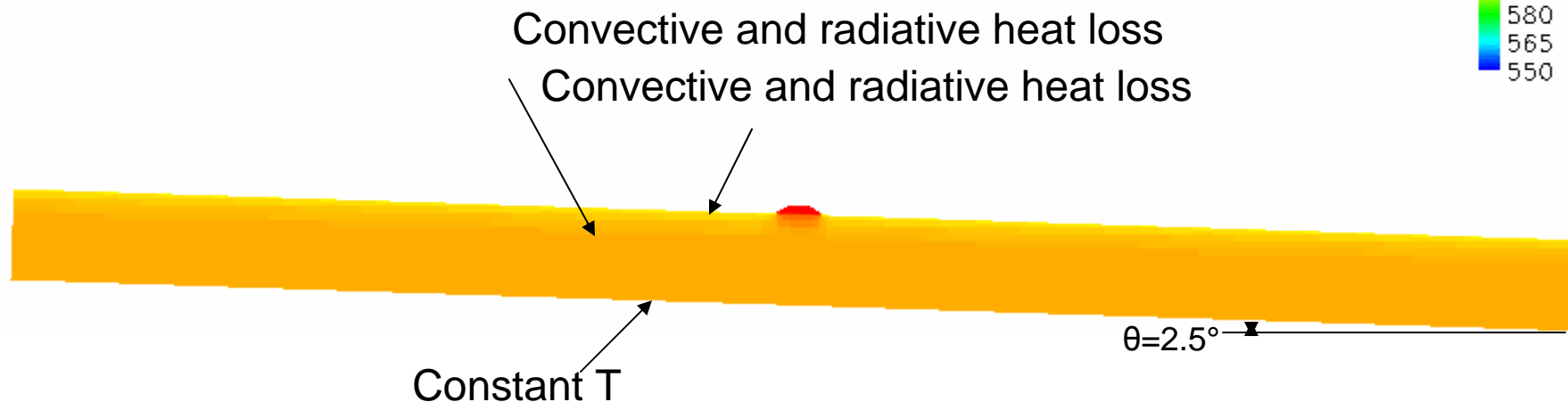
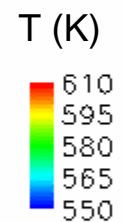
- ⊕ Free convection heat loss on free surface included; The catch surface of the catch plate not covered by polymer melt is adiabatic; Uniform catch plate initial T at 600K; Catch plate backside temperature at constant 600K
- ⊕ Reduced computational domain ($L = 0.1\text{m}$) w.r.t NIST experiment ($L = 0.24\text{ m}$) to save computational time
- ⊕ 2-dimensional grid: 200 X 30 (L X H)

Case T3



- ⊕ Dimension of catch plate the same as NIST experiment
- ⊕ Free convection and radiative heat loss on the free surface of the melt and the surface of the catch plate included; Uniform catch plate initial T at 600K; Catch plate backside temperature at constant 600K
- ⊕ 2-dimensional grid: 400 X 30 (L X H)

Case T4

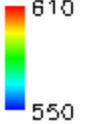


- ⊕ Dimension of catch plate the same as experiment
- ⊕ Free convection and radiative heat loss on the free surface and the catch surface of the catch plate included; Uniform catch plate initial T at 600K; Catch plate backside temperature at constant 600K; Plate tilt angle 2.5°
- ⊕ 2-dimensional grid: 400 X 30 (L X H)

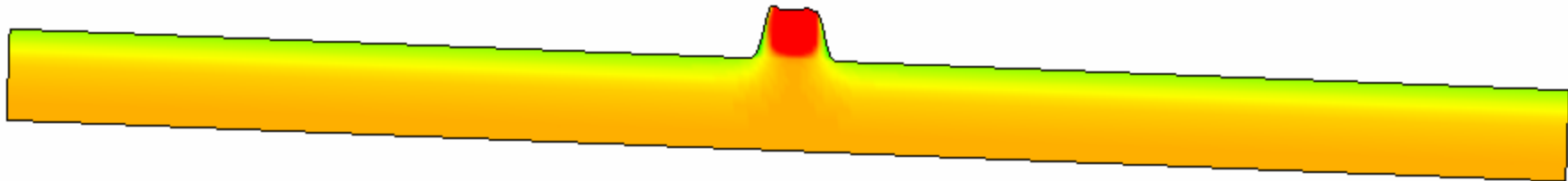


Case T4 - Snapshots

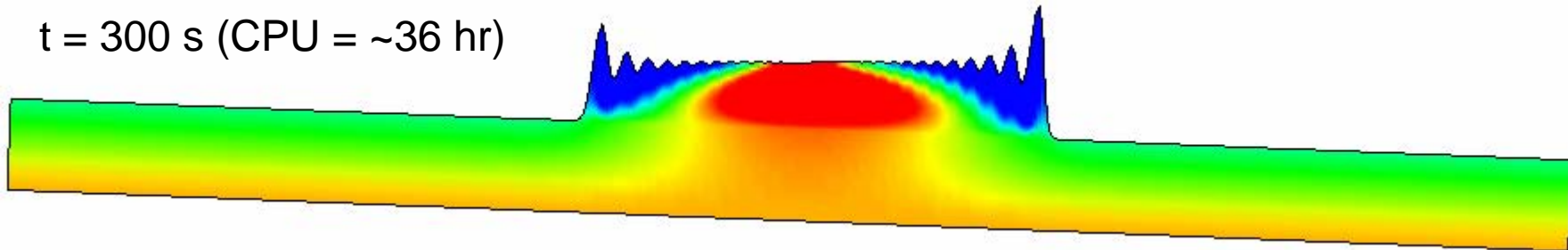
T (K)
610
550



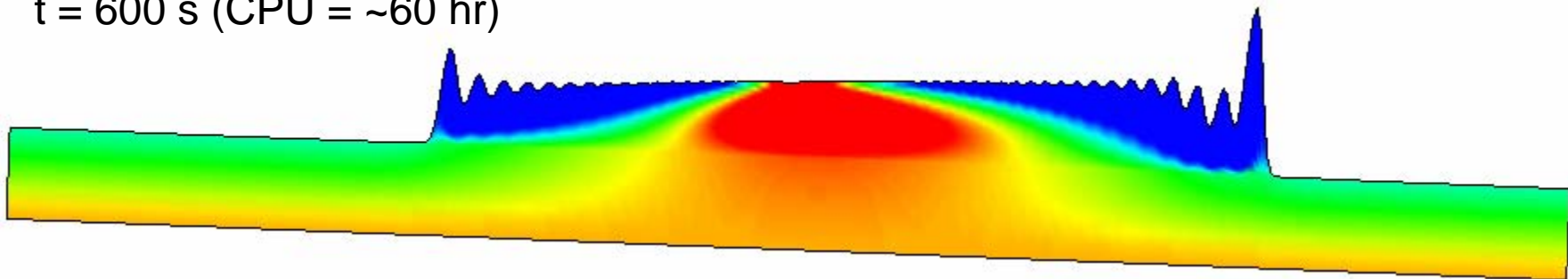
t = 30 s (CPU = ~12 hr)



t = 300 s (CPU = ~36 hr)



t = 600 s (CPU = ~60 hr)



- ⊕ Calculation time steps were limited to 0.01s for t=0 ~ 30 s
- ⊕ Maximum time steps after t = 300 s is 0.05 s
- ⊕ Simulation was run on a 2.8 GHz Intel workstation



Summary

- ⊕ Test results from simulations using realistic boundary conditions demonstrate the feasibility of the modeling methodology
- ⊕ Melt free surface becomes corrugated when applying heat loss BCs
- ⊕ There are two large peaks at the two ends of the melt in all 4 cases reported in this presentation
- ⊕ Heated catch surface with initial temperature above $\sim 570\text{K}$ is crucial to the success of the simulations
- ⊕ Simulation diverged when setting tilt angle to 5°
- ⊕ Computational time steps at the beginning of the simulations ($t < \sim 30$ sec) are very small (in the order of 10^{-3} s). CFL = 0.1 was used in all simulations and maximum time step was set to 0.05 s. It took about 12 hrs to complete a 30 s simulation and about 60 hr to complete a 600 s simulation on a 2.8 GHz Intel workstation.



Future Work

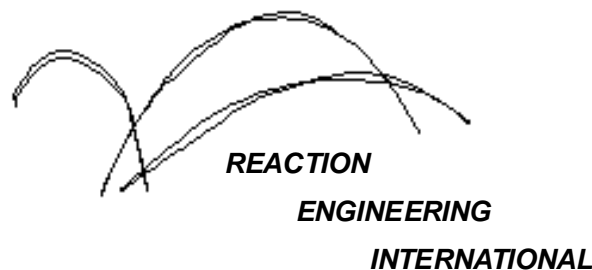
- ⊕ Implement realistic initial temperature distribution in catch plate
 - ⊕ Steady state
 - ⊕ Convective and radiative heat losses at catch surface
 - ⊕ Constant T at backside
- Test the possibility of reducing the catch plate backside temperature
- Combine simulations of the vertical resin and the catch basin
- Simulate PP6523 (feasibility study without surface tension model)
- ⊕ Implement surface tension boundary condition on free surface
- ⊕ Repeat simulations of PP702N and PP6523



A Computational Model For Fire Growth and Spread On Thermoplastic Objects

Task 4: Include Melt Pool on Catch Surface

(04/26/07)

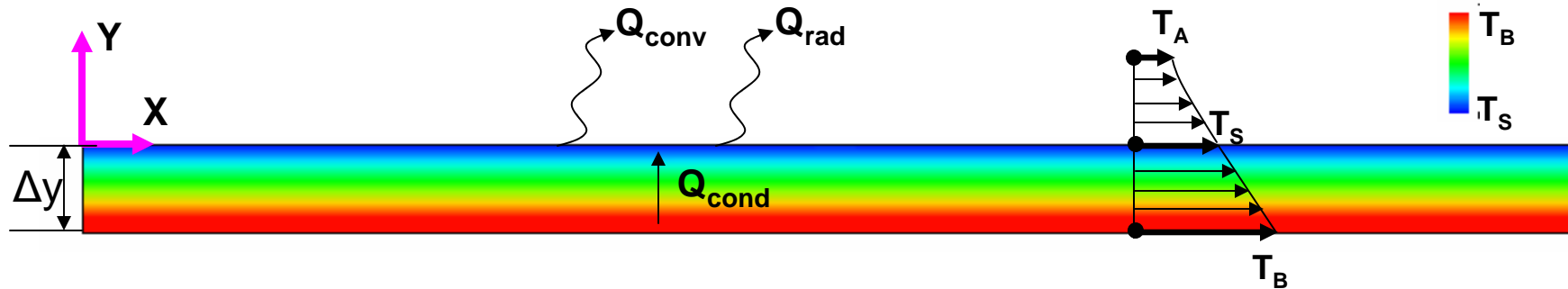


Outline

- ⊕ Initial Temperature Distribution inside the catch plate
- ⊕ Case Summary
- ⊕ Case T5: PP702 Simulation
 - ⊕ Movie of polymer melt shape
 - ⊕ Temperature contour snap shots
- ⊕ Case T6: PP6523 Simulation
 - ⊕ Movie of polymer melt shape
 - ⊕ Temperature contour snap shots
- ⊕ Surface tension model
 - ⊕ Surface tension force normal to the free surface
 - ⊕ Surface tension gradient effects
 - ⊕ Calculation of free surface curvature
- ⊕ Summary and future work



Temperature Distribution of Catch Plate



⊕ 1-D Steady State Energy Balance Equation:

$$k \frac{dT}{dy} = h(T_S - T_A) + \varepsilon\sigma(T_S^4 - T_A^4)$$

$$k = 1.26 \text{ w/m-K}; \quad h = 8.0 \text{ w/m}^2 \cdot \text{K}; \quad \varepsilon = 1.0; \quad \sigma = 5.67 \times 10^{-8} \text{ w/m}^2 \cdot \text{K}^4;$$

$$T_A = 298 \text{ K}; \quad \Delta y = 0.0127 \text{ m}$$

⊕ Initial catch plate temperature distribution in PP702N Simulation (T5):

$$T = T_B - 6860.63 \cdot (y + 0.0127)$$

$$T_B = 675 \text{ K}; \quad T_S = 588 \text{ K}; \quad -0.0127 \leq y \leq 0$$

⊕ Initial catch plate temperature distribution in PP6523 Simulation (T6):

$$T = T_B - 7570.87 \cdot (y + 0.0127)$$

$$T_B = 700 \text{ K}; \quad T_S = 604 \text{ K}; \quad -0.0127 \leq y \leq 0$$

Case Summary

Case #	Description	Report
T1	Adiabatic BC; Uniform T0=600K; Reduced dimension; $\theta = 0^\circ$; PP702N	03-22-2007
T2	Convective heat loss; Uniform T0=600K; Backside constant T=600K; Reduced dimension; $\theta = 0^\circ$; PP702N	
T3	Convective and radiative heat losses; Uniform T0=600K; Catch plate included; Backside constant T=600K; NIST experiment dimension; $\theta = 0^\circ$; PP702N	
T4	Convective and radiative heat losses; Uniform T0=600K; Catch plate included; Backside constant T=600K; NIST experiment dimension; $\theta = 2.5^\circ$; PP702N	
T5	Convective and radiative heat losses; Realistic initial catch plate temperature distribution; Backside constant T = 675K; NIST experiment dimension; $\theta = 2.5^\circ$; PP702N	04-26-2007 (current)
T6	Convective and radiative heat losses; Realistic initial catch plate temperature distribution; Backside constant T = 700K; NIST experiment dimension; $\theta = 2.5^\circ$; PP6523	



Case T5: PP702N – Shape Change



Movie time period: 2 – 360 seconds

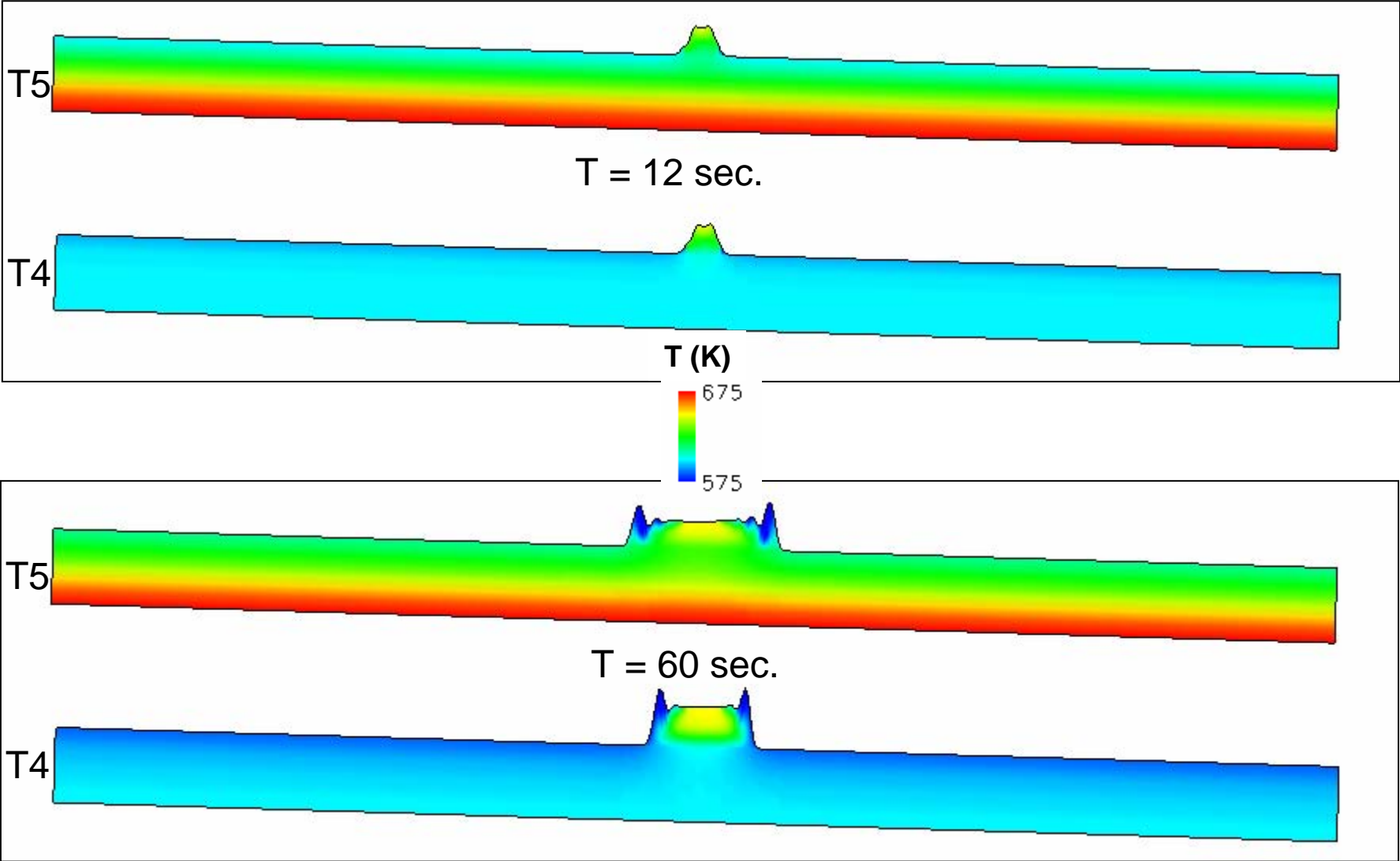
Computation time (0 – 360 secs): 15 hrs (CFL = 0.05, $\Delta t_{\max} = 0.05$ sec)

⊕ Initial catch plate temperature distribution:

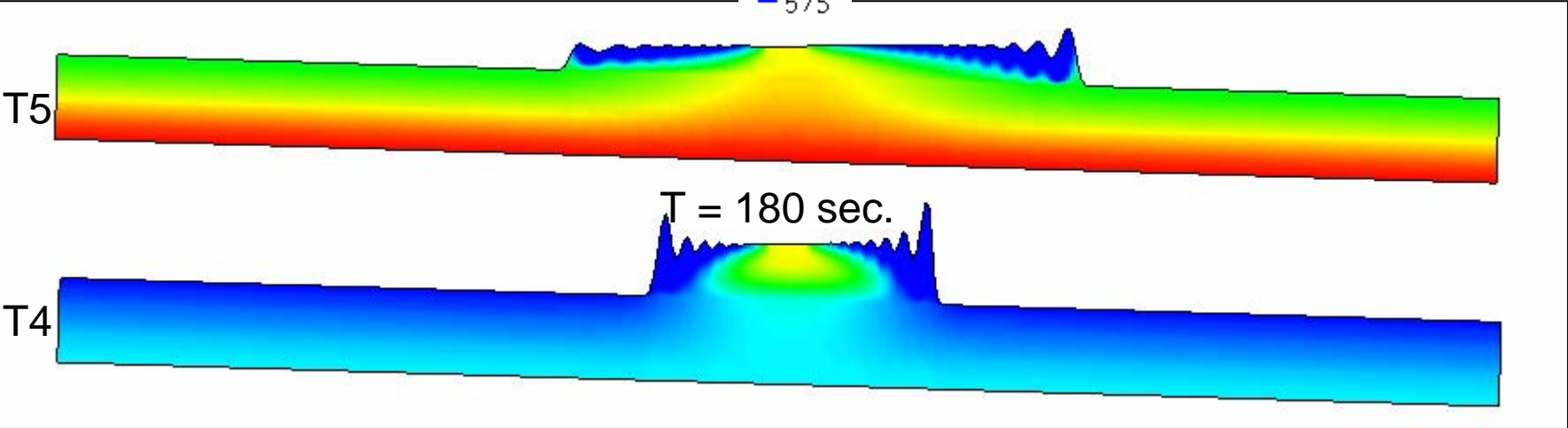
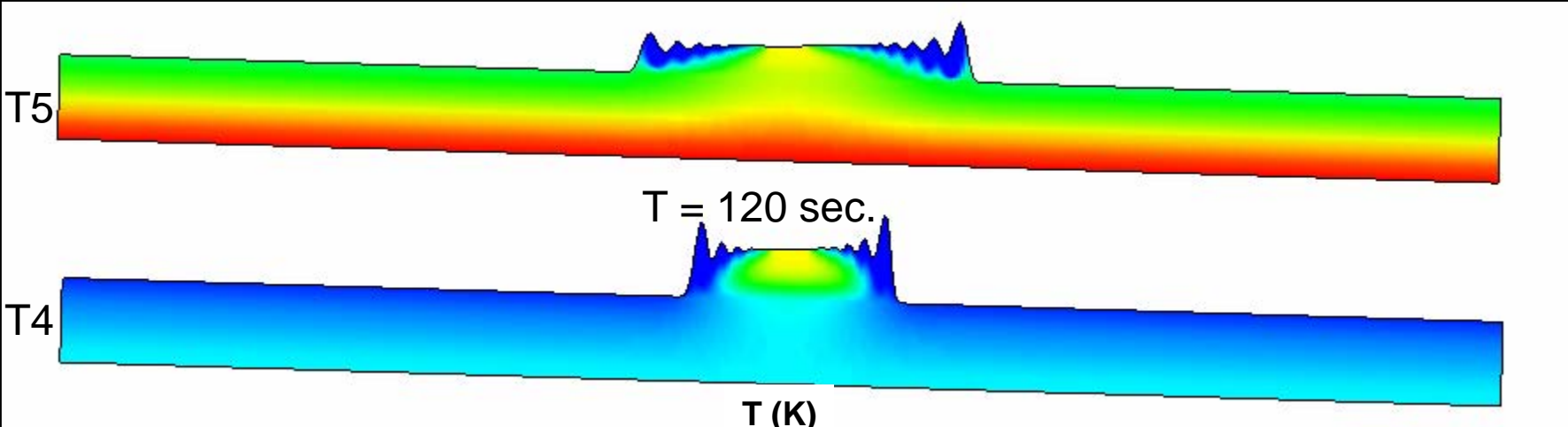
$$T = T_B - 6860.63 \cdot (y + 0.0127)$$

$$T_B = 675 \text{ K}; T_S = 588 \text{ K}; -0.0127 \leq y \leq 0$$

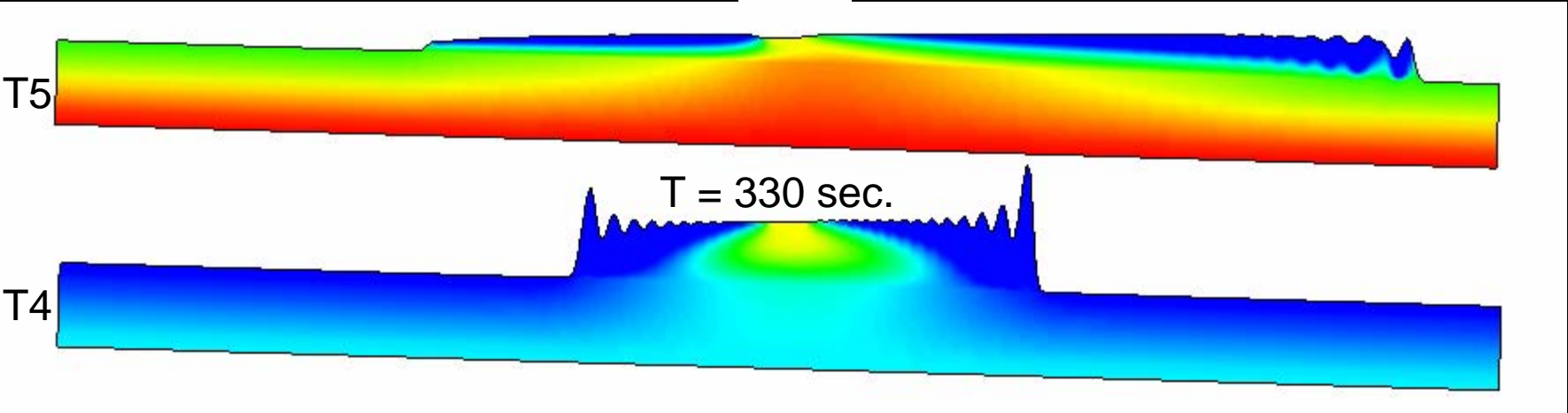
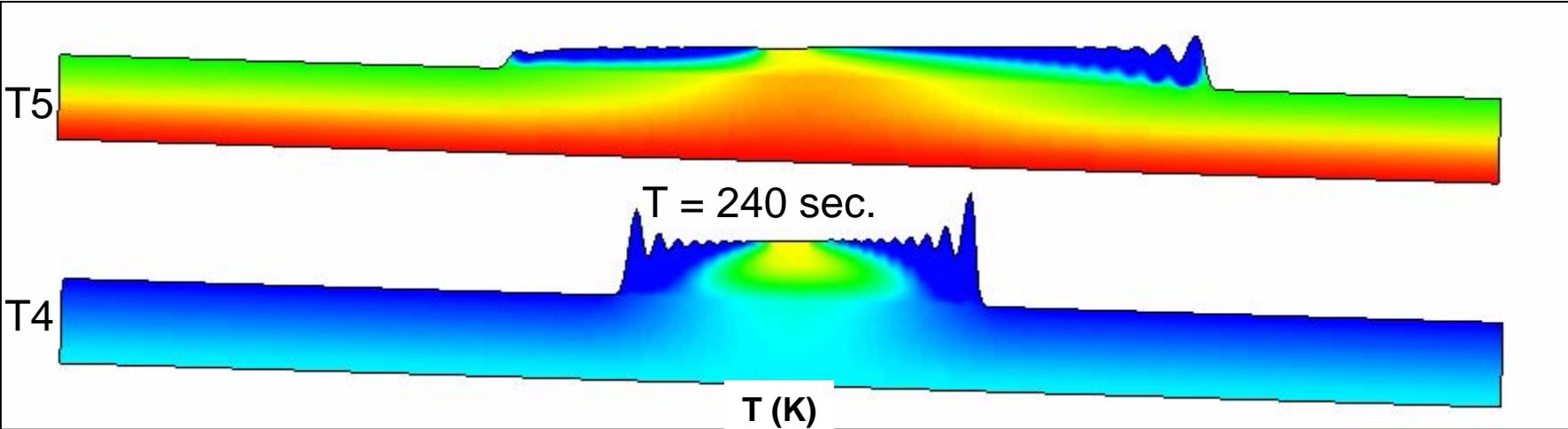
Case T5: PP702N – Temperature Snap Shots



Case T5: PP702N – Temperature Snap Shots



Case T5: PP702N – Temperature Snap Shots



Case T6: PP6523 – Shape Change



Movie time period: 2 – 240 seconds

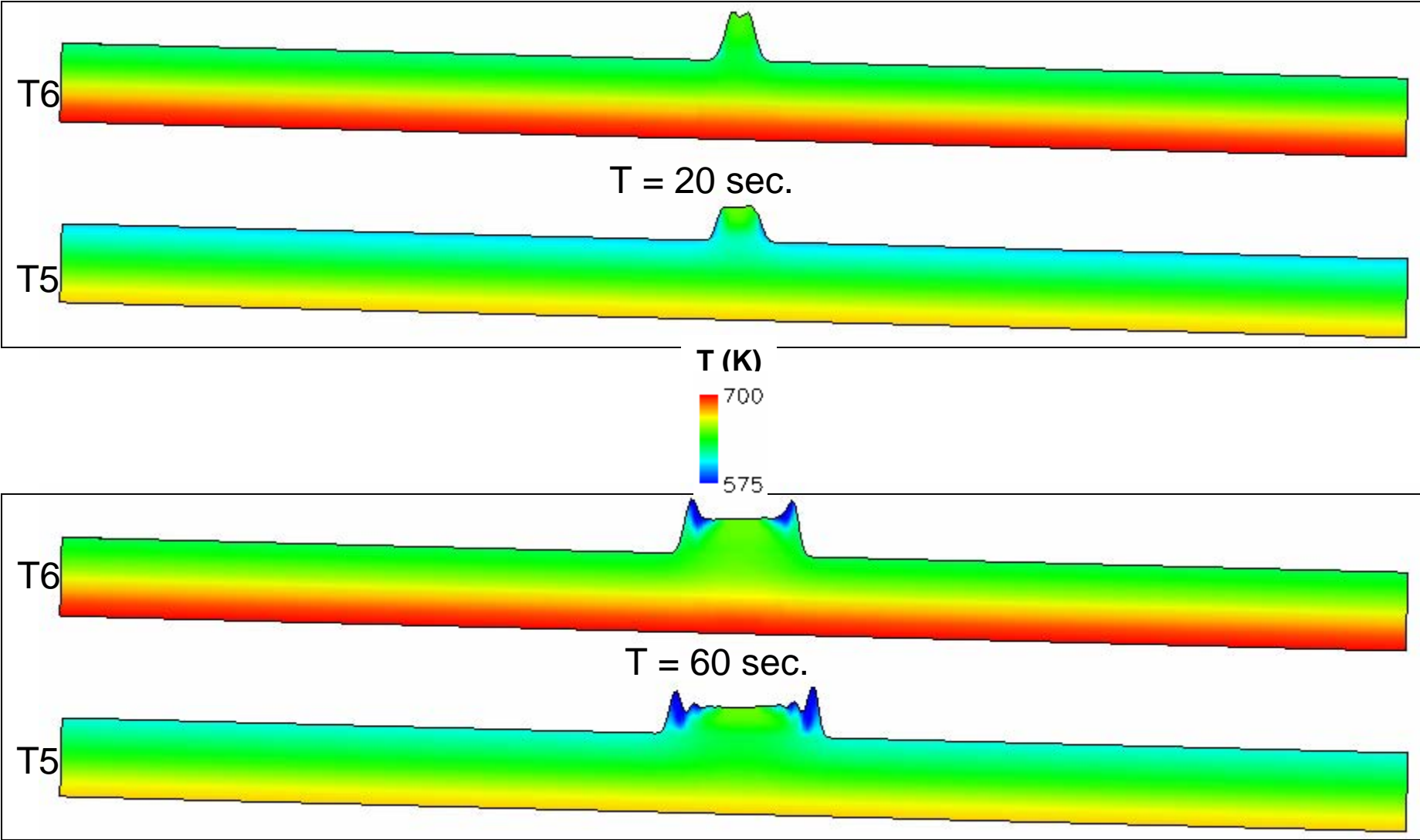
Computation time (0 – 240 secs) : 18 hrs (CFL = 0.05, $\Delta t_{\max} = 0.05$ sec)

⊕ Initial catch plate temperature distribution:

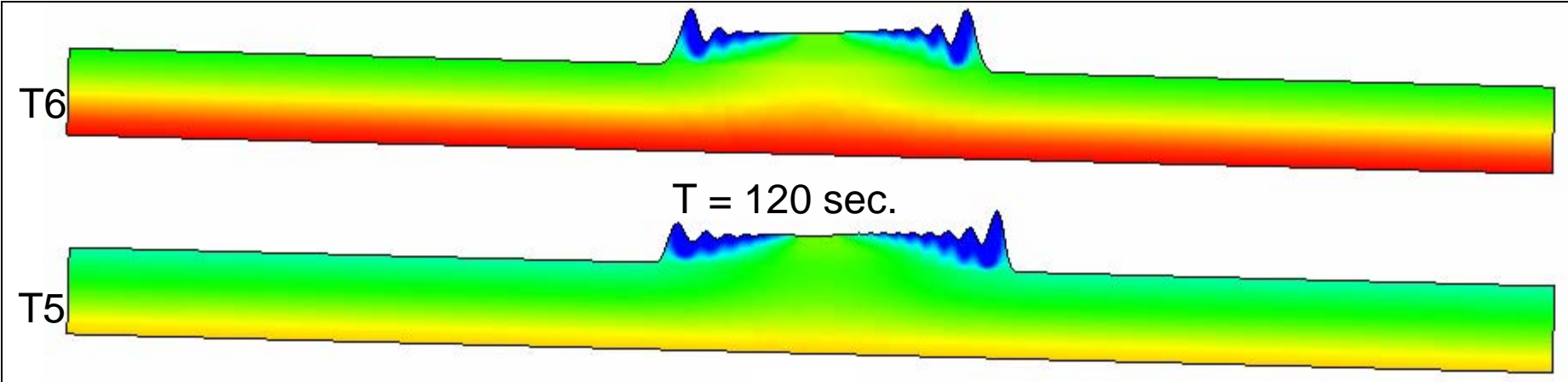
$$T = T_B - 7570.87 \cdot (y + 0.0127)$$

$$T_B = 700 \text{ K}; T_S = 604 \text{ K}; -0.0127 \leq y \leq 0$$

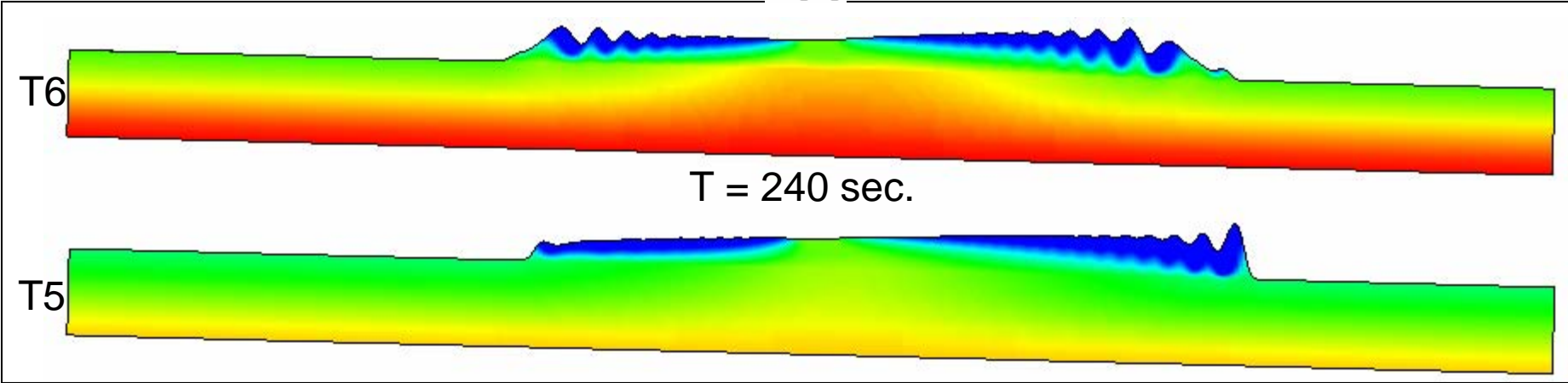
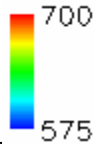
Case T5: PP6523 – Temperature Snap Shots



Case T5: PP6523 – Temperature Snap Shots



T (K)



Surface Tension as Function of Temperature - Theory

⊕ Two empirical equations for surface tension of liquids

Eotvos:

$$\gamma = \kappa(T_c - T) / V^{2/3}$$

where, V is the molar volume of that substance

T_c is the critical temperature

κ is a constant for each substance.

Guggenheim-Katayama

$$\gamma = \gamma^0 (1 - T / T_c)^n$$

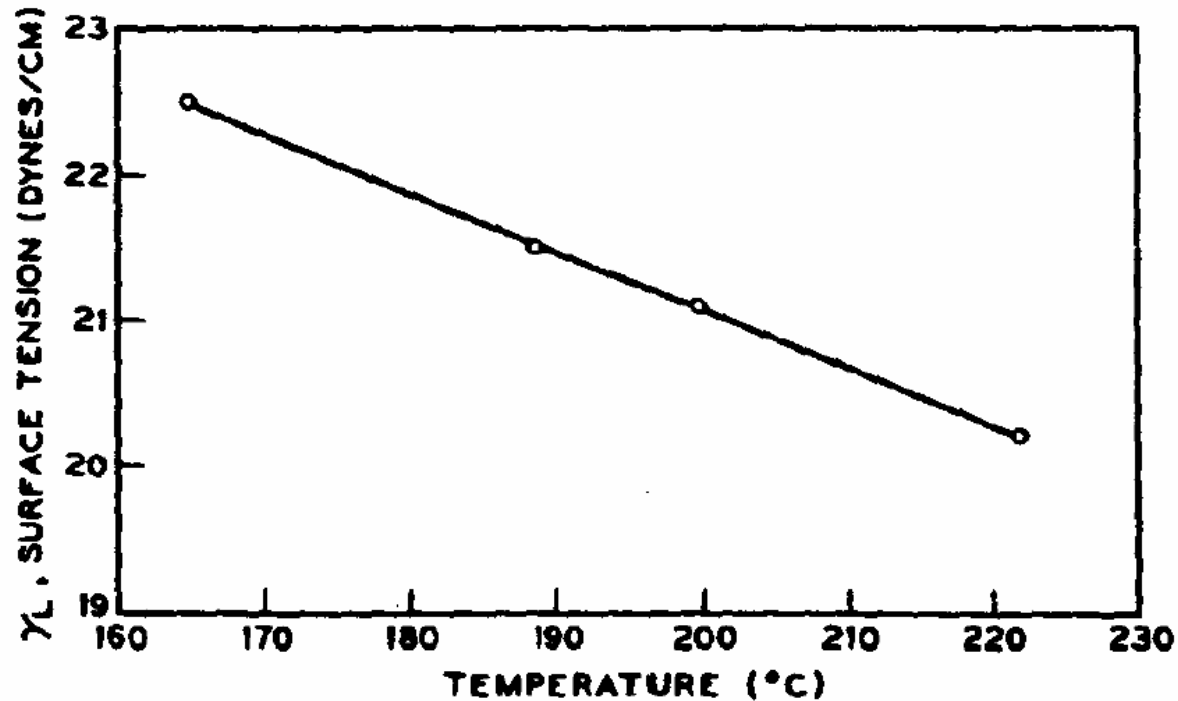
where, γ^0 is a constant for that substance

n is an empirical factor, whose value is 11/9 for organic liquids

http://en.wikipedia.org/wiki/Surface_tension, The critical temperature, T_c , of a material is the temperature above which distinct liquid and gas do not exist



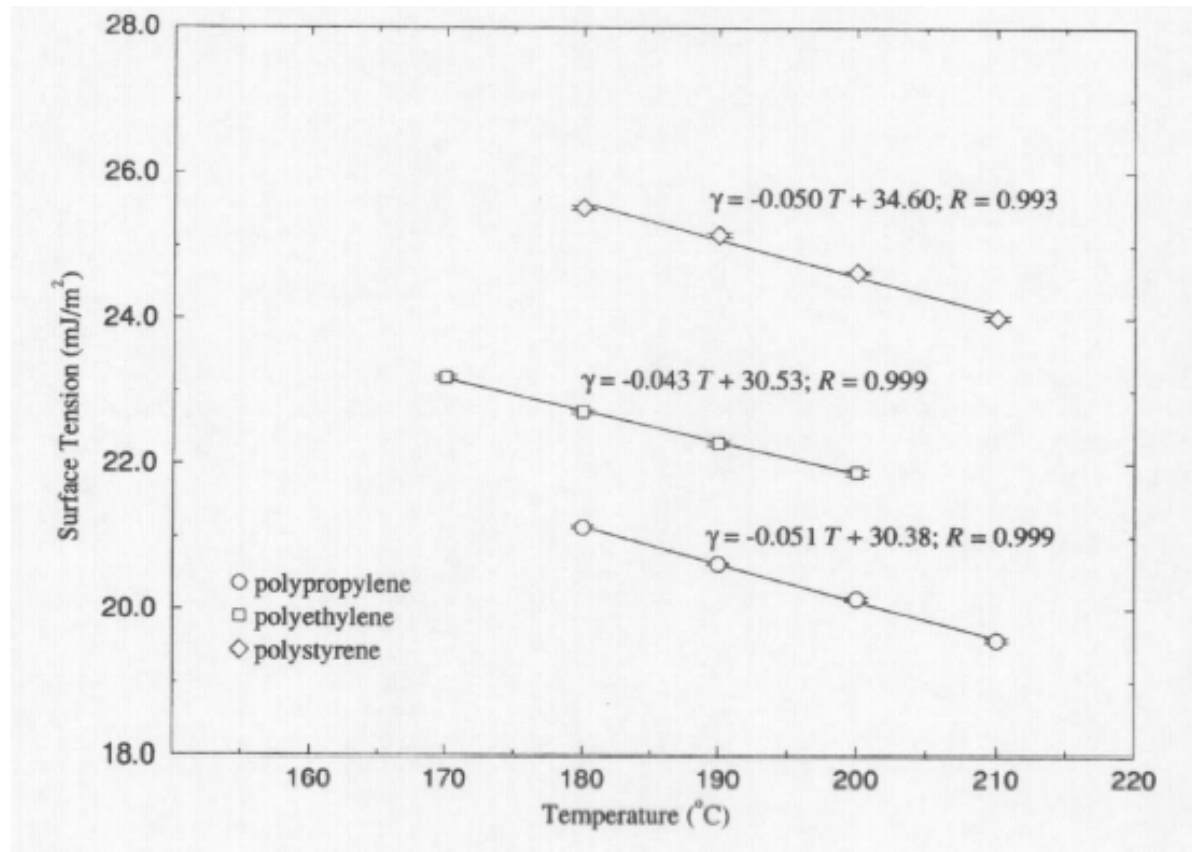
Surface Tension of Polypropylene - Experiments



$$\gamma = -0.04 T(^{\circ}C) + 29.10 \quad (165 - 220^{\circ}C)$$

Schonhorn, H., and Scharpe L., "Surface tensions of Molten Polypropylene," Polymer Letters, Vol.3, 1965, p.235.

Surface Tension of Polypropylene - Experiments



$$\gamma = -0.051T(^{\circ}C) + 30.38 \quad (180 - 210^{\circ}C)$$

Kwok, D, et al., "Study on the surface tensions of polymer melts using axisymmetric drop shape analysis", Polymer Engineering and Science, Vol.38, 1998, p.757



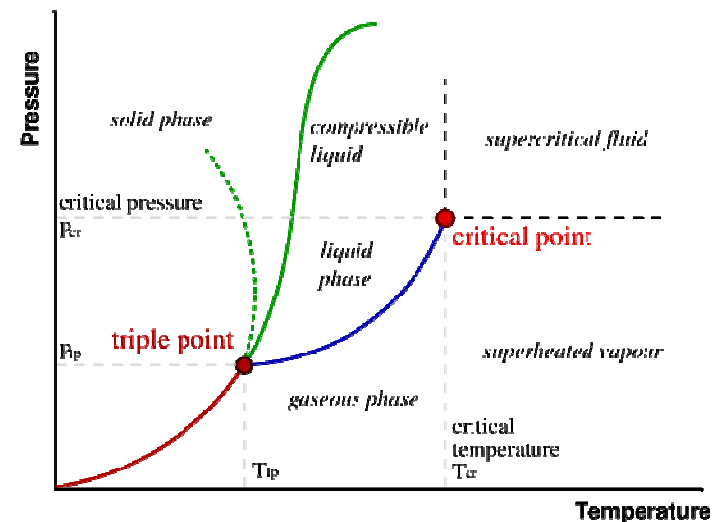
Surface Tension of Polypropylene - Summary

- ⊕ The critical temperature, T_c , of a material is the temperature above which distinct liquid and gas do not exist.
- ⊕ Both Eotvos and Guggenheim-Katayama's empirical expressions comply with the fact that the surface tension reduced to zero at/above the critical temperature..

- ⊕ **What's is the critical temperature of PP702 and PP6523 ?**
 Schonhorn-Scharpe's correlation suggests that $T_c = 728 \text{ }^\circ\text{C}$
 Kwok's correlation suggests that $T_c = 596 \text{ }^\circ\text{C}$.

higher than the surface temperatures seen in the CFD simulations

- ⊕ Both Schonhorn-Scharpe and Kwok's model are based on linear correlation, and the temperature range from 165-220 $^\circ\text{C}$ (438 - 493 K). Eotvos's expression suggests that linear correlation might be applicable for higher temperature (but below the critical temperature).



Phase diagram



Surface Tension CFD Mode – Surface Tension Forces

⊕ Surface Tension Forces (in the normal direction of the free surface)

⊕ Young-Laplace:

$$\Delta P = \gamma \left(\frac{1}{R_1} + \frac{1}{R_2} \right)$$

*ΔP is the pressure difference over the interface;
 R_1, R_2 are the principal radii of curvature of the surface;
 γ is the surface tension*

⊕ Implementation in CFD as a body force

$$\vec{F}_{vol} = -\Delta P \cdot A \cdot \hat{n} = -\gamma \cdot \kappa \cdot A \cdot \hat{n}$$

$$\kappa = \nabla \cdot \hat{n}; \quad \hat{n} = \frac{\vec{n}}{|\vec{n}|}$$

*κ is the curvature of the free surface;
 \vec{n} is the normal vector of the free surface
 A is the surface area*

⊕ Surface tension γ as a function of temperature (Thomas J. Ohlemiller 1/16/07 email)

$$\gamma = -0.051T + 30.38 \quad (180 - 210 \text{ }^\circ\text{C}) \quad \text{Philips HNZ020 polypropylene}$$

$$\gamma = -0.040T + 29.10 \quad (165 - 220 \text{ }^\circ\text{C}) \quad \text{Eastman Epolene D-10 atactic PP}$$

⊕ Model only applies to cells forming the free surface



Surface Tension CFD Mode – Surface Tension Gradient

⊕ Surface Tension Gradient Effects (in the tangential direction of the free surface)

⊕ Shear stress at the surface resulting from the variation of surface tension*:

$$\mu \frac{\partial U}{\partial n} = \frac{d\gamma}{d\tau} \equiv \gamma_\tau$$

*μ is the viscosity;
 U is the tangential velocity component;
 n is the normal direction of the free surface
 τ is the tangential direction of the free surface*

⊕ Implementation in CFD as a momentum source

$$\vec{S} = \gamma_\tau \cdot \hat{\tau} = \gamma_x \vec{i} + \gamma_y \vec{j}$$

$$S_u = \gamma_x \cdot V$$

$$S_v = \gamma_y \cdot V$$

$$\hat{\tau} = \frac{\vec{\tau}}{|\vec{\tau}|}$$

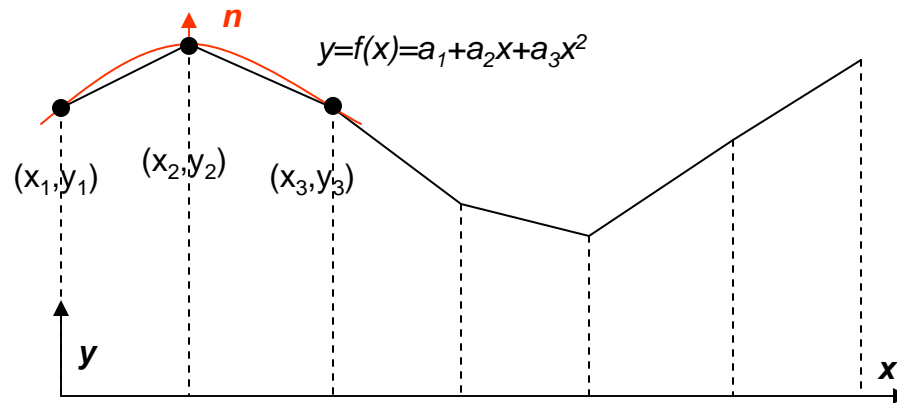
*S_u , S_v are the additional source terms in the u - and v -momentum equations, respectively ;
 $\vec{\tau}$ is the tangential vector of the free surface
 V is the cell volume*

⊕ Model only applies to cells forming the free surface

* W.A. Sirignano and I. Glassman, *Combustion Sci. and Tech.*, Vol. 1, pp307-312, 1970.



Surface Tension CFD Mode – Calculate Surface Curvature



Reference:
<http://web.mit.edu/1.63/www/lecnote.html>

- ⊕ Define the free surface passing through (x_1, y_1) , (x_2, y_2) , (x_3, y_3) using parabolic curve $y=g(x)=a_1+a_2x+a_3x^2$.

- ⊕ Solve linear algebraic equations for coefficients a_i

$$y_1=a_1+a_2x_1+a_3x_1^2.$$

$$y_2=a_1+a_2x_2+a_3x_2^2.$$

$$y_3=a_1+a_2x_3+a_3x_3^2.$$

- ⊕ Define a functional $f(x,y)=y-g(x)=y-a_1-a_2x-a_3x^2$, the normal to the surface is thus,

$$\hat{n} = \frac{\nabla f}{|\nabla f|} = \frac{\vec{j} - g'(x)\vec{i}}{(1 + g'(x)^2)^{1/2}}$$

- ⊕ The curvature of the free surface may be expressed as:

$$\kappa = \nabla \cdot \hat{n} = \frac{g_{xx}}{(1 + g_x^2)^{3/2}}$$



Summary

- ⊕ Realistic initial condition of catch plate has been implemented in the CFD model

- ⊕ Starting from the realistic initial condition, two test cases (T5 and T6) have been performed for PP702N and PP6523. Comparing the results with that of a previous case (T4, see 3/22/07 report) that started from a uniform temperature initial condition, the following observations can be made
 - In order for the CFD code to run with realistic initial condition, the backside temperature must be increased from 600 K (used in T4) to 675 K and 700 K for T5 and T6, respectively
 - Comparing to case T4, the melt flow in T5 and T6 expands much faster due to the higher backside temperatures, and
 - The free surfaces are much smoother in T5 and T6 than that in T4
 - Because of the different viscosity-temperature relationships, the predicted behaviors of the two polymer melts are different in terms of free surface shapes and expansion speeds

- Surface tension model has been developed



Future Work

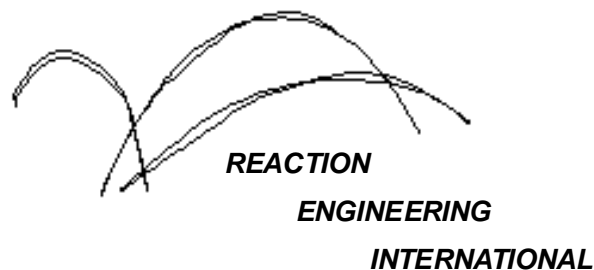
- ⊕ Implement surface tension model into CPCFD
- ⊕ Repeat test cases T5 and T6 with surface tension effects
- ⊕ Combined simulations of the vertical resin and the catch basin for both PP702N and PP6523



A Computational Model For Fire Growth and Spread On Thermoplastic Objects

Task 4: Include Melt Pool on Catch Surface

(05/30/07)



Outline

- ⊕ Implement Surface Tension Model
- ⊕ Case Summary
- ⊕ Study the Impact of Time Step Size
 - ⊕ Snap shots of free surface shape at certain time points
 - ⊕ Mean expansion velocities vs. time
- ⊕ Study the Impact of Surface Tension Effects
 - ⊕ Movie of polymer melt shape
 - ⊕ Temperature contour snap shots
 - ⊕ Mean expansion velocities vs. time
 - ⊕ Momentum source terms due to surface tension effects
- ⊕ Summary and future work



Surface Tension CFD Mode – Surface Tension Forces

⊕ Surface Tension Forces (in the normal direction of the free surface)

⊕ Young-Laplace:

$$\Delta P = \gamma \left(\frac{1}{R_1} + \frac{1}{R_2} \right)$$

*ΔP is the pressure difference over the interface;
 R_1, R_2 are the principal radii of curvature of the surface;
 γ is the surface tension*

⊕ Implementation in CFD as a body force

$$\vec{F}_{vol} = -\Delta P \cdot A \cdot \hat{n} = -\gamma \cdot \kappa \cdot A \cdot \hat{n}$$

$$\kappa = \nabla \cdot \hat{n}; \quad \hat{n} = \frac{\vec{n}}{|\vec{n}|}$$

*κ is the curvature of the free surface;
 \vec{n} is the normal vector of the free surface
 A is the surface area*

⊕ Surface tension γ as a function of temperature (Thomas J. Ohlemiller 1/16/07 email)

$$\gamma = -0.040T + 29.10 \quad (165 - 220 \text{ }^\circ\text{C}) \quad \text{Eastman Epolene D-10 atactic PP}$$

⊕ Model only applies to cells forming the free surface



Surface Tension CFD Mode – Surface Tension Gradient

⊕ Surface Tension Gradient Effects (in the tangential direction of the free surface)

⊕ Shear stress at the surface resulting from the variation of surface tension*:

$$\mu \frac{\partial U}{\partial n} = \frac{d\gamma}{d\tau} \equiv \gamma_\tau$$

*μ is the viscosity;
 U is the tangential velocity component;
 n is the normal direction of the free surface
 τ is the tangential direction of the free surface*

⊕ Implementation in CFD as a momentum source

$$\vec{S} = \gamma_\tau \cdot \hat{\tau} = \gamma_x \vec{i} + \gamma_y \vec{j}$$

$$S_u = \gamma_x \cdot A$$

$$S_v = \gamma_y \cdot A$$

$$\hat{\tau} = \frac{\vec{\tau}}{|\vec{\tau}|}$$

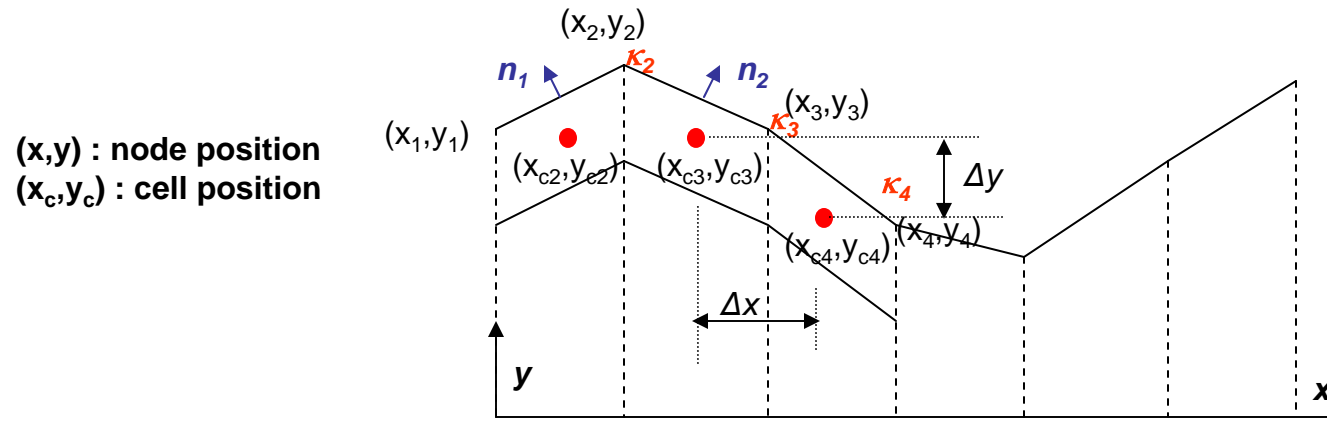
*S_u , S_v are the additional source terms in the u - and v -momentum equations, respectively ;
 $\vec{\tau}$ is the tangential vector of the free surface
 V is the cell volume*

⊕ Model only applies to cells forming the free surface

* W.A. Sirignano and I. Glassman, *Combustion Sci. and Tech.*, Vol. 1, pp307-312, 1970.



Surface Tension CFD Model – Calculate Surface Curvature - A



- ⊕ Calculate \mathbf{n}_1 the normal vector to line passing through (x_1, y_1) , (x_2, y_2) , and calculate \mathbf{n}_2 the normal vector to line passing through (x_2, y_2) , (x_3, y_3) . \mathbf{n} can be computed from τ
- ⊕ Then the curvature at node point (x_2, y_2) can be approximated as.

$$\begin{aligned} \kappa_2 &= \nabla \cdot \mathbf{n} = \frac{\partial n_x}{\partial x} + \frac{\partial n_y}{\partial y} = \frac{\Delta n_x}{\Delta x} + \frac{\Delta n_y}{\Delta y} \\ &= \frac{n_{x2} - n_{x1}}{\Delta x} + \frac{n_{y2} - n_{y1}}{\Delta y} \end{aligned}$$

- ⊕ Similarly, we can obtain the curvature at node point (x_3, y_3) , (x_4, y_4) If we want to get the curvature at a cell center, we may just simply take the average of curvature of nearby node points.



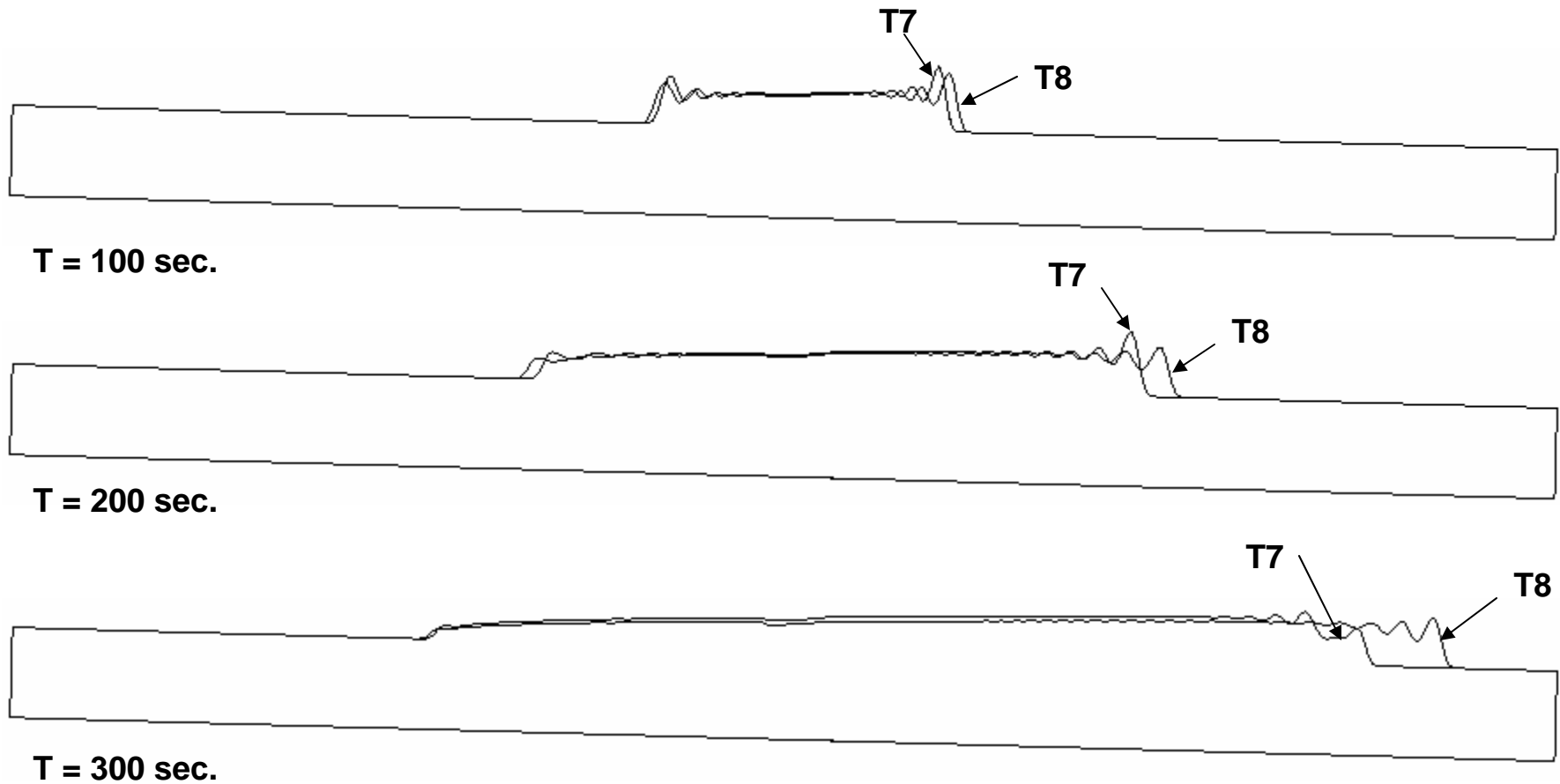
Case Summary

Cases	Boundary and Initial Conditions	Time Step	Surface Tension effect (normal direction)	Surface Tension effect (tangential direction)	Polymer
T7	Convective and radiative heat losses; Backside constant $T = 675\text{K}$; $\theta = 2.5^\circ$; $T = T_B - 6860.63 \cdot (y + 0.0127)$	$\Delta t_{\max} = 0.1$ CFL = 0.5	Not included	Not included	PP702N
T8	Same as T7	$\Delta t_{\max} = 0.02$ CFL = 0.5	Not included	Not included	PP702N
T9	Same as T7	$\Delta t_{\max} = 0.02$ CFL = 0.5	Included	Included	PP702N
T10	Same as T7	$\Delta t_{\max} = 0.02$ CFL = 0.5	Included	Not Included	PP702N
T11	Convective and radiative heat losses; Backside constant $T = 700\text{K}$; $\theta = 2.5^\circ$; $T = T_B - 7570.87 \cdot (y + 0.0127)$	$\Delta t_{\max} = 0.02$ CFL = 0.5	Not Included	Not Included	PP6523
T12	Same as T11	$\Delta t_{\max} = 0.02$ CFL = 0.5	Included	Included	PP6523

Cases	T7	T8	T9	T10	T11	T12
Time Period (second)	30 - 250	30 - 250	30 - 250	30 - 250	30 - 250	30 - 250
CPU time (hr)	8.5	16.5	21.0	21.0	16.0	46.0



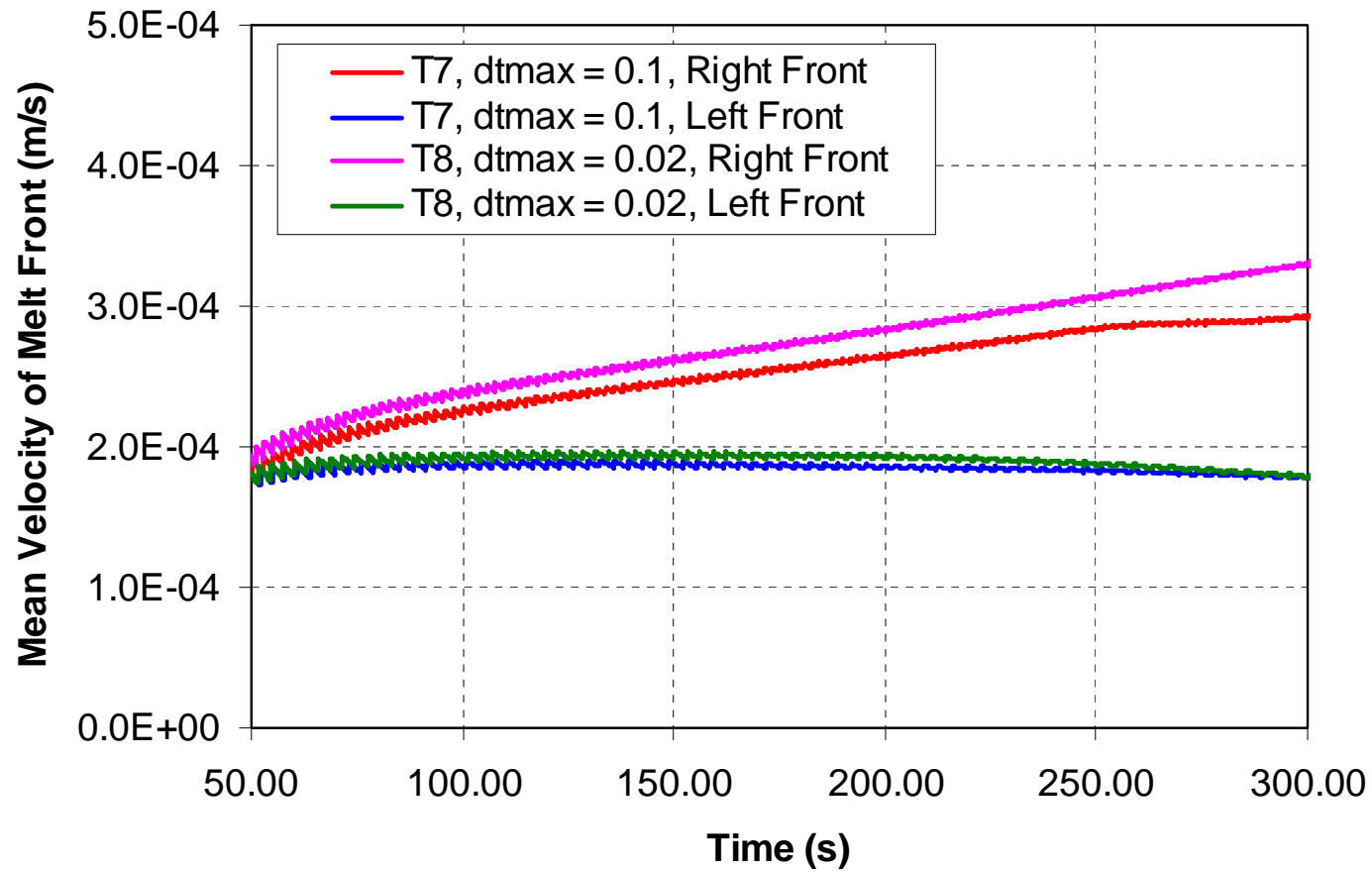
Case T7 vs T8: Impact of Time Step



CPU time (30 – 300 sec):
Case T7 – 8.5 hr
Case T8 – 19.5 hr



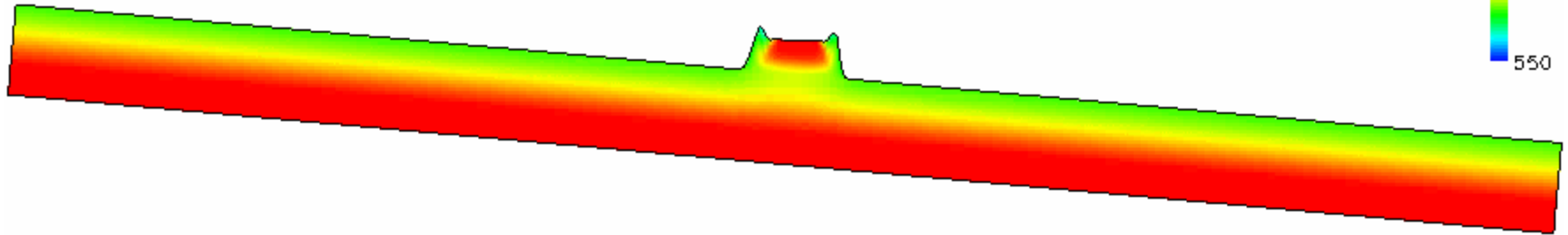
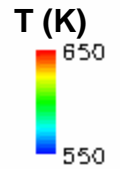
Case T7 vs T8: Impact of Time Step



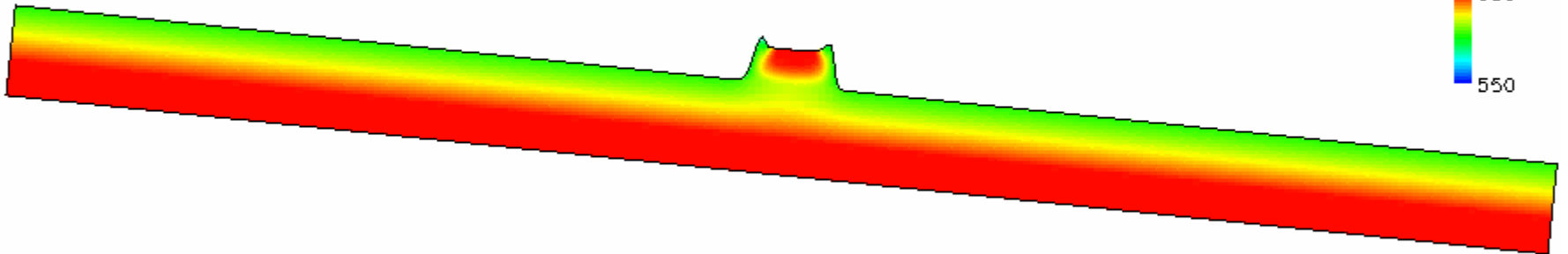
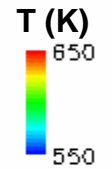
Case T8 vs T9: Impact of Surface Tension Effects

Case T8, 30 – 250 sec, CPU time = 16.5 hr

PP702N



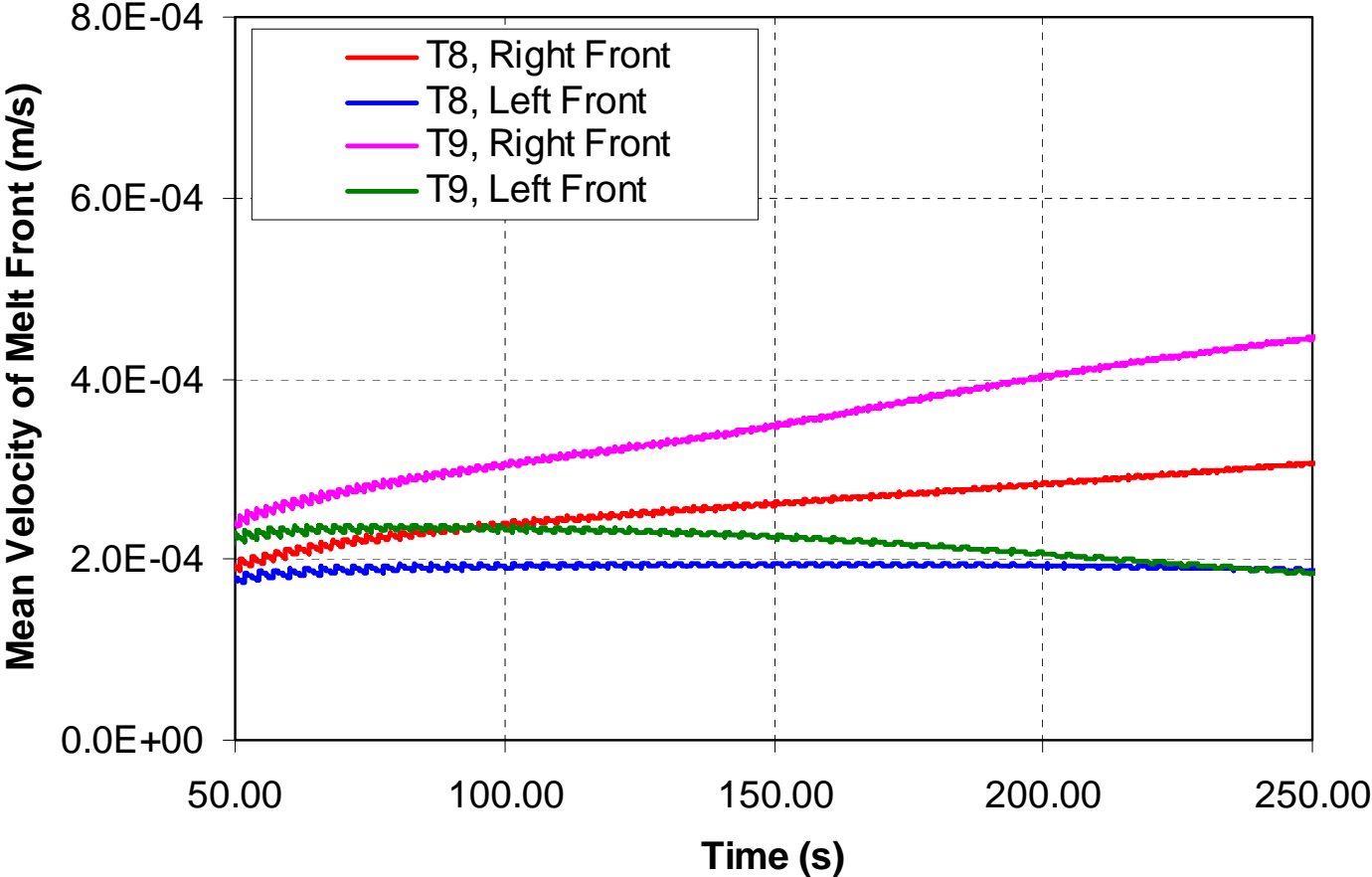
Case T9, 30 – 250 sec, CPU time = 21 hr



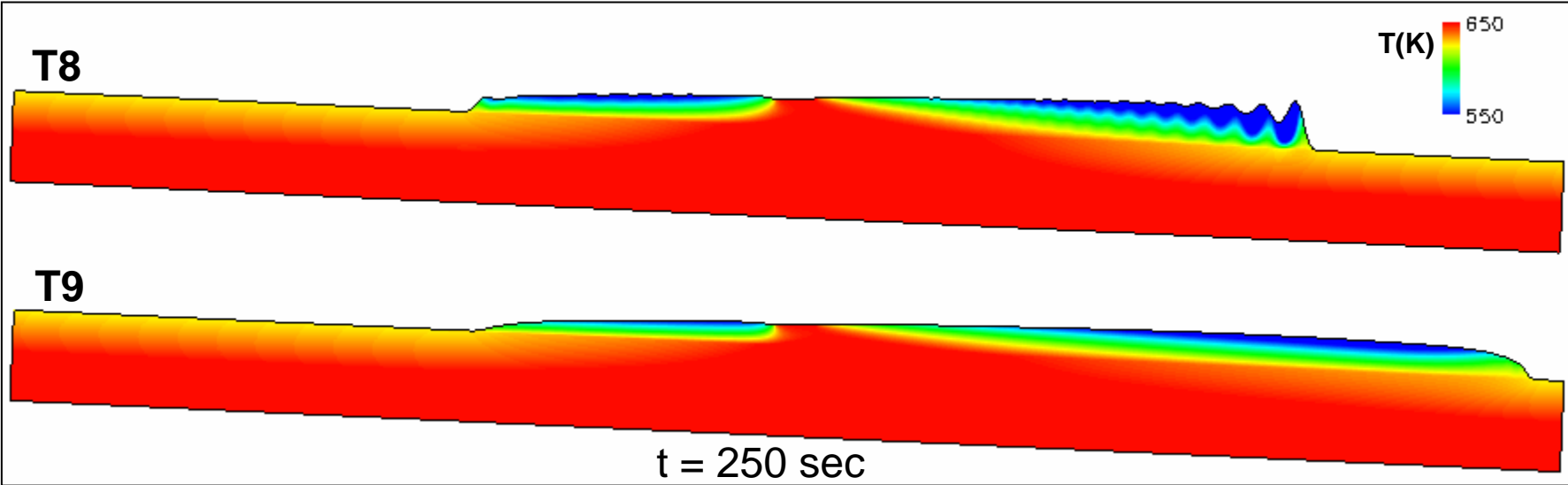
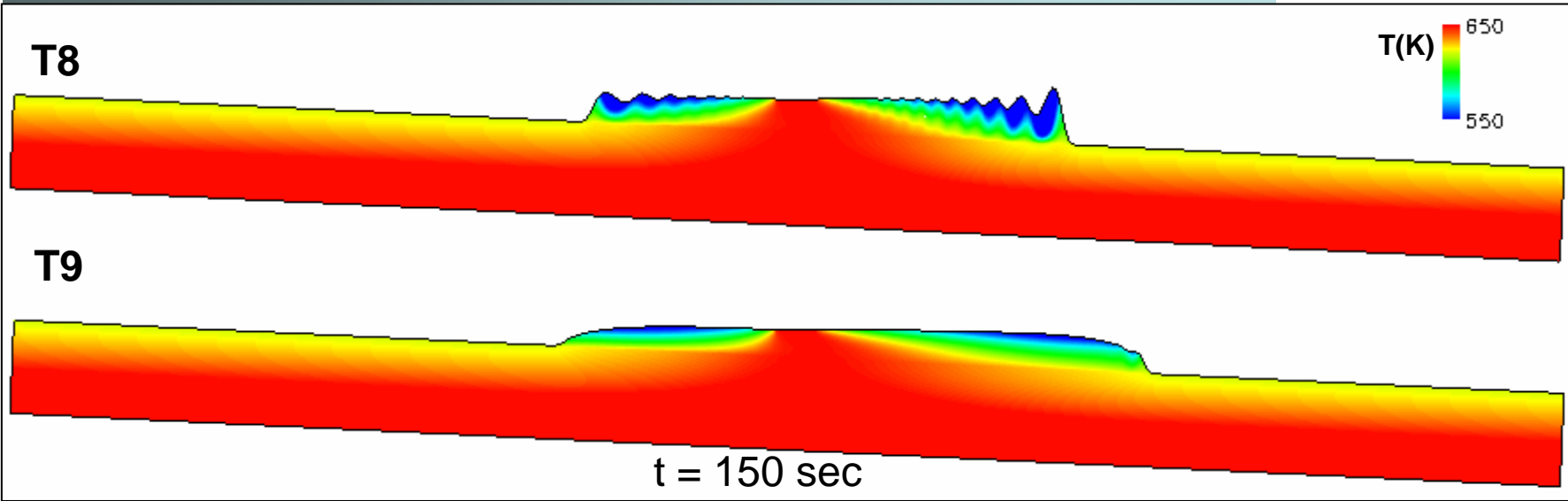
A handwritten mark or signature in the bottom right corner of the slide.

Case T8 vs T9: Impact of Surface Tension Effects

PP702N

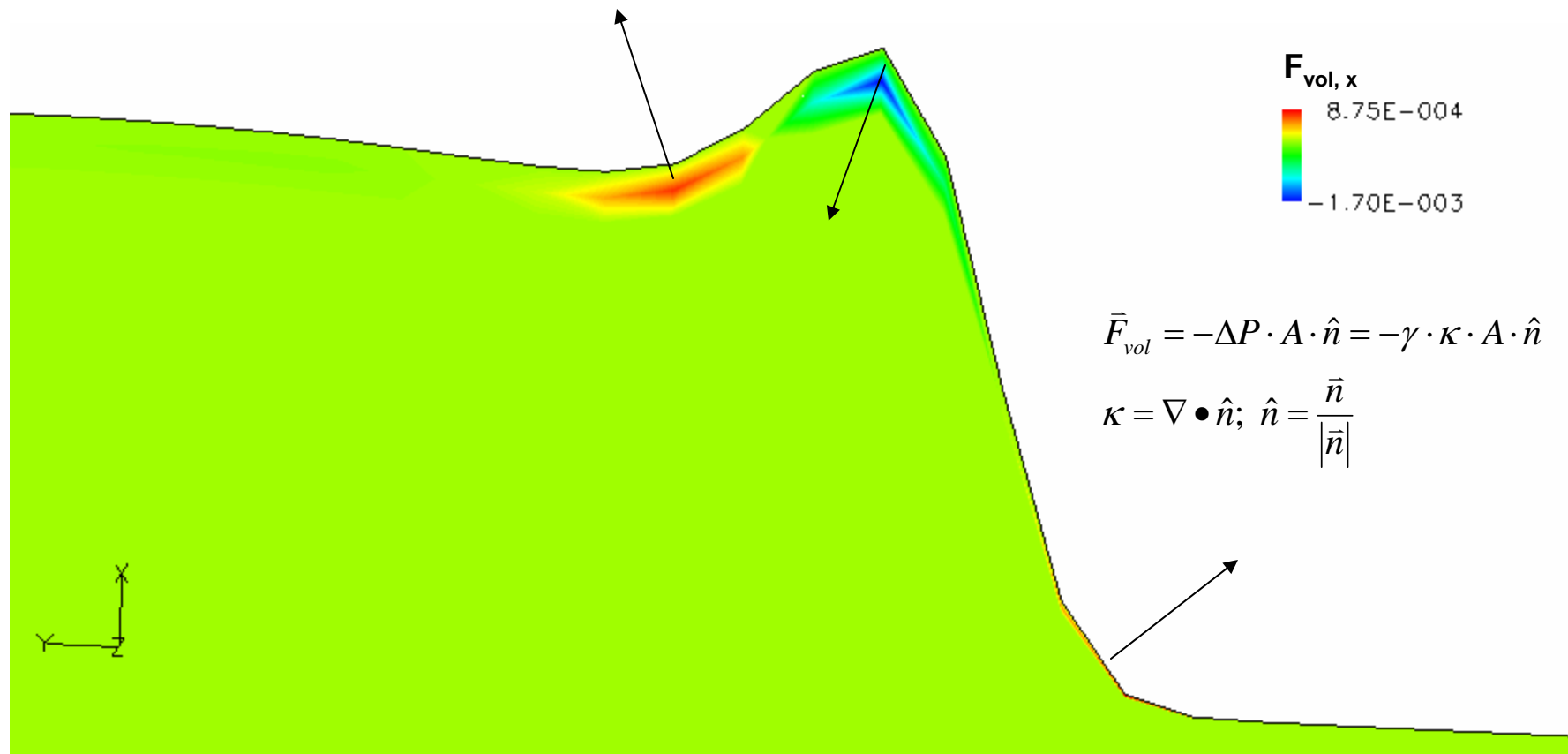


Case T8 vs T9: Snap Shots of Temperature Contour PP702N



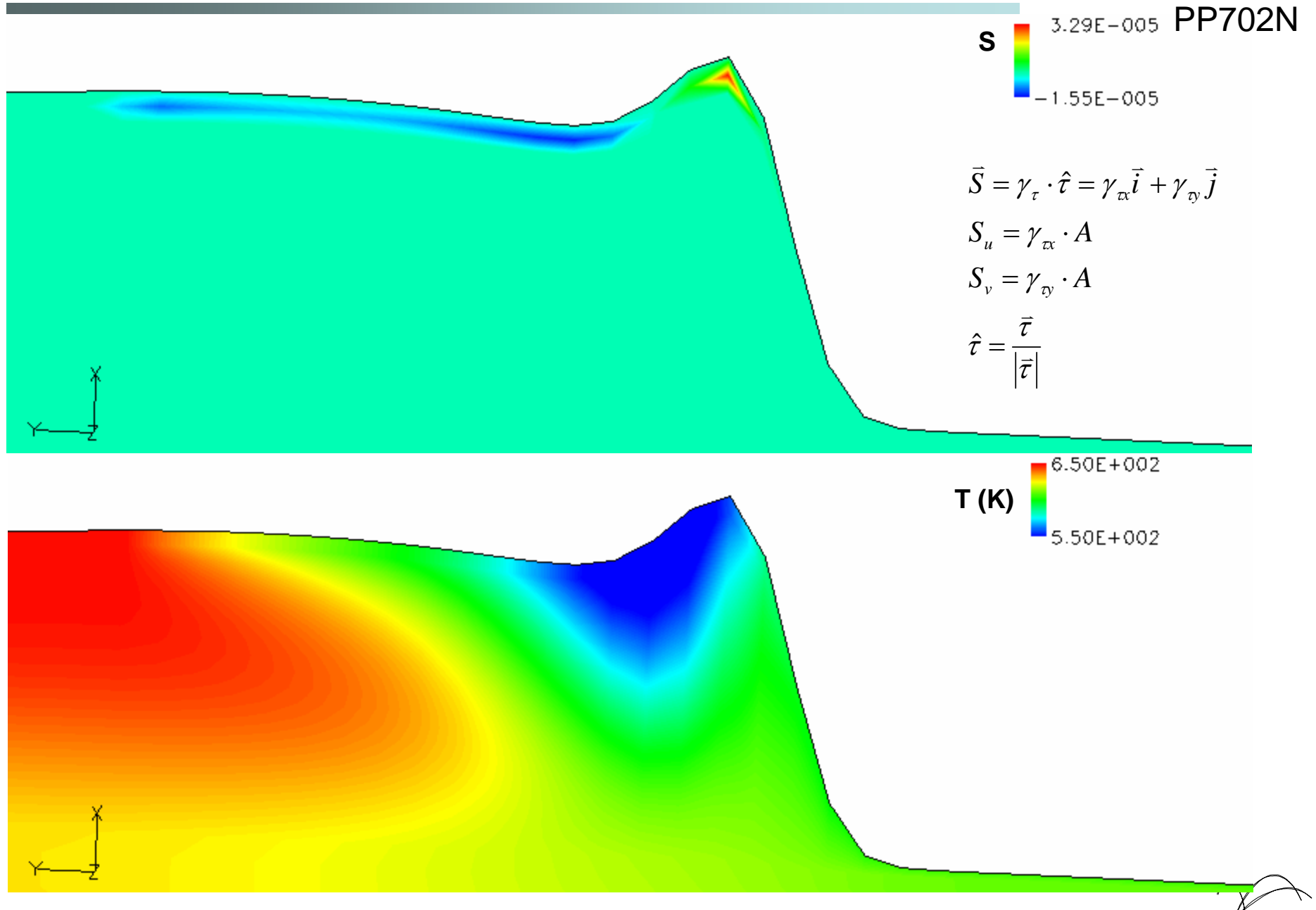
Case T9: Source Terms due to Surface Tension Force

PP702N



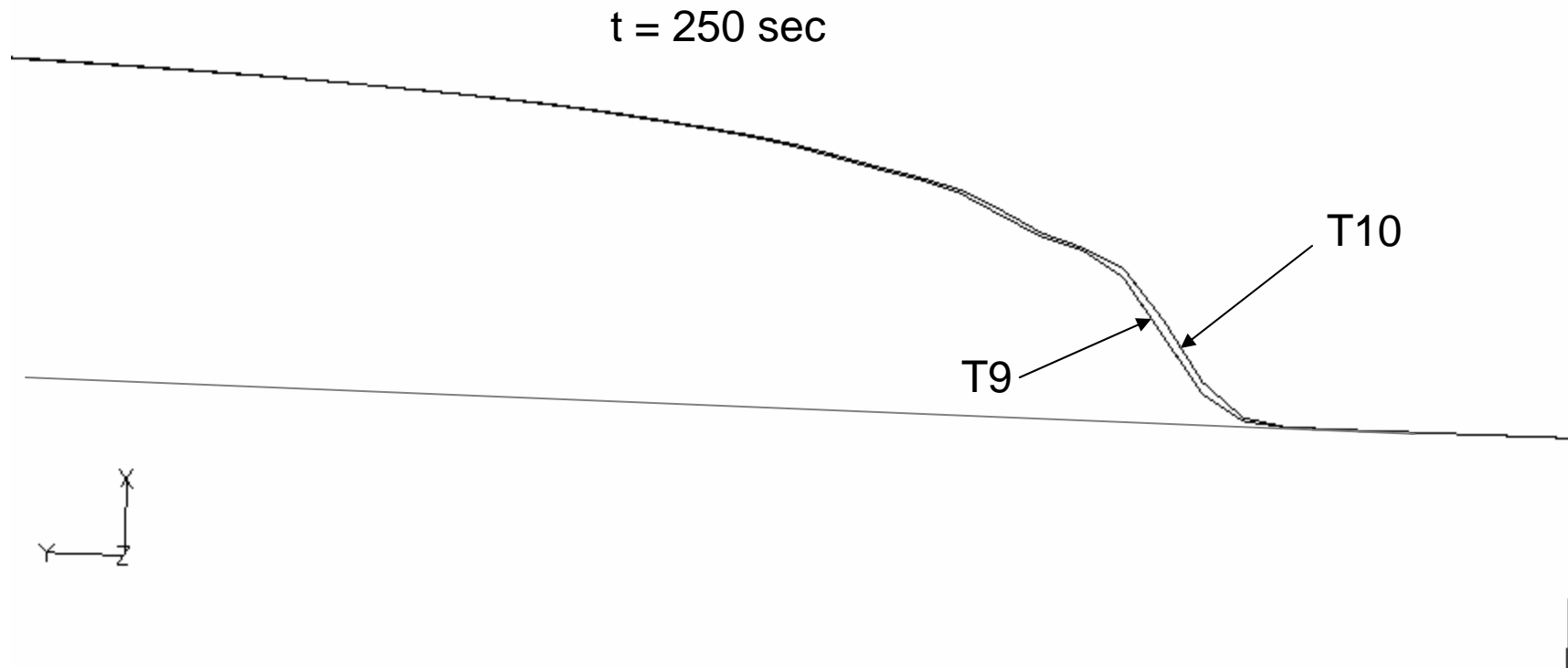
t = 50 sec

Case T9: Source Terms due to Surface Tension Gradient



Case T9 vs. T10: Effects of Surface Tension Gradient

PP702N

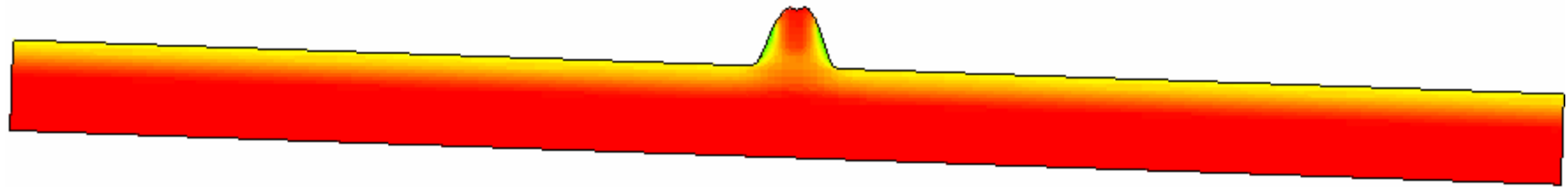


- ⊕ The magnitude of the surface tension gradient source terms are much smaller than that of the surface tension force source terms
- ⊕ The impact of neglecting the surface tension gradient effects is negligible under the simulated condition.

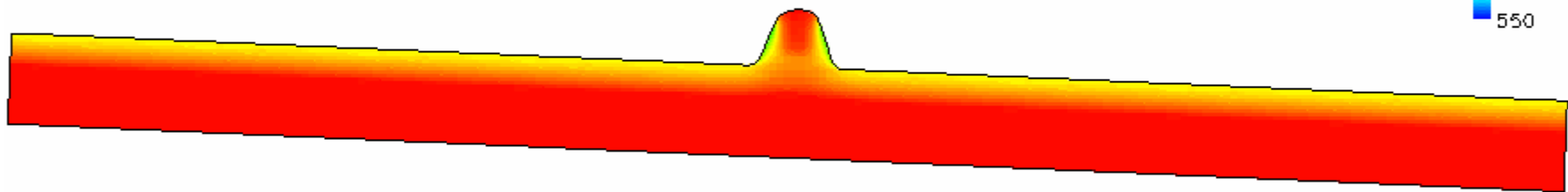
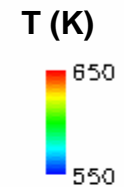
Case T11 vs T12: Impact of Surface Tension Effects

Case T11, 30 – 250 sec, CPU time = 16.0 hr

PP6523

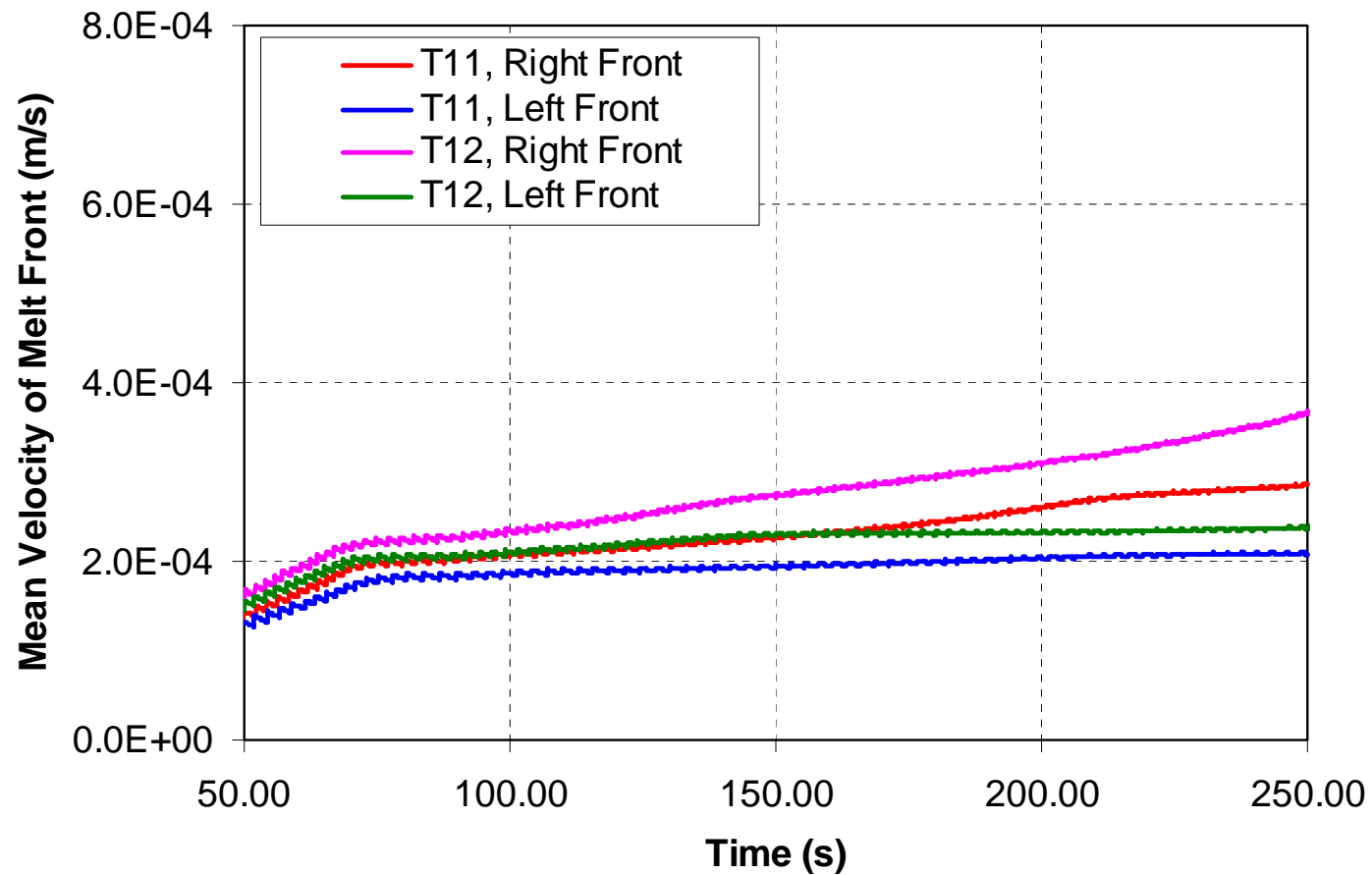


Case T12, 30 – 250 sec, CPU time = 40 hr



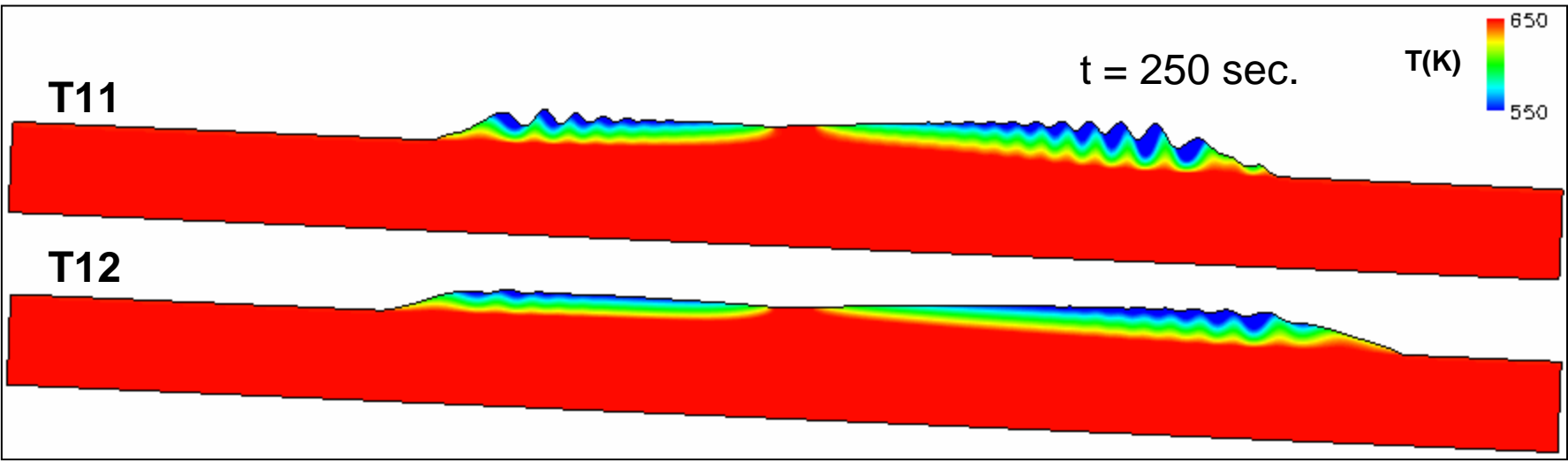
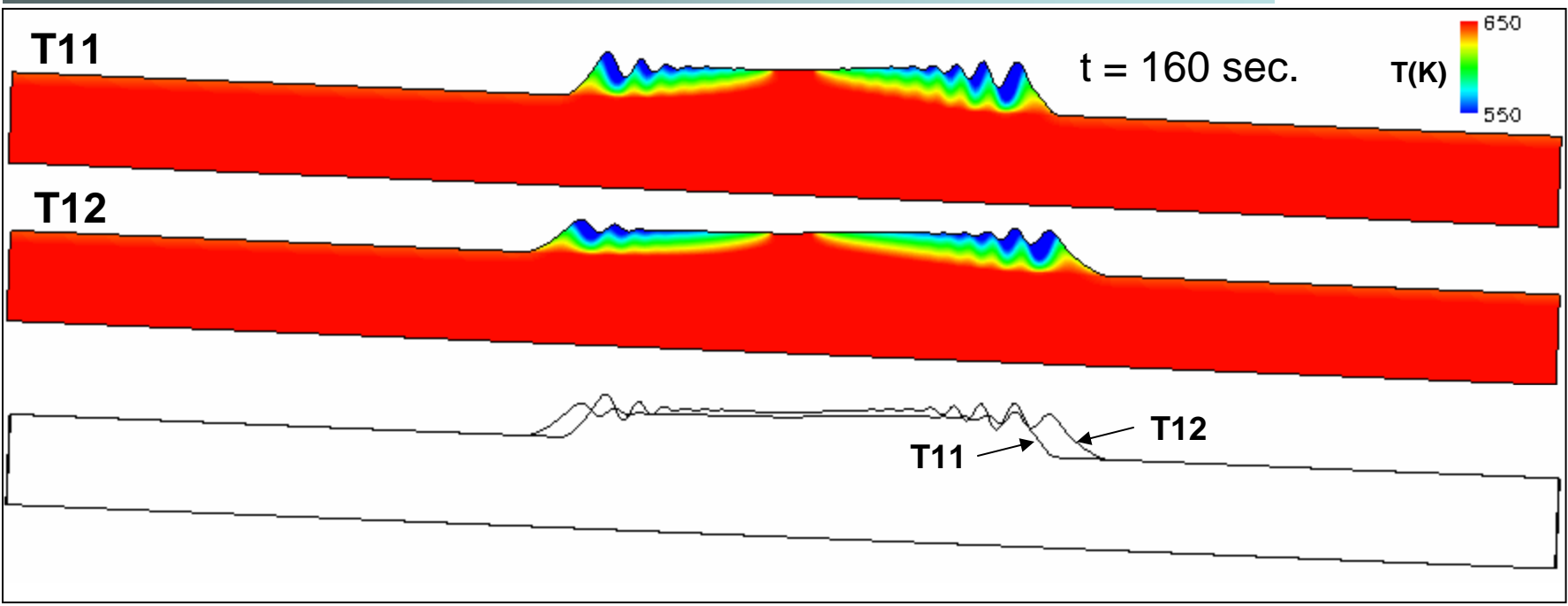
Case T11 vs T12: Impact of Surface Tension Effects

PP6523



Cases T11 & T12: PP6523 – Temperature Snap Shots

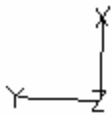
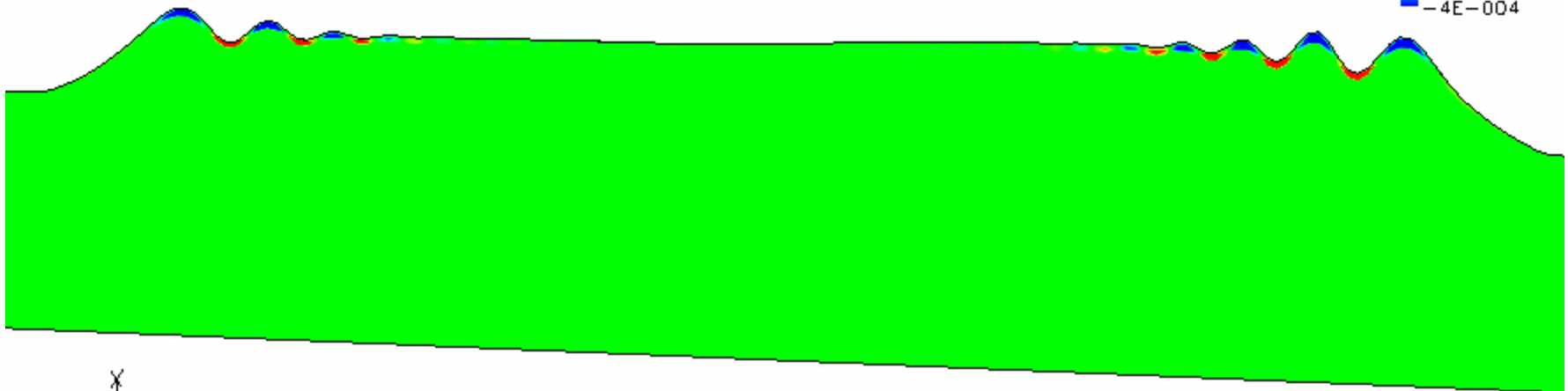
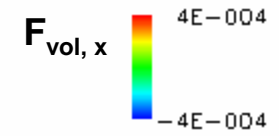
PP6523



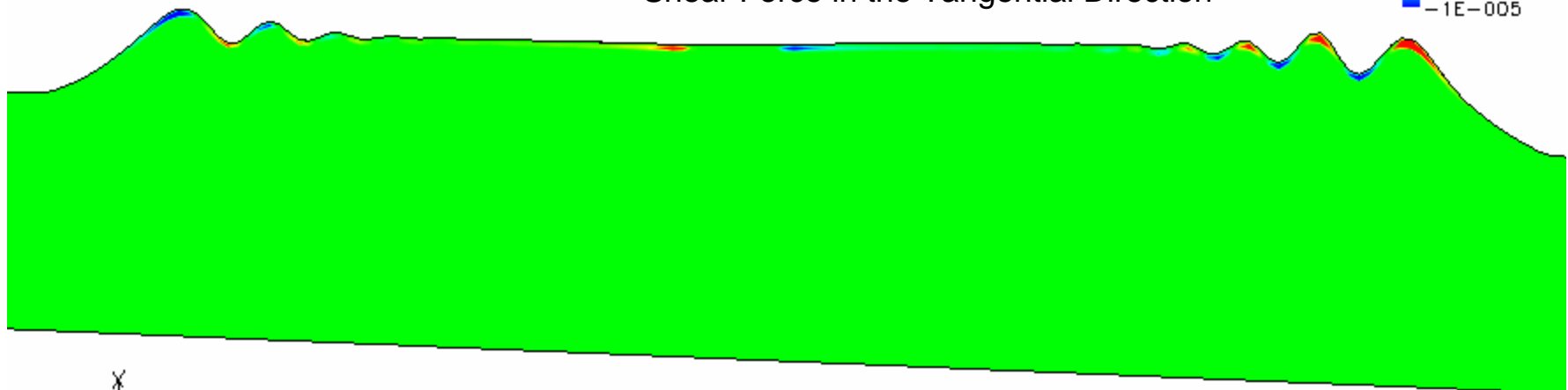
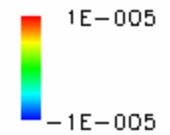
Case T12: PP6523N – Surface Tension Source Terms PP6523

t = 160 sec.

Force in the Normal Direction

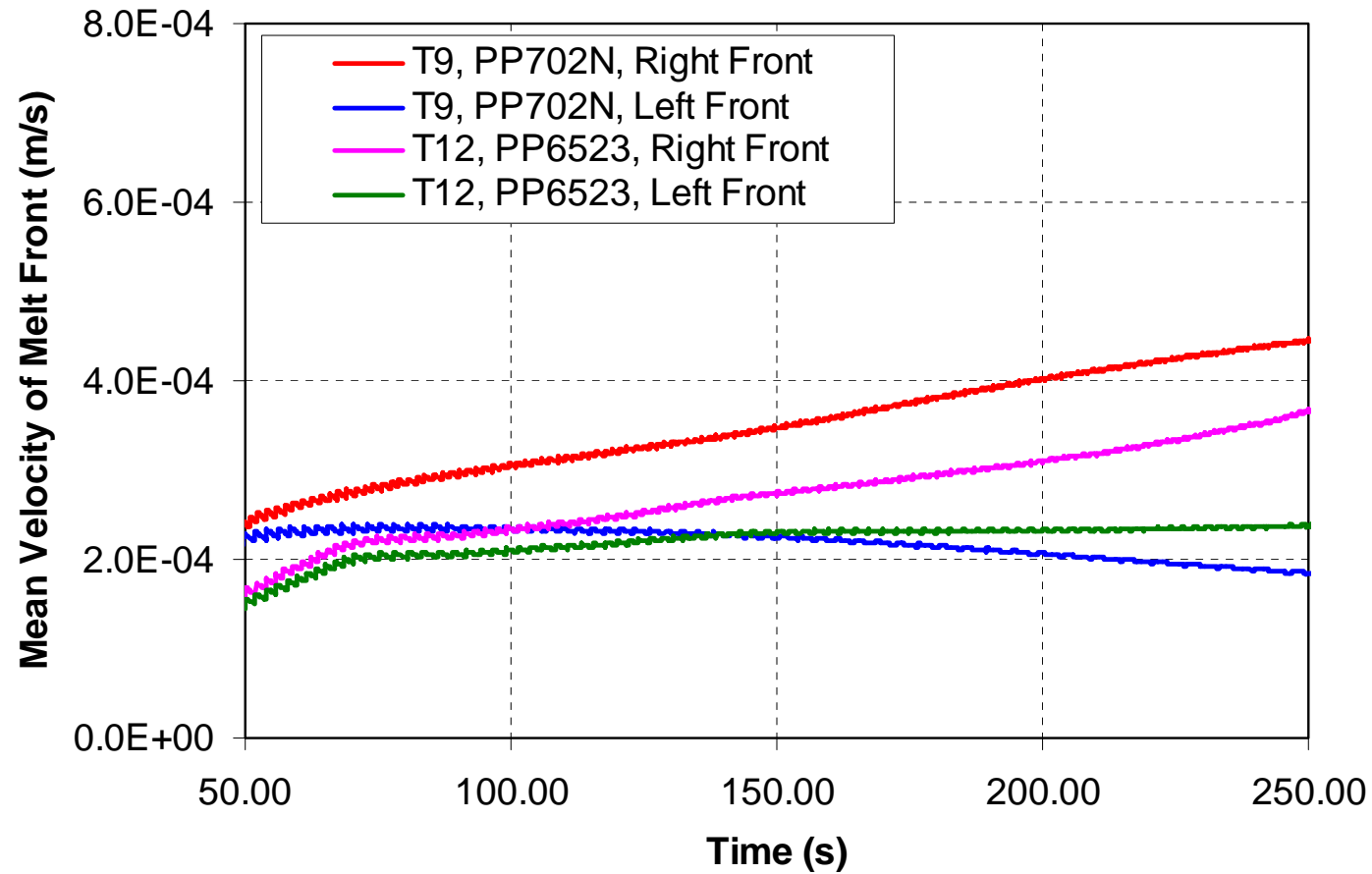


Shear Force in the Tangential Direction



A handwritten mark or signature in the bottom right corner of the page.

Case T9 vs T12: Expansion Rates Comparison

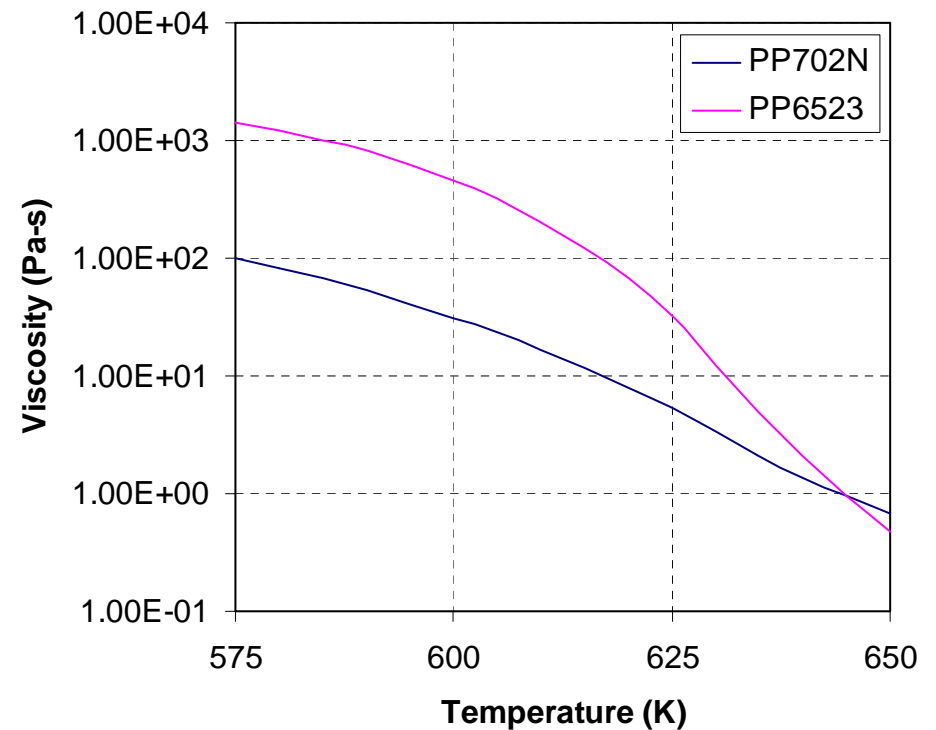
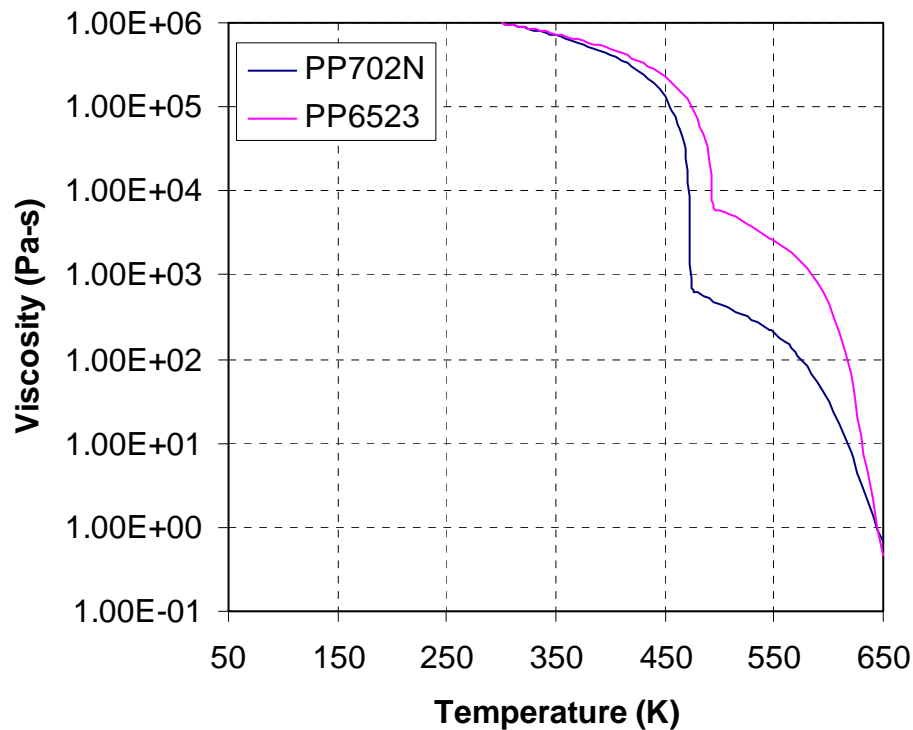


Summary

- ⊕ Surface tension model has been implemented into CPCFD
- ⊕ A parametric study on time step size has been performed
 - ⊕ reducing maximum time step size from 0.1s to 0.02s increases the mean expansion velocity by 2% at 50 s and by 10% at 300 s.
 - ⊕ reducing maximum time step size from 0.1s to 0.02s doubles the run-time
- ⊕ The inclusion of surface tension effects
 - ⊕ makes the free surface much smoother
 - ⊕ increases the expansion velocities (moving downward) by 30% for PP702N and by 20% for PP6523 at the end of the calculations (i.e., $t = 250$ sec)
- ⊕ The melt front (moving downward) of PP6523 moves faster than PP702N under the simulated conditions
- ⊕ The surface tension gradient effect owing to surface temperature variation is negligible comparing to the surface tension force in the normal direction of the free surface under the simulated condition.



Viscosity vs. Temperature



- ⊕ Free surface temperature varies in the range of 575 K to 650 K,
- ⊕ Viscosity of PP6523 is much larger (by one order of magnitude) than that of PP702N from 575 K to about 645 K
- ⊕ For temperature greater than 645 K, viscosity of PP6523 becomes smaller than that of PP702N

Future Work

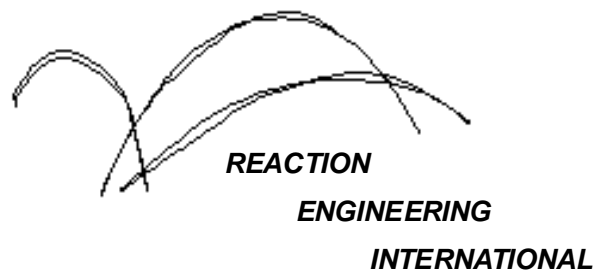
- ⊕ Parametric study of grid resolution
- ⊕ Combined simulations of the vertical resin and the catch basin for both PP702N and PP6523
- ⊕ Simulation of gasification process without flow?
- ⊕ Finalize source code and documentation
- ⊕ Final report



A Computational Model For Fire Growth and Spread On Thermoplastic Objects

Task 4: Include Melt Pool on Catch Surface

(06/27/07)



Outline

- ⊕ Time Step Sensitivity Study
 - ⊕ Snap shots of free surface shape at certain time points
 - ⊕ Mean expansion velocities vs. time
- ⊕ Grid Sensitivity Study
 - ⊕ Snap shots of free surface shape at certain time points
 - ⊕ Mean expansion velocities vs. time
- ⊕ Summary and future work



Case Summary

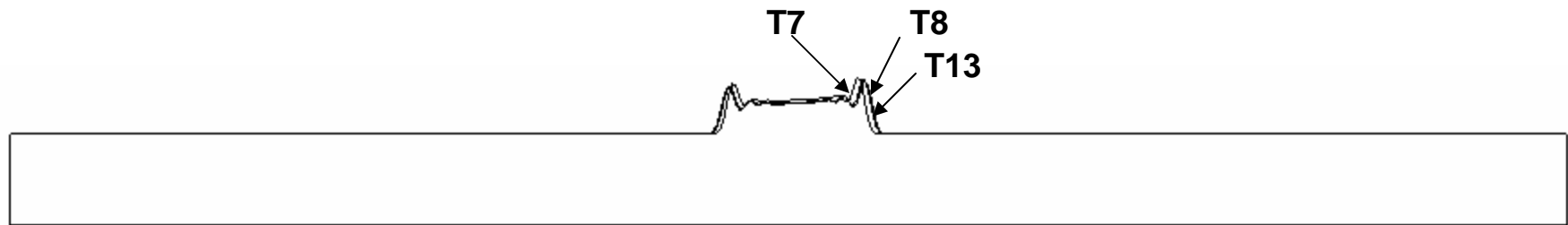
Cases	Time Step	Grid	CPU time (hr)*	Surface Tension effect
T7	$\Delta t_{\max} = 0.1$; CFL = 0.5	400X30	8.5	Not included
T18	$\Delta t_{\max} = 0.045$; CFL = 0.5	400X30	15.0	Not included
T8	$\Delta t_{\max} = 0.02$; CFL = 0.5	400X30	15.0	Not included
T13	$\Delta t_{\max} = 0.01$; CFL = 0.5	400X30	34.0	Not Included
T19	$\Delta t_{\max} = 0.02$; CFL = 0.5	533X30	15.0	Not Included
T14	$\Delta t_{\max} = 0.02$; CFL = 0.5	600X30	17.0	Not Included
T15	$\Delta t_{\max} = 0.02$; CFL = 0.5	800X30	21.0	Not Included
T9	$\Delta t_{\max} = 0.02$; CFL = 0.5	400X30	21.0	Included
T16	$\Delta t_{\max} = 0.02$; CFL = 0.5	600X30	36.0	Included
T17	$\Delta t_{\max} = 0.02$; CFL = 0.5	800X30	48.0	Included

* estimated, physical time period from 30 s to 250 s

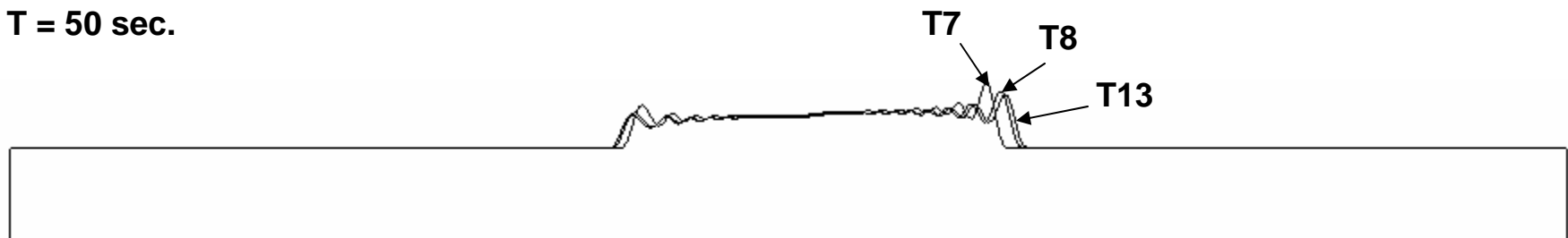
** all calculations are for PP702N



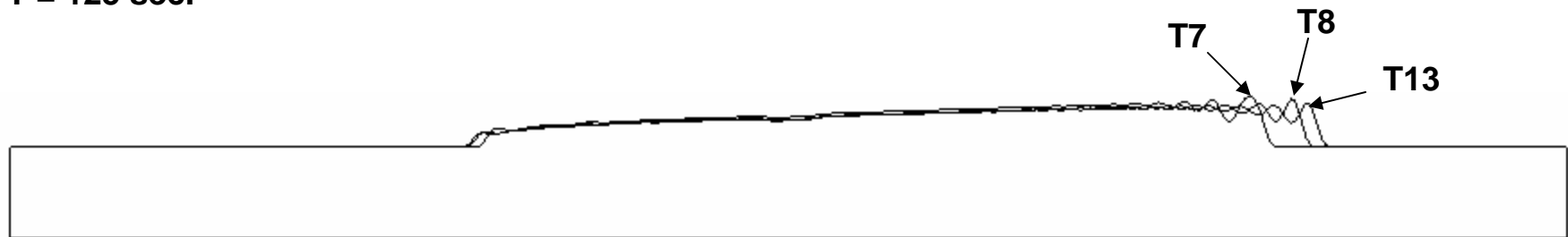
Impact of Time Step on Free Surface Shape



T = 50 sec.



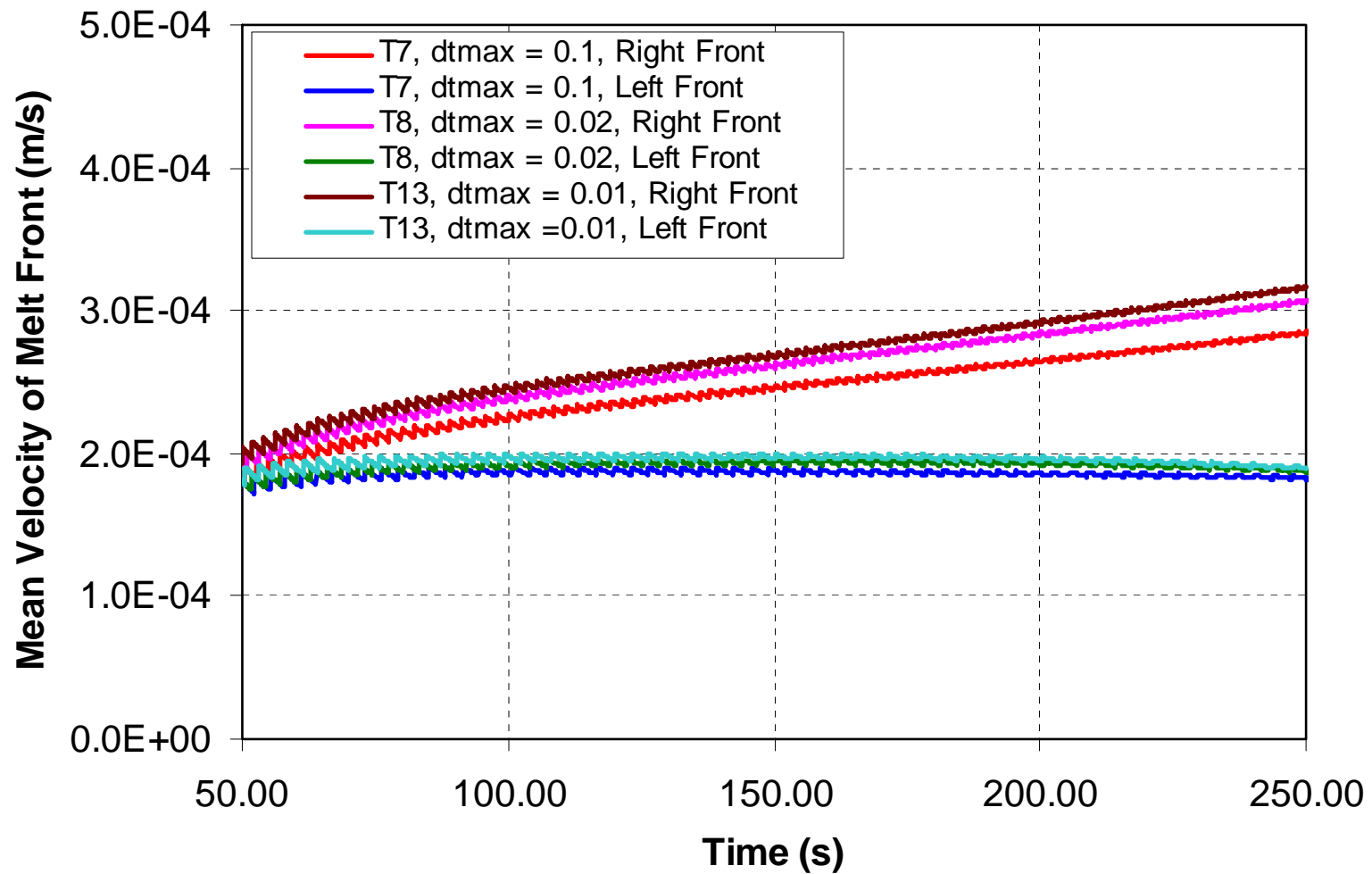
T = 125 sec.



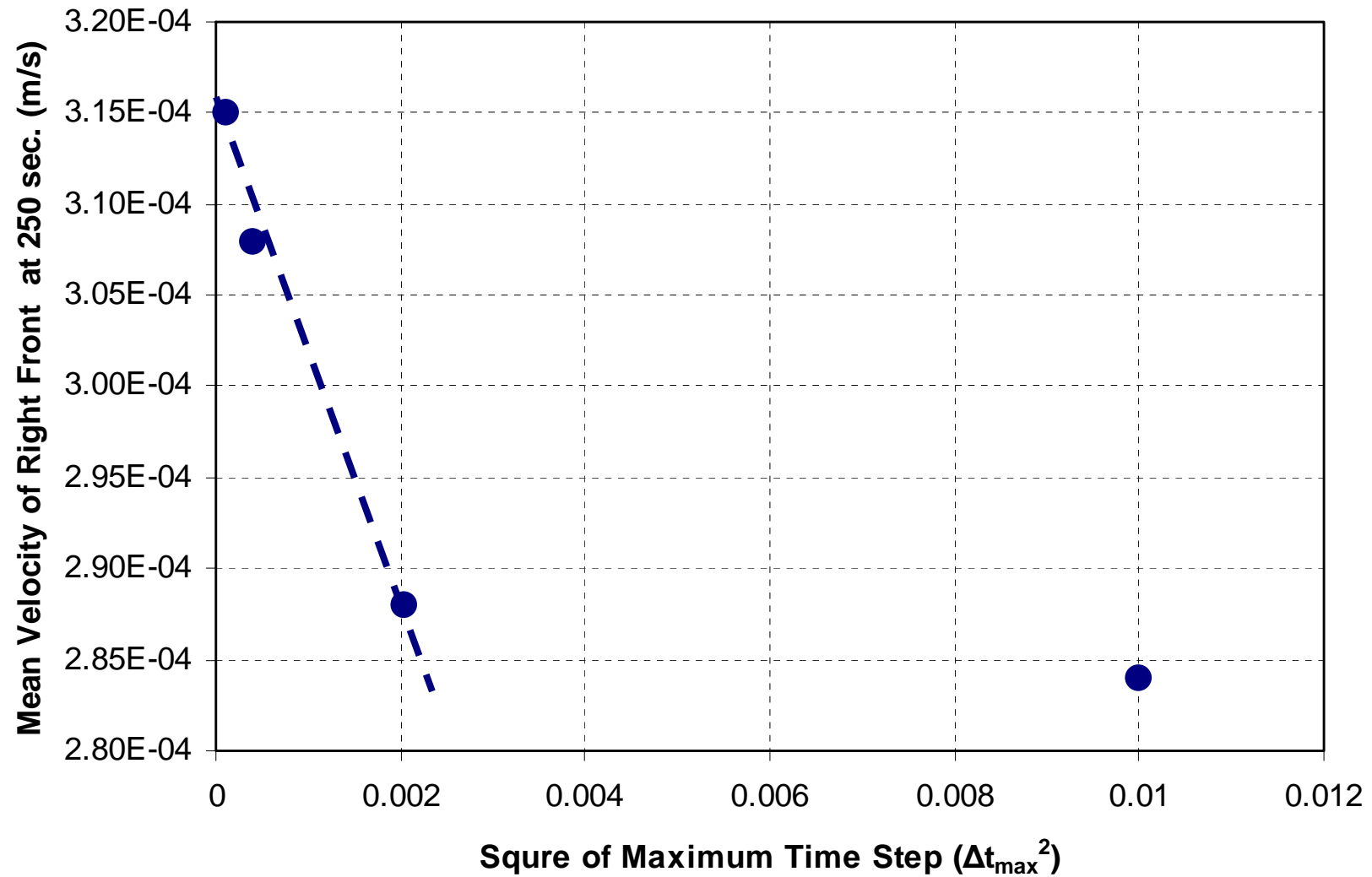
T = 250 sec.



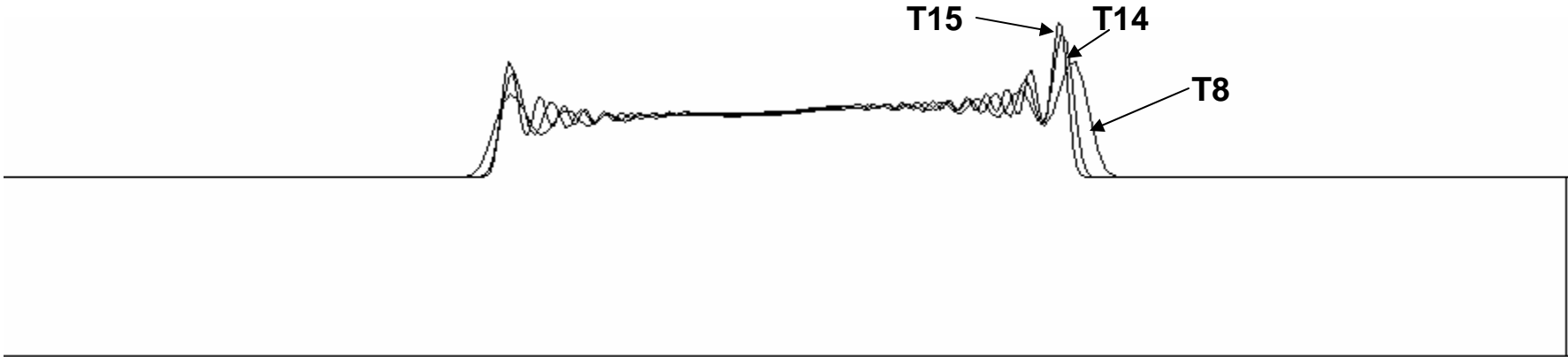
Impact of Time Step on Spreading Velocity



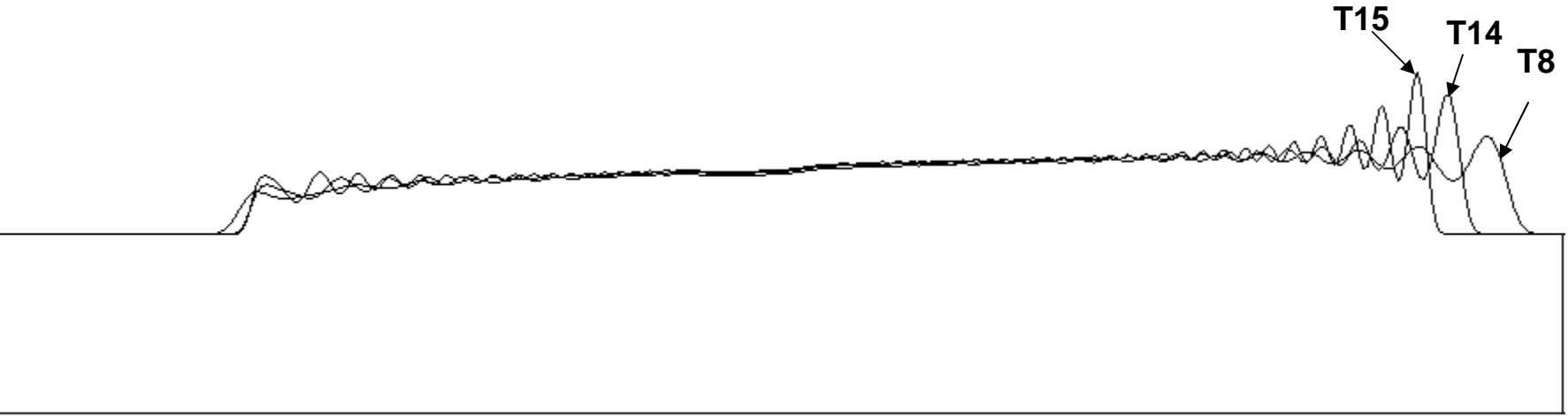
Impact of Time Step on Spreading Velocity



Impact of Grid Size on Free Surface Shape



T = 100 sec.



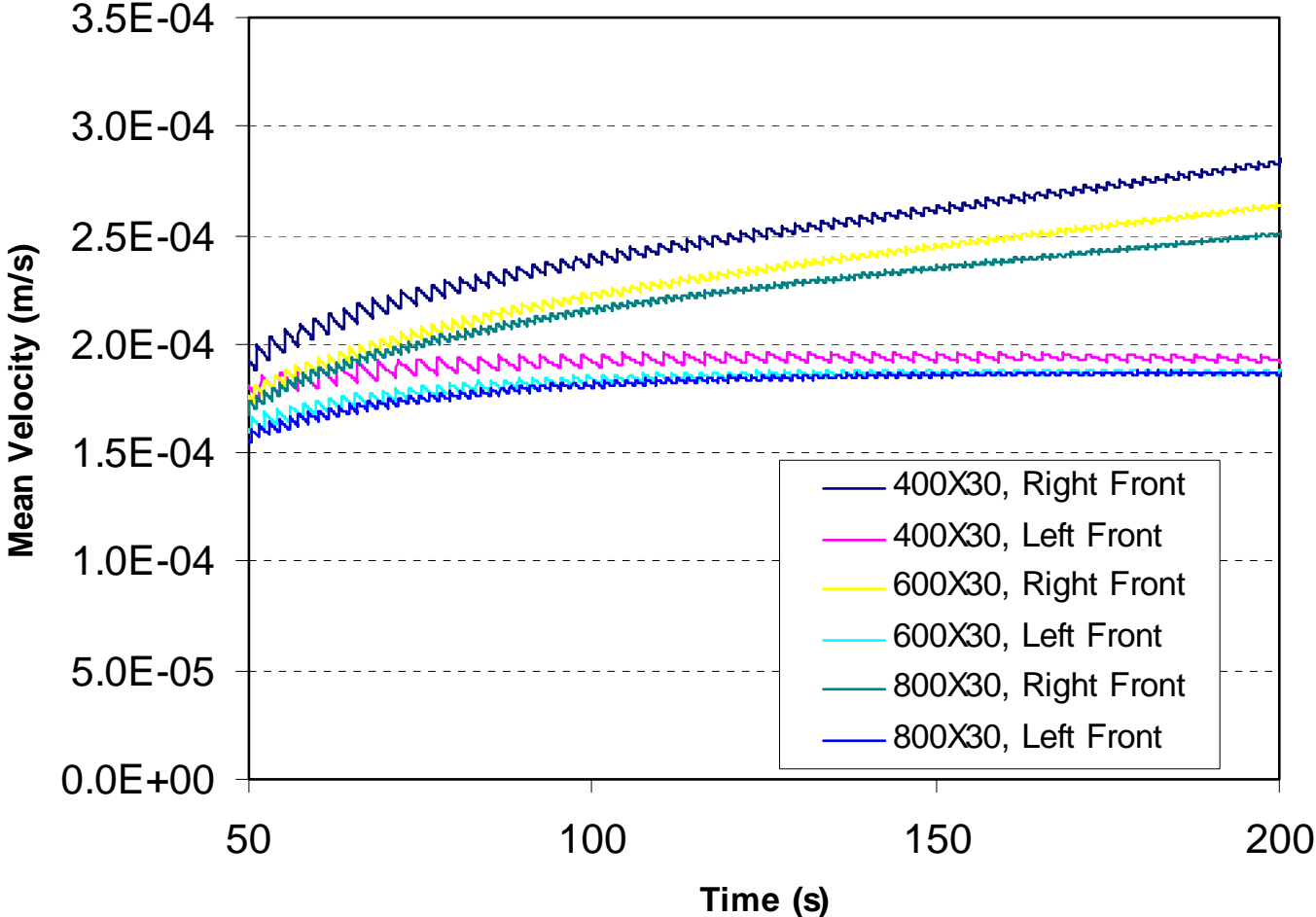
T = 200 sec.

Surface Tension Effects not included

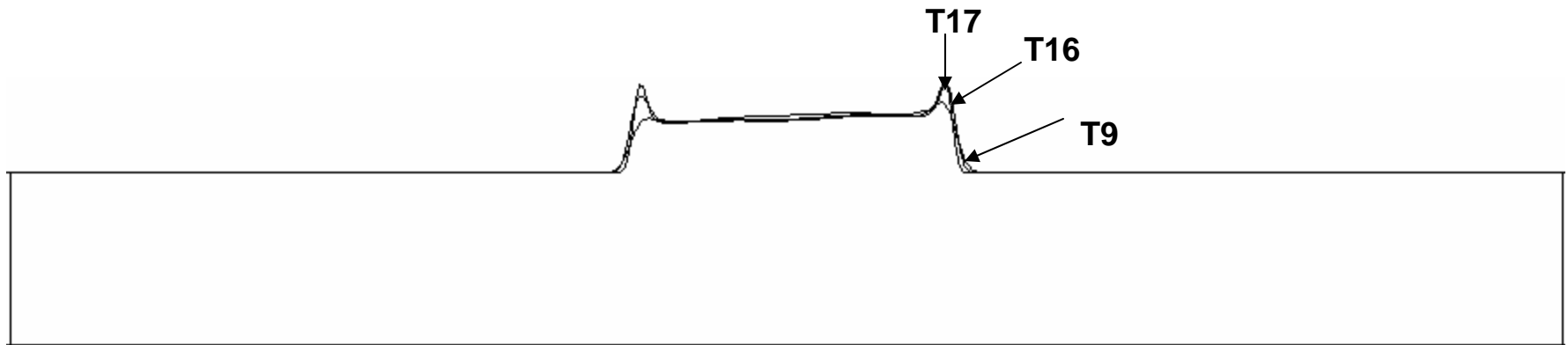


Impact of Grid Size on Spreading Velocity

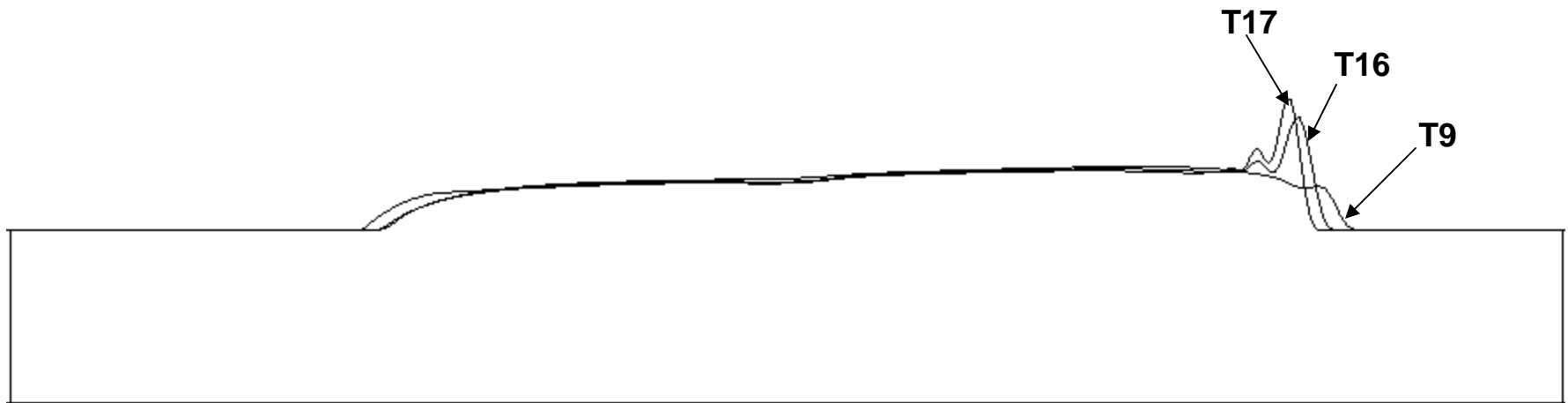
Surface Tension Effects not included



Impact of Grid Size on Free Surface Shape



$T = 50$ sec.



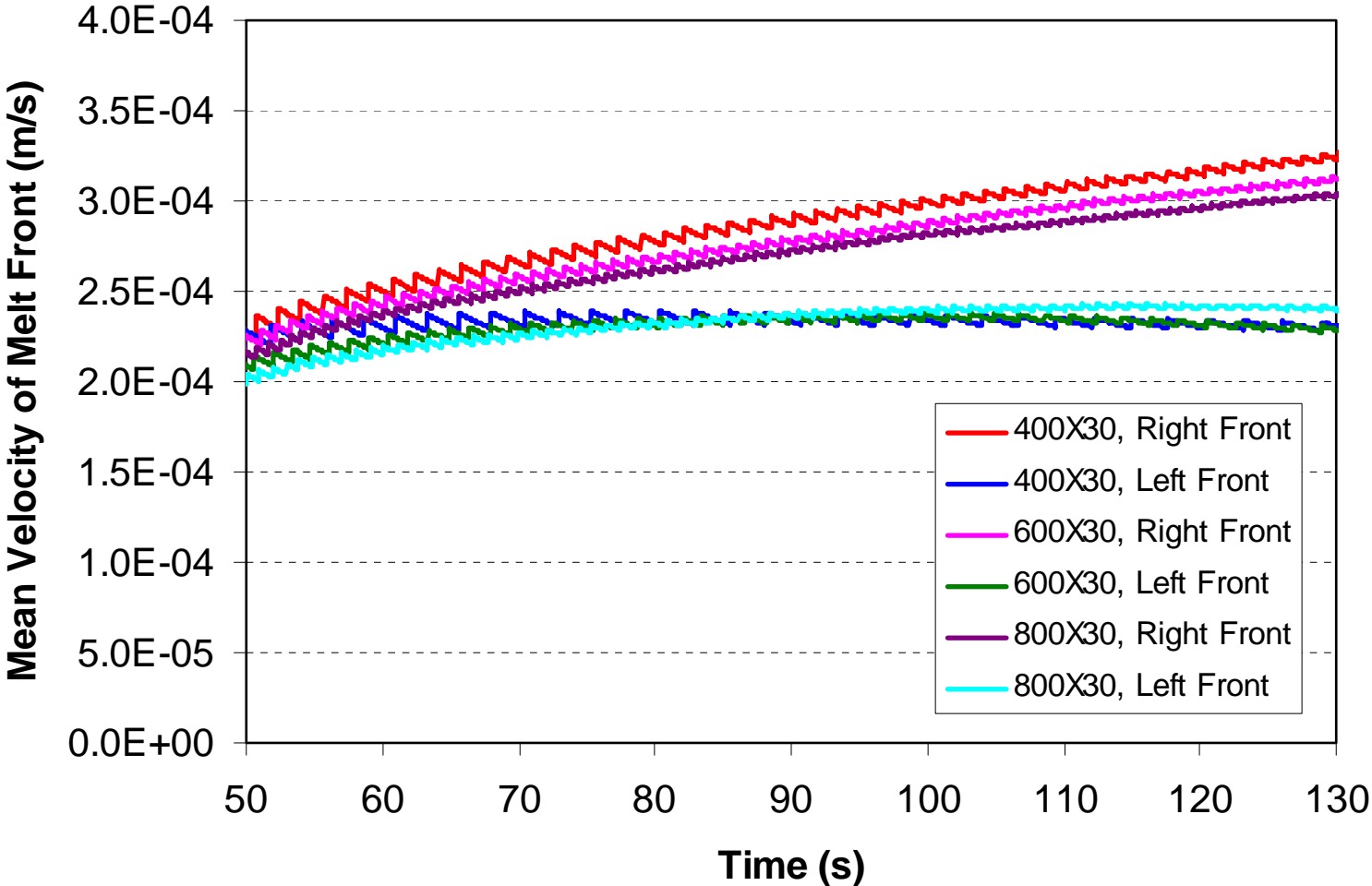
$T = 130$ sec.

Surface Tension Effects included

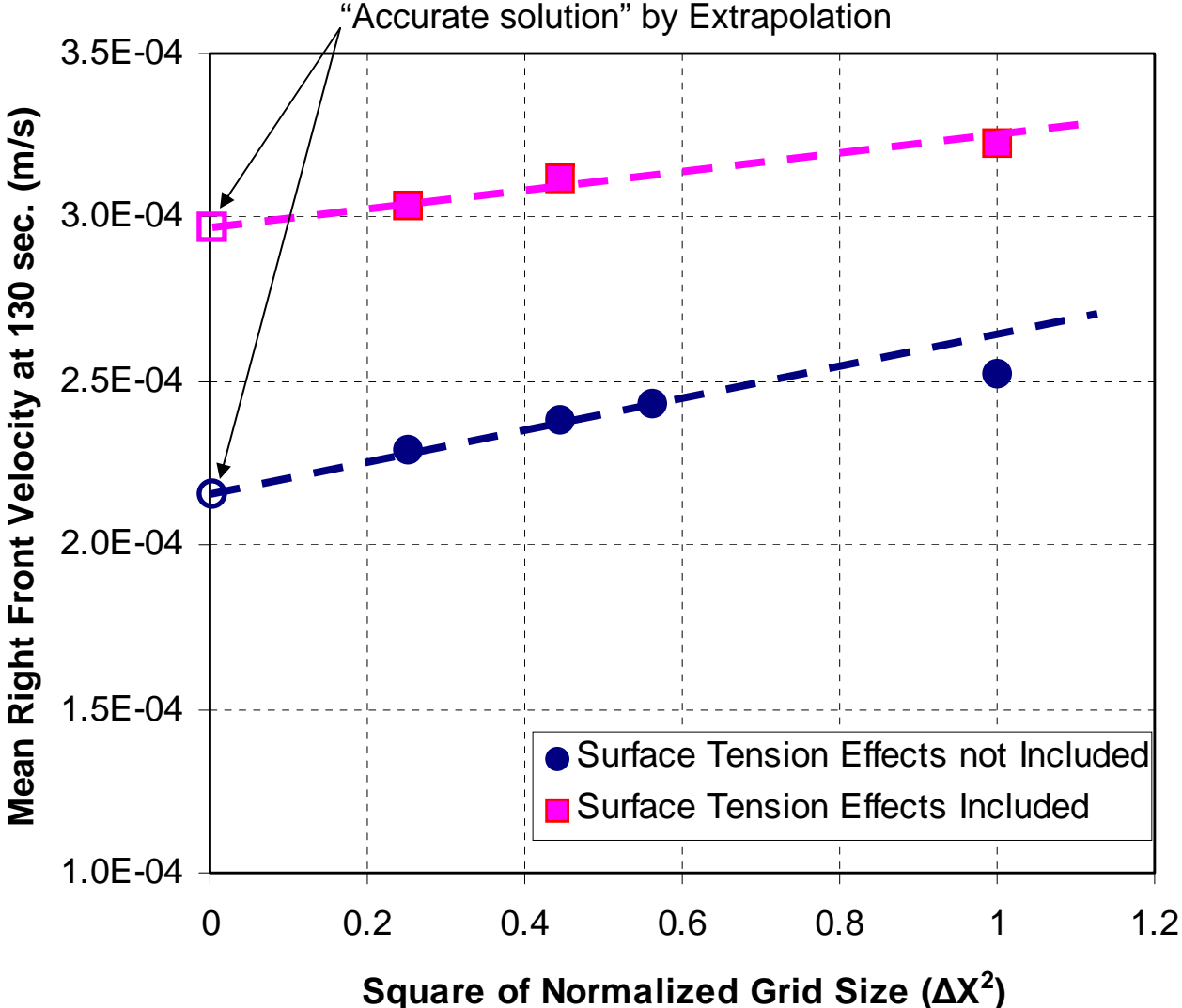


Impact of Grid Size on Spreading Velocity

Surface Tension Effects included



Impact of Grid Size on Spreading Velocity



Summary

- ⊕ A parametric study on time step size has been performed
 - ⊕ reducing maximum time step size increases the mean expansion velocity
 - ⊕ reducing maximum time step size from 0.1s to 0.02s doubles the run-time

- ⊕ A grid sensitivity study has been performed
 - ⊕ Fluctuations of free surface become stronger as grid size decreases
 - ⊕ The inclusion of surface tension effects suppresses the fluctuations
 - ⊕ The inclusion of surface tension effects leads to smaller differences among front moving velocities using different grids



Future Work

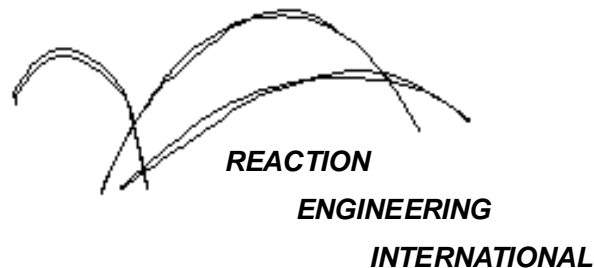
- ⊕ Combined simulations of the vertical resin and the catch basin for both PP702N and PP6523
- ⊕ Simulation of gasification process without flow?
- ⊕ Finalize source code and documentation
- ⊕ Final report



A Computational Model For Fire Growth and Spread On Thermoplastic Objects

Task 4: Include Melt Pool on Catch Surface

(07/20/07)



Outline

- ⊕ Task 4A – model PP702
 - ⊕ Time dependent melt flow rate obtained from Task3 (Case 3R, see 12/05/06 report)
 - ⊕ Catch plate tilt angle = 2.5°
- Task 4B – model PP6523
 - Time dependent melt flow rate obtained from Task3 (Case 3I, see 09/26/06 report)
 - Catch plate tilt angle = 2.5°
- Task 4C – model PP702 with a different tilt angle
 - Melt flow rate the same as Task 4A
 - Catch plate tilt angle = 0.0°
- Summary and future work



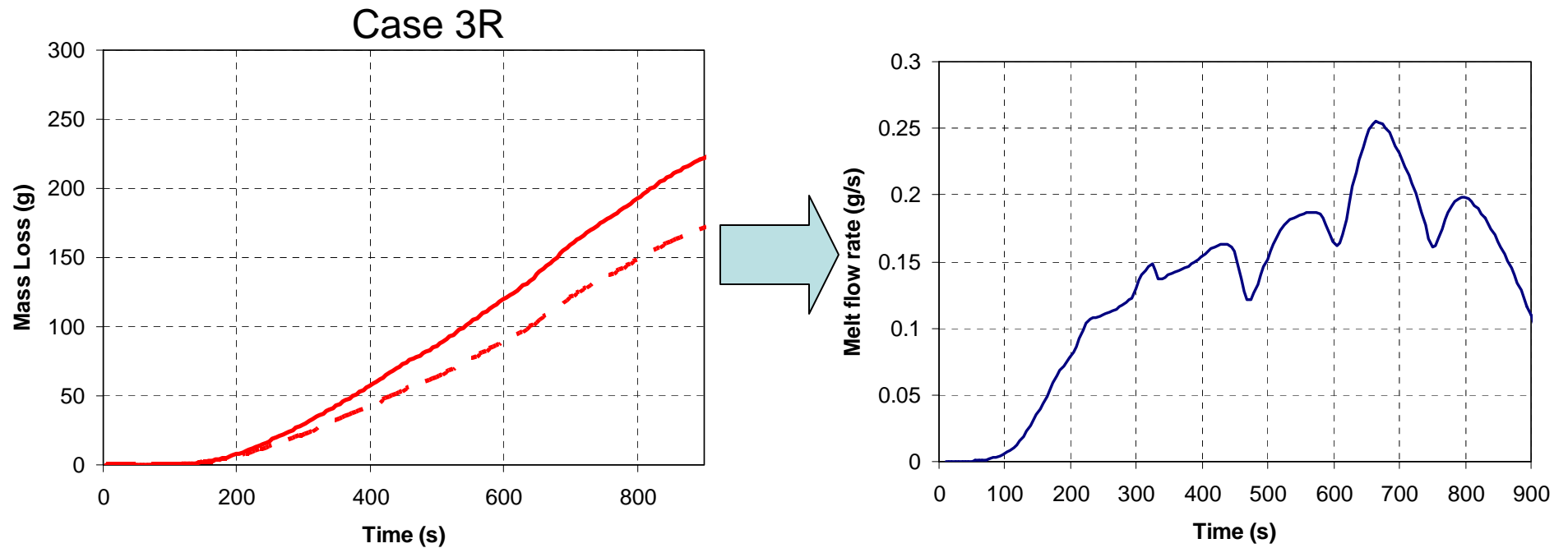
Case Summary

Case	Polymer	Melt flow rate	Time step	Grid	Tile angle
4A	PP702N	From Case 3R	0.02 s	400X30	2.5°
4B	PP6523	From Case 3I	0.02 s	400X30	2.5°
4C	PP702N	From Case 3R	0.01 s	400X30	0.0°

* Surface tension model included in all simulations



Task 4A – Melt flow rate



Mass loss history

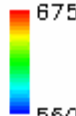
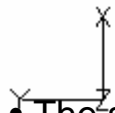
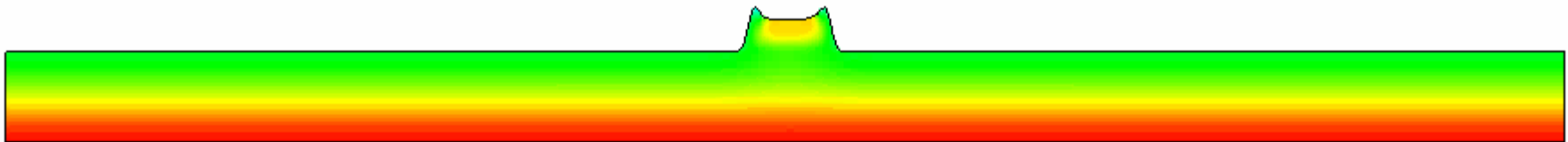
- solid line = total mass loss
- dashed line = mass loss occurring as melt flow
- difference between solid and dashed line = mass loss due to gasification

Melt flow rate calculated as the first derivative of the dashed line

Task 4A – Melt flow on catch plate

Physical time period: 200 sec – 460 sec
CPU time: 19 hrs

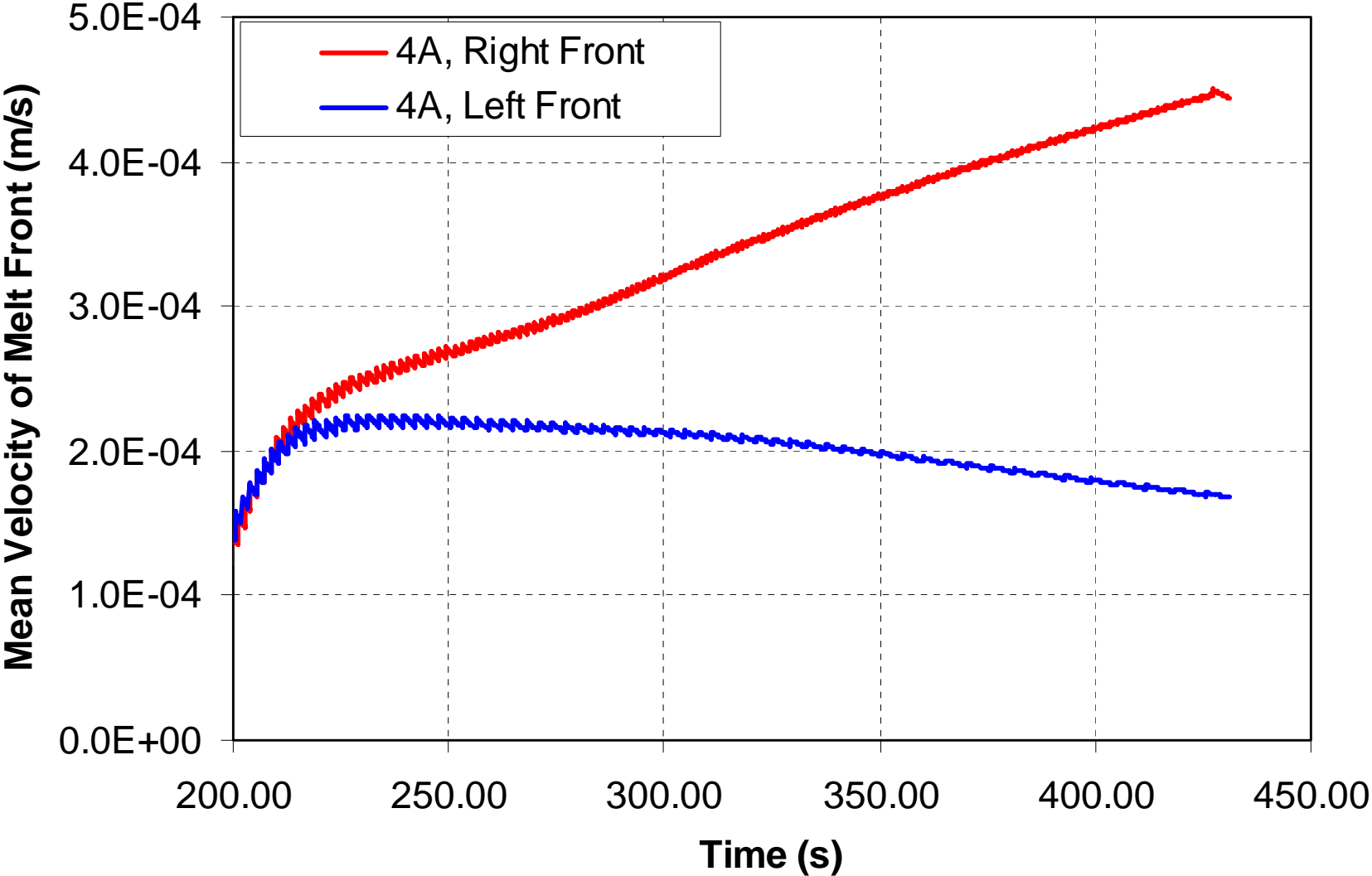
T (K)
675
550

- The small melt flow rate onto the catch plate at the beginning (< 100 sec.) caused case to crash
 - melt temperature became too low due to heat loss and small flow rate
- To overcome the difficulty, the melt flow rate on to the catch plot from 0 sec. to 200 sec. was modeled using a constant melt flow rate to create an initial amount of mass on the catch plate:
 - 1) Compute the melt flow using a large constant melt flow rate (i.e., 0.14 g/s) for 30 seconds. This will result in about 5 grams of melt on the catch plate.
 - 2) Stop simulation
 - 3) Restart simulation using the time dependent melt flow rate profile, starting at 200 sec.
 - 4) Continue simulation until melt front approaches end of plate

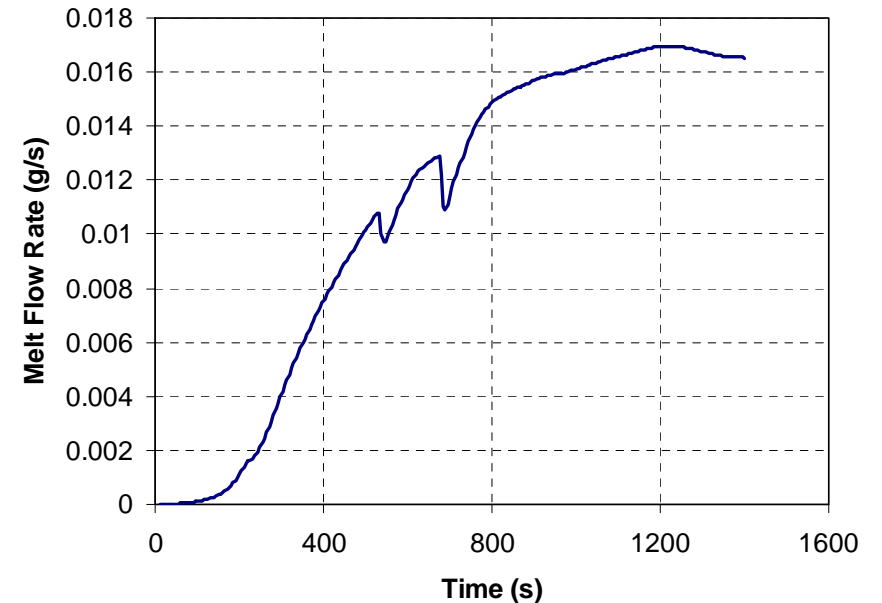
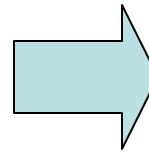
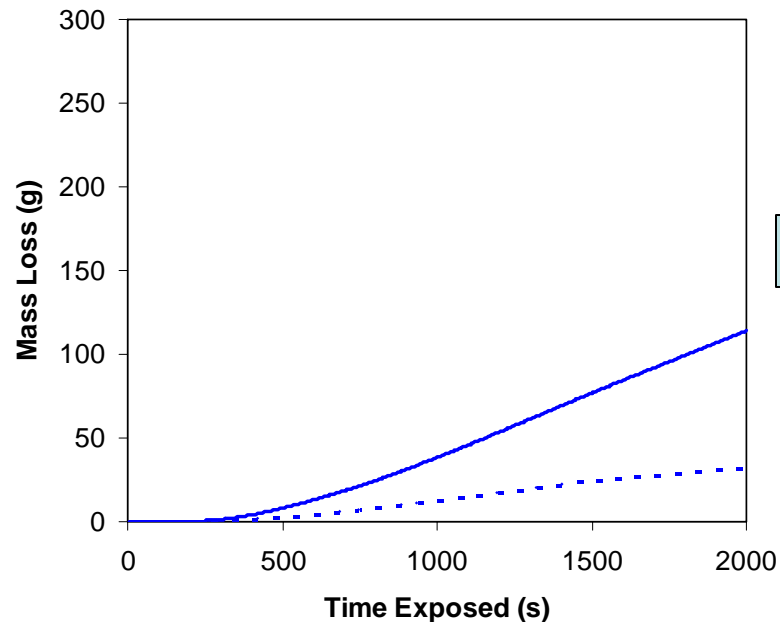


Task 4A - Spreading velocity



Task 4B – Melt flow rate

Case 3I



Mass loss history

- solid line = total mass loss
- dashed line = mass loss occurring as melt flow
- difference between solid and dashed line = mass loss due to gasification

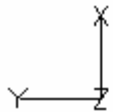
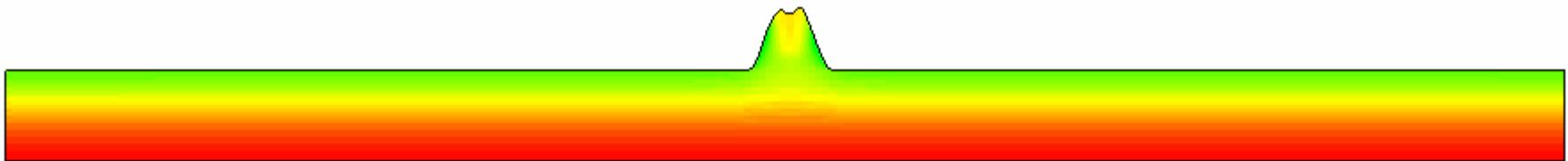
Melt flow rate calculated as the first derivative of the dashed line

Note: The melt flow rate in Case 3I is one order of magnitude smaller than that in Case 3R

Task 4B – Melt flow on catch plate

Physical time period: 700 sec – 1400 sec
CPU time: 36 hrs

T (K)
675
550



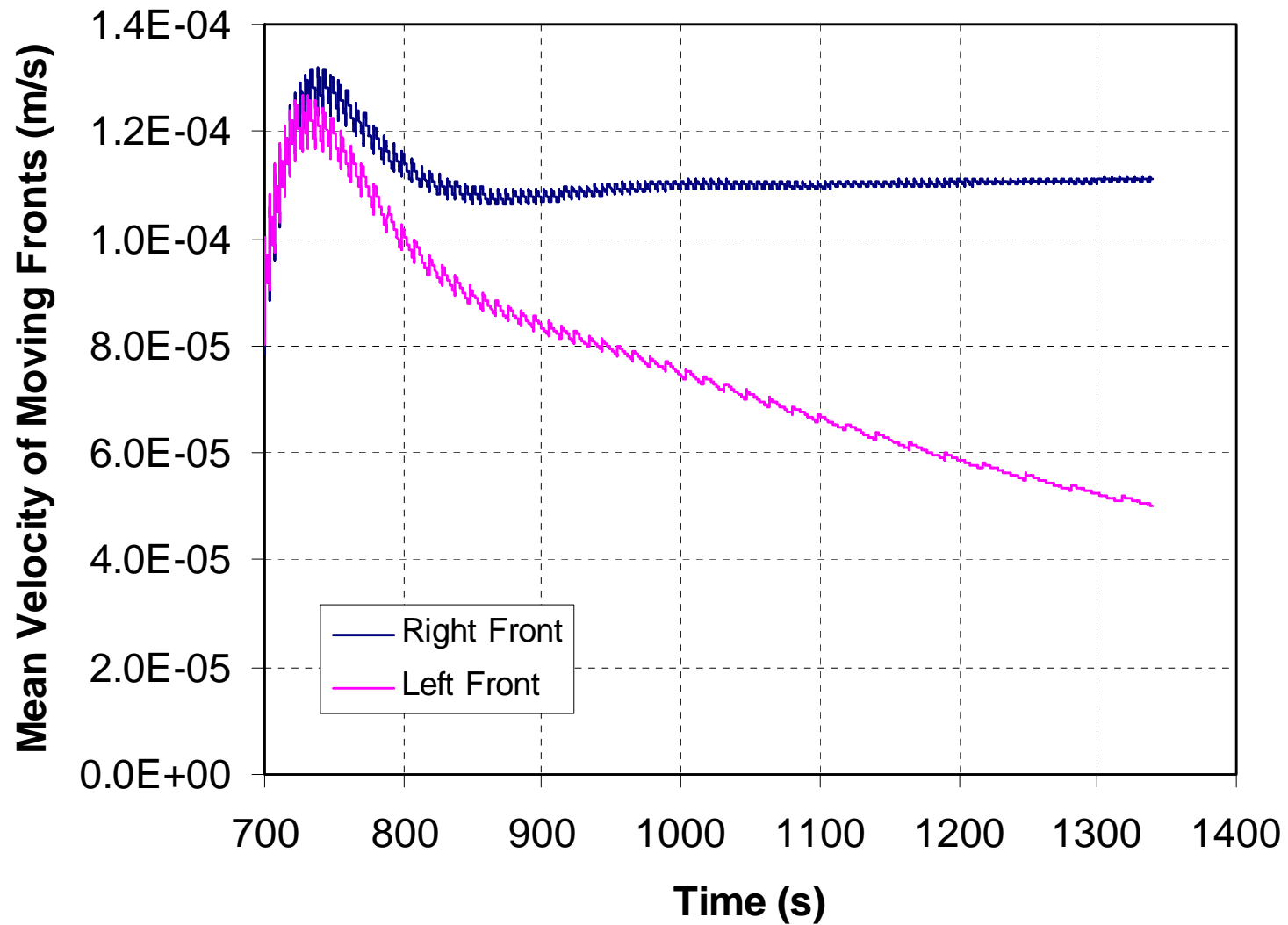
- The small melt flow rate at the beginning (< 500 sec.) caused case to crash
 - melt temperature became too low due to heat loss and small flow rate

To overcome the difficulty, the melt flow rate on to the catch plot from 0 sec. to 700 sec. was modeled using a constant melt flow rate to create an initial amount of mass on the catch plate:

- 1) Compute the melt flow using a large constant melt flow rate (i.e., 0.14 g/s) for **30 seconds**. This will result in about **5 grams** of melt on the catch plate.
- 2) Stop simulation
- 3) Restart simulation using the time dependent melt flow rate profile, starting at 700 sec.
- 4) Continue simulation until melt front approaches end of plate



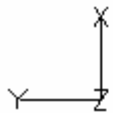
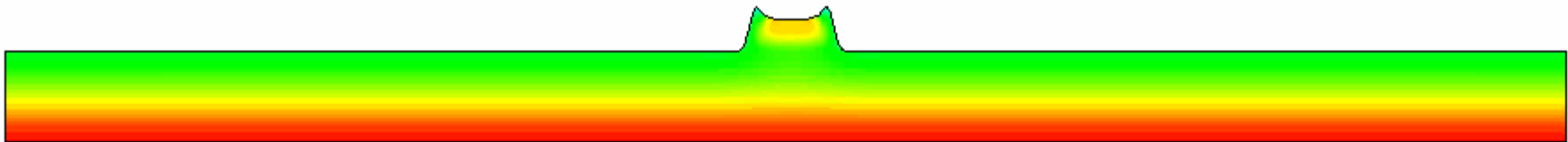
Task 4B - Spreading velocity



Task 4C – Melt flow on catch plate

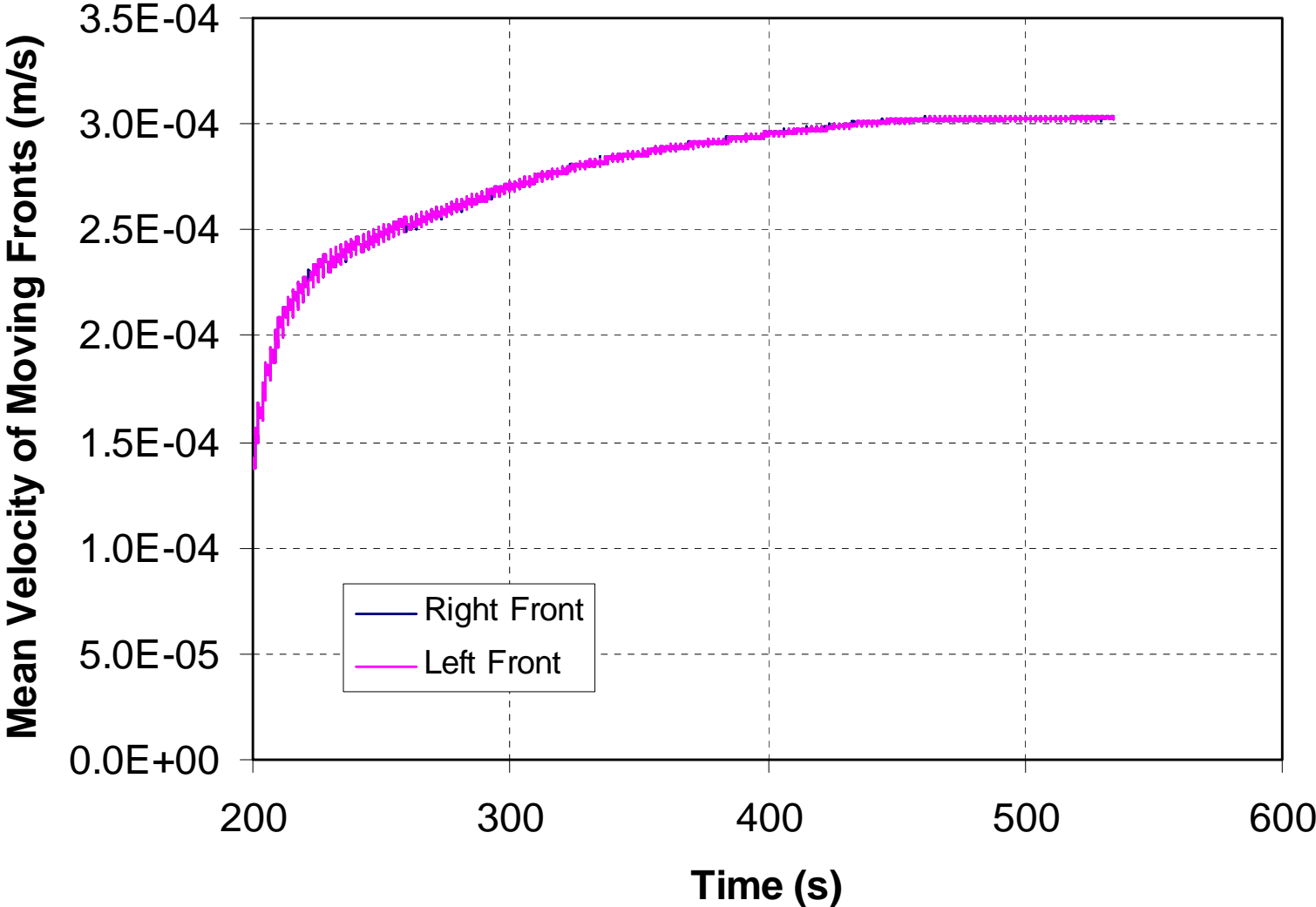
Physical time period: 200 sec – 460 sec
CPU time: 40 hrs

T (K)
675
550



- Melt flow rate the same as that in Task 4A
- Used same start-up procedure as Task 4A.

Task 4C - Spreading velocity



Note: identical curves for right front and left front



Summary and Future Work

⊕ Required Simulations in Task4 have been performed

- ⊕ Code encountered problem when started with time dependent melt flow rate because the rate is too small at the early stage, which leads to low melt temperature due to heat loss
- ⊕ A restart methodology was developed to overcome the problem. We first run the simulation using a relatively large constant melt rate for a certain time period. We then restart the simulation with the time dependent melt rate. Mass conservation is used to determine the restart point of the time dependent melt rate

Future Work

- ⊕ Finalize source code and documentation
- ⊕ Final report



APPENDIX B

CPCFD Code Documentation

1.0 Instructions for using the CPCFD code to solve problems of Task 1, 2 and 3

1) Initial Grid Generation

Before running CPCFD, the user must edit, compile and run mesh.f to generate the initial computational grid. The grid is stored in two input files GRID and INLET. Currently, the code is written for the Task 1 problem and the grid is 19X200 (ghost cells not included) for the demo case.

2) Input File

File input.dat stores all the parameters that control the simulation. The format of a typical input.dat for Task 1 is listed below:

```

T T F T F F F      !sol_u v w p tk ep om
0 0 0              !nrs nmf itcm
1 1 1 1 1 1       !NSWPu p tk ep om scalars
0.85 1.00 0.8 0.8 0.3 1.00 !RELAXu p tk ep den scalars
3 1 1 1 3        !ISCMu tk ep om scalars
1.013e5 0 20 1 0  !p_ref i,j,k,ib_init
0.0 -9.8 0.0      !gx, gy, gz
2000 2.5          !itermax sormax
0 1000 1 1       !restart nitout nitflow nitsca
1                !is_unsteady
400.0 2.d-0 1.0d0 1 !t_end dt t_outp time_level
1.d-1           !CFL number
2.4d3 2.98d2 9.0d2 2.5d-1 !Cp, temp_init, density, heat conductivity
30000.d0 1.25d6    !incident heat flux, gasification heat
2                !ipolymer, 1 - PP23K; 2 - PP702N; 3 - PP6523

```

The first line contains logical flags that determine which equations are to be solved. For 2-D polymer melting problem, the user must not change this line. For 3-D problem, the third parameter should be changed to "T" that enables the code to solve the "w velocity".

The second line contains parameters related to reactive flow simulation, and should be kept the same when modeling polymer melting problems.

The third line contains the number of TDMA sweeps used in solving the linear equations.

The fourth line contains the under-relaxation factors used in solving different equations. The first under-relaxation factor corresponds to the momentum equation, which may need adjustments during calculation to avoid divergence or to speed up convergence. This can be done by changing the value in the ACTIVE file. The other relevant under-relaxation factors are the second one and the last one, corresponding to the pressure equations and the temperature equation, respectively. Currently they are set to be 1.0 (i.e., no under-relaxation), and have not caused any problem in all the test runs.

The fifth line controls the differencing schemes for the equations. 1 – upwind scheme; 2 -- central differencing scheme; 3 -- mixing scheme; 4 -- exponent scheme.

The sixth line contains the reference pressure (Pa), and the index of the reference grid point.

The seventh line contains the components of the gravity vector

The eighth line contains the maximum number of outer iteration in each time step (itermax) and the residual limit (sormax) used to determine convergence. For example, if sormax=1.0, then the solutions must converge to a level that at least six significant digits remain unchanged from iteration to iteration. Whereas if sormax = 6, only one significant digit remain unchanged.

The ninth line contains, from left to right, the flag for restart, the iteration interval for diagnostic output, the number of inner iterations for solving the momentum and pressure equations, and the number of inner iterations for solving the temperature equation. If the restart flag is 1, then the code will try to read in the restart files at the beginning of the simulation. If it is 0, the simulation will start from scratch. For restart, see section 8) for detail.

The tenth line contains the flag for simulating unsteady problem, 1 for time accurate unsteady problem and 0 for steady problem. For Task 1, the flag should remain 1.

The eleventh line contains, from left to right, the ending time of the simulation, the maximum time step allowed, the time interval for solution output, and the time marching scheme (0 for first order backward Euler scheme, and 1 for second order 3-level scheme).

The twelfth line contains the CFL number used to determine time step. Larger CFL number leads to longer time step.

The last two lines assigns case parameters: specific heat, initial temperature, density, heat conductivity, and incident heat flux, gasification heat and a flag for choosing polymer.

3) ACTIVE File

Once the simulation starts, an ACTIVE file will be written out, and can be used to control the simulation in the fly. A typical ACTIVE file reads

```

1000.0      !End time
2000       !Max iteration #
1          !Max flow iteration #
1          !Max temperature iteration #
0.3        !density under-relaxation factor
100        !number of outer iterations between diagnostic screen output
0.85  1.0  !under-relaxation factors for momentum and pressure equations
1.0        !under-relaxation factor for temperature equation
2.0        !maximum time step

```

0.2	!CFL number
1.0	!output time interval
2.5	!residual upper limit

See comments at the end of each line for explanation.

The minimum number of global iterations (default value) in each time step is 10.

4) Case Dependent Source Files

The Fortran source code includes the following files:

```
cpcfd.f -- main program
fmb3.f -- containing all driving subroutines
fblock.f -- implementations of models and solver.
```

A Makefile can be used to compile and link the source code. The user may need to modify the Makefile based on the available operating system and Fortran compiler. At REI, the code is compiled under Linux system using a Portland Group Fortran Compiler (pgf90).

Certain parts of the source code are case dependent, and need modification when setting up different cases. They are contained in fblock.f and are listed below. For more detail, see the code.

```
subroutine fbck_setup --- set material properties such as k, Cp, density, and initial
                           temperature.
subroutine fbck_mvlg --- implement re-meshing scheme
subroutine fbck_pcorrcr --- implement cell face mass flux correction due to moving
                           mesh and boundary
subroutine fbck_bc_sca --- apply heat flux boundary condition
function vislam --- implement viscosity-temperature relation
```

In the demo, the code is configured to mode PP702 exposed to 30,000 W/m² constant heat flux with radiative and convective heat loss.

5) Run the Simulation from Scratch

Following are the steps to run the demo simulation from scratch

- Create two sub-directories (./FV and ./output) under working directory.
- Compile and run mesh.f. Copy GRID and INLET to the working directory.
- Compile the source code and copy the executable CPCFD.exe to working directory.
- Edit and Copy input.dat to working directory. Make sure the restart flag is turned off.
- launch CPCFD.exe

Typical screen output looks like the following:


```

.....
.....
.....
Time = 0.20868E+03 W(y=0) = 0.28049E-01 W(y=0.25) = 0.99674E-02
Time = 0.20868E+03 totv = 0.58634E-03 Mass Loss Ratio = 0.61879E-01 Total mass loss
rate = 0.21649E+00 Melt flow fraction = 0.82360E+00
mass conservation: 0.34031181E-03 0.35697476E-08 0.76451802E-09 0.13137932E-03
0.28340087E-04 0.50003122E-03
0.51208481E-02 0.29436213E-09 0.51208481E-01 0.29436213E-09

TIME STEP: 4800 time = 208.69372 dt = 0.00512

TIME STEP: 4800 time = 208.69372 dt = 0.00512
ITER = 1 Iter_flow = 1 RESIDUAL: M, U, V, W
1.09237 0.17468 0.69568 -22.96195

TIME STEP: 4800 time = 208.69372 dt = 0.00512
ITER = 1 Iter_scalar = 1 Residual: SCALARS
1.62199

MUVS 1 1.09237 0.17468 0.69568 1.62199
MUVS 10 0.96373 0.29299 0.70663 -4.84325

Time = 0.20869E+03 W(y=0) = 0.28049E-01 W(y=0.25) = 0.99669E-02
Time = 0.20869E+03 totv = 0.58634E-03 Mass Loss Ratio = 0.61893E-01 Total mass loss
rate = 0.21649E+00 Melt flow fraction = 0.82360E+00
mass conservation: 0.34030748E-03 0.35694999E-08 0.76450220E-09 0.13138289E-03
0.28340851E-04 0.50003122E-03
0.51201375E-02 0.29437275E-09 0.51201375E-01 0.29437275E-09
.....
.....
.....

```

The first line shows, from left to right, the current time, object thickness at $y=0$ (bottom) and at $y=0.25$ (top).

The second line shows, from left to right, the current time, volume of the calculation domain, mass loss ratio, total mass loss rate and melt flow fraction during the current time step.

The third line shows information regarding mass conservation. From left to right, they are volume remaining in the domain, volume flowing out during the previous time step, volume gasifying into the environment, cumulated volume flowing out of the domain, cumulated volume gasifying into the environment, and the sum of the remaining volume and the cumulated volumes leaving the domain.

The fourth line shows information regarding time step selection. From left to right, they are actual time step used, maximum time step based on diffusion, maximum time step based on convection, and maximum time step based on both diffusion and convection.

The fifth line shows the current time step, current time, and time step size.

The sixth to eighth lines show the residuals of the continuity and momentum equations (listed in the eighth line) after one global iteration.

The ninth to eleventh lines show the temperature equation residual.

The interval of global iterations for residual output can be adjusted in the ACTIVE file

The next two lines are summary of the residuals for each solved equations.

6) Output Data

The solutions that can be visualized by graphic tools are written to the ./FV directory. The data are in PLOT3D format. The data are written out every n seconds, where n is the output time interval defined in input.dat file and can be adjusted in the ACTIVE file. The files are organized as follows:

f3dmbXXX.fun --- stores the solution
f3dmbXXX.grd --- stores the multi-block grid
f3dmb.nam --- stores the name of the solved quantities

In the file name, "XXX" represents the time in seconds. For example, f3dmb500.fun contains the solution at t=500 sec. In addition to these data files, file f3dmb0.fun and f3dmb0.grd always store the latest solution after each time step, which can be used to monitor the solution without having to wait the solution to reach a specific time point.

When the simulation completes, the final solution is written to the following files: f3dmb.fun and f3dmb.grd

In REI, FieldView is used to visualize the data. When reading the data, choose FORMATTED for FILE FORMAT; choose 3-D for COORDINATES; and choose MULTI-GRID for DATA FORMAT.

7) Other Diagnostic Output

Several files are written to the working directory to monitor the simulation process.

File surf.dat contains information about the free surface location. The data are organized into three columns. The first column stores the elevation of the grid points on the free surface, and the second and third columns store the corresponding coordinates in the horizontal direction at the beginning and at the end of the current time step.

File massloss.dat contains information about mass conservation, which are also shown on the screen. See section 5) for detail.

8) Restart

Restart file are stored in the ./output directory. After each output time point, two files are written out, they are

GRIDXXX and RESTRTXXX

where "XXX" represents the time in seconds.

To restart, the user must copy these files to the working directory and rename them as GRID and RESTRT, respectively. For example, if the user wants to restart the simulation at t=140 sec. the files GRID140 and RESTRT140 must be copied to the working directory and renamed to GRID and RESTRT.

Before restart, make sure the restart flag in input.dat is set to 1.

Delete GRID and RESTRT if the simulation is intended to start from scratch. In this case, GRID must be generated by executing the initial mesh generator. See section 1) for detail.

2.0 Instructions for using the CPCFD code to solve problems of Task 4

1) Initial Grid Generation

Before running CPCFD, the user must edit, compile and run mesh.f to generate the initial computational grid. The grid is stored in two input files GRID and INLET. For the Task 4 demo case, there are 30 grid points in the X direction and 400 grid points in the Y direction (ghost cells not included). The catch plate consists of 10X400 fixed grid points. The polymer melt has 20X400 grid points and these points are allowed to move in the X direction. The initial thickness of the polymer melt is set to be 1.e-4 m. For more details about the computational grid, see final reports.

2) Input File

File input.dat stores all the parameters that control the Task 4 simulation. The format of a typical input.dat for Task 4 is listed below:

```

T T F T F F F      !sol_u v w p tk ep om
0 0 0              !nrs nmf itcm
1 1 1 1 1 1       !NSWPu p tk ep om scalars
0.85 1.00 0.8 0.8 0.3 1.00 !RELAXu p tk ep den scalars
3 1 1 1 3         !ISCMu tk ep om scalars
1.013e5 0 20 1 0  !p_ref i,j,k,ib_init
0.0 -9.8 0.0      !gx, gy, gz
2000 2.5          !itermax sormax
0 1000 1 1       !restart nitout nitflow nitsca
1                !is_unsteady
400.0 2.d-0 1.0d0 1 !t_end dt t_outp time_level
1.d-1            !CFL number
2.4d3 2.98d2 9.0d2 2.5d-1 !Cp, temp_init, density, heat conductivity
30000.d0 1.25d6   !incident heat flux, gasification heat
2                !ipolymer, 1 - PP23K; 2 - PP702N; 3 - PP6523
-1.0 650.0       !mass flow rate, melt temperature
1                !surface tension model

```

The first line contains logical flags that determine which equations are to be solved. For 2-D polymer melting problem, the user must not change this line. For 3-D problem, the third parameter should be changed to "T" that enables the code to solve the "w velocity".

The second line contains parameters related to reactive flow simulation, and should be kept the same when modeling polymer melting problems.

The third line contains the number of TDMA sweeps used in solving the linear equations.

The fourth line contains the under-relaxation factors used in solving different equations. The first under-relaxation factor corresponds to the momentum equation, which may need

adjustments during calculation to avoid divergence or to speed up convergence. This can be done by changing the value in the ACTIVE file. The other relevant under-relaxation factors are the second one and the last one, corresponding to the pressure equations and the temperature equation, respectively. Currently they are set to be 1.0 (i.e., no under-relaxation), and have not caused any problem in all the test runs.

The fifth line controls the differencing schemes for the equations. 1 -- upwind scheme; 2 -- central differencing scheme; 3 -- mixing scheme; 4 -- exponent scheme.

The sixth line contains the reference pressure (Pa), and the index of the reference grid point.

The seventh line contains the components of the gravity vector - gx, gy, and gz. The catch plate tilt angle beta is also defined by the gravity vector as $\tan(\beta) = gy/gx$.

The eighth line contains the maximum number of outer iteration in each time step (itermax) and the residual limit (sormax) used to determine convergence. For example, if sormax=1.0, then the solutions must converge to a level that at least six significant digits remain unchanged from iteration to iteration. Whereas if sormax = 6, only one significant digit remain unchanged.

The ninth line contains, from left to right, the flag for restart, the iteration interval for diagnostic output, the number of inner iterations for solving the momentum and pressure equations, and the number of inner iterations for solving the temperature equation. If the restart flag is 1, then the code will try to read in the restart files at the beginning of the simulation. If it is 0, the simulation will start from scratch. For restart, see section 8) for detail.

The tenth line contains the flag for simulating unsteady problem, 1 for time accurate unsteady problem and 0 for steady problem. For Task 1, the flag should remain 1.

The eleventh line contains, from left to right, the ending time of the simulation, the maximum time step allowed, the time interval for solution output, and the time marching scheme (0 for first order backward Euler scheme, and 1 for second order 3-level scheme).

The twelfth line contains the CFL number used to determine time step. Larger CFL number leads to longer time step.

The thirteenth to fifteenth lines assign case parameters: specific heat, initial temperature, density, heat conductivity, and incident heat flux, gasification heat and a flag for choosing polymer. It should be noted that, when simulating melt flow on the catch plate, the initial temperature in the data file is only used to set the backside temperature of the catch plate. Initial temperature distribution within the catch plate is hardwired in the code currently (see lines 794 - 800 of fblock.f) and the final report

The sixteenth line assigns a constant mass flow rate of the melt (kg/s) and the melt temperature (K). To use time dependent mass flow rate in the calculation, the user must do the following:

- A. set the mass flow rate in the input file to -1.0
 B. create an ASCII data file "massrate.dat" in the following format

11		----- Total number of table entry
0.0	7.81E-05	----- Time (s) and mass flow rate (kg/s)
5.01332	8.16E-05	
10.0187	8.60E-05	
15.02898	9.20E-05	
20.03494	9.84E-05	
25.03807	1.04E-04	
30.04405	1.07E-04	
35.04669	1.08E-04	
40.05655	1.08E-04	
45.06237	1.09E-04	
50.07059	1.10E-04	

The code will tabulate the table contained in "massrate.dat" to determine the time dependent mass flow rate

The last line is a flag for the surface tension model. To apply the surface tension model, set the flag to 1. Otherwise, set it to 0.

3) ACTIVE File

Once the simulation starts, an ACTIVE file will be written out, and can be used to control the simulation in the fly. A typical ACTIVE file reads

1000.0		!End time
2000		!Max iteration #
1		!Max flow iteration #
1		!Max temperature iteration #
0.3		!density under-relaxation factor
100		!number of outer iterations between diagnostic screen output
0.85	1.0	!under-relaxation factors for momentum and pressure equations
1.0		!under-relaxation factor for temperature equation
2.0		!maximum time step
0.2		!CFL number
1.0		!output time interval
2.5		!residual upper limit

See comments at the end of each line for explanation.

The minimum number of global iterations (default value) in each time step is 10.

4) Case Dependent Source Files

The Fortran source code includes the following files:

```
cpcfd.f -- main program
fmb3.f  -- containing all driving subroutines
fblock.f -- implementations of models and solver.
```

A Makefile can be used to compile and link the source code. The user may need to modify the Makefile based on the available operating system and Fortran compiler. At REI, the code is compiled under Linux system using a Portland Group Fortran Compiler (pgf90).

Certain parts of the source code are case dependent, and need modification when setting up different cases. They are contained in fblock.f and are listed below. For more detail, see the code.

```
subroutine fbck_setup --- set material properties such as k, Cp, density, and initial
                        temperature.
subroutine fbck_mvlg  --- implement re-meshing scheme
subroutine fbck_pcorrc --- implement cell face mass flux correction due to moving
                        mesh and boundary
subroutine fbck_bc_sca --- apply heat flux boundary condition
function vislam --- implement viscosity-temperature relation
subroutine SurfCurveA --- calculates free surface curvature
```

The surface tension model is implemented in fbck_bc_sca, fbck_calcu, and fbck_calcv

In the demo, the code is configured to mode the Task 4 problem and can not be used for Task 1 to 3.

5) Run the Simulation from Scratch

Following are the steps to run the demo simulation from scratch

- a) Create two sub-directories (./FV and ./output) under working directory.
- b) Compile and run mesh.f. Copy GRID and INLET to the working directory.
- c) Compile the source code and copy the executable CPCFD.exe to working directory.
- d) Edit and Copy input.dat to working directory. Set t_end to 30.0, mass flow rate to 1.4e-4. Make sure the restart flag and the surface tension model flag are turned off.
- e) Launch CPCFD.exe

Once the simulation of the first 30 seconds completed, do the following

- a) Copy GRID29 and RESTR29 from ./output to the working directory and rename them as GRID and RESTR

- b) Open input.dat. Set t_{end} to 400.0 and mass flow rate to -1.0. Turn on the restart flag and the surface tension model flag. Save input.dat.
 c) Copy massrate.dat to the working directory.
 c) Launch CPCFD.exe again.

Typical screen output looks like the following:

```

.....
.....
.....
Time = 0.32455E+02 W(j=2) = 0.10000E-03 W(j=200) = 0.45568E-02 VR = 0.14790E-03
VL = 0.16639E-03
melt flow rate = 1.0748186883438162E-004
0.20000000E-01 0.35000003E-09 0.99929105E-01 0.35000003E-09

TIME STEP: 149 time = 32.49467 dt = 0.02000

TIME STEP: 149 time = 32.49467 dt = 0.02000
ITER = 1 Iter_flow = 1 RESIDUAL: M, U, V, W
2.42088 1.73416 2.11876 -22.40645

TIME STEP: 149 time = 32.49467 dt = 0.02000
ITER = 1 Iter_scalar = 1 Residual: SCALARS
1.43313

MUVS 1 2.42088 1.73416 2.11876 1.43313
MUVS 10 2.49579 1.77480 2.13870 0.31786

Time = 0.32475E+02 W(j=2) = 0.10000E-03 W(j=200) = 0.45544E-02 VR = 0.14781E-03
VL = 0.16628E-03
melt flow rate = 1.0748586672349618E-004
0.20000000E-01 0.35000003E-09 0.10109939E+00 0.35000003E-09
.....
.....
.....

```

The first line shows, from left to right, the current time, the thickness of the melt layer at the edge of the catch plate, the thickness of the melt layer at the center of the catch plate, the moving velocity of the right front and the moving velocity of the left front.

The second line shows the melt flow rate at the current time step.

The third line shows information regarding time step selection. From left to right, they are actual time step used, maximum time step based on diffusion, maximum time step based on convection, and maximum time step based on both diffusion and convection.

The fourth line shows the current time step, current time, and time step size.

The fifth to seventh lines show the residuals of the continuity and momentum equations (listed in the seventh line) after one global iteration.

The eighth to tenth lines show the temperature equation residual.

The interval of global iterations for residual output can be adjusted in the ACTIVE file

The next two lines are summary of the residuals for each solved equations.

6) Output Data

The solutions that can be visualized by graphic tools are written to the ./FV directory. The data are in PLOT3D format. The data are written out every n seconds, where n is the output time interval defined in input.dat file and can be adjusted in the ACTIVE file. The files are organized as follows:

f3dmbXXX.fun --- stores the solution
f3dmbXXX.grd --- stores the multi-block grid
f3dmb.nam --- stores the name of the solved quantities

In the file name, "XXX" represents the time in seconds. For example, f3dmb500.fun contains the solution at t=500 sec. In addition to these data files, file f3dmb0.fun and f3dmb0.grd always store the latest solution after each time step, which can be used to monitor the solution without having to wait the solution to reach an specific time point.

When the simulation is completed, the final solution is written to the following files: f3dmb.fun and f3dmb.grd

In REI, FieldView is used to visualize the data. When reading the data, choose FORMATTED for FILE FORMAT; choose 3-D for COORDINATES; and choose MULTI-GRID for DATA FORMAT.

7) Other Diagnostic Output

File surf.dat contains information about the free surface location. The data are organized into three columns. The first column stores the elevation of the grid points on the free surface, and the second and third columns store the corresponding coordinates in the horizontal direction at the beginning and at the end of the current time step.

8) Restart

Restart file are stored in the ./output directory. After each output time point, two files are written out, they are

GRIDXXX and RESTRTXXX

where "XXX" represents the time in seconds.

To restart, the user must copy these files to the working directory and rename them as GRID and RESTRT, respectively. For example, if the user wants to restart the simulation at t=140 sec. the files GRID140 and RESTRT140 must be copied to the working directory and renamed to GRID and RESTRT.

Before restart, make sure the restart flag in input.dat is set to 1.

Delete GRID and RESTRT if the simulation is intended to start from scratch. In this case, GRID must be generated by executing the initial mesh generator. See section 1) for detail.

3.0 Instructions for adjusting control parameters to avoid divergence

It is possible that, during the course of a simulation, the code diverges. To solve the problem, it is always helpful to make sure that all the restart files are properly stored. If a divergence happens, one can always restart the case from a previous time step after adjusting some of the control parameters in the input data file. The following steps can be taken to make the code less prone to divergence:

1. reducing the maximum time step size
2. reducing the CFL number that also controls the time step size
3. reducing the under-relaxation factors used in solving the momentum, pressure, and energy equations

If the problem persists, try to restart from an even earlier time step and repeat the above steps. The proper values of these control parameters are case dependent. It is necessary to adjust these numbers on a trial-and-error base.

The control parameters can also be adjusted in the ACTIVE file without terminating the case. By monitoring the screen output or the output log file, it is often possible to spot the on-set of divergence. For example, if the number of iterations to reach convergence in a time step increases significantly compared to the number of iterations required in previous time steps, it may indicate that the simulation has become unstable and divergence may occur within the next couple time steps. To avoid the divergence, try the three steps mentioned above in the ACTIVE file.

Sometimes, divergence is caused by factors such as using extreme boundary conditions and thus divergence can not be solved by simply adjusting the control parameters. For example, in the simulations performed for Task 4 if the backside temperature of the catch plate is below a certain value, the case will diverge due to the worsening grid quality (i.e., grid skewness) developed during the simulation. If this occurs, one has to study the exact cause of the problem and fix it.